



IMPERIAL INSTITUTE  
OF  
AGRICULTURAL RESEARCH, PUSA.







PROCEEDINGS  
OF THE  
ROYAL SOCIETY OF LONDON

SERIES A—MATHEMATICAL AND PHYSICAL SCIENCES

VOL CXLIX

LONDON

Printed and published for the Royal Society  
By Harrison & Sons, Ltd., 44-47, St. Martin's Lane  
Printers in Ordinary to His Majesty

April, 1935

LONDON :  
HARRISON AND SONS, LTD., PRINTERS IN ORDINARY TO HIS MAJESTY  
ST. MARTIN'S LANE

# CONTENTS

## SERIES A VOL CXLIX

No. A 866—March 1, 1935

PAGE

A Theory of the Rotations of Molecules in Solids and of the Dielectric Constant of Solids and Liquids. By R. H. Fowler, F.R.S.....	1
Raman Spectra of Certain Organo-Metallic Compounds. By N. Gopala Pai. Communicated by Sir Venkata Raman, F.R.S. (Plate 1).....	29
The Effect of Temperature on the Thermal Conductivity and the Accommodation Coefficient of Hydrogen. By H. S. Gregory. Communicated by G. P. Thomson, F.R.S. ....	35
Investigations on the Spectrum of Selenium. V—Structure of Se II. By S. G. Krishnamurty and K. R. Rao. Communicated by M. N. Saha, F.R.S. (Plates 2 and 3).....	56
The Electromagnetic Equations of the Supraconductor. By F. and H. London. Communicated by F. A. Lindemann, F.R.S. ....	71
Shear Waves through the Earth's Core. By L. Bastings. Communicated by Lord Rutherford, O.M., F.R.S.....	88
The Accommodation Coefficient and the Evaporation Coefficient of Water. By T. Alty and C. A. Mackay. Communicated by R. H. Fowler, F.R.S...	104
Contributions to the Theory of Specific Heat. III—On the Existence of Pseudo- $T^3$ Regions in the Specific Heat Curve of a Crystal. By M. Blackman. Communicated by S. Chapman, F.R.S.....	117
Contributions to the Theory of Specific Heat. IV—On the Calculation of the Specific Heat of Crystals from Elastic Data. By M. Blackman. Communicated by S. Chapman, F.R.S.....	126
The Photoelectric Absorption of $\gamma$ -Rays in Heavy Elements. By H. R. Hulme, J. McDougall, R. A. Buckingham, and R. H. Fowler, F.R.S.....	131
Experiments at Very Low Temperatures obtained by the Magnetic Method. I—The Production of the Low Temperatures. By N. Kürti and F. Simon. Communicated by F. A. Lindemann, F.R.S.....	152
The Scattering of Neutrons by Protons. By H. A. Bethe and R. Peierls. Communicated by D. R. Hartree, F.R.S.....	176
On the Direction of Approach of Microseismic Waves. By A. W. Lee. Communicated by G. C. Simpson, F.R.S.....	183
The Transmutation of Heavy Hydrogen Investigated by the Cloud-Track Method. By P. I. Dee and C. W. Gilbert. Communicated by Lord Rutherford, O.M., F.R.S. (Plates 4 and 5).....	200

	PAGE
Results of Calculations of Atomic Wave Functions. III—Results for Be, Ca, and Hg. By D. R. Hartree, F.R.S., and W. Hartree.....	210
The Interaction of Hydrogen with Micro-Crystalline Charcoal—I. By R. M. Barrer and E. K. Rideal, F.R.S.....	231
The Interaction of Hydrogen with Micro-Crystalline Charcoal. II—Activated Sorption of Hydrogen and Methane by Carbon. By R. M. Barrer. Communicated by E. K. Rideal, F.R.S.....	253
The Nuclear Spin of Iodine. I—Fine Structure in the First Spark Spectrum. By S. Tolansky. Communicated by W. L. Bragg, F.R.S.....	269
X-Ray Study of the Inter-Diffusion of Copper and Zinc. By E. A. Owen and L. Pickup. Communicated by Sir William Bragg, O.M., F.R.S.....	282
The Diurnal Variation of Magnetic Disturbance in High Latitudes. By J. M. Stagg. Communicated by G. C. Simpson, F.R.S.....	298
The Behaviour of Three Single Crystals of Aluminium in Fatigue under Complex Stresses. By H. L. Cox and W. J. Clenshaw. Communicated by H. J. Gough, F.R.S. (Plates 6 and 7).....	312
Investigations of Raman Spectra. Part I—The Raman Spectra of Sulphuric, Nitric, and Nitrosylsulphuric Acids. By W. R. Angus and A. H. Leckie. Communicated by F. G. Donnan, F.R.S. ....	327
The Thermal Decomposition of Acetone Vapour. By C. A. Winkler and C. N. Hinshelwood, F.R.S. ....	340
The Thermal Decomposition of Acetaldehyde. By C. A. Winkler and C. N. Hinshelwood, F.R.S. ....	355
Adsorption on Measured Surfaces of Vitreous Silica. By W. G. Palmer and R. E. D. Clark. Communicated by Sir William Pope, F.R.S.....	360
On Gauss' Theorem and the concept of Mass in General Relativity. By E. T. Whittaker, F.R.S. ....	384
The Isotopic Constitution and Atomic Weights of Hafnium, Thorium, Rhodium, Titanium, Zirconium, Calcium, Gallium, Silver, Carbon, Nickel, Cadmium, Iron, and Indium. By F. W. Aston, F.R.S.....	396
The Accurate Determination of the Energy Released in Certain Nuclear Transformations. By M. L. E. Oliphant, A. R. Kempton, and Lord Rutherford, O.M., F.R.S. ....	406

Ship Waves: The Relative Efficiency of Bow and Stern. By T. H. Havelock, F.R.S.....	417
The Variation of the Mobility of Gaseous Ions with Temperature. I—Positive Ions in their own Gas. By A. M. Tyndall, F.R.S., and A. F. Pearce.....	426

	PAGE
Electronic Spectra of Polyatomic Molecules. I—Saturated Aldehydes. By E. Eastwood and C. P. Snow. Communicated by T. M. Lowry, F.R.S. (Plate 8).....	434
Electronic Spectra of Polyatomic Molecules. II—Acrolein. By E. Eastwood and C. P. Snow. Communicated by T. M. Lowry, F.R.S. (Plates 9 and 10).....	446
Statistical Error in Counting Experiments. By R. Peierls. Communicated by R. H. Fowler, F.R.S. ....	467
On the Spectrum of the Normal Frequencies of a Polar Crystal Lattice. I—General Theory. By J. H. C. Thompson. Communicated by E. A. Milne, F.R.S. ....	487
International Frequency Comparisons by Means of Standard Radio Frequency Emissions. By L. Essen. Communicated by Sir Joseph Petavel, F.R.S... ..	506
The Rotational Dispersion of Sound in Hydrogen. By A. S. Roy and M. E. Rose. Communicated by H. S. Allen, F.R.S.....	511
Artificial Radioactivity produced by Neutron Bombardment—II. By E. Amaldi, O. D'Agostino, E. Fermi, B. Pontecorvo, F. Rasetti and E. Segrè. Communicated by Lord Rutherford, O.M., F.R.S. ....	522
The Theoretical Determination of the Lift Coefficient for a Thin Elliptic Cylinder. By L. Howarth. Communicated by G. I. Taylor, F.R.S.....	558
The Secondary Cathode Rays Expelled from Metals by Molybdenum K $\alpha$ Radiations. By H. R. Robinson, F.R.S., and C. J. B. Clews.....	587
The Kinetics of Photosynthesis. (Abstract.) By E. C. C. Baly, F.R.S.....	596
Index .....	597

---



# A Theory of the Rotations of Molecules in Solids and of the Dielectric Constant of Solids and Liquids

By R. H. FOWLER, F.R.S.

(Received 21st December, 1934)

## § 1—INTRODUCTION

It is well known that Rochelle salt,  $\text{NaKC}_4\text{H}_4\text{O}_6 \cdot 4\text{H}_2\text{O}$ , for a limited range of temperature may, for practical purposes, be said to have an infinite dielectric constant analogous to the infinite permeability of iron in its ferromagnetic state. Such states, it is now realized, occur in a number of phenomena and a common description is of value; we shall refer to them as *co-operative states*. The co-operative state in Rochelle salt is limited by an upper critical temperature  $T_u$  (or Curie Point) such that for  $T > T_u$  the susceptibility though large is finite and decreases rapidly as  $T$  increases. Unlike the corresponding magnetic substances there is also a lower critical temperature  $T_l$  such that for  $T < T_l$  the susceptibility is again finite and decreases as  $T$  decreases. It is agreed\* that these phenomena are to be explained by the orientation of polar molecules in the crystal—the polar molecules in these particular crystals being undoubtedly water molecules present as water of crystallization. The co-operative state and the upper critical temperature  $T_u$  can be explained by an exact analogy of the Weiss-Langevin theory of ferromagnetism, and no difficulties are raised by the large size of the necessary molecular field. The interaction energy of electrical dipoles is so large that it supplies precisely the necessary term which it fails to do in the magnetic case. The explanation of this part of the phenomenon requires the polar water molecules to be orientating freely under the influence of the effective applied electric field. The lower critical temperature  $T_l$  can and must then be explained, it is believed, by a failure of the free rotations at lower temperatures which can so cut down the efficiency of the response to the applied field that the material is no longer self-polarizing.†

Again the dielectric constant of ice or water is finite at all temperatures, and falls to low values even for low frequencies as the temperature is

\* See, e.g., Kobeko and Kurtschatow, 'Z. Physik,' vol. 66, p. 192 (1930).

† B. and I. Kurtschatow, 'Phys. Z. Sowjet.,' vol. 3, p. 320 (1933).



decreased below 150° K. This can only be understood, assuming that the  $\text{H}_2\text{O}$  molecule in ice or water carries the same dipole as in steam, or even a comparable one, if its orientations are not free but severely restricted by the local field of its neighbours, even at the highest temperatures for which the dielectric constant of water has been investigated. The water dipoles are so numerous and so strong that water and ice would be co-operative at all temperatures if the dipole carriers were even approximately free. Somewhat similar phenomena occur for other polar liquids such as some of the alcohols and nitrobenzene which are believed to be explicable in the same way. Rochelle salt, and its variants in which ammonium replaces potassium, are the only known substances with a co-operative state. While there is probably general agreement about these qualitative explanations, it seems that no quantitative discussion has yet been given, even of any simplified model, which really displays behaviour of the types observed. Such a discussion of a simple model will be given in this paper. The exact results for the simple model reproduce many of the features observed, but naturally the model is too much simplified to expect it to provide a faithful representation of every detail. It is, however, possible to see the modifications necessary in the model to make it the better fit the facts, and to see, moreover, that these modifications are physically reasonable. The need for such a quantitative theory was first brought clearly to my notice at a conference on the solid state held in Leningrad in 1932. As will appear, however, an essential feature of the theory is an application of the ideas of order and disorder in metallic alloys, where the ordered state is typically co-operative, recently put forward by Bragg and Williams.\* As soon as their ideas are incorporated the theory "goes."

Any attempt to discuss these dielectric constants on the basis of the orientations (and rotations) of molecular dipoles naturally raises the whole question of the rotations of molecules in solids, and, in fact, this question must and can be disposed of satisfactorily by the same theory before we pass on to the dielectric constant. It has again long been recognized that in certain solids there are definite transition points to be associated with a change from oscillation to rotation of the molecules, setting in rather suddenly. The matter was first discussed theoretically by Pauling, who gave a satisfactory qualitative explanation. He conceived of a model in which the molecules rotate about their centres of gravity in a field of potential energy —  $W \cos \theta$ , where  $\theta$  is the angle made by the figure axis of the molecule with some fixed direction. He sug-

\* 'Proc. Roy. Soc.,' A, vol. 145, p. 699 (1934).

gested that the transition point occurred when  $kT = 2W$ ; for lower temperatures the molecules all oscillate about  $\theta = 0$ ; for higher they all rotate practically freely. Pauling makes it quite clear that this can only happen if the rotations themselves destroy the field so that  $W$  depends on  $T$ , but makes no attempt at a more exact theory. A more accurate theory for Pauling's model, incorporating the essential ideas of Bragg and Williams will be the first main result of this paper.

After this theoretical study of the vibration-rotation transition point for this simple model its dielectric constant is evaluated in detail. The properties of the model are then compared with the properties of various actual substances and it is shown that the general features are properly accounted for. The discussion throughout uses classical partition functions. It is shown that these must be sufficiently accurate for a study of the critical temperatures and at low temperatures the necessary corrections are easily made roughly. A more accurate version of the theory using quantum partition functions is under investigation, but it does not seem likely that this added accuracy is important. A more refined theory must probably use a more accurate representation of the rotating molecule, allowing it all its three rotations, and of the field of potential energy in which it moves. The theory can probably not be applied to the very low temperature transition in solid methane,  $\text{CH}_4$ , for which a quantum mechanical treatment is probably essential.

## § 2—THE CLASSICAL RIGID ROTATOR IN A FIELD — $W \cos \theta$

The model we propose to discuss in detail in this paper is the symmetrical rigid rotator without spin about its axis of figure, rotating about its centre of gravity in a field of potential energy —  $W \cos \theta$ , due to the surrounding molecules. In later sections, when the dielectric constant is studied, we shall suppose that the molecule carries a dipole directed along its axis of figure. The Hamiltonian energy function  $H$  of this system is

$$H = \frac{1}{2I} \left( p_\phi^2 + \frac{p_\theta^2}{\sin^2 \theta} \right) - W \cos \theta, \quad (1)$$

where  $\theta$ ,  $\phi$  are the usual Eulerian angles defining the direction of the axis of figure,  $p_\theta$ ,  $p_\phi$  their conjugated momenta and  $I$  the transverse moment of inertia. The classical partition function  $f(T)$  is then

$$f(T) = \frac{1}{h^2} \iiint \exp \left[ -\frac{1}{kT} \left\{ \frac{1}{2I} \left( p_\theta^2 + \frac{p_\phi^2}{\sin^2 \theta} \right) - W \cos \theta \right\} \right] dp_\theta dp_\phi d\theta d\phi. \quad (2)$$

The  $\phi$ ,  $p_\theta$ ,  $p_\phi$  integrations can be carried out immediately giving

$$f(T) = \frac{4\pi^2 I k T}{h^2} \int_{-1}^{+1} e^{Wq/kT} dq, \quad (3)$$

where  $q = \cos \theta$ ; this gives

$$f(T) = \frac{8\pi^2 I k T}{h^2} \frac{kT}{W} \sinh \frac{W}{kT}. \quad (4)$$

The most important quantity is the contribution of these rotations to the specific heat. By standard formulæ we have, for  $N$  molecules,

$$\begin{aligned} \overline{E}_{\text{rot}} &= NkT^2 \frac{\partial}{\partial T} \log f(T) \\ &= NkT \left[ 2 - \frac{W}{kT} \coth \frac{W}{kT} \right]; \end{aligned} \quad (5)$$

$$C_{\text{rot}} = \frac{d\overline{E}_{\text{rot}}}{dT} = Nk \left[ 2 - \frac{W^2}{k^2 T^2 \sinh^2 W/kT} \right]. \quad (6)$$

The energy content given by formula (5) starts at  $-NW + 2NkT$  for very low temperatures (where, in fact, the classical term in  $T$  will be wrong), and becomes  $NkT - \frac{1}{3}NW^2/kT$  at high. There is, however, if the curve is plotted, no sign of any sharp transition for  $kT \approx W$ , and it is clear that no sharp transition can be given by any such model for which  $W$  is strictly constant as we have so far assumed.

We have, however, following Pauling, no reason to assume that  $W$  is constant, rather every reason to the contrary. The directive power of the field to which each molecule is subject, specified by  $W$ , is, of course, mainly due to the lack of spherical symmetry in the fields of the neighbouring molecules. This lack of symmetry must be entirely destroyed by a sufficient degree of rotation among these molecules. The state of affairs is strictly analogous to Bragg's problem of order and disorder among the molecules of a metallic alloy in a homogeneous phase. In that problem the energy required to increase the disorder by interchanging one pair of molecules cannot be a constant, but must depend on the degree of disorder, vanishing entirely when the disorder is complete. So here  $W$  must depend on the amount of rotation present and vanish when that is sufficiently large.

Any specification of the amount of rotation is somewhat arbitrary, but a possible rough specification can be provided as follows. We might say that the molecule is non-rotating if

$$\frac{1}{2I} \left( p_\phi^2 + \frac{p_\theta^2}{\sin^2 \theta} \right) < \beta W, \quad (7)$$

where  $\beta$  is constant. If  $f_0(T)$  is that part of the partition function which satisfies (7) we define the degree of non-rotation  $S$  by the equation

$$S = f_0(T)/f(T), \quad (8)$$

and assume that

$$W = W_0 S. \quad (9)$$

When  $S = 1$  (as  $T \rightarrow 0$ ) non-rotation is complete and  $W$  has its full value  $W_0$ . The actual value of  $f_0(T)$  is easily calculated. It is

$$f_0(T) = \frac{2\pi}{h^2} \int_0^\pi e^{W \cos \theta / kT} d\theta \iint_{p_\theta^2 + p_\phi^2 / \sin^2 \theta < 2IkT} e^{-(p_\theta^2 + p_\phi^2 / \sin^2 \theta) / 2IkT} dp_\theta dp_\phi,$$

which reduces by obvious substitutions to

$$f_0(T) = \frac{4\pi IkT}{h^2} \int_{-1}^1 e^{Wq/kT} dq \iint_{x^2 + y^2 < \beta W / kT} e^{-x^2 - y^2} dx dy, \quad (10)$$

$$= \frac{8\pi^2 IkT}{h^2} \frac{kT}{W} \sinh \frac{W}{kT} (1 - e^{-\beta W / kT}). \quad (11)$$

Thus, under specification (7)

$$S = f_0(T)/f(T) = 1 - e^{-\beta W / kT} \quad (W = SW_0). \quad (12)$$

It is perhaps formally more accurate to specify non-rotation, instead of by (7), by the inequality

$$\frac{1}{2I} \left( p_\theta^2 + \frac{p_\phi^2}{\sin^2 \theta} \right) < \beta W (1 + \cos \theta), \quad (13)$$

which asserts that the kinetic energy at any  $\theta$  is less than a certain fraction of that necessary to allow the axis of the molecule to reach the pole  $\theta = \pi$ . In that case formula (10) is unaffected except that  $\beta$  is replaced by  $\beta(1 + q)$ . It is easily shown that

$$f_0(T) = \frac{8\pi^2 IkT}{h^2} \frac{kT}{W} \left[ \sinh \frac{W}{kT} - \frac{e^{W(1-2\beta)/kT} - e^{-W/kT}}{2(1-\beta)} \right],$$

so that, under (13),

$$S = 1 - \frac{e^{W(1-2\beta)/kT} - e^{-W/kT}}{2(1-\beta) \sinh W/kT} \quad (W = SW_0). \quad (14)$$

If  $1 > \beta > \frac{1}{2}$  no essential difference is introduced by using (14) rather than (12) and we shall make some use of (12) on account of its greater simplicity. The special case of (14),  $\beta = \frac{1}{2}$ , has, however, peculiar properties of considerable importance. For then equation (14) reduces to

$$S = \tanh \frac{1}{2} W / kT = \tanh \frac{1}{2} W_0 S / kT. \quad (15)$$

Equation (15) yields a much more rapid variation of  $S$  near  $T_c$  than equation (12) and we shall study this case in detail later on. Still more striking variations occur near  $T_c$  if  $\beta < \frac{1}{2}$  (see § 2, para. c).

Any one of these implicit equations at once determines  $S$  as a function of  $T$ , and  $S$  can be studied in the manner customary in ferromagnetic theory. For example, using equation (12) one can plot the curves  $y = 1 - e^{-x}$ ,  $y = (kT/\beta W_0)x$ . Their intersections give the possible value of  $S$ . When

$$T > T_c = \beta W_0/k, \quad (16)$$

then  $S \equiv 0$ . When  $T < T_c$  then a non-zero value of  $S$  is possible and as we shall show in § 2.4 represents stable equilibrium provided it exists. The temperature  $T_c = \beta W_0/k$  is the transition temperature. For values of  $T$  near  $T_c$   $S$  is given approximately by

$$S = \frac{2T}{T_c} \left(1 - \frac{T}{T_c}\right) \quad (T \rightarrow T_c - 0), \quad (17)$$

so that as  $T \rightarrow T_c - 0$ ,  $S \rightarrow 0$ , and

$$dS/dT \rightarrow -2/T_c. \quad (18)$$

It remains to determine the energy content of the rotations and their contribution to the specific heat. Formula (5) still applies if  $W$  is replaced by  $W_0 S$ . Hence

$$\bar{E}_{\text{rot}} = NkT \quad (T > T_c), \quad (19)$$

$$= NkT \left[ 2 - \frac{W_0 S}{kT} \coth \frac{W_0 S}{kT} \right] \quad (T < T_c). \quad (20)$$

$$C_{\text{rot}} = Nk \quad (T > T_c) \quad (21)$$

$$= Nk \left[ 2 - \frac{x^2}{\sinh^2 x} \right] - N W_0 \frac{dS}{dT} \left[ \frac{\cosh x \sinh x - x}{\sinh^2 x} \right] \\ \left( x = \frac{W_0 S}{kT}, \quad T < T_c \right). \quad (22)$$

These formulæ are general and can be used, however  $S$  is specified, provided that the relevant values of  $S$  and  $dS/dT$  are substituted in them.

When  $S$  is determined by equation (12) and therefore satisfies (17) and (18) we find that  $C_{\text{rot}} \rightarrow Nk$  ( $T \rightarrow T_c - 0$ ).  $C_{\text{rot}}$  is therefore continuous at  $T_c$ . Though there is a break in the form of the energy-temperature curve at  $T = T_c$  its slope is there continuous. The general form of the energy curve is shown in fig. 1. The dotted curve shows roughly the

modification required by the quantum theory which may be estimated as follows. At low temperatures when  $S \approx 1$  and the excursions of the axis are small, the motion is approximately that of a simple harmonic oscillator in two dimensions with equal frequencies

$$\frac{1}{2\pi} \sqrt{\frac{W_0}{I}}.$$

Thus while  $T_0 = \beta W_0/k$  the characteristic temperature  $\Theta$  for the oscillations below which quantization is important is  $(h/2\pi)(W_0/I)^{1/2}$ . If  $W_0$

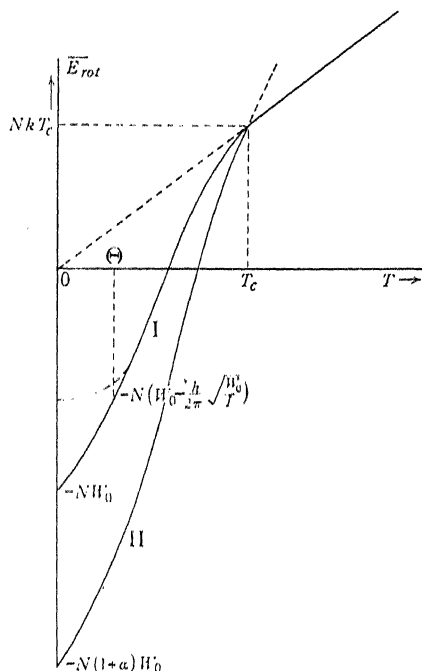


FIG. 1.—General form of the rotational energy content. The broken curve shows the modification required by quantum theory

is about 1/20th electron-volt, then  $T_c \approx 600 \beta^\circ$  while  $\Theta \approx 60^\circ$ . Since  $\beta$  presumably is unlikely to be much less than 1/4,  $\Theta$  remains well below  $T_c$  so long as  $W_0$  is not less than 0.02 electron-volts (or less if  $\beta$  is larger), and quantization cannot be important near the transition temperature.

(a) *A Model with a Discontinuous  $C_{rot}$* —When  $S$  is determined by (12), or by (14) with  $1 > \beta > \frac{1}{2}$ ,  $C_{rot}$  is continuous at  $T = T_c$ , but a small change in the model which is physically possible *a priori* introduces a finite discontinuity. If we may assume that the field of potential energy in which the axis of the molecule moves is not  $-W \cos \theta$ , which is zero

in the mean, but rather  $-\alpha W = W \cos \theta$ , so that there is some degree of mean binding which vanishes with  $S$ , such a discontinuity occurs. For the only effect of the extra energy  $-\alpha W$  is to add a term  $-N\alpha W = -N\alpha W_0 S$  to  $E_{\text{rot}}$  and therefore a term

$$N\alpha W_0 (-dS/dT)$$

to  $C_{\text{rot}}$ . When  $S$  is determined by (12) and  $T = T_c = 0$  this tends to the limit  $Nk(2\alpha/\beta)$ ; when  $T > T_c$  it is identically zero. The energy for this form of the model is shown by the curve II in fig. 1. When  $S$  is determined by (14) with  $1 > \beta > \frac{1}{2}$  we obtain results exactly similar in form, but the discontinuity in  $-dS/dT$  increases steadily without limit as  $\beta$  approaches the value  $\frac{1}{2}$ .

(b) *A Model for which  $C_{\text{rot}} \rightarrow \infty$  as  $T \rightarrow T_c = 0$ .* Still more striking phenomena are exhibited if we assume that  $\beta = \frac{1}{2}$  in (14), i.e., that  $S$  is given by (15). Here

$$S = \tanh \frac{1}{2} W_0 S / kT = \tanh T_c S / T. \quad (23)$$

Formulae (19) to (22) are still applicable, but when  $T \propto T_c$

$$S \propto \sqrt{3} \frac{T}{T_c} \left(1 - \frac{T}{T_c}\right)^{\frac{1}{2}}, \quad -T_c \frac{dS}{dT} \propto \frac{\sqrt{3}}{2} \left(1 - \frac{T}{T_c}\right)^{-\frac{1}{2}}. \quad (24)$$

According to (19) and (20)  $E_{\text{rot}}$  is continuous at  $T = T_c$ , but  $C_{\text{rot}}$  is discontinuous. It is easy to show that

$$C_{\text{rot}} = Nk \quad (T > T_c), \quad C_{\text{rot}} = 5Nk \quad (T = T_c = 0). \quad (25)$$

If we add an extra energy term  $-\alpha W_0 S$  as in § 2.1, then  $E_{\text{rot}}$  contains the extra term  $-N\alpha W_0 S$  as before and  $C_{\text{rot}}$  the extra term  $N\alpha W_0 (-dS/dT)$ . This is identically zero for  $T > T_c$  and tends to infinity like

$$\sqrt{3} Nk\alpha (1 - T/T_c)^{-\frac{1}{2}} \quad (T = T_c = 0) \quad (26)$$

the energy remains continuous.

(c) *A Model with a Non-zero Latent-heat*—If in equation (14) for  $S$  we take  $\beta < \frac{1}{2}$  the behaviour of the resulting function  $S(T/T_c)$  changes entirely. The type of behaviour that now occurs has already been noticed by Bragg and Williams, though they have not made the interpretation of it which appears to be relevant here. Equation (14) used to determine  $S$  in the usual way gives  $S$  as an intersection of the two curves

$$(S =) y = 1 - \frac{e^{(1-2\beta)x} - e^{-x}}{2(1-\beta) \sinh x}, \quad y = \frac{kT}{W_0} x. \quad (27)$$

So long as  $1 > \beta > \frac{1}{2}$  the intersections occur as for equation (12) or (15) and  $T_c = \beta W_0/k$  as shown in fig. 2 *a*. When, however,  $\beta < \frac{1}{2}$  the initial curvature of the curve for  $y$  changes sign, the curve is concave upwards and the intersections occur as in fig. 2 *b*. The critical temperature  $T_c$  is fixed by the first line through the origin which touches the curve, and the point of contact occurs for a non-zero value of  $y$ . The slope at the origin is still  $\beta$  so that  $T_c > \beta W_0/k$ , but as  $T \rightarrow T_c - 0$  it is no longer true that  $S \rightarrow 0$ . Instead  $S \rightarrow S_0 > 0$  and  $-T_c dS/dT \rightarrow +\infty$ . On referring to (20) we see that  $\overline{E}_{\text{rot}}$  is discontinuous at  $T_c$ , the amount being given by

$$\Delta \overline{E}_{\text{rot}} = \overline{E}_{\text{rot}}(T_c + 0) - \overline{E}_{\text{rot}}(T_c - 0) = Nk \left[ \frac{W_0 S_0}{k} \coth \frac{W_0 S_0}{k T_c} - 1 \right]. \quad (28)$$

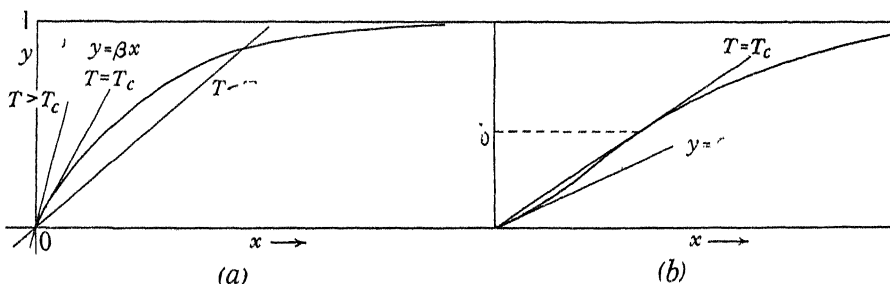


FIG. 2—The determination of  $S$ ; (a)  $\beta > \frac{1}{2}$ , (b)  $\beta < \frac{1}{2}$

Ideally this should appear as a true latent heat of transition over and above the contributions of the locally abnormally great values of  $C_v$ .

Fig. 3 shows  $S$  as a function of  $T/T_c$  for the various implicit equations which may determine it. Curves I show  $S$  and  $(-T_c dS/dT)$  for equation (15),  $\beta = \frac{1}{2}$ . Curve II shows  $S$  for equation (14),  $\beta = \frac{1}{4}$ . Curve III shows  $S$  for equation (12). Curves for equation (14),  $\beta > \frac{1}{2}$ , are of the same general form as III, but of steeper slope at  $T/T_c = 1$  and tend to curve I as  $\beta \rightarrow \frac{1}{2}$ . The energy and specific heat are shown as functions of  $T/T_c$  in a number of special cases in fig. 4, *a*, *b*, *c*.

We shall return to the comparison of these formulæ with experiment after completing the formal theory for the dielectric constant.

(*d*) *Stability of the Non-zero Value of  $S$ , when  $T < T_c$* —We have still to show that the non-zero root of equations (12), (14), or (15) when it exists necessarily gives the stable state, but this is not difficult. The partition function  $f(T)$  has the value (from (4))

$$\frac{8\pi^2 I k T}{h^2} \frac{k T}{W_0 S} \sinh \frac{W_0 S}{k T},$$

and for given  $T$  and  $W_0$  is a steadily increasing function of  $S$ . But



$Nk \log f(T)$  is the contribution made by these rotations to Planck's characteristic function for the assembly, so that  $-NkT \log f(T)$  is the contribution to the Helmholtz free energy ( $\equiv$  work function)  $F$ . As between two possible states with different  $S$  the stable one at given temperature and volume must always be that of least  $F$ ; that is, of greatest

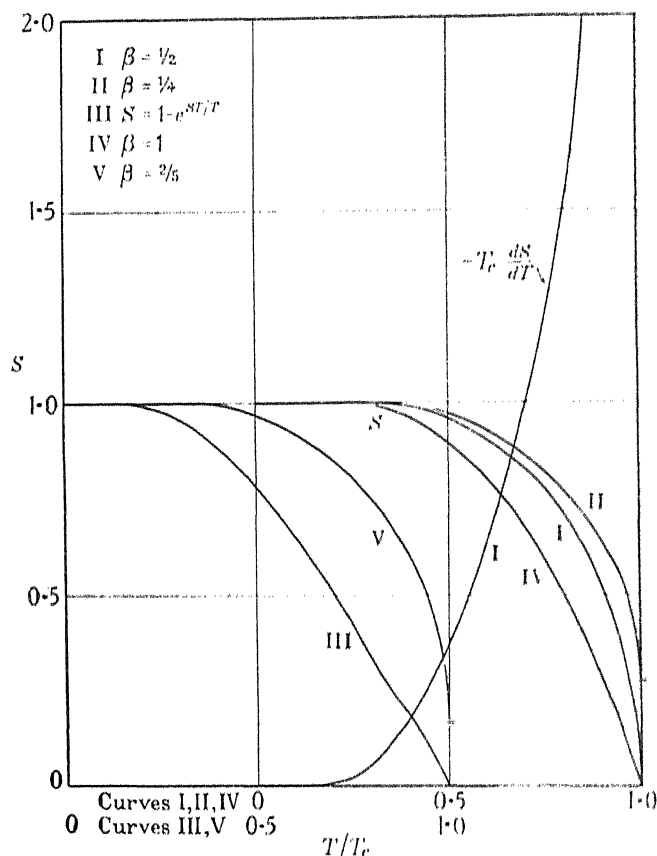


FIG. 3—Curves showing  $S$  as a function of  $T/T_e$  for various implicit equations. Curves I, II, IV, and V refer to equation (14) for the values of  $\beta$  shown in the diagram. For  $\beta = \frac{1}{2}$  the value of  $-T_e dS/dT$  is also shown

$f(T)$ . Thus the stable state has the greater (or greatest) value of  $S$ , permitted by the implicit equation, as we have already assumed.

### § 3—THE DIELECTRIC CONSTANT OF A MEDIUM COMPOSED OF DIPOLE CARRIERS ROTATING ACCORDING TO THE THEORY OF § 2

If we assume that the systems of § 2 all possess the same natural direction of equilibrium orientation, the assembly would be permanently polarized in that direction independently of any applied field, and the more com-

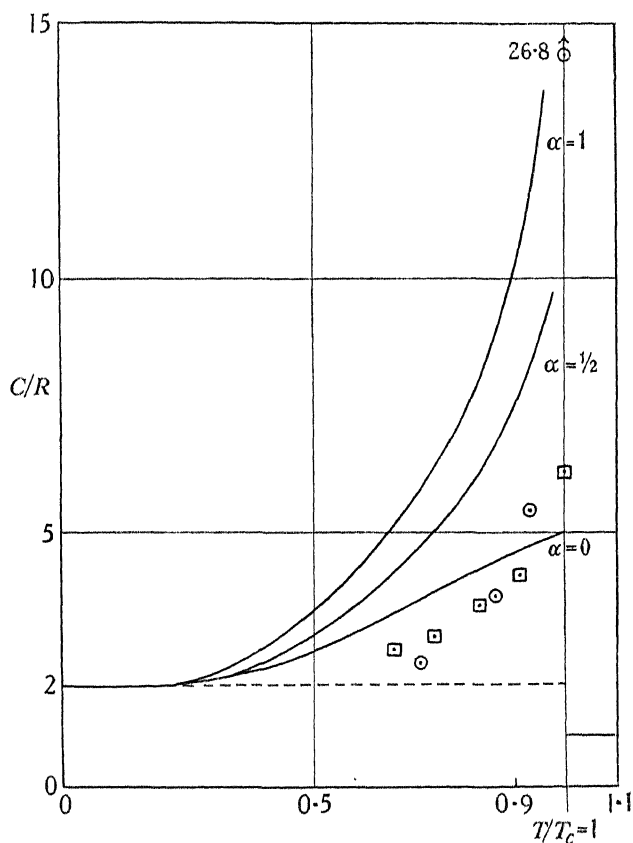


FIG. 4 *a*—Curves showing  $C_{\text{rot}}$  as a function of  $T/T_c$  for  $\beta = \frac{1}{2}$  and various values of  $\alpha$  defining the additional binding. The plotted points represent observations for HI analysed as described in § 5

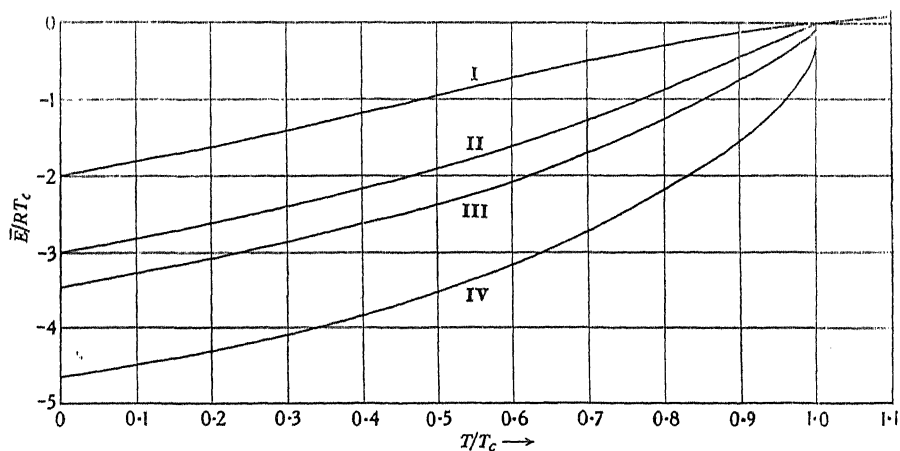


FIG. 4 *b*—Curves showing  $\overline{E}_{\text{rot}}/RT_c$  as a function of  $T/T_c$  for  $\alpha = 0$  and I,  $\beta = 1$ ; II,  $\beta = \frac{1}{2}$ ; III,  $\beta = \frac{2}{3}$ ; IV,  $\beta = \frac{3}{4}$

pletely the lower the temperature. To achieve a model acceptable as a starting point it is therefore necessary at least to divide the systems into two equal groups whose natural equilibrium orientations are in opposite directions. We shall, therefore, start by assuming that the assembly consists of  $\frac{1}{2}N$  systems in the field of potential energy  $-W \cos \theta$  and  $\frac{1}{2}N$  in  $W \cos \theta$ . The extra term  $-\alpha W$  (if present) is here without effect

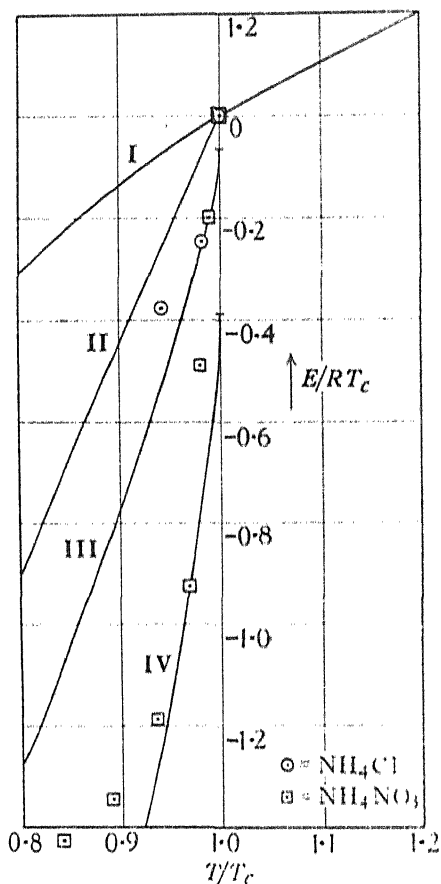


FIG. 4 c—Curves showing  $\overline{E}_{rot}/RT_c$  on an enlarged scale for  $T \propto T_c$ . The plotted observations are discussed in § 5

and need not be considered. An effective field  $F'$  acts on the systems in the direction  $\theta = 0$  so that the total potential energies are  $-(W + \mu F') \cos \theta$  and  $(W - \mu F') \cos \theta$  respectively, where  $\mu$  is the dipole moment of each system. This very simple special arrangement will be generalized later. The partition functions are then

$$\frac{8\pi^2 I k T}{h^2} \frac{k T}{W + \mu F'} \sinh \frac{W + \mu F'}{k T}, \quad \frac{8\pi^2 I k T}{h^2} \frac{k T}{W - \mu F'} \sinh \frac{W - \mu F'}{k T}, \quad (29)$$

respectively. Using the general statistical relationship for the polarization  $P$ , which here becomes

$$P = \frac{1}{2}NkT \frac{\partial}{\partial F'} (\log f_1 + \log f_2), \quad (30)$$

it then follows at once that

$$P = NkT\mu \left[ \frac{\mu F'}{W^2 - \mu^2 F'^2} - \frac{1}{kT} \frac{\sinh 2\mu F'/kT}{\cosh 2W/kT - \cosh 2\mu F'/kT} \right]. \quad (31)$$

Assuming that  $F'$  is small ( $\mu F' \ll W$ ) this reduces easily to

$$\frac{P}{F'} = \frac{N\mu^2}{kT} \left[ \frac{k^2 T^2}{W^2} - \frac{1}{\sinh^2 W/kT} \right], \quad (32)$$

which has the correct limiting form  $N\mu^2/3kT$  when  $W \rightarrow 0$ . For further application it is convenient to write (32) in the form

$$\frac{P}{F'} = \frac{N\mu^2}{3kT} g(x) \quad \left( x = \frac{W}{kT} \right), \quad (33)$$

so that  $g(x)$  is a reducing factor which the binding imposes on the effective value of  $N\mu^2$ . As  $x \rightarrow 0$ ,  $g(x) \rightarrow 1$ ; as  $x \rightarrow \infty$ ,  $g(x) \propto 3/x^2 \rightarrow 0$ .

In order to deduce the dielectric constant  $\eta$  we have now to use the usual relationships between  $\eta$ ,  $P$ ,  $F'$  and  $F$ , the ordinary electric force in the medium. The first of these is, of course,

$$\eta = 1 + 4\pi P/F. \quad (34)$$

The second relating  $F$  and  $F'$  is, by Lorentz's lemma,

$$F' = F + \frac{4}{3}\pi P, \quad (35)$$

for any medium to which Lorentz's lemma applies. The lemma does not apply to non-cubic crystalline media such as Rochelle salt. We shall therefore use it at present in the general form

$$F' = F + \gamma P, \quad (36)$$

where  $\gamma$  will depend on the direction of  $P$  in the crystal. We shall only consider principal directions for which  $P$ ,  $F'$ , and  $F$  are all parallel. It follows that

$$\eta = 1 + \frac{4\pi N\mu^2 g(x)/3kT}{1 - \gamma N\mu^2 g(x)/3kT}, \quad (37)$$

provided that  $F'$  and therefore  $P$  can be regarded as small. We can therefore write

$$\eta = 1 + \frac{4\pi}{\gamma} \frac{T_d}{T - T_d} \left( T_d = \frac{\gamma N\mu^2}{3k} g(x) \right), \quad (38)$$

provided that  $T > T_d$ . If  $T < T_d$ , then the approximation leading from (31) to (32) is illegitimate. We have, then, strictly to solve (31) together with (36) for  $P$  in terms of  $F$ . It turns out, of course, just as in the theory of ferromagnetism that  $P$  no longer vanishes with  $F$  and that we are concerned with a co-operative state of permanent polarization in zero field with an "infinite" dielectric constant.

The binding  $W$  in these equations must not, however, be thought of as a constant. To a first approximation it will be governed by equation (12), (14), or (15) so that the complete behaviour of the dielectric constant is to be regarded as controlled by the equations

$$\eta = 1 + \frac{4\pi}{\gamma} \frac{T_d}{T - T_d}, \quad T_d = \frac{\gamma N \mu^2}{3k} g\left(\frac{SW_0}{kT}\right) = T_d^0 g, \quad S = S\left(\frac{T}{T_c}\right), \quad (39)$$

with

$$g(x) = 3 \left| \frac{1}{x^2} - \frac{1}{\sinh^2 x} \right|. \quad (40)$$

It can be seen at once that when  $T \rightarrow 0$ ,  $S \rightarrow 1$ ,  $x \rightarrow \infty$ ,  $T_d \rightarrow 0$  ( $T^2$ ). Hence at low temperatures we have certainly  $T > T_d$  and  $\eta \rightarrow 1$ . For very large values of  $T$ ,  $S \rightarrow 0$ ,  $g(x) \rightarrow 1$ , and  $T_d$  assumes a constant value so that  $\eta$  behaves according to the ordinary dipole theory of Debye and eventually  $\eta \rightarrow 1$  again. At intermediate temperatures  $\eta$  will increase to a finite maximum and then decrease again provided that we always have  $T > T_d$ . But if as  $T$  increases we arrive at  $T_d = T$  then we must have a range in which  $\eta$  is infinite, bounded by upper and lower critical temperatures. This is just what is observed for Rochelle salt along the  $a$ -axis, but the model is still somewhat too specialized for actual applications.

(a) *A More General Model*—Before proceeding to the exact numerical study of these equations, we should study an arrangement of the equilibrium orientations less restricted than that in § 3. This may be done most simply as follows. Let us consider the same model, but subject it to an effective field  $F'$  at right angles to the directions of equilibrium orientation. This adds the potential energy  $-\mu F' \sin \theta \cos \phi$  to the Hamiltonian, and the partition function for either group of systems becomes

$$\begin{aligned} f(T) &= \frac{1}{h^2} \iiint \exp \left[ -\frac{1}{kT} \left\{ \frac{p_\theta^2 + p_\phi^2 / \sin^2 \theta}{2I} - W \cos \theta \right. \right. \\ &\quad \left. \left. - \mu F' \sin \theta \cos \phi \right\} \right] dp_\theta dp_\phi d\theta d\phi, \\ &= \frac{2\pi I k T}{h^2} \int_{-1}^{+1} e^{Wq/kT} dq \int_0^{2\pi} e^{(\mu F'/kT) \sin \theta \cos \phi} d\phi. \end{aligned} \quad (41)$$

This can be evaluated explicitly in finite terms by changing to new Eulerian angles and the corresponding momenta, but it is unnecessary to do this as it will suffice for our purposes to expand in powers of  $F'$  and retain  $F'^2$ . We then find\*

$$f(T) = \frac{8\pi^2 I kT}{h^2} \frac{kT}{W} \sinh \frac{W}{kT} \left[ 1 + \frac{1}{2} \frac{\mu^2 F'^2}{kTW} \left\{ \coth \frac{W}{kT} - \frac{kT}{W} \right\} \right]. \quad (42)$$

The usual formula then gives

$$\frac{P}{F'} = \frac{N\mu^2}{kT} \left( \frac{kT}{W} \coth \frac{W}{kT} - \frac{k^2 T^2}{W^2} \right), \quad (44)$$

in place of (32) for  $F'$  parallel to  $\theta = 0$ .

It is now possible to combine (44) and (32) to give the  $P, F'$  relation for the more general case in which the equilibrium orientations of the dipole axes are arranged at random in space. It is easily verified that for any set of dipoles whose equilibrium directions are half-and-half in opposite directions the effects of imposed fields parallel and perpendicular to the equilibrium directions are independent of each other to the order of accuracy of (32) and (44). Moreover, instead of averaging the response for all equilibrium directions we can equally well average it for all directions of  $F'$ . But it is then clear that the average must be obtained by taking for  $P/F'$  two-thirds of (44) plus one-third of (32) since there are two independent directions normal to  $\theta = 0$  and only one parallel. (Alternatively one may recover these factors by remembering that the parallel component has the factor  $\cos^2 \theta$  averaged over the sphere while the perpendicular one has  $\sin^2 \theta$ .) Thus in general

$$\frac{P}{F'} = \frac{N\mu^2}{3kT} \left[ 2 \frac{kT}{W} \coth \frac{W}{kT} - \frac{k^2 T^2}{W^2} - \frac{1}{\sinh^2 W/kT} \right]. \quad (45)$$

It is probably correct therefore to discuss the dielectric constant of liquids or solids of high symmetry using equation (39) with (in place of (40))

$$g(x) = 2 \frac{\coth x}{x} - \frac{1}{x^2} - \frac{1}{\sinh^2 x}. \quad (46)$$

For solids of lower symmetry equation (40) might be more appropriate. The functions  $g(x)$  defined by (46) and (40) are shown in fig. 5.

A greater variety of behaviour is now possible as  $T \rightarrow 0$ . Equations (39) and (40) do not require that  $\eta \rightarrow 1$  and do not even necessarily make

\* The exact formula is

$$f(T) = \frac{8\pi^2 I kT}{h^2} \frac{kT}{(W^2 + \mu^2 F'^2)^{1/2}} \sinh \frac{(W^2 + \mu^2 F'^2)^{1/2}}{kT}. \quad (43)$$

$\eta$  finite as  $T \rightarrow 0$ . It is possible to examine how  $\eta$  will behave for small values of  $g$  as  $T \rightarrow 0$  with some ease, since when  $1/x$  is small

$$g(x) \approx \frac{2}{x} - \frac{1}{x^2} = \frac{2kT}{SW_0} \left(1 - \frac{kT}{2SW_0}\right) \quad (47)$$

is a good approximation. We shall write

$$W_0/k = T_c/\beta', \quad (48)$$

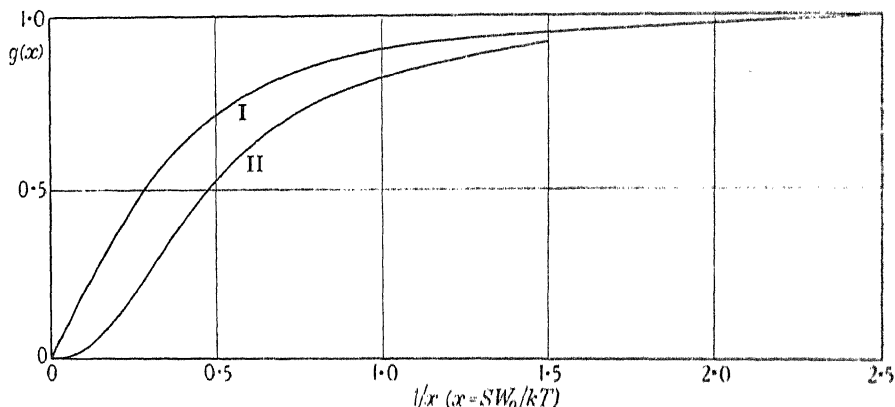


FIG. 5—Curves showing  $g(x)$  as a function of  $x$  for

I 
$$g(x) = 2 \frac{\coth x}{x} - \frac{1}{x^2} - \frac{1}{\sinh^2 x}.$$

II 
$$g(x) = 3 \left( \frac{1}{x^2} - \frac{1}{\sinh^2 x} \right)$$

where  $\beta' = \beta$  when  $\beta \gg \frac{1}{2}$ , but is somewhat greater than  $\beta$  when  $\beta \approx \frac{1}{2}$ . We may also in this region put  $S = 1$ . Thus

$$g(x) \approx \frac{2\beta'T}{T_c} \left(1 - \frac{\beta'T}{2T_c}\right). \quad (49)$$

Then

$$\eta = 1 + \frac{4\pi}{\gamma} \frac{1 - \beta'T/2T_c}{T_c/(2\beta'T_d^0) - 1 + \beta'T/2T_c}. \quad (50)$$

There are two critical temperatures in this formula,  $T_c$  the critical temperature for the vanishing of  $S$  and the onset of free rotations and  $T_d^0$  ( $= \gamma N \mu^2 / 3k$ ) the critical temperature for the co-operative state of polarization among these freely rotating dipole carriers. We see from (50) that  $\eta$  steadily increases as  $T$  diminishes and remains finite if and only if

$$T_c > 2\beta'T_d^0. \quad (51)$$

A large variety of possible curves for  $\eta$  is illustrated in fig. 6.

§ 4—THE VALUE OF  $\gamma^*$ 

We have already stated that the usual value of  $\gamma$  is  $4\pi/3$ , but that this value may not apply to crystals of lower symmetry, such as Rochelle salt for example, for which  $\gamma$  may have very different values along different axes. This fact is of great importance because Rochelle salt is only abnormally polarizable along its  $a$ -axis, and it seems almost certain that

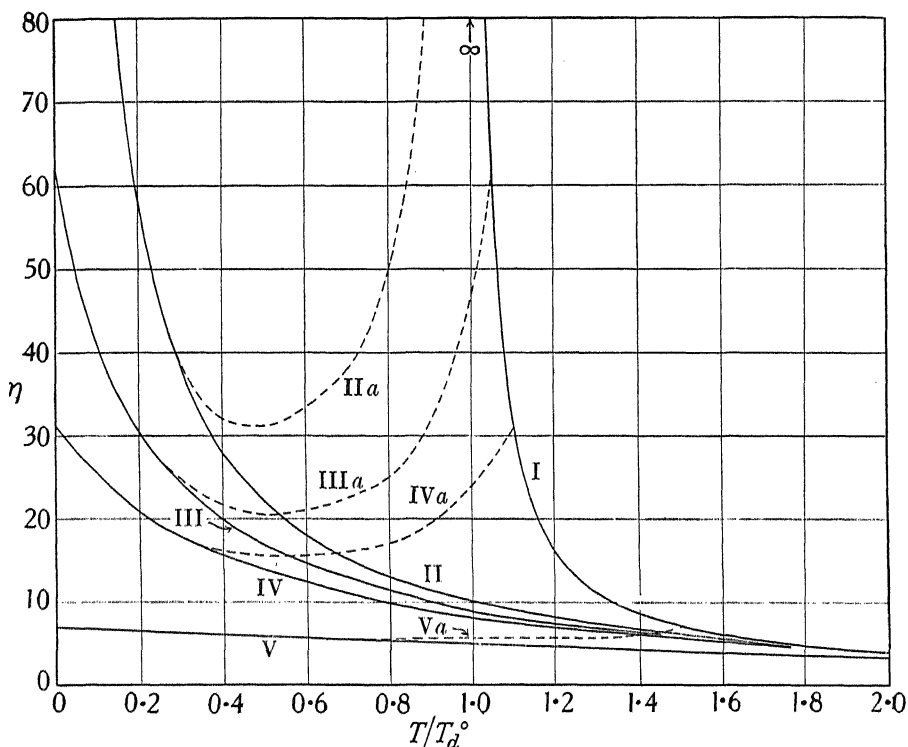


FIG. 6 *a*—Curves showing  $\eta$  as a function of  $T/T_d^0$  for  $\beta = \beta' = 1$  and I,  $T_c = T_d^0$ ; II,  $T_c = 2T_d^0$ ; III,  $T_c = 2.1T_d^0$ ; IV,  $T_c = 2.2T_d^0$ ; V,  $T_c = 3T_d^0$ ; also for  $\beta = \beta' = \frac{1}{2}$  and I + IIa,  $T_c = T_d^0$ ; I + IIIa,  $T_c = 1.05T_d^0$ ; I + IVa,  $T_c = 1.1T_d^0$ ; I + Va,  $T_c = 1.5T_d^0$ .

The second set of curves are shown broken only where they are distinct from parts of those of the first set. The function  $g(x)$  used is that shown in I, fig. 5

this selectivity is to be referred merely to the different values of  $\gamma$  along the different axes—values which are themselves a simple consequence of the arrangement in the lattice of the water of crystallization which carries the dipoles. The actual arrangement of the water is not yet known, but is capable of direct determination by X-ray analysis, by which the

\* I have great pleasure in thanking Herr H. Grönewold for help over this section.



assumptions to be made later in this paper can be tested. In the meantime it seems worth while to calculate  $\gamma$  roughly for a simple arrangement of dipoles which gives just the type of variation of  $\gamma$  with direction which we require.

Suppose the dipole carriers are arranged along strings parallel to one of the axes of co-ordinates ( $z$ -axis). The strings themselves are in square array with a spacing  $d$ . The spacing of the dipoles along any one string is  $d/n$ . This we shall call arrangement A, shown in fig. 7. It is convenient to compare the effect of these dipoles with dipoles of strength  $n$

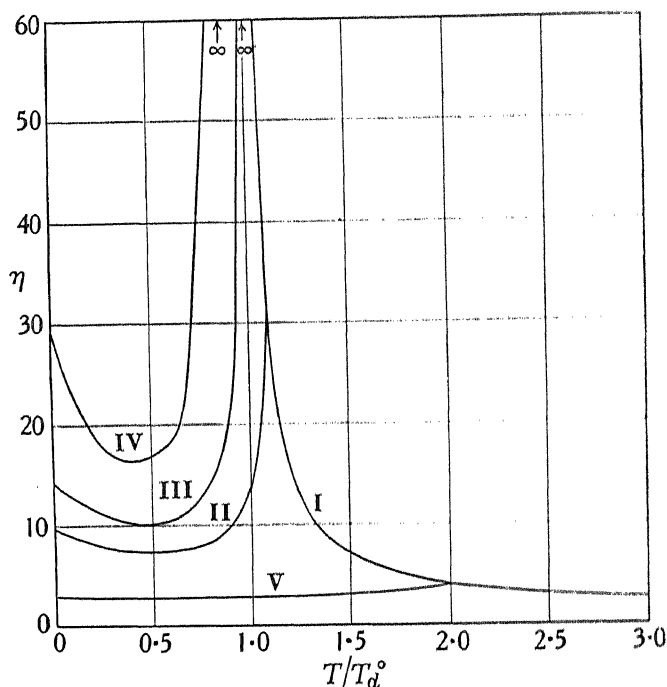


FIG. 6 *b*—Curves showing  $\eta$  as a function of  $T/T_d^0$  for  $\beta = \frac{1}{2}$ ,  $\beta' = 0.4355$  and I + III,  $T_c = T_d^0$ ; I + II,  $T_c = 1.1 T_d^0$ ; I + IV,  $T_c = 0.9 T_d^0$ ; I + V,  $T_c = 2 T_d^0$ . The function  $g(x)$  used is that shown in I, fig. 5

times as great in true cubical array of spacing  $d$ , for which we know that  $\gamma = 4\pi/3$ . This we shall call arrangement B. The actual value of  $\gamma$  for the arrangement in strings is then  $4\pi/3 + \omega$  where  $\omega$  is the difference between the effects of the two different arrangements. It is then easy to show that

$$\omega_z = \frac{d^3}{n} \sum_A' \left( -\frac{1}{r^3} + \frac{3z^2}{r^5} \right) - d^3 \sum_B' \left( -\frac{1}{r^3} + \frac{3z^2}{r^5} \right),$$

$$\omega_y = \omega_x = \frac{d^3}{n} \sum_A' \left( -\frac{1}{r^3} + \frac{3x^2}{r^5} \right) - d^3 \sum_B' \left( -\frac{1}{r^3} + \frac{3x^2}{r^5} \right),$$

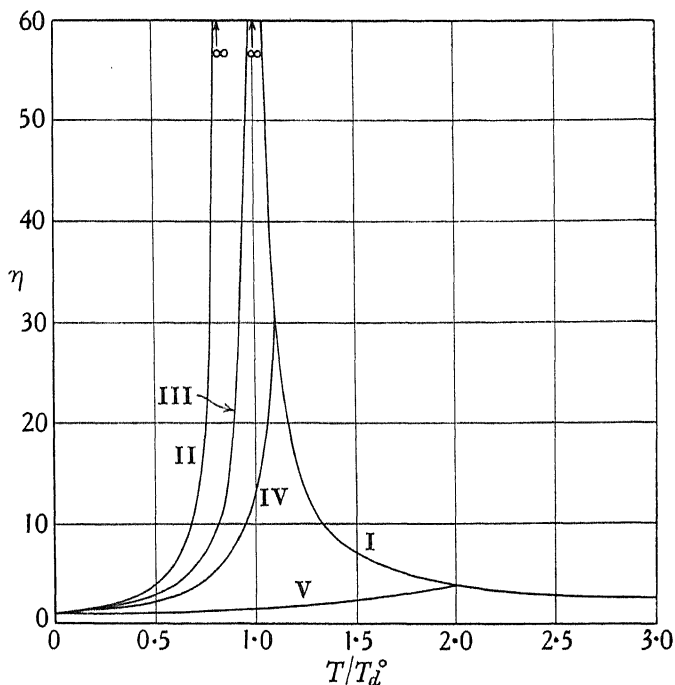


FIG. 6 c—Curves showing  $\eta$  as a function of  $T/T_d^0$  for  $\beta = \beta' = \frac{1}{2}$  and I + III,  $T_c = T_d^0$ , I + II,  $T_c = 0.9 T_d^0$ ; I + IV,  $T_c = 1.1 T_d^0$ ; I + V,  $T_c = 2 T_d^0$ . The function  $g(x)$  used is that shown in II, fig. 5

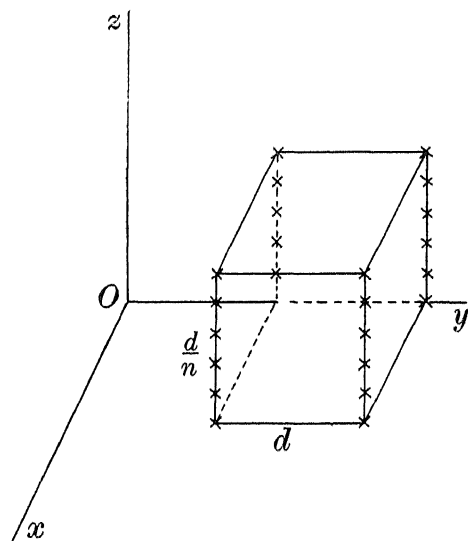


FIG. 7—A probable arrangement of dipole carriers in strings in a crystal of Rochelle salt

where  $\Sigma'_A$  denotes summation over the locations of all the dipoles in arrangement A omitting the dipole at the origin, and  $\Sigma'_B$  has a similar meaning. From these equations it follows that  $\omega_x + \omega_y + \omega_z = 0$ , so that

$$-\omega_x = -\omega_y = \frac{1}{2}\omega_z = (\omega_z - \omega_x)/3 = \omega_0. \quad (52)$$

From the last form for  $\omega_0$  it follows that

$$\omega_0 = \frac{d^3}{n} \Sigma'_A \frac{z^2 - x^2}{r^5},$$

the corresponding summation over the arrangement B vanishing by symmetry. This can be turned into

$$\omega_0 = \Sigma_{k,l} \Sigma'_m \cdot \frac{1}{n} \frac{(k^2 + l^2 + m^2/n^2) - \frac{3}{2}(k^2 + l^2)}{(k^2 + l^2 + m^2/n^2)^{5/2}} \dots, \quad (53)$$

where the summations run over all integral values of  $k, l, m$ , the single value  $(0, 0, 0)$  being excluded. This sum may be broken up into two parts,  $\omega'_0$  for  $k = l = 0$ , and  $\omega''_0$  when not both  $k$  and  $l$  are zero. When  $n = 1$  (and  $\omega_0 = 0$ )

$$\omega'_0(1) = -\omega''_0(1) = \Sigma' \frac{1}{m^3} = 2.404 \dots$$

When  $n > 1$   $\omega'_0(n) = n^2 \omega'_0(1)$  and  $\omega''_0(n)$  eventually tends to zero as  $n \rightarrow \infty$ . It seems probable that  $\omega''_0(n)$  increases steadily from  $-2.404 \dots$  to 0 as  $n$  increases. Assuming this, which is not easily proved, we should have as a lower limit for  $\omega_0$  and probably also as a fair approximation for order of magnitude

$$\omega_0 = (n^2 - 1) 2.404 \dots \quad (54)$$

Using these results we see that a value of  $n$  quite near unity is ample to make substantial differences in the factor  $\gamma$  and thus introduce entirely different critical temperatures for polarization along different crystalline axes.

#### § 5—COMPARISON OF OBSERVED AND CALCULATED ENERGIES OF MOLECULAR ROTATION

Typical examples of substances showing abnormal specific heats, which should presumably be accounted for by a theory on the lines of that proposed here, are the halogen hydrides and certain ammonium salts. Specific heat curves for the halogen hydrides are shown in fig. 8. These

are reproduced from the papers of Giauque and Wiebe.\* It is at once apparent that the *general* form of the breaks in these curves is similar to the calculated curves for the specific heat shown in fig. 4 *a*. There are, however, for HI two similar breaks and for HBr one single and one double one. For HCl the breaks are so violent and so close together that specific heat values are not recorded—only a heat of transition. It

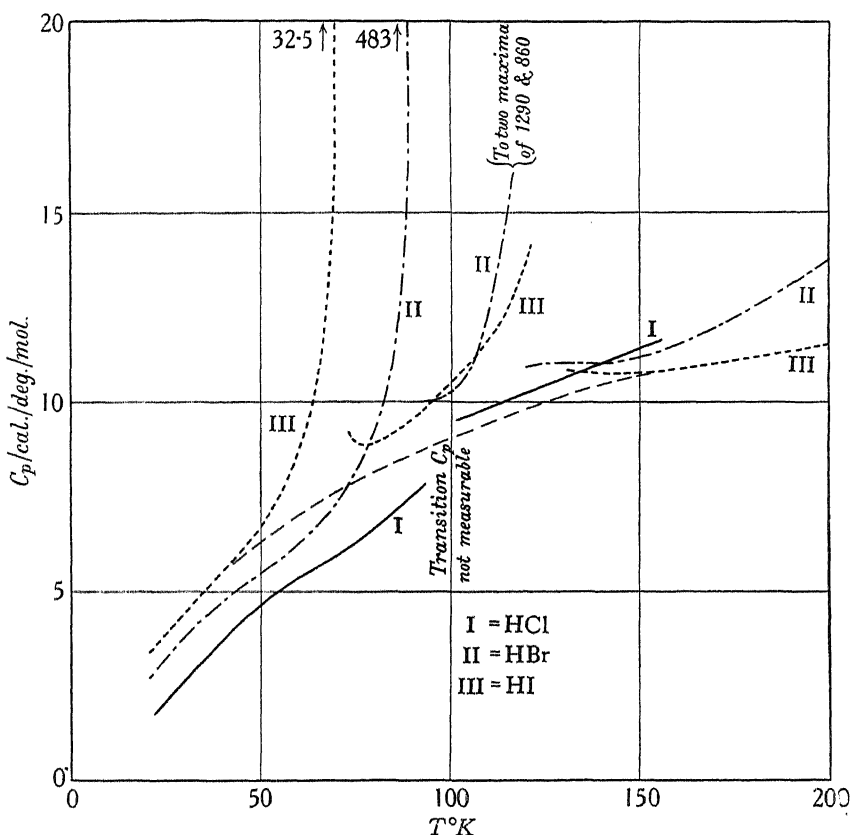


FIG. 8—Observed values of specific heat for the halogen hydrides at low temperatures

appears, therefore, as if the rotational degrees of freedom do not set in together, but that perhaps rotations about the various crystal axes set in separately (see also § 8). This, of course, makes impossible any strict comparison between the theory here given and these observations. It seems reasonable, however, to assume that these observed breaks refer to one rotational freedom each instead of two, and therefore to abstract from the observed curve the “abnormal” part of the specific heat, call

\* ‘J. Amer. Chem. Soc.’ vol. 50, pp. 101, 2193 (1928); vol. 51, p. 1441 (1929).

this  $C_{\text{rot}}$  and calculate  $C_{\text{rot}}/(\frac{1}{2}R)$  as a function of  $T/T_c$  for comparison with the theoretical  $C_{\text{rot}}(T/T_c)/R$ .

Observed points derived in this way for HI are plotted in fig. 4 *a*. There is a good deal of arbitrariness in the abstraction from the observed curves of the abnormal part. This has been achieved by drawing a smooth curve below the observed curve leaving the latter well below the lower critical temperature and joining it smoothly just above the higher critical temperature. In the theoretical curves of  $C_{\text{rot}}/R$ , however, the corresponding abnormal part must be reckoned as the excess above 2. To the observed values obtained above 2 has been added before they were plotted.

On considering the points so plotted on fig. 4 *a* one must conclude that though they give a curve of the same sort of shape as the theory the variation is definitely restricted to a smaller range of  $T/T_c$ . This extra sharpness of the transition is still more marked for HBr and HCl so that the theory must somehow be bettered by making the transition sharper.

Specific heat and energy content curves\* for  $\text{NH}_4\text{Cl}$  and  $\text{NH}_4\text{NO}_3$  are shown in fig. 9. For these substances and especially for  $\text{NH}_4\text{Cl}$  the specific heat varies so violently that it is almost impossible to compare the specific heats satisfactorily. As the energy itself is almost discontinuous a better comparison can be made between the theory and observation by comparing these energy content curves with the curves of figs. 4, *b*, *c*. These theoretical curves show  $\bar{E}_{\text{rot}}/RT_c$  plotted against  $T/T_c$ . In order to compare theory and experiment it is therefore only necessary to reduce the observed energy curve to these variables† and plot the points so obtained in fig. 4 *c*, adjusting one point on the observed energy curve arbitrarily to lie at the break of the calculated curves, the point (0, 1) in fig. 4 *c*. It is again evident that while the general form of the agreement is fairly good, the abnormal variation of the energy is more sharply concentrated near  $T/T_c = 1$  than the theory indicates. Nevertheless, it seems fair to conclude that the theory proposed is along the right lines and accounts satisfactorily in a rough way for the energy content and specific heat observed.

\* For  $\text{NH}_4\text{Cl}$ , Simon, Simson, and Ruhemann, 'Z. phys. Chem.,' vol. 129, p. 339 (1927); for  $\text{NH}_4\text{NO}_3$ , Crenshaw and Ritter, *ibid.*, B, vol. 16, p. 143 (1932).

† It might be better, as  $\text{NH}_4$  has three equal moments of inertia and three degrees of rotational freedom to take  $2E/3RT_c$  and plot it as a function of  $T/T_c$ . The proposed model using a polar type of field,  $-W \cos \theta$ , is, however, entirely unable to cope with more than two rotational freedoms; to do so a much more complicated field must be used, with, for example, tetrahedral symmetry. This refinement has, therefore, not been introduced. If it were used, it would diminish the ordinates of all the observed points in fig. 4 *c* by a factor 2/3 and have little effect on the general nature of the agreement.

## § 6—THE DIELECTRIC PROPERTIES OF ROCHELLE SALT

The observed value of  $\eta$  for Rochelle salt along the  $a$ -axis\* may be described by saying that  $\eta \rightarrow \infty$  as  $T$  decreases to  $T_d^0 = 298^\circ \text{K}$ , remains infinite until  $T$  falls to  $0.865 T_d^0$  and then decreases rapidly, reaching ordinary values by about  $0.83 T_d^0$ . In order to compare this behaviour with this theory it is necessary to assume that the water molecules of

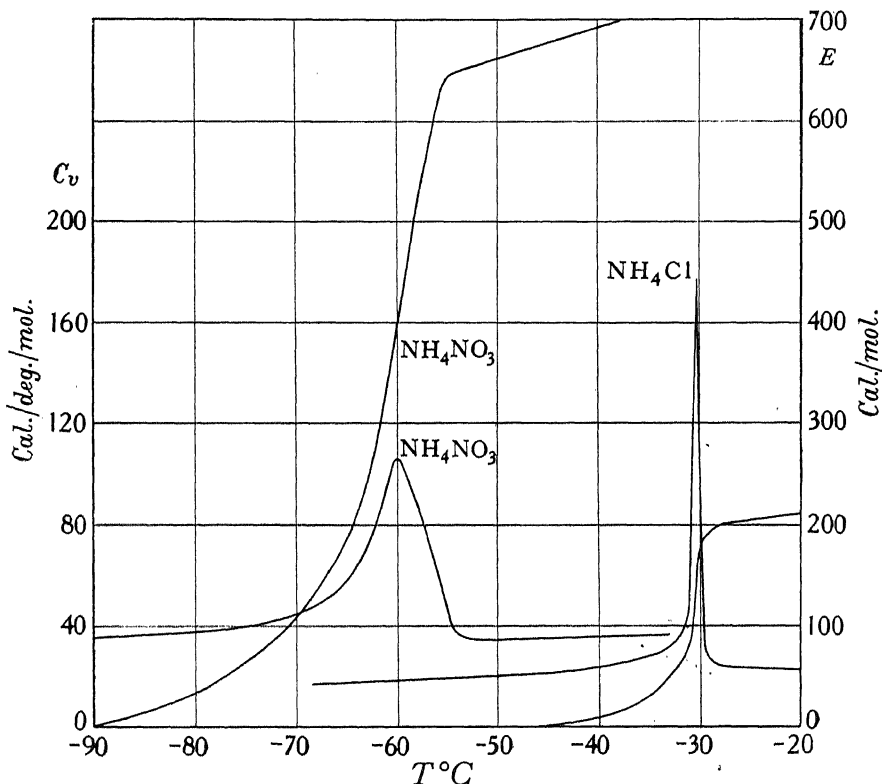


FIG. 9—Observed values of specific heat and energy content as a function of  $T$  for the ammonium salts  $\text{NH}_4$ ,  $\text{NO}_3$ , and  $\text{NH}_4\text{Cl}$

crystallization carry the orientating dipoles. If their dipole is equal to the dipole of the molecule in steam, the  $T_d^0$  would have the value  $550^\circ \text{K}$  for  $\gamma = \frac{4}{3}\pi$ , and a proportionately greater value if  $\gamma$  is greater. As we shall see  $\gamma$  must be appreciably greater than  $\frac{4}{3}\pi$  so that  $N\mu^2$  for the water of crystallization must be some two and a half to three times smaller than the value for steam leads one to expect. It is unfortunate that this

\* Kobeko and Kurtshatov, *loc. cit.*, esp. fig. 6.

change occurs as it makes the application of the theory less definite. The possibility of such a change, however, cannot be excluded *a priori*.

The source of the anisotropy must first be considered. The two curves for  $g(x)$  in fig. 5 show that it is always easier to polarize a medium by deflecting the dipoles by a force at right angles to their ordinary directions of equilibrium. Thus any anisotropy due to  $g(x)$  combined with special natural directions of equilibrium must make it easier to polarize the substance *in* a plane, whereas it is actually more easily polarized *normal* to a plane. Such anisotropy could, however, be due to  $\gamma$  if the molecules are arranged in strings (parallel to the  $a$ -axis) as in fig. 7. They would then probably have their natural directions of orientation in one or other direction along the string. We must then use the  $g(x)$  of equation (40) for polarization along the  $a$ -axis and a  $g(x)$  derived from (44) for polarization at right angles. This  $g(x)$  will not differ greatly from the  $g(x)$  of (46). The curves of fig. 6 *c* apply therefore along the  $a$ -axis and those of figs. 6 *a, b* at right angles. If, for example,  $\beta = \beta' = \frac{1}{2}$  and  $T_c \cong 0.9 T_d^0$  (||) while  $T_c \cong 1.5 T_d^0$  ( $\perp$ ) the observed characteristics of Rochelle salt will be remarkably well reproduced by the theory. It remains to be seen whether the corresponding values of  $\gamma$  are confirmed by the X-ray analysis of the positions of the water molecules. Our theory requires  $\gamma$  (||)/ $\gamma$  ( $\perp$ ) = 1.666.

#### § 7—THE DIELECTRIC CONSTANTS OF TYPICAL POLAR LIQUIDS (AND SOLIDS)

Curves showing  $\eta$  as a function of  $T$  for a number of substances are shown in fig. 10. At first sight, except for a steeper fall at temperatures below that at which they develop their greatest value of  $\eta$ , these curves look not unlike the curves of fig. 6 *c*. These curves, however, are calculated for the value of  $g(x)$  given by (40) and cannot possibly apply to a liquid or to a solid for which  $\eta$  is isotropic. Similar peaks near  $T = T_d^0$  are shown by the curves of fig. 6 *a, b*, but these are followed at low temperatures by another rise of  $\eta$  to high values, and of this there is experimentally no sign. On the existing evidence it appears, therefore, that we must conclude that the complete curve of the dielectric constant for a substance such as ice-water, for example, cannot be accounted for by any simple form of the present theory—that is, by any theory in which the binding forces resisting rotation are destroyed solely by the degree of rotation present. There is another difficulty in such a comparison, namely, that the calculated values of  $T_d^0$ , using (38) with  $\gamma = 4\pi/3$ , are in all cases higher and in some cases much higher than the temperatures of

the observed  $\eta$ -peaks, as is shown by the following table. Though some such reduction must be assumed to occur in Rochelle salt (§ 6) we shall see that no assumption of such drastic reduction can be applied with success to ordinary polar liquids. Before, therefore, we can make any detailed comparison of theory and experiment for  $\eta$  for these polar liquids we must examine whether there is any acceptable physical reason

TABLE I—SHOWING THE TEMPERATURE  $T_d^0$  AND THE TEMPERATURE OF MAXIMUM DIELECTRIC CONSTANT FOR CERTAIN POLAR LIQUIDS. THESE VALUES OF  $T_d^0$  ARE OBTAINED BY USING IN (38) THE VALUE OF THE DIPOLE FOUND FOR THE SAME MOLECULE IN VAPOUR OR IN DILUTE SOLUTION

Substance	$T_d^0$	Temperature of maximum $\eta$
H <sub>2</sub> O .....	1200	273
C <sub>6</sub> H <sub>5</sub> NO <sub>2</sub> .....	920	263
CH <sub>3</sub> OH .....	410	163
CH <sub>2</sub> Cl <sub>2</sub> .....	375	286
C <sub>6</sub> H <sub>5</sub> NO <sub>2</sub> .....	185	147

for the entry of some hitherto omitted effect. On studying fig. 10 it will be seen that though the  $\eta$ -peak and the melting point do not occur at identical temperatures yet they are obviously closely associated. Now the process of melting must be connected with a rapid weakening of the binding forces between neighbours, particularly the directive effect of such forces, a weakening which can be attributed to the increasing *oscillations* of the molecules about their mean positions. That melting ensues when the amplitude of oscillation reaches a certain critical value is the basis of Lindemann's melting point formula. It seems, therefore, reasonable, or rather physically necessary, to suppose that the field controlling the rotations of a molecular dipole is not to be expected to be precisely of the form  $SW_0$  where  $S$  is controlled by the rotations themselves, but rather of the form  $SW_0 + S'W'_0$ , where  $S'$  is controlled by the degree of linear oscillations of the neighbouring molecules and vanishes at or near the melting point, attaining rapidly a value comparable with unity, as the temperature falls. The rapid fall of  $\eta$  on the low temperature side of the peak will therefore be attributed to the establishment of extra directional binding forces as the liquid solidifies. It remains to examine in detail the observed values of  $\eta$  on the high temperature side of the peak where  $S' = 0$  and the present simple theory should apply.

A satisfactory analysis cannot be made by assuming that  $T_d^0$  is modified so as to correspond to the temperature of the observed peak for the



reason that if any such identification is made, or made approximately, the greater part of the observed curve must be correlated with part of curve I, namely,

$$\eta = 1 + \frac{3T_d^0}{T - T_d^0},$$

and no such correlation fits the facts for constant  $T_d^0$ .

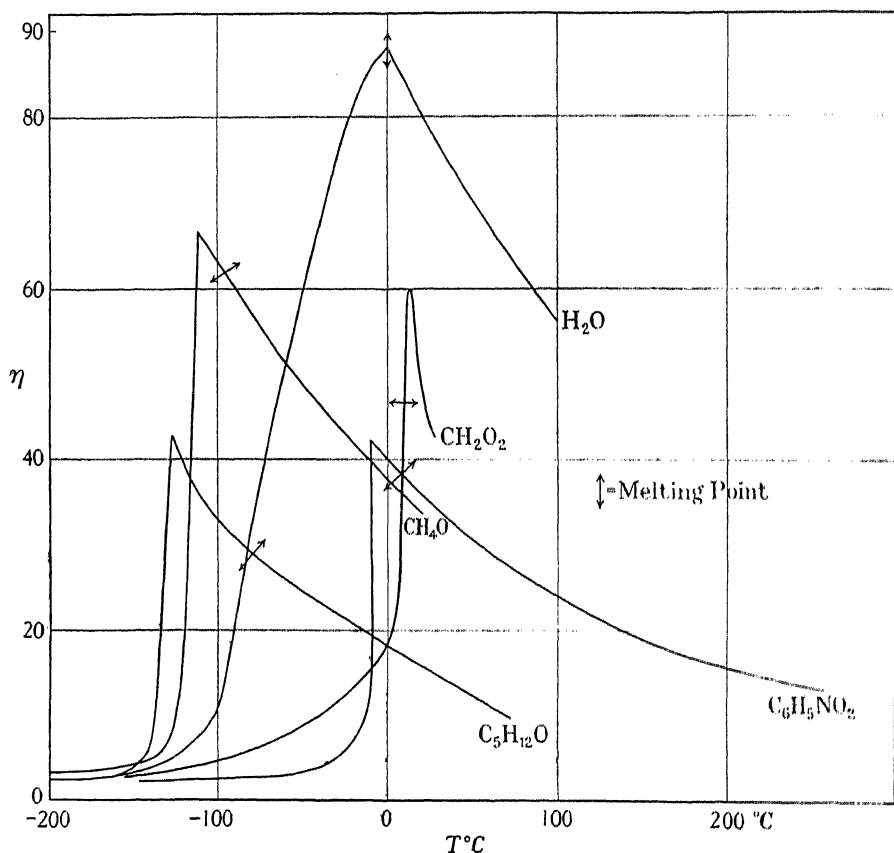


FIG. 10—Observed values of the dielectric constant as a function of  $T$  for the substances specified. The cross arrows mark the melting point temperature on each curve for that substance

*The Analysis for  $\text{H}_2\text{O}$* —The range of values of  $T/T_d^0$  concerned is  $0.23$ – $0.31$ , in which  $\eta$  falls from  $88$  to  $56$ . In this range formula (50) with  $\gamma = 4\pi/3$  can be used; it contains the single parameter  $T_o/\beta'$  so that  $\beta$  or  $\beta'$  is scarcely relevant. In that case if  $T_o/\beta' = 2336$  the observed curve for  $\eta$  is reproduced faithfully. [ $\eta(273) = 91$ ,  $\eta(373) = 53$ .] The slightly too great variation of  $\eta$  can be partially compensated by

using a small value of  $\beta$  as the exact curves are just beginning to diverge in the upper temperature range.

If it is held that the discrepancy is significant, then no fit can be obtained with this value of  $T_d^0$ , but with a somewhat reduced value of  $T_d^0$  and a suitable value of  $\beta$  a good fit is possible. There are then, however, too many available parameters to allow of convincing discussion.

*The Analysis for  $C_6H_5NO_2$* —The range of values of  $T/T_d^0$  concerned is  $0.286$ – $0.558$  in which  $\eta$  falls from  $42$  to  $14$ , taking the value  $24$  at  $0.41$ . If these points are compared with the curves of fig. 6 *a* it will be found that there is unmistakable evidence that (according to our theory)  $T_d^0$  is too large. The points can only be accommodated by one of the curves of these families if  $T_d^0$  is reduced to about  $645$ . The observed points then lie close to a member of the family of curves  $\beta = 1$  if  $T_c$  is approximately  $1.95 \times 645 = 1260$ .

*The Analysis for  $CH_4O$* —The range of values of  $T/T_d^0$  plotted in fig. 10 is  $0.397$ – $0.715$  in which  $\eta$  falls from  $67$  to  $34$ . These values could probably be reproduced with the calculated value of  $T_d^0$  for a suitable  $T_c$  if  $\beta$  is rather less than  $1$  but greater than  $\frac{1}{2}$ . Insufficient  $\eta$  curves have been calculated to allow of any closer discussion.

*The Analysis for  $C_5H_{12}O$* —Here, rather surprisingly, the calculated value of  $T_d^0$  ( $185^\circ$ ) is too small and must be increased to at least  $260^\circ$  before any successful comparison with the theory is possible. It is then apparent that a fair representation must be possible, but closer discussion requires many more calculated curves.

To sum up this rather tentative discussion one may say that the theory appears to be competent to describe the types of curve that are actually observed for polar liquids, but only if  $T_d^0$  is allowed to be an adjustable parameter. Much more numerical work would be necessary to decide precisely how good a fit can be obtained since there are three adjustable parameters in the present stage of the theory; it is, however, likely that such an elaborate test would be worth while. The theory also gives the right sort of dielectric properties for Rochelle salt. From the very nature of its initial assumptions it cannot claim to be better than a very rough approximation to the truth, but it may provide a rational scheme on the basis of which the observations may be discussed, and in that way lead to a better understanding of molecular orientations and solutions in liquids and solids.

## § 8—ADDENDUM

During the last stages of preparing this paper an article by Frenkel, Todes, and Ismailow\* came to hand. In this the transition points observed by Giauque for the halogen hydrides are discussed as in the present paper, but from a rather different aspect, so that the two treatments hardly overlap. Frenkel and his collaborators treat the transition as sharp and discuss the temperature of its occurrence by calculating and equating the free energy (which they calculate) for the two phases of rotating and non-rotating molecules. They are not primarily concerned with the gradual nature of the transition. Here we have attempted to develop a molecular theory to account for just this gradualness. Our theory makes the transitions on the whole too slow. Frenkel's idealization treats them as perfectly sharp. It seems quite possible that a combination of both sets of ideas may produce a really satisfactory theory.

## § 9—SUMMARY

A molecular theory of the rotations of molecules in liquids and solids is proposed, which enables calculations to be made of the transition from the non-rotating to the rotating form in solids. Calculations can be made according to the theory of the changes of the specific heat and energy content in the transition region of a solid and of the dielectric constant of a polar liquid and of Rochelle salt in fair agreement with the observed facts. The theory proceeds by applying to molecular rotations the idea, equivalent to that recently applied so successfully by Bragg and Williams to order and disorder in metallic alloys, that the potential energy of the rotating molecule must be a function of the amount of rotation already present. This leads at once to a critical temperature for the disappearance of the controlling field, and the main body of the paper consists merely in working out accurately the consequences of this idea for simple models.

\* 'Acta Physicochemica U.S.S.R.,' vol. 1, p. 97 (1934).

---

## Raman Spectra of Certain Organo-Metallic Compounds

By N. GOPALA PAI, M.A., Research Scholar, Indian Association for the Cultivation of Science, Calcutta

(Communicated by Sir Venkata Raman, F.R.S.—Received June 19, 1934)

[PLATE 1]

### 1—INTRODUCTION

The Raman effect in a large variety of substances, both organic and inorganic, has been studied in detail in relation to molecular structure. There is, however, an important class of organo-metallic compounds, namely, the metallic alkyls, etc., that have not been properly studied. These compounds would be of special interest, firstly, in view of the peculiar nature of the chemical bonds between carbon and the metallic atoms, and secondly, because of the effect of the very large mass of the metallic atoms on the frequencies of oscillation. The dearth of investigations on these compounds is due mainly to the extremely poisonous nature of their vapours and the spontaneous inflammability of some of them in air. Using a special technique, the Raman spectra of the following compounds of the above class have been studied by the present writer, namely, of zinc dimethyl and diethyl, mercury dimethyl and diethyl, bismuth trimethyl, tin tetramethyl and lead tetraethyl. This paper gives an account of these investigations.

### 2—EXPERIMENTAL

The liquids\* were contained in the usual double-chambered vessel consisting of a flask intended to contain the undistilled liquid, and a cylindrical Wood's tube into which the liquid is distilled over from the flask.

The introduction of the liquids into the above double chamber is a matter of some difficulty, especially with the zinc dialkyls owing to their spontaneous inflammability when exposed to air. These liquids were

\* The two zinc alkyls were obtained from Schering-Kahlbaum and all the other substances from Fraenkel and Landau.

manipulated in the following manner. The liquids as obtained from the makers were contained in small capsules. These were placed at the bottom of a suitable steel cylinder with small holes at the bottom; the cylinder was fitted with a piston worked by a screw. The capsules, *immersed in an atmosphere of carbon dioxide*, were smashed by screwing down the piston, and the liquid was allowed to flow into the double chamber. The chamber was then exhausted and sealed.

After a few distillations into the Wood's tube and washing back, the final dust-free distillate was collected in the Wood's tube. The distillation presented no difficulties, except for lead tetraethyl. With this substance, the distillation could not be carried on easily when the double chamber was evacuated and sealed. The chamber had to be connected to a pump which was working continuously during the process of distillation. Even then, the liquid showed signs of decomposition, the final distillate being slightly yellowish in colour.

Some of the liquids showed a tendency to photo-decomposition under the action of the light used for exciting the Raman spectra, and consequently developed in the course of exposure a strong continuous spectrum in the scattered light. This is naturally a disadvantage, since the continuous spectrum masks some of the weak Raman lines. The usual method of eliminating such a continuous radiation, viz., continued replenishing of the liquids in the Wood's tube, by allowing it to distil all the time into the tube and overflow back to the flask, could not be adopted for these liquids, since the quantities available were very small, e.g., about 2 cc for bismuth trimethyl. With such substances, therefore, we had to resort to the tedious but unavoidable procedure of continuing the exposure in stages of one hour, the liquid being redistilled into the Wood's tube after each such exposure. In such cases, the incident radiations were limited by the use of a Zeiss blue filter to the 4358 group of lines alone; the ultra-violet radiations thus being eliminated, and the photo-chemical action minimized. With lead tetraethyl, even these precautions were not quite efficient, and the continuous spectrum could not be eliminated. It is not necessary to describe the details of the optical arrangement for the study of the Raman radiations since they are well known. The spectrograms are reproduced in figs. 1 to 5, Plate 1.

### 3—RESULTS

The various Raman frequencies of these substances and their intensities in arbitrary units are tabulated below. The infra-red absorption frequencies are available for two of the liquids, viz., tin tetramethyl and lead

tetraethyl, from the recent measurements of Kettering and Sleator,\* and they are also included in the Table for comparison with the Raman frequencies of these liquids.

The correspondence between the infra-red and the Raman frequencies is not particularly striking, especially in the case of the tin alkyl.

#### 4—DISCUSSION OF RESULTS

The most striking feature of the Raman spectra of these various metallic alkyls is the exceptionally large intensity of some of the lines. Among the known compounds only the iodides approach them. The intensities are so large that the antistokes lines corresponding to such large frequency shifts as  $\Delta\nu = 500 \text{ cm}^{-1}$  appear very prominently. The intensity of the Raman spectra is presumably connected with the high molecular weight of these compounds, since the iodides which have intense Raman lines

TABLE I

Zn(CH <sub>3</sub> ) <sub>2</sub>		Hg(CH <sub>3</sub> ) <sub>2</sub>		Hg(C <sub>2</sub> H <sub>5</sub> ) <sub>2</sub>		Zn(C <sub>2</sub> H <sub>5</sub> ) <sub>2</sub>		Bi(CH <sub>3</sub> ) <sub>3</sub>	
144	2d	156	2d	140	1	111(?)	2	171	4
				212	2	176	2		
248	1	255	0	259	3	255	2		
				329	0				
								460	8
488	2								
505	8	515	8	486	8	476	5		
		565	1	562	0	533	1		
						579	2		
620	4d			633	0d				
		700	3					784	0d
				958	1	938	2		
				1008	3	990	2		
				1055	2				
1159	6d	1182	6	1178	6d	1175	5	1147	2
		1258	1					1165	3
1346	0					1336	0	1230	1d
				1370	1			1347	0
				1421	3	1403	1		
				1455	3	1458	1		
2897	3	2879	1	2857	1	2879	3		
				2896	3				
		2910	2					2915	1
		2965	1	2942	1				

\* 'Physics,' vol. 4, p. 39 (1933).

TABLE I—(continued)

Sn(CH <sub>3</sub> ) <sub>4</sub>				Pb(C <sub>2</sub> H <sub>5</sub> ) <sub>4</sub>			
Raman		Infra-red		Raman		Infra-red	
152	7			96	4		
262	4			165	2		
506	8			237	1		
526	5			444	4		
				462	3		
		776	10				
952	0d	943	2	941	1	952	10
				1014	2	1016	9
1046	0	1051	2				
		1063	1				
				1170	3	1169	9
1200	5	1205	7				
1262	0						
		1369	3				
		1470	5				
		1724	2	1781	1	1778	5
		2464	1				
2915	3			2869	1	2949	9
2979	2						
		3038	6				
		3730	1				

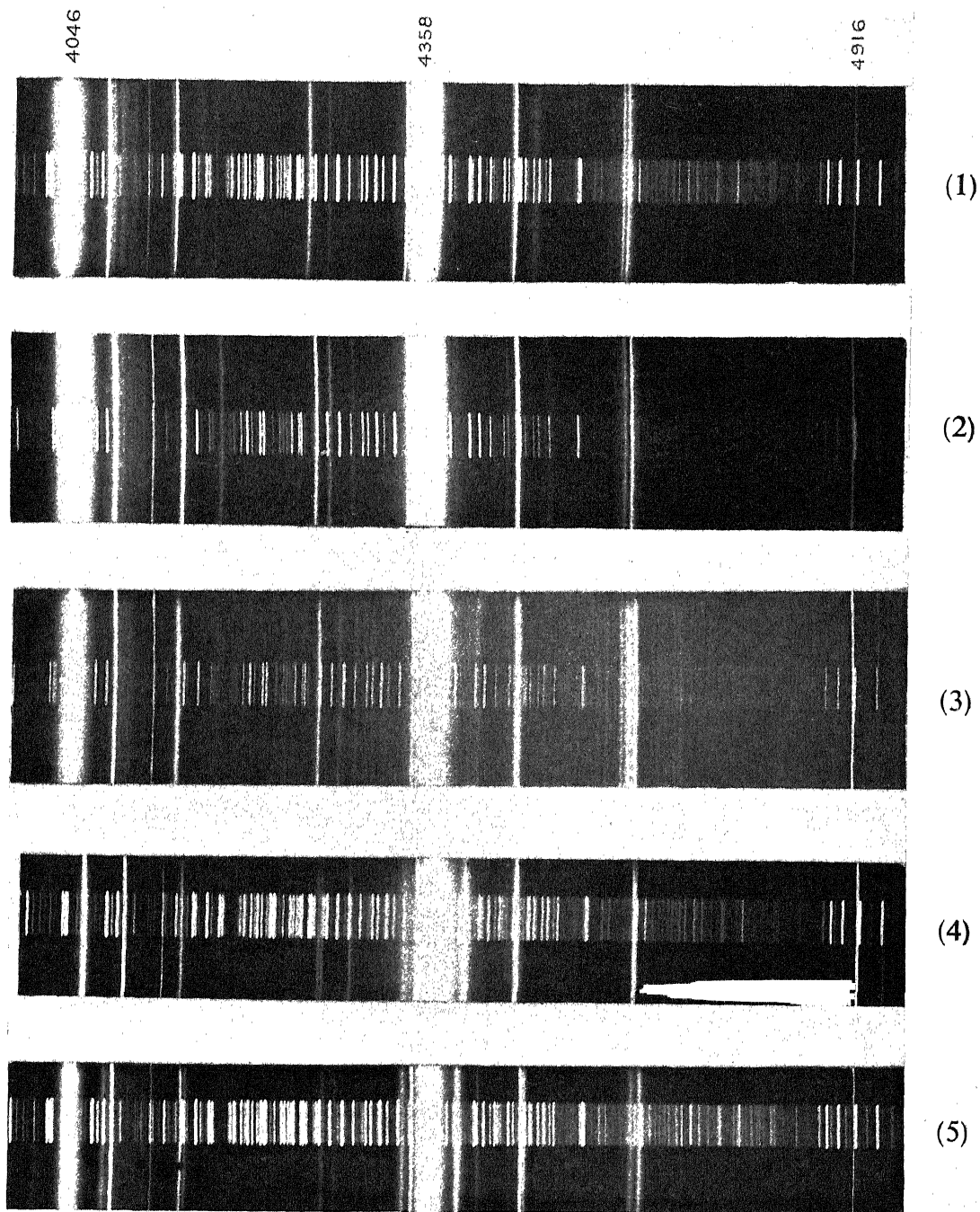
are also very massive. Another feature is the occurrence of a number of low Raman frequencies. This is indeed to be expected owing to the large mass of the metallic atoms.

There are other features which may also be mentioned here. Owing to the C—H bond which is present in all the compounds, there are naturally some frequencies—about  $\Delta\nu = 3000 \text{ cm}^{-1}$  characteristic of this bond, which are common to all the compounds. An examination of the data shows that, in addition, the frequencies in the neighbourhood of 1200 and 1400, which are common to all the compounds, are also to be attributed to the same bond.

We now proceed to discuss the individual compounds in some detail.

*The Dialkyls*—Among the compounds studied here, zinc dimethyl and diethyl have already been studied by Venkateswaran.\* Our measurements confirm the values of the Raman frequencies obtained by him and further show two new lines at  $\Delta\nu = 144$ , and  $248 \text{ cm}^{-1}$ . Also the strong line obtained by him at  $\Delta\nu = 505 \text{ cm}^{-1}$  is found to be a doublet whose components are at 488 and 505, the latter component being much stronger than the former.

\* 'Ind. J. Phys.,' vol. 5, p. 145 (1930).



(1)  $\text{Zn}(\text{CH}_3)_2$

(2)  $\text{Hg}(\text{CH}_3)_2$

(3)  $\text{Hg}(\text{H}_2\text{C}_5)_2$

(4)  $\text{Bi}(\text{CH}_3)_3$

(5)  $\text{Sn}(\text{CH}_3)_4$

(Facing p. 32.)





Considering first zinc dimethyl, its Raman frequencies are 144 (2), 248 (1), 488 (2), 505 (8), 620 (4), 1159 (6), 1346 (0), and 2897 (3). Of these, the last three frequencies are due to C—H bonds. If we ignore the weak line at 248 and further consider the doublet at 488–505 as a single line, we are left with three frequencies, which are presumably

the fundamental frequencies of oscillation of the system  $\text{Zn} \begin{array}{l} \nearrow \text{CH}_3 \\ \searrow \text{CH}_3 \end{array}$ , which

may be treated as equivalent to a non-linear triatomic molecule.

The theory of oscillations of a non-linear triatomic molecule has been worked out by Dennison\* and others. Let us denote by  $F$  and  $F'$  the binding forces corresponding to the Zn—C and C—C bonds respectively in the molecule, and by  $2\alpha$  the valency angle of the Zn atom. Then on the basis of Dennison's theory it is possible to calculate from the above three frequencies the values of  $2\alpha$  and of  $F$  and  $F'$ . Calculating in this manner we find that the valency angle =  $136^\circ$ ;  $F$  and  $F'$  are equal to  $1.60 \times 10^5$  and  $0.94 \times 10^5$  dyne/cm respectively.  $F'$  is much smaller than  $F$  as we should expect, since there is no chemical linkage between C and C, and the forces between them must naturally be weak. The large valency angle is also consistent with the small values for the dipole-moments obtained with the dialkyls.

The above value of  $F$  would correspond to the heat of dissociation of the Zn—C bond being about 32 kilocalories per gram mol. Sufficient thermo-chemical data are not available to confirm this value; it may be mentioned, however, that it is of the proper magnitude.

It is not clear why one of the above fundamental frequencies should have a doublet structure. The explanation is probably similar to the one usually offered for the doublet nature of the 760–791 fundamental frequency of  $\text{CCl}_4$ , namely, that it is close to the value obtained by the combination of two other frequencies.

We next consider  $\text{Hg}(\text{CH}_3)_2$ . Treating this molecule also as a symmetrical non-linear triatomic molecule of the type  $\text{XY}_2$ , and taking 515, 156, and  $700 \text{ cm}^{-1}$  as its fundamental frequencies, we obtain as in the case of zinc dimethyl,  $F$  (corresponding to the Hg—C bond) to be  $2.1 \times 10^5$  dyne  $\text{cm}^{-1}$  and  $F'$  (corresponding to C—C bond) to be  $1.2 \times 10^5$ . The valency angle of Hg comes out as  $133^\circ$ .

We should mention here that the fundamental frequencies of  $\text{Hg}(\text{CH}_3)_2$  are considerably *higher* than those of  $\text{Zn}(\text{CH}_3)_2$  in spite of the much

\* 'Phil. Mag.', vol. 1, p. 195 (1926).

larger atomic weight of mercury. This is remarkable, since in the case of all homologous series of compounds, the corresponding frequencies show a *diminution* with increase in atomic weight. The observed higher frequencies for the mercury compound are evidently to be attributed to the unique properties of mercury which differentiate it from zinc and the other elements of its group in the Periodic Table. Whereas mercury forms covalent links of great stability with a large number of elements, e.g., halogens, oxygen, carbon, etc., zinc has to be forced to enter into combination with radicals which could be attached by such covalent linkages only, and the resulting compounds are also extremely unstable. If in the dimethyls that we are considering, the linkages between Hg and C and between Zn and C may be taken to be of the covalent type, the much larger value of  $F$  for the Hg—C bond and the consequent larger value of the oscillational frequencies of the mercury compound are readily understood.

The diethyl derivatives of Hg and Zn show the same general characteristics, and need not be considered here.

*Bismuth trimethyl*—The Raman spectrum of this compound is very similar to the well-known spectra of the series of trichlorides  $\text{PCl}_3$ ,  $\text{AsCl}_3$ ,  $\text{SbCl}_3$ , and  $\text{BiCl}_3$  on the one hand and to the spectra of  $\text{N}(\text{CH}_3)_3$  and  $\text{NH}_3$  on the other. Its four fundamental frequencies are 1147, 171, 460, and 171 respectively, two of which are identical, as in the case of  $\text{BiCl}_3$ . Like the other compounds mentioned here,  $\text{Bi}(\text{CH}_3)_3$  has presumably a pyramidal structure, the three methyl groups forming the triangular base of the prism, and the Bi atom being located at the apex. The binding forces between the atoms and the vertical angle of the pyramid can be calculated in the usual manner from the above values of the fundamental frequencies.

*The Tetra-alkyls*—The Raman spectra of the two tetra-alkyls resemble, as we should expect, those of the tetra-chlorides of C, Si, Ti, and Sn, which have been studied by a number of workers; their fundamental frequencies are 506, 152, 526, and 262  $\text{cm}^{-1}$  for  $\text{Sn}(\text{CH}_3)_4$  and 444, 96, 462, and 165  $\text{cm}^{-1}$  for  $\text{Pb}(\text{C}_2\text{H}_5)_4$ , corresponding to a regular tetrahedral model. Preliminary polarization measurements on the Raman lines of  $\text{Sn}(\text{CH}_3)_4$  show that the line  $\Delta\nu = 506 \text{ cm}^{-1}$  is strongly polarized, while the other lines are feebly so, as we should expect from the tetrahedral structure.

In conclusion, the author desires to express his thanks to Professor K. S. Krishnan, and Sir C. V. Raman for their kind interest in the work.

## SUMMARY

An account is given of the Raman spectra of the following metallic alkyls : zinc dimethyl and diethyl, mercury dimethyl and diethyl, bismuth trimethyl, tin tetramethyl and lead tetraethyl. The Raman frequencies are discussed in relation to the structure of the molecules. It is found that the dialkyls may be treated as symmetrical non-linear triatomic molecules of the type  $XY_2$ , in which the metallic atom X has a large valency angle. Bismuth trimethyl conforms to a pyramidal model, while the tetra-alkyls have a regular tetrahedral structure.

---

## The Effect of Temperature on the Thermal Conductivity and the Accommodation Coefficient of Hydrogen

By H. S. GREGORY, A.R.C.S., Ph.D., Assistant Professor of Physics,  
Royal College of Science

(Communicated by G. P. Thomson, F.R.S.—Received October 12, 1934)

## INTRODUCTION

Comparatively little work has been attempted on the subject of the effect of temperature on the conduction of heat through hydrogen.

Eucken\*† carried out investigations on the thermal conductivity of hydrogen for a range of temperature between  $-252.2^\circ$  and  $100^\circ$  C. A modification of the hot wire method was employed in which his final values were obtained relative to a predetermined value for the thermal conductivity of air, viz.,  $566 \times 10^{-7}$  cal  $\text{cm}^{-1}$   $\text{sec}^{-1}$   $\text{deg}^{-1}$ . The values thus determined at various temperatures are given in Table I and compared with those of other observers.

All methods which have been used to investigate the heat conduction through gases, with one exception, are complicated by the existence of the errors due to convective losses or mass motions of the gas itself. Although these mass motions are diminished to a great extent by decreasing the gas pressure, this procedure restricts the measurements to a gas in

\* 'Phys. Z.', vol. 14, p. 324 (1913).

† 'Phys. Z.', vol. 12, p. 1101 (1911).

more or less a state of rarefaction and at the same time—in particular in the hot wire method—the troublesome temperature drop effect is enhanced by reason of the low pressure and also by the extremely small dimensions of the wires used. Further, the calculation of the convective losses has not yet been found theoretically possible.

TABLE I

Temperature	$K \times 10^7$	Observer
-252.2	322	Eucken*
-191.5	1324	
0	3970	
-191.5	1331	Eucken†
-182.6	1481	
-78.4	3065	
0	3960	
100	4994	
0	4165	Weber, S.‡
0	4100	Schleiermacher§
100	5228	
0	4190	Schneider
0	4180	Schneider¶

\* 'Phys. Z.,' vol. 12, p. 1101 (1911).

† 'Phys. Z.,' vol. 14, p. 324 (1913).

‡ 'Ann. Physik,' vol. 54, p. 437 (1917).

§ 'Wied. Ann.,' vol. 34, p. 623 (1888).

|| 'Ann. Physik,' vol. 79, p. 177 (1926).

¶ 'Ann. Physik,' vol. 80, p. 215 (1926).

The problem of disentangling experimentally the convective losses from those due to pure conduction was the subject of an investigation by Gregory and Archer.\*\* This was effected by the use of a double system of tubes and wires which in conjunction with the bridge system used enabled them to eliminate experimentally these losses from their measurements. This and other investigations which have since been carried out by other observers have firmly substantiated the truth of their arguments in this respect. It is emphasized that the success in this instance was due to the important modification imposed on the hot wire method in which an electrically heated wire is maintained at constant temperature to a high degree of accuracy while the pressure of the gas is lowered by successive amounts, a procedure only possible with a bridge

\*\* 'Proc. Roy. Soc.,' A, vol. 110, p. 91 (1926).

system and not with a potentiometer method as adopted by Weber\* and other observers in their researches on the subject.

### THEORY OF METHOD

Kundt and Warburg,† who were led to predict, by analogy with the “slip” effect in viscosity, the existence of a temperature discontinuity at the surface of separation of a heated solid and a gas, defined such temperature drop by the relation

$$\delta\theta = -\mu \frac{d\theta}{dn}, \quad (1)$$

where  $d\theta/dn$  represents the normal temperature gradient at a point on the solid, and  $\mu$  a quantity which was found to be proportional to the mean free path of the gas molecules.

More recently the subject has been developed along theoretical lines by Smoluchowski‡ who, making use of Maxwell’s§ hypothesis that molecules can be regarded as centres of forces of repulsion varying inversely as the fifth power of the distance of separation, found the temperature drop to be represented by the relation

$$\begin{aligned} \delta\theta &= -\gamma\lambda \frac{d\theta}{dn} \\ &= -\frac{15}{2\pi} \frac{2-a}{2a} \lambda \frac{d\theta}{dn}, \end{aligned} \quad (2)$$

where  $a$  is the accommodation coefficient as defined by Knudsen,||  $\lambda$  the mean free path of the gas molecules and  $d\theta/dn$  the normal temperature gradient at a point in the gas near the heated surface.

A second calculation of  $\delta\theta$  by Smoluchowski¶ was based on a hypothesis, also used by Maxwell in his theoretical investigation of “slip” in gases, in which it was assumed that amongst all molecules striking a surface only a fraction  $\beta$  attain thermal equilibrium, while the remainder  $(1 - \beta)$  are reflected without change of temperature. These two aspects give results which are indistinguishable from one another in their application to experimental practice. Equation (1) applies only to small tempera-

\* ‘Ann. Physik,’ vol. 54, p. 437 (1917).

† ‘Pogg. Ann.,’ vol. 156, p. 177 (1875).

‡ ‘Ann. Physik,’ vol. 35, p. 983 (1911).

§ ‘Phil. Trans.,’ vol. 170, p. 231 (1879).

|| ‘Ann. Physik,’ vol. 34, p. 593 (1911).

¶ ‘Ann. Physik,’ vol. 35, p. 983 (1911).

ture discontinuities and to heat transfer between surfaces where the curvature is large compared with the mean free path.

If  $T_1$  and  $T_2$  represent the temperatures of the wire and the internal surface of the tube when thermal equilibrium is attained, and if  $T''_1$  and  $T'_1$  denote the average temperatures of the molecules approaching and leaving the wire, fig. 1, then  $T_1 - T''_1$  is termed the temperature drop at the wire and  $T''_2 - T_2$  the corresponding discontinuity of temperature at the wall of the tube. The average temperature of the molecules leaving the wire will depend on the extent to which the impinging molecules accommodate themselves with the temperature of the wire.

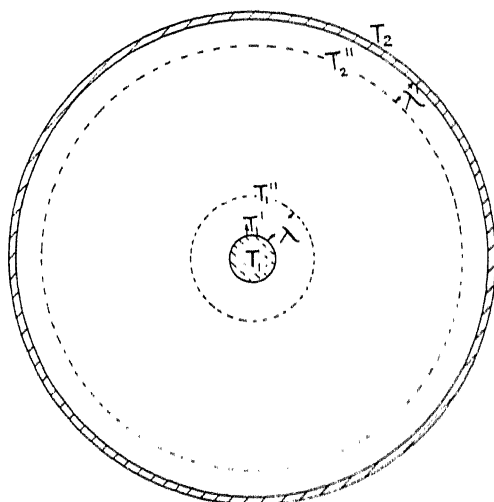


FIG. 1

Knudsen\* has defined such an effect in terms of the mean energies of the approaching and receding molecules. If  $E_1$ ,  $E'_1$  and  $E''_1$  are the mean energies of the molecules at the temperatures  $T_1$ ,  $T'_1$  and  $T''_1$  respectively, then

$$\frac{E'_1 - E''_1}{E_1 - E''_1} = \text{constant} = a, \quad (3)$$

where  $a$  is known as the accommodation constant.

If the velocity distribution of the molecules leaving the wire corresponds to a Maxwellian distribution, then equation (3) can be written

$$a = \frac{E'_1 - E''_1}{E_1 - E''_1} = \frac{T'_1 - T''_1}{T_1 - T''_1}, \quad (4)$$

\* 'Ann. Physik,' vol. 34, p. 593 (1911).

If, however, a Maxwellian distribution does not exist, equation (4) no longer holds in respect of the emitted molecules. On this account, Langmuir and Blodgett\* in their investigation of the effect of temperature on the accommodation constant of hydrogen have avoided Knudsen's definition of  $a$ .

For a cylindrical temperature distribution, as in the hot wire method, the equation expressing thermal equilibrium in the absence of convection can be written in the form

$$\begin{aligned} Q \log \frac{r_2 - \lambda'}{r_1 + \lambda} &= 2\pi K l (T''_1 - T''_2) \\ &= 2\pi K l (T_1 - \delta\theta_1 - \overline{T_2 + \delta\theta_2}) \\ &= 2\pi K l (T_1 - T_2 - \delta\theta_1 - \delta\theta_2), \end{aligned} \quad (5)$$

where  $T_1$  and  $T_2$  are the wire and wall temperatures,  $\delta\theta_1$  and  $\delta\theta_2$  the temperature drop at the wire and the wall respectively,  $\lambda$  and  $\lambda'$  the mean free paths corresponding to the temperatures of the wire and the wall,  $r_1$  and  $r_2$  the radii of the wire and internal tubewall and  $K$  the absolute thermal conductivity at a mean temperature across the gas layer.  $Q$  represents the heat transfer per second, corrected for radiation, from a wire of length  $l$  whose temperature, from consideration of the principle of compensation, is considered constant throughout its length, a point fully discussed in previous papers.

From (2) above

$$\delta\theta_1 = \frac{\lambda_0 P_0}{P} \frac{15}{2\pi} \frac{2-a}{2a} \frac{Q_0}{2\pi K_1 l r_1} \quad (6)$$

and

$$\delta\theta_2 = \frac{\lambda'_0 P_0}{P} \frac{15}{2\pi} \frac{2-a'}{2a'} \frac{Q_0}{2\pi K_2 l r_2}, \quad (7)$$

where  $P_0$  denotes a pressure of 1 atmosphere in cm of mercury and  $P$  the existing gas pressure in the tubes measured in the same units,  $\lambda_0$  and  $\lambda'_0$  the mean free paths of the gas molecules at atmospheric pressure and at the temperatures of the wire and wall respectively. The accommodation constants  $a$  and  $a'$  will differ slightly by reason of the different temperatures of the wire and internal wall surface.  $Q_0$  represents the heat transfer operative in the absence of temperature drop and convection,  $K_1$  and  $K_2$  the absolute thermal conductivity of the gas at the wire and wall temperatures.

\* 'Phys. Rev.,' vol. 40, p. 78 (1932).



Substituting (6) and (7) in (5)

$$\begin{aligned} Q \log \frac{r_2 - \lambda'}{r_1 + \lambda} &= 2\pi K l (T_1 - T_2) - 2\pi K l (\delta \theta_1 + \delta \theta_2) \\ &= 2\pi K l \theta - \frac{15}{2\pi} \frac{2\pi K l P_0}{P} \frac{Q_0}{2\pi l} \left( \frac{2-a}{2a} \frac{\lambda_0}{K_1 r_1} \right. \\ &\quad \left. + \frac{2-a'}{2a'} \frac{\lambda'_0}{K_2 r_2} \right). \end{aligned} \quad (8)$$

Since the ratio of  $r_2 : r_1$  is of the order of 250 : 1 in the present instance, the term

$$\frac{2-a'}{2a'} \frac{\lambda'_0}{K_2 r_2}$$

is small compared with

$$\frac{2-a}{2a} \frac{\lambda_0}{K_1 r_1}$$

and also since  $a'$  will differ only slightly from  $a$  on account of the small variation of  $a$  with temperature, it is sufficiently exact to write  $a$  for  $a'$  in (8) and hence

$$\frac{Q}{\theta} \log \frac{r_2 - \lambda'}{r_1 + \lambda} = 2\pi K l - \frac{15}{2\pi} \frac{2-a}{2a} \frac{P_0}{P \theta} \frac{2\pi K l Q_0}{2\pi l} \left( \frac{\lambda_0}{K_1 r_1} + \frac{\lambda'_0}{K_2 r_2} \right). \quad (9)$$

For reasons considered below,  $\theta$ , the temperature difference between the wire and the wall, will vary progressively with time during the course of the experiment.

Since

$$Q_0 = \frac{2\pi K l \theta}{\log \frac{r_2}{r_1}},$$

equation (9) can be written

$$\begin{aligned} \frac{Q}{\theta} \log \frac{r_2 - \lambda'}{r_1 + \lambda} &= 2\pi K l \\ &\quad - \frac{I^2}{\log \frac{r_2}{r_1}} \frac{15}{2\pi} \frac{P_0}{P} \frac{2-a}{2a} \left( \frac{\lambda_0}{K_1 r_1} + \frac{\lambda'_0}{K_2 r_2} \right), \end{aligned} \quad (10)$$

where  $I = 2\pi K l$ .

A linear relation therefore holds between

$$\frac{Q}{\theta} \log \frac{r_2 - \lambda'}{r_1 + \lambda} \quad \text{and} \quad \frac{1}{P},$$

the intercept value of which corresponds to the term  $2\pi Kl = I$ , from which the absolute conductivity of the gas corresponding to an average temperature  $\frac{T_1 + T_2}{2}$  can be calculated.

The slope of the line is a measure of the quantity

$$\frac{I^2}{\log \frac{r_2}{r_1}} \frac{15}{2\pi} P_0 \frac{2-a}{2a} \left( \frac{\lambda_0}{K_1 r_1} + \frac{\lambda'_0}{K_2 r_2} \right),$$

from which  $a$  at the temperature of the wire is determined

The values of  $\lambda_0$  and  $\lambda'_0$  at their appropriate temperatures are calculable in terms of viscosity data.

Equation (10) would appear to require a correction to allow for the variations of  $K$  with possible variations in  $T_2$  the wall temperature, since  $K$  corresponds to the average temperature  $\frac{T_1 + T_2}{2}$ ,  $T_1$  being constant.

If it be supposed that observations commence when the wire and internal wall temperatures are  $T_1$  and  $T_2$ , the correcting factor is  $1 \pm \alpha \cdot \delta\theta$ , where  $\delta\theta$  represents a maximum alteration in  $T_2$  during the time of the experiment and the maximum possible change in  $K$  is given by

$$K \pm \delta K = K (1 \pm \alpha \cdot \delta\theta),$$

$\alpha$  being the temperature coefficient of change of thermal conductivity.  $\alpha$  for a large range of temperature is of the order 0.003 and therefore the factor  $1 \pm \alpha \cdot \delta\theta$  is of negligible effect for possible variations of wall temperature of  $0.5^\circ$ , which was the maximum change of temperature permitted during the total time occupied in the observations.

The quantities  $K_1$  and  $K_2$  corresponding to the wire and wall temperatures will differ by an amount of the order of 5% in the present experiments and a further modification of the working equation (10) is possible, since the magnitude of the terms  $\lambda'_0/K_2 r_2$  and  $\lambda_0/K_1 r_1$  are in the ratio of 1:250 approximately. Hence, to this order of accuracy, we can write  $K_1 = K_2$  and the relation reduces to

$$\begin{aligned} \frac{Q}{\theta} \log \frac{r_2 - \lambda'}{r_1 + \lambda} &= \frac{Q}{\theta} \log \frac{r_2}{r_1} \left( \frac{P - \frac{\lambda'_0 P_0}{r_2}}{P + \frac{\lambda_0 P_0}{r_1}} \right) \\ &= 2\pi Kl \\ &\quad - \frac{15}{2\pi} \frac{P_0}{P} \frac{2-a}{2a} \frac{I}{\log \frac{r_2}{r_1}} \frac{K}{K_1} \left( \frac{\lambda_0}{r_1} + \frac{\lambda'_0}{r_2} \right). \end{aligned} \quad (11)$$

In actual practice, the existence of a uniformly heated wire can be realized by means of the compensating device used by Gregory and Archer\* in the earlier experiments on the subject. The system adopted in the present investigation consisted of two similarly constructed tubes and wires, dimensionally the same, except in length and disposed in opposite arms of a Callendar and Griffiths bridge. It has been shown from theoretical considerations by Gregory and Archer† in a previous paper, that the resistance associated with such a balanced bridge system is that corresponding to a wire equal in length to the difference between the main and compensating wires, and which is uniform in temperature throughout its length, provided the design of the tube system is such that the quantities

$$e^{-2l_1/\sqrt{P}} \quad \text{and} \quad e^{-2l_2/\sqrt{P}}$$

are negligibly small compared with unity, where  $2l_1$  and  $2l_2$  are the lengths of the main and compensating wires and  $P$  a quantity depending on the dimensions of the system and the heat losses from the surfaces of the wires.

When such conditions are satisfied, the system is termed to be compensating in that the temperature distribution along each of the two wires is the same and the heat losses by conduction through the leading wires connected to each of the two wires are equal.

In addition to the effects considered above, two others are of especial consequence as associated with the present experimental procedure. As an example of one of these effects, the case is considered of a tube system when immersed in the vapour of a boiling liquid. In this instance a failure of attainment of the stationary state was observed, and was found to be directly due to a progressive accumulation of heat on the tube wall, which, if the internal wire is maintained at a constant temperature, leads to a steadily decreasing temperature difference between the wire and wall, and the latter, being at a higher temperature than the vapour, a large error is possible in the calculated thermal conductivity of the gas, if equality of the wall and vapour temperatures is assumed. The existence of such an effect first led the author to consider the advantage of directly measuring the temperature of the external surface of the tube by fusing platinum wire to the surface. The procedure of covering the wire with a thin coating of pyrex glass, and then fusing the same to the tube wall, was found to be satisfactory. This is shown diagrammatically in fig. 2.

\* 'Proc. Roy. Soc.,' A, vol. 110, p. 91 (1926).

† 'Phil. Mag.,' vol. 3, p. 931 (1927).

A series of experiments was undertaken to test the constancy of the wall temperature under the conditions associated with the use of the ice and water thermostat, designed by the author and used in conjunction with Mr. Archer in previous experiments, and also with a similar thermostat using oil at various temperatures over a range of some 300 degrees. In all cases, except that of the ice and water thermostat, a heating effect was found to exist and to be of greater magnitude for gases of high thermal conductivity.

Such an effect is specially noticeable with the present bridge system in which the heating current through the wires is raised or lowered in order to maintain constancy of the wire temperature. In every case the effect was accompanied by a lowering of the current strength which pointed to a progressive heating of the tube wall.

The use of the oil thermostat was complicated by the difficulty of adjusting and maintaining a constant temperature throughout the mass of oil, which temperature was found to vary intermittently, however carefully the current through the heaters was adjusted. This was due to the uncertainty from time to time of the atmospheric conditions prevailing in the laboratory and external to the thermostat, and the sensitivity of the bridge used was such that it was found impossible to secure an exact balance for the current flowing through the hot wire system. The procedure was adopted of so adjusting the current through the heaters in the thermostat that the oil was allowed to cool at a rate sufficiently small to permit of accurate adjustment of the bridge current and at the same time, to overcome the heating effect referred to above. By this means the temperature of the wall surface could be caused to decrease sufficiently slowly with time to enable an accurate experimental procedure to be carried out, and in many instances a rate of decrease of less than  $0.5^{\circ}$  per hour was observed. The term "wall effect" has been introduced by the author to denote the resultant temperature change of the wall due to the two thermal effects considered above, such temperature changes being measured during the course of the experiments by the platinum thermometer in intimate fusion with the tube wall.

The thermostat was constructed of a welded steel inner vessel of 10 gallons capacity surrounded by an outer vessel also of steel, the intervening space being packed with slag wool. The inner vessel was fitted with a brass frame to which was bolted six 100-ohm heating coils con-

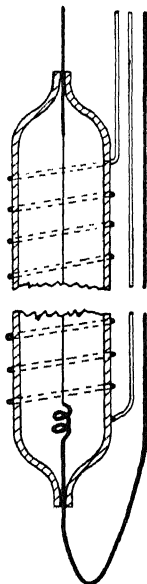


FIG. 2

nected in parallel and disposed symmetrically as shown diagrammatically in fig. 3. The arrangement for producing turbulence in the thermostatic fluid consisted of an L-shaped tube open at both ends, the lower end carrying a bevel gear operated by a vertical driving shaft to which was attached a horizontal pulley driven by an electric motor. The other end of the bevel gear was in rigid connection with a propeller by which means the oil was drawn from the tank in the neighbourhood of the heaters and caused to flow along the vertical portion of the L-tube in which was fixed the tube system used in the experiments.

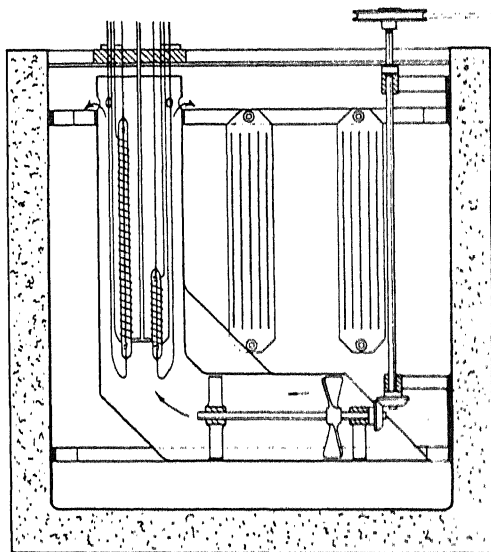


FIG. 3

It was found necessary during the course of the experiments to supplement the fixed heaters by the addition of another movable heater of about 2000 watts capacity. This was because of the large amount of heat required for the experiments in the neighbourhood of  $300^{\circ}\text{C}$ . The tank was closed by two steel half-plates covered by asbestos cement with an aperture through which the experimental system passed into the tank. The oil used was a thermostatic substance supplied by Messrs. C. C. Wakefield and Co., Ltd., and termed Special Thermostat Oil.

#### WALL TEMPERATURE CORRECTION

An appreciable correction to the internal wall temperature was found necessary on account of the large thickness of the walls of the tubes employed.

If the temperatures of the internal and external surfaces are represented by  $T_2$  and  $T_3$ , then  $T_2$  can be found from the relation

$$T_2 = T_3 + \frac{Q \log \frac{r_3}{r_2}}{2\pi K_g l},$$

where  $Q$  is the heat loss (corrected for radiation) from a wire of length  $l$ ,  $r_2$  and  $r_3$  the internal and external radii of the tube and  $K_g$  the thermal conductivity at an average temperature  $\frac{T_2 + T_3}{2}$  of the glass used. Values of  $K_g$  at the appropriate temperatures were calculated in terms of the data obtained by Stephens,\* who showed that the conductivity of Pyrex glass could be represented accurately by the relation

$$K_g^T = -0.00352 + 0.00245 \log_{10} T$$

over a range of temperature from  $-182^\circ$  to  $250^\circ$  C, where  $T$  is temperature on the absolute scale.

#### RADIATION CORRECTION

The correction to be applied for the emission of heat by radiation from a wire maintained at a certain temperature to a coaxial surface maintained at a lower temperature is not of very serious importance in the hot wire method, owing to the very small dimensions of the wires used. In the present series of experiments, the maximum correction was found to be of the order of 0.5% of the total heat transfer.

An exact determination is one of great difficulty. The experimental procedure as originally adopted by Gregory and Archer† was to evacuate the tubes as completely as possible and determine the heat loss under similar conditions of temperature as those imposed in the presence of a gas. It should be pointed out, however, that the temperature distribution along an electrically heated wire is not the same in the two cases and for this reason the present method of compensating end effects by using a long and short system of tubes and wires no longer holds. In addition, even in the best vacuum experimentally attainable, there is a heat transfer by conduction through a strongly rarefied gas which according to Knudsen is directly proportional to the gas pressure and comparable in magnitude with the radiation loss.

\* 'Phil. Mag.', vol. 14, p. 897 (1932).

† 'Proc. Roy. Soc., A', vol. 110, p. 91 (1926).

If  $Q$  denotes the total heat loss from a wire of length  $l$  and radius  $r_1$  maintained at a temperature  $T_1$  to a surrounding tube at a temperature  $T_2$ , then

$$Q = 2\pi r_1 l \varepsilon (T_1 - T_2) aP + \phi (T_1, T_2),$$

where  $\varepsilon$  represents the molecular conductivity,  $P$  the gas pressure and  $a$  the coefficient of accommodation, while  $\phi (T_1, T_2)$  is the loss by radiation corresponding to the existing temperature conditions. If  $T_1$  and  $T_2$  are constant, then a linear relation holds between  $Q$  and  $P$  since  $a$  and  $\varepsilon$  are independent of pressure, from which  $\phi (T_1, T_2)$  is known from the intercept on the  $Q$  axis. The procedure can be repeated for various values of  $T_1$  and  $T_2$  ( $T_1 > T_2$ ) and  $\phi$  determined for any chosen temperatures of the wire and wall and which represents a criterion of application in the present experiments.

Such an investigation was carried out by Milverton\* with respect to the radiation from bright platinum and his results were expressed by a formula of the type

$$\phi (T_1, T_2) = 1.87 (T_1^{3.82} - T_2^{3.82}) 10^{-14} \text{ calories per cm of wire,}$$

in which  $T_1$  and  $T_2$  refer to the absolute temperatures of the wire and wall.

The above expression was employed to calculate the corrections applied to the results in the present paper.

The author has also calculated the radiation correction by using a formula deduced from theoretical considerations by Helfgott,† viz.,

$$E = \sigma T^4 (1 - e^{-\alpha T}),$$

where  $\sigma = 5.72 \times 10^{-12}$  watts per  $\text{cm}^2$  and  $\alpha$  has the value  $1.25 \times 10^{-4}$  for platinum,  $T$  denoting temperature on the absolute scale. The substitution of such data in place of the values calculated from Milverton's relation introduces a change in the thermal conductivity of the order of 1/15%, which is beyond the estimated accuracy of the present investigation.

#### EXPERIMENTAL PROCEDURE

Apart from the important modifications referred to above, the arrangement of the experimental apparatus is similar to that employed by Gregory and Archer‡ in their experiments on the truth of Maxwell's

\* 'Phil. Mag.', vol. 17, p. 397 (1934).

† 'Z. Phys.', vol. 49, p. 555 (1928).

‡ 'Phil. Mag.', vol. 1, p. 593 (1926).

law of heat conduction. The procedure followed in a typical set of observations corresponding to a definite temperature of the wire is outlined below.

If the fundamental interval of the compensated platinum wire of length  $l$  has been determined, the bridge setting for any fixed wire temperature  $T_1$  is known in terms of this along with the resistance at  $0^\circ \text{C}$ . If now the heating current in the thermostat is adjusted until a definite rate of cooling of the oil is operative, the current in the bridge circuit is adjusted by means of the rheostats in the battery circuit to a point where the balancing current through the tubes is slightly too high, as indicated by a definite deflection of the galvanometer. Such a deflection, if the balancing current is kept constant, will gradually be nullified in view of the increasing magnitude of  $(T_1 - T_2)$  with time due to the cooling of the thermostat and eventually balance of the bridge circuit is effected. The temperature of the external wire is observed simultaneously with a measure of the balancing current, obtained with the potentiometer. The gas pressure is then decreased by a known amount and the procedure repeated. It is then found that in the absence of convection a definite change of balancing currents results, a change which is due to the increase of the temperature drop effect by reason of the decrease of gas pressure. The same holds for all other decreases in the gas pressure. It is found that the effect rapidly increases as the pressure is lowered by successive amounts and a point is ultimately attained where the time required for balance changes from an interval of about 5 minutes to a period of some hours; the current is found to require repeated adjustment in value to maintain constancy of the wire temperature. Since the cooling of the bath is in a direction such as to require the current to be increased, this effect must depend on some change occurring at the wire surface and is interpreted as being due alone to progressive changes in the film of gas adsorbed on the surface of the wire. The author has sought to express such changes in terms of the variation with time of the surface energy of the associated gas solid phase and this will be discussed in a subsequent paper from the aspect of the variation of the accommodation constant with pressure. In passing, it is emphasized that the method employed is such as to show conclusively that such effects are dependent alone on a change of surface conditions of the gas solid phase.

Typical sets of such observations are recorded in Tables II and III, and are expressed as a change of the balancing current with pressure.

The quantities  $\frac{Q}{\theta} \log \frac{r_2 - \lambda'}{r_1 + \lambda}$  and  $\frac{1}{P}$  can be calculated from such data and plotted to exhibit their dependence on each other in a linear relation.



TABLE II

Resistance of wire = 8.739 ohms; radiation = 0.00125 cal; ( $\theta_p$ ) temperature of wire = 328.91° C.

1/P	Current amps	$\theta_w$ ° C	$\theta_p$ ° C	$\frac{Q}{\theta} \log \frac{r_2 - \lambda'}{r_1 + \lambda}$
0.01257	0.3789	311.67	0.20	0.08678
0.01925	0.3771	311.72	0.20	0.08611
0.03008	0.3755	311.67	0.20	0.08505
0.04476	0.3733	311.61	0.20	0.08362
0.06477	0.3700	311.56	0.19	0.08163
0.09488	0.3649	311.52	0.19	0.07902
0.13812	0.3574	311.47	0.18	0.07521
0.19455	0.3475	311.42	0.17	0.07043

Mean temperature = 320.4° C.

Intercept =  $2\pi K l = 0.0875$

$K = 708 \times 10^{-6}$  cal cm<sup>-1</sup> sec<sup>-1</sup> deg<sup>-1</sup>.

Slope = 0.0868.

$a = 0.236$ .

TABLE III

Resistance of wire = 6.107 ohms; radiation = 0.000355 cal; ( $\theta_p$ ) temperature of wire = 145.94° C.

1/P	Current amps	$\theta_w$ ° C	$\theta_p$ ° C	$\frac{Q}{\theta} \log \frac{r_2 - \lambda'}{r_1 + \lambda}$
0.01250	0.3573	132.42	0.14	0.07260
0.01595	0.3588	132.32	0.14	0.07298
0.02000	0.3593	132.22	0.14	0.07259
0.02487	0.3591	132.18	0.14	0.07227
0.03413	0.3582	132.15	0.14	0.07169
0.04464	0.3572	132.13	0.14	0.07112
0.05984	0.3558	132.10	0.14	0.07029
0.08842	0.3527	132.02	0.14	0.06854
0.18149	0.3412	132.00	0.13	0.06353

Mean temperature = 139.25° C.

Intercept =  $2\pi K l = 0.0736$ .

$K = 595 \times 10^{-6}$  cal cm<sup>-1</sup> sec<sup>-1</sup> deg<sup>-1</sup>.

Slope = 0.055.

$a = 0.239$ .

The values of  $\lambda'$  and  $\lambda$  corresponding to known wall and wire temperatures are calculated from the recent data of Trautz and Stauf\* on the effect of temperature on the viscosity of hydrogen, the formula employed being

$$\lambda = \frac{2 \cdot 02 \cdot \eta}{\sqrt{P\rho}},$$

where  $\eta$  is the viscosity of the gas at the appropriate temperature,  $P$  one atmosphere in dynes per  $\text{cm}^2$  and  $\rho$  the density of the gas at N.T.P.

#### APPARATUS AND RESULTS

The single compensated tube system used in the present series of experiments was made of Pyrex glass, and the principal constants of the apparatus were as follows:—

- radius of platinum wire ( $r_1$ ), 0·00397 cm;
- length of principal wire, 24·81 cm;
- length of compensating wire, 5·13 cm;
- effective length of wire ( $l$ ), 19·68 cm;
- internal radius of tube ( $r_2$ ), 0·757 cm;
- external radius of tube ( $r_3$ ), 0·992 cm;
- resistance of internal wire at 0° C, 3·899 ohms;
- resistance of internal wire at 99·64° C, 5·417 ohms;
- fundamental interval, 1·518 ohms;
- resistance of external wire at 0° C, 1·083 ohms;
- resistance of external wire at 100·49° C, 1·498 ohms;
- fundamental interval, 0·415 ohms.

In Tables II and III showing typical sets of observations the following symbols are used:—

- $P$  the pressure of the gas in cm of mercury;
- $\theta_w$  ° C, the temperature of the external wall of tubes;
- $\theta_g$  ° C, the temperature correction for the wall of the tubes;
- $\theta$  ° C, the temperature difference between the wire and the internal wall of the tubes;
- $Q$ , the total heat loss in calories from the wire, given by  $C^2 R_{\theta_r} / J$ , corrected for radiation;
- $\theta_p$  ° C, the temperature of the wire.

$$\theta = \theta_p - (\theta_w + \theta_g).$$

\* 'Ann. Physik,' vol. 2, p. 737 (1929).

The lines obtained for various wire and bath temperatures are shown in fig. 4 and indicate the accuracy of the observations.

The intercepts of such lines enable  $K$  to be found corresponding to a mean temperature between those of the wire and internal surface of the tube, the latter temperature being determined as explained above.

The slopes of the lines are the measures of the quantity from which the accommodation constant  $a$  is known. The linear form of equation (11) above for the range of pressures considered is a proof that  $a$  is independent of pressure over this range and depends only on temperature.

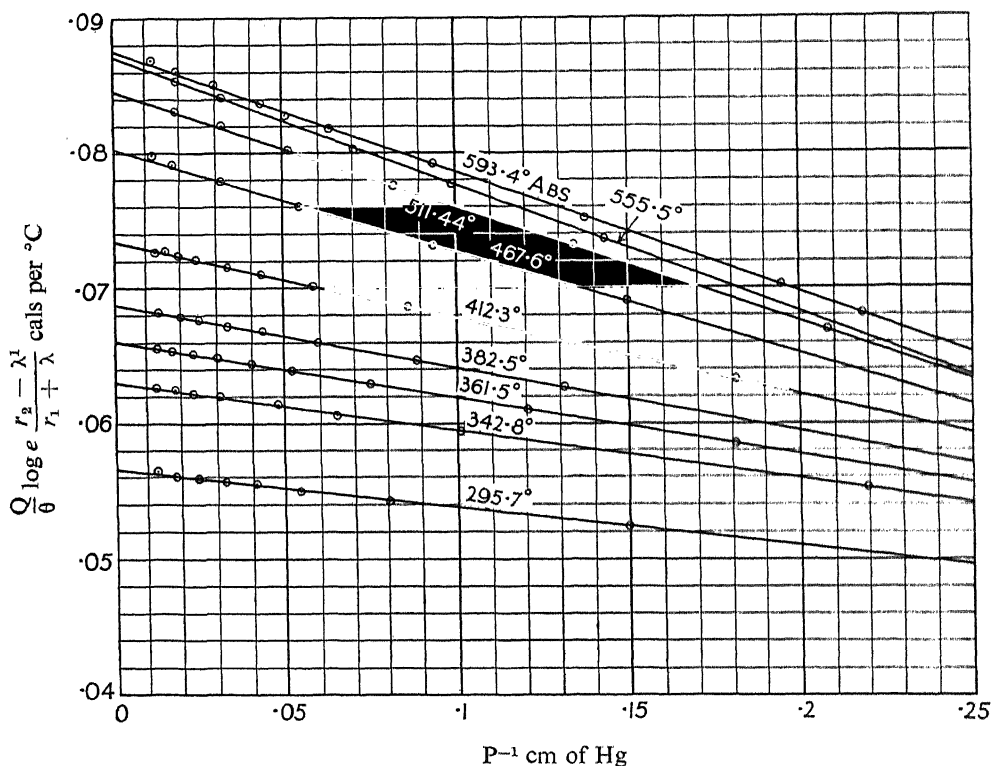


FIG. 4

The values of  $K$  referred to a mean gas temperature are tabulated in Table IV and are represented graphically in terms of such temperatures in fig. 5.

The graph in fig. 5 is marked by a definite change of  $dK/dT$  in the neighbourhood of about  $230^{\circ}$  C. Such a change might be reasonably interpreted as an effect due to gas impurities in the hydrogen associated with a lower thermal conductivity than in the pure state. The point

TABLE IV

Mean absolute temperature of gas $T^{\circ}$	$K \times 10^6$	Absolute temperature of wire $T_1^{\circ}$	$a$
593.4	708	601.9	0.236
555.5	704	564.2	0.213
511.4	689	520.2	0.211
467.6	651	475.5	0.216
412.3	595	418.9	0.239
382.5	558	389.4	0.252
361.5	534	368.0	0.259
342.8	512	349.4	0.269
295.1	459	299.4	0.282

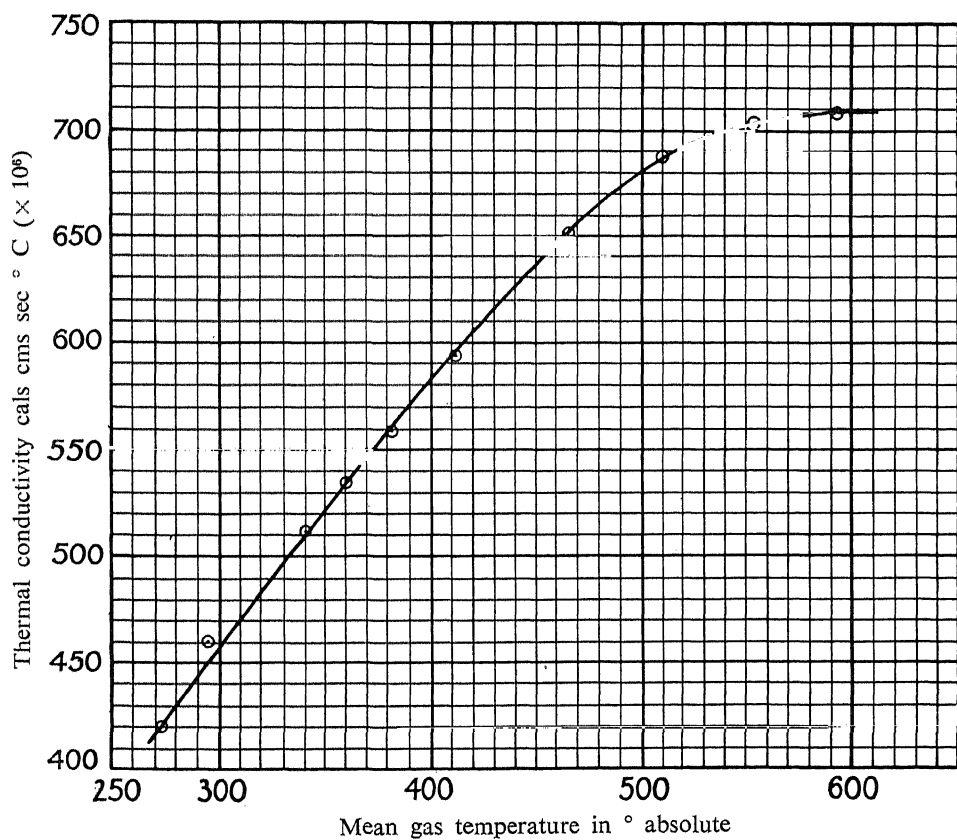


FIG. 5

was investigated by the author from the aspect of repeated observations, but no discrepancy of more than 0.5% was found amongst the determinations.

If the values of  $\log K$  are plotted against the values of  $\log T$ , where  $T$  is the absolute mean gas temperature, then for a range of about 230° a linear relation is found to hold. Beyond this range a linear law is still operative, but the line makes a smaller angle with the  $\log T$  axis.

The equations expressing the above variations are found to be

$$K_T = 5.68 \times 10^{-6} \cdot T^{0.77}$$

between 270° K and 502° K, and

$$K_T = 2.2 \times 10^{-4} \cdot T^{0.19}$$

above 500° K.

In a paper on the effect of temperature on the viscosity of carbon dioxide Ibbs and Wakeman\* discuss a similar effect. In this case the graphical representation of  $\log \eta$  and  $\log T$  reveals two lines intersecting at a small angle, and this has been interpreted as being due to a change in the molecular structure of the gas.

The point can be investigated from another standpoint. If  $K$ ,  $\eta$  and  $C_v$  are the thermal conductivity, the viscosity and the specific heat at constant volume per gram of the gas at the same temperature, then it has been shown theoretically by Chapman and others that a relation exists between these quantities of the form

$$K = f\eta C_v,$$

where  $f$  is a constant independent of temperature and which depends on the force operative in molecular collision. The author has applied the results obtained for  $K$  together with what are considered to be the most accurate data available for  $\eta$  and  $C_v$  in order to calculate the corresponding values of  $f$ . The results are shown in Table V and an average value of  $f$  obtained from these is found to be 2.2.

#### COEFFICIENT OF ACCOMMODATION

Values of  $a$  calculated as indicated above are tabulated in Table IV and represented graphically in fig. 6 at various temperatures of the wire. The results are similar over the same temperature range to those obtained by Langmuir and Blodgett† for a tungsten filament in an atmosphere of

\* 'Proc. Roy. Soc.,' A, vol. 134, p. 613 (1932).

† 'Phys. Rev.,' vol. 40, p. 78 (1932).

TABLE V

Absolute temperature of wire $T_1$	$K \times 10^6$	$\eta \times 10^7$	$C_v$	$f$
601.9	708	1437	2.50	1.97
564.2	705	1369	2.49	2.07
520.2	692	1290	2.47	2.18
475.5	658	1211	2.46	2.21
418.9	602	1109	2.44	2.23
389.4	567	1057	2.43	2.21
368.0	542	1019	2.42	2.20
349.4	519	986	2.41	2.18
299.4	464	896	2.40	2.16

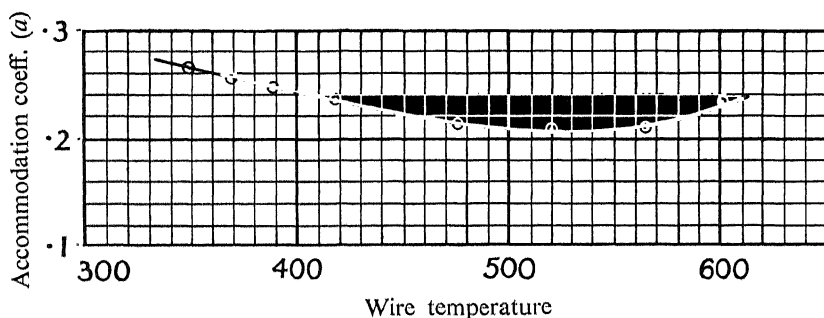


FIG. 6

hydrogen, and also by Mann\* in a recent investigation. In the latter instance it was shown that the magnitude of the coefficient of accommodation depends to a great extent on the actual condition of the surface of the wire at the time of the experiment.

Roberts,† using tungsten filaments surrounded by strongly rarefied helium, found the accommodation coefficient to change from 0.057, the value found for a newly flashed surface, to 0.19 after 24 hours' exposure to the gas.

These results suggest that the increase in the value of  $a$  is associated with the formation of adsorption films by molecules drawn from the surrounding gas, the upper surface of which would consist of a loosely bound configuration of molecules for which  $a$  would be correspondingly

\* 'Proc. Roy. Soc.,' A, vol. 146, p. 776 (1934).

† 'Proc. Roy. Soc.,' A, vol. 129, p. 146 (1930).

large. Such conclusions are in agreement with the investigations of Knudsen\* in relation to roughened and blackened surfaces.

During the course of the present series of observations it was found that below a certain pressure, and this again depends on the temperature, the time required for attainment of the steady state changed from a period of several minutes to one of many hours. The current strength required to maintain constancy of the wire temperature was found to decrease rapidly at first and after some hours remained fixed in value. Such changes in the current at constant temperature and constant pressure point to progressive changes in the condition of the surface film with time. Although the agreement between various observers does not lead to any definite conclusion on the subject, yet the results at various pressures lower than those considered by the author suggest a variation of  $a$  with pressure at constant temperature.

In comparing the results of Mann (*loc. cit.*) with those of the author, it is emphasized that the former vary from an extrapolated small value corresponding to a perfectly clean surface to the higher values associated with the surface when contaminated with adsorbed gas, and that these latter results are of the same order of magnitude as were obtained by the author relative to gases at much higher pressures and with regard to surfaces which had been exposed to the contaminating influence of the gas for some time before the observations were recorded.

The importance of an accurate investigation of the temperature variation of thermal conduction in gases is emphasized in special relation to measurements of the coefficient of accommodation and the associated examination of the gas-solid phase.

The recent development of such measurements for hydrogen by Langmuir and Blodgett† may be considered from the point of view of comparison between their method and that used by the author. In their investigation of the accommodation coefficient for the hydrogen-solid phase, a modified hot wire method was employed.

Langmuir, in common with other investigators of the accommodation constant  $a$ , has regarded a state of rarefaction to exist adjacent to the wire, and  $a$  is defined as being the ratio of the experimentally observed heat loss  $Q_e$  to the calculated loss  $Q$ .

$$\text{i.e.,} \quad a = Q_e/Q, \quad (12)$$

where  $Q$  is known in terms of the temperature drop  $T_1 - T'$ , the molecular conductivity  $\epsilon_k$  and the pressure  $P$  of the gas.

\* 'K. danske vidensk. Selsk. Skr.,' vol. 9, p. 1 (1930).

† 'Phys. Rev.,' vol. 40, p. 78 (1932).

$\alpha$  can be calculated from (12) since  $T'$  can be found from the relation

$$Q_o = \frac{2\pi l \int_{T_2}^{T'} K \cdot dT}{\log_{\frac{r_2}{r_i + \lambda}}},$$

where  $T_2$  is the temperature of the tube wall and  $K$  is known as a function of the temperature from the equation

$$K = A \cdot T^n,$$

$A$  and  $n$  being constants.

In Langmuir's experiments use was made of Eucken's\* data on the thermal conductivity of hydrogen between the temperature of liquid nitrogen and 100° C.

The excellence of the method lies in the fact that although the wire temperatures extended as high as 1600° K, the bath temperature being 92° K, in no case was the calculated value of  $T'$  greater than 226° K, corresponding to a temperature drop of 1374°. In this way it was sufficient to make use of data on thermal conduction only over a limited range of temperatures and at temperatures lower than 0° C. The author has calculated  $T'$  in Langmuir's experiments from data obtained at low temperatures in conjunction with Mr. Dock; the effect is to change the temperature drop from 1374° to 1356° and, when applied to a calculation of  $\alpha$ , gives a value which differs from that obtained by Langmuir by an amount of only 1%.

In Langmuir's experiments the variation of  $K$  with temperature was of secondary importance only in the calculation of  $\alpha$ , whereas in the author's experiments it is of primary importance.

#### SUMMARY

The paper describes a modification of the hot wire method of investigating thermal conduction in gases in which the influence of convection and the temperature drop effect are eliminated in one operation. The method is applied to hydrogen over a range of temperature up to about 300° C.

An electrically heated oil thermostat was used as a constant temperature bath, the temperature of the tube wall being determined by means of a platinum wire fused on to the wall. Allowance was made experimentally for the gradual heating of the tube wall by regulating the heating current in the thermostat.

\* 'Phys. Z.,' vol. 14, p. 324 (1913); vol. 12, p. 1101 (1911).



Corrections were applied for the loss of heat by radiation through the gas, and also for the temperature fall across the tube wall.

The values of the thermal conductivity of hydrogen, varying from  $0.000459 \text{ cal cm}^{-1} \text{ sec}^{-1} \text{ deg}^{-1}$  at  $295.1^\circ \text{ K}$  to  $0.000708$  at  $593.4^\circ \text{ K}$ , and of the accommodation coefficient for the hydrogen-platinum phase are given.

The variation of the thermal conductivity of hydrogen with temperature is expressed in the form

$$K_T = A \cdot T^n.$$

The accommodation coefficient is found to have a minimum value of  $0.21$  at  $520^\circ \text{ K}$  and to be independent of pressure over the range of pressures considered.

## Investigations on the Spectrum of Selenium V—Structure of Se II

By S. G. KRISHNAMURTY, M.A., and K. R. RAO, D.Sc., Andhra  
University, Waltair, India

(Communicated by M. N. Saha, F.R.S.—Received October 15, 1934)

[PLATES 2 AND 3]

### INTRODUCTION

Besides the very early work summarized in Kayser's 'Handbuch' the first considerable list of lines due to singly ionized selenium was given by L. and E. Bloch\* in 1930. These authors used an electrodeless discharge through selenium vapour and ascribed the lines to the several stages of ionization of the atom by inserting a variable auxiliary gap in series with the discharge tube. Lacroute† also investigated the spectrum from  $\lambda 2200$  to  $\lambda 1200$ . These measurements, however, were not sufficiently complete, and did not extend far enough into the extreme ultra-violet to enable an analysis of the spectrum of Se II to be undertaken, and up to the present there are no published records of any attempts at such an analysis.

\* 'C. R. Acad. Sci. Paris,' vol. 185, p. 761 (1927) ; vol. 187, p. 562 (1928) ; 'Ann. Physique,' vol. 13, p. 233 (1930).

† 'J. Phys. Radium,' vol. 9, p. 180 (1928).

The present paper, one of a series,\* deals with the essential features of the quartet and doublet systems found to be characteristic of the singly ionized atom of Se. More than 200 lines have been classified, comprising a majority of the important lines of the spectrum and several of the faint ones. There are, however, some definite groups of lines which are not accounted for by the set of identified terms; these groups lie chiefly in the extreme quartz and the fluorite regions and it would seem that they probably arise from double electron transitions and combinations with  $sp^4$  terms. When the analysis had been obtained, a very irregular feature was observed regarding the intensity of the fundamental resonance group  $4p\ ^4S-5s\ ^4P$ ; this is discussed in a later section.

### EXPERIMENTAL

The excitation of the spectrum Se II, chiefly in the visible and quartz regions, presents little difficulty. Even the ordinary spark in air produced by a small induction coil, with a suitable series self-inductance to suppress the air lines, is rich in the lines characteristic of Se II. The discharge through a rather wide capillary tube of about 1 to  $1\frac{1}{2}$  mm bore could be used with great advantage, as a slight adjustment of the series spark gap ensures the excitation of the lines attributable to Se II only. This latter source alone has been used for purposes of measurement on account of the comparative sharpness of the lines. The general experimental work was described fully in Part I. In addition to this, spectra have since been taken with a Fuess glass prism spectrograph and an extra dense glass prism in a Littrow mount. These have been used to record some of the fainter lines of the spectrum found necessary for the progress of the analysis.

### PREDICTED TERMS

Three families of predicted terms are set out in Table I, corresponding to the addition of an electron to the three different states ( $^3P$ ,  $^1D$ ,  $^1S$ ) of the Se III core. The first family consists of quartet and doublet terms based on  $^3P$  state and the other two families, of doublets alone. Of these many of the terms due to the  $4p$ ,  $5s$ ,  $4d$  configurations and their higher Rydberg members have been identified, as also those due to the inner transition  $sp^4$ .

\* K. R. Rao and others: I, Se IV and Se V, 'Proc. Roy. Soc.,' A, vol. 131, p. 154 (1931); II, Se III, *ibid.*, vol. 140, p. 387 (1933); III, Se III, *ibid.*, vol. 145, p. 681 (1934); IV, Se I and Se VII, *ibid.*, vol. 145, p. 694 (1934).

TABLE I—PREDICTED TERMS OF Se II

3 <sub>1</sub>	3 <sub>2</sub>	3 <sub>3</sub>	4 <sub>1</sub>	4 <sub>2</sub>	4 <sub>3</sub>	4 <sub>4</sub>	5 <sub>1</sub>	5 <sub>2</sub>	5 <sub>3</sub>	6 <sub>1</sub>	Term prefix	Terms						
											Limit <sup>3</sup> P			<sup>1</sup> D		<sup>1</sup> S		
2	6	10	2	3							4 <i>p</i>	<sup>4</sup> S			<sup>2</sup> D		<sup>2</sup> P	
2	6	10	2	2			1				5 <i>s</i>	<sup>4</sup> P	<sup>2</sup> P		<sup>2</sup> D		<sup>2</sup> S	
2	6	10	2	2	1						4 <i>d</i>	<sup>4</sup> F	<sup>4</sup> D	<sup>4</sup> P	<sup>2</sup> G	<sup>2</sup> F <sub><i>a</i></sub>	<sup>2</sup> D <sub><i>a</i></sub>	<sup>2</sup> D <sub><i>b</i></sub>
												<sup>2</sup> F	<sup>2</sup> D	<sup>2</sup> P	<sup>2</sup> P <sub><i>a</i></sub>	<sup>2</sup> S <sub><i>a</i></sub>		
2	6	10	2	2				1			5 <i>p</i>	<sup>4</sup> D	<sup>4</sup> P	<sup>4</sup> S	<sup>2</sup> F	<sup>2</sup> D <sub><i>a</i></sub>	<sup>2</sup> P <sub><i>b</i></sub>	
										1		<sup>2</sup> D	<sup>2</sup> P	<sup>2</sup> S	<sup>2</sup> P <sub><i>a</i></sub>			
2	6	10	2	2							6 <i>s</i>	<sup>4</sup> P	<sup>2</sup> P		<sup>2</sup> D		<sup>2</sup> S	
2	6	10	1	4							<i>sp</i> <sup>1</sup>	<sup>4</sup> P	<sup>2</sup> P		<sup>2</sup> D		<sup>2</sup> S	

## ANALYSIS\*

Since no Zeeman Effects or other such criteria are available for the absolute identification of the Se II lines, the classification of these into multiplets had to be based mainly on the general evidence furnished by recurring constant wave number differences, line intensities, and analogies with other spectra whose structures are theoretically the same as, or similar to, that of Se II, such as As I or O II and S II. From the theoretical terms set forth in Table I, it is to be expected that the most important of the lines attributable to Se II will result from the transition  $4p \rightarrow 5s$ . But as the terms  $^4P$  and  $^4D$  of the  $4p$  configuration are excluded by Pauli's principle, the only quartet due to the above transition is  $4p \ ^4S \rightarrow 5s \ ^4P$ . As this fundamental multiplet consists of only three lines, without including any recurring constant difference such as occurs in a many lined multiplet, and as the intervals between these lines are presumably large, it was difficult to obtain the first clue to the analysis. In the arc spectrum of arsenic, which is iso-electronic with Se II, this group of three lines is most outstanding and unmistakable, being self-reversed in a somewhat heavy current arc and appearing in absorption by a column of non-luminous vapour. A search for this group with an identical behaviour in the spectrum of Se II, however, led to what seemed for a long time an almost insuperable difficulty.

The following comparison indicates

$mp \ ^4S - \overline{m+1} \ s \ ^4P$				
	$\nu_1$		$\nu_2$	$\nu_2/\nu_1$
N I	83366	O II	185506	2.226
P I	56344	S II	110269	1.957
As I	52895	Se II	98676	1.866

\* A preliminary report appeared in 'Current Science,' vol. 2, p. 384 (1934).

clearly that in Se II this member should occur in the region  $\lambda$  1000. Photographs of the discharge tube containing selenium have consistently revealed the existence of only two lines, which are very prominent and attributable to Se II, at  $\lambda$  1033 and  $\lambda$  1049, with  $\delta\nu = 1483$ . These appeared even under a very weak stimulus in uncondensed discharges. If these two were taken as part of the group  $4S-4P$ , the absence of the third line seemed inexplicable. Another possible choice was the group of three strong lines at  $\lambda\lambda$  1119, 1099, and 1080, which exhibited identical behaviour under all conditions, but they could not be so easily excited as the former two lines and therefore belong more probably to Se III than to Se II. The assignment of these to the spectrum Se III by one of the writers (Part III) has definitely excluded this possibility. Further light was thrown on the data by the very high dispersion spectrograms of the vacuum spark spectrum of selenium taken under varying intensities of excitation. The line  $\lambda$  1049 was found to be a very close doublet, the components being equally intense; this led to the suspicion that the group  $4p\ 4S-5s\ 4P$  might show an anomaly in the magnitude and ratio of the intervals. But even with this assumption the group of levels

TABLE II—MULTIPLETS IN Se II

$4p$	$4S_{1\frac{1}{2}}$ 174904	$2D_{1\frac{1}{2}}$ 13169 161825	$2D_{2\frac{1}{2}}$ 616 161209	$2P_{\frac{1}{2}}$ 9252 151957	$2P_{3\frac{1}{2}}$ 858 151090
$5s\ 4P_{\frac{1}{2}}$ = 79724.3	95270 (10)	82102 (2)			71372 (1)
$4P_{1\frac{1}{2}}$ = 78240.7 <i>1483.6</i>	96753 (10)	83586 (0)	82068 (4)		72855 (2)
$4P_{2\frac{1}{2}}$ = 76320.0 <i>1920.7</i>	98676 (4)		84880 (4)		
$2P_{\frac{1}{2}}$ = 76098.0	98894 (1)	85720 (9)		75859 (7)	75001 (2)
$2P_{1\frac{1}{2}}$ = 73638.3 <i>2459.7</i>	101358 (1)	88184 (2)	87568 (9)	78318 (5)	77463 (8)
$2D_{1\frac{1}{2}}$ = 66544.4	—	95283 (10)	—	85411 (3)	84556 (5)
$2D_{2\frac{1}{2}}$ = 66638.3 <i>-93.9</i>	108349 (1)	95189 (5)	94574 (6)		84462 (6)
$sp^4\ 4P_{\frac{1}{2}}$ = 88556.7	86485 (6)			63404 (1)	
$4P_{1\frac{1}{2}}$ = 89414.8 <i>-853.1</i>	85578 (8)				
$4P_{2\frac{1}{2}}$ = 91117.6 <i>1702.8</i>	89875 (9)		70089 (2)		59981 (1)
$2P_{1\frac{1}{2}}$ = 74699.1		—	86507 (9)	77259 (3)	76402 (8)
$6s\ 4P_{\frac{1}{2}}$ = 40951.0	134043 (1)				
$\alpha$ = 71707.4			—	80254 (6)	79391 (3)
$\beta$ = 70120.2		91704 (0)	—	81833 (2)	80978 (8)
$\gamma$ = 69019.9	105982 (1)	92806 (1)		82933 (5)	
$\delta$ = 66160.4	108836 (1)	95666 (4)	95051 (3)		
$\epsilon$ = 53260		108565 (3)	107950 (1)	98697 (4)	97839 (3)

TABLE II—MULTIPLETS

$5p$	$4D_{\frac{1}{2}}$	$4D_{\frac{3}{2}}$	$4D_{\frac{5}{2}}$	$4D_{\frac{7}{2}}$	$4P_{\frac{1}{2}}$	$4P_{\frac{3}{2}}$	$4P_{\frac{5}{2}}$
	60695.0	412.5 60282.5	1356.6 58925.9	1729.9 57196.0	61945.3	3727.6 58217.7	1621.6 56596.1
$5s\ 4P_{\frac{1}{2}}$ = 79724.3 <i>1483.6</i>	19029.3 (8)	10441.9 (9)			17779.0 (10)	21506.6 (9)	
$4P_{\frac{1}{2}}$ = 78240.7 <i>1920.7</i>	17545.7 (6)	17958.4 (9)	10314.9 (10)		10205.6 (4)	20023.2 (8)	21644.6 (5)
$4P_{\frac{3}{2}}$ = 76320.0		16037.3 (2)	17304.3 (7)	10124.4 (10)		18103.0 (9)	19723.8 (10)
$2P_{\frac{1}{2}}$ = 76098.0 <i>2459.7</i>	15402.6 (5)	—			—	17880.5 (8)	
$2P_{\frac{3}{2}}$ = 73638.3	—	—	—			15421.4 (4)	17042.2 (6)
$2D_{\frac{1}{2}}$ = 66544.4 <i>— 93.9</i>							
$2D_{\frac{3}{2}}$ = 66638.3							
$6s\ 4P_{\frac{1}{2}}$ = 40951.0 <i>1592.1</i>	19744.1	19331.3 (3)			20994.4 (3)	17266.6 (3)	
$4P_{\frac{1}{2}}$ = 39858.9 <i>2033.9</i>	21336.4 (1)	20424.0 (2)	19567.3 (4)		22587.3 (2)	18859.2 (1)	17237.8 (2)
$4P_{\frac{3}{2}}$ = 37325.0		22917.1 (00)	21601.0 (0)	19870.6 (4)		20892.4 (1)	19271.2 (3)
$sp\ 4P_{\frac{1}{2}}$ = 88556.7 <i>— 358.1</i>	27861.5 (0)	28273.8 (1)			26611.5 (1)	—	
$4P_{\frac{1}{2}}$ = 89414.8 <i>— 1702.8</i>	28719.5 (0)	29132.2 (2)	30488.7 (3)		27469.3 (2)	31196.5 (4)	32819.3 (4)
$4P_{\frac{3}{2}}$ = 91117.6		30834.6 (2)	32191.1 (3)	33922.2 (4)		32899.9 (6)	34522.1 (5)
$2P_{\frac{1}{2}}$ = 74699.1	—	—	15773.3 (1)			16481.4 (2)	
$4d\ 4F_{\frac{1}{2}}$ = 82830.6 <i>2919.1</i>	22136.2 (5)	22548.1 (2)	23904.1 (0)				
$4F_{\frac{1}{2}}$ = 79911.2 <i>2019.8</i>		19628.5 (8)	20985.5 (8)	—			
$4F_{\frac{3}{2}}$ = 77891.4 <i>1079.5</i>			18966.1 (9)	20694.8 (3)			
$4F_{\frac{5}{2}}$ = 76811.9				19615.9 (10)			
$5d\ 4F_{\frac{1}{2}}$ = 36468.6 <i>397.4</i>	24226.4 (8)	23813.7 (3)	—		25476.8 (0)	21749.2 (00)	
$4F_{\frac{1}{2}}$ = 36071.2 <i>1088.7</i>		24211.3 (9)	22854.7 (4)	21124.8 (0)		22146.6 (0)	
$4F_{\frac{3}{2}}$ = 34982.5 <i>1697.6</i>			23943.4 (10)	22213.2 (2)			21613.8 (1)
$4F_{\frac{5}{2}}$ = 33284.9				23911.1 (10)			
$4D_{\frac{1}{2}}$ = 36628.3 <i>2580.1</i>	24066.8 (5)	23654.1 (2)	22297.8 (1)		25316.9 (3)	21589.6 (1)	—
$4D_{\frac{3}{2}}$ = 34048.2 <i>1182.9</i>		—	24877.7 (5)	23147.5 (1)		24169.5 (7)	22548.1 (2)
$4D_{\frac{5}{2}}$ = 32865.3			26059.6 (3)	24331.0 (9)			23731.6 (8)
$4P_{\frac{1}{2}}$ = 34054.1 <i>2401.5</i>	—	26228.1 (1)	24871.8 (2)		27891.4 (1)	24163.5 (5)	22541.9 (2)
$4P_{\frac{3}{2}}$ = 31652.6			—	25543.3 (2)		26565.3 (3)	24943.6 (9)
$\alpha$ = 71707.4							
$\beta$ = 70120.2							
$\gamma$ = 69019.9							
$\delta$ = 66160.4							

## IN Se II—(continued)

$4S_{1\frac{1}{2}}$	$2D_{1\frac{1}{2}}$	$2D_{2\frac{1}{2}}$	$2P_{\frac{1}{2}}$	$a$	$b$	$c$	$d$
55685.5	57254.7	$2647.6$ 54607.1	53611.9	53720.7	50104.1	47072.8	43828.8
24038.4 (1)	22469.8 (5)						
22555.1 (5)	20985.5 (8)	23633.6 (2)					34412.6 (3)
20634.6 (10)	—	21712.6 (7)					
20412.8 (1)	18843.8 (10)		22486.0 (6)	22376.9 (10)	25993.8 (2)	29024.9 (4)	
—	16384.0 (5)	19031.3 (9)	20026.1 (4)	19917.3 (3)	23533.7 (7)	26565.3 (3)	29809.5 (2)
						19471.5 (7)	22715.6 (9)
						19565.5 (6)	22809.5 (10)
16326.3 (3)							
18360.5 (4)		? 17282.3 (2)					
32871.7 (6)							
33729.8 (6)	32160.0 (2)	34808.0 (2)					
35432.0 (5)		36510.2 (2)					
	17444.6 (2)	20092.0 (9)	21087.0 (10)	20978.3 (3)		27626.2 (3)	30870.1 (2)
	20785.9 (1)	18138.7 (0)	17143.6 (0)				
	21183.6 (0)						
	20626.0 (0)	17978.9 (1)	16984.0 (2)				
21637.5 (1)							
21631.6 (1)							
24033.0 (4)		22954.7 (2)	21959.1 (0)				
16022.0 (00)						24634.4 (2)	
		15512.6 (9)	16508.3 (9)	16399.7 (3)		23047.6 (1)	
			15408.0 (4)				
						19087.6 (2)	22331.6 (1)

$5p\ ^4D$ ,  $^4P$ ,  $^4S$ , which should strongly combine with  $5s\ ^4P$ , could not be identified. It remained, however, very definite that the difference  $\delta\nu = 1483\text{ cm}^{-1}$  must be characteristic of Se II, as there have been found as many as six or eight pairs having this interval and involving some of the strongest of the Se II lines in the visible region. In addition to this, two more intervals, 616 and 858, have been found to be characteristic of Se II; these latter occur among the lines in the Lyman region. The correlation of these data, however, remained a difficulty till, at the suggestion of one of the writers (S. G. K.), it was recognized that the difference  $\delta\nu = 1483$  corresponds to  $5s\ (^4P_{\frac{1}{2}} - ^4P_{\frac{3}{2}})$  and the usually strongest line  $4p\ ^4S_{\frac{1}{2}} - 5s\ ^4P_{\frac{3}{2}}$  must have been faint and lying among the faint lines in the region. With this clue the important interval  $1920\cdot7$  was then discovered and the building up of the multiplet scheme represented in Table II proceeded very rapidly. As originally surmized the differences 616 and 858 proved to be those of  $4p\ ^2D$  and  $4p\ ^2P$ ; this identification is well established by the existence of many intercombination lines with the appropriate intensities and also by Table III of the intervals of these metastable states in the known spectra of the same outer electronic constitution.

TABLE III—INTERVALS OF METASTABLE DOUBLET TERMS

Spectrum	$mp\ (^2D_{\frac{1}{2}} - ^2D_{\frac{3}{2}})$	$mp\ (^2P_{\frac{1}{2}} - ^2P_{\frac{3}{2}})$
N I .....	unresolved	unresolved
O II .....	28·8	4·5
F III .....	31	—
P I .....	15·5	25·5
S II .....	31·5	48·6
Cl III .....	62	98
As I .....	322·3	461·2
Se II .....	615	855

In P I and As I-like spectra the intervals are approximately doubled with increasing ionization.

The configuration next to the deepest is that designated as “ $5s$ ” giving  $^4P$  and  $^2P$ ,  $^2D$ , and  $^2S$ . These are found to be exactly analogous to those of other similar spectra. The intervals,

$$5s\ ^4P_{\frac{1}{2}} - 5s\ ^4P_{\frac{3}{2}} = 3404\cdot4$$

$$6s\ ^4P_{\frac{1}{2}} - 6s\ ^4P_{\frac{3}{2}} = 3626\cdot0$$

are definitely tending towards their limiting value 3937 of  $4p\ ^3P_0 - ^3P_2$  of Se III. Further, the ratio between  $5s\ (^4P_{\frac{1}{2}} - ^4P_{\frac{3}{2}})$  and  $5s\ (^2P_{\frac{1}{2}} - ^2P_{\frac{3}{2}})$

which is  $3404.4/2459.9$  or  $3:2.01$  is very nearly equal to the theoretical ratio  $3:2$  and hence confirms the following scheme of limits:—

$5s\ ^4P_{2\frac{1}{2}},\ ^2P_{1\frac{1}{2}}$ of Se II	$4p\ ^3P_2$ of Se III
$^4P_{1\frac{1}{2}},\ ^2P_{\frac{1}{2}}$ of Se II	$^3P_1$ of Se III
$^4P_{\frac{1}{2}}$ of Se II	$^3P_0$ of Se III

The small but inverted interval of the  $5s\ ^2D$  term is a characteristically common feature of all the spectra of this type hitherto known.

In contrast to the above set of terms, those due to the higher lying configurations such as  $5p$ , or  $4d$ , do not show any marked similarities with the corresponding terms of the analogous spectra. Of these many of the doublets have not yet been identified in Se II. Among the quartets described in this paper the most abnormal feature so far observed is the very large interval  $5p\ (^4P_{\frac{1}{2}}—^4P_{1\frac{1}{2}})$  which, in fact, even makes the component  $5p\ ^4P_{\frac{1}{2}}$  to be the deepest of all the  $5p$  energy states. Interchanging  $5p\ ^4P_{\frac{1}{2}}$  and  $5p\ ^4D_{\frac{1}{2}}$  would reduce this abnormality to a certain extent and also improve the interval ratio between the components of the  $5p\ ^4D$  term, but the change would disturb the identification of the terms  $5d\ ^4F$  and  $4d\ ^4F$ , which have been based on a very careful scrutiny of the nature and behaviour of the lines rather than on a mere equality of wave number differences. Hence the present assignment. The identification of  $sp^4\ ^4P$  is also considered to be quite certain from the prominence of the group  $4p\ ^4S—sp^4\ ^4P$  and the other combinations it gives with the  $5p$  terms. The designations of  $4d\ ^4D$  and  $4d\ ^4P$ , which are but partially identified, must be considered as only provisional. A few other terms whose denomination cannot yet be decided are denoted by the symbols  $a$ ,  $b$ ,  $c$ , etc., and  $\alpha$ ,  $\beta$ , etc., according as they are supposed even or odd. A full consideration of these and other doublet terms depending on the  $^1D$  and  $^1S$  states of the Se III core will be made in a succeeding part of these investigations.

#### INTENSITIES

The intensities of some of the lines show marked irregularities. Thus in the doublet  $4p\ ^2P—5s\ ^2D$  the component  $^2P_{\frac{1}{2}}—^2D_{1\frac{1}{2}}$  is very much weaker than  $^2P_{1\frac{1}{2}}—^2D_{1\frac{1}{2}}$  which is nearly as intense as  $^2P_{1\frac{1}{2}}—^2D_{2\frac{1}{2}}$ . This feature is markedly noticeable also in the spectrum of As I. The outstanding anomaly in intensity occurs in the fundamental member  $4p\ ^4S—5s\ ^4P$ . In a quartet group like this, in which one of the terms is single, the intensities are proportional, according to Burger and Dorgelo, to the statistical weights of the components of the multiple term, *i.e.*,



in the ratio 2:4:6. Actually the intensities have been found to be in the ratio 10:10:4, the component  $^4S_{11}$ — $^4P_{21}$ , which ought to be the strongest of the group being very faint. The experimental intensities mentioned above are visual estimates, no quantitative measurements being practicable in the region  $\lambda$  1000 at the present stage of development of the technique of intensity measurement. The multiplet itself is shown in fig. 2, Plate 3. In spite of this qualitative estimate, it is believed that the relative order of the intensities of the lines is correct, and that the anomaly is genuine, since it is difficult to ascribe it to variations in the sensitivity of the plate or any other such causes leading to spurious intensities of spectral lines.

Anomalies in the intensities of spectral lines are often encountered and sometimes found to be due to the electrical condition of the emitting source. For example, the anomalous intensities of some doublets in the spectrum of O II are said to be produced probably as a result of successive electron impact occurring in heavy current discharges such as a hollow cathode or the positive column,\* and the enhancement of certain lines of the Lyman series of hydrogen† has been accounted for as arising from simultaneous transfer to the neutral atom of one kind of the energy of *ionization and excitation* of the excited atom of another kind. In many instances like the above the so-called anomaly in intensity has thus been observed to be dependent upon the nature and condition of the emitting source. In Se II the dependence of the intensity of the lines on the nature of the source was not specially investigated so as to warrant any definite conclusions, but it may be stated that the anomaly described above was observed under all the conditions in which the spectrum was photographed. These sources of the spectrum were (a) high potential sparks in vacuum, with the secondary voltages varying between 20 to 50 kV, and with varying amounts of additional inductance (a maximum of 0.05 m.h.) in series with the spark; (b) the positive column in an ordinary discharge through selenium vapour, described in Part I, with varying amounts of capacity and inductance in the secondary circuit. It is therefore presumed that the cause of the intensity anomaly does not lie in the condition of the emitting source.

According to quantum mechanics, mutual interactions occur between adjacent spectral terms of the same J value arising from similar electron configurations. These interactions have a perturbing influence both on the magnitude of the series terms and on the intensities of the resulting

\* Emeleus, 'Proc. Nat. Acad. Sci., Wash.,' vol. 20, p. 115 (1934).

† K. R. Rao and Badami, 'Proc. Roy. Soc.,' A, vol. 138, p. 540 (1932).

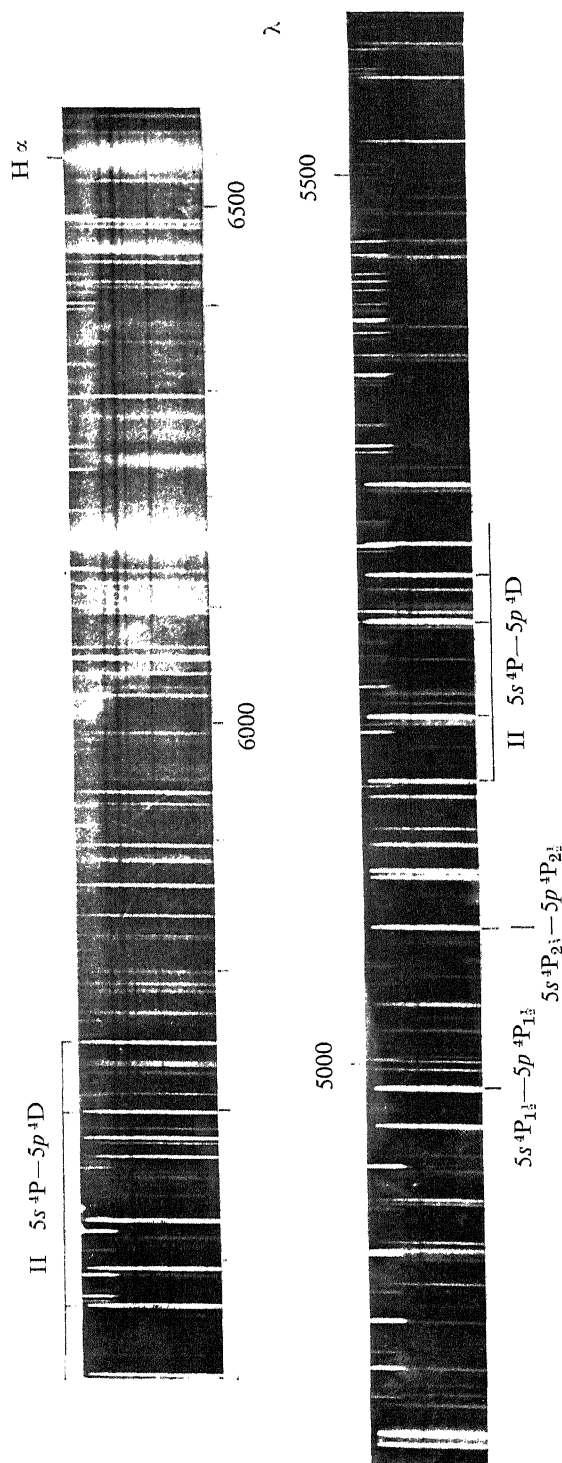


FIG. 1—Discharge tube spectrum of selenium

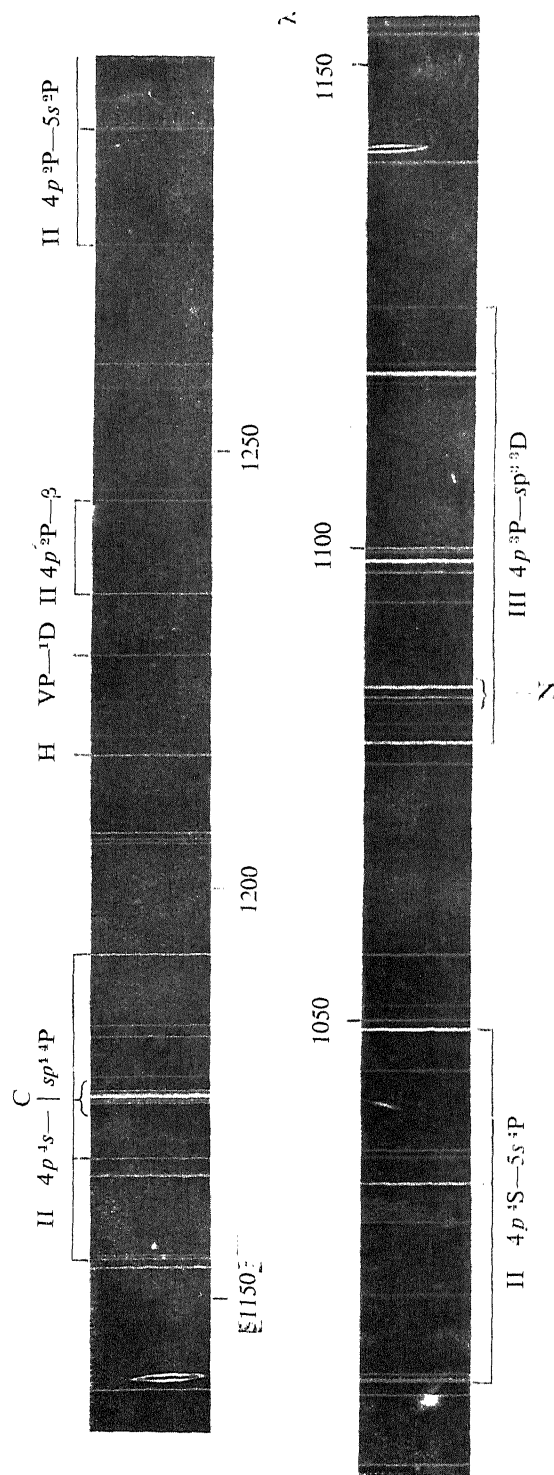


FIG. 2—Vacuum spark spectrum of selenium with inductance

lines, thus giving rise to a violation of the ordinary interval and intensity rules in multiplets. It is considered that the intensity anomaly under consideration arises from such an interaction of spectral terms. If so, the term  $5s^2P_{2\frac{1}{2}}$  must have been perturbed by the terms  $sp^44P_{2\frac{1}{2}}$ ,  $4d^4F_{2\frac{1}{2}}$ ,  $4D_{2\frac{1}{2}}$  or other terms of the same kind in its vicinity having the same  $J$  value. It is not possible to determine this conclusively until a complete and exhaustive term analysis of the spectrum is obtained and the parent electron configurations of all the perturbing terms are known. We hope to describe this in a later communication in which also a complete catalogue of the lines ascribed to Se II will be included. Table IV contains a list only of the lines of Se II which have so far been classified.

TABLE IV—LIST OF CLASSIFIED LINES IN Se II

$\lambda$ I.A. (int.)	$\nu$ (vac.)	Classification	$\lambda$ I.A. (int.)	$\nu$ (vac.)	Classification.
6490.60 (5)	15402.6	$5s^2P_{\frac{1}{2}}-5p^4D_{\frac{1}{2}}$	5300.99 (1)	18859.2	$5p^4P_{1\frac{1}{2}}-6s^4P_{1\frac{1}{2}}$
6488.34 (4)	15408.0	$5p^2P_{\frac{1}{2}}-\gamma$	5271.11 (9)	18966.1	$4d^4F_{3\frac{1}{2}}-5p^4D_{2\frac{1}{2}}$
6482.70 (4)	15421.4	$5s^2P_{1\frac{1}{2}}-5p^4P_{1\frac{1}{2}}$	5253.60 (8)	19029.3	$5s^4P_{\frac{1}{2}}-5p^4D_{\frac{1}{2}}$
6444.60 (6)	15512.6	$5p^2D_{2\frac{1}{2}}-\beta$	5253.05 (9)	19031.3	$5s^2P_{1\frac{1}{2}}-5p^2D_{2\frac{1}{2}}$
6338.14 (1)	15773.3	$sp^42P_{1\frac{1}{2}}-5p^4D_{2\frac{1}{2}}$	5237.56 (2)	19087.6	$c-8$
6239.70 (00)	16022.0	$5p^4S_{1\frac{1}{2}}-\alpha$	5227.48 (10)	19124.4	$5s^4P_{2\frac{1}{2}}-5p^4D_{3\frac{1}{2}}$
6233.73 (2)	16037.3	$5s^4P_{2\frac{1}{2}}-5p^4D_{1\frac{1}{2}}$	5187.66 (3)	19271.2	$5p^4P_{2\frac{1}{2}}-6s^4P_{2\frac{1}{2}}$
6134.94 (4)	16295.6	$4P_{1\frac{1}{2}}-4P_{\frac{1}{2}}$	5175.90 (10)	19314.9	$5s^4P_{1\frac{1}{2}}-5p^4D_{2\frac{1}{2}}$
6123.41 (3)	16326.3	$5p^4S_{1\frac{1}{2}}-6s^4P_{1\frac{1}{2}}$	5171.51 (3)	19331.3	$5p^4D_{1\frac{1}{2}}-6s^4P_{\frac{1}{2}}$
6101.82 (5)	16384.0	$5s^2P_{1\frac{1}{2}}-5p^2D_{1\frac{1}{2}}$	5142.10 (9)	19441.9	$5s^4P_{\frac{1}{2}}-5p^4D_{1\frac{1}{2}}$
6095.99 (3)	16399.7	$a-\beta$	5134.28 (7)	19471.5	$5s^2D_{1\frac{1}{2}}-c$
6065.77 (2)	16481.4	$sp^42P_{1\frac{1}{2}}-5p^4P_{1\frac{1}{2}}$	5109.61 (6)	19565.5	$5s^2D_{2\frac{1}{2}}-c$
6055.87 (9)	16508.3	$5p^2P_{\frac{1}{2}}-\beta$	5109.15 (4)	19567.3	$5p^4D_{2\frac{1}{2}}-6s^4P_{1\frac{1}{2}}$
5886.26 (2)	16984.0	$5p^2P_{\frac{1}{2}}-5d^4D_{1\frac{1}{2}}$	5096.50 (10)	19615.9	$4d^4F_{4\frac{1}{2}}-5p^4D_{3\frac{1}{2}}$
5866.16 (6)	17042.2	$5s^2P_{1\frac{1}{2}}-5p^4P_{2\frac{1}{2}}$	5093.22 (8)	19628.5	$4d^4F_{2\frac{1}{2}}-5p^4D_{1\frac{1}{2}}$
5831.47 (0)	17143.6	$5p^2P_{\frac{1}{2}}-5d^4F_{1\frac{1}{2}}$	5068.61 (10)	19723.8	$5s^4P_{2\frac{1}{2}}-5p^4P_{2\frac{1}{2}}$
5799.60 (2)	17237.8	$5p^4P_{2\frac{1}{2}}-6s^4P_{1\frac{1}{2}}$	5063.39 (1)	19744.1	$5p^4D_{\frac{1}{2}}-6s^4P_{\frac{1}{2}}$
5789.94 (3)	17266.6	$5p^4P_{1\frac{1}{2}}-6s^4P_{\frac{1}{2}}$	5031.15 (4)	19870.6	$5p^4D_{3\frac{1}{2}}-6s^4P_{2\frac{1}{2}}$
*5784.68 (2)	17282.3	$5p^2D_{2\frac{1}{2}}-6s^4P_{2\frac{1}{2}}$	5019.36 (3)	19917.3	$5s^2P_{1\frac{1}{2}}-a$
5747.43 (7)	17394.3	$5s^4P_{2\frac{1}{2}}-5p^4D_{2\frac{1}{2}}$	4992.83 (8)	20023.2	$5s^4P_{1\frac{1}{2}}-5p^4P_{1\frac{1}{2}}$
5730.84 (2)	17444.6	$sp^42P_{1\frac{1}{2}}-5p^2D_{1\frac{1}{2}}$	4992.10 (4)	20026.1	$5s^2P_{1\frac{1}{2}}-5p^2P_{\frac{1}{2}}$
5697.81 (6)	17545.7	$5s^4P_{1\frac{1}{2}}-5p^4D_{\frac{1}{2}}$	4975.72 (9)	20092.0	$sp^42P_{1\frac{1}{2}}-5p^2D_{2\frac{1}{2}}$
5623.07 (10)	17779.0	$5s^4P_{\frac{1}{2}}-5p^4P_{\frac{1}{2}}$	4897.53 (1)	20412.8	$5s^2P_{1\frac{1}{2}}-5p^4S_{1\frac{1}{2}}$
5591.13 (8)	17880.5	$5s^2P_{\frac{1}{2}}-5p^4P_{1\frac{1}{2}}$	4846.90 (0)	20626.0	$5p^2D_{1\frac{1}{2}}-5d^4D_{1\frac{1}{2}}$
5566.87 (9)	17958.4	$5s^4P_{1\frac{1}{2}}-5p^4D_{1\frac{1}{2}}$	4844.88 (10)	20634.6	$5s^4P_{2\frac{1}{2}}-5p^4S_{1\frac{1}{2}}$
5560.54 (1)	17978.9	$5p^2D_{2\frac{1}{2}}-5d^4D_{1\frac{1}{2}}$	4830.78 (3)	20694.8	$4d^4F_{3\frac{1}{2}}-5p^4D_{3\frac{1}{2}}$
5522.42 (9)	18103.0	$5s^4P_{2\frac{1}{2}}-5p^4P_{1\frac{1}{2}}$	4809.61 (1)	20785.9	$5p^2D_{1\frac{1}{2}}-5d^4F_{1\frac{1}{2}}$
5511.56 (0)	18138.7	$5p^2D_{2\frac{1}{2}}-5d^4F_{1\frac{1}{2}}$	4785.10 (1)	20892.4	$5p^4P_{1\frac{1}{2}}-6s^4P_{2\frac{1}{2}}$
5444.97 (4)	18360.5	$5p^4S_{1\frac{1}{2}}-6s^4P_{2\frac{1}{2}}$	4777.88 (2)	20924.0	$5p^4D_{1\frac{1}{2}}-6s^4P_{1\frac{1}{2}}$
5305.31 (10)	18843.8	$5s^2P_{\frac{1}{2}}-5p^2D_{1\frac{1}{2}}$	4765.51 (3)	20978.3	$sp^42P_{1\frac{1}{2}}-a$

\* Doubtful; classified as Se III line, cf. Part III.

TABLE IV—(continued)

$\lambda$ I.A. (int.)	$\nu$ (vac.)	Classification	$\lambda$ I.A. (int.)	$\nu$ (vac.)	Classification
4763.87 (8)	20985.5	$\left\{ \begin{array}{l} 4d^4 F_{2\frac{1}{2}} - 5p^4 D_{2\frac{1}{2}} \\ 5s^4 P_{1\frac{1}{2}} - 5p^2 D_{1\frac{1}{2}} \end{array} \right.$	4159.77 (4)	24033.0	$5p^4 S_{1\frac{1}{2}} - 5d^4 P_{2\frac{1}{2}}$
4761.85 (3)	20994.4	$5p^4 P_{\frac{1}{2}} - 6s^4 P_{\frac{1}{2}}$	4158.84 (1)	24038.4	$5s^4 P_{\frac{1}{2}} - 5p^4 S_{1\frac{1}{2}}$
4740.94 (10)	21087.0	$sp^4 {}^2P_{1\frac{1}{2}} - 5p^2 P_{\frac{1}{2}}$	4153.93 (5)	24066.8	$5p^4 D_{1\frac{1}{2}} - 5d^4 D_{1\frac{1}{2}}$
4732.46 (0)	21124.8	$5p^4 D_{3\frac{1}{2}} - 5d^4 F_{2\frac{1}{2}}$	4137.31 (5)	24163.5	$5p^4 P_{1\frac{1}{2}} - 5d^4 P_{1\frac{1}{2}}$
4719.32 (0)	21183.6	$5p^4 D_{1\frac{1}{2}} - 5d^4 F_{2\frac{1}{2}}$	4136.28 (7)	24169.5	$5p^4 P_{1\frac{1}{2}} - 5d^4 D_{2\frac{1}{2}}$
4685.53 (1)	21336.4	$5p^4 D_{3\frac{1}{2}} - 6s^4 P_{1\frac{1}{2}}$	4129.15 (9)	24211.3	$5p^4 D_{1\frac{1}{2}} - 5d^4 F_{2\frac{1}{2}}$
4648.44 (9)	21506.6	$5s^4 P_{\frac{1}{2}} - 5p^4 P_{1\frac{1}{2}}$	4126.57 (8)	24226.4	$5p^4 D_{1\frac{1}{2}} - 5d^4 F_{1\frac{1}{2}}$
4630.56 (1)	21589.6	$5p^4 P_{1\frac{1}{2}} - 5d^4 D_{1\frac{1}{2}}$	4108.82 (9)	24331.0	$5p^4 D_{3\frac{1}{2}} - 5d^4 D_{3\frac{1}{2}}$
4628.12 (0)	21601.0	$5p^4 D_{2\frac{1}{2}} - 6s^4 P_{2\frac{1}{2}}$	4058.23 (2)	24634.4	$c - \alpha$
4625.37 (1)	21613.8	$5p^4 P_{2\frac{1}{2}} - 5d^4 F_{3\frac{1}{2}}$	4019.48 (2)	24871.8	$5p^4 D_{2\frac{1}{2}} - 5d^4 P_{1\frac{1}{2}}$
4621.58 (1)	21631.6	$5p^4 S_{1\frac{1}{2}} - 5d^4 P_{1\frac{1}{2}}$	4018.53 (5)	24877.7	$5p^4 D_{2\frac{1}{2}} - 5d^4 D_{2\frac{1}{2}}$
4620.32 (1)	21637.5	$5p^4 S_{1\frac{1}{2}} - 5d^4 D_{2\frac{1}{2}}$	4007.91 (9)	24943.6	$5p^4 P_{2\frac{1}{2}} - 5d^4 P_{2\frac{1}{2}}$
4618.80 (5)	21644.6	$5s^4 P_{1\frac{1}{2}} - 5p^4 P_{2\frac{1}{2}}$	3948.81 (3)	25316.9	$5p^4 P_{1\frac{1}{2}} - 5d^4 D_{1\frac{1}{2}}$
4604.33 (7)	21712.6	$5s^4 P_{2\frac{1}{2}} - 5p^2 D_{2\frac{1}{2}}$	3924.04 (0)	25476.8	$5p^4 P_{1\frac{1}{2}} - 5d^4 F_{1\frac{1}{2}}$
4596.59 (00)	21749.2	$5p^4 P_{1\frac{1}{2}} - 5d^4 F_{1\frac{1}{2}}$	3913.81 (2)	25543.3	$5p^4 D_{3\frac{1}{2}} - 5d^4 P_{2\frac{1}{2}}$
4552.64 (0)	21959.1	$5p^4 P_{\frac{1}{2}} - 5d^4 P_{2\frac{1}{2}}$	3845.98 (2)	25993.8	$5s^2 P_{\frac{1}{2}} - b$
4516.22 (5)	22136.2	$4d^4 F_{1\frac{1}{2}} - 5p^4 D_{1\frac{1}{2}}$	3836.27 (3)	26059.6	$5p^4 D_{2\frac{1}{2}} - 5d^4 D_{3\frac{1}{2}}$
4514.11 (0)	22146.6	$5p^4 P_{1\frac{1}{2}} - 5d^4 F_{2\frac{1}{2}}$	3811.62 (1)	26228.1	$5p^4 D_{1\frac{1}{2}} - 5d^4 P_{1\frac{1}{2}}$
4500.57 (2)	22213.2	$5p^4 D_{3\frac{1}{2}} - 5d^4 F_{3\frac{1}{2}}$	3763.25 (3)	26565.3	$\left\{ \begin{array}{l} 5s^2 P_{1\frac{1}{2}} - c \\ 5p^4 P_{1\frac{1}{2}} - 5d^4 P_{2\frac{1}{2}} \end{array} \right.$
4483.48 (1)	22297.8	$5p^4 D_{2\frac{1}{2}} - 5d^4 D_{1\frac{1}{2}}$	3756.71 (1)	26611.5	$sp^4 {}^4P_{\frac{1}{2}} - 5p^4 P_{\frac{1}{2}}$
4476.70 (1)	22331.6	$d - \delta$	3639.40 (2)	27469.3	$sp^4 {}^4P_{1\frac{1}{2}} - 5p^4 P_{\frac{1}{2}}$
4467.64 (10)	22376.9	$5s^2 P_{\frac{1}{2}} - a$	3618.72 (3)	27626.2	$sp^4 {}^2P_{1\frac{1}{2}} - c$
4449.17 (5)	22469.8	$5s^4 P_{\frac{1}{2}} - 5p^2 D_{1\frac{1}{2}}$	3588.16 (0)	27861.5	$sp^4 {}^4P_{\frac{1}{2}} - 5p^4 D_{1\frac{1}{2}}$
4445.97 (6)	22486.0	$5s^4 P_{\frac{1}{2}} - 5p^2 P_{\frac{1}{2}}$	3584.32 (1)	27891.4	$5p^4 P_{1\frac{1}{2}} - 5d^4 P_{1\frac{1}{2}}$
4434.94 (2)	22541.9	$5s^4 P_{2\frac{1}{2}} - 5d^4 P_{1\frac{1}{2}}$	3535.84 (1)	28273.8	$sp^4 {}^4P_{\frac{1}{2}} - 5p^4 D_{1\frac{1}{2}}$
4433.73 (2)	22548.1	$\left\{ \begin{array}{l} 4d^4 F_{1\frac{1}{2}} - 5p^4 D_{1\frac{1}{2}} \\ 5p^4 P_{2\frac{1}{2}} - 5d^4 D_{2\frac{1}{2}} \end{array} \right.$	3480.96 (0)	28719.5	$sp^4 {}^4P_{1\frac{1}{2}} - 5p^4 D_{1\frac{1}{2}}$
4432.35 (5)	22555.1	$5s^4 P_{1\frac{1}{2}} - 5p^4 S_{1\frac{1}{2}}$	3444.27 (4)	29024.9	$5s^2 P_{1\frac{1}{2}} - c$
4426.02 (2)	22587.3	$5p^4 P_{\frac{1}{2}} - 6s^4 P_{1\frac{1}{2}}$	3431.65 (2)	29132.2	$sp^4 {}^4P_{1\frac{1}{2}} - 5p^4 D_{1\frac{1}{2}}$
4401.02 (9)	22715.6	$5s^2 D_{1\frac{1}{2}} - d$	3353.68 (2)	29809.5	$5s^2 P_{1\frac{1}{2}} - d$
4382.91 (10)	22809.5	$5s^2 D_{2\frac{1}{2}} - d$	3278.96 (3)	30488.7	$sp^4 {}^4P_{1\frac{1}{2}} - 5p^4 D_{2\frac{1}{2}}$
4374.24 (4)	22854.7	$5p^4 D_{2\frac{1}{2}} - 5d^4 F_{2\frac{1}{2}}$	3242.18 (2)	30834.6	$sp^4 {}^4P_{2\frac{1}{2}} - 5p^4 D_{1\frac{1}{2}}$
4355.19 (2)	22954.7	$5p^2 D_{2\frac{1}{2}} - 5d^4 P_{2\frac{1}{2}}$	3238.45 (2)	30870.1	$sp^4 {}^4P_{1\frac{1}{2}} - d$
4354.64 (00)	22957.6	$5p^4 D_{1\frac{1}{2}} - 6s^4 P_{2\frac{1}{2}}$	3204.56 (4)	31196.5	$sp^4 {}^4P_{1\frac{1}{2}} - 5p^4 P_{1\frac{1}{2}}$
4337.63 (1)	23047.6	$c - \beta$	3108.55 (2)	32160.0	$sp^4 {}^4P_{1\frac{1}{2}} - 5p^2 D_{1\frac{1}{2}}$
4318.91 (1)	23147.5	$5p^4 D_{3\frac{1}{2}} - 5d^4 D_{2\frac{1}{2}}$	3105.55 (3)	32191.1	$sp^4 {}^4P_{2\frac{1}{2}} - 5p^4 D_{2\frac{1}{2}}$
4248.03 (7)	23533.7	$5s^2 P_{1\frac{1}{2}} - b$	3046.10 (4)	32819.3	$sp^4 {}^4P_{1\frac{1}{2}} - 5p^4 P_{2\frac{1}{2}}$
4230.08 (2)	23633.6	$5s^4 P_{1\frac{1}{2}} - 5p^2 D_{2\frac{1}{2}}$	3041.25 (6)	32871.7	$sp^4 {}^4P_{1\frac{1}{2}} - 5p^4 S_{1\frac{1}{2}}$
4226.41 (2)	23654.1	$5p^4 D_{1\frac{1}{2}} - 5d^4 D_{1\frac{1}{2}}$	3038.64 (6)	32899.9	$sp^4 {}^4P_{2\frac{1}{2}} - 5p^4 P_{1\frac{1}{2}}$
4212.61 (8)	23731.6	$5p^4 P_{2\frac{1}{2}} - 5d^4 D_{3\frac{1}{2}}$	2963.87 (6)	33729.8	$sp^4 {}^4P_{1\frac{1}{2}} - 5p^4 S_{1\frac{1}{2}}$
4198.08 (3)	23813.7	$5p^4 D_{1\frac{1}{2}} - 5d^4 F_{1\frac{1}{2}}$	2947.06 (4)	33922.2	$sp^4 {}^4P_{2\frac{1}{2}} - 5p^4 D_{3\frac{1}{2}}$
4182.20 (0)	23904.1	$4d^4 F_{1\frac{1}{2}} - 5p^4 D_{2\frac{1}{2}}$	2905.06 (3)	34412.6	$5s^4 P_{1\frac{1}{2}} - d$
4180.98 (10)	23911.1	$5p^4 D_{3\frac{1}{2}} - 5d^4 F_{4\frac{1}{2}}$	2895.85 (5)	34522.1	$sp^4 {}^4P_{2\frac{1}{2}} - 5p^4 P_{2\frac{1}{2}}$
4175.34 (10)	23943.4	$5p^4 D_{2\frac{1}{2}} - 5d^4 F_{3\frac{1}{2}}$	2872.06 (2)	34808.0	$sp^4 {}^4P_{1\frac{1}{2}} - 5p^2 D_{2\frac{1}{2}}$
			2821.48 (5)	35432.0	$sp^4 {}^4P_{2\frac{1}{2}} - 5p^4 S_{1\frac{1}{2}}$

TABLE IV—(continued)

$\lambda$ I.A. (int.)	$\nu$ (vac.)	Classification	$\lambda$ (vac.)	$\nu$ (vac.)	Classification
2738.15 (2)	36510.2	$sp^4\ ^4P_{2\frac{1}{2}}—5p\ ^2D_{2\frac{1}{2}}$	1170.81 (3)	85411	$4p\ ^2P_{\frac{1}{2}}—5s\ ^2D_{1\frac{1}{2}}$
			1168.52 (8)	85578	$4p\ ^4S_{1\frac{1}{2}}—sp^4\ ^4P_{1\frac{1}{2}}$
			1166.51 (9)	85726	$4p\ ^2D_{1\frac{1}{2}}—5s\ ^2P_{\frac{1}{2}}$
			1156.94 (6)	86435	$4p\ ^4S_{1\frac{1}{2}}—sp^4\ ^4P_{\frac{1}{2}}$
			1155.97 (9)	86507	$4p\ ^2D_{2\frac{1}{2}}—sp^4\ ^2P_{1\frac{1}{2}}$
			1141.97 (9)	87568	$4p\ ^2D_{2\frac{1}{2}}—5s\ ^2P_{1\frac{1}{2}}$
			1134.00 (2)	88184	$4p\ ^2D_{1\frac{1}{2}}—5s\ ^2P_{1\frac{1}{2}}$
			1090.46 (0)	91704	$4p\ ^2D_{1\frac{1}{2}}—\beta$
			1077.52 (1)	92806	$4p\ ^2D_{1\frac{1}{2}}—\gamma$
			1057.37 (6)	94574	$4p\ ^2D_{2\frac{1}{2}}—5s\ ^2D_{2\frac{1}{2}}$
			1052.07 (3)	95051	$4p\ ^2D_{2\frac{1}{2}}—\delta$
			1050.54 (5)	95189	$4p\ ^2D_{1\frac{1}{2}}—5s\ ^2D_{2\frac{1}{2}}$
			1049.65 (10)	95270	$4p\ ^4S_{1\frac{1}{2}}—5s\ ^4P_{\frac{1}{2}}$
			1049.51 (10)	95283	$4p\ ^2D_{1\frac{1}{2}}—5s\ ^2D_{1\frac{1}{2}}$
			1045.30 (4)	95666	$4p\ ^2D_{1\frac{1}{2}}—\delta$
			1033.56 (10)	96753	$4p\ ^4S_{1\frac{1}{2}}—5s\ ^4P_{1\frac{1}{2}}$
			1022.09 (3)	97839	$4p\ ^2P_{1\frac{1}{2}}—\epsilon$
			1013.42 (4)	98676	$4p\ ^4S_{1\frac{1}{2}}—5s\ ^4P_{2\frac{1}{2}}$
			1013.20 (4)	98697	$4p\ ^2P_{\frac{1}{2}}—\epsilon$
			1011.18 (1)	98894	$4p\ ^4S_{1\frac{1}{2}}—5s\ ^2P_{\frac{1}{2}}$
			986.60 (1)	101358	$4p\ ^4S_{1\frac{1}{2}}—5s\ ^2P_{1\frac{1}{2}}$
			943.56 (1)	105982	$4p\ ^4S_{1\frac{1}{2}}—\gamma$
			926.35 (1)	107950	$4p\ ^2D_{2\frac{1}{2}}—\epsilon$
			922.94 (1)	108349	$4p\ ^4S_{1\frac{1}{2}}—5s\ ^2D_{2\frac{1}{2}}$
			921.11 (3)	108565	$4p\ ^2D_{1\frac{1}{2}}—\epsilon$
			918.81 (1)	108836	$4p\ ^4S_{1\frac{1}{2}}—\delta$
			746.03 (1)	134043	$4p\ ^4S_{1\frac{1}{2}}—6s\ ^4P_{\frac{1}{2}}$

## TERM VALUES

Absolute term values in Se II can be estimated from two members of any of the series  $4p\ ^4S—ms\ ^4P$  or  $5s\ ^4P—mp\ ^4S$  or other doublets. But, as is very well known, such an estimate can be only approximate, the probable error possibly being as large even as a few thousands. With this limitation, a mean value was obtained of the term  $5s\ ^4P_{2\frac{1}{2}}$  from the identified members of the various above-mentioned series. The term values so obtained are given in Table V. As many intercombination lines between the quartet and doublet terms have been located, the relative values of the two systems are known accurately.

TABLE V—TERM VALUES IN Se II

Term	$\nu$	$\Delta\nu$	Term	$\nu$	$\Delta\nu$
$4p\ ^4S_{1\frac{1}{2}}$	174994		$5p\ ^4P_{\frac{1}{2}}$	61945.3	
					<i>3727.6</i>
$\quad\quad\quad\ ^2D_{1\frac{1}{2}}$	161825		$\quad\quad\quad\ ^4P_{1\frac{1}{2}}$	58217.7	
		<i>616</i>			<i>1621.6</i>
$\quad\quad\quad\ ^2D_{2\frac{1}{2}}$	161209		$\quad\quad\quad\ ^4P_{2\frac{1}{2}}$	56596.1	
$\quad\quad\quad\ ^2P_{\frac{1}{2}}$	151957		$\quad\quad\quad\ ^4S_{1\frac{1}{2}}$	55685.5	
		<i>858</i>			
$\quad\quad\quad\ ^2P_{1\frac{1}{2}}$	151099		$\quad\quad\quad\ ^2D_{1\frac{1}{2}}$	57254.7	
					<i>2647.6</i>
			$\quad\quad\quad\ ^2D_{2\frac{1}{2}}$	54607.1	
$5s\ ^4P_{\frac{1}{2}}$	79724.3				
		<i>1483.6</i>	$\quad\quad\quad\ ^2P_{\frac{1}{2}}$	53611.9	
$\quad\quad\quad\ ^4P_{1\frac{1}{2}}$	78240.7				
		<i>1920.7</i>			
$\quad\quad\quad\ ^4P_{2\frac{1}{2}}$	76320.0		$6s\ ^4P_{\frac{1}{2}}$	40951.0	
					<i>1592.1</i>
$\quad\quad\quad\ ^2P_{\frac{1}{2}}$	76098.0		$\quad\quad\quad\ ^4P_{1\frac{1}{2}}$	39358.9	
		<i>2459.7</i>			<i>2033.9</i>
$\quad\quad\quad\ ^2P_{1\frac{1}{2}}$	73638.3		$\quad\quad\quad\ ^4P_{2\frac{1}{2}}$	37325.0	
$\quad\quad\quad\ ^2D_{1\frac{1}{2}}$	66544.4		$5d\ ^4F_{1\frac{1}{2}}$	36468.6	
		<i>-93.9</i>			<i>397.4</i>
$\quad\quad\quad\ ^2D_{2\frac{1}{2}}$	66638.3		$\quad\quad\quad\ ^4F_{2\frac{1}{2}}$	36071.2	
					<i>1088.7</i>
$sp^4\ ^4P_{\frac{1}{2}}$	88556.7		$\quad\quad\quad\ ^4F_{3\frac{1}{2}}$	34982.5	
		<i>-858.1</i>			<i>1697.6</i>
$\quad\quad\quad\ ^4P_{1\frac{1}{2}}$	89414.8		$\quad\quad\quad\ ^4F_{4\frac{1}{2}}$	33284.9	
		<i>-1702.8</i>			
$\quad\quad\quad\ ^4P_{2\frac{1}{2}}$	91117.6		$\quad\quad\quad\ ^4D_{1\frac{1}{2}}$	36628.3	
					<i>2580.1</i>
$\quad\quad\quad\ ^2P_{1\frac{1}{2}}$	74699.1		$\quad\quad\quad\ ^4D_{2\frac{1}{2}}$	34048.2	
					<i>1182.9</i>
			$\quad\quad\quad\ ^4D_{3\frac{1}{2}}$	32865.3	
$4d\ ^4F_{1\frac{1}{2}}$	82830.6				
		<i>2919.4</i>	$\quad\quad\quad\ ^4P_{1\frac{1}{2}}$	34054.1	
$\quad\quad\quad\ ^4F_{2\frac{1}{2}}$	79911.2				<i>2401.5</i>
		<i>2019.8</i>	$\quad\quad\quad\ ^4P_{2\frac{1}{2}}$	31652.6	
$\quad\quad\quad\ ^4F_{3\frac{1}{2}}$	77891.4				
		<i>1079.5</i>	$a$	53720.7	
$\quad\quad\quad\ ^4F_{4\frac{1}{2}}$	76811.9				
			$b$	50104.1	
$5p\ ^4D_{\frac{1}{2}}$	60695.0				
		<i>412.5</i>	$c$	47072.8	
$\quad\quad\quad\ ^4D_{1\frac{1}{2}}$	60282.5				
		<i>1356.6</i>	$d$	43828.8	
$\quad\quad\quad\ ^4D_{2\frac{1}{2}}$	58925.9				
		<i>1729.9</i>			
$\quad\quad\quad\ ^4D_{3\frac{1}{2}}$	57196.0				

TABLE V—(continued)

Term	$\nu$	$\Delta\nu$
$\alpha$	71707·4	
$\beta$	70120·2	
$\gamma$	69019·9	
$\delta$	66160·4	
$\varepsilon$	53260	

## COMPARISON OF TERMS

As I, Se II, and Br III form an iso-electronic series and these spectra are expected to be exactly similar. The doublets and quartets of As I have been investigated in detail. The following table gives a comparison of the term intervals in this spectrum with those in Se II. It would seem that the ratio is more nearly equal to 2 with  $4p$  and the  $sp^4$  terms than in  $5s$  or  $6s$  terms. The analysis of Br III has been published by Deb,\* who gives the  $5s\ ^4P$  interval as  $1354\text{ cm}^{-1}$ ; this appears to be entirely out of step in the above sequence. A modification† of the analysis is under investigation by the writers, and will be reported in detail in a separate communication.

TABLE VI—INTERVALS IN As I AND Se II

Term	As I $\delta\nu$	Se II $\delta\nu$	Ratio
$4p\ ^2D$	322·3	616	1·91
$\ ^2P$	461·2	858	1·86
$5s\ ^4P$	2203·5	3404·3	1·54
$\ ^2P$	1469·6	2459	1·67
$\ ^2D$	—19·1	—93·9	4·92
$6s\ ^4P$	2304·3	3626·0	1·57
$sp^4\ ^4P$	—1229·4	—2560·9	2·08

In conclusion, the authors desire to express their best thanks to Professor M. N. Saha, D.Sc., F.R.S., for his interest in their work and encouragement.

\* 'Proc. Roy. Soc.,' A, vol. 127, p. 208 (1930).

† In this new scheme the difference  $5s\ ^4P_{\frac{3}{2}} - 5s\ ^4P_{\frac{1}{2}}$  has a value of about  $4839\text{ cm}^{-1}$ , which is perfectly in keeping with the sequence of values of As I and Se II. It also agrees with the value  $4p\ ^3P_0 - 4p\ ^3P_2$  of Br IV (Rao and Krishnamurty, 'Proc. Phys. Soc., Lond.,' vol. 46, p. 531 (1934)).



## SUMMARY

By studying the spectra of selenium excited under various conditions and photographed in the entire region between  $\lambda$  8000 to  $\lambda$  450 many lines have been ascribed to the singly ionized atom. Of these about 200 lines, comprising a majority of the strong lines and several faint lines of the spectrum, have been classified as belonging to the quartet and doublet systems which are theoretically predicted according to Hund. The absolute term values have been determined from a consideration of several series. The largest term,  $4p\ ^4S_{1\frac{1}{2}} = 174994\text{ cm}^{-1}$ , gives the ionization potential of Se II to be about 21.6 volts.

Interesting anomalous intensities have been met with; the most prominent of which is that exhibited by the fundamental resonance group  $4p\ ^4S - 5s\ ^4P$ ; this is considered to be due to the mutual interaction of adjacent spectral terms, *e.g.*,  $4d$  or  $sp^4$  with the  $5s\ ^4P$  term.

## EXPLANATION OF PLATES 2 AND 3

FIG. 1—Spectrum of the discharge through Selenium vapour in the region between  $\lambda$  6500 and  $\lambda$  5000 and Fe arc comparison, showing the important supermultiplet  $5s\ ^4P - 5p\ ^4D$ .

FIG. 2—Vacuum spark spectrum of Selenium between  $\lambda$  1250 and  $\lambda$  1000, showing the fundamental groups  $4p\ ^4S \rightarrow 5s\ ^4P$ ,  $sp^4\ ^4P$ . The intensity anomaly in the former group is obvious. ( $\lambda$  1049 is a blend.)

---

## The Electromagnetic Equations of the Supraconductor

By F. and H. LONDON, Clarendon Laboratory, Oxford

(Communicated by F. A. Lindemann, F.R.S.—Received October 23, 1934)

Electric currents are commonly believed to persist in a supraconductor without being maintained by an electromagnetic field. Thus the relation between the field strength  $\mathbf{E}$  and the current density  $\mathbf{J}$  in a supraconductor has sometimes been described† by means of an “acceleration equation,” of the form

$$\Lambda \dot{\mathbf{J}} = \mathbf{E} ; \quad \Lambda = m/ne^2. \quad (1)$$

This equation, which might replace Ohm’s law for supraconductors, simply expresses the influence of the electric part of the Lorentz force on freely movable electrons of the mass  $m$  and charge  $e$ , the number per  $\text{cm}^3$  being  $n$  (we use rational units). By definition the constant  $\Lambda$  must be positive. As a direct consequence of this equation (1) stationary currents in supraconductors are possible when  $\mathbf{E} = 0$ .

We shall see, however, that actually equation (1), which we will refer to as the “acceleration theory,” implies more than is verified by experiment; moreover, presupposing an acceleration without any friction it implies a premature theory, the development of which has presented a hopelessly insoluble problem to mathematical physicists. Apparently a model was wanted which would explain that in its most stable state the supraconductor has always a persistent current. We shall give a formulation which is somewhat more restricted in this respect. On the other hand it includes one more important fact, namely, the experiment of Meissner and Ochsenfeld.‡ In this way we get a new description of the electromagnetic field in a supraconductor, which is consistent and, as it eliminates unnecessary statements, is in closer contact with experiment. This new description seems to provide an entirely new point of view for a theoretical explanation.

† Becker, Heller, and Sauter, ‘Z. Physik,’ vol. 85, p. 772 (1933); Braunbeck, ‘Z. Physik,’ vol. 87, p. 470 (1934); London, ‘Nature,’ vol. 133, p. 497 (1934).

‡ ‘Naturw.,’ vol. 21, p. 787 (1933).

## § 1—THE FUNDAMENTAL EQUATIONS

Although we intend to abandon the “acceleration equation” (1) we shall take this equation as a provisional basis in order to find out the point where it must be corrected. Taking the curl of (1) and using

$\text{curl } \mathbf{E} = -\frac{1}{c} \dot{\mathbf{H}}$  we obtain

$$\text{curl } \Lambda \dot{\mathbf{J}} = -\frac{1}{c} \dot{\mathbf{H}}, \quad (2)$$

or since  $\frac{1}{c} \mathbf{J} = \text{curl } \mathbf{H}$  (neglecting the displacement current)

$$\text{curl curl } \Lambda \dot{\mathbf{H}} = -\frac{1}{c^2} \dot{\mathbf{H}}$$

and as  $\text{div } \mathbf{H} = 0$

$$\Lambda c^2 \nabla^2 \dot{\mathbf{H}} = \dot{\mathbf{H}}. \quad (3)$$

Here we can integrate with respect to time and obtain:

$$\Lambda c^2 \nabla^2 (\mathbf{H} - \mathbf{H}_0) = \mathbf{H} - \mathbf{H}_0. \quad (4)$$

(4) is a nonhomogeneous equation for  $\mathbf{H}$ .  $\mathbf{H}_0$  denotes the magnetic field at the time  $t = 0$ . The general solution of (4) follows by superposition of any particular solution on the general solution of the homogeneous equation

$$\Lambda c^2 \nabla^2 \mathbf{H} = \mathbf{H}. \quad (5)$$

The solutions of (5) which behave regularly inside the superconductor decrease exponentially very quickly as one recedes from the surface, where they are fitted into the values of the external field.  $\Lambda c^2 = mc^2/ne^2$  is of the order of magnitude  $10^{-11} \text{ cm}^2$ . A particular solution of (4) may be written down immediately, namely,

$$\mathbf{H} = \mathbf{H}_0.$$

Now the general solution of (4) follows by superposition of this solution (*i.e.*, of the original field  $\mathbf{H}_0$ ) on our general solution of the homogeneous equation, which is not appreciably different from zero except near the surface.

The general solution means, therefore, that practically the original field persists for ever in the superconductor. Only in a layer of the order  $10^{-5} \text{ cm}$  below the surface all disturbances take place reversibly, provided the threshold value is not exceeded. The field  $\mathbf{H}_0$  is to be regarded as “frozen in” and represents a permanent memory of the field which

existed when the metal was last cooled below the transition temperature.

Until recently the existence of "frozen in" magnetic fields in superconductors was believed to be proved theoretically and experimentally. By Meissner's experiment,<sup>†</sup> however, it has been shown that this point of view cannot be maintained. It results clearly from the thermodynamic discussion of Gorter<sup>‡</sup> that at the transition to the superconducting state any magnetic field which may have existed before in the conductor is pushed out of it so that experiments which seemed to show that magnetic fields are frozen in are to be explained by the existence of non-superconducting inclusions, in which the magnetic lines of force are pressed together.

Since magnetic fields under no circumstances can be found in the superconducting phase, one is tempted to give the integration constant  $\mathbf{H}_0$  of (3) in (4) the value zero. But if not all solutions of a differential equation exist in reality, the equation gives too general a description. One should not use a differential equation like (1) which contains too many possibilities, as it gives nature more freedom than it wants. If in reality  $\mathbf{H}_0$  is always confined to the value zero, then this means that

$$\Lambda c^2 \nabla^2 \mathbf{H} = \mathbf{H}$$

is to be considered as a fundamental law and not to be treated as a particular integral of a differential equation in consequence of (1). Hence we abandon (1). Since  $\text{curl } \mathbf{H} = \frac{1}{c} \mathbf{J}$  we can write (5) in the form

$$\text{curl } \Lambda \mathbf{J} = -\frac{1}{c} \mathbf{H}. \quad (6)$$

This we postulate as the fundamental equation which replaces Ohm's law in superconductors.

Equation (6) says more than (2), so far as it includes Meissner's effect. Proceeding from (6) to (2) by differentiating with respect to the time we

<sup>†</sup> Meissner and Ochsenfeld, 'Naturw.,' vol. 21, p. 787 (1933); 'Z. ges. Kälte-industr.,' vol. 11, p. 125 (1934) 'Phys. Z.,' vol. 35, p. 954 (1934); de Haas and Casimir, 'Physica,' vol. 1, p. 291 (1934); Mendelssohn and Babbitt, 'Nature,' vol. 133, p. 459 (1934); Mendelssohn and Moore, 'Nature,' vol. 133, p. 413 (1934). Schubnikoff and Rjalinin, 'Phys. Z. Sowjet,' vol. 5, p. 671 (1934); 'Nature,' vol. 134, p. 286 (1934). Keeley and Mendelssohn, 'Nature,' vol. 134 p. 773 (1934).

<sup>‡</sup> 'Arch. Musée Teyler,' ser. III, vol. 7, p. 378 (1933); 'Nature,' vol. 132, p. 931 (1933). Gorter and Casimir, 'Physica,' vol. 1, p. 306 (1934), *see also* Ehrenfest and Rutgers, 'Comm. Phys. Lab., Leiden,' Supp. 75b. (Nachtrag).

lose this content. The logical relation between the three propositions (1), (2) and (6) may be represented by the following scheme:

$$\begin{array}{ccc}
 (1) \quad \Lambda \dot{\mathbf{J}} = \mathbf{E} & & (6) \quad \text{curl } \Lambda \mathbf{J} = -\frac{1}{c} \dot{\mathbf{H}} \\
 \swarrow & & \swarrow \\
 (2) \quad \text{curl } \Lambda \dot{\mathbf{J}} = -\frac{1}{c} \dot{\mathbf{H}}. & & 
 \end{array}$$

The propositions (1) and (6) possess, so to speak, the same degree of generality. Assuming (6) instead of (1) we comprehend more in *one* respect, namely, Meissner's Effect, but less in another respect, for we cannot deduce (1) from (6); but we obtain from (2) the weaker statement:

$$\text{curl } (\Lambda \dot{\mathbf{J}} - \mathbf{E}) = 0.$$

Inasmuch as (1) says more than (2) it expresses a prejudice which, in our opinion, is not tested by experience. We are only enabled to conclude, that  $\Lambda \dot{\mathbf{J}} - \mathbf{E}$  can be represented as the gradient of a quantity  $\mu$ :

$$\Lambda \dot{\mathbf{J}} - \mathbf{E} = \text{grad } \mu. \quad (7)$$

Now the question arises whether  $\mu$  is merely an integration constant or whether it represents a real physical quantity. Comparing (6) with (7) (which may be written in the form  $\Lambda (\dot{\mathbf{J}} - \text{grad } \mu/\Lambda) = \mathbf{E}$ ) we see that we can put together these six equations in the form of an equation for an antisymmetrical tensor:

$$\Lambda \left( \frac{\partial J_i}{\partial x_k} - \frac{\partial J_k}{\partial x_i} \right) = \frac{1}{c} f_{ik}. \quad (8)$$

Here we have named the field strengths  $E_x, E_y, E_z, H_x, H_y, H_z$  as usual by  $if_{14}, if_{24}, if_{34}, f_{23}, f_{31}, f_{12}$  and the co-ordinates  $x, y, z, ict$  by  $x_1, x_2, x_3, x_4$ . Then the quantity  $\mu/\Lambda$  has to be regarded as the time-like supplement of the current density  $\mathbf{J}$ . As is well known from ordinary electrodynamics, this is the density of charge  $\rho$ .

Therefore the relativistic covariance would require

$$J_4 = \frac{\mu}{ic\Lambda} = ic\rho. \quad (9)$$

This interpretation by the principle of covariance† now gives to equation (7) the quality of an *independent physical statement*

$$\Lambda (\dot{\mathbf{J}} + c^2 \text{grad } \rho) = \mathbf{E}, \quad (10)$$

where  $\rho$  is connected with  $\mathbf{E}$  by

$$\rho = \text{div } \mathbf{E}. \quad (11)$$

Here for the sake of simplicity we have taken the value of the dielectric constant  $\epsilon$  equal to one as we do not know anything about it. This may subsequently have to be corrected.

Putting (11) in (10) we get

$$\Lambda (\dot{\mathbf{J}} + c^2 \text{grad div } \mathbf{E}) = \mathbf{E},$$

or since  $\text{grad div } \mathbf{E} = \nabla^2 \mathbf{E} + \text{curl curl } \mathbf{E} = \nabla^2 \mathbf{E} - \frac{1}{c^2} \dot{\mathbf{J}},$

$$\Lambda c^2 \nabla^2 \mathbf{E} = \mathbf{E} \quad (12)$$

and by taking the divergence we get

$$\Lambda c^2 \nabla^2 \rho = \rho. \quad (13)$$

Thus we see the 10 quantities  $\mathbf{E}, \mathbf{H}, \mathbf{J}, \rho$  obey the same equation.

So far we have neglected throughout the displacement current. If one considers it, these equations follow:

$$\left. \begin{aligned} \nabla^2 \mathbf{E} - \frac{1}{c^2} \frac{\partial^2 \mathbf{E}}{\partial t^2} &= \frac{1}{\Lambda c^2} \mathbf{E} \\ \nabla^2 \mathbf{H} - \frac{1}{c^2} \frac{\partial^2 \mathbf{H}}{\partial t^2} &= \frac{1}{\Lambda c^2} \mathbf{H} \\ \nabla^2 \mathbf{J} - \frac{1}{c^2} \frac{\partial^2 \mathbf{J}}{\partial t^2} &= \frac{1}{\Lambda c^2} \mathbf{J} \\ \nabla^2 \rho - \frac{1}{c^2} \frac{\partial^2 \rho}{\partial t^2} &= \frac{1}{\Lambda c^2} \rho \end{aligned} \right\}. \quad (14)$$

The field strength  $\mathbf{E}$  and  $\mathbf{H}$  may be derived as usual from a scalar potential  $\phi$  and a vector potential  $\mathbf{A}$  by

$$\left. \begin{aligned} \mathbf{E} &= - \text{grad } \phi - \frac{1}{c} \dot{\mathbf{A}} \\ \mathbf{H} &= \text{curl } \mathbf{A} \end{aligned} \right\}. \quad (15)$$

† It is very remarkable that equation (6) has a four-dimensional supplement, which does not explicitly contain the velocity of the supraconductor. Of course (10) is not the only possible form of a covariant supplement, but it is apparently distinguished by its simplicity and there is no reason to consider more complicated ones.

Comparing (15) with (10) and (6) we see, that it is possible† to choose the potentials—which are not absolutely uniquely determined by the field—so that they become proportional to the density of current and charge:

$$\left. \begin{aligned} \Lambda c \mathbf{J} &= -\mathbf{A} \\ \Lambda c^2 \rho &= -\phi \end{aligned} \right\}. \quad (16)$$

These equations, which could also be employed as the fundamental equations of the theory do not contain any dynamics as equation (1) nor any other explicit statements about temporal variations. Like the specific resistance in Ohm's law  $\Lambda$  is a constant depending on the material. There is no particular reason now, for attributing to it the value given in (1) although for the atomistic explanation no very different interpretation is to be expected (see equation 32)).

The additional condition for the vector potential

$$\operatorname{div} \mathbf{A} + \frac{1}{c} \dot{\phi} = 0$$

corresponds, because of (16), to the equation of continuity:

$$\operatorname{div} \mathbf{J} + \dot{\rho} = 0.$$

Putting the second equation (16) in (10), which expresses the modified equation of acceleration, the latter becomes

$$\Lambda \dot{\mathbf{J}} = \mathbf{E} + \operatorname{grad} \phi. \quad (17)$$

We learn from it that the acceleration of  $\mathbf{J}$  is only due to that part of  $\mathbf{E}$  which remains when the potential part ( $-\operatorname{grad} \phi$ ) has been subtracted. When  $\mathbf{E}$  is merely a potential field it has therefore no influence on the superconducting current.

## § 2—THE LAW OF CONSERVATION OF ENERGY, PRODUCTION OF HEAT, BOUNDARY CONDITIONS

As usual the law of conservation of energy follows from Maxwell's equations. But now in the equation

$$\operatorname{div} c [\mathbf{E}\mathbf{H}] = -\frac{\partial}{\partial t} \left\{ \frac{1}{2} (\mathbf{H}^2 + \mathbf{E}^2) \right\} - (\mathbf{J}\mathbf{E}),$$

† Here we consider only simply connected superconductors. As to the generalization for multiply connected superconductors see a paper in "Physica."

the term  $(\mathbf{J}\mathbf{E})$  has not simply the significance of Joule heat. From the equation  $\mathbf{E} = \Lambda (\dot{\mathbf{J}} + c^2 \text{grad } \rho)$  we find:

$$\begin{aligned} (\mathbf{J}\mathbf{E}) &= \Lambda \{ \mathbf{J}\dot{\mathbf{J}} + c^2 (\mathbf{J} \text{grad } \rho) \} \\ &= \Lambda \left\{ \frac{d}{dt} \left( \frac{\mathbf{J}^2}{2} \right) + c^2 \text{div} (\rho \mathbf{J}) - c^2 \rho \text{div } \mathbf{J} \right\} \\ &= \frac{d}{dt} \left( \frac{\Lambda}{2} \mathbf{J}^2 \right) + c^2 \Lambda \left\{ \text{div} (\rho \mathbf{J}) + \frac{d}{dt} \left( \frac{\rho^2}{2} \right) \right\}. \end{aligned}$$

Therefore the energy principle may be written in the following form:

$$\text{div } c [\mathbf{E}\mathbf{H}] = - \frac{\partial}{\partial t} \left\{ \frac{1}{2} (\mathbf{H}^2 + \mathbf{E}^2) + \frac{\Lambda}{2} (\mathbf{J}^2 + c^2 \rho^2) \right\} - \Lambda c^2 \text{div } \rho \mathbf{J}. \quad (18)$$

In addition to the usual terms for the magnetic and the electric energy there is a term  $\frac{\Lambda}{2} \mathbf{J}^2$ , a kind of kinetic energy of the persistent currents and another term  $\frac{\Lambda}{2} c^2 \rho^2$ , which may be interpreted as an additional potential energy connected with the density of electric charges in the supraconductor.

The last term  $(- \Lambda c^2 \text{div } \rho \mathbf{J})$  is the most interesting one. Its significance may become clearer by integrating over the whole of the supraconducting phase and transforming the integrals of the divergences into surface integrals:

$$c \int [\mathbf{E}\mathbf{H}]_n d\sigma = - \frac{\partial}{\partial t} \int \left[ \frac{1}{2} \mathbf{H}^2 + \mathbf{E}^2 \right] dS + \frac{\Lambda}{2} \int (\mathbf{J}^2 + \rho^2 c^2) dS - \Lambda c^2 \int \rho \mathbf{J}_n d\sigma.$$

In consequence of the continuity of the tangential components of  $\mathbf{E}$  and  $\mathbf{H}$  we can substitute on the left-hand side the components of the field outside the supraconductor, where  $c [\mathbf{E}\mathbf{H}]$  is known to be the Poynting vector, *i.e.*, the flow of electromagnetic energy. The term

$$Q = \Lambda c^2 \int \rho \mathbf{J}_n d\sigma, \quad (19)$$

therefore, must be an amount of energy, which balances the flow of electromagnetic energy particularly for stationary processes ( $\partial/\partial t \dots = 0$ ), where the state of the supraconductor does not change.  $Q$  must be a non-electromagnetic form of energy and as such heat is the only form of energy which comes into question.



In the interior of the superconductor the law of conservation of energy can be written in the form

$$\operatorname{div} \mathbf{S} + \frac{\partial W}{\partial t} = 0. \quad (20)$$

Here the quantities

$$W = \frac{1}{2}(\mathbf{H}^2 + \mathbf{E}^2) + \frac{\Lambda}{2}(\mathbf{J}^2 + c^2 \rho^2) \quad (21)$$

and

$$\mathbf{S} = c [\mathbf{EH}] + \Lambda c^2 \rho \mathbf{J} \quad (22)$$

are to be interpreted as the density and as the flow of the total energy in the superconductor.

Equation (20) states that *inside* the superconductor no energy disappears, *i.e.*, changes into heat. The production of heat is therefore to be localized exactly on the surface of the superconductor. There the flow of energy, changing discontinuously from  $\Lambda c^2 \rho \mathbf{J} + c[\mathbf{EH}]$  to  $c[\mathbf{EH}]$ , has a surface divergence. (19) shows that the production of heat occurs where the electric current has a normal component to the surface and meets there an electric density. It can easily be shown that the heat  $Q$  produced, where the current  $\mathbf{I}$  enters and leaves the superconductor, is always positive and is exactly equal to  $\mathbf{VI}$ ,  $V$  being the difference of voltage through which the current passes. Joule's law, therefore, is fulfilled, at least for the superconductor as a whole.

For the sake of completeness we announce the components of the Maxwell stresses  $T_{ik}$  in the superconductor:

$$T_{ik} = T_{ik}(\mathbf{E}) + T_{ik}(\mathbf{H}) - T_{ik}(\mathbf{J}) - \frac{\delta_{ik}}{2} \Lambda c^2 \rho^2.$$

Here

$$T_{ik}(\mathbf{E}) = E_i E_k - \frac{1}{2} \delta_{ik} E^2, \text{ etc.}$$

$$\delta_{ik} = \begin{cases} 1 & \text{for } i = k \\ 0 & \text{for } i \neq k. \end{cases}$$

Then the energy impulse tensor  $\Theta_{ik}$  comprehending as usual the stresses, the flow and the density of energy in its four-dimensional scheme may be written in the form:

$$\Theta_{ik} = \sum_{r=1}^4 f_{ir} f_{kr} - \frac{1}{4} \delta_{ik} \sum_{r,s=1}^4 f_{rs}^2 - \Lambda \left( \mathbf{J}_i \mathbf{J}_k - \frac{\delta_{ik}}{2} \sum_{r=1}^4 \mathbf{J}_r^2 \right).$$

Here we use the same notation as in equation (8). The four-dimensional divergence of this tensor vanishes identically:

$$\sum_{k=1}^4 \frac{\partial \Theta_{ik}}{\partial x_k} = 0.$$

That means that no *ponderomotiv* volume forces are acting inside the supraconductor, even when charges and currents are present in its interior.

It remains to establish the *boundary conditions* for the transition from the supraconductor to the adjacent insulator or normal conductor respectively. Of course, as always in Maxwell's theory, the tangential components of  $\mathbf{E}$  and the normal components of  $\mathbf{H}$  and of  $\mathbf{J} + \dot{\mathbf{E}}$  (or  $\mathbf{J} + \dot{\mathbf{D}}$ ) must be continuous. Further, we think it reasonable to postulate continuity of the normal component of  $\mathbf{E}$  (or  $\mathbf{D}$ ) and of the tangential component of  $\mathbf{H}$  in order to get a unique solution. Discontinuity of these components would mean the possibility of mathematical surface charges of an arbitrary amount. As the space charges lie always so near the surface that they appear macroscopically to be superficial ones it does not seem physically plausible to assume mathematical surface densities in addition. In contrast to normal conductors surface currents and surface charges of a finite amount would lead to an infinite value of the additional energy term  $\frac{\Lambda}{2} (\mathbf{J}^2 + c^2 \rho^2)$  in the supraconductor and therefore they are excluded by the theory itself. But applying these boundary conditions (continuity of *all* components of  $\mathbf{E}$  and  $\mathbf{H}$ ) there is some consideration necessary, as the smallest normal conducting layer on the surface would give rise to surface charges according to Maxwell's theory. A special question will be the boundary conditions at the boundary between supraconducting and non-supraconducting phase in the same metal. We shall treat this in § 4.

### § 3—SUPRACONDUCTING SPHERE ON A HOMOGENEOUS ELECTRIC FIELD

As a simple application of this theory we consider a supraconducting sphere in a homogeneous electric field. Let  $R$  be the radius of the sphere and  $r_0 \vartheta_0 \psi$  spherical polar co-ordinates with the axis coinciding with the direction of the field.

(1) *The adjacent medium is an insulator*—Then we have the equations

$$\nabla^2 \phi = 0 \text{ outside the sphere,}$$

$$\nabla^2 \phi = \beta^2 \phi \quad \beta^2 = \frac{1}{\Lambda c^2} \text{ inside the sphere.}^\dagger$$

<sup>†</sup> In the supraconductor  $\phi$  can always be chosen so that it becomes proportional to  $\rho$  (see equation (16)) and then, like the latter, obeys equation (13).

The potential is completely determined from its asymptotic values at great distances by the postulate that  $\phi$  and  $\partial\phi/\partial r$  shall be continuous on the surface of the sphere. We obtain

$$\phi = \begin{cases} \left(\frac{A}{r^2} - rE\right) \cos \vartheta & \text{or } r \gg R \\ \frac{B}{\beta r} \left(\cosh \beta r - \frac{\sinh \beta r}{\beta r}\right) \cos \vartheta & \text{for } r \leq R \end{cases}$$

$E$  is the asymptotic field strength and

$$A = ER^3 \left[ 1 - \frac{3}{\beta R} \left( \operatorname{ctgh} \beta R - \frac{1}{\beta R} \right) \right]$$

$$B = -\frac{3RE}{\sinh \beta R}.$$

For  $r \leq R$  the potential gives immediately the electric charges according to  $\rho = -\frac{1}{\Lambda c^2} \phi$ . It is easy to see that the distribution of these charges near to the surface is practically the same as the distribution of charges induced on the surface of a normal conducting sphere in a homogeneous electric field. The lines of the electric field strength end on the charges below the surface.

(2) *Now the adjacent medium may be a conductor of the conductivity  $\sigma$ .* Then the equations and boundary conditions of  $\phi$  are exactly the same as before and we obtain the same electric field and charges. But now outside the sphere a current  $\mathbf{J}$  is connected with the field by  $\mathbf{J} = -\sigma \operatorname{grad} \phi$ . Since  $\operatorname{div} \mathbf{J} = 0$  we have to postulate the continuity of  $J_r$  on the surface of the sphere. Now the current  $\mathbf{J}$  inside is uniquely determined by its normal component on the surface and by the equations

$$\operatorname{curl} \operatorname{curl} \mathbf{J} + \beta^2 \mathbf{J} = 0 \quad \text{and} \quad \operatorname{div} \mathbf{J} = 0.$$

We obtain

$$J_r = -\frac{k \cos \vartheta}{\beta r^2} \left( \cosh \beta r - \frac{\sinh \beta r}{\beta r} \right)$$

$$J_\vartheta = \frac{k \sin \vartheta}{2r} \left[ \left( 1 + \frac{1}{\beta^2 r^2} \right) \sinh \beta r - \frac{1}{\beta r} \cosh \beta r \right]$$

$$k = \frac{3\sigma ER}{\sinh \beta R} \left[ 2 + \frac{\beta^2 R^2}{1 - \beta R \operatorname{ctgh} \beta R} \right].$$

In the supraconductor the distribution of current is not parallel to the electric field. The streamlines of  $\mathbf{J}$  are broken at the surface in contrast to the electric lines of force, which are continuous.

§ 4—SUPRACONDUCTING WIRE. THE TRANSITION CURVE

As another application we shall consider the problem of the distribution of a given current in a circular supraconducting wire of infinite length.

We use cylindrical co-ordinates  $z, r, \vartheta$  with the  $z$ -axis coinciding with the axis of the wire. Let  $a$  be the radius of the wire and  $R$  that of the boundary surface between the supraconducting and the normally conducting phase.

1—As long as  $I < I_T = 2\pi acH_T$  ( $H_T$  is the threshold value) only the supraconducting phase exists. With the notation  $\beta^2 = \frac{1}{\Lambda c^2}$  the equation for the current density  $\mathbf{J}$  may be written

$$\text{curl curl } \mathbf{J} + \beta^2 \mathbf{J} = 0. \quad (23)$$

From reasons of symmetry  $\mathbf{J}$  has only a  $z$ -component, which can only depend on  $r$ . Then  $\mathbf{J} = J_z(r)$  obeys the equation

$$\frac{\partial^2 J}{\partial r^2} + \frac{1}{r} \frac{\partial J}{\partial r} - \beta^2 J = 0.$$

This is the Bessel differential equation for  $J_0(i\beta r)$ .† This solution has still to be normalized. This gives

$$\mathbf{J} = I \frac{i\beta}{2\pi a} \frac{J_0(i\beta r)}{J_1(i\beta a)}. \quad (24)$$

For  $\mathbf{H}$  we get

$$\mathbf{H} = H_\phi = -\frac{1}{\beta^2 c} \text{curl}_\phi \mathbf{J} = \frac{I}{2\pi ac} \frac{J_1(i\beta r)}{J_1(i\beta a)}. \quad (25)$$

Current and field are near the surface in a layer of the thickness  $\frac{1}{\beta} \sim 10^{-5}$  cm.

If  $r \gg 10^{-5}$  cm we may replace the Bessel functions by exponential functions and we get

$$\left. \begin{aligned} \mathbf{J} = J_z &= I \frac{\beta}{2\pi \sqrt{ar}} e^{\beta(r-a)} \\ \mathbf{H} = H_\phi &= I \frac{1}{2\pi c \sqrt{ar}} e^{\beta(r-a)} \end{aligned} \right\} \text{ for } r \ll a.$$

Outside the wire  $\mathbf{H}$  is given, as usual, by  $\text{div } \mathbf{H} = 0$ ,  $\text{rot } \mathbf{H} = 0$  and the postulate of continuity on the surface.

The well-known solution is

$$\mathbf{H} = H_\phi = I \frac{1}{2\pi rc} \quad \text{for } r \gg a.$$

† Confusion between current density  $J$  and the Bessel functions  $J$  should not arise since the latter have always numbers as indices.

In the superconductor the electric field is not connected with the current; it is only determined by the equations  $\nabla^2 \mathbf{E} = \beta^2 \mathbf{E}$  and  $\text{curl } \mathbf{E} = 0$ . If we assume continuity of all components of  $\mathbf{E}$  on the boundaries these equations involve only a very short continuation of the external fields at the ends into a layer of the superconductor about  $10^{-5}$  cm thick. In this layer  $\mathbf{E}$  decreases exponentially from the adjacent normal conducting leads, so that in practice one would find no *potential-difference in a superconductor*, in agreement with the classical experiment of superconductivity.

2—Suppose now  $I > I_T = 2\pi acH_T$ .

From the centre to a radius  $R$  we have  $H < H_T$ . Here the equations of § 1 are valid, beyond  $R$ , where  $H \geq H_T$ , we will assume Ohm's law.†

Then the total current  $I$  is divided into

$$I = I^{(i)} + I^{(e)}.$$

On the surface of the inner current  $I^{(i)}$  the magnetic field produced by it will have just the value  $H_T$ , therefore we get for  $I^{(i)}$  the equation

$$I^{(i)} = 2\pi cRH_T. \quad (26)$$

The part  $I^{(e)}$  flowing on the outside as an ordinary conduction current is necessarily accompanied by an electric field strength  $E = E_z$  according to Ohm's law

$$\sigma E \cdot \pi(a^2 - R^2) = I^{(e)} = I - 2\pi cRH_T = I - I_T \frac{R}{a},$$

or

$$E = \frac{I - I_T \frac{R}{a}}{\sigma \pi a^2 \left[ 1 - \left( \frac{R}{a} \right)^2 \right]}. \quad (27)$$

This field strength  $\mathbf{E}$  has to be continued through the boundary into the superconducting part. If the equation of acceleration (1) were true, the current  $I^{(i)}$  in the superconducting phase would be accelerated by the electric fields. The magnetic field connected with the current would increase and rise above the threshold value  $H_T$  below the separating surface. The latter would, therefore, shrink inwards and the process would continue until no superconducting phase would be left.

† This condition for the boundary between both phases of the superconductor is to be regarded as quite provisional, as possibly the whole conception of these two separated phases is too simple.

But during this process in the non-supraconducting part the magnetic field would decrease. An elementary calculation shows that as soon as  $R$  is smaller than a certain value  $R_0$  given by

$$R_0 = a \left( \frac{I}{I_T} - \sqrt{\left( \frac{I}{I_T} \right)^2 - 1} \right), \quad (28)$$

the magnetic field in the non-supraconducting phase would not everywhere exceed  $H_T$ . There supraconductivity should appear again, in contradiction with the mechanism we have described, provided that we accept the conception that supraconductivity appears where the magnetic field is smaller than the threshold value.

In contrast to that our equations do not imply any acceleration by an electrostatic field in a supraconductor. We will consider how far this enables us to avoid these difficulties.

For current density  $\mathbf{J}^{(i)}$  and magnetic field  $\mathbf{H}^{(i)}$  we can simply take the solution (24), (25) replacing  $a$  by  $R$ :

$$\begin{aligned} J &= J_z = i\beta c H_T \frac{J_0(i\beta r)}{J_1(i\beta R)} \\ H &= H_\phi = H_T \frac{J_1(i\beta r)}{J_1(i\beta R)}. \end{aligned}$$

Since  $\dot{H}^{(i)} = 0$  the electric field  $\mathbf{E}^{(i)}$  has no curl and therefore it may be represented by a potential  $\phi$ , the latter obeying the equation,

$$\nabla^2 \phi - \beta^2 \phi = 0,$$

and the boundary condition on the surface,

$$-\left( \frac{\partial \phi}{\partial z} \right)_{r=R} = E_z = E.$$

The only regular solution is

$$\phi = -Ez \frac{J_0(i\beta r)}{J_0(i\beta R)}. \quad (29)$$

Therefrom we derive the components of the electric field  $\mathbf{E}^{(i)}$

$$\left. \begin{aligned} E_z^{(i)} &= E \cdot \frac{J_0(i\beta r)}{J_0(i\beta R)} \\ E_r^{(i)} &= i\beta z E \frac{J_1(i\beta r)}{J_0(i\beta R)} \end{aligned} \right\}. \quad (30)$$

As this field is derived from a potential it has no influence on the distribution of current calculated before. In contrast to the "theory of acceleration" we have now stationary conditions.

It seems important to emphasize that the field  $\mathbf{E}^{(s)}$  could not be determined unless the normal component of  $\mathbf{E}$  on the boundary surface between supraconducting phase and normal conducting phase is discontinuous. It is evident that the boundary between two phases of one substance is a quite different thing from the boundary between two substances and therefore the same boundary conditions may not be expected in both cases. If  $E_n$  were postulated to be continuous on the surface between both phases no solution would exist as long as we maintain the conception that  $H < H_T$  or  $H > H_T$  decides where supraconductivity occurs and where not.

It seems to be remarkable that our solution has charges linearly increasing along the wire. The order of magnitude of the electric fields belonging to them are, however, very small compared with the magnetic fields, at least for such lengths of supraconducting wire as have been investigated until now. For longer wires it may be necessary to consider an influence of these charges and fields on equation (26). On the other hand it would be interesting to calculate the conditions at the ends of a finite wire where the current enters. But here we shall defer the consideration of such details.

The radius  $R$  of the boundary surface is not yet determined. We see only that any radius  $R > R_0$  (see equation (28)) would agree with our electrodynamics and could give us a stationary distribution of current with a certain field strength  $E$ .  $R$  functions here as a parameter and therefore cannot be determined by the differential equations of the problem. In order to determine  $R$  we need a further condition. Whether this condition can be derived from thermodynamics or whether the present theory requires still another supplement as to the electrodynamics at the boundary between both phases is a question which must be the subject of a more thorough and general consideration, with which we cannot deal in this paper. But one is tempted to guess that in our special case only the value  $R = R_0$  (equation (28)) can come into question. It is distinguished from any other possible value of  $R$ . For instance, it could be characterized as giving the minimum of the surface charges or of the Joule-heat. Taking the Joule-heat,

$$Q = IE = \frac{1}{\sigma \pi a^2} \cdot I^2 \frac{1 - \frac{I R}{I_T a}}{1 - \left(\frac{R}{a}\right)^2},$$

we get for its minimum the equation,

$$\left(\frac{R}{a}\right)^2 - 2\left(\frac{R}{a}\right)\left(\frac{I}{I_T}\right) + 1 = 0.$$

The only solution of this equation which comes into question ( $R < a$ ) is  $R = R_0$  (equation (28)).

Though this supposition requires further examination we will shortly consider its consequences.

Putting  $R = R_0$  into (27) we get the resistance  $\omega$  as a function of the current  $I$  ( $\omega_0 = \frac{1}{\sigma\pi a^2}$  being the resistance per cm length of the wire in the non-supraconducting state),

$$\begin{aligned}\omega &= \frac{E}{I} = \frac{\omega_0}{I} \frac{I - I_T \frac{R_0}{a}}{1 - \frac{R_0^2}{a^2}} \\ &= \frac{\omega_0}{2} \left(1 + \sqrt{1 - \left(\frac{I_T}{I}\right)^2}\right).\end{aligned}\tag{31}$$

This can be used, of course, only for  $I \geq I_T$ . For  $I = I_T$  this solution gives the value  $\omega_0/2$ . For  $I < I_T$  we have the solution which was calculated at the beginning of this paragraph with  $E = 0$ ; that means  $\omega = 0$ . Therefore the resistance drops discontinuously from its half value to zero.

Considered as a function of  $I_T$  (31) gives the transition curve as a function of temperature. Possibly  $\Lambda$  is to be regarded as dependent on temperature. But the result (31) is not dependent on the value of  $\Lambda$ .  $I_T$  is given by the curve of the threshold value of the critical magnetic field  $H_T$  which, near the critical temperature  $T_0$ , can be represented linearly in the form

$$H_T = k (T_0 - T).$$

Therefore analogously

$$I_T = 2\pi caH_T = b (T_0 - T).$$

This gives

$$\omega = \frac{\omega_0}{2} \left\{1 + \sqrt{1 - b^2 \left(\frac{T - T_0}{I}\right)^2}\right\}.$$

In the limit for very weak currents the resistance curve therefore drops absolutely vertically from its value at the temperature  $T_0$  to the value zero (see fig. 1). The comparison with the measurements of de Haas and



Voogd† shows qualitative conformity, but it seems premature to discuss the experiments without considering further details.

### CONCLUDING REMARKS

In considering the equations (16) one is very strongly reminded of Gordon's formulæ for electric current and charge in his relativistic formulation of Schrödinger's Theory:

$$\left. \begin{aligned} \mathbf{J} &= \frac{he}{4\pi im} (\psi \text{ grad } \psi^* - \psi^* \text{ grad } \psi) - \frac{e^2}{mc} \psi \psi^* \mathbf{A} \\ \rho &= \frac{he}{4\pi im c^2} \left( \psi^* \frac{\partial \psi}{\partial t} - \psi \frac{\partial \psi^*}{\partial t} \right) - \frac{e^2}{mc^2} \psi \psi^* \phi \end{aligned} \right\}. \quad (32)$$

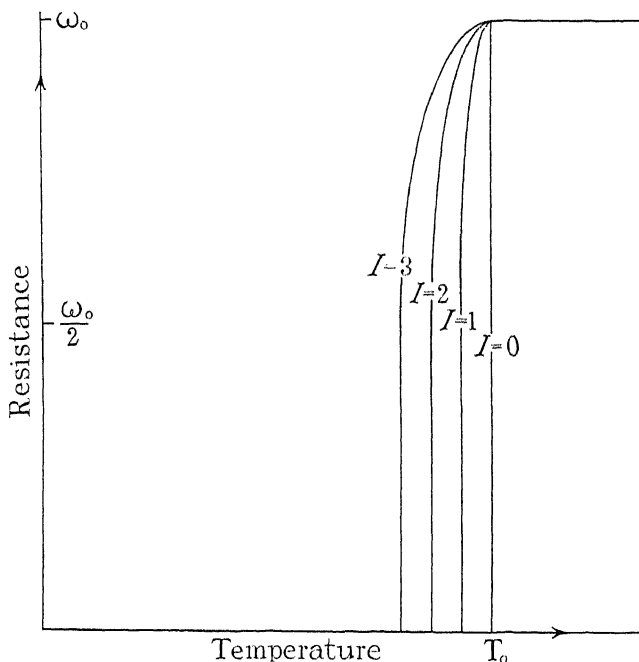


FIG. 1.—The transition curve for different values of the current  $I$ .  $I$  in arbitrary units

Let  $\psi$  be the wave function of a single electron in the self-consistent field of the others; then in Gordon's formulation  $\psi \psi^*$  gives at least approximately the value of the statistical expectation for an electron at every point of the space. Summing over all electrons  $\Sigma \psi \psi^*$  gives the number of electrons per  $\text{cm}^3$ , varying about its average only in very small spaces.

† 'Comm. Phys. Lab. Leiden,' No. 214c.

Therefore macroscopically, since  $\Lambda = \frac{m}{ne^2}$ , the last terms in (32) are equal to  $\frac{1}{\Lambda c} \mathbf{A}$  and  $\frac{1}{\Lambda c^2} \phi$  respectively.

Using the original eigenfunctions of the free electrons in the metal the terms in brackets in (32) would vanish by summing over all electrons and (32) would become exactly identical with (16). This follows for  $\mathbf{J}$  from reasons of symmetry, for  $\rho$  from the compensating presence of the positive ions. But actually the eigenfunctions of the electrons in the metal are disturbed by the magnetic field and therefore the terms in brackets in (32) do not vanish. Moreover, they compensate almost completely the terms containing the potentials and only a very small diamagnetism results, the so-called Landau-Peierls diamagnetism.<sup>†</sup>

But now suppose the electrons to be coupled by some form of interaction. Then the lowest state of the electrons may be separated by a finite distance from the excited ones and the disturbing influence of the field on the eigenfunctions can only be appreciable if it is of the same order of magnitude as the coupling forces. As long as the magnetic field is sufficiently weak there should not be more than a negligible disturbance of the eigenfunctions, and therefore equations (32) would be approximately identical with (16). With increasing magnetic field the very highly degenerate excited states, which are partly paramagnetic, split up. Some of them decrease and, being already at a lower temperature than would be possible without field, suddenly become occupied and supraconductivity disappears. Of course these last remarks are to be taken as indicating roughly a programme which requires a detailed quantum mechanical investigation.

In conclusion we should like to express our thanks to Professor F. A. Lindemann, F.R.S., for his kind hospitality at the Clarendon Laboratory and for his interest in our work. We should also like to thank Imperial Chemical Industries whose generous assistance to one of us has enabled us to undertake this work.

#### SUMMARY

A new formulation of the dependence of current on field in supraconductors is established.

$$\mathbf{E} = \Lambda (\dot{\mathbf{J}} + c^2 \text{grad } \rho) \tag{10}$$

$$\mathbf{H} = - \Lambda c \text{curl } \mathbf{J}. \tag{6}$$

<sup>†</sup> Landau, 'Z. Physik,' vol. 64, p. 629 (1930); Peierls, 'Z. Physik,' vol. 80, p. 763 (1933).

A characteristic feature of this formulation is the possibility of electrostatic fields existing in superconductors. In contrast to the customary conception that in a superconductor a current may persist without being maintained by an electric or magnetic field, the current is characterized as a kind of diamagnetic volume current, the existence of which is necessarily dependent upon the presence of a magnetic field. That magnetic field itself may be produced reciprocally by the current (§ 1).

The law of conservation of energy is discussed. The production of Joule-heat is localized on the surface of the superconductor, where the current enters and leaves it (§ 2).

As examples the field, boundary surfaces, and distribution of currents in a superconducting sphere and a wire are treated and the transition curve is calculated (§§ 3, 4).

## Shear Waves through the Earth's Core

By L. BASTINGS, M.Sc., F.Inst.P., Associate in Seismology, Dominion Observatory, Wellington, N.Z.

(Communicated by Lord Rutherford, O.M., F.R.S.—Received October 27, 1934)

### 1—GROWTH OF THE CORE THEORY

Seismological evidence of a central core to the earth was first pointed out by Oldham in 1906.\* From his analysis of travel-time data regarding longitudinal (P) and transverse (S) waves observed at great distances from earthquake epicentres, he concluded that at a depth equal to about three-fifths of the radius there occurs a transition to material possessing radically different physical properties from that external to this boundary.

With the aid of more extensive data assembled by Turner† and others, the problem was later re-examined independently by Knott‡ and by Gutenberg.§ The latter concluded that at a depth of 2900 km the

\* 'Quart. J. Geol. Soc.,' vol. 62, p. 456 (1906).

† "The Large Earthquakes of 1913," 'Rep. Brit. Ass.' (1917).

‡ 'Proc. Roy. Soc. Edin.,' vol. 39, p. 157 (1919).

§ 'Nachr. Ges. Wiss. Göttingen,' p. 1 (1914). This paper was probably not available to Knott in 1918. It has long been out of print, and no copy is available in N.Z. I am indebted to Professor Gutenberg for the loan of his own copy.

velocity of P waves suddenly decreases from over 13 km per sec to about  $8\frac{1}{2}$ . The theory involves the appearance of a delayed P wave at epicentral distances beyond  $143^\circ$ , and the chief characteristics predicted for this wave have been amply verified by Gutenberg,\* by Macelwane† and by Lehmann.‡ Also Wadati§ has lately confirmed the earlier estimates of the core depth from observations on  $S_cS$ . Mean density considerations suggest that this core is metallic; and the magnetic properties of the earth are consistent with a nickel-iron composition resembling that found in many meteors.

Gutenberg (*loc. cit.*) in 1914 carried his deductions a stage further. Assuming that shear waves would penetrate the core and maintain a velocity ratio to the P waves of 1 to 1.8, as travel-times in the mantle

TABLE I

$i_0$	$\Delta$	Times		$i_0$	$\Delta$	Times	
°	°	m	s	°	°	m	s
17.7	$184\frac{1}{2}$	39	22	10	144	35	47
17	$160\frac{1}{2}$	37	56	8	146	35	53
16	151	36	53	6	151	36	06
15	147	36	16	4	159	36	24
14	$145\frac{1}{2}$	35	58	2	169	36	36
12	$143\frac{1}{2}$	35	42	0	180	36	44

indicate, he predicted characteristics for these shear waves very similar to those of the P waves. Numerical details are indicated in Table I, adapted from the original paper.

$i_0$  is the angle between the ray at the focus and the downward normal. the ray  $i_0 = 0^\circ$  goes straight through without refraction. For  $i_0 = 12^\circ$ ,  $\Delta$  is a minimum ( $143\frac{1}{2}^\circ$ ), and for larger angles, the travel-time curve follows a later branch. The ray  $i_0 = 17.7^\circ$  grazes the core, and after refraction arrives at the maximum distance of  $184\frac{1}{2}^\circ$ . In consequence of the concentration of energy in the neighbourhood of the turning-point, unusually large amplitudes are to be expected near  $143\frac{1}{2}^\circ$ ; while at shorter distances, the phase should be entirely absent—the earth's surface being, as it were, in the shadow of the core for this movement.

\* 'Abh. senckenb. naturf. Ges.,' vol. 40, p. 57 (1925).

† 'Beitr. Geophys.,' vol. 28, p. 165 (1930).

‡ 'Beitr. Geophys.,' vol. 26, p. 402 (1930).

§ 'Proc. imp. Acad. Japan,' vol. 9, p. 494 (1933).

## 2—A REVISED NOMENCLATURE

Gutenberg originally referred to the P wave through the core by the symbol  $P_4P_4P$ , later by  $P_cP_cP$ , and more recently by  $P'$ . Turner\* substituted  $[P]$ ; and Macelwane† introduced numerical suffixes to distinguish the two branches, thus:— $P'_1$  and  $P'_2$ . Recently, the Seismological Committee of the British Association‡ has given its approval to the use of K instead of  $P_c$  for P waves through the core. Thus  $PKP = P_cP_cP = P'$ . One objection to the dashed notation is that the dash has received wide support to indicate phases registered beyond  $180^\circ$ . And

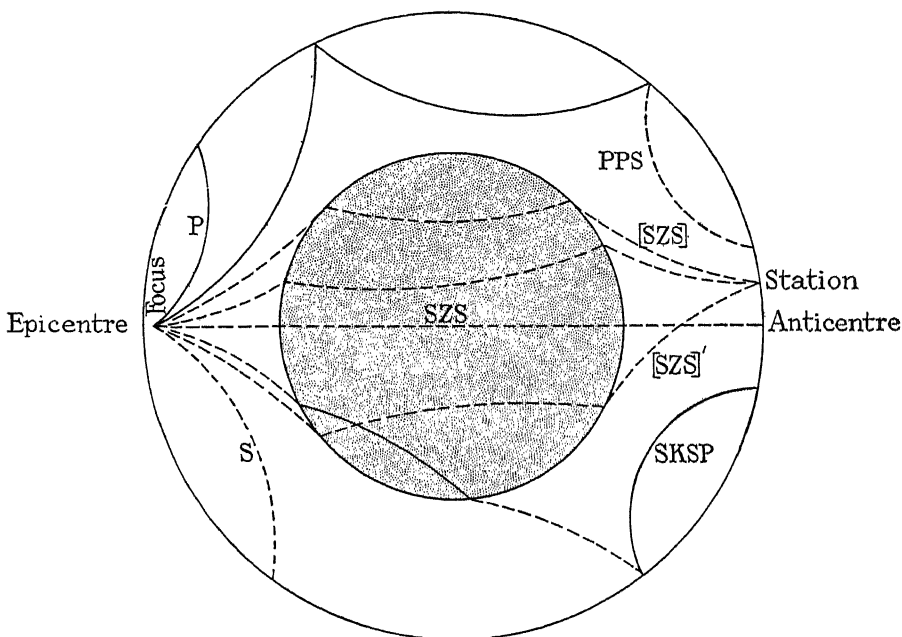


FIG. 1—Diagrammatic view of paths of various core waves. —, compressional waves; ----, shear waves.

the desirability of using it in this connection will emerge shortly. I have suggested elsewhere§ the use of the square bracket to indicate the later branch of such phases as PKP, thus:— $[PKP]$  to  $180^\circ$  and  $[PKP]'$  beyond.

The shear waves have similarly been represented by  $S_4S_4S$ ,  $S'$ , etc. In order to maintain a uniform notation, it is here proposed to employ Z

\* 'Int. seis. Summ.,' May, 1923.

† 'Beitr. Geophys.,' vol. 28, p. 165 (1930).

‡ 'Rep. Brit. Ass.' (1933).

§ 'Nature,' vol. 134, p. 216 (1934).

for shear waves through the core: so that  $S'$  becomes SZS. The later branch will similarly be referred to as [SZS] within  $180^\circ$  and [SZS]' beyond. In fig. 1 the paths of these and other waves mentioned later are represented diagrammatically.

### 3—THE LIQUID CORE HYPOTHESIS

For many years subsequent to the publication of Gutenberg's paper, no observations were discovered to agree with his predictions for SZS, despite the repeated appearance of PKP. And gradually the conviction grew among seismologists that their absence pointed to the core material being liquid—or at least sufficiently fluid to damp out transverse vibrations before they could penetrate it. At the same time were emerging other lines of evidence which pointed to a similar conclusion. Jeffreys\* showed that the magnitude of the lunar tides in the earth implies a lower average rigidity than is indicated by the seismological evidence. But he pointed out that the data can be reconciled by assuming the high rigidity to be confined to the mantle, with a vanishingly small or zero rigidity for the core. This takes for granted, of course, that rigidity has the same meaning for short-period waves as for stresses of much longer period.

The liquid core hypothesis is also consistent with the fluid theory of the origin of the earth, as generally accepted. Taking the age of the earth to be of the order of  $10^9$  years, and temperature gradients and other factors governing cooling as indicated by surface evidence, it appears highly probable that solidification has not yet proceeded as far as the deep interior.

Some or all of these arguments have brought general support for the fluid core hypothesis from such varied authorities as Turner,† Gregory‡ and Daly.§

### 4—FIRST EVIDENCE FOR A RIGID CORE

One important seismological contribution of a positive nature had, however, appeared in the meantime. Macelwane|| in 1925 announced the discovery of evidence from the S. Pacific Earthquake of June 26,

\* 'Mon. Not. R. astr. Soc., geophys. Suppl.,' vol. 1, p. 371 (1926).

† 'Mon. Not. R. astr. Soc., geophys. Suppl.,' vol. 1, p. 425 (1926).

‡ "Earthquakes and Volcanoes," p. 76 (Benn) 1929.

§ 'Bull. Geol. Soc. Amer.,' vol. 44, p. 243 (1933).

|| 'Phys. Rev.,' vol. 25, p. 721 (1925); 'Bull. Geol. Soc. Amer.,' vol. 27, p. 209 (1926).

1924, for shear waves transmitted through the core. Later\* he found the phase to be missing in the records from European stations considered by him to be favourably situated. Eventually he published his complete evidence,† consisting of 15 values for SZS and 21 for [SZS] between  $146.7^{\circ}$  and  $167.3^{\circ}$ . The difference between observed and predicted values are mostly negative for SZS and positive for [SZS]. They are also very varied in magnitude, so that many of them must be more than 20 seconds removed from the mean line through them. Further, he found no evidence for a focal zone. Summarizing the investigation in 1930, he concludes:—"In 1925 the writer was led, by the discovery of these S' waves in the shadow zone and beyond it, to state that they were shear waves transmitted through the core of the earth . . . However, the failure to find a pronounced focal zone and the meagre energy of the waves near the antipodes now give him pause."

Imamura‡ has lately recorded a large amplitude movement at Tokyo at an epicentral distance of  $160.4^{\circ}$ , which he identifies with SZS. But the evidence offered by Macelwane and by Imamura in support of a rigid core has not brought general conviction.§

#### 5—NEW EVIDENCE FROM A NEW ZEALAND EARTHQUAKE

The critical evidence for which Macelwane and others have sought in vain appears to be present in European records of the Buller (New Zealand) Earthquake of 1929. I have elsewhere|| discussed some aspects of this earthquake, and placed its epicentre at  $41^{\circ} 43' \text{ S.}$ ,  $172^{\circ} 15' \text{ E.}$ , and the time at the epicentre June, 16d 22h 47m 35s G.M.T.¶

Before presenting the details of the record readings, it may be advisable to point out that among the numerous movements recorded at great distances, two of special prominence occur at about the time predicted by Gutenberg for SZS, viz., SKSP and PPS, the former a couple of minutes before SZS and the latter very shorter after [SZS].

Both phases appear in the records of the present earthquake at nearly thirty stations, and in both cases the points lie closely on the mean curve

\* 'Bull. Seis. Soc. Amer.,' vol. 19, p. 135 (1929).

† 'Beitr. Geophys.,' vol. 28, p. 165 (1930).

‡ 'Proc. Imp. Acad. Japan,' vol. 8, p. 354 (1932).

§ See e.g., Daly, *loc. cit.*; Byerly, 'Bull. nat. Res. Council. Wash.,' No. 90, p. 179 (1933).

|| 'N.Z. J. Sci. Tech.,' vol. 15, p. 128 (1933).

¶ Lehmann has also discussed several aspects of this earthquake in some detail, *loc. cit.*

through them. Their prominence renders the identification of any feeble new movements in the neighbourhood difficult; and any other impulse comparable in magnitude with them must be regarded as of outstanding importance. A weak movement at about the expected time for SZS is readable on both components of a Wiechert instrument at Ksara,  $145^{\circ}0'$ , fig. 2. It is a little too early for PPS, although the next movement to emerge is a little late for this phase. The large amplitudes for which we are searching is certainly absent here.

At the next station, Abisco ( $149^{\circ}9'$ ), PPS arrives at the expected time, and is preceded by a clearly readable movement on all three components

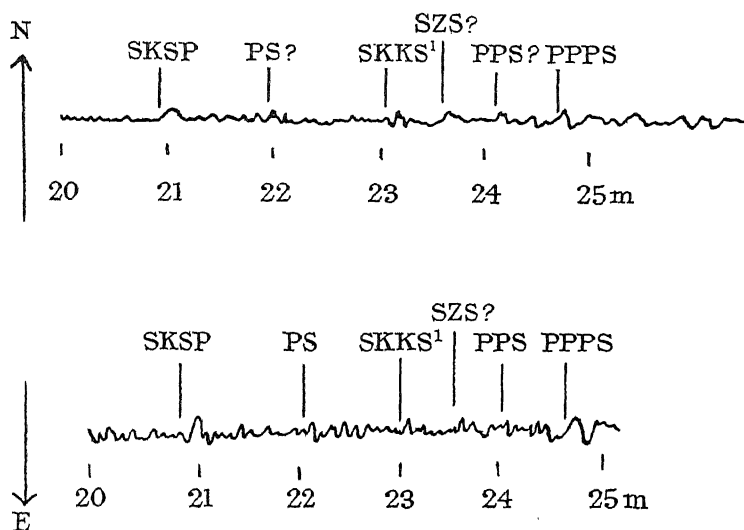


FIG. 2—Ksara,  $\Delta = 145^{\circ}0'$ ;  $\Delta t = - 8$  sec

of a Galitzin seismograph. The north component emergence is specially prominent, and carries the largest amplitude so far on the record—excepting only the phases SKSP and PP, which are both very prominent movements on all records at this distance. Fig. 3 shows clearly the relationship of the phase to PPS and to the prior movement (which may be PS).

Next in order of distance comes Sebastopol,  $150^{\circ}1'$ , the International Seismological Summary for which lists only the first phase to appear and one other, a movement interpreted in the Summary as “L.” It is obviously prominent at this station, and falls into line with neighbouring readings for SZS.

At Pulkovo,  $150^{\circ}6'$ , the phase is very prominent on N. and E. Galitzins. It is marked by the Station as “ $i_2$ ” on the E. record, and is listed without



identification in the brief accompanying bulletin. The double amplitude on the record is 66 mm—almost the largest movement on the diagram prior to the arrival of the long waves. It completely obliterates the succeeding PPS. The turning-points only are visible for the first few excursions of the light spot in the contact copy supplied, and are reproduced as they appear in fig. 4. On the N. component, the phase emerges

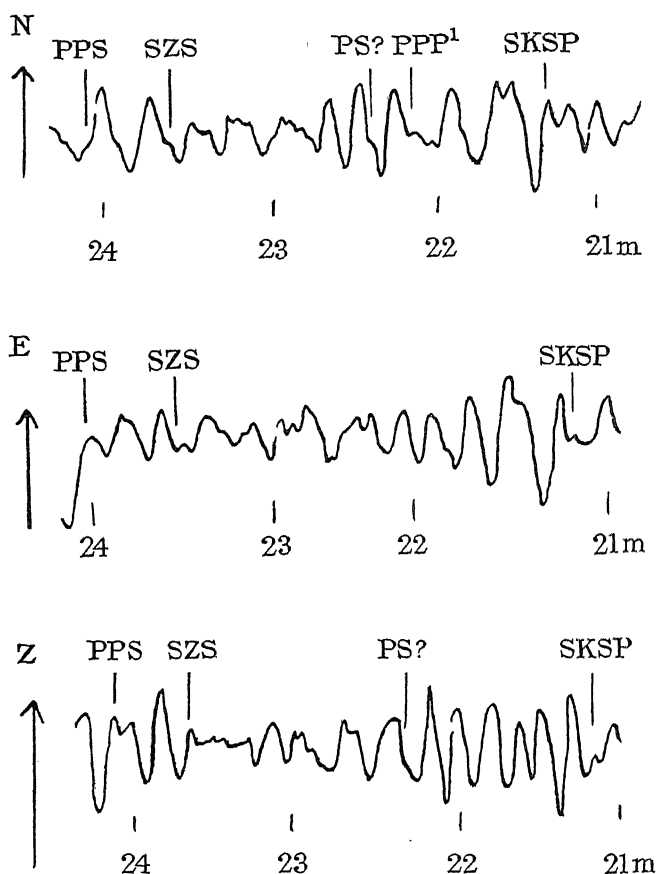


FIG. 3—Abisco,  $\Delta = 149.9^\circ$ ;  $\Delta t = -6$  sec

out of the prior movement (PS?); its double amplitude is 26 mm, or about equal to that of the very prominent SKSP and considerably larger than the prominent PPS which follows. The Z component is unreadable about this time, owing to the overlay of subsequent lines which carry the long wave movements.

The next nearest station is Upsala,  $156.1^\circ$ , by which distance the phase has begun to subside into comparative insignificance, see fig. 5. And

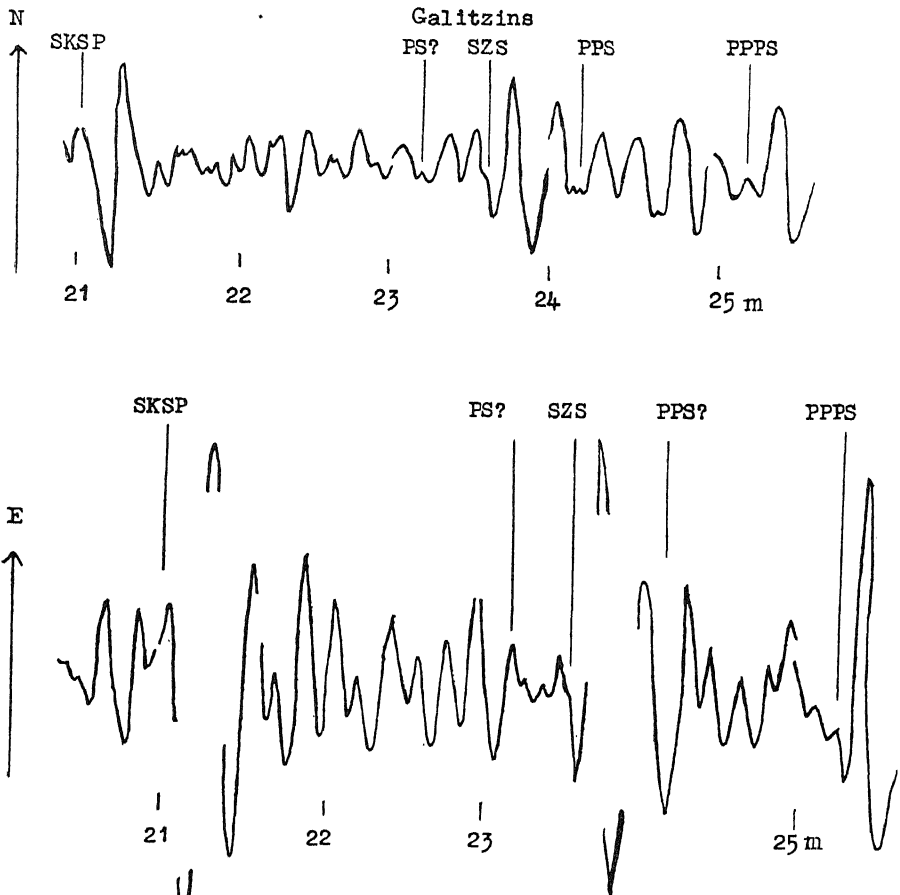


FIG. 4—Pulkovo,  $\Delta = 150.6^\circ$ ;  $\Delta t = + 14$  sec

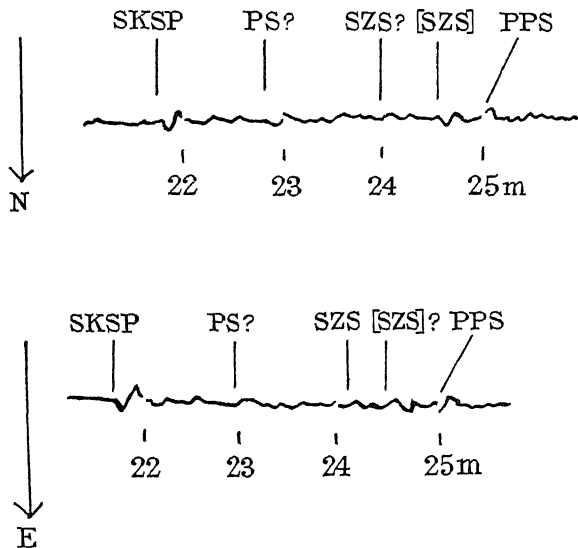


FIG. 5—Upsala,  $\Delta = 156.1^\circ$ ;  $\Delta t = + 3$  sec

thereafter it has been read without ambiguity only on sensitive instruments furnishing abundant detail. Ten reliable values have been secured between  $160^\circ$  and  $175^\circ$ , and one bulletin entry has been correlated with the phase.

In reading these records, weights were assigned to the arrival-times according to the apparent reliability of the emergences and the number and quality of the records bearing them. These weights were incorporated in a least square analysis of the data, leading to the following equation for the mean line through the points:—

$$T = 23\text{h } 24\text{m } 05\text{ s} + (\Delta - 165^\circ) \times 1.6\text{s.}$$

The mean deviation of the 16 points from the line is under 8 seconds. Combining these arrival-times with the epicentral time already quoted, we obtain travel-times which agree with the values interpolated from Gutenberg's table to within less than 15 seconds in every case. The lower curves in fig. 6 show Gutenberg's points joined by a broken line, along with the values here presented.

The second branch, [SZS], first emerges at Upsala,  $156.1^\circ$ , from which station comes the first detailed data beyond the focal zone revealed above. The Wiechert instruments here are of small magnification, and the readings gain significance only when taken in conjunction with those of later stations. Records from Sofia,  $157.1^\circ$ , Königsberg,  $157.3^\circ$ , and Belgrade,  $159.3^\circ$ , all show unmistakable signs of a new movement in this neighbourhood, and prior to PPS; though in none of these records is SZS readable. At Lund,  $160.6^\circ$ , and later, both movements are discernable; while at both Copenhagen,  $160.8^\circ$ , and Vienna,  $162.0^\circ$ , the second movement rises to considerable prominence, especially on the E. components, see figs. 7 and 8. From here onwards to  $175^\circ$ , 12 further clearly marked emergences of [SZS] have been logged, either with or without SZS—but always overshadowed by the closely following PPS, and the prominent SKSP somewhat earlier. At Dyce,  $164.1^\circ$ , the later branch appears to occur a second time, arriving by the major arc, fig. 9; and at six further stations, movements are readable which fit the extension of the line through the earlier [SZS] points. All three movements are very clearly shown on the N. component Galitzin at Uccle, fig. 10. It is to be observed that these later points all occur beyond the limiting distance indicated by Gutenberg.

The readings from  $164^\circ$  to  $196^\circ$  all closely conform to the line

$$T = 23\text{h } 25\text{m } 55\text{s} + (\Delta - 165^\circ) \times 5.3\text{s.}$$

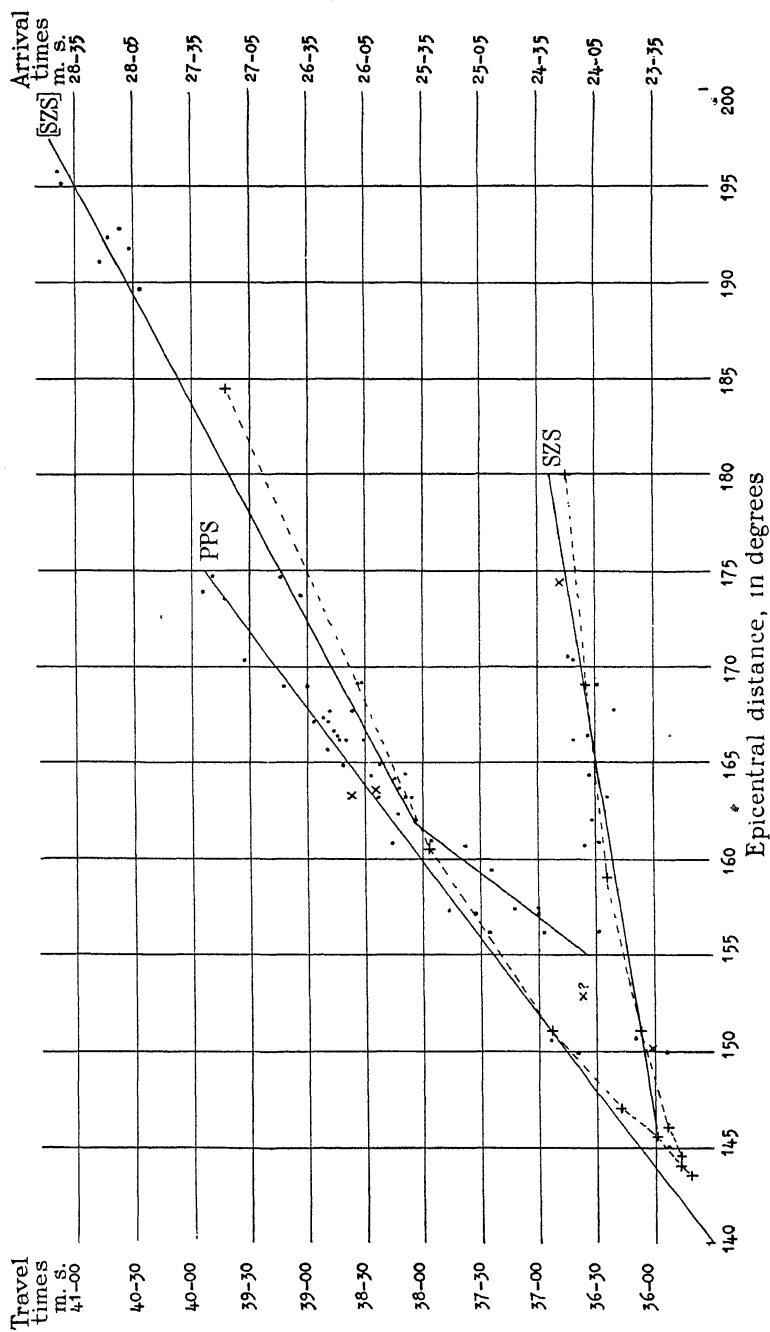


FIG. 6—SZS, [SZS], [SZS]' with PPS. +, Gutenberg, 1914; •, readings from bulletins, etc.

This agrees initially with Gutenberg to within a few seconds, but rises somewhat more steeply, so that the values differ by 16 seconds at  $180^\circ$ .

The first six points in [SZS] disagree with the prediction, and lie closely on a line

$$T = 23\text{h } 25\text{m } 15\text{s} + (\Delta - 160^\circ) \times 13\text{s},$$

### Galitzins

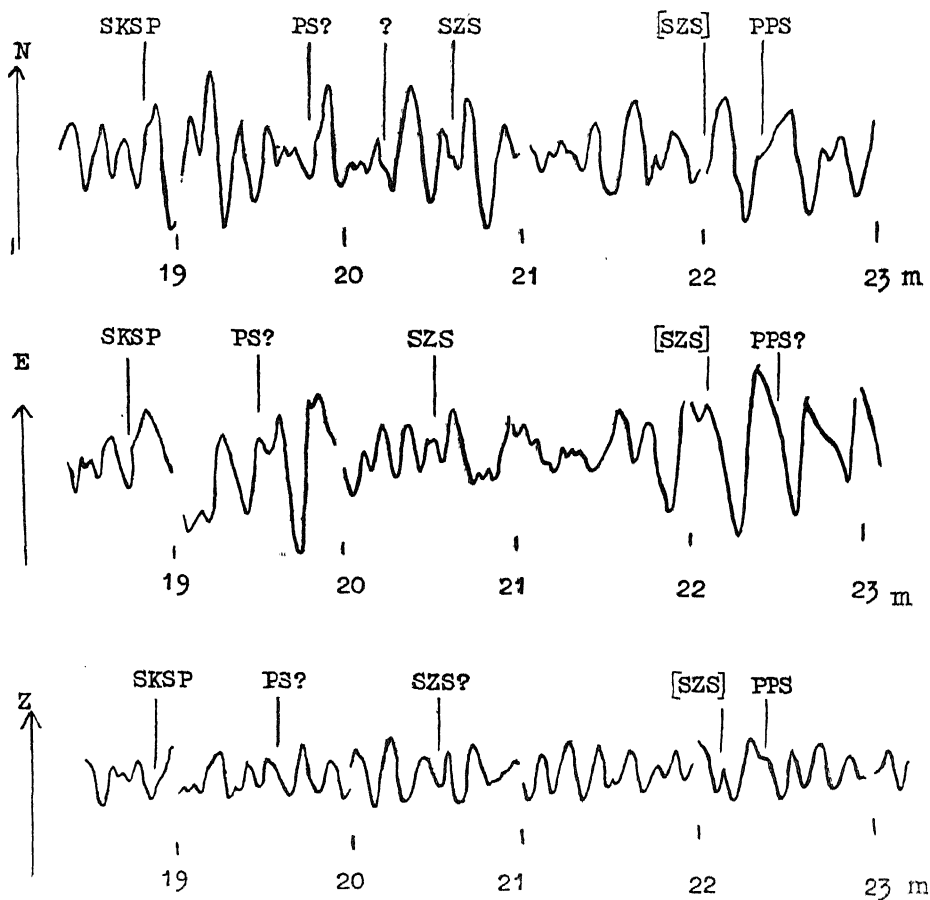


FIG. 7—Copenhagen,  $\Delta = 160.8^\circ$ ,  $\Delta t = + 3 \text{ min } 30 \text{ sec}$

which slopes much more steeply than the later portion. There are not sufficient stations between  $150^\circ$  and  $162^\circ$  to settle the shape of the curve there or its relationship to the SZS line. But the data, taken in conjunction with the large amplitudes in the  $150^\circ$  area, suggest that the focal zone and the second branch occur a little beyond the distance predicted by Guten-

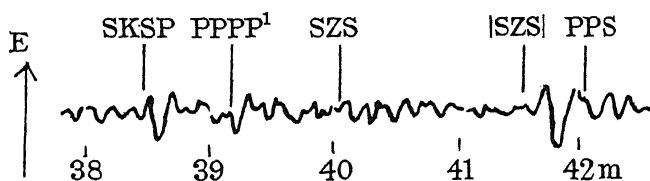
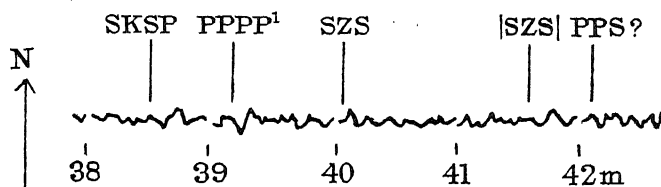


FIG. 8—Vienna,  $\Delta = 162.0^\circ$ ,  $\Delta t = -15$  min 56 sec

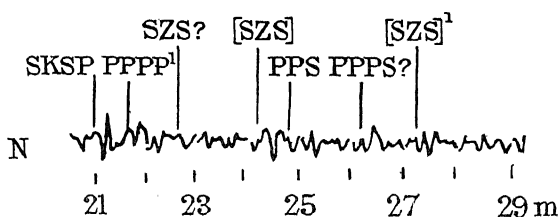


FIG. 9—Dyce,  $\Delta = 164.1^\circ$ ,  $\Delta t = +1$  min 33 sec

Galitzin.

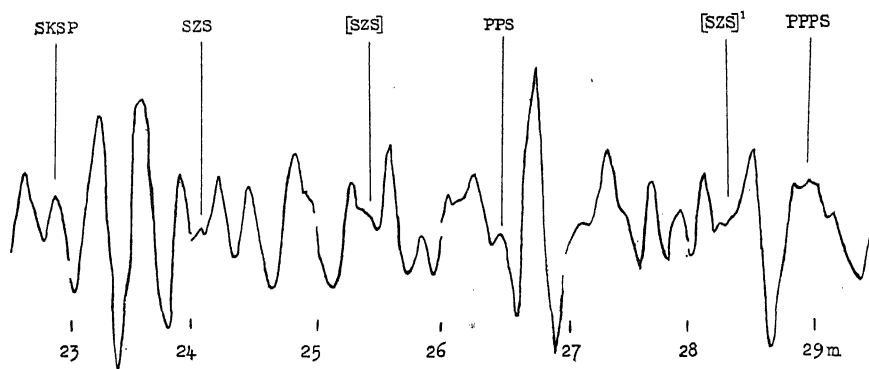


FIG. 10—Uccle,  $\Delta = 167.7^\circ$ ,  $\Delta t = -8$  sec

berg. This and the minor divergence in [SZS] and [SZS]' at the further distances would seem to demand minor detailed adjustments in the assumptions underlying the theory.

Table II gives a complete list of the stations whose records have provided data for the above analysis (stations in brackets supplied bulletins only). Where readings alter on more than one component, the arrival-times tabulated are weighted means. The weights assigned in the analysis to these mean times are also given, together with the differences ( $O - C$ ) between observed times and those calculated from the equations above.

Selecting now the travel-times for both branches at  $165^\circ$  (where they are most accurately delineated), and comparing them with the corresponding times for both branches of PKP, as read on the same collection of records, we have

$$\frac{T_{szs}}{T_{pkp}} = \frac{36\text{m } 30\text{s}}{20\text{m } 13\text{s}} = 1.80 \quad \text{and} \quad \frac{T_{[szs]}}{T_{[pkp]}} = \frac{38\text{m } 20\text{s}}{21\text{m } 10\text{s}} = 1.81.$$

These ratios agree most satisfactorily with the corresponding ratios, 1.79 to 1.84, for P and S arriving at various epicentral distances without penetrating the core; and indicated a value for Poisson's ratio for the core material approximately the same as for the mantle.

#### 7—PERIODS AND AMPLITUDES OF THE SHEAR WAVES

The periods or quasi-periods of the shear waves vary appreciably from station to station, being as low as 9 seconds and as high as 19. The average is  $11\frac{1}{2}$  for SZS and  $12\frac{1}{2}$  for [SZS]. There is no indication of the amplitudes being unduly enlarged by resonance—a point of special importance in assessing the value of the large movements—except on the vertical Galitzin at Abisco. Here the period of the movement is about  $11\frac{1}{2}$  seconds, and of the instrument 11.6. The prominence of the vertical movement in SZS at this station is no doubt due largely to this synchronism. The phase is not readable with certainty on any other vertical instrument in the range; which is to be expected of a transverse vibration arriving at the high vertical angles which our interpretation of the impulses would imply.

The amplitudes of these movements are in almost every case distinctly smaller than those of the corresponding P waves which have penetrated the core. Even in their respective focal zones—as far as the present evidence goes—the shear waves are distinctly less prominent. The focal zone for PKP has been definitely shown by Gutenberg and

TABLE II—ARRIVAL-TIMES IN MINUTES AND SECONDS, AFTER 23H G.M.T.

Station	$\Delta$ °	SZS			[SZS]			[SZS]'		
		Time m s	Wt	O - C s	Time m s	Wt	O - C s	Time m s	Wt	O - C s
Ksara .....	145.0	23 27	1	-6	—	—	—	—	—	—
Abisco .....	149.9	23 28	3	-13	—	—	—	—	—	—
(Sebastopol) .....	150.1	23.6	1	-5	—	—	—	—	—	—
Pulkovo .....	150.6	23 45	3	+3	—	—	—	—	—	—
Upsala .....	156.1	24 04	1	+13	24 32	2	+8	—	—	—
Sofia .....	157.1	—	—	—	24 35	1	-2	—	—	—
Königsberg .....	157.3	—	—	—	24 48	3	+8	—	—	—
Belgrade .....	159.3	—	—	—	25 00	1	-6	—	—	—
Lund .....	160.8	24 11	3	+13	25 13	3	-10	—	—	—
Copenhagen .....	160.8	24 04	2	+5	25 31	3	+6	—	—	—
Vienna .....	162.0	24 07	3	+7	25 39	3	+1	—	—	—
Leipzig .....	163.2	—	—	—	25 41	1	+2	—	—	—
Hamburg .....	163.2	24 04	1	+3	25 44	2	+5	—	—	—
Cheb .....	163.7	—	—	—	25 47	1	±0	—	—	—
Dyce .....	164.1	—	—	—	25 49	1	-1	28 43	1	+4
Göttingen .....	164.4	24 08	1	+4	25 44	1	-7	—	—	—
Munich .....	164.9	—	—	—	25 57	1	+3	28 42	2	+8
Heidelberg .....	166.2	—	—	—	26.1	1	+6	—	—	—
Hohenheim .....	166.2	24 16	1	+9	—	—	—	—	—	—
De Bilt .....	166.4	24 09	2	+2	—	—	—	—	—	—
Zürich .....	167.1	—	—	—	—	—	—	—	—	—
Uccle .....	167.7	23 55	3	-14	26 11	—	—	28 11	1	-12
(Moncalieri) .....	168.3	—	—	—	—	—	—	28 18	2	-2
Kew .....	169.0	24 04	1	-7	—	—	—	28 06	1	-11
Oxford .....	169.0	—	—	—	26 09	3	-6	—	—	—
Algiers .....	170.3	24 16	1	+3	26 07	3	-8	28 21	1	+8
Tortosa .....	173.7	—	—	—	—	—	—	28 01	2	+13
(Malaga) .....	174.4	24 23	1	+3	26 38	2	-2	—	—	—
San Fernando .....	174.6	—	—	—	26.8	1	+3	—	—	—



others to occur at about  $143^\circ$ . In the present earthquake, no records are available between  $135^\circ$  and  $145^\circ$ . In the Ksara records at the latter distance, PKP is prominent, and [PKP] is the largest movement prior to the long waves, being approximately 50% larger than SKSP, with which the shear wave amplitudes have here been repeatedly compared.

This relationship between the two classes of movements after penetrating the core is in marked contrast to their relative importance at shorter distances, where their trajectories have been confined entirely to the mantle. This fact is in harmony with the recognized prominence of  $S_cS$  as compared with  $P_cP$  at short distances; and points to a much larger proportion of the energy of the S wave being reflected at the core boundary than in the case of the P wave.

#### 7—CONCLUSION

The recurrence of these movements in another earthquake, the identification of the two branches, the general agreement of the travel-times with Gutenberg's calculations, the evidence from Poisson's ratio, and above all, the discovery of the large amplitudes in the  $150^\circ$  neighbourhood appear to establish the possibility of shear waves penetrating the central core. The core material thus seems to possess, at least for shearing stresses of short period, a rigidity such as it is usual to associate only with a solid.

It is not difficult to see why the discovery has eluded investigators for so long. The confirmation of the theory could be derived only from a major earthquake occurring in a locality permitting abundant recording in the  $150^\circ$ – $160^\circ$  neighbourhood, and also having its epicentre and time at the origin accurately determinable. Moreover, the focal zone is probably narrow, and may easily be missed, if not punctuated by stations with sensitive and reliable instruments. Beyond this zone, the movements are not conspicuous, and being sandwiched between large amplitudes throughout the range, they are liable to be overlooked. It seems probable that the present earthquake is the first in seismological history in which these favourable conditions have been even approximated to; and until seismological stations are much more widely scattered throughout the world, it may be difficult to find a counterpart to this one. It says much for the quality of Gutenberg's original material and for the accuracy of his analysis that his theory, after waiting twenty years for adequate confirmation, should thus prove to be in such good agreement with the discovered facts.

My thanks are due to the Directors of the various seismological stations who have sent diagrams or bulletins; to the Editors of the International Summary for an advanced copy of the Summary for this earthquake; and to Dr. C. E. Adams, Dominion Seismologist, for placing all this material at my disposal and for proffering valued advice and encouragement throughout. It is intended to publish further aspects of this earthquake at a later date.

#### 8—SUMMARY

A detailed analysis of the travel-times for the waves arriving at great distances from a major earthquake led Gutenberg in 1914 to the conclusion that the interior of the earth contains a central core at a depth of about 2900 km. His predictions regarding the characteristics of compressional (P) waves transmitted through this core have been abundantly verified. But until lately, no signs have been forthcoming of the existence of distortional (S) waves that had penetrated this central mass. In consequence it has gradually come to be accepted that the core is in a fluid or semi-fluid state, and so is incapable of transmitting shear waves that reach its boundary. Jeffreys has deduced evidence from tidal theory indicating a similar lack of rigidity in the core, at least for long-period stresses.

Recently, fragmentary evidence has been published by Macelwane and by Imamura in support of the existence of shear waves transmitted through the core (S') and conforming to Gutenberg's predictions.

The present contribution is based on a detailed study of the European records of the 1929 Buller (N.Z.) earthquake, in which signs have been found of S' at 16 stations between 145° and 175° from the epicentre. Travel-times agree closely with Gutenberg's values, and in other respects the evidence conforms to his theory—the phase shows large amplitudes in the 150° neighbourhood, and later develops into two branches. The identification of the phase is further strengthened by the fact that PPS (which closely follows the later branch of S') is also distinguishable, and a separate curve has been plotted for it. A comparison between the travel-times for the two branches of S' with the corresponding times for the two branches of P' gives ratios in close agreement with the ratio for P and S waves which have not penetrated the core. The rigidity of the core, at least for vibrations of short period, thus seems to be definitely established.

---

## The Accommodation Coefficient and the Evaporation Coefficient of Water

By T. ALTY, D.Sc. and C. A. MACKAY, Ph.D., University of Saskatchewan, Canada

(Communicated by R. H. Fowler, F.R.S.—Received October 30, 1934)

### INTRODUCTION

Previous experiments\* have already indicated that the maximum rate of evaporation of water into a vacuum is not so great as would be expected theoretically. The ratio of the experimental to the theoretical rate is defined as the evaporation coefficient  $f$  and has been found to have a value of about 0.04 for pure water at temperatures about 0° C. This result would indicate that, of the vapour molecules striking the liquid surface, about 96% must return to the vapour without entering the liquid. It is therefore of interest to enquire whether these vapour molecules attain temperature equilibrium with the surface or rebound at once before this equilibrium can be established. In the present paper experiments are described in which vapour molecules are incident on a liquid surface which is at a temperature lower than that of the vapour itself and the energy transferred to the surface by the vapour molecules is measured. If  $\alpha$ , the accommodation coefficient, is defined as usual as the ratio of the energy actually transferred to the maximum possible transfer, it is found that for water at 10° C—

$$\alpha = 1.0$$

$$f = 0.036$$

so that, while only a very small fraction of the vapour molecules enter the liquid, all of them reach temperature equilibrium with the surface before re-evaporating into the vapour.

### METHOD

If a drop of water is allowed to form on a glass tip in a vessel maintained at a pressure ( $p$ ) which is lower than the saturated vapour pressure corresponding to the temperature of the drop, steady evaporation takes place from the surface of the latter throughout the period of its formation.

\* Alty, 'Phil. Mag.', vol. 15, p. 82 (1933).

This evaporation cools the surface. When the drop is fully formed it falls from the tip and may be collected and the drop weight determined. The surface tension can be deduced therefrom and hence the surface temperature of the evaporating drop and the saturated vapour at this temperature may be obtained. This data makes possible the direct calculation of  $f$  as follows.

If the temperature is sufficiently low and therefore the saturated vapour pressure not too great, the rate at which molecules leave the liquid will not be affected appreciably by the presence of the surrounding vapour. Further, the rate of transfer of molecules from a liquid to its saturated vapour must be equal to the rate from the vapour to the liquid so that

$$\begin{aligned}
 & \text{the number of molecules leaving the liquid at temperature } T \text{ and} \\
 & \text{entering a vacuum per sec} \\
 = & \text{the number leaving the liquid and entering the saturated vapour} \\
 & \text{at temperature } T \text{ per sec} \\
 = & \text{the number leaving the saturated vapour and entering the liquid} \\
 = & \text{the number striking the liquid surface} \times f \\
 = & \frac{1}{4}Ncf \text{ per sq cm, if } N \text{ is the number of vapour molecules per cc} \\
 & \text{and } c \text{ is their average velocity.}
 \end{aligned}$$

Thus if  $A$  is the area of the drop surface at time  $t$ , the total mass evaporating into a vacuum during the formation of the drop will be

$$\begin{aligned}
 m &= \frac{1}{4}Ncf \int_0^{t_0} A dt \text{ gm} \\
 &= 0.2439 \frac{P_s}{\sqrt{T_s}} \cdot f \cdot \int_0^{t_0} A dt \text{ gm}
 \end{aligned}$$

if the saturated vapour pressure ( $P_s$ ) at the temperature ( $T_s$ ) of the drop surface is expressed in millimetres of mercury;  $\int_0^{t_0} A dt$  is given in square centimetres per second, and  $t_0$  is the total time of formation of the drop in seconds.

When the evaporation takes place into a space at a pressure  $p$  instead of into a vacuum, some molecules return to the liquid and the net amount of evaporation will be

$$\bar{m} = 0.2439 \frac{P_s - p}{\sqrt{T_s}} f \int_0^{t_0} A dt. \quad (1)$$

The mass  $\bar{m}$  may be equated to the mass actually evaporated from the drop. This may be determined experimentally as the difference between

the drop weight and the mass of water supplied to the drop during its formation. When the experimental values of the different quantities are inserted in equation (1), the value of the evaporation coefficient  $f$  may be derived at once.

Suppose now that the water supplied to the drop enters it at a known temperature  $T_b$ . Then it appears that the drop may acquire heat in three ways, viz. :—

- (1) from the warm water entering the drop ;
- (2) by conduction of heat along the glass tip ;
- (3) from the gas surrounding the drop (since this gas will be at a temperature higher than that of the evaporating surface).

Let these three heat quantities be  $W_1, W_2, W_3$  cal. Then the total amount of heat supplied to any drop must be equal to the total amount leaving the tip during the life time of the drop, *i.e.*, to the sum of the latent heat of vaporization required by the evaporating liquid and the amount of heat carried away by the falling drop itself. Hence if  $\bar{m}$  gm evaporates from the drop and  $M$  gm is the total mass of water entering it, we must have

$$W_1 + W_2 + W_3 = \bar{m}L + (M - \bar{m}) T_a \quad (2)$$

if  $L_T$  is the latent heat of vaporization at  $T^\circ \text{C}$  and  $T_a^\circ \text{C}$  is the mean temperature of the falling drop.

But  $W_1 = MT_b$ , and  $W_2$  may be calculated at once from the dimensions of the tip so that

$$W_3 = \bar{m}L_{T_s} + (M - \bar{m}) T_a - MT_b - W_2.$$

But  $W_3 =$  heat supplied by the vapour striking the surface = mass of gas striking the surface  $\times$  specific heat at constant pressure  $\times (T_g - T_s) \times \alpha$  if  $T_g$  is the temperature of the vapour at a distance of one mean free path from the drop surface.

Therefore

$$W_3 = 0.2439 \frac{p}{\sqrt{T_g}} \int_0^{t_0} A dt \cdot C_p \cdot (T_g - T_s) \cdot \alpha,$$

or, equating the two values of  $W_3$ , we have

$$\alpha = \frac{\bar{m}L_{T_s} + (M - \bar{m}) T_a - MT_b - W_2}{0.2439 \frac{p}{\sqrt{T_g}} \int_0^{t_0} A dt \cdot C_p (T_g - T_s)} \quad (3)$$

This is the expression used in the calculation of  $\alpha$ .

## EXPERIMENTAL

In the earlier work, water was used at temperatures about  $0^{\circ}\text{C}$  and at these temperatures the amount of evaporation from a drop is not very large (about 4 mg). It is clear that, if this evaporation could be increased, the accuracy of the experiment would also be increased considerably. This increase in evaporation is particularly necessary for the determination of  $\alpha$ , as equation (3) reduces to the ratio of two rather small quantities if  $\bar{m}$  is small. If, however,  $\bar{m}$  is large, it is possible to make a more reliable estimate of  $\alpha$ .

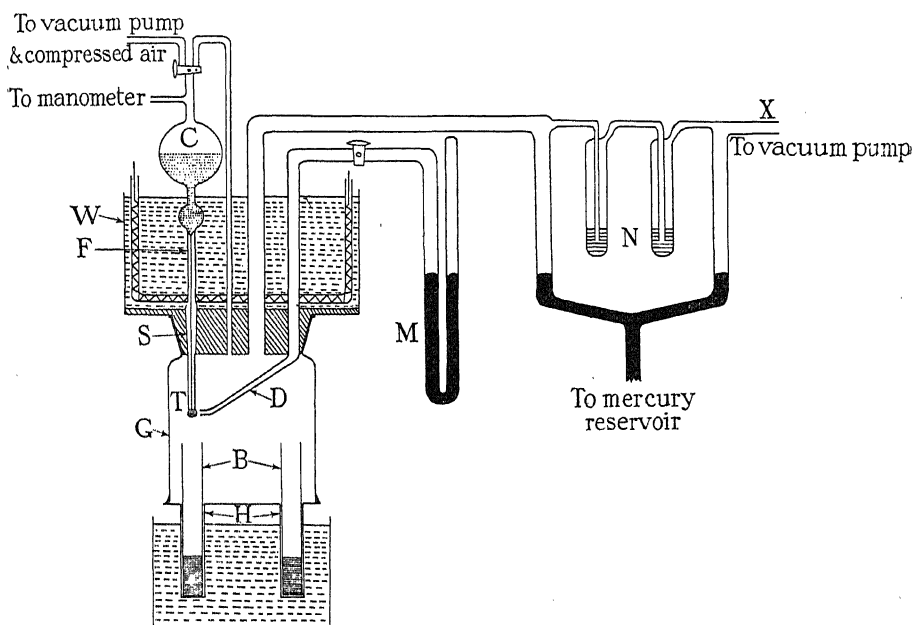


FIG. 1

For these reasons the earlier apparatus was modified in several particulars and the essential features of the new apparatus are shown in fig. 1. Pure water is stored in the container C and passes through the fine capillary F to the tip T on which the drop is formed. The glass vessel G is connected at X to a high speed oil pump which keeps the pressure in G sufficiently low. The pressure in this vessel is measured by means of a travelling microscope and the manometer M. The general method of conducting an experiment was described in the earlier paper (*loc. cit.*) and will not be repeated.

The simplest method of increasing the amount of evaporation is to raise the temperature of the water entering the drop and thus supply

more heat to the latter. For this purpose the capillary F was surrounded by an electrically controlled thermostat W, whose temperature could be varied up to  $80^{\circ}\text{C}$ . This increase in temperature introduced a new experimental difficulty. The drops were previously collected in small glass vessels containing a layer of light oil to prevent further evaporation after the drop entered the oil. When the warmer water was supplied to the drops, the temperature of the oil slowly increased during the course of an experiment until it was considerably above the temperature whose saturated vapour pressure was equal to the pressure in G. When this happened, the oil-water mixture boiled explosively and ruined the experiment. The glass vessels previously used were therefore replaced by the brass containers B. These fitted into brass cylinders H, soldered into a brass plate as shown in fig. 1, and good thermal contact was ensured by placing a little oil in H before introducing the containers B. The outer cylinders were immersed in a thermostat whose temperature was adjusted to be about  $1^{\circ}\text{C}$  higher than the temperature whose saturated vapour pressure was equal to the actual pressure in G. This temperature had to be fixed rather carefully. If it was too high, the oil exploded out of the container; if it was too low, water vapour condensed on to the cylinder and so made it impossible to determine the drop weight. On the other hand, once the correct temperature for any particular experiment was attained, the experiment could proceed without further trouble and with no sign of condensation. In order to avoid any errors from this source the brass containers were highly polished so that the first signs of condensation could be easily detected. With this arrangement it was possible to increase the number of drops collected in an experiment to about 50. In the earlier work no more than 10 could be collected safely; in most of the present experiments the number was 30 to 50.

By means of these modifications it was found that the amount of evaporation could be increased satisfactorily. Now, when a considerable mass of vapour leaves the drop per second, there must be rather violent convection currents in the container G and it was considered advisable to measure the pressure in G as near to the drop surface as possible. In the earlier work, the pressure was determined by a manometer attached to the stopper S but, with the larger rates of evaporation used in the present experiments, this type of measurement might lead to some error in  $p$ . Consequently the manometer was connected to the tube D whose open end was within 1 mm of the drop surface. The actual pressure in G was varied from experiment to experiment by means of the mercury bubblers N (glycerine was used for the low pressure work).

The driving pressure in C was measured by means of a cathetometer reading to 0.001 cm, and was corrected for the slight change in pressure during an experiment caused by the removal of some water from C. Condensation of warm water on the glass of the apparatus was prevented by winding the whole with resistance wire and keeping it at a higher temperature than that of the water being used.

## RESULTS

*Preliminary Experiments*—Before the determination of  $f$  and  $\alpha$  can be carried out a number of preliminary experiments must be completed.

A—Firstly the radius of the tip must be accurately known. This was measured directly and also deduced from the weight of very slowly formed drops at a known temperature at which the surface tension was already known. This method gives the effective tip radius and agreed well with that directly determined. The average of a number of measurements was

$$r = 0.17485 \text{ cm.}$$

From the weight of any given drop and the radius of the tip the surface tension can be determined and thence the surface temperature. For the particular tip used, the relation between drop weight and surface temperature could be represented by the equation

$$T_s = -20.52 + 9.8064 m - 0.1677 m^2. \quad (4)$$

B—The mass of liquid flowing through the capillary F at a temperature of 25.00° C was measured as a function of the driving pressure P (cm of Hg at 0° C) and could be represented by the equation

$$M = (9.450 P + 16.725) \text{ mg/min.} \quad (5)$$

The mass flowing at any other thermostat temperature may be derived from this by applying a correction for the change of viscosity.

C—Finally it is known that the weight of a falling drop only gives the true surface tension of a liquid when the drop is formed extremely slowly. When, as in these experiments, the drop is formed more rapidly, its mass is greater than normal and, before inserting the drop weight in equation (4), it must be corrected for this hydrodynamical effect. This is done by measuring the drop weight as a function of the rate of flow. If  $w$  is the drop weight when the rate of flow is  $M$  gm/min, and  $w_0$  the weight for a very small rate of flow, then the percentage increase in weight is  $\frac{100(w-w_0)}{w}$  =  $\Delta$  (say), and this quantity is shown in fig. 2 as a function of  $M$ . This



curve was obtained with water at  $20.9^{\circ}\text{C}$  and, of course, will be valid only at this temperature. In view of the fact that the thermostat temperature used in the experiments ranged from  $20^{\circ}\text{C}$  to  $70^{\circ}\text{C}$  it was no longer possible to ignore the temperature variation of  $\Delta$  as was previously done (*loc. cit.*). Instead  $\Delta$  was measured at a number of temperatures and the result is shown in fig. 3 in which the ratio  $(\Delta_x/\Delta_{20.9})$  is plotted against the temperature. From these two curves the measured drop weight may be corrected for the rate of flow before being inserted in equation (4) to give the surface temperature.

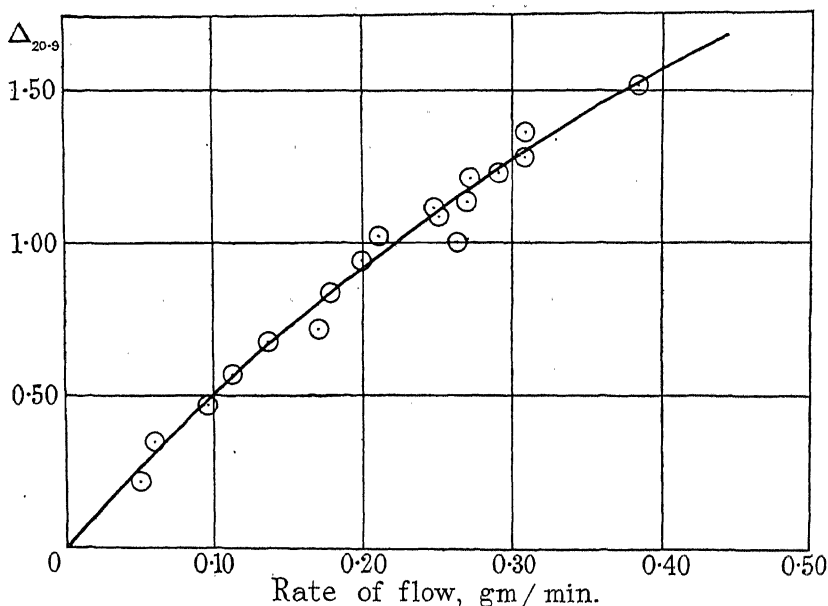


FIG. 2

D—The area of the evaporating surface is required. This was determined, as in the former work, by obtaining a number of photographs of the drop during its formation and deducing the area and  $\int_0^{t_0} A dt$  therefrom.

*Calculation of  $f$  and  $\alpha$* —The calculation of  $f$  was performed in exactly the same manner as in the earlier work and the results obtained are included in Table I which also gives all the data required in the calculation. In spite of the fact that the drop itself was smaller than in the earlier experiments it will be seen that the amount of evaporation per drop was much greater than formerly, being as great as 40 mg in one experiment.

The pressure in the experimental vessel is very considerably lower than the saturated vapour pressure corresponding to the temperature of the surface as is shown in the column  $(P_s - p)$ . This increase in  $\bar{m}$  should increase the accuracy of the determination of the experimental rate of evaporation while that in  $(P_s - p)$  should likewise increase the accuracy of the theoretical estimate.

For the calculation of  $\alpha$  equation (3) must be rearranged somewhat. We have

$$\alpha = \frac{\bar{m}L_{T_s} + (M - \bar{m}) T_a - MT_b - W_2}{0.2439 \frac{p}{\sqrt{T_g}} C_p (T_g - T_s) \int_0^{t_0} Adt},$$

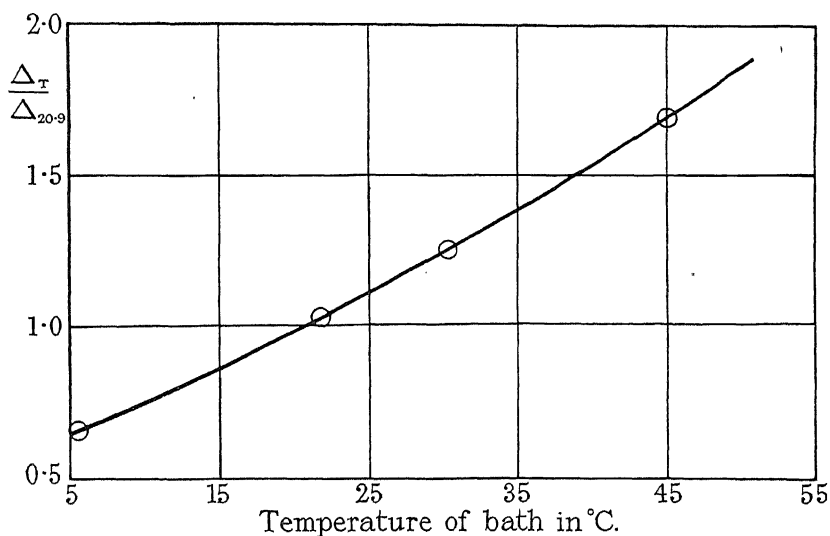


FIG. 3

or

$$\alpha (T_g - T_s) = \frac{[\bar{m}L_{T_s} + (M - \bar{m}) T_a - MT_b - W_2] \sqrt{T_g}}{0.2439 p C_p \int_0^{t_0} Adt},$$

and

$$\alpha \left( \frac{T_g - T_s}{T_b - T_s} \right) = \frac{[\bar{m}L_{T_s} + (M - \bar{m}) T_a - MT_b - W_2] \sqrt{T_g}}{0.2439 p C_p (T_b - T_s) \int_0^{t_0} Adt}, \quad (6)$$

and  $C_p = 0.465$  for water vapour.

Now  $T_g$ , the temperature of the gas striking the drop surface, is unknown. It must, however, be between  $T_s$ , the lowest temperature in the system, and  $T_b$ , the highest temperature in the system, and since in the experiments  $(T_b - T_s)$  is never very large, we may replace  $\sqrt{T_g}$  on

TABLE I

Expt No	$p$ mm	$(P_s - p)$	Driving pressure cm	M mg	$T_b$ °C	$T_s$ °C	$\bar{m}$ mg	$t_0$ secs	$\frac{\bar{m}}{pt} \times 10^6$	100 f	$\left[ \alpha \left( \frac{T_g - T_s}{T_b - T_s} \right) \right]_{\min}$
1	16.971	3.487	10.496	58.507	38.43	22.68	4.243	22.76	1.10	0.61	0.060
2	17.038	4.458	12.691	59.940	40.75	23.50	5.623	18.95	1.74	0.76	0.095
3	15.724	5.260	14.551	59.469	41.30	23.10	5.005	16.49	1.93	0.66	0.092
4	23.999	6.494	11.572	63.434	42.32	29.43	9.875	21.12	1.94	0.84	0.179
5	24.901	11.676	17.708	60.089	50.43	32.62	6.385	11.94	2.14	0.53	0.117
6	25.614	6.821	14.702	62.955	47.23	30.47	9.231	15.59	2.31	1.01	0.152
7	23.063	7.926	14.338	63.869	43.50	29.71	10.176	17.23	2.56	0.86	0.167
8	23.447	9.165	14.039	88.908	42.93	30.60	35.367	24.71	6.10	1.87	0.64
9	24.128	10.674	15.911	85.398	43.89	31.74	31.892	20.82	6.34	1.67	0.67
10	10.645	4.417	12.234	90.336	39.72	17.72	35.364	30.07	11.04	3.00	0.63
11	10.845	5.607	15.721	95.802	39.81	19.13	40.854	25.48	14.80	3.23	0.90
12	10.890	5.469	21.626	89.034	39.45	19.04	33.866	17.83	17.42	3.92	1.06
13	5.378	3.921	21.264	75.683	43.28	10.26	19.324	14.35	25.05	3.80	0.89
14	5.316	6.400	31.610	70.108	41.34	13.68	13.862	9.50	27.45	2.54	1.03
15	6.141	5.928	29.001	75.577	43.16	14.24	19.398	10.75	29.40	3.40	1.11

the right-hand side by  $\sqrt{T_s}$ . The error will then not be large and the resulting value of  $\alpha \left( \frac{T_g - T_s}{T_b - T_s} \right)$  will be too small.

Similarly, the exact value of  $T_a$ , the average temperature of the falling drop, is not known. If we replace  $T_a$  by  $T_s$ , *i.e.*, if we assume that all the mass of the falling drop is at the temperature of its surface, we shall once more obtain a value of  $\alpha \left( \frac{T_g - T_s}{T_b - T_s} \right)$  which is too small.

With these simplifications equation (6) may be replaced by the inequality

$$\alpha \left( \frac{T_g - T_s}{T_b - T_s} \right) \geq \frac{8.816 \sqrt{T_s}}{p (T_b - T_s) \int_0^{t_0} Adt} [\bar{m} (L_{T_s} - T_s) - M (T_b - T_s) - W_2].$$

Now the conduction term  $W_2$  will depend on the temperature difference between the tip and the thermostat. It would have a maximum value if the tip were at the temperature  $T_s$ , when the actual value of  $W_2$  for the tip used in the experiments would be

$$W_2 = \frac{AK (T_b - T_s) t_0}{d},$$

where

$A$  is the area of cross-section of the glass capillary in sq cm,

$K$  is the specific thermal conductivity of the glass, and

$d$  is the length in cm of the glass capillary projecting from the thermostat.

Inserting the values of the constants we find

$$W_2 = 4.26 \times 10^{-5} (T_b - T_s) t_0 \text{ cal}$$

if  $t_0$  is the time of formation of the drop in seconds.

In just the same way as for the previous approximations, we shall obtain a minimum value for  $\alpha (T_g - T_s)/(T_b - T_s)$  by giving  $W_2$  its maximum value. Hence the value of  $\alpha (T_g - T_s)/(T_b - T_s)$  may be written

$$\alpha \left( \frac{T_g - T_s}{T_b - T_s} \right) \geq \frac{8.816 \sqrt{T_s}}{p (T_b - T_s) \int_0^{t_0} Adt} [\bar{m} (L_{T_s} - T_s) - (T_b - T_s) (M + 4.26 \times 10^{-5} t_0)] \quad (7)$$

In this expression every term on the right-hand side is measurable and so the minimum value of  $\alpha (T_g - T_s)/(T_b - T_s)$  may be determined. This value may be written  $[\alpha (T_g - T_s)/(T_b - T_s)]_{\min}$ .

The value of  $T_g$ , the temperature of the gas striking the drop surface, will vary from one experiment to another. When the rate of evaporation ( $\bar{m}/t$ ) is small, or the pressure ( $p$ ) in the experimental vessel is high,  $T_g$  will not differ very markedly from  $T_s$ . If, however,  $\bar{m}/t$  becomes large, convection currents will become more and more pronounced in the vessel and warm vapour may be swept towards the drop surface. Similarly, if  $p$  becomes small the mean free path in the gas increases and it becomes less and less difficult for the warmer gas to approach the surface. For these reasons it may be expected that  $T_g$  and therefore  $\left[ \alpha \left( \frac{T_g - T_s}{T_b - T_s} \right) \right]_{\min}$  will increase with the quantity  $(\bar{m}/tp)$ , and the two quantities are plotted against each other in fig. 4. The curve clearly shows the well-marked relation between them.

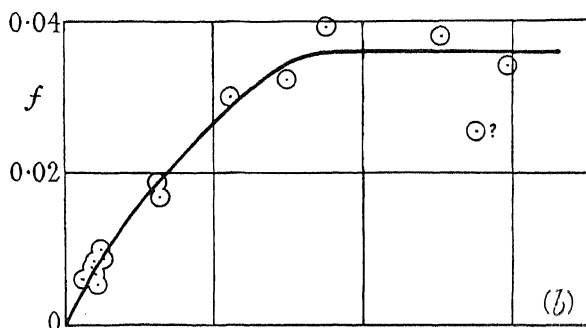


FIG. 5

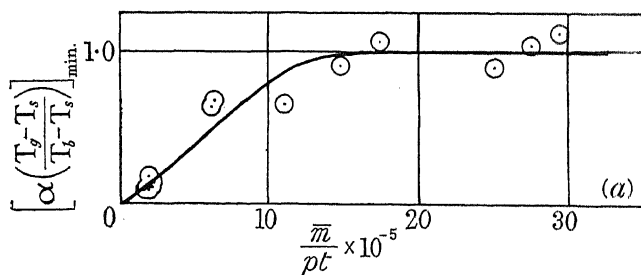


FIG. 4

Now it is not possible under any circumstances for  $T_g$  to exceed  $T_b$ , since  $T_b$  is the temperature of the brass stopper S and so is the highest temperature with which the gas in G is in contact. Hence at all times

$$T_g \leq T_b$$

and therefore, since  $\alpha$  can never exceed unity,

$$\alpha \left( \frac{T_g - T_s}{T_b - T_s} \right) \leq 1.$$

But from fig. 4 it appears that for large values of  $(\bar{m}/tp)$ ,

$$\left[ \alpha \left( \frac{T_g - T_s}{T_b - T_s} \right) \right]_{\min} = 1,$$

so that in such experiments it must follow that

$$T_g = T_b$$

and

$$\alpha = 1.$$

Therefore in experiments with a rapid rate of evaporation into a vessel at low pressure, it seems that the temperature of the gas close to the drop is equal to that of the hottest part of the system and that the heat exchange between the gas and the surface is exactly what would be expected from a theoretical point of view if every impinging vapour molecule reaches thermal equilibrium before leaving the surface and returning to the vapour.

Since the accommodation coefficient of water vapour at a liquid water surface is thus found to be unity, fig. 4 shows the variation of  $[(T_g - T_s)/(T_b - T_s)]_{\min}$  with  $(\bar{m}/tp)$ . It appears that for small values of  $(\bar{m}/tp)$ , the gas temperature  $T_g$  does not differ greatly from  $T_s$ , and only when  $(\bar{m}/tp)$  is greater than about  $15 \times 10^{-5}$  does  $T_g$  become equal to  $T_b$ . When the drop is surrounded by stagnant vapour, as in experiments at low  $(\bar{m}/tp)$ , this stagnant layer may affect the rate of evaporation and hence the value of  $f$ , and, in fact, it may be seen from Table I, or fig. 5 that this is so,  $f$  being quite definitely reduced in the experiments for which  $(\bar{m}/tp)$  is small. No effect of this nature could, however, be present in the experiments in which  $T_g = T_b$ , as there is clearly no difficulty in vapour molecules from the body of the gas reaching or leaving the surface. Consequently the best value of  $f$  is probably obtained by taking the average of all experiments for values of  $(\bar{m}/tp)$  greater than  $15 \times 10^{-5}$ . In this way the value

$$f = 0.034$$

is obtained or, if the exceptionally low value 2.54 should be rejected,  $f = 0.036$ .

## DISCUSSION

The results as a whole show that the rate of evaporation of water is only about 0.036 of that deduced from kinetic theory considerations. Therefore more than 96% of the vapour molecules striking the surface return to the vapour without entering the liquid. They do, however,

remain on the surface long enough to reach temperature equilibrium with it. This behaviour is very unexpected for a liquid, as any molecule condensing on the surface would be expected automatically to become part of the liquid. The result suggests that the surface behaves rather like a semi-solid on which adsorption and re-evaporation of the vapour molecules may take place, the chance of an adsorbed molecule entering the liquid during its lifetime on the surface being small. The idea of the liquid surface obtained in this way would appear to fit in well with the theory of the structure of water recently proposed by Fowler and Bernal.\*

In conclusion, we wish to thank Mr. H. H. Penley and Mr. J. H. Buck who obtained for us the data from which fig. 3 was drawn.

#### SUMMARY

The evaporation coefficient of water and the accommodation coefficient for water at a liquid water surface have been measured and it has been shown that

$$\begin{aligned} \text{the evaporation coefficient} &= 0.036, \\ \text{while the accommodation coefficient} &= 1.0. \end{aligned}$$

These results indicate that, so far as the interaction with the vapour molecules is concerned, the surface behaves more like a solid than a liquid. Most of the vapour molecules incident on it are unable to penetrate into the liquid, but, on the other hand, they are able to attain temperature equilibrium with the surface before re-evaporating into the vapour phase.

\* 'J. Chem. Phys.,' vol. 1, No. 8, p. 515 (1933).

---

# Contributions to the Theory of Specific Heat

## III—On the Existence of Pseudo- $T^3$ Regions in the Specific Heat Curve of a Crystal

By M. BLACKMAN, Beit Scientific Research Fellow, Imperial College,  
South Kensington

(Communicated by S. Chapman, F.R.S.—Received November 1, 1934)

This paper is a continuation of the previous investigation (Part II)\* on the vibrational spectrum of a crystal. The influence of the maxima of the density of the vibrations on the form of the  $\theta_D - T$  diagram is discussed in some detail. The main result is the discovery that more than one region of constant  $\theta_D$  value is possible—which is equivalent to the possibility of pseudo- $T^3$  regions in the specific heat curve. A further result is an explanation of the discrepancies hitherto found between the  $\theta_D$  values derived from thermal and from elastic data at low temperatures.

1—We shall start with an examination of the one-dimensional case which is important because it provides a striking example of the influence of the lattice structure on the specific heat curve.

The general one-dimensional case where we have two kinds of particles, leads to the density curve shown in fig. 1. The density of the vibrations is constant for small frequencies and has three maxima, two of which disappear when the masses of the particles are equal.

The important feature of the spectrum is, for our purpose, the fact that the density increases immediately outside† of the continuum‡ region (where it is constant). The fact interpreted in terms of a  $\theta_D - T$  diagram (one-dimensional Debye theory, *cf.* Part I) means that the  $\theta_D$  value must decrease outside of the continuum region, where it is constant.

This leads to the important conclusion that it is possible for the  $\theta_D - T$  curve to go through a minimum outside of the continuum region, *e.g.*, in the case where the  $\theta_D - T$  curve tends to rise as a whole. Such a case has been dealt with in Part I, *viz.*, when the masses of the particles

\* 'Proc. Roy. Soc.,' A, vol. 148, Part I, p. 365; II, p. 384 (1934).

† This holds generally as can be seen from the formulæ given in Part I.

‡ For the sake of clarity the use of the phrase "continuum region" will be defined; it is that region where the lattice behaves exactly like an elastic continuum. For the density of the vibrations this means the region of constant density in the one-dimensional case, the  $\nu$  and  $\nu^2$  regions in the two- and three-dimensional cases respectively, for the specific heat the  $T$ ,  $T^2$ ,  $T^3$  regions in the three cases respectively.



are very different (*cf.* fig. 2, Part I). The investigation did not show the minimum, but as the accuracy was not sufficiently good to exclude the possibility of a small minimum, the investigation was repeated in the case of  $m/M = 8$ , an accuracy of under 1% being aimed at. Fig. 2, shows the result—a small but quite definite minimum.

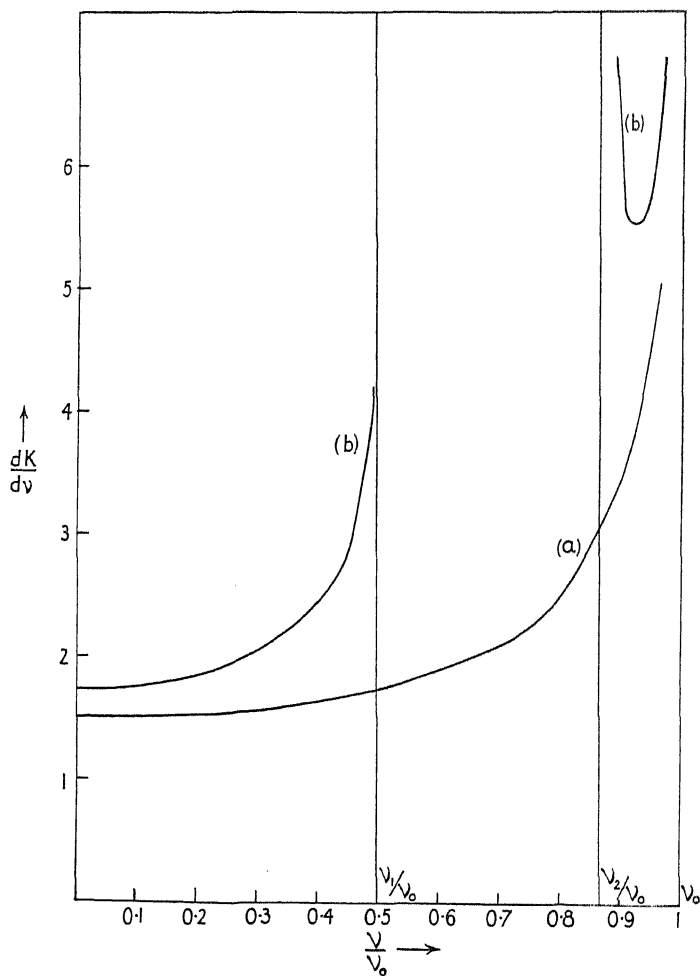


FIG. 1—The density of the vibrations of a one-dimensional lattice. (a).  $m/M = 1$ ; (b).  $m/M = 3$

This is a clear example of a case where there are two regions of constant  $\theta_D$  value. In both these regions the specific heat will be proportional to  $T$ , not, however, in the intermediate region.

2—The two-dimensional density curve is shown in fig. 3. The same features, *i.e.*, the increase of the density outside of the continuum region

is noticeable, and conclusions similar to those deduced above hold for the  $\theta_D - T$  curve where  $\theta_D$  is now the two dimensional  $\theta_D$  value. The important feature of the spectrum is the prominent maximum which adjoins the continuum region. If we go to temperatures which are low enough, the influence of this maximum is negligible and we obtain a constant  $\theta_D$  value, which is the true continuum value. The specific heat will vary as  $T^2$  here. As soon as we raise the temperature somewhat, so that only the first maximum is important, and not the higher frequencies, we obtain a relatively large increase in the specific heat; for the specific heat of the new part of the spectrum rises exponentially

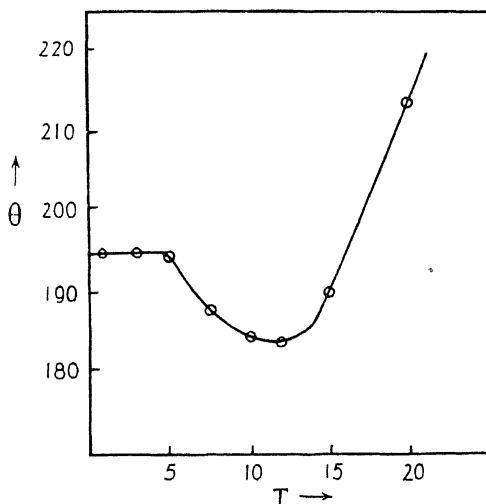


FIG. 2— $\theta$ - $T$  diagram for a one-dimensional lattice ( $m/M = 8$ )

instead of according to a  $T^2$  law. This means that the  $\theta_D$  value will drop appreciably, the value depending, of course, on the weight of the maximum.

The further change in the  $\theta_D$  value will now depend on the particular form of the spectrum. We can divide the whole spectrum into several parts, a Debye spectrum and portions labelled plus and minus; the plus denotes that the part is to be added to, the minus that it is to be subtracted from, the Debye spectrum in order to give the real spectrum. The  $\theta_D$  variation now depends on the relative sizes of the first plus and minus regions. If the minus region is the larger the  $\theta_D$  value has a minimum and rises again; if it is very much larger,  $\theta_D$  attains a maximum value and then falls to a value roughly about  $\theta_{\max}$  (where  $\theta_{\max} = \frac{h\nu_{\max}}{K}$ ; otherwise the  $\theta_D$  value rises slowly to its final value without going through a maximum (fig. 4)).

In the case where the plus region is larger than the minus the  $\theta_D$  value will probably vary slowly with temperature after the initial fall; it may rise or fall, this depending to some extent on the second maximum. Hence in this case there are two possible types of curves, fig. 4.

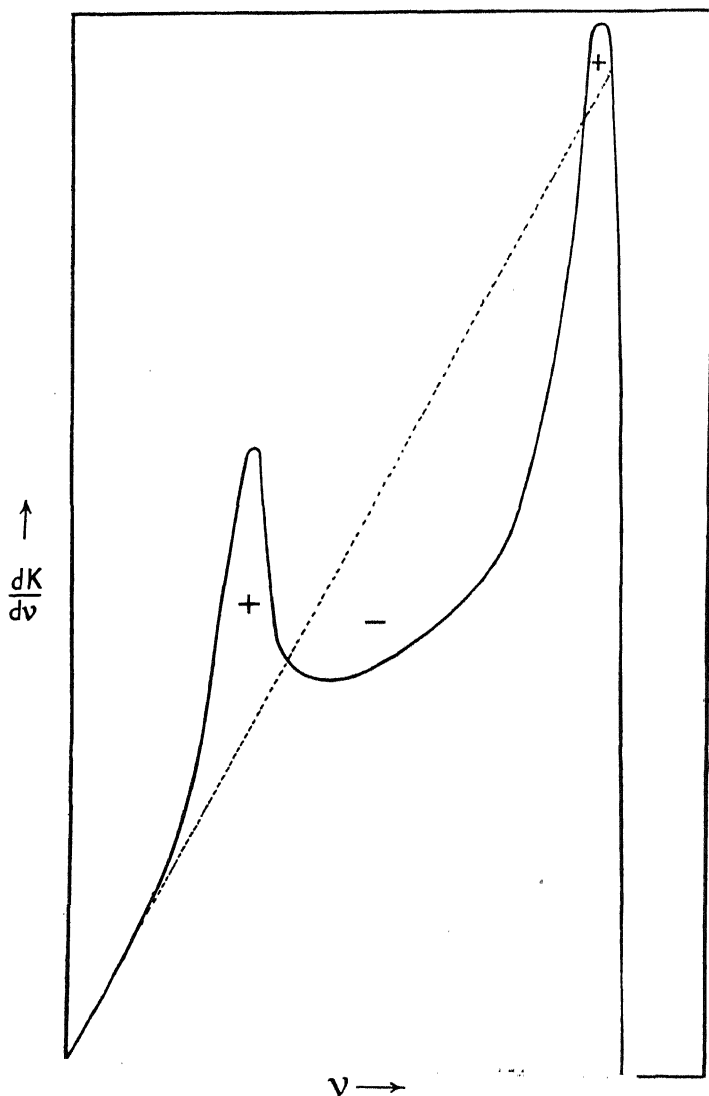


FIG. 3—Density of the vibrations in a two-dimensional square lattice

The actual lattice used for the purposes of calculation\* consisted of particles arranged at the corners of squares; the forces between particles

\* Cf. Part II, figs. 2 (a) and 2 (b).

at a distance  $a$  and at a distance  $a\sqrt{2}$  are considered ( $a$  is the lattice constant). The restoring forces in the two cases are  $\alpha$  and  $\gamma$  respectively, and their ratio was taken to be  $1/20$ . The distribution of the vibrations is shown in fig. 3; it is obvious that the first plus region is much smaller than the first minus region. Hence a  $\theta_D$  curve with a maximum as well as a minimum value is to be anticipated. This is confirmed by calculation.

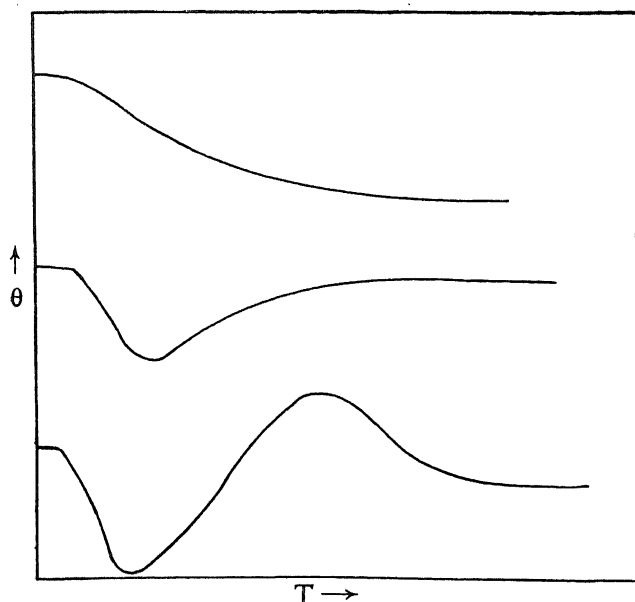


FIG. 4—Possible Types of  $\theta$ - $T$  diagrams

TABLE I

Temperature ° K	$C_v$	$\theta_D$	$\sqrt{C_v}/T$
5	0.002089	260	0.0091
8	0.0053	254	0.0093
10	0.0113	213	0.0106
12.5	0.0220	200	0.0119
15	0.0398	180	0.0133
17.5	0.0560	178	0.0135
20	0.0709	180	0.0133
25	0.0845	206	0.0116
30	0.1029	225	0.0107
50	0.1583	300	
150	0.396	370	
150	1.1274	260	

A striking feature of the curve is the very large drop in the  $\theta_D$  value outside the continuum region. A further point of importance is the second region where  $\theta_D$  is constant at low temperatures.

As seen from the table,  $\sqrt{C_v}/T$  is fairly constant in this region.

We have here a concrete example of the existence of a "spurious continuum" region and, in this case, of the existence of a pseudo- $T^2$  region.

3—The vibrational spectrum of the three dimensional cubical crystal does not differ in essentials from that of the two dimensional case, as was shown in Part II. The  $\nu^2$  law replaces the  $\nu$  law and there are more maxima of the density, but these factors will not alter the deductions as regards the variation of the  $\theta_D$  value with temperature. For instance, the first maximum at low frequencies will cause a fall of the  $\theta_D$  value outside of the continuum region, and the general form of the  $\theta_D - T$  curves must be the same as those deduced from the consideration of the two-dimensional spectrum.\*

In particular, the conclusion as to the possible existence of a pseudo- $T^3$  region holds here just as well as in the one- and two-dimensional cases.

The above conclusions lead to a rather surprising result, when applied to the case of NaCl, and similar ionic crystals. The experimental  $\theta_D - T$  curves for NaCl, KCl and AgCl for instance, show a falling  $\theta_D$  value as the temperature is decreased, and a more or less constant  $\theta_D$  value at the lowest temperatures. Since these results clash with the above prediction that the  $\theta_D$  value will always decrease outside of the continuum region ( $\theta_D$  seems to rise steadily in the above cases), we are forced to conclude that the constant  $\theta_D$  value at low temperatures does not represent the final  $\theta_D$  value, but is the minimum value of  $\theta_D$ , and that measurements of  $\theta_D$  at still lower temperatures would reveal a rise in  $\theta_D$ , until it reached the final  $\theta_D$  value, where it would again become constant in the true continuum region.

The conclusion we reach is that the  $T^3$  region in the case of the above cubic crystals is spurious.

The Debye theory predicts the beginning of the  $T^3$  region at  $\theta/T$  values of about 10; according to the above theory the beginning should be roughly at about 50, but would vary from case to case. For an average crystal, it should not start before a few degrees absolute.

\* The fact that the  $\theta_D - T$  curves deduced in the two-dimensional case hold also for a more complicated spectrum, is best illustrated by a consideration of the general one-dimensional case where there are three maxima. A consideration of the curves given in Part I (fig. 3) (with the correction mentioned in § 1) shows that all the forms given in fig. 4 are present.

At the time the theory was developed the only evidence which existed pertained to measurements at very low temperature by Keesom\* and his collaborators. In the case of silver the  $\theta_D$  value drops from 220 to 209 as we lower the temperature becoming fairly constant at about 17° K, with a  $\theta_D$  value of 209. Measurements at still lower temperatures show a rise of  $\theta_D$  to a value 226 at  $T = 5.5^\circ$  K, and then a falling  $\theta_D$  value. A similar behaviour is found in the case of zinc and copper. The final drop in the  $\theta_D$  value can be interpreted as being due to the electrons, but the rise in  $\theta_D$  is not explained thereby; it seems likely that this is the effect predicted by our theory, though independent evidence would be more convincing.

Such evidence could be obtained from the study of the specific heat of NaCl, etc., at very low temperatures, especially as the theory has been worked out for cubical crystals only. Such experiments are fortunately in progress† at the Physical Chemistry Institute in Göttingen, and the experiments of Clusius, Goldman and Perlick give to some extent the desired confirmation.

These investigators have found that the  $\theta_D$  value of NaCl starts to rise again at very low temperatures reaching a value of 305 ( $\theta_D$  (minimum) = 275); the experimental curves seem to indicate that the  $\theta_D$  value will become constant at a value slightly higher than 305, but this region of temperature has not yet been investigated. Similar results were obtained with LiF, the  $\theta_D$  value rising from 610 (where it was practically constant over a few degrees) to 690 as the temperature was decreased, the curve showing, however, no signs of rounding off.

Experiments at still lower temperatures (helium temperatures) are necessary in order to show definitely that the  $\theta_D$  value does become constant again. Should this be found the existence of the pseudo- $T^3$  region will be demonstrated.

The case of silver chloride would be particularly interesting because the  $\theta_D$  value falls very sharply with decreasing temperature, so that the minimum in  $\theta_D$  should show up very well.

The evidence which exists at present does seem confirmatory to the theory; it is particularly interesting that the first predictions as regards

\* W. H. Keesom and J. v. d. Ende, 'Proc. Acad. Sci. Amst.,' vol. 35, p. 143 (1932); W. H. Keesom and J. A. Kok, 'Proc. Acad. Sci. Amst.,' vol. 35, p. 301 (1932).

† After the conclusion of the above paper in outline, I had the opportunity of discussing the results with Dr. Clusius, in Göttingen. I then became aware that the experiments were already in progress. I am greatly indebted to Dr. Clusius for his kindness in permitting me to use the experimental results.

the NaCl crystal type should have been confirmed, but more experimental evidence is required before it can be taken as established.

4—The above considerations throw some light on the rather puzzling discrepancy between the  $\theta_D$  values calculated from elastic data, and those found experimentally from thermal data.\* The discrepancies are in some cases (Zn, ZnS) of the order of 50%, the  $\theta_D$  (elastic) value always being the higher. In the case of NaCl, KCl, CaF<sub>2</sub> the agreement seems at first sight satisfactory; when, however, we notice that the elastic data at ordinary temperatures are used and that these are about 30% larger at low temperatures,† the agreement disappears. It is clear that we can compare the results only at low temperatures because only there does a crystal behave like an elastic continuum. In these cases we are also left with the result that  $\theta_D$  (elastic) is larger than  $\theta_D$  (thermal).

In order to explain these discrepancies Grüneisen and Goens‡ have proposed a theory which gives a correction of the right order. This has been discussed in Part I, where it was shown that the theory cannot be accepted; no explanation for the discrepancy could, however, be offered there.

What we now suggest is that there is no discrepancy, but that the wrong values of  $\theta_D$  (thermal) have been used. The minimum value of  $\theta_D$  has been used instead of the true  $\theta_D$  value in the continuum region. Since this  $\theta_D$  value will always be larger than the old  $\theta_D$  value, the correction is in the right direction.

The rise in  $\theta_D$  from its maximum value can be very appreciable as is instanced in the case of LiF quoted above; the two-dimensional case (cf. Table I) dealt with shows a rise of about 50% too. It seems likely, therefore, that the correction can be of the right size to explain the discrepancies.

According to our theory, there will be no discrepancy between elastic and thermal  $\theta_D$  values if we use the values in the continuum region. This means that where  $\theta_D$  rises when the temperature is lowered, the  $\theta_D$  value at the lowest temperatures should coincide with  $\theta_D$  (elastic), where the elastic data at low temperature are to be used. It is encouraging that in the case of tungsten, which shows such a behaviour, the results seem to point to the correctness of our conclusions.§

\* Cf. A. Eucken, 'Handbuch der Exper. Phys.,' vol. 8 (a); E. Schrödinger, 'Handbuch der Phys.,' vol. 10.

† T. Steinebach, 'Z. Physik,' vol. 33, p. 664 (1925).

‡ 'Z. Physik,' vol. 26, p. 250 (1924).

§ A. Eucken, 'Handbuch der Exper. phys.,' vol. 81, p. 252, 4th footnote.

Further experimental measurements can, however, settle this point definitely. The theory would require for instance a marked rise in the  $\theta_D$  value of zinc sulphide at low temperatures, as this is a case where there is a marked discrepancy. This is a definite prediction of the theory and the experiments on the thermal and elastic properties at low temperatures will decide as to its correctness.

#### SUMMARY

From the general form of the vibrational spectrum of a cubical lattice, the possibility of pseudo- $T^3$  regions in the specific heat curve are deduced. From the form of the experimental specific heat curves of NaCl, AgCl, etc., it is deduced that the  $\theta_D$  values will rise at still lower temperatures than those attained; the latest experimental results seem to confirm this prediction.

The theoretical predictions are also used to account for the apparent discrepancy between the  $\theta_D$  values calculated from elastic data (at low temperatures) and those deduced from thermal data.

---



## Contributions to the Theory of Specific Heat

### IV—On the Calculation of the Specific Heat of Crystals from Elastic Data

By M. BLACKMAN, Beit Scientific Research Fellow, Imperial College,  
South Kensington

(*Communicated by S. Chapman, F.R.S.—Received November 1, 1934*)

This paper contains a development of a method of calculating  $\theta_D$  values from elastic data (at low temperatures) originally given in Part II.\*

1—The general problem is that one is given the equation of motion of a continuum, and hence the velocity of the elastic waves as a function of the direction of the waves in a crystal and of the elastic constants; for specific heat purposes it is necessary to obtain from this equation the mean value of the velocity, and this is correlated fairly easily with the Debye  $\theta_D$  value.

The strict solution of this problem in its general form seems extremely difficult; the methods given are all interpolation methods, due to Hopf and Lechner† and to Försterling‡, following the earlier work of Born and v. Kármán,§ who gave a method applicable in the case of a nearly isotropic crystal. Debye had solved the problem for an isotropic medium, but this is hardly applicable to the ordinary crystal which is definitely anisotropic.

The advantage of the method developed here is that simple formulæ are obtained, and that a geometrical method is used which gives greater insight into the problem. The method is developed for regular crystals only.

2—The new idea which is introduced into this treatment, as compared with the older investigations, is that we can take advantage of the fact that we are really dealing with a crystal, and not an elastic continuum.

The crystal is built up of a large number of like cells. If we choose the basis to be a cube containing  $s$  particles, we can build up a crystal out of

\* ‘Proc. Roy. Soc.,’ A, vol. 148, p. 384 (1935).

† ‘Verh. deuts. Phys. Ges.,’ vol. 16, p. 643 (1914).

‡ ‘Z. Physik,’ vol. 3, p. 9 (1920).

§ ‘Phys. Z.,’ vol. 14, p. 15 (1913).

$n^3$  such cells; the crystal is a cube having a length of side  $na$ , where  $a$  is the side of the elementary cube. The total number of particles is  $Ns = n^3s$ , and the number of normal vibrations  $3Ns$ .

If we consider the vibration of such a crystal we may assume solutions of the form\*

$$u_{l_1l_2l_3} = u' e^{i(2\pi\nu t + l_1\phi_1 + l_2\phi_2 + l_3\phi_3)}, \text{ etc.}, \quad (1)$$

where

$$\phi_1 = \frac{2\pi a_1}{n}, \quad \phi_2 = \frac{2\pi a_2}{n}, \quad \phi_3 = \frac{2\pi a_3}{n},$$

and  $a_1, a_2, a_3$  vary from 1 to  $n$ .

We have here  $N = n^3$  vibrations, and since there are three directions of motion for each particle, and  $s$  particles in the unit cell, we have  $3sN$  vibrations in all which is the correct number.

This solution satisfies the condition of periodicity which is substituted for boundary conditions.

We have of course in the general case a determinant giving the frequency  $\nu$  as a function of  $\phi_1, \phi_2, \phi_3$ . Here we will deal only with the region of small frequencies where we have only the three acoustical branches.

In this region the crystal behaves like an elastic continuum and we may describe any wave in a continuum in the form

$$u = u' e^{2\pi i \left( \frac{t}{T} + \frac{nx + y + rz}{\lambda} \right)}. \quad (2)$$

The equation of motion of the regular crystal in this region is given by

$$\begin{vmatrix} c_{11}p^2 + c_{44}q^2 + c_{44}r^2 - \rho c^2 & (c_{12} + c_{44})pq & (c_{12} + c_{44})pr \\ (c_{12} + c_{44})qp & c_{11}q^2 + c_{44}r^2 + c_{44}p^2 - \rho c^2 & (c_{12} + c_{44})qr \\ (c_{12} + c_{44})rp & (c_{12} + c_{44})rq & c_{11}r^2 + c_{44}p^2 + c_{44}q^2 - \rho c^2 \end{vmatrix} = 0. \quad (3)$$

Now since (1) and (2) are perfectly equivalent methods of describing a wave in a crystal we have the relations

$$\phi_1 = \frac{2\pi}{\lambda} ap, \quad \phi_2 = \frac{2\pi}{\lambda} aq, \quad \phi_3 = \frac{2\pi}{\lambda} ar. \quad (4)$$

$$(x = l_1a, y = l_2a, z = l_3a).$$

The main point is now to substitute these relations back in (3) and

\* Cf. Born and v. Kármán, 'Phys. Z.,' vol. 13, p. 297 (1912), where this method was first introduced.

obtain a new equation in which we have the frequency  $\nu$  as a function of  $\phi_1, \phi_2, \phi_3$ .

$$\left| \begin{array}{ccc} -\nu^2 + \frac{c_{11}\phi_1^2}{4\pi^2a^2\rho} + \frac{c_{44}\phi_2^2}{4\pi^2a^2\rho} + \frac{c_{44}\phi_3^2}{4\pi^2a^2\rho} & \frac{(c_{12} + c_{44})\phi_1\phi_2}{4\pi^2a^2\rho} & \frac{(c_{12} + c_{44})\phi_1\phi_3}{4\pi^2a^2\rho} \\ \frac{(c_{12} + c_{44})\phi_2\phi_1}{4\pi^2a^2\rho} & -\nu^2 + \frac{c_{11}\phi_2^2}{4\pi^2a^2\rho} + \frac{c_{44}\phi_3^2}{4\pi^2a^2\rho} + \frac{c_{44}\phi_2^2}{4\pi^2a^2\rho} & \frac{(c_{12} + c_{44})\phi_2\phi_3}{4\pi^2a^2\rho} \\ \frac{(c_{12} + c_{44})\phi_3\phi_1}{4\pi^2a^2\rho} & \frac{(c_{12} + c_{44})\phi_3\phi_2}{4\pi^2a^2\rho} & -\nu^2 + \frac{c_{11}\phi_3^2}{4\pi^2a^2\rho} + \frac{c_{44}\phi_1^2}{4\pi^2a^2\rho} + \frac{c_{44}\phi_2^2}{4\pi^2a^2\rho} \end{array} \right| = 0. \quad (5)$$

This is a form which permits us to take advantage of the fact that we are dealing with a crystal.

3—In the region of low frequencies we know that the density of the vibrations is proportional to  $\nu^3$ . If we count the number of vibrations ( $n_1$ ) between  $\nu = 0$  and  $\nu = \nu_1$ , we can obtain an expression for the Debye maximum frequency  $\nu_D$  in the form

$$\nu_D^3 = \nu_1^3 \frac{n_0}{n_1}, \quad (6)$$

where  $n_0$  = total number of the vibrations =  $3sN$ .

The advantage of using (5) is that we can evaluate  $n_0$  and  $n_1$  fairly simply on the same scale, in certain cases.

The method now followed is essentially that adopted in Part II. The justification of the method adopted is given there. The advance made here is that we do not need to refer our considerations to a model as done there, and hence we have a greater generality.

For small values of  $c_{12} + c_{44}/c_{11}$  (about  $\frac{1}{3}$ ) we may neglect the non-diagonal terms and obtain for the surfaces of constant frequency three ellipsoids\* of the form

$$1 = \frac{\frac{\phi_1^2}{4\pi^2a^2\rho}}{c_{11}} + \frac{\frac{\phi_2^2}{4\pi^2a^2\rho}}{c_{44}} + \frac{\frac{\phi_3^2}{4\pi^2a^2\rho}}{c_{44}}. \quad (7)$$

The volume of the ellipsoids lying between  $\nu = 0$  and  $\nu = \nu_1$  is proportional to the number of vibrations lying between  $\nu = 0$  and  $\nu = \nu_1$ . Using the range  $0 \leq \phi \leq \pi$  in each case, the total number of vibrations is proportional to  $3s\pi^3$ .

\* Cf. Part II.

The value of  $\nu_D$  obtained is given by\*

$$\nu_D^3 = \frac{3}{4\pi} \frac{s}{a^3 \rho^{\frac{1}{3}}} \sqrt{c_{11} c_{44}^2}. \quad (8)$$

To obtain the result in Part II (*i.e.*, an orthocubic lattice with particles of one type only) we put

$$s = 1, \quad \rho = \frac{m}{a^3}, \quad c_{11} = \frac{\alpha + 4\gamma}{a}, \quad c_{12} = c_{44} = \frac{2\gamma}{a},$$

where  $\alpha$  and  $\gamma$  are the binding forces defined in Part II.† This gives

$$\nu_D^3 = \frac{3}{4\pi} \sqrt{\frac{4\gamma^2 (\alpha + 4\gamma)}{m^3}},$$

which we obtained in Part II, and which follows as a special case of the more general theory.

In the case where  $c_{12} + c_{44}/c_{11}$  is larger than assumed here the surfaces become very complicated, and explicit formulæ can be obtained only in one special case, where the wave surfaces become spherical. We assume the Cauchy Relation  $c_{12} = c_{44}$  for simplicity and then find

$$\nu_D^3 = \frac{3s}{3 \cdot 57 \sqrt{3\pi} a^3 \rho^{\frac{1}{3}}} \sqrt{c_{11} c_{44}^2} \quad (c_{44} = \frac{1}{3} c_{11}). \quad (9)$$

This equation is so written in order to illustrate the fact that it is really the constant of the equation which has been changed, and that this is about 50% smaller.

Now the equation (1) with its constant  $3/4\pi$  will hold for  $c_{44}/c_{11} \leq \frac{1}{10}$  as is evidenced by the comparison of the value for KCl with the accurate calculations of Hopf and Lechner (see Table I below). Now it will be assumed that the change in the constant is linear between  $c_{44}/c_{11}$  values of  $\frac{1}{10}$  and  $\frac{1}{3}$ ; this is perhaps not strictly justified, but it will suffice if we desire results of a few per cent. accuracy, as will be shown in Table I.

For values of  $c_{44}/c_{11}$  between  $\frac{1}{10}$  and  $\frac{1}{3}$  we use this method of finding the constant, and also the value of  $\frac{1}{2}(c_{12} + c_{44})$  instead of  $c_{12}$  and  $c_{44}$  in the case where these are found not to be quite equal. In the case of formula (8) the  $c_{44}$  values only are used.

\* It is interesting that Hopf and Lechner found extremely complicated integrals in this case so that a direct computation was not possible. This illustrates the superiority of the geometrical consideration.

† Cf. also Born and v. Kármán, *loc. cit.*

4—The following table shows a comparison of the results obtained here with Hopf and Lechner's results, also the data relevant to the calculation. The elastic data used were those due to Voigt and are the same as those used by Hopf and Lechner.

TABLE I

Substance	$s$	$a$	$\rho$	$\theta_D$ (calculated)	$\theta_D$ (Hopf and Lechner)	$\theta_D$ (Born and v. Kármán)
KCl .....	1	3.14	1.987	227	230	—
NaCl.....	1	2.81	2.161	282	296	302
CaF <sub>2</sub> .....	12	5.45	3.11	496	499	—
FeS <sub>2</sub> .....	12	5.38	5.03	662	682	—

The method can be made more accurate by the use of Born and v. Kármán's method in conjunction with formula (8). It may also be pointed out that a similar analysis holds for any type of crystal; an investigation shows, however, that the large number of elastic constants render the treatment rather complicated, and it has been thought better to confine this paper to essentially simple crystals.

## SUMMARY

A new method is deduced by which  $\theta_D$  values can be calculated from elastic data; this is based on considerations of lattice theory as well as on the geometrical form of the wave surfaces.

The numerical results in particular cases are compared with those due to other investigators.

## The Photoelectric Absorption of $\gamma$ -Rays in Heavy Elements

By H. R. HULME, J. MCDUGALL, R. A. BUCKINGHAM, and R. H. FOWLER, F.R.S.

(Received November 2—Revised December 18, 1934)

### § 1—INTRODUCTION

The photoelectric effect in hydrogen-like atoms has been treated by various authors, and the object of this paper is to co-ordinate the various results and to obtain values of  $\sigma$ , the absorption coefficient, which should be valid for all ranges of  $h\nu_0$ , the energy of a quantum of the incident light, and for all values of  $Z$ , the atomic number of the atom. To this end we shall develop a method which is applicable in the range not previously examined—where  $Z$  is large and  $h\nu_0 \sim mc^2$ ,  $m$  being the mass of the electron and  $c$  the velocity of light.

The problem may be stated briefly as follows. The nucleus of the atom is a heavy particle and may therefore be regarded as fixed at the origin of co-ordinates. We shall neglect exchange interaction between the atomic electrons, assuming that each K-electron may be treated separately. We may then consider the absorption by a simplified model consisting of a fixed nucleus and one K-electron, so that the results obtained have to be doubled to give the total absorption by the K-shell. The system is then perturbed by a beam of  $\gamma$ -rays travelling along the  $Z$ -axis, the perturbing potentials being given by

$$\begin{aligned} A_y &= b_0 [e^{2\pi i\nu_0(t-z/c)} + e^{-2\pi i\nu_0(t-z/c)}], \\ A_x &= A_z = 0, \quad A_0 = 0. \end{aligned}$$

Under the influence of this perturbation the K-electron absorbs a quantum of energy and jumps into a free state, appearing as a photoelectron, and we are interested in the number of such transitions per second when the  $\gamma$ -ray beam is of unit intensity. This is defined to be the absorption coefficient per K-electron, and is given by†

$$\frac{2\pi ce^2}{h\nu_0} \sum_{k', u'} |(E', k', u' | - \rho_1 \sigma_y e^{2\pi i\nu_0 z/c} | E'', k'', u'')|^2. \quad (\text{A})$$

† Hulme 'Proc. Roy. Soc.,' A, vol. 133, p. 381 (1931), equation (33). This paper will be referred to as I.

It is a sum of matrix elements representing transitions from the initial state,  $\psi(E'', k'', u'')$ , to all possible final states,  $\psi(E', k', u')$  of the electron.  $E, k, u$  are the energy, azimuthal and magnetic quantum numbers respectively, and  $\nu_0$  the frequency of the incident  $\gamma$ -ray. The relativistic wave functions of Dirac are used, so that the wave function  $\psi$  has four components, and  $\rho_1\sigma_y$  is a matrix of four rows and columns.

When  $h\nu_0 \ll mc^2$ , a non-relativistic treatment is adequate, as all the velocities concerned are small compared with  $c$ . In this case we may use Schrödinger wave functions in (A), and replace  $\rho_1\sigma_y$  by unity. The problem can then be treated fairly simply if we assume that  $h\nu_0/mc^2$  is so small that  $\lambda/a_0 \gg 1$ , where  $\lambda$  is the wave-length of the incident light and  $a_0$  is the radius of the first Bohr orbit, given by  $a_0 = h^2/4\pi^2 mZe^2$  ( $Z$  being the atomic number). We write

$$e^{2\pi i \nu_0 z/c} = e^{2\pi i z/\lambda} = 1 + 2\pi i z/\lambda,$$

since  $z/\lambda$  is now small in the region of the K-shell, and to this approximation there are definite selection rules for  $u$  and  $k$ . We need, therefore, only consider a small number of final states for the electron, and the absorption coefficient may be obtained easily.†

It is possible, however, to obtain closed formulæ for the absorption coefficient without having recourse to this approximation, provided we neglect relativistic effects. These have been given by Stobbe‡ and Sauter,§ using polar co-ordinates, and by Fischer|| using parabolic co-ordinates.

For heavy atoms, for absorption in the K-shell,  $h\nu_0$  must be greater than the binding energy of the electron. For lead, for example, we must have  $h\nu_0/mc^2 > 0.200$ , and so even here a relativistic treatment is desirable, not because the velocity of the photoelectron is large, but because the velocity of the electron in its initial bound state is not small compared with  $c$ . For harder  $\gamma$ -rays the velocity of the photoelectron may also be of order  $c$ , and in this case it is essential to use a relativistic theory.

When we come to deal with the relativistic case, it is no longer possible to separate the wave equation in parabolic co-ordinates, which are best suited to the problem, nor is it possible to use the methods of Stobbe or Sauter without some approximation. It is necessary to use spherical polar co-ordinates, and so express the wave functions of the photoelectron in terms of  $E, k, u$ . If we include the retardation factor there

† See, for example, A. Sommerfeld, 'Wellenmechanisches Ergänzungsband,' p. 211.

‡ 'Ann. Physik,' vol. 7, p. 661 (1930).

§ 'Ann. Physik,' vol. 9, p. 217 (1931).

|| 'Ann. Physik,' vol. 8, p. 821 (1931).

is now no selection rule for  $k$ , and we must sum over all the possible final states. This summation cannot be carried out in the relativistic treatment without some approximation, since  $k$  occurs in the form  $(k^2 - \gamma^2)^{\frac{1}{2}}$ , where  $\gamma = Z/137$ . A possible method is to expand the retardation factor  $\exp(2\pi iz/\lambda)$  in terms of Bessel functions with coefficients  $P_n^0(\cos \theta)$ . Putting  $z = r \cos \theta$  we have

$$e^{2\pi ir \cos \theta/\lambda} = \sum_{n=0}^{\infty} (2n+1) \frac{i^n}{n!} \left( \frac{\pi}{2r \cdot 2\pi/\lambda} \right)^{\frac{1}{2}} J_{n+\frac{1}{2}}(2\pi r/\lambda) P_n^0(\cos \theta), \quad (\text{B})$$

where  $P_n^0$  is the Legendre polynomial as defined by Darwin, and is  $n!$  times the ordinary one.

We then find<sup>†</sup> that, when  $Z \ll 137$ , we may put  $(k^2 - \gamma^2)^{\frac{1}{2}} = k$ , and the matrix elements giving the transition probability to a particular final state can be evaluated, and contain a factor  $\tau^k$ , where  $k$  is the azimuthal quantum number of the final state and  $\tau$  is given approximately by

$$\tau = (1 + 2mc^2/h\nu_0)^{-\frac{1}{2}}.$$

It is found that  $\tau$  is the factor dominating the convergence, that is, determining the number of final states which it is necessary to take into consideration. For long wave-lengths  $mc^2/h\nu_0$  is large and  $\tau$  is so small that we need only consider the first two terms,  $k = 1$  and  $2$ , which is equivalent to the previous approximation of replacing  $\exp(2\pi ir \cos \theta/\lambda)$  by  $1 + 2\pi ir \cos \theta/\lambda$ . For short wave-lengths the convergence is slow, and in the region  $h\nu_0 \sim mc^2$  it is necessary to take about six or eight terms. The calculation has been carried out in I for the case of light elements, when  $Z \ll 137$ , using the relativistic equation of Dirac.

A more elegant method, subject to the same restriction on  $Z$ , has been used by Sauter<sup>‡</sup> to obtain closed formulæ for the total absorption and space distribution of electrons for values of  $h\nu_0/mc^2$  of order unity or greater. It has the disadvantage that  $\gamma (= Z/137)$  is neglected from the beginning, and it is very difficult to decide how small  $Z$  must be in order that the results may constitute a decent approximation to the exact ones. They certainly are not good enough for the heavier elements like lead, and we do find that the predicted variation of  $\sigma$  with  $Z$  is not in agreement with experiment when  $Z^5$  is large. Both the above-mentioned calculations are correct to the zero-order approximation in  $Z/137$ , and give an absorption proportional to  $Z$  per K-electron, whereas the experi-

<sup>†</sup> Hulme, *loc. cit.* I.

<sup>‡</sup> 'Ann. Physik,' Ser. 5, vol. 11, p. 454 (1931).



mental results† favour a law with the fourth power of  $Z$ . It is therefore evident that these two methods are only valid for small values of  $Z$ , but unfortunately it is impossible to estimate the error for any particular value of  $Z$ .

While the present calculations were in progress, Harvey Hall‡ gave a method which he applies to all atoms, with the restriction that  $h\nu_0 \gg mc^2$ . The essential part of Hall's method consists in expanding  $\psi(E, k, u)$ , the wave function of the photoelectron, in powers of  $1/k$ . When  $h\nu_0/mc^2 \gg 1$ , the electrons are emitted in states with all possible azimuthal quantum numbers, but it is found that most of the electrons go into states where  $k \sim h\nu_0/mc^2$ . It is thus permissible to expand in powers of  $1/k$  when  $h\nu_0/mc^2 \gg 1$ , as the expansion is then valid for the important transitions.

In this way it is possible to sum over all values of  $k$  before performing the final integration, and we are left with an expression for  $\sigma$  as a double integral (equation (3), *loc. cit.*) when we neglect terms of order  $\epsilon$ , where  $\epsilon = h\nu_0/mc^2 + (1 - \gamma^2)^{\frac{1}{2}}$ .§

This integral is of the form,

$$\sigma = \phi(\gamma) \iint \psi(u, v, \gamma) \chi(u, v, \gamma^2) du dv,$$

where the functions  $\phi$ ,  $\psi$  and  $\chi$  have no particular physical significance, and are intended only to show the powers of  $\gamma$  involved. The function  $\chi$  has a sharp maximum when  $u = v = 1 - 2/\epsilon$ , and Hall observes that we can take the value of  $\chi(u, v, \gamma^2)$  at this point and remove this quantity outside the integral sign, so that

$$\sigma = \phi(\gamma) \chi(u, v, \gamma^2)_{u=v=1-2/\epsilon} \iint \psi(u, v, \gamma) du dv.$$

Now Sauter (*loc. cit.*) has evaluated the absorption coefficient, correct to the zero order of approximation in  $\gamma$ , so that if we retain only the lowest power of  $\gamma$  in the above expression we should get Sauter's result—

$$\sigma_{\text{sauter}} = \sigma_0 = \phi(0) \chi(0) \iint \psi(u, v, 0) du dv,$$

† Rutherford, Chadwick and Ellis, "Radiations from Radioactive Substances," p. 464.

‡ 'Phys. Rev.,' vol. 45, p. 620 (1934). We are indebted to Mr. Hall for the opportunity of seeing the manuscript of the full calculations before publication, and for his friendly correspondence.

§ In Hall's notation  $\epsilon = h\nu/mc^2 + (1 - \alpha^2)^{\frac{1}{2}}$  and  $\alpha = Z/137$ .

so that

$$\sigma = \sigma_0 \frac{\phi(\gamma) \chi(\gamma^2)}{\phi(0) \chi(0)} \cdot \frac{\iint \psi(u, v, \gamma) du dv}{\iint \psi(u, v, 0) du dv}.$$

The quantity

$$\iint \psi(u, v, \gamma) du dv$$

cannot be evaluated explicitly and Hall appears to have overlooked the presence of  $\gamma$  in it, and to have put the ratio of the two integrals equal to unity, thus obtaining a closed expression for  $\sigma$ .

Actually his formula (see § 5) gives results in good agreement with those obtained in the present paper by rigorous calculation, even in the region  $h\nu_0 \sim mc^2$ . The main part of the correction seems to be included in  $\phi(\gamma) \chi(\gamma^2)$ , but we feel that there is no justification for neglecting  $\gamma$  in the integrand. In any case the formula must be regarded as empirical in the region where  $h\nu_0/mc^2$  is of order unity, since the approximations made are only valid when  $h\nu_0 \gg mc^2$ . As may be seen from the table in § 5, the differences between the two sets of results decreases as  $h\nu_0$  increases, and even for lead with  $h\nu_0/mc^2 = 0.7$ , the difference is only 13%. This must mean that the form of correction required by Sauter's formula is approximately the same over a large range of wave-lengths. We shall, therefore, use Hall's formula, given in equation (24), to supplement the present calculations in the region  $h\nu_0 \gg mc^2$ .

It is of considerable importance to know the absorption coefficients of the heavy elements for  $\gamma$ -rays, as this knowledge is required in a number of experiments, the determination of the internal conversion coefficients of radioactive metals being an example. It therefore seemed worth while to treat the problem rigorously, even though a considerable amount of numerical work is necessary, and it was decided to carry out the calculations for large values of  $Z$  by a method which is an extension of the one used in the calculation of the internal conversion coefficients of the radioactive elements.†

We expand the perturbation term as in equation (B) and we then find that the term in  $J_{n+\frac{1}{2}}$ , for example, induces transitions to final states with azimuthal quantum numbers  $k = n \pm 1$ . Each matrix element in (A) is therefore of the form

$$(\psi_0 | f(\theta \phi) \{ \lambda J_{k+1+\frac{1}{2}}(r) + \mu J_{k-1+\frac{1}{2}}(r) \} | \psi_k),$$

† H. R. Hulme, 'Proc. Roy. Soc.,' A, vol. 138, p. 643 (1932), referred to as II; H. M. Taylor and N. F. Mott, 'Proc. Roy. Soc.,' A, vol. 138, p. 665 (1932).

where  $\psi_0$  and  $\psi_k$  are the wave functions of the initial and final states. The matrix element is an integral over all space, and the integration over the angular co-ordinates is trivial. The radial integration can be carried out rigorously, since it is possible to expand a Bessel function of half integral order in a finite number of terms. The result of the integration is then expressible as the sum of a number of hypergeometric functions as in II, and these may be evaluated to any desired degree of accuracy.

This method, therefore, does not make use of any uncontrollable approximations, but the labour involved in the computation makes it impossible to apply it in a reasonable time to more than a few wavelengths and a few values of  $Z$ . The complexity of the calculation increases as  $h\nu_0/mc^2$  increases, and it is very difficult to deal with values of this quantity greater than about 4.

We now have at our disposal four distinct sets of results, of which we give the authors and ranges of validity below—

- (1) Non-relativistic calculations by Sauter and Fischer, valid for all  $Z$  when  $h\nu_0/mc^2 \ll 1$ .
- (2) Relativistic calculations by Sauter and Hulme, valid for all  $h\nu_0$  when  $Z/137 \ll 1$ .
- (3) Relativistic calculations by H. Hall, which we shall use when  $h\nu_0/mc^2 \gg 1$ , for all values of  $Z$ .
- (4) Calculations of the present paper, valid for all  $Z$  and all  $h\nu_0$ , but impracticable when  $h\nu_0/mc^2$  is greater than about 4.

We see that a complete survey of the absorption in the K-shell is thus possible, and we shall endeavour to co-ordinate the last three sets of results and give values of  $\sigma$  for all  $Z$  and  $h\nu_0$  in the  $\gamma$ -ray region.

The approximations mentioned above are essentially attempts to reduce the complication of the mathematics, which arises from the circumstances (1) that there is no selection rule for  $k$ , and (2) that  $k$  occurs in the form  $(k^2 - \gamma^2)^{1/2}$ , and it is therefore not possible to obtain a closed formula for the summation over  $k$ , unless  $\gamma$  be neglected. Of a somewhat different type is the approximation used by Hall and Oppenheimer,<sup>†</sup> who treat the outgoing electron as a free electron. This approximation is rather uncontrollable, and fails completely when  $h\nu_0/mc^2$  is of order unity. It is criticized in Hall's more recent paper. It is also not to be expected that the use of the asymptotic expressions for the final states would lead to essentially better results, since these expressions are not valid near the nucleus.

<sup>†</sup> 'Phys. Rev.', vol. 38, p. 57 (1931).

We now pass on to develop the actual formulæ on which the numerical work has been based. The reader who is interested chiefly in the results can turn at once to § 5.

## § 2. CALCULATION OF THE MATRIX ELEMENTS

We shall use the notation of I and II referring to equation (26) of I as I (26), etc. The absorption coefficient is given by equation (A) of the previous section, and the matrix elements involved are the sums of four terms, given by I (48). Our object is to show how these may be calculated without the restriction  $Z \ll 137$ . The initial state of the K-electron is a combination of two states, representing the spin in opposite directions. The perturbation, however, is symmetrical with regard to these two directions, and it is immaterial whether we consider the electron to be in either one of the two states, or a combination of both. We shall therefore take the electron to be initially in the state of type I (3A), given by  $k = 0, u = 0$ . From the table, I, p. 395, we see that the selection rule for  $u$  is  $\Delta u = \pm 1$ , while the azimuthal quantum number of the final state,  $k$ , may take any (integral) value. Combining the contributions from the four columns of the table we obtain the following results:—

$$\begin{aligned}
 m_{-1, k}^a &= i^k \sqrt{k+1} \int_0^\infty \left[ F_k (\beta + 2) J_{k+1+\frac{1}{2}}(qr) \right. \\
 &\quad \left. + \gamma G_k \frac{(k+1) J_{k+1+\frac{1}{2}}(qr) - k J_{k-1+\frac{1}{2}}(qr)}{(2k+1)} \right] Q_k dr \\
 m_{1, k}^a &= -i^k \gamma \int_0^\infty G_k [J_{k+1+\frac{1}{2}}(qr) \\
 &\quad + J_{k-1+\frac{1}{2}}(qr)] \frac{\sqrt{\{k(k+1)(k+2)\}}}{(2k+1)} Q_k dr \\
 m_{-1, k}^b &= i^k \sqrt{k} \int_0^\infty \left[ F_{-k-1} (\beta + 2) J_{k-1+\frac{1}{2}}(qr) \right. \\
 &\quad \left. - \gamma G_{-k-1} \frac{(k+1) J_{k+1+\frac{1}{2}}(qr) - k J_{k-1+\frac{1}{2}}(qr)}{(2k+1)} \right] Q_{-k-1} dr \\
 m_{1, k}^b &= -i^k \gamma \int_0^\infty G_{-k-1} [J_{k+1+\frac{1}{2}}(qr) \\
 &\quad + J_{k-1+\frac{1}{2}}(qr)] \frac{\sqrt{\{k(k+1)(k-1)\}}}{(2k+1)} Q_{-k-1} dr, \quad (1)
 \end{aligned}$$

where  $m_{u, k}^a$ ,  $m_{u, k}^b$ , are the matrix elements for the transitions from  $k = 0, u = 0$  to the final states of types I (3A) and I (3B) with quantum

numbers  $u$  and  $k$ , and the other symbols have the same meaning as in I, namely—

$$\gamma = Z/137, \quad \beta = (1 - \gamma^2)^{\frac{1}{2}} - 1, \quad a_0 = h^2/4\pi^2 mZe^2, \quad (2A)$$

and  $q = 2\pi/\lambda$ , where  $\lambda$  is the wave-length of the incident light.  $Q_k$  is given by

$$Q_k = r^{\beta+2} e^{-r/a_0} (\beta + 2)^{-1} (2\pi^2/qr)^{\frac{1}{2}} \xi(E_0) \xi(E, k), \quad (2B)$$

where  $\xi(E_0)$  is the normalizing factor for the initial state, and  $\xi(E, k)$  that for the radial part of the wave function of the final state, of energy  $E$ . The normalizing factors and the radial wave functions,  $F_k$ ,  $G_k$ , etc. are taken from I, § 2, and are given by

$$\left. \begin{aligned} \mathfrak{G}_k &= AF_k + i |B| G_k \\ \mathfrak{G}_k &= [(k-s)-i(b+c)] r^s a^{2s+2} e^{-\pi b} \int_{-1}^{+1} (1-u)^{s-ib+1} (1+u)^{s+ib} e^{iaru} du \\ A^2 &= \frac{2\pi}{hc} (mc^2 + E), \quad B^2 = \frac{2\pi}{hc} (mc^2 - E) \end{aligned} \right\}, \quad (2C)$$

$$\left. \begin{aligned} s &= \{(k+1)^2 - \gamma^2\}^{\frac{1}{2}} - 1, \\ a &= -iAB = 2\pi p/h, \\ b &= \frac{i\gamma}{2} \left( \frac{A}{B} - \frac{B}{A} \right) = \frac{\gamma E}{pc}, \\ c &= \frac{i\gamma}{2} \left( \frac{A}{B} + \frac{B}{A} \right) = \frac{\gamma mc}{p}, \end{aligned} \right\} \quad (2D)$$

where  $p$  is the magnitude of the momentum of the photoelectron. We have further

$$\left. \begin{aligned} \xi(E, k) &= \left( \frac{2\pi E}{hc^2 a} \right)^{\frac{1}{2}} \frac{A \cdot |B|}{(A^2 + |B|^2)^{\frac{1}{2}}} K^{-1}, \\ \text{with} \quad K &= \frac{1}{2} \sqrt{[(k-s)^2 + (b+c)^2]} |\Gamma(s+ib+1)| e^{-\frac{3\pi b}{2}} (2a)^{s+1}. \end{aligned} \right\} \quad (2E)$$

For states of type I (3B) we have

$$\left. \begin{aligned} \mathfrak{G}_{-k-1} &= [(b-c) + i(k-1-s')] r^{s'} a^{2s'+2} e^{-\pi b} \\ &\quad \times \int_{-1}^{+1} (1-u)^{s'-ib+1} (1+u)^{s'+ib} e^{iaru} du \\ \text{with} \quad s' &= (k^2 - \gamma^2)^{\frac{1}{2}} - 1. \end{aligned} \right\} \quad (2F)$$

Corresponding expressions are obtained for the normalizing factor.

From equations (1) and (2B) we see that the integrals involved are all of the form

$$\int_0^\infty (\pi/2qr)^{\frac{1}{2}} r^{\beta+2} e^{-r/a_0} J_{p+\frac{1}{2}}(qr) (\lambda_1 F_k + \mu_1 G_k) dr,$$

or a similar integral with  $F_{-k-1}$ ,  $G_{-k-1}$ , where  $p = k \pm 1$ . If we put  $\delta = 1/aa_0$  and  $q/a = \tau$ , as in II (17), the integral becomes

$$a^{-(\beta+3)} \int_0^\infty (\pi/2\tau ar)^{\frac{1}{2}} (ar)^{\beta+2} e^{-\delta ar} J_{p+\frac{1}{2}}(\tau ar) (\lambda_1 F_k + \mu_1 G_k) d(ar).$$

We now change the variable of integration by writing  $r$  for  $ar$ , at the same time expressing the integral in terms of the complex quantities  $\mathfrak{G}_k$  and  $\mathfrak{G}_k^*$  obtaining

$$a^{-(\beta+3)} \int_0^\infty (\pi/2\tau r)^{\frac{1}{2}} r^{\beta+2} e^{-\delta r} J_{p+\frac{1}{2}}(\tau r) (\lambda_2 \mathfrak{G}_k + \mu_2 \mathfrak{G}_k^*) dr. \quad (3)$$

We use the following *finite* expansion for  $J_{p+\frac{1}{2}}(\tau r)$

$$J_{p+\frac{1}{2}}(\tau r) = \frac{1}{(2\pi\tau r)^{\frac{1}{2}}} \left[ e^{i\tau r} \sum_{l=0}^p \frac{i^{l-p-1} (p+l)!}{l! (p-l)! (2\tau r)^l} + \text{conjugate} \right]. \quad (4)$$

The integral (3) can now be found in terms of a number of convergent integrals of the form

$$\left( \frac{1}{2\tau} \right)^{l+1} a^{-(\beta+3)} \int r^{\beta+1-l} e^{-\delta r \pm i\tau r} (\lambda_2 \mathfrak{G}_k + \mu_2 \mathfrak{G}_k^*) dr, \quad (5)$$

where  $l$  is a positive integer  $\leq p$ . We shall show how to calculate the integrals

$$R_{l,k} = \frac{a^{-(\beta+3)}}{(2\tau)^{l+1} \cdot K} \int_0^\infty r^{\beta+1-l} e^{-\delta r + i\tau r} \mathfrak{G}_k dr \quad (6)$$

and

$$S_{l,k} = \frac{a^{-(\beta+3)}}{(2\tau)^{l+1} \cdot K} \int_0^\infty r^{\beta+1-l} e^{-\delta r + i\tau r} \mathfrak{G}_k^* dr, \quad (7)$$

where  $K$  is given by (2E), and the variable  $ar$  is replaced by  $r$  in  $\mathfrak{G}_k$  and  $\mathfrak{G}_k^*$ . It is convenient to include in this way the part of  $\xi(E, k)$  which depends on  $k$ . We note that when  $l = 0$  the integrals (6) and (7) are  $(2a\tau K)^{-1}$  times the integrals II (15) and II (21).

The integrals involving  $e^{-i\tau r} \mathfrak{G}_k^*$  and  $e^{-i\tau r} \mathfrak{G}_k$  are the conjugates of (6) and (7) respectively, so that every integral of the type (5) can be calculated provided we know the values of (6) and (7). Let us consider

the first one. Change the variable of integration from  $ar$  to  $r$  in the expression (2c) for  $\mathfrak{G}_k$  and substitute in (6). We find

$$R_{l,k} = \frac{2^{-s} a^{-(\beta+2)} e^{\pi b/2}}{(2\tau)^{l+1} |\Gamma(s+ib+1)|} e^{i\omega_k} \int_0^\infty e^{-(\delta-i\tau-iu)r} r^{\beta+s+1-l} \\ \times \int_{-1}^{+1} (1-u)^{s-ib+1} (1+u)^{s+ib} du,$$

where

$$\omega_k = \arg [(k-s) - i(b+c)]. \quad (8)$$

These integrals are convergent for all the values of  $l$  and  $k$  involved, since  $\beta+s+1 > k$ , and  $l \leq p \leq k+1$ , so that  $\beta+s+1-l > -1$  in all cases, which ensures the convergence at the origin. The integral (8) is evaluated as in II, and we find

$$R_{l,k} = \frac{a^{-(\beta+2)} e^{\pi b/2} e^{i\omega_k}}{|\Gamma(s+ib+1)| (2\tau)^{l+1}} \Gamma(s+\beta+2-l) \frac{2^{s+2}}{[\delta-i(\tau-1)]^{s+\beta+2-l}} \\ \times \frac{\Gamma(s+ib+1) \Gamma(s-ib+2)}{\Gamma(2s+3)} F(s+\beta+2-l, s+ib+1, 2s+3; z), \quad (9)$$

where  $z = 2/(\delta-i\tau-i\delta)$ . For the integral (7) we have

$$S_{l,k} = \frac{a^{-(\beta+2)} e^{\pi b/2} e^{-i\omega_k}}{|\Gamma(s+ib+1)| (2\tau)^{l+1}} \Gamma(s+\beta+2-l) \frac{2^{s+2}}{[\delta-i(\tau-1)]^{s+\beta+2-l}} \\ \times \frac{\Gamma(s+ib+2) \Gamma(s-ib+1)}{\Gamma(2s+3)} F(s+\beta+2-l, s+ib+2, 2s+3; z). \quad (10)$$

By using the relations between contiguous hypergeometric functions we may now calculate  $R_{l+1,k}$  and  $S_{l+1,k}$  from  $R_{l,k}$  and  $S_{l,k}$ . We have from II (27), replacing  $\beta$  by  $\beta-l$

$$2\tau [\delta-i(\tau-1)]^{-1} (s-\beta+l+1) (s+\beta-l+1) R_{l+1,k} \\ = (-ib-\beta+l) R_{l,k} + (s-ib+1) (1-z) S_{l,k} e^{2i\omega_k}, \quad (11)$$

and

$$2\tau [\delta-i(\tau-1)]^{-1} (s-\beta+l+1) (s+\beta-l+1) S_{l+1,k} \\ = (s+ib+1) R_{l,k} e^{-2i\omega_k} + (ib-\beta+l) (1-z) S_{l,k}. \quad (12)$$

These two relations enable us to express all the integrals in terms of  $R_{0,k}$  and  $S_{0,k}$  and hence the integral (3) in terms of these two. We shall not give any closed formula for the general integral (3) as it is simplest to calculate all the integrals of type (6) and (7) successively and then substitute in (3) after expanding the Bessel function as in (4).

The integrals  $R_{0,k}$  and  $S_{0,k}$  are calculated by transforming the hypergeometric function in (9) from the variable  $z$  to the variable  $1/z$ , which is small in the region in which we are interested. The expressions (9) and (10) for  $R_{0,k}$  and  $S_{0,k}$  are equal to the expressions II (18) and II (22) multiplied by  $(2a\tau K)^{-1}$ , so that on transforming to  $1/z$  we find

$$R_{0,k} = e^{i\omega_k} U \left[ F(s + ib + 1, ib - s - 1, ib - \beta; z^{-1}) + \frac{\Gamma(s + \beta + 2) \Gamma(ib - \beta - 1) \Gamma(s + 2 - ib)}{\Gamma(s + 1 - \beta) \Gamma(s + ib + 1) \Gamma(\beta + 1 - ib)} \times (-z)^{-(\beta+1-ib)} F(s + \beta + 2, \beta - s, \beta + 2 - ib; z^{-1}) \right], \quad (13)$$

$$S_{0,k} = e^{-i\omega_k} U \left[ \frac{s + ib + 1}{\beta - ib} (-z)^{-1} F(s + ib + 2, ib - s, ib + 1 - \beta; z^{-1}) + \frac{\Gamma(s + \beta + 2) \Gamma(ib - \beta) \Gamma(s - ib + 1)}{\Gamma(s + 1 - \beta) \Gamma(s + ib + 1) \Gamma(\beta + 1 - ib)} \times (-z)^{-(\beta+1-ib)} \Gamma(\beta + s + 2, \beta - s, \beta + 1 - ib; z^{-1}) \right], \quad (14)$$

where

$$U = \frac{\Gamma(\beta + 1 - ib)}{\tau a^{\beta+2} [\delta - i(\tau - 1)]^{\beta+1-ib}}, \quad (15)$$

and is independent of  $l$ . We shall write (13) and (14) as

$$R_{0,k} = U (R)_{0,k}, \quad (16)$$

$$S_{0,k} = U (S)_{0,k}, \quad (17)$$

and since  $U$  is independent of  $l$  we see that the recurrence formulæ (11) and (12) hold for  $(R)_{l,k}$  and  $(S)_{l,k}$  also. In the numerical work it is convenient to separate out the parts which are independent of  $l$  and  $k$  as above, and to work with  $(R)_{l,k}$  and  $(S)_{l,k}$ .

When the final state is of type I (3B), the results of this section hold provided we replace  $s$  by  $s'$  and

$$\{(k - s) - i(b + c)\} \text{ by } \{(b - c) + i(k - 1 - s')\}$$

in all the above formulæ.

We may, therefore, express the integrals (1) for  $m_{-1,k}^a$ , etc., in terms of  $(R)_{0,k}$  and  $(S)_{0,k}$  and their conjugate complexes. The final expression for the absorption coefficient is too cumbersome to write down, but we



can separate out the part which is independent of  $k$  as follows. In the expressions (1) for the matrix elements we separate out the part

$$\xi(E_0) \xi(E, k) K (4\pi)^{\frac{1}{2}} (\beta + 2)^{-1} |U|,$$

where  $U$  is given by (15). The integrals which remain are then all of the form

$$\frac{(R)_{l,k} \text{ or } (S)_{l,k}}{A}, \quad \frac{(R)_{l,k} \text{ or } (S)_{l,k}}{|B|}, \quad (18)$$

we write

$$m_{u,k}^a = \xi(E_0) \xi(E, k) \cdot K \cdot (4\pi)^{\frac{1}{2}} (\beta + 2)^{-1} |U| (m)_{u,k}^a, \quad (18)$$

where  $(m)_{u,k}^a$  is now a pure number and the factor of it is independent of  $k$ , since  $\xi(E, k) \times K$  does not contain  $k$ . We then find on substituting in the formula A of § 1 for the absorption coefficient

$$\begin{aligned} \left. \begin{array}{l} \text{Absorption coefficient} \\ \text{per K-electron} \end{array} \right\} &= \frac{\pi b \gamma \theta}{(\beta + 2) \Gamma(2\beta + 3) Z} \left( \frac{c}{2\pi \nu_0} \right)^2 \\ &\times \frac{2A^2 |B|^2}{A^2 + |B|^2} \frac{(2\gamma)^{2\beta+2} |\Gamma(\beta + 1 - i b)|^2}{\left| \left[ \gamma + \frac{i}{\theta} \left( \frac{a}{q} - 1 \right) \right]^{2(\beta+1-ib)} \right|} \\ &\times \sum_{\substack{k=0 \\ u=\pm 1}}^{\infty} [| (m)_{u,k}^a |^2 + | (m)_{u,k}^b |^2], \end{aligned} \quad (19)$$

where  $\theta = mc^2/h\nu_0$ .

This has the dimensions of  $(c/\nu_0)^2$ , or an area, as it must have.

The chief difficulty in the treatment according to Dirac's relativistic equation arises from the fact that the numbers  $s$  and  $s'$ , occurring in  $F_k$  and  $G_k$ , are not integers. This necessitates the separate calculation of all the matrix elements for the different values of  $s, s'$ . When the atomic number is small we may approximate by putting  $\beta = 0$  and  $s = k$ . The calculation is then much simpler and explicit formulæ for the absorption coefficient and space distribution of photoelectrons can be found (Sauter, *loc. cit.*).

It is not possible to obtain much idea of the variation of the absorption coefficient with  $Z$  and  $\lambda$  from the above formulæ, as the quantities  $(m)_{-1,k}^a$ , etc., are functions of  $\gamma$  and  $\theta$ . Let us consider the limit  $\lambda \rightarrow 0$ . We find that

$$|m_{1,k}^b|^2 \sim \frac{k(k+1)(k-1)}{2(k+1)^2} \sim k \quad \text{when } k \text{ is large,}$$

and similarly for the other matrix elements, so that the sum in (19) is

apparently divergent. This, however, is not the case. It means that we must take a higher approximation. When  $k$  is large and *fixed* and  $\theta$  is small, a second approximation to the expression  $(R)_{j,k}$ , is of the form

$$(1 + \varepsilon k \theta^{\beta+1} + \varepsilon' k^2 \theta),$$

where  $\varepsilon$  and  $\varepsilon'$  are complex quantities of order unity if  $\beta$  is small. We then have

$$|(m)_{1,k}^b|^2 \sim k |(1 - \varepsilon k \theta^{\beta+1} + \varepsilon' k^2 \theta)|^2. \quad (20)$$

It is, however, impossible to use an approximation of this form because we cannot consider  $k$  as fixed, as we may see from the following. Suppose, for example, that the correct asymptotic expression for  $|(m)_{1,k}^b|^2$  were of the form  $k(1 - \theta)^k$  or  $k(1 - k\theta + \dots)$ . We then find that the sum is convergent

$$\begin{aligned} \sum_{k=0}^{\infty} |(m)_{1,k}^b|^2 &\sim \frac{1}{[1 - (1 - \theta)]^2} \\ &\sim 1/\theta^2 \\ &\sim \nu_0^2, \end{aligned}$$

which gives a term in the absorption coefficient proportional to  $\lambda$ . This is the asymptotic form of the result given by Sauter (*loc. cit.*) for the case  $\beta \rightarrow 0$ , so that the above is quite a possible assumption. We now see as  $\theta$  ( $\sim \lambda$ ) decreases, the importance of the transitions to final states with large  $k$  becomes greater. Assuming  $|(m)_{1,k}^b|$  to be of the form stated when  $\theta$  is small, we see that the maximum value of  $|(m)_{1,k}^b|^2$  occurs when  $k\theta \simeq 1$ , so that the final states with quantum numbers in this region are the most important. It is then difficult to obtain expressions for the hypergeometric functions in (13) and (14) when  $s \simeq k \rightarrow \infty$  and  $z^{-1} \simeq \theta \rightarrow 0$ , so that  $k\theta \rightarrow 1$ . The formulæ given by Watson† for hypergeometric functions of the form  $F(a + n, b - n; c; x)$ , where  $n \gg 1$ , are not valid when  $x \rightarrow 0$ , as the constants  $c_1$ , etc., occurring in the expansion tend to infinity. It is therefore impossible to consider  $k$  as fixed, and any equation of the form (20) is quite useless as an asymptotic approximation. A more extended examination of the asymptotic form of  $F(a + n, b - n; c; x)$ , when  $n \rightarrow \infty$  and  $x \rightarrow 0$ , is necessary before we can consider the absorption as  $\lambda \rightarrow 0$ .

This difficulty has been avoided by Harvey Hall (*loc. cit.*) who has used an expansion (not asymptotic) of the wave function in terms of  $1/k$  before carrying out the integration.

† 'Trans. Cam. Phil. Soc.,' vol. 22, p. 277 (1917).

The expression (19) for the absorption coefficient is suitable for the same range of wave-lengths as in I, *i.e.*,  $\theta = mc^2/h\nu_0 > 1/4$ . It is theoretically possible to use it for all values of  $\theta$ , but the series converges very slowly when  $\theta < 1/4$ .

### § 3—ABSORPTION COEFFICIENT AT THE SERIES LIMIT

If it is required to find the absorption coefficient at, or near the series limit, the above calculations must be modified. In the expressions (9) and (10) the hypergeometric functions may be calculated without further transformation, and the numerical work is considerably simplified.

It may be shown that the absorption coefficient tends to a definite value at the series limit, and we shall show how to calculate this.

Let us consider a beam of light whose wave-length is given by

$$h\nu_0 = mc^2(-\beta + \Delta), \quad (21)$$

so that  $\theta = 1/(\Delta - \beta)$ . Here  $\Delta$  is a small positive quantity which tends to zero as we approach the series limit with  $\theta$  increasing. We shall express the values of the various constants in terms of  $\Delta$ , and then we shall take the limit as  $\Delta \rightarrow 0$ . We find that it is necessary to go some distance with the calculation before we can proceed to the limit.

On putting in the value of  $h\nu_0$  we find, to the first order,

$$\frac{1}{\tau^2} = \left(\frac{a}{q}\right)^2 = \frac{2\Delta}{\beta^2},$$

$$c = \delta = b = \gamma/\sqrt{2\Delta}$$

but

$$(b - c) = \gamma^2/2b$$

and

$$\frac{|B|^2}{A^2} = \frac{\Delta}{2} = \frac{\gamma^2}{2b}.$$

Let us consider the values of the hypergeometric function in (9) and (10), putting

$$F_1 = F(s + \beta + 2, s + ib + 1, 2s + 3; z)$$

and

$$F_2 = F(s + \beta + 2, s + ib + 2, 2s + 3; z).$$

Now

$$z = \frac{2}{1 - \tau - i\delta} = \frac{2\sqrt{\Delta}}{\beta - i\gamma} \quad \text{and} \rightarrow 0 \text{ as } \Delta \rightarrow 0,$$

whilst  $b \rightarrow \infty$ , so that  $bz$  is finite. Consider now  $F_1$ . We have

$$F_1 = 1 + \frac{(s + \beta + 2)(s + i\beta + 1)}{(2s + 3)1!} z \\ + \frac{(s + \beta + 2)(s + \beta + 3)(s + i\beta + 1)(s + i\beta + 2)}{(2s + 3)(2s + 4)2!} z^2 + \dots,$$

and as  $\Delta \rightarrow 0$

$$F_1 \rightarrow 1 + \frac{(s + \beta + 2)}{(2s + 3)1!} (ibz) + \frac{(s + \beta + 2)(s + \beta + 3)}{(2s + 3)(2s + 4)2!} (ibz)^2 + \dots \\ = {}_1F_1(s + \beta + 2; 2s + 3; ibz), \dagger \quad (22)$$

and  $F_1 - F_2 \rightarrow 0$ .

We may not, however, put  $F_1 = F_2$  immediately, as  $F_1 - F_2$  occurs multiplied by factors which tend to infinity.

We have

$$F_1 - F_2 = -\frac{(s + \beta + 2)}{(2s + 3)} z F(s + \beta + 3, s + i\beta + 2, 2s + 4; z) \\ \rightarrow -\frac{(s + \beta + 2)}{(2s + 3)} z {}_1F_1(s + \beta + 3, 2s + 4; ibz), \quad (23)$$

and further

$$ibz = \left( \frac{2\gamma^2}{|\beta|} \right)^{\frac{1}{2}} e^{i\lambda}$$

with  $\lambda = \pi + \tan^{-1}(|\beta|/\gamma)$ .

We can calculate  $F_1$ ,  $F_2$  and  $F_1 - F_2$ .

We put

$$F_1 + F_2 \simeq 2F_1 = \lambda, \\ b(F_1 - F_2) = \mu,$$

so that  $\lambda$  and  $\mu$  are both of order unity,  $\mu$  being given by

$$\mu = (ibz) \frac{i(s + \beta + 2)}{(2s + 3)} {}_1F_1(s + \beta + 3, 2s + 4; ibz).$$

Previously we have worked with  $R_{l,k}$  and  $S_{l,k}$ , but now we have  $R_{l,k} \simeq S_{l,k}$ . Again we may not put  $R_{l,k} - S_{l,k} = 0$ , for it occurs multiplied by  $b$ . We therefore work with  $R_{l,k} + S_{l,k}$  and  $b(R_{l,k} - S_{l,k})$ . These are easily expressed in terms of  $\lambda$  and  $\mu$ , both of which are finite, and we can

$$\dagger {}_1F_1(a, b; z) = 1 + \frac{a}{b} z + \frac{a(a+1)}{b(b+1)} \frac{z^2}{2!} + \dots$$

derive recurrence formulæ for  $R_{l,k} + S_{l,k}$  and  $b(R_{l,k} - S_{l,k})$  by addition and subtraction of the formulæ for  $R_{l,k}$  and  $S_{l,k}$ . Finally, we have

$$F_k = (\mathcal{G}_k + \mathcal{G}_k^*)/2A$$

$$G_k = (\mathcal{G}_k - \mathcal{G}_k^*)/2 |B|,$$

which enables us to express the integrals (1) in terms of  $R_{l,k} + S_{l,k}$  and  $b(R_{l,k} - S_{l,k})$  since  $1/|B| \sim 0(b)$ . The limits of the various factors as  $\Delta \rightarrow 0$  are easily found, and we shall not reproduce the work here, as it is quite straightforward provided we work with the quantities  $\lambda$ ,  $\mu$ ,  $(R_{l,k} + S_{l,k})$  and  $b(R_{l,k} - S_{l,k})$  throughout.

In comparing with experiment the value of  $\sigma$  so obtained, we must remember that the calculated value of  $h\nu_0$  at the series limit does not agree with the experimental value, largely owing to the shielding effect of the outer shells. In lead for example the calculated value of  $h\nu_0/mc^2$  is 0.200 and the experimental value 0.175. We can take some account of this as follows.

In the integrals (1), expressing the transition probabilities, the main contribution comes from the regions near the nucleus, and those not far removed from the K-shell, provided that most of the photoelectrons are to be found in states with  $k = 0$  or 1. This condition is fulfilled for the soft  $\gamma$ -rays at the series limit, so that the region inside the L-shell is the most important. We can therefore consider the electron to be in a field of which the potential is given approximately by  $Ze/r - V_0$ , where  $V_0$  is the potential due to the presence of the outer shells, which is considered constant in the important region inside the L-shell. The additional term  $-V_0$ , does not alter the solutions of the wave equation, but only the energies. Consider now a  $\gamma$ -ray of energy  $h\nu_k$ , equal to the theoretical binding energy of a K-electron, *i.e.*, neglecting all screening effects. Since the wave functions in the important region inside the L-shell are unaffected by the presence of the  $V_0$  term, we may use the method given, and the result should give the absorption coefficient correctly. This absorption coefficient is then to be compared with the experimental value for  $\gamma$ -rays of energy  $h\nu_k$ , and not the value at the actual series limit, where  $h\nu_0 = h\nu_l < h\nu_k$ .

This argument is somewhat crude and it does not enable us to say anything about the absorption coefficients for  $\gamma$ -rays with energies between  $h\nu_l$  and  $h\nu_k$ . However, it does show that we must expect the absorption coefficient at the actual series limit ( $h\nu_l$ ) to be appreciably greater than that calculated for  $\gamma$ -rays of energy  $h\nu_k$ , as has been shown to be the case.†

† H. Hall, 'Phys. Rev.', vol. 38, p. 57 (1931).

## § 5—RESULTS

The values of the absorption coefficient, measured in  $\text{cm}^2$  for the *two* electrons of the K-shell for values of  $Z$ , the atomic number, and  $h\nu_0$ , the energy of the  $\gamma$ -ray, have been calculated and are given in the table, where  $\theta = mc^2/h\nu_0$ .

$\begin{array}{c} Z \\ \theta \end{array}$	26	50	84
0.452	$2.3 \times 10^{-26}$ (2.45)	$4.6 \times 10^{-25}$ (4.87)	$4.61 \times 10^{-24}$ (4.36)
1.443	$3.9 \times 10^{-25}$ (4.19)	$7.1 \times 10^{-24}$ (7.67)	$6.02 \times 10^{-23}$ (5.23)

In the brackets we give for comparison the values calculated using the formula of H. Hall:

$$\left. \begin{array}{l}
 \text{where} \\
 \text{and} \\
 \text{with}
 \end{array} \right\} \begin{array}{l}
 \sigma_{\text{K-shell}} = \sigma_0 / \alpha^{2\gamma^2} e^{\gamma(\pi-2\gamma)} \\
 \sigma_0 = 4\pi a_0^2 \alpha_0^8 Z^5 R \cdot mc^2 / h\nu_0 \\
 R = \frac{k'_0{}^3}{\kappa'^4} \left[ \frac{4}{3\varepsilon} + \frac{\varepsilon-2}{\varepsilon+1} \left\{ 1 + \frac{1}{2\varepsilon k'_0} \log \frac{\varepsilon-k'_0}{\varepsilon+k'_0} \right\} \right] \\
 \gamma = Z/137 \qquad a_0 = h^2/4\pi^2 me^2 \\
 \varepsilon = \kappa' + (1 - \alpha^2)^{\frac{1}{2}} \\
 \kappa' = h\nu_0/mc^2 \qquad \alpha_0 = 2\pi e^2/hc \\
 k'_0 = (\varepsilon^2 - 1)^{\frac{1}{2}}
 \end{array} \quad (24)$$

It will be seen that the differences are small, and decrease as  $h\nu$  increases, so that even though we feel that there is no justification for Hall's formula, we shall use it to supplement the above values in the region  $mc^2/h\nu_0 < 0.452$ .

In fig. 1, we plot  $\sigma_{\text{K}}/Z^5$  against  $Z$  for the two wave-lengths calculated, using Sauter's formula for  $\sigma_0$  at the point  $Z = 0$ , which is accurate in the limit  $Z \rightarrow 0$ .

From these two curves we can now find the value of  $\sigma_{\text{K}}$  for each of the two wave-lengths for any element, with an accuracy the same as that of the computation. With the aid of the values so obtained, together with the values for  $\sigma_{\text{K}}/\theta$  when  $\theta = 0$  and  $0.194$  as given by Hall's formula, we can find the values of  $\sigma$  for all values of  $\theta$  up to  $\theta = 1.443$ . In fig. 2 we plot  $\sigma_{\text{Atom}}/Z^5\theta$  against  $\theta$  as being most convenient, since it tends to

a finite non-zero limit as  $Z \rightarrow 0$  and also as  $\theta \rightarrow 0$ .  $\sigma_{\text{Atom}}$  is the absorption coefficient per atom and is obtained from  $\sigma_K$  by multiplying by a fraction  $5/4$  so as to include approximately the effect of the outer shells. This fraction  $5/4$  is taken from Rutherford, Chadwick and Ellis (*loc. cit.*, p. 464) who state that experiment shows that about  $4/5$  to  $5/6$  of the total absorption is due to the K-shell. Hall and Rarita† have recently calculated the absorption in the L-shell when  $h\nu_0 \gg mc^2$ , and find it about  $1/5$

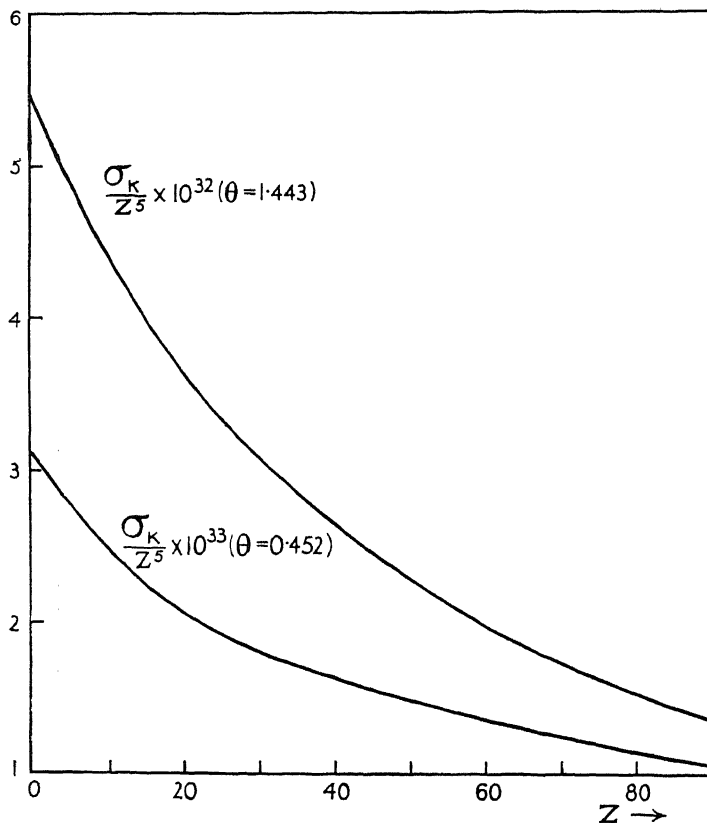


FIG. 1

that of the K-shell. This result is therefore in agreement with experiment, since the absorption in the outer shells is very small. The curves are given for various values of  $Z$ , which are indicated in the figure.

The three points marked in the figure are the experimental values of  $\sigma_{\text{Atom}}$  for lead ( $Z = 82$ ), and are taken from the empirical curve of L. H. Gray.‡ The agreement is very satisfactory.

† 'Phys. Rev.,' vol. 46, p. 143 (1934).

‡ 'Proc. Cam. Phil. Soc.,' vol. 27, p. 103 (1931).

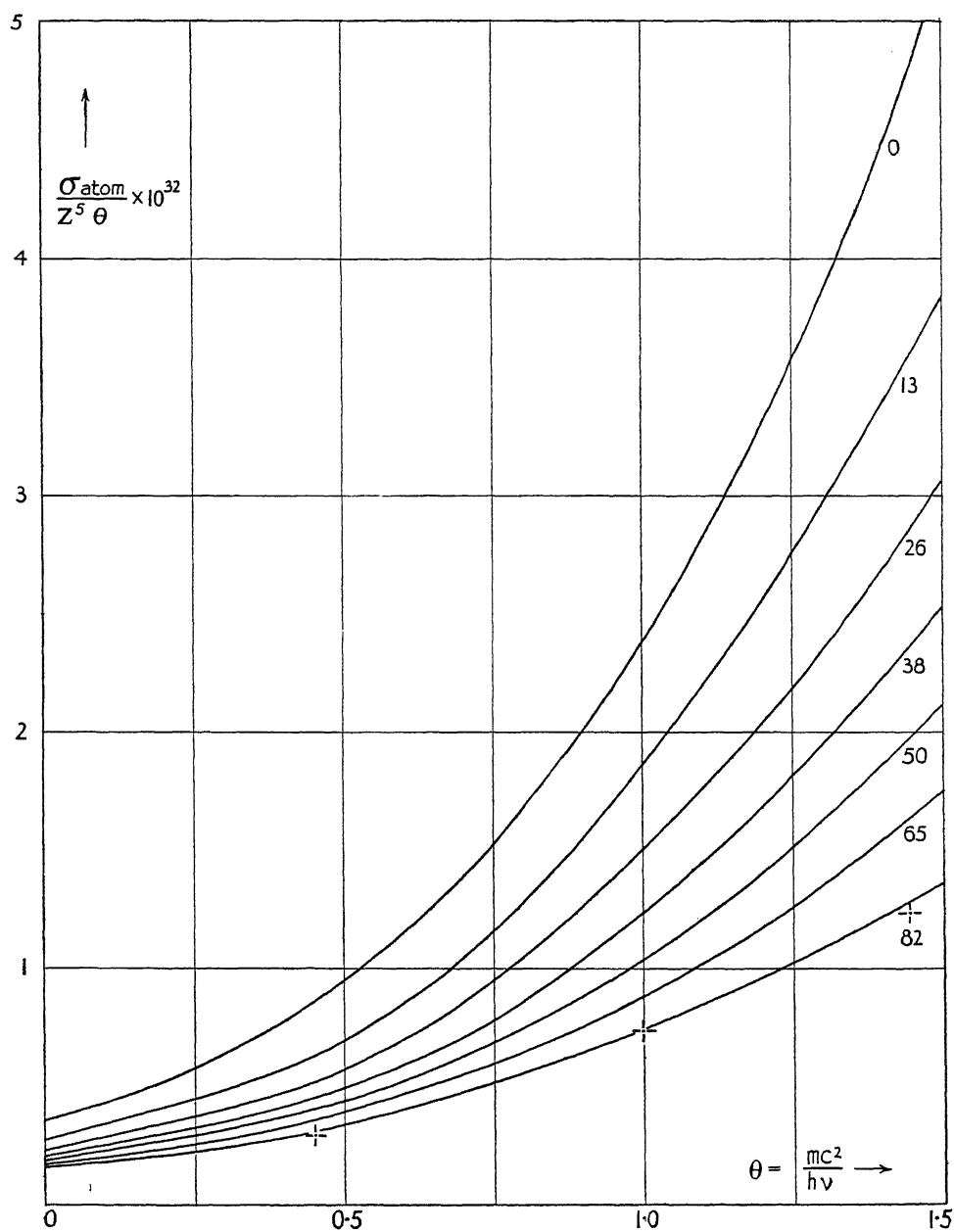


FIG. 2



The results expressed in this figure should be accurate to within about 8%, the results for lead in particular being probably accurate to within 4%.

It is also of interest to see the number of photoelectrons in the various final states, as shown in fig. 3.

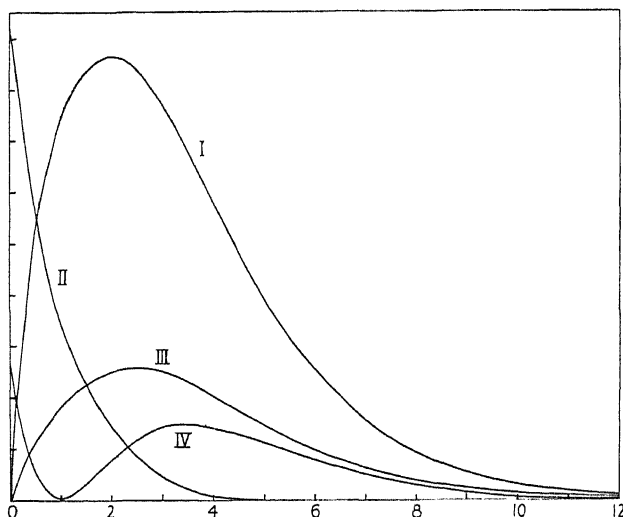


FIG. 3

We have plotted the number of electrons ejected in the four possible types of final state against  $k$ , the azimuthal quantum number, for the case  $Z = 84$ ,  $\theta = 0.452$ . The graphs marked I, II, III and IV represent the values of

$$|(m)_{1,k^a}|^2, \quad |(m)_{-1,k^a}|^2, \quad |(m)_{1,k+1^b}|^2 \quad \text{and} \quad |(m)_{-1,k+1^b}|^2$$

respectively. Of course the ordinates only exist for integral values of  $k$ , but the dependence is best exhibited in the form of a graph. The values for  $k \geq 9$  have been obtained by extrapolation.

For the  $h\nu_0/mc^2 = 0.210$  (which is the value at the theoretical series limit for  $Z = 84$ ) the calculation with  $Z = 84$  gives  $\sigma_{\text{Atom}} = 1.66 \times 10^{-21}$ , so that for lead we have

$$\begin{aligned} \sigma_{\text{Atom}} &= (82/84)^4 \cdot 1.66 \times 10^{-21} \\ &= 1.51 \times 10^{-21}. \end{aligned}$$

This may be compared with the experimental value given by J. A. Gray's empirical formula,<sup>†</sup>

$$\sigma_{\text{Atom}} = 1.92 (1 + 0.008Z) (1 - \lambda/4\lambda_K - \lambda/50 \lambda_K^2) Z^4 \lambda^3 10^{-26},$$

<sup>†</sup> J. A. Gray, 'Proc. Roy. Soc. Canada,' vol. 21, p. 179 (1927)

where  $\lambda_K$  is the wave-length at the series limit given in Angstroms. For lead  $\lambda_K = 0.139 \text{ \AA}$  and we find

$$\sigma_{\text{Atom}} = 1.51 \times 10^{-21},$$

in good agreement with the calculated value.

We have to thank the Department of Scientific and Industrial Research for grants extending over the three academic years 1931-34, which have enabled two of us (J. M. and R. A. B.) to devote our time to these calculations. Without this help these results could not have been obtained.

#### SUMMARY

A method is developed for finding the photoelectric absorption coefficient for the K-shell,  $\sigma_K$ . The calculations are rigorous and are not subject to the restriction  $Z \ll 137$ , where  $Z$  is the atomic number. Theoretically it is possible to apply the method for all values of  $h\nu_0$ , the energy of the quantum absorbed, but, as a considerable amount of numerical work is necessary, it is not practical for large values of  $h\nu_0/mc^2$ .

Values of  $\sigma_K$  are given for  $h\nu/mc^2 = 0.693$  and  $2.21$  for elements with atomic numbers 26, 50 and 84. The values obtained do not differ much from those given by H. Hall (*loc. cit.*), using a method which is discussed in the text. We have therefore used his expression for  $\sigma_K$  in the region  $h\nu_0 > 5mc^2$ , and have constructed graphs giving the photoelectric absorption *per atom* for various elements in the range  $h\nu_0 > 0.7 mc^2$  or  $3.4 \times 10^5 \text{ e.v.}$  The values obtained for lead are in excellent agreement with the experimental results as given by L. H. Gray's empirical formula (*loc. cit.*).

---

# Experiments at Very Low Temperatures obtained by the Magnetic Method

## I—The Production of the Low Temperatures

By N. KÜRTI and F. SIMON, Clarendon Laboratory, Oxford University

(Communicated by F. A. Lindemann, F.R.S.—Received November 6, 1934)

The lowest limit of temperature obtainable by the hitherto usual method of evaporating liquid helium lies at about  $0.7^{\circ}$ .† At this temperature the vapour pressure of helium is already so small that it does not seem possible to proceed to appreciably lower temperatures in this way.

In the course of last year the first successful experiments in attaining still lower temperatures were carried out using the magnetic method proposed by Debye‡ and Giauque.§ This method is based on the possibility of diminishing considerably the entropy of some paramagnetic salts by isothermal magnetization. The subsequent demagnetization, if carried out adiabatically, then results in a lowering of the temperature.||

A suitable substance for this method will be one with magnetic dipoles which are relatively free. That is to say, one in which the possible orientations of the dipoles all have nearly the same energy. In this case an external magnetic field will be able to produce a big change in the order of the dipoles, thus diminishing the entropy.¶ Such a substance can be recognized by the fact that it follows the Curie-Langevin law very closely, since this law is derived from the assumption of perfectly free elementary magnets. A substance, however, possessing perfectly free dipoles, and therefore following the Curie-Langevin law at *all* temperatures (*i.e.*, an “ideal” substance) cannot exist. For in such a substance there would have to be, at all temperatures, a random distribution of the dipoles in the different directions in the absence of an external field. In this case its entropy would not vanish at absolute zero, and this is contradictory to Nernst's theorem.

† Keesom, ‘Comm. Phys. Lab., Leiden,’ No. 219a, vol. XX (1932).

‡ ‘Ann. Physik,’ vol. 81, p. 1154 (1926).

§ ‘J. Amer. Chem. Soc.,’ vol. 49, p. 1864 (1927).

|| At high temperatures this method is of no use for the following two reasons: (1) at high temperatures exceedingly strong magnetic fields would have to be applied in order to obtain high magnetization (*i.e.*, a fairly large entropy change), and (2) the specific heats being high, the corresponding cooling would be very small.

¶ See, for instance, Simon, ‘Z. Physik,’ vol. 81, p. 824 (1933).

Actually, in a real substance, there must be a tendency to establish an order with respect to the dipole orientations, due to the existence of an interaction between the ions and the neighbouring particles. The resulting deviations from the ideal behaviour will begin when the temperature falls to the order of magnitude of a characteristic temperature  $\theta_m$ ,  $\theta_m$  being defined by the relation  $k\theta_m = U$  ( $U$  = interaction energy,  $k$  = Boltzmann's constant).

This characteristic temperature is the most important thing to know if one wishes to determine how suitable a substance will be for this procedure, since the lower the characteristic temperature, the lower the temperature that can be obtained by demagnetization.† At the present time it does not seem possible to predict the value of  $\theta_m$  for the various substances from purely theoretical considerations, though the theory may give some useful indications. Of course, the substance must be one which behaves ideally at least down to the temperatures obtainable with liquid helium (about 1°). The fact that it does this, however, gives no indication as to the value of the characteristic temperature. But there is a method which allows us to calculate the value of  $\theta_m$  from experiments carried out at temperatures much higher than  $\theta_m$  itself. The existence of energy levels implies an anomaly of the specific heats,‡ noticeable up to temperatures much higher than  $\theta_m$ , as the normal specific heat due to the lattice vibrations is very small at these temperatures. From the measurement of this anomaly one can derive the value of  $\theta_m$ . In this way, two years ago,§ we determined the characteristic temperature of gadolinium sulphate, and were enabled to predict the cooling effects to be expected.

Soon afterwards the first direct cooling experiments were carried out by Giauque and MacDougall,|| and by de Haas, Wiersma, and Kramers.¶ Giauque and MacDougall used gadolinium sulphate, and our predictions were in quite good agreement with their results. De Haas, Wiersma, and Kramers worked with several other substances, and found chromium potassium alum very suitable. Early this year we also started direct

† The complete demagnetization of a substance with  $\theta_m = 0$ , *i.e.*, an ideal substance, would lead to the attainment of absolute zero.

‡ Cf. Simon, 'Ergebn. exakt. Naturwiss.', vol. 9, p. 253 ff (1930).

§ Kürti, Simon, 'Naturwiss.', vol. 21, p. 178 (1933); Kürti, 'Z. phys. Chem.,' B, vol. 20, p. 305 (1933).

|| 'Phys. Rev.', vol. 43, p. 768 (1933); 'Phys. Rev.', vol. 44, p. 235 (1933).

¶ 'Physica,' vol. 13, p. 175 (1933); 'Nature,' vol. 131, p. 719 (1933); 'Naturwiss.', vol. 21, p. 467 (1933); 'Physica,' vol. 1, p. 1 (1933); de Haas, 'Nature,' vol. 132, p. 372 (1933); 'Naturwiss.', vol. 21, p. 732 (1933); de Haas and Wiersma, 'Physica,' vol. 1, p. 779 (1934). See also the report of Meissner, 'Phys. Z.', vol. 35, p. 303 (1934).

cooling experiments,† partly with the intention of finding out how suitable different substances would be, but chiefly in order to develop the experimental technique. Before entering into a description of our experiments, some theoretical considerations, which will be useful in the interpretation of the results, may be set forth.

### THEORETICAL CONSIDERATIONS

As the cooling in the magnetic method is brought about by an adiabatic and reversible demagnetization, a knowledge of the entropy as a function of temperature and magnetic field ( $H$ ) will give all the necessary information. We shall restrict the calculations to the case of demagnetization to the field zero, as this is the most important case in practice. Then one need only know the entropy as a function, firstly, of the temperature in the field zero, and, secondly, of the field at the initial temperature. Anticipating, we give in fig. 1 as an example, these data for iron ammonium alum.

The curve represents the entropy in a field zero; the entropy at the initial temperature of  $1^\circ$  as a function of the field is shown by the points on the line  $F$ . One can derive from this diagram the cooling that would be obtained by starting from different initial conditions. For example, starting at  $1^\circ$  with a field of 10,000 gauss (the point  $X$  in fig. 1, the parallel to the temperature axis, representing the isentropic demagnetization, ends at the field zero in the point  $Y$ . The abscissa of this point gives then the temperature attained (being  $0.045^\circ$  in the present case).

We shall now show how this diagram can be obtained. We shall neglect the entropy corresponding to the thermal vibrations in these calculations, the justification for this being given later. There is no difficulty in calculating the entropy as a function of  $H$  at the initial temperature, as, for the present, we are only interested in substances behaving ideally down to the initial temperature. The entropy is given by the formula,

$$S_{T, H} = S_{H=0} + \int_0^H \left( \frac{\partial \sigma}{\partial T} \right)_H dH$$

( $\sigma$  = magnetic moment per gram-ion), and an ideal substance  $(\partial \sigma / \partial T)_H$  can be easily derived.

The entropy in the field zero ( $S_{H=0}$ ) would possess in an ideal substance, at *any* temperature, the value  $R \log_e (2J + 1)$  per gram-ion, where

† Kürti and Simon, 'Nature,' vol. 133, p. 907 (1934).

$J$  stands for the total angular momentum of the ion concerned, according to the  $(2J + 1)$ -fold spacial degeneracy of the basic level of each individual ion. (In fig. 1 this value is represented by the dotted line,  $J$  for  $\text{Fe}^{+++} = 5/2$ .) In a real substance, however, the degeneracy is removed owing to the interaction between the ions and the neighbouring particles. Then at high temperatures ( $kT$  being large compared with the energy intervals between the resulting terms), the entropy will still be practically the same as for an ideal substance. But at lower temperatures the entropy decreases and, according to Nernst's theorem, vanishes at absolute zero as represented by the curve.

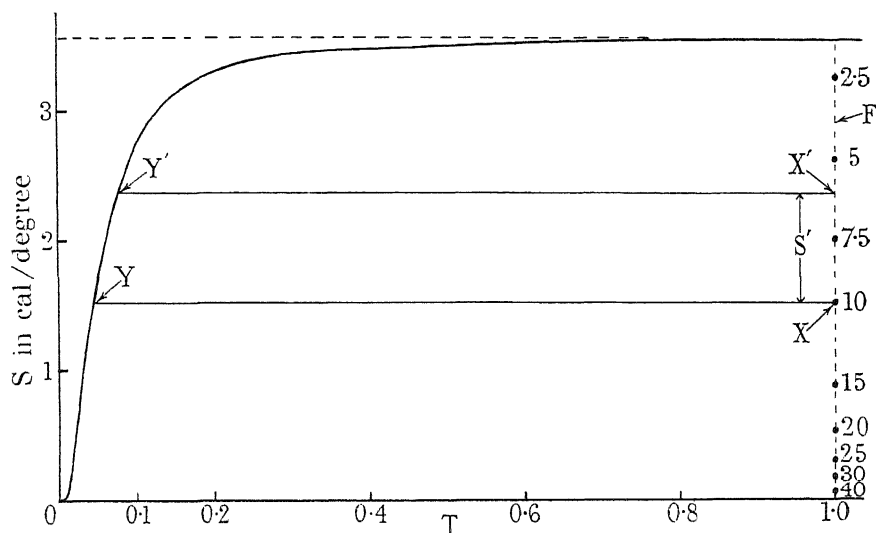


FIG. 1—Entropy of 1 gm-ion iron ammonium alum ( $\theta = 0.061^\circ$ ); the field strengths on line F are given in kilogauss

To calculate the S-curve, one requires a knowledge of the splitting pattern of the ground state. There are two causes† for the removal of the degeneracy, one being the influence of the electric field of the lattice, the other the direct interaction between the magnetic ions. Kramers has shown that if the number of electrons in the ion is odd, then an electric field cannot completely remove the degeneracy. A twofold degeneracy will be left which can only be removed by an interaction between the ions. Thus in the first case one would be justified in considering the ions independent of each other, and knowing the splitting pattern one would be enabled to calculate the corresponding entropy. For the

† Cf. Kramers, 'Proc. Acad. Sci. Amst.,' vol. 32, p. 1189 (1929).

second case, however, one can no longer assume that the ions are independent and the problem becomes more complicated.

But as even a rough knowledge of the entropy and of the specific heats derived from it would be a great help for the planning of the experiments, it seemed useful to derive an approximative formula. For this purpose we assumed that the basic level of each individual ion is split into  $(2J + 1)$  levels, which are separated by equal energy differences  $U = k\theta_m$ .

The relation between the temperature obtained by demagnetization and the initial conditions can then be derived in the following way.† Let  $T_i$  and  $H_i$  denote the initial temperature and field, and  $T_f$  the final temperature after demagnetization to field zero. In the initial conditions the ground state is split by the magnetic field into  $(2J + 1)$  levels, separated from each other by energy differences  $g\mu_B H$  ( $\mu_B$  = Bohr's magneton,  $g$  = Landé splitting factor). The distribution on the different levels, and consequently also the entropy, is a function only of  $\frac{g\mu_B H_i}{kT_i}$ . This is valid as long as the substance behaves ideally under the initial conditions, i.e.,  $T_i \gg \theta_m$ ,  $\mu_B H_i \gg k\theta_m$ , and these conditions are fulfilled in all cases of practical interest. Now, according to our assumption, the splitting of the final state reached after demagnetization is the same as that of the initial state, the only difference being that the  $(2J + 1)$  levels are now separated by the energy differences  $k\theta_m$ . Thus the entropy in the final state is the same function of  $k\theta_m/kT_f$ , as it was in the initial conditions of  $g\mu_B H_i/kT_i$ . Since during demagnetization the entropy remains constant, it follows that

$$\frac{T_f}{T_i} = \frac{k}{g\mu_B} \frac{\theta_m}{H_i}, \quad (I)$$

† The S-curve, which we shall not need explicitly for the derivation of the formula, is easily calculated with the above assumption. The entropy is given by

$$S = R \left[ T \frac{d \log_e Q_{(2J+1), \theta_m}}{dT} + \log_e Q_{(2J+1), \theta_m} \right],$$

where

$$Q_{(2J+1), \theta_m} = 1 + e^{-\frac{\theta_m}{T}} + e^{-\frac{2\theta_m}{T}} + \dots + e^{-\frac{2J\theta_m}{T}}.$$

For the numerical evaluation, we note that

$$Q_{(2J+1), \theta_m} = \frac{Q^{E_{(2J+1)\theta_m}}}{Q^{E_{\theta_m}}},$$

where  $Q^{E_{(2J+1)\theta_m}}$  and  $Q^{E_{\theta_m}}$  are the analogous expressions for one-dimensional har-

or, putting in the numerical values of  $k$  and  $\mu_B$

$$\frac{T_f}{T_i} = \frac{14 \cdot 9}{g} \frac{\theta_m}{H_i} \quad (\text{IA})$$

( $H_i$  being measured in kilogauss).

The above-mentioned limitations are fulfilled sufficiently accurately for  $T_i > 4\theta_m$ , and  $T_f/T_i < 0 \cdot 4$ .

If  $g = 2$ , as for  $Gd^{+++}$ , and according to the theory of Bose and Stoner for the ions in the first part of the iron group, the formula becomes

$$\frac{T_f}{T_i} = 7 \cdot 5 \frac{\theta_m}{H_i}. \quad (\text{II})$$

As in all the substances we are concerned with  $g = 2$ , we shall refer in future to formula (II), thus characterizing the substance by  $\theta_m$  instead of by  $\theta_m/g$ .

According to this formula† the final temperature is proportional to the initial temperature and inversely proportional to the initial field. The latter is of especial importance, as it shows that, in accordance with Nernst's theorem, the absolute zero cannot be attained by finite magnetic fields. The specific individual properties of the substance considered are represented in this formula by the proportionality of the final temperature to  $\theta_m$ .‡

In applying the formula one has, of course, to bear in mind the limits of its validity. The simplifications we introduced are in some ways

monic oscillators, with frequencies  $\frac{k}{h}(2J+1)\theta_m$  and  $\frac{k}{h}\theta_m$ . Hence for the entropy of the system we find

$$S = \frac{1}{3} [S^{E_{(2J+1)\theta_m}} - S^{E_{\theta_m}}],$$

$S^{E_{(2J+1)\theta_m}}$  and  $S^{E_{\theta_m}}$  are the corresponding entropies of a solid body according to Einstein, the numerical values of which can be found in tables. The coefficient  $\frac{1}{3}$  is due to the fact that  $Q$  relates to a one-dimensional oscillator, whereas the  $S$  values in the tables are given for a three-dimensional oscillator. In this way the  $S$ -curve in fig. 1 was calculated, taking for  $\theta_m$   $0 \cdot 061^\circ$  as derived from our measurements.

The same formula can be used for the calculation of the entropy of an ideal paramagnetic substance for different fields by simply replacing  $\theta_m$  by  $g\mu_B H/k$ .

† It was with this formula that we calculated the final temperatures to be expected for gadolinium sulphate ('Naturwiss.', vol. 21, p. 178 (1933)).

‡ The value of  $J$  does not enter into the formula at all so that with substances having different values of  $J$ , but the same  $\theta_m$ , the same final temperatures should be obtained. Of course,  $J$  does exert some influence, so far as  $\theta_m$  depends upon it. It seems that an increase in  $J$  would give rise to an increase in  $\theta_m$ , so that a substance with high  $J$  would be less favourable.



analogous to those which one makes in representing the specific heat of a non-regular crystal by a single Debye function. It is true that it will be possible to characterize roughly the properties of such a crystal in this way, but one cannot expect to represent the details; especially in extrapolating to very low temperatures, differences may appear in both cases.

Now one does not wish to cool only the salt itself, but the chief aim will be to cool other substances by this method in order to investigate their properties. For this reason we shall consider the influence of a second substance in contact with the paramagnetic salt, and we shall assume that the thermal contact is so perfect that we have reversible conditions.

Let us denote the entropy of the second substance at the initial temperature by  $S'$ . Then the entropy of the whole system will no longer be given by the point X, fig. 1, but by the point  $X'$ , where the distance  $XX' = S'$ . If the second substance follows Debye's  $T^3$  law, its entropy at the final temperature can be neglected and the final temperature is then given by the abscissa of the point  $Y'$ ,  $Y'$  being the intersection of the parallel to the temperature axis through  $X'$  with the  $S$ -curve.

For our numerical calculation, we shall consider the influence of the addition of an equal volume of lead† to iron ammonium alum in demagnetizing from  $1^\circ$  and 10,000 gauss. The entropy of 1 cc of lead at  $1^\circ$  is  $2 \times 10^{-5}$  calories/degree. This is negligible compared with the entropy of 1 cc (1/258 gram-ion) of iron ammonium alum, which, under these conditions, amounts to  $5 \times 10^{-3}$  calories/degree. In other words, practically the same temperature is reached with the additional substance as without it, and this gives us at the same time the justification for neglecting the entropy of the lattice vibrations in the derivation of the formula.

For very high fields, however, conditions are somewhat different. The entropy of the paramagnetic salt then becomes very small (see fig. 1) so that the entropy of the added substance, or of the lattice vibrations, may no longer be negligible. In order to obtain a numerical estimate, we have calculated the additional field that must be applied starting at  $1^\circ$  so that the same final temperature is reached after an equal volume of lead has been added. This additional field will be 33 gauss for an initial field of 10,000 gauss, for 20,000 gauss it becomes 100 gauss, for 30,000 gauss 250 gauss, and for 40,000 gauss it is already 1000 gauss. At 60,000 gauss the entropy of 1 cc of iron ammonium alum is only  $2 \times 10^{-3}$

† We take lead for the numerical example because of its high specific heat.

calories/degree at this temperature. That is the same value as that of the entropy of the added substance. So one would have to apply an infinite field in order to compensate the influence of the added substance. As the order of magnitude of the additional entropy in our example is the same as that of the lattice vibrations in the paramagnetic salt itself, we see that in deriving a formula for very high magnetic fields it is necessary to take into account the influence of the entropy of the lattice vibrations, whereas for fields obtainable in practice the influence is negligible.†

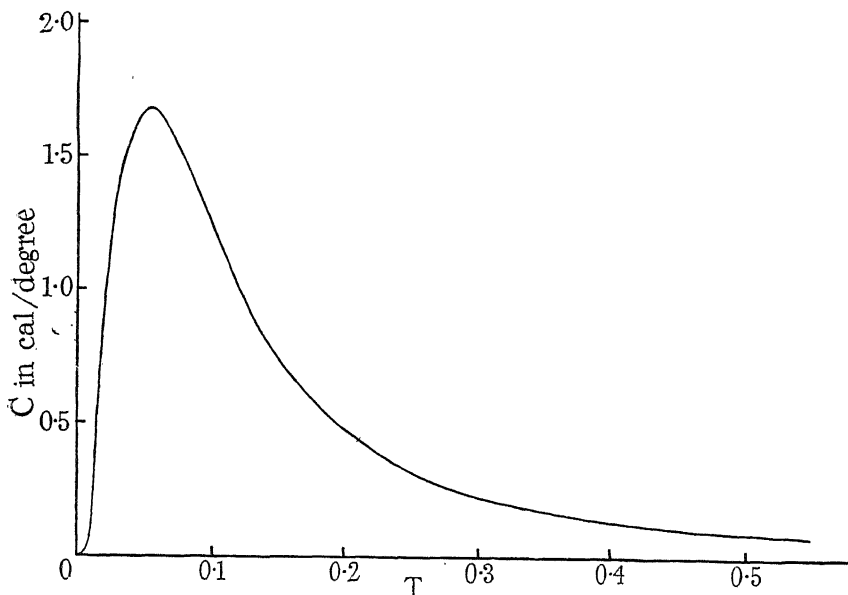


FIG. 2—Heat capacity of 1 gm-ion iron ammonium alum ( $\theta_m = 0.061^\circ$ )

Nothing has been said yet about the *specific heats* of these paramagnetic substances, which are of very great practical importance, as they give us an idea of the rate at which the temperature will rise after cooling. The change in the distribution of the ions amongst the different levels occurring in the neighbourhood of the temperature  $\theta_m$  is accompanied, as we have already mentioned, by a big anomaly of the specific heats due to the fact that an additional energy is necessary to lift the ions on to the higher energy levels.‡ In fig. 2 the heat capacity of 1 gram-ion of iron

† The existence of the lattice vibrations gives the lowest limit for the temperatures obtainable. Even the use of an infinitely large magnetic field would result in attaining only a temperature of about  $0.005^\circ$  (for a substance with  $\theta_m = 0.06^\circ$ , and making a reasonable estimate for the lattice entropy), whereas according to the formula absolute zero would be attained in this case.

‡ See Simon, 'Ergbn. exakt. Naturwiss.', vol. 9, p. 253 ff. (1930).

ammonium alum is given, calculated from the curve S in fig. 1 by means of the relation

$$C = T \left( \frac{\partial S}{\partial T} \right)_{H=0}.$$

The maximum of the anomaly is situated in this case at about  $0.05^\circ$ , the height of it amounting to 1.7 calories/gram-ion degree. With other substances conditions are similar, the position of the anomaly on the  $T$  axis obviously depending on the value of  $\theta_m$ , and the shape depending to a certain extent on  $J$ .

It is instructive to compare the magnitude of this specific heat with that of normal substances. 1 cc (equals 1/258 gram-ion) of iron ammonium alum has at the maximum (*i.e.*, at about  $0.05^\circ$ ) a heat capacity of 0.006 calories/degree. This corresponds to the heat capacity of 16 tons of lead at this temperature, or of 2 kilograms at  $1^\circ$ . This is very important from the experimental point of view, since a heat flow would warm up a substance whose specific heat varies according to the  $T^3$  law very quickly, and one could scarcely hope to maintain for an appreciable time the low temperatures obtained in the first moment. The fact mentioned above, however, changes this situation entirely and one can expect to keep for a reasonable period even small amounts of substances at the low temperatures obtained. To have the most favourable conditions, a substance must be chosen as cooling material whose characteristic temperature lies in the region in which it is desired to make investigations. For instance, a substance with a characteristic temperature of  $0.01^\circ$  would not be very suitable for investigations in the region between  $0.1^\circ$  and  $1^\circ$ , since its heat capacity in this region is small and it would warm up very quickly.†

#### DETERMINATION OF THE TEMPERATURE

We have now to say a few words on the determination of the temperatures obtained within this new region. The general way of determining the absolute temperature consists in measuring the pressure-volume relation of a gas, extrapolating it to the density zero, and getting the absolute value of  $T$  by applying the laws for an ideal gas. Within the

† Of course, this is true only for the heating up in an external field zero; in a finite external field the heat capacity is enlarged considerably. So it would be possible to get low rates of heating up at temperatures much above the characteristic temperature by demagnetizing to a finite field instead of to the field zero. But then it would be necessary to measure the temperatures in an external field, and this would usually complicate the experiment to an undesirable extent.

new temperature region with which we are concerned, no method relying upon a gas can be of any use. One might, however, make use of some other quantity for which a well-founded theoretical law exists, allowing an extrapolation down to the lowest temperatures. For instance, one could consider using Debye's  $T^3$  law for the specific heat, or any other quantity directly connected with it, such as the thermal expansion. But apart from other considerations,<sup>†</sup> the absolute change of these magnitudes following the  $T^3$  law becomes immeasurably small at these very low temperatures.

The last objection, however, would not apply when making use of the change of the paramagnetic susceptibility. But, as we have already seen, the magnetic method brings us just into those temperature regions in which Curie's law, well founded for higher temperatures, ceases to be valid.<sup>‡</sup>

The only way to obtain a really sound foundation would be to establish a temperature scale by thermodynamical measurements. We have seen that the thermal changes accompanying the change of magnetization of the paramagnetic salts used for this method are considerable. Therefore, it is obvious that the best way to obtain the thermodynamical scale is to apply the laws of thermodynamics to the process of magnetization.<sup>§</sup> But before this can be done one must be thoroughly familiar with the magnetic method. In the present stage of development, therefore, those who have carried out experiments of this kind have confined themselves to the use of an arbitrary temperature scale based upon the susceptibility of the salt itself. An arbitrary temperature  $T^*$  was thus introduced by extrapolating the susceptibility according to Curie's law. It is likely that at temperatures higher than  $\theta_m$  Curie's law will be followed fairly well, so that  $T^*$  will not differ appreciably from  $T$ . In the neighbourhood of  $\theta_m$  and below, however, it is difficult to say at present how great the deviations are likely to be.

<sup>†</sup> Cf. Cristescu and Simon, 'Z. phys. Chem.,' B, vol. 25, p. 273 (1934).

<sup>‡</sup> According to formula (II), starting from  $1^\circ$  a field of 7500 gauss brings us to the temperature  $\theta_m$ .

<sup>§</sup> The simplest way seems to us to be to determine the entropy in a field zero by demagnetizing from different initial conditions, and to measure the energy in a field zero, both quantities as a function of the arbitrary temperature  $T^*$ . The absolute temperature can then be derived by means of the known thermodynamical formula

$$T = \left( \frac{\partial U}{\partial T^*} \right)_{H=0} / \left( \frac{\partial S}{\partial T^*} \right)_{H=0}.$$
 See also Keesom, 'J. Phys. Rad.,' vol. 5, p. 373 (1934).

## THE APPARATUS

*General Remarks*

The construction of the apparatus depends largely upon the way in which the susceptibility is to be measured. One can either do this by measuring the force exerted on the sample when in an unhomogeneous field, or by using an inductance method. As the first way implies the necessity of having movable parts within the apparatus, and as, moreover, the sensitivity of the inductance method can be increased sufficiently, we have chosen the latter. In principle our method consisted in measuring the change in the mutual inductance of two coils placed round the paramagnetic salt.†

Another point affecting the construction of the apparatus is the size of the available magnets. We have already seen that the temperatures reached are inversely proportional to the initial field. As we had only small magnets at our disposal, it was necessary to use small pole gaps in order to obtain sufficiently strong fields. The part of the apparatus containing the substance had therefore to be as narrow as possible, and for this reason only a small amount of substance could be used. But this is not an appreciable disadvantage, since the heat capacities of these salts are so exceptionally high.

Every apparatus for this process must be constructed so that one can carry out, first an isothermal magnetization at a temperature as low as possible, and then an adiabatic demagnetization. In other words, one must be able first to bring the substance into thermal contact with a bath of liquid helium which takes up the heat of magnetization, and afterwards to remove the contact. This can be realized most simply by using as the heat transmitter a gas (which in future we shall refer to as the “exchange gas”), which can be pumped off in order to isolate the substance, as is usual for calorimetric measurements at low temperatures.‡ Now it is desirable to shorten the time necessary for conducting away the heat of magnetization and for the subsequent establishment of a high vacuum,

† An inductance method has already been used by Giaque and MacDougall, but no details are given in their papers. De Haas, Wiersma, and Kramers originally worked with the balance method, but in their last experiments they have also used an inductance method.

‡ For some purposes, especially when working with bigger amounts of the paramagnetic salt, it might prove useful to immerse the salt directly in a small quantity of liquid helium which remains in contact with the salt during demagnetization. Under our conditions, however, this does not appear favourable.

particularly because during this time the magnet has to remain switched on. If this time is short, one can overload the magnet and obtain higher fields. But there is a difficulty in making a quick change from the isothermal to the adiabatic arrangement, because at these low temperatures the helium gas is adsorbed on the substance and on the walls of the apparatus in considerable amounts, and it takes a long time to obtain a good vacuum.

For this reason we have chosen our experimental arrangement so that we need not rely upon removing the last traces of exchange gas by pumping. At the low temperatures reached by demagnetization the vapour pressure of helium becomes so small that the residual gas must condense on the surface of the substance. Table I gives the vapour pressures of helium, as calculated from the vapour pressure equation of Keesom.<sup>†</sup>

TABLE I—VAPOUR PRESSURES OF HELIUM

T	<i>p</i> (mm)	T	<i>p</i> (mm)
1.0	$1.5 \times 10^{-1}$	0.3	$7 \times 10^{-10}$
0.7	$3.2 \times 10^{-3}$	0.2	$3 \times 10^{-15}$
0.6	$4.2 \times 10^{-4}$	0.1	$3 \times 10^{-31}$
0.5	$2.5 \times 10^{-5}$	0.05	$4 \times 10^{-62}$
0.4	$5.0 \times 10^{-7}$	0.03	$6 \times 10^{-103}$

We see from the table that below 0.3° to 0.4° the vapour pressure is so small that the gas in equilibrium<sup>‡</sup> cannot transfer an appreciable amount of heat. (It may be of interest to mention that the vapour pressure of helium at 0.05° is about the same as that of iron at room temperature.) In a closed space having a temperature of even as much as 0.1° there is a much higher vacuum than can be obtained in any other way.

For this reason it is possible to establish a high vacuum by using the cooling substance itself as a pump. The experimental arrangement must then be adapted so that the free space filled with exchange gas is not too large. In this case the heat of condensation developed on the substance cannot do any harm. For instance, the condensation of an amount of helium gas contained in a volume of 10 cc at 1° and under a pressure of 1/1000 mm corresponds to a transfer of entropy of  $2 \times 10^{-6}$  calories/degree, taking 0.5° as the mean condensing temperature. As we saw above such an amount is negligible.

<sup>†</sup> 'Comm. Phys. Lab. Leiden,' No. 219a, vol. 20 (1932).

<sup>‡</sup> The values given for the vapour pressure are maximum values, since, on account of the adsorption on the substance the pressure will be appreciably reduced.

Of some importance in the construction of the apparatus was an observation made in the first experiments, namely, that the container for the salt did not cool down with the salt, even when the substance was touching the container at many points, and that the rate of warming up was also very slow in spite of such direct contact. This failure to conduct heat at the points of contact made it possible to simplify the construction considerably since the container could be directly connected with the helium bath, so that the heat exchange in the presence of the exchange gas was very efficient.

It is perhaps worth mentioning that it is necessary to avoid soft soldering any parts which are cooled down to the temperature of liquid helium, if in the neighbourhood of the substance. Soft solder is a superconductor at these temperatures, and gives rise to persistent currents that would disturb the measurement of the susceptibility.

### *The Construction of the Apparatus*

The same apparatus used by Kürti† for measuring the specific heat of gadolinium sulphate was used for this work, after some slight alterations. It contained a small Linde-liquefier,‡ in principle similar to that first described by Ruhemann.§ Only the parts used for the magnetic process need be described.

In fig. 3, V is the lower part of the helium liquefier; its temperature can be reduced to about  $1.6^{\circ}$  by pumping off the liquid helium. In order to obtain still lower initial temperatures, a second container C is used, into which liquid helium can be condensed through the thin-walled German silver tube G. This container is surrounded by the metal shield S, which is soldered to the helium liquefier so that it takes up its temperature. Consequently, the heat flow to C is very small, and it is possible to reduce the temperature to about  $1^{\circ}$  by connecting it through G to a mercury diffusion pump with a pumping speed of 3 litres/second. The lower part of C is also the inner part of a ground joint, the outer part being the upper end of B, the container for the substance. This container is connected to C, the ground joint being smeared with tap grease. This kind

† 'Z. phys. Chem.,' B, vol. 20, p. 308 (1933).

‡ During the last few years we changed to the expansion method for the liquefaction of helium (Simon, 'Z. ges. Kälteindustr.,' vol. 39, p. 89 (1932); Simon and Ahlberg, 'Z. Physik,' vol. 81, p. 816 (1933)). But in this case we kept to the older arrangement in order to make use of this available apparatus, which needed only a few alterations.

§ 'Z. Physik,' vol. 65, p. 67 (1930).

of joint turned out to be tight enough, even at low temperatures, for the very small pressure differences with which one is concerned. The container B can be filled with helium gas or can be evacuated through the tube R.

All these parts are surrounded by the copper vessel A, which is

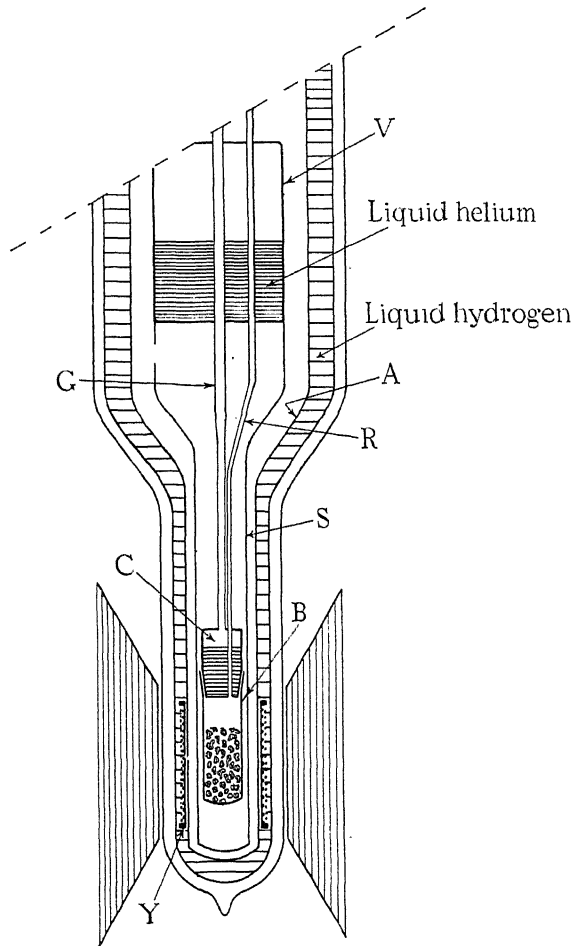


FIG. 3—Sketch of the apparatus

situated in a bath of liquid hydrogen. It is evacuated at the beginning of the helium liquefaction and remains so during the whole experiment.

The two coils for the susceptibility measurements are wound on a brass bobbin (Y) 2 cm long. The secondary coil consists of 2160 turns



of copper wire of 0.12 mm diameter, the primary of 20 turns of copper wire of 0.7 mm diameter. The bobbin is attached to A at the same height as the substance, thus being immersed in liquid hydrogen.

The measurement consists in reading the ballistic deflection of a galvanometer connected with the secondary coil, when a current is switched on in the primary. Of course, the deflection corresponding to the effect of the coils themselves has to be compensated, and this is done by a system of two adjustable coils situated outside the apparatus.

In the course of our experiments we worked with two different magnets. In the beginning we had at our disposal only a very old electromagnet of horseshoe form which gave, with a pole gap of 37 mm and a diameter of the pole pieces of 30 mm, a maximum field of 5000 gauss.†

In the later experiments we worked with a specially made electromagnet of the Weiss form. Fitted provisionally with uncooled coils, it gave with the same pole dimensions as above about 8000 gauss for a considerable time, or by overloading up to 15,000 gauss for about 1 minute.‡

As during the susceptibility measurements no iron can be allowed to be in the neighbourhood of the apparatus, both magnets were mounted on wheels so that they could easily be moved away.

#### DESCRIPTION OF AN EXPERIMENT

We shall omit a description of the operations necessary to obtain the temperature of liquid helium, which was reached about 1 hour after the precooling with liquid air had been started. Once the boiling point of helium was attained about 1 cc of liquid helium was condensed into the chamber C. Then the helium in C was pumped off and the susceptibility of the salt was measured at a number of points between  $4.2^{\circ}$  and  $1.4^{\circ}$ , the temperature being determined by the vapour pressure of the helium. B was filled with exchange gas at about 0.1 mm pressure.

Then the helium in C was pumped off to as low a pressure as possible, which reduced the temperature to between  $1.0^{\circ}$  and  $1.2^{\circ}$  according to the prevailing experimental conditions.

Next the magnet was moved into place, and the field switched on. The liberation of the heat of magnetization was indicated by the increased rate of evaporation of the liquid helium in C. After a few seconds, however, the stationary state was re-established, showing that the heat of

† In some experiments, by using a narrower Dewar vessel, we could reduce the pole gap to 30 mm thus obtaining about 6000 gauss.

‡ We hope soon to replace these provisional coils by cooled ones.

magnetization was quickly conducted away.† Therefore we could start pumping off the exchange gas immediately after switching on the magnet. With our experimental arrangement we had to pump from 5 to 8 minutes in order to obtain a vacuum of  $10^{-3}$  mm, which proved to be high enough. We found that at a pressure of this order the amount of gas still remaining in the apparatus was small enough to condense quickly on the substance during demagnetization.

Then the magnet was switched off and moved away. The first temperature measurement could be carried out about 20 to 30 seconds later.

Only the earlier of our experiments were carried out in the manner described. Though the time during which the current through the magnet had to be switched on was already very short,‡ we wished to reduce this time still more in our later experiments, in order to be able to overrun the magnet and use stronger fields. We succeeded in doing this when we found that a vacuum too high to give a good heat contact, nevertheless did not prevent the heat of magnetization being carried off in a short time. This is due to the fact that when the magnet is switched on the temperature of the substance rises considerably in the first moment.§ This causes the desorption of a large amount of gas, which carries away the heat of magnetization in a few seconds, so that it is possible to work with still smaller pressures. On switching on the magnet, with an exchange gas pressure of only  $10^{-2}$  mm, it was sufficient to pump for 1 or 2 minutes in order to obtain the vacuum necessary for an adiabatic demagnetization. As stated above, the heat of magnetization was carried away completely in this case. A cooling of the right order of magnitude is obtained even when the magnet is switched on only for 3 to 5 seconds, starting with an exchange gas pressure of  $10^{-4}$  mm||¶.

† We may mention that if a field of 10,000 gauss is applied at  $1^{\circ}$  to 1 gm of iron ammonium alum (the amount generally used in our experiments) the heat developed causes the evaporation of 8 mm<sup>3</sup> of liquid helium.

‡ The only data given by other experimenters is that of de Haas, Wiersma, and Kramers in their earlier experiments (see 'Naturwiss.,' vol. 21, p. 732 (1933)). In these experiments the magnet had to be switched on for some hours.

§ One can calculate that on switching on 10,000 gauss at  $1^{\circ}$  adiabatically, iron ammonium alum would heat up to about  $9^{\circ}$ .

|| We think it will be possible, by carefully choosing the dimensions, both for the parts containing the substance and for the pumping leads of the helium bath, to shorten still more the time during which the magnet has to be switched on. In this case it should be possible to work with much stronger fields by applying a method similar to that used by Kapitza.

¶ Based upon the experiences described above, we have designed a very simple arrangement which retains many advantages though it is not fit for such general use as our usual apparatus. A description is given in 'Physica,' vol. 1, p. 1107 (1934).

The compensation of the two systems of coils for the susceptibility measurement was adjusted at the boiling point of helium.<sup>†</sup> Then in the temperature range between  $4.2^{\circ}$  and  $1.6^{\circ}$  the ballistic deflections of the galvanometer were determined as a function of the helium vapour pressure, using always the same measuring field. The galvanometer deflections gave in this region, for all the substances we used, a straight line when plotted against  $1/T$ .

The following example gives an idea of the sensitivity of the arrangement: using 1 gm of iron ammonium alum the change of the galvanometer deflection between  $4.2^{\circ}$  and  $1.6^{\circ}$  (*i.e.*, a change in  $1/T$  of about 0.4) was 30 mm, applying a measuring field of 25 gauss. Once the low temperature was obtained by demagnetization, the measuring field had to be weakened in order to avoid too big deflections. These small measuring fields do not perceptibly affect the final temperature, so that one measures practically the same temperature as that obtained in demagnetizing to the field zero.

## THE RESULTS

We shall restrict ourselves to a general survey of the investigation of different substances, omitting a description of the experiments carried out in order to develop the apparatus and the experimental method. We shall characterize the different substances by giving the value of  $\theta_m$  as derived in applying formula (II); in this way the variations in the initial conditions are eliminated. We have to emphasize, of course, that in calculating  $\theta_m$  the values of  $T^*$  only are available and not those of the absolute temperature  $T$ . Thereby an uncertainty is involved when calculating with a very low final temperature  $T^*$ . But our  $\theta_m$  values are only intended to characterize the properties of the substance roughly for practical purposes, postponing the theoretical discussion until we have a sound foundation for the temperature after having established the thermodynamical scale.

In choosing the substance, we were guided principally by the extensive experimental work done in Leiden on the susceptibility of paramagnetic

<sup>†</sup> In the metal parts between the measuring coil and the substance eddy, currents are produced on switching on the measuring field. But as their time constant is small compared with the period of the galvanometer they give rise only to a very short kick which does not affect the reading of the deflection.

substances† and by the fundamental theoretical considerations of Kramers‡ and van Vleck.§

As our first substance we took gadolinium sulphate, the “classical” substance, in order to compare its  $\theta_m$  with the value obtained from our specific heat measurements and with that calculated from Giauque’s results. On looking for other suitable substances, we thought of taking some salts of the ions  $Mn^{++}$  and  $Fe^{+++}$ , as the ground state of these two, like  $Gd^{+++}$ , is an S-term. On theoretical grounds the unhomogeneous electric field in the crystal should have a much smaller effect on an S-term, owing to its high symmetry, than on other terms. We took, therefore, iron ammonium alum and manganese ammonium sulphate, both of which, according to the Leiden measurements,|| follow Curie’s law down to  $14^\circ$ . In addition, we knew from unpublished measurements of the specific heat of the former, that its  $\theta_m$  is considerably smaller than that of gadolinium sulphate. Furthermore, for the sake of comparison we investigated chromium potassium alum with which, in Leiden, the lowest temperatures had been obtained. Finally, we did some experiments with mixed crystals in order to determine the influence of the magnetic dilution on  $\theta_m$ .

All these substances were used in the form of a coarse powder, in amounts ranging from 0.3 to 1.0 gm.

In calculating the susceptibilities we did not make any correction for the demagnetizing factor and the Lorentz factor, as these two corrections should cancel out to a first approximation in the conditions prevailing in our experiments.¶

(a) *Iron ammonium alum*,  $FeNH_4(SO_4)_2 \cdot 12H_2O$  (1 gm-ion = 462 gm, corresponding to 258 cc of compact material).

In Table II we give the result of a set of measurements.

We see that the values of  $\theta_m$  obtained from demagnetizations starting with different initial fields and initial temperatures give sufficiently

† See, for instance, the survey on this subject by Gorter, ‘Arch. Mus. Teyler,’ vol. 7, p. 183 (1933).

‡ ‘Leipziger Vorträge,’ p. 43 (1933), where references to earlier publications can be found.

§ “The Theory of Electric and Magnetic Susceptibilities.” (Oxford 1932).

|| Kamerlingh Onnes and Oosterhuis, ‘Comm. Phys. Lab. Leiden,’ No. 129b, vol. 11, (1912); Jackson and Kamerlingh Onnes, ‘Comm. Phys. Lab. Leiden,’ No. 168b, vol. 15, (1923).

¶ Breit, ‘Comm. Phys. Lab. Leiden,’ Suppl. No. 46; see also Gorter, ‘Arch. Mus. Teyler,’ vol. 7, p. 194 (1933). This point, which can in any case only give rise to an appreciable error in demagnetizing to the lowest temperatures, will be discussed in detail in a subsequent paper.

TABLE II

$T_i$	$H_i$ (Kgauss)	$T_f^*$	$\theta_m$
1.23	14.1	0.038	0.059
1.23	11.1	0.053	0.064
1.23	10.3	0.055 <sub>5</sub>	0.062 <sub>5</sub>
1.23	8.3 <sub>0</sub>	0.071 <sub>5</sub>	0.065
1.23	6.5 <sub>5</sub>	0.085 <sub>7</sub>	0.061
1.23	4.9 <sub>5</sub>	0.114	0.061 <sub>5</sub>
1.23	2.9 <sub>0</sub>	0.187	0.059
2.23	10.3	0.099	0.059
2.23	8.2 <sub>3</sub>	0.119	0.061

consistent values of  $\theta_m$ . The mean value of  $\theta_m$  derived from this table is 0.061<sub>3</sub>. This value was used for calculating the entropy and specific heat given in figs. 1 and 2. As a further illustration, we show in fig. 4

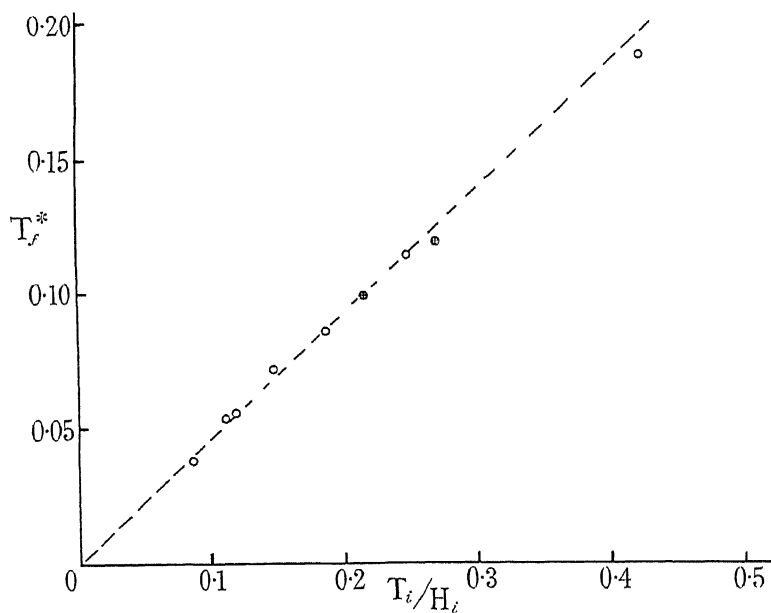


FIG. 4—Final temperatures  $T_f^*$  obtained with iron ammonium alum as function of initial temperature over initial field.  $\circ$  initial temperature = 1.23°;  $\oplus$  initial temperature = 2.23°

the final temperatures ( $T_f^*$ ) as a function of  $T_i/H_i$ . In agreement with the formula, the points lie on a straight line passing through the origin.

It was with this substance that the lowest temperature in our experiments were obtained, namely,  $T^* = 0.038^\circ$ , reached under the conditions shown in the table.

(b) *Manganese ammonium sulphate*,  $\text{MnSO}_4(\text{NH}_4)_2\text{SO}_4 \cdot 6\text{H}_2\text{O}$ . (1 gm-ion = 381 gm, corresponding to 208 cc of compact material)—It was this salt that we used in the experiments concerned with the development of the apparatus and the experimental technique. Therefore not all the experiments have the same weight, and we do not think it worth while to give the data of the numerous demagnetizations carried out with this salt. We found that down to final temperatures of  $0.2^\circ$  the results can be well represented by formula (II), with  $\theta_m = 0.11^\circ$ . Starting with higher initial fields, however, lower final temperatures are reached than those calculated with a  $\theta_m$  of  $0.11^\circ$ . These deviations are quite appreciable; for example, with  $T_i = 1.23^\circ$  and  $H_i = 8000$  gauss, a temperature of  $0.09^\circ$  is obtained, instead of  $0.12^\circ$ . On increasing the initial field still further, the final temperature remains stationary, at least when fields up to 14 kilogauss are applied.

It seems probable that this is due to a phenomenon analogous to the Curie point; a question we are still investigating. It may be mentioned here, however, that as has been specially emphasized by Debye,<sup>†</sup> these paramagnetic substances should become ferromagnetic, provided one takes into account only the pure magnetic interaction of the ions. The corresponding Curie points are then given, on taking  $4\pi/3$  as the constant of the molecular field, by  $4\pi/3\rho \cdot C$  ( $\rho$  = density,  $C$  = Curie constant). For manganese ammonium sulphate this expression gives  $0.086^\circ$ , a temperature in the region of the above anomalies. But, on the other hand, with iron ammonium alum which, according to the above formula, ought to have a Curie point at  $0.068^\circ$ , there is no indication of an anomaly in this temperature region.

(c) *Gadolinium sulphate*,  $\frac{1}{2}\text{Gd}_2(\text{SO}_4)_3 \cdot 8\text{H}_2\text{O}$ . (1 gm-ion = 373 gm, corresponding to 124 cc of compact material)—The sample used was the same as that with which specific heat measurements had been carried out. We are much indebted to Professor G. Urbain for placing this sample at our disposal. We made only one demagnetization ( $T_i = 1.15^\circ$ ,  $H_i = 5.4$  kilogauss) reaching a temperature  $T_f^* = 0.35^\circ$ , which leads to a value  $\theta_m = 0.22^\circ$ . The agreement with  $\theta_m = 0.26^\circ$  calculated from the specific heats seems sufficiently close, taking into consideration the fact that the latter value had to be derived from the last portion of the specific heat anomaly. From the demagnetization experiments of Giauque we derive  $\theta_m = 0.19^\circ$ .

(d) *Chromium potassium alum*,  $\text{KCr}(\text{SO}_4)_2 \cdot 12\text{H}_2\text{O}$ . (1 gm-ion = 479 gm, corresponding to 261 cc of compact material)—With this sub-

<sup>†</sup> 'Ber. sächs. Akad. Wiss.,' vol. 86, p. 105 (1934).

stance, too, we only carried out one experiment ( $T_i = 1.14^\circ$ ,  $H_i = 5.5$  kilogauss,  $T_f^* = 0.16^\circ$ ), which gives  $\theta_m = 0.10^\circ$ . The experiment of de Haas and Wiersma ( $T_i = 1.16^\circ$ ,  $H_i = 24.6$  kilogauss,  $T_f^* = 0.031^\circ$ ) gives  $\theta_m = 0.09^\circ$ . [Note added in proof—Further experiments demagnetizing to lower temperatures ( $0.055^\circ$ ) have shown that the  $\theta_m$  values diminish as with manganese ammonium sulphate.]

(e) *Mixed Crystal of Manganese Ammonium Sulphate and Magnesium Ammonium Sulphate*—The well-known Leiden investigations on the influence of paramagnetic dilution on susceptibility suggest that the interaction, and consequently  $\theta_m$ , can be diminished by diluting the ions further, and this can be realized by working with mixed crystals.† In doing this, of course, the proportion of the vibration entropy to that of the magnetic ions is changed in the unfavourable direction. However, our calculation above shows that this fact does not become serious until a proportion of 1:50 to 1:100 is reached. Of course, a dilution will be an advantage only if the interaction between the magnetic ions themselves is responsible for splitting the terms. If, however, it is the electric field of the lattice which removes the degeneracy, then only the neighbouring particles would have an influence; as their effect is scarcely changed by dilution nothing would be gained.

To get an idea of the efficiency of this method, we made a trial with a mixed crystal of  $1\text{MnSO}_4(\text{NH}_4)_2\text{SO}_4 \cdot 6\text{H}_2\text{O}$  diluted with  $20\text{MgSO}_4(\text{NH}_4)_2\text{SO}_4 \cdot 6\text{H}_2\text{O}$ . Five demagnetizations were carried out with this substance with final temperatures between  $0.05^\circ$  and  $0.08^\circ$ . From these experiments  $\theta_m = 0.08^\circ$ , which is 25% smaller than  $\theta_m$  for pure manganese ammonium sulphate.

The fact that a dilution in the proportion 1 to 20 causes only such a relatively small decrease in  $\theta_m$ , i.e., in the interaction energy, seems to indicate that the removal of the degeneracy is in the first place due to the crystalline field, and only to a smaller extent to the direct interaction of the magnetic ions on one another. We propose to continue these experiments, especially with mixed crystals of iron ammonium alum and aluminium ammonium alum.

*Comparison of the different Substances*—We ought to include here those substances investigated by de Haas, Wiersma, and Kramers with their first apparatus,‡ namely, cerium fluoride, dysprosium ethyl sulphate, and cerium ethyl sulphate. But as in their experiments the rate of warming up immediately after demagnetization was very high, it is not possible

† Cf. Gorter, 'Arch. Mus. Teyler,' vol. 7, p. 274 (1933).

‡ 'Physica,' vol. 1, p. 1 (1933).

to give the actual lowest temperatures and, moreover, as the demagnetizations were not carried through to the field zero, the values of  $\theta_m$  cannot be calculated.

In Table III we give  $\theta_m$  for pure substances in order of increasing  $\theta_m$ .

TABLE III

Substance	$\theta_m$
Iron ammonium alum .....	0·061
Chromium potassium alum .....	0·095
Manganese ammonium sulphate .....	0·11
Gadolinium sulphate .....	0·21

In characterizing a substance by  $\theta_m$  one assumes that the entropy due to the lattice vibrations is negligible. In going to lower temperatures, however, or in cooling down other substances (especially in those most interesting cases which show an anomaly in the specific heat) this is no longer true. In such cases it is desirable to have a substance which, *ceteris paribus*, has a magnetic entropy density as high as possible. This will be the case (a) if the concentration of the ions is high, or (b) if the entropy per gm-ion is high, and this depends upon the value of  $J$  (for an ideal substance  $S = R \log_e (2J + 1)$ ), which in this case has to be considered.

In Table IV we give for the substances mentioned above, as a measure for the magnetic entropy density, the value of  $A = \frac{R \log_e (2J + 1)}{\text{ionic volume}}$  in calories per degree per  $\text{cm}^3$ .

We see that the variation of  $A$  for these substances is not very large. Furthermore, one has to bear in mind that the values of  $\theta_m$  and  $A$  are not independent of each other, though there is no simple quantitative relation between them.

TABLE IV

Substance	$A$
Gadolinium sulphate .....	0·033
Manganese ammonium sulphate .....	0·017
Iron ammonium alum .....	0·014
Chromium potassium alum .....	0·011

*Rate of Warming Up*—It is not only important to obtain low temperatures, but one must also be able to keep them. The rate of warming up depends on the specific heat and on the heat flow to the substance. The specific heat is a maximum in the neighbourhood of  $\theta_m$ , so the conditions



become more and more favourable down to this temperature. More important still is the effect of the rapid lowering of the vapour pressure which acts in the same direction. For example, at about  $0.4^\circ$  the vapour pressure is already so small that the gas in equilibrium cannot give rise to a heat contact of practical importance. Below these temperatures conditions are such that even small amounts of substances can be kept for a long time at low temperatures. Care must be taken, however, not to make a mechanical heat contact between the substance and the container, unless the latter is very well insulated from parts at helium temperatures. One must, therefore, avoid pressing the substance against the container or letting it freeze on to it.

The absolute values of the rate of warming up depend on the experimental conditions. In our arrangement, for instance, the rate of heating up in the temperature region below  $0.4^\circ$  was usually about 1 millidegree per minute; we could reduce this to  $\frac{1}{4}$  millidegree by changing the dimensions. With these high vacua and the complete lack of radiation it would be possible, of course, to get as low a value as one wished; but up to the present it has not been necessary to reduce the rate of warming up, as the values mentioned above allow the carrying out of practically isothermal measurements. Rather there is a difficulty in warming up a cooled substance to a specified temperature. We found the simplest way was to let the temperature of the container rise temporarily; the gas desorbed in this way causes a bigger heat flow which can be stopped at the desired point by cooling the container again.

To keep a constant temperature in the region about  $0.4^\circ$  is more difficult for the two reasons mentioned above. One can improve the conditions by choosing a substance with a higher  $\theta_m$ , thus, for example, gadolinium sulphate seems to be quite suitable for this temperature region. A better way, however, is to work with greater amounts of a substance with small  $\theta_m$ . In this case small magnetic fields are sufficient (for example, a field of 1.5 kilogauss suffices to cool iron ammonium alum from  $1.2^\circ$  to  $0.4^\circ$ ) so that one can afford to increase the size of the apparatus.

The next step in the further development of experiments of this kind will have to be the establishment of the thermodynamical temperature scale, as only then can one have a solid basis for temperature measurements. Furthermore, this will provide the necessary data for discussing the properties of the paramagnetic substances from the theoretical point of view.

Future experiments will be chiefly those in which another substance is cooled down with the paramagnetic salt. We shall report on a first

attempt in this direction in a subsequent paper which will deal with an investigation on different metals to find out whether they become supra-conductive in this temperature region. A more important application, however, than the extension of these investigations into the new temperature region will be the study of phenomena originating in the existence of a nuclear spin.<sup>†</sup> For these phenomena the new temperature region will be characteristic, since appreciable effects can only be observed at extremely low temperatures owing to the small value of the interaction energy and of the nuclear magnetic moments.<sup>‡</sup> Besides the theoretical interest, the nuclear paramagnetism may be of practical interest for the magnetic method, as probably the very lowest temperatures will be reached with a multiple stage apparatus, of which the last stage will work with a substance exhibiting nuclear paramagnetism.<sup>§</sup>

In conclusion, we should like to express our thanks to Imperial Chemical Industries, Ltd., whose generous assistance has enabled us to continue our researches in England.

We also wish to thank all the members of the laboratory, and especially Professor Lindemann and Mr. T. C. Keeley for their hospitality and their assistance in many phases of the work.

Finally, we are much indebted to Dr. H. London for his kind help in carrying out the experiments.

#### SUMMARY

(1) The production of very low temperatures by the magnetic method is discussed from the theoretical point of view, especially the influence of the initial conditions of field and temperature and of the characteristic properties of the substance. In addition, the effect of adding another substance and cooling it with the paramagnetic salt is calculated.

(2) An apparatus and the technique of the experiments are described permitting, quickly and simply, extremely low temperatures to be attained and used. In particular, it is shown that it is possible even with small amounts of substance to maintain the low temperatures obtained for a

<sup>†</sup> [*Note added in proof*—A preliminary account of some researches on these points has been published in 'Nature,' vol. 135, p. 31 (1935).]

<sup>‡</sup> It might be mentioned that in some cases, *e.g.*, with orthohydrogen, the nuclear paramagnetism could already be detected in the temperature region of liquid helium.

<sup>§</sup> [*Note added in proof*—From the account of the discussion on low temperatures at the Deutscher Physikertag, 1934 (initiated with a very interesting paper by Professor Debye), which was published in 'Phys. Z.,' vol. 35, p. 923 (1934) it appears that Dr. Gorter made a similar suggestion.]

very long time so that one can now carry out measurements in this temperature region quite easily.

(3) Iron ammonium alum, manganese ammonium sulphate, chromium potassium alum, and gadolinium sulphate have been investigated as working substances. Of these salts iron ammonium alum is the most nearly ideal, *i.e.*, the interaction of the magnetic ions is the smallest, so that the salt is the most suitable for this method. With this substance, starting at  $1.2^\circ$  and 14 kilogauss, a temperature of  $0.038^\circ$  was reached.

(4) Experiments with a substance in which the magnetic ions were diluted by forming a mixed crystal indicated that the greater part of the interaction is due to the crystalline field and not to direct interaction.

## The Scattering of Neutrons by Protons

By H. A. BETHE and R. PEIERLS, University of Manchester

(Communicated by D. R. Hartree, F.R.S.—Received November 19, 1934)

1. The mass defects of the lightest nuclei, particularly the ratio between that of the dipion and the  $\alpha$ -particle, make it very probable that the range of the interaction force between proton and neutron is very small, of the order of about  $10^{-13}$  cm.\* Therefore, in all experiments in which scattering of neutrons by protons has been observed, their wave-length is larger than the range of the interaction force. In these circumstances it is well known that the scattering intensity will be independent of angle for that co-ordinate system in which the centre of gravity is at rest.† For much higher energies, of course, this will no longer be true and one will expect then an anisotropy in the scattered intensity. This effect will become appreciable for energies for which the wave-length is of the same order as the range of the forces. Exact measurements of the angular distribution of scattered fast neutrons would therefore afford a direct check of the assumption of a short range and an estimate of this range. The existing experiments‡ show an isotropic scattering within

\* Wigner, 'Phys. Rev.', vol. 43, p. 252 (1933).

† Wigner, 'Z. Physik,' vol. 83, p. 253 (1933); Chadwick, 'Proc. Roy. Soc.,' A, vol. 142, p. 1 (1933).

‡ Chadwick, *loc. cit.*; Auger and Monod-Herzen, 'C. R. Acad. Sci., Paris,' vol. 196, p. 1102 (1933); Kurie, 'Phys. Rev.,' vol. 43, p. 672 (1933).

the limits of error, but are not accurate enough to allow very definite conclusions.

2. The importance of such experiments is further increased by the fact that, as was pointed out by Wick,\* the sign of the asymmetry in the scattering depends on whether the interaction is of the ordinary type or an exchange force as proposed by Heisenberg† and Majorana,‡ and observations of the asymmetry could therefore decide this question.

For very high energies of the scattered particles (wave-length small compared with range) for "ordinary" forces§ this asymmetry is always such that most of the particles are scattered through small angles (*i.e.*, most of the observed protons move at right angles to the incident neutron beam). For exchange forces one gets the opposite behaviour, *i.e.*, the neutrons will preferentially be scattered backwards in the co-ordinate system of relative motion (in the ordinary co-ordinate system the protons will then mostly go forward). This behaviour can be interpreted as the incident particle going on with a small deflection, but in the process of scattering it has changed role with the scattering particle and has become a proton.

It has been tacitly assumed that this will be quite generally true and that a forward maximum in the scattering will always indicate ordinary forces, while a backward maximum would require exchange.

We shall show, however, that just for the proton-neutron interaction this assumption fails for not very high energies. For these we just get a backward maximum with ordinary and a forward maximum with exchange forces, whereas the effect reverses its sign at a certain rather high energy.|| This behaviour is closely connected with the fact that the interaction forces admit a state in which the particles are bound together, as we know from the existence of the dipion.

3. In the following we denote by  $r$  the length of the radius vector between proton and neutron and by  $\theta$  its angle with the incident beam, by  $E$ ,  $v$ ,  $k$  the energy, velocity and wave number of the incident neutrons in the relative co-ordinate system and by  $E_0$ ,  $v_0$ ,  $k_0$  the same quantities for the system where the proton is initially at rest.

\* 'Z. Physik,' vol. 84, p. 799 (1933).

† 'Z. Physik,' vol. 77, p. 1 (1932).

‡ 'Z. Physik,' vol. 82, p. 137 (1933).

§ We use here and subsequently the word "ordinary" forces as distinct from exchange forces, for interactions corresponding to wave mechanical operators that do not interchange the co-ordinates of protons and neutrons.

|| The calculations of Wigner ('Z. Physik,' *loc. cit.*) led to different results, but they contained an error in the rather complicated analysis.

$M$  is the mass of the proton or the neutron,  $V(r)$  the interaction potential, which for definiteness we first suppose to be an "ordinary" one, and  $\varepsilon$  the binding energy of the dipton.

The Schrödinger equation then separates in polar co-ordinates; we write

$$r\psi = \sum_l u_l(r) P_l(\theta), \quad (1)$$

where  $P_l$  is the spherical harmonic of order  $l$  and  $u_l$  has to satisfy the equation\*

$$\frac{\hbar^2}{M} \left( \frac{d^2 u_l}{dr^2} - \frac{l(l+1)}{r^2} u_l \right) + (E - V(r)) u_l = 0, \quad (2)$$

and asymptotically for large  $r$  has the form

$$u_l = \text{const.} \sin(kr - \frac{1}{2}l\pi + \delta_l). \quad (3)$$

The phases  $\delta_l$  have to be determined by integration of (2). Then the effective cross-section for scattering through an angle  $\theta$  becomes†

$$d\sigma = \frac{\pi}{2k^2} \left| \sum_l (2l+1) P_l(\theta) (e^{2i\delta_l} - 1) \right|^2 \sin \theta d\theta. \quad (4)$$

We now assume  $V$  to have a range of order  $a$  which is small compared with the wave-length  $\lambda = 1/k$ . In this case all phases  $\delta_l$  will be small except for  $l=0$ , because the centrifugal force  $\hbar^2 l(l+1)/Mr^2$  already makes the eigen-function very small for radii  $r < l\lambda$ .

4. We begin with the discussion of  $\delta_0$ . We know of the potential  $V$  that the equation (2<sub>0</sub>) admits a solution with a negative energy, viz.,  $-\varepsilon$ . There will be only one negative eigen-value, because the difference between the levels must be of the order  $\hbar^2/Ma^2$  which with the assumed value of  $a \sim 10^{-13}$  cm becomes of the order  $10^3$  volts. The eigen-function  $u_0$  belonging to this bound state will increase quickly for  $r < a$ , and for large  $r$  will show a slow exponential drop,‡ of the form

$$\left. \begin{aligned} u_0 &= \text{const.} e^{-\alpha r} \\ \alpha &= \sqrt{M\varepsilon}/\hbar \sim 2.3 \cdot 10^{12} \text{ cm}^{-1} \end{aligned} \right\}. \quad (5)$$

In the transitional region  $r \sim a$  the expression  $\frac{1}{u_0} \frac{du_0}{dr}$  must therefore be slightly negative and of the order  $-\alpha$ .

\*  $\frac{1}{2}M$  = reduced mass.

† Mott and Massey, "Atomic Collisions," Oxford Press, 1933, p. 24.

‡ Bethe and Peierls, 'Proc. Roy. Soc.,' A, vol. 148, p. 146 (1935).

If we now consider a small positive energy, the value of  $\frac{1}{u_0} \frac{du_0}{dr}$  for  $r = a$  will be practically the same as for the small negative energy  $-\varepsilon$ . This can be shown in the following way: by writing (2<sub>0</sub>) for two different values of  $E$  one can easily derive the following relation for the corresponding wave functions  $u_0$  and  $u'_0$ :

$$\left[ u_0 \frac{du'_0}{dr} - u'_0 \frac{du_0}{dr} \right]_{r=a} = \frac{M}{\hbar^2} (E - E') \int_0^a u_0 u'_0 dr. \quad (6)$$

If the difference  $E - E'$  is small, we have

$$\frac{d}{dE} \left( \frac{1}{u_0} \frac{du_0}{dr} \right)_{r=a} = - \frac{M}{\hbar^2} \frac{1}{u_0^2(a)} \int_0^a u_0^2(r) dr. \quad (7)$$

The integral on the right-hand side is of the order  $au_0^2(a)$ . It actually is somewhat smaller, since  $u_0^2(r)$  vanishes at  $r = 0$  and its value at  $r = a$  is practically equal to its maximum value. Therefore

$$\left( \frac{1}{u_0} \frac{du_0}{dr} \right)_{r=a} \sim -\alpha - (E + \varepsilon) \frac{\gamma Ma}{\hbar^2}; \quad 0 < \gamma < 1. \quad (8)$$

For the special case of a potential hole of rectangular shape, we find  $\gamma = \frac{1}{2}$ . The right-hand side of (8) differs appreciably from  $\alpha$  only if

$$E \sim \frac{\hbar^2 \alpha}{Ma} = \sqrt{\varepsilon \cdot \frac{\hbar^2}{Ma^2}}, \quad (9)$$

which is of the order  $1 \times 10^7$  volts (corresponding to a neutron energy  $E_0 = 2 \times 10^7$  volts).

If, therefore, the energy is smaller than (9) we have essentially

$$\left( \frac{1}{u_0} \frac{du_0}{dr} \right)_a = -\alpha,$$

and since  $u_0$  will already have the form (3<sub>0</sub>) for  $r = a$ , we see that

$$k \frac{\cos(ka + \delta_0)}{\sin(ka + \delta_0)} = -\alpha, \quad (10)$$

which yields

$$\begin{aligned} \delta_0 &= -ka + \operatorname{tg}^{-1}(-k/\alpha) \\ &= \pi/2 + \operatorname{tg}^{-1}(\alpha/k) - ka. \end{aligned}$$

According to (4) the differential and total cross-sections then become

$$\left. \begin{aligned} d\sigma &= \frac{2\pi}{\alpha^2 + k^2} \sin \theta \, d\theta \\ \sigma &= \frac{4\pi}{\alpha^2 + k^2} = 24 \times 10^{-25} \frac{\varepsilon}{\varepsilon + \frac{1}{2}E_0} \text{ cm}^2 \end{aligned} \right\}, \quad (11)$$

where  $E_0 = 2E$  is the energy of the incident neutron and  $\varepsilon = 2 \cdot 2 \cdot 10^5$  volts.

The cross-section (11) is rather larger than the experimental values of Chadwick. For  $E_0 = 4 \cdot 3 \cdot 10^6$  volts ( $v = 2 \cdot 9 \cdot 10^3$  cm/sec) Chadwick finds a cross-section between  $5$  and  $8 \times 10^{-25}$  cm<sup>2</sup> (radius  $4$  to  $5 \times 10^{-13}$ ), whereas (11) gives  $12 \times 10^{-25}$ ; for  $E_0 = 2 \cdot 1 \times 10^5$  volts ( $v = 2 \cdot 10^3$  cm/sec) the corresponding figures are  $11$  to  $15 \times 10^{-25}$  (experimental) and  $16 \times 10^{-25}$  (theoretical). Considering the very indirect experimental method the agreement can, however, be considered as fair.

The assumption of a short range for the potential can thus be checked both by the isotropy and by the absolute magnitude of the cross-section (11).

For energies that are small compared with (9),  $\delta_0$  is larger than  $\pi/2$  since  $k^2 \ll \alpha/a$ , but above a certain energy of the order (9),  $\delta_0$  will become smaller than  $\pi/2$ . In order to see this we remark that  $\delta_0 = \pi/2$  is equivalent to

$$\left( \frac{1}{u_0} \frac{du_0}{dr} \right)_a = -k \operatorname{tg} ka \sim -k^2 a,$$

and according to (8)

$$- \alpha - (E + \varepsilon) \gamma M a / \hbar^2 = - \alpha - \gamma a (k^2 + \alpha^2) = - k^2 a,$$

i.e.,

$$k^2 (1 - \gamma) = \alpha/a - \alpha^2 \gamma$$

$$E_s = \frac{1}{1 - \gamma} \sqrt{\varepsilon \frac{\hbar^2}{M a^2}}. \quad (12)$$

Since  $1 - \gamma$  is positive and of order unity this energy is of the order (9).

5. For the evaluation of  $\delta_1$ , we compare the behaviour of the function  $u_1$  and the function  $w_1$  that is a solution of (2<sub>1</sub>) when  $V$  is put equal to zero. One easily derives that

$$\left( w_1 \frac{du_1}{dr} - u_1 \frac{dw_1}{dr} \right)_{r=R} = \frac{M}{\hbar^2} \int_0^R V(r) u_1(r) w_1(r) dr,$$

where  $R$  is an arbitrary large distance. Inserting (3<sub>1</sub>), we find

$$- \operatorname{tg} (kR + \delta_1) + \operatorname{tg} kR = \frac{M}{\hbar^2 k} \frac{1}{u_1(R) w_1(R)} \int_0^\infty V u_1 w_1 dr.$$

It is convenient to choose such a distance  $R$  that  $tg \, kR = 0$ , then  $w_1(R)$  has just its relative maximum value and

$$tg \, \delta_1 = - \frac{M}{\hbar^2 k u_1(R) w_1(R)} \int_0^\infty V(r) u_1 w_1 dr. \quad (13)$$

The right-hand side is positive since  $V < 0$ , and  $u_1$  and  $w_1$  have equal sign.

The expression (13) is small, since  $V$  is only appreciable in regions where both the functions  $u$  and  $w_1$  are much smaller than outside because of the centrifugal force. For an estimate of (13) we may identify  $u_1$  with

$$w_1 = \frac{\sin kr}{kr} - \cos kr,$$

and obtain

$$\delta_1 = - \frac{M}{\hbar^2 k} \int_0^\infty V(r) (\tfrac{1}{3} k^2 r^2)^2 dr.$$

From the existence of a small negative eigen-value of the equation (2<sub>0</sub>) one can conclude that

$$- \int V(r) r^4 dr \propto \tfrac{1}{2} \frac{\hbar^2}{M} a^3$$

$$\delta_1 \propto \tfrac{1}{18} (ka)^3.$$

Actually the form of  $u_1$  will differ from that of  $w_1$  and therefore the numerical factor will be even less certain; we may write

$$\delta_1 = \frac{\beta}{18} (ka)^3, \quad (14)$$

where  $\beta$  is of order unity. For the special case of a rectangular potential, it may be shown that

$$\beta = \frac{72}{\pi^2} - 6 = 1.32.$$

6. We see that  $\delta_1$  is very small and positive,  $\delta_2$ ,  $\delta_3$ , etc., are proportional to still higher powers of  $ka$ , and therefore in calculating the deviations from the isotropic distribution we may confine ourselves to the first two terms in (4), and also neglect higher powers of  $\delta_1$  than the first:

$$d\sigma = \frac{\pi}{2k^2} |(\cos 2\delta_0 - 1) + i(\sin 2\delta_0 + 3\delta_1 \cos \theta)|^2 \sin \theta d\theta$$

$$= \frac{\pi}{2k^2} (4 \sin^2 \delta_0 + 6\delta_1 \sin 2\delta_0 \cos \theta) \sin \theta d\theta.$$



We therefore see that the sign of the asymmetry depends on the product  $\delta_1 \sin 2\delta_0$ . According to the properties of  $\delta_0$  and  $\delta_1$  derived above, we get a maximum backward ( $\cos \theta = -1$ ) for energies smaller than (12), since for these  $\delta_0 > \pi/2$ , *i.e.*,  $\sin 2\delta_0 < 0$ . At higher energies we have a maximum forward, and the asymmetry vanishes for the energy  $E_s$  given by (12).

The highest absolute value of the asymmetry for energies below (12) is obtained for  $E = \frac{1}{2}E_s$ ; then the difference between forward and backward scattering, divided by the average scattering, becomes

$$\beta (a\alpha)^2/12 (1 - \gamma),$$

which is approximately 1%. Such a small asymmetry is difficult to observe and the anisotropy would become easily observable\* only for neutron energies above (12), *i.e.*, about  $4 \cdot 10^7$  volts, which at the present moment seem impossible to obtain.

It would, however, be very important to measure the angular distribution with neutron energies up to the highest available, in order to ascertain that our original assumptions are at least approximately correct.

If the interaction force is not an "ordinary" one but of the exchange type, the calculation of  $\delta_0$  remains unchanged. In the differential equation for  $\delta_1$ , however, the sign of the potential will be reversed.† To that accuracy with which we considered this potential as a perturbation on  $u$  we simply have to reverse the sign of  $\delta_1$ . Actually also the coefficient  $\beta$  will be smaller than it would be with an "ordinary" force. (With a rectangular potential,  $\beta = \frac{36}{\pi} \frac{1 + e^{-\pi}}{1 - e^{-\pi}} - 6 \left(1 + \frac{12}{\pi^2}\right) = -0.89$ ). Then we shall have a forward maximum for  $E < E_s$  and a backward maximum for  $E > E_s$ .

#### SUMMARY

The cross-section and the angular distribution are calculated for the scattering of neutrons by protons. The result is practically independent of the special law of force assumed between neutron and proton, it depends only on the known binding energy of the dipton. The cross-section obtained is about 50% larger than the rather uncertain experi-

\* For energies comparable with  $V$ , *i.e.*, of the order  $10^8$  volts, the asymmetry would become of the order unity.

† Bethe and Peierls, *loc. cit.*

mental value. The scattering is almost isotropic (in the relative co-ordinate system) for all neutron energies up to about 40 million volts. Only for still higher energies, which are at present unavailable, an experimental determination of the sign of the anisotropy would decide whether the force between neutron and proton is of the exchange type or an ordinary force.

---

## On the Direction of Approach of Microseismic Waves

By A. W. LEE, M.Sc., D.I.C., Kew Observatory

(Communicated by G. C. Simpson, F.R.S.—Received November 20, 1934)

### 1—INTRODUCTION

It has been thought for some time that an examination of the relation between the phases of the horizontal and vertical displacements in microseisms would be of interest in showing how closely the oscillations compare with Rayleigh waves, but a practicable scheme for making the observations has only recently been developed. In the earlier attempts the turning points of consecutive oscillations were timed during several minutes, but the accuracy attained by interpolation between the minute breaks was not high enough for reliable comparisons between the components. A solution of this difficulty has now been found in a modification of the method adopted by Leet,\* who has examined the relation between the horizontal and vertical phases of the microseisms recorded at Harvard Observatory, using comparisons of the movements *exactly at the minute breaks*. The application of this new method to the seismograms of Kew Observatory is described in the present paper.

### 2—TABULATION OF THE PHASES OF THE MICROSEISMS

Fig. 1 shows portions of the records obtained from the Galitzin seismographs at Kew on January 11, 1930, when the microseisms were very large. Upward movements on the seismograms correspond with ground

\* 'Gerl. Beitr. Geophys.,' vol. 42, p. 232 (1934).

movements to the north, to the east, and upwards. The direction of recording is from right to left.

For the purposes of this investigation the phases at the beginning of the minute breaks have been allotted numbers according to a scale, fig. 2, from 0 to 15. The entries 0 and 8 indicate that the beginning of

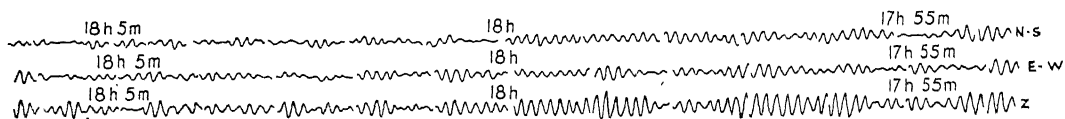


FIG. 1—Large microseisms recorded at Kew Observatory, January 11, 1930

the break coincides with the crest and trough respectively. Four examples illustrating readings of 12, 0, 7 and 3 are shown in the figure. The procedure adopted in the tabulations is to estimate the phases at fifty consecutive time breaks, the series beginning 25 minutes before the specified hour.

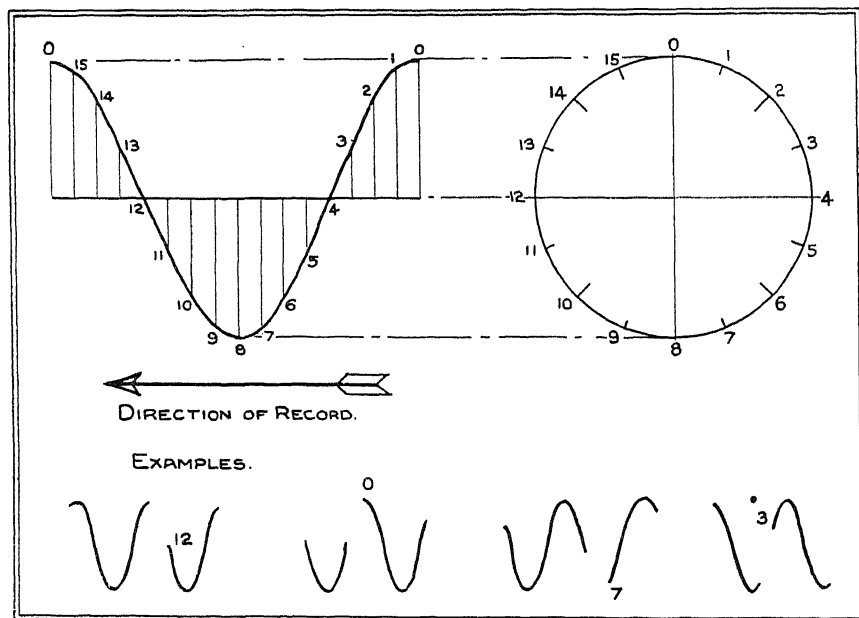


FIG. 2—Scale of tabulation for phase angles

The free periods of the horizontal and vertical seismographs being 25 sec and 13 sec, the "lag" of the ground movements behind the corresponding oscillations in the records is not the same for the three components, and the phases of the horizontal and vertical ground movements are not directly comparable from the seismograms.

In Galitzin's notation the formula for the time lag with simple harmonic earth movements is:—

$$\text{Time lag } (\tau + \tau_1) = \frac{T_p}{2\pi} \cdot \tan^{-1} \left\{ \sqrt{(1 - \mu^2)} \cdot \frac{2u}{u^2 - 1} \right\} + \frac{T_p}{2\pi} \left\{ \tan^{-1} \left( \frac{2u_1}{u_1^2 - 1} \right) + \frac{\pi}{2} \right\}.$$

Here  $T_p$  is the period of the earth wave,  $\mu^2$  the damping coefficient,  $u$  and  $u_1$ , the ratios of period of the earth-wave to the periods of the pendulum and of the galvanometer, and the inverse tangents are between 0 and  $\pi$ .\*

The phase differences between earth movements of periods 0 to 10 seconds and the recorded oscillations, for the Galitzin seismographs at Kew are as given in Table I.

TABLE I

Period of earth movement, seconds . . . . .	0	2	4	6	8	10
Horizontal phase correction, degrees . . . . .	450	431	413	395	378	362
Vertical phase correction, degrees . . . . .	450	415	382	351	324	300

These values are appropriate for critical damping and with the free period of each pendulum equal to that of the corresponding galvanometer; the effects of slight departures from these ideal conditions are not appreciable. The differences between the phase corrections of the horizontal and vertical seismographs, for oscillations of periods 4, 6 and 8 seconds, are  $31^\circ$ ,  $44^\circ$  and  $54^\circ$ ; consequently in dealing with the microseisms this difference may be taken as  $45^\circ$ . The sign of the difference is such that when the horizontal and vertical records are in phase the vertical earth movement is  $45^\circ$  in advance of the horizontal movement. To allow for this difference between the instruments  $45^\circ$  is subtracted from the phases of the vertical component, before the values are compared with the phases of the horizontal components.

A specimen of the tabulations, showing values for 1930, January 11d 18h, is given in Table II.

### 3—DATA

The microseisms associated with depressions over different parts of the eastern Atlantic and western Europe have been investigated. The

\* The phase difference is called a "lag" implying that the movements of the recorder follow the corresponding movements of the ground. Actually when the movements are not simple harmonic the changes in amplitude of the recorder precede the changes in amplitude of the ground movement. The lag,  $\tau + \tau_1$ , given by the Galitzin formula should therefore be decreased by  $2\pi$ . In other words the lag of the earth movement behind the movement of the light spot of the seismograph is  $2\pi - (\tau + \tau_1)$ . Cf. Scrase, 'London Proc. Phys. Soc.,' vol. 43, p. 259 (1931).

TABLE II—TABULATION OF PHASES OF THE MICROSEISMS AND PHASE DIFFERENCES BETWEEN THE COMPONENTS. 1930. JANUARY 11D 18H, PHASE UNIT =  $\pi/8$

Time, G.M.T.	Phases as read			Z phase corrected	Phase differences		
	N—S	E—W	Z		Z and N—S	Z and E—W	N—S and E—W
h m							
17 35	15	9	5	3	12	6	10
36	9	14	14	12	13	2	5
37	15	11	9	7	8	4	12
38	0	6	5	3	13	3	6
39	8	2	15	13	11	5	10
40	3	4	6	4	15	0	1
41	13	6	5	3	10	3	9
42	1	5	7	5	12	0	4
43	7	11	9	7	0	4	4
44	0	6	3	1	15	5	6

occasions were selected from the synoptic weather maps (British Daily Weather Reports). The occasions chosen,\* together with the positions of the depressions and the bearings from Kew to the disturbed regions, are set out in Table III.

TABLE III—OCCASIONS SELECTED FOR TABULATION OF THE PHASES OF THE MICROSEISMS

Date	Figure	Position of depressions	Bearing of centres of depressions from Kew
1930, January 11d 18h ..	5	North-west of Scotland . . . .	North-west.
		North-west of Azores . . . . .	West.
1932, December 10d 7h	6	Atlantic Ocean off northern Portugal	South-west.
		Barent's Sea . . . . .	North-north-east.
1933, December 13d 7h	7	Bay of Biscay to Ligurian Sea	South.
		Northern Norway . . . . .	North-north-east.
1934, January 18d 7h. . . .	8	Between the Shetlands and Norway	North-north-east.
1934, January 23d 7h. . . .	9	Greenland Sea . . . . .	North.
		Atlantic Ocean west of Ire- land	West.
1934, February 8d 7h ..	10	Southern Norway and Kanai Peninsula	North-north-east.

\* A comparison of the microseismic amplitudes and the meteorological conditions on the first of these dates has already been published—London, Meteorological Office, Geophysical Mem., No. 62 (1934).

Fifty measurements of the phases were made in each case, and after applying the "lag correction" of  $45^\circ$  to the values for the vertical component, the phase differences between the components were tabulated. The significance of a few of the measurements is uncertain owing to juxtaposition of two periods at the minute breaks, but such values do not occur often enough to have an appreciable effect upon the complete series.

Table IV shows the distribution of the phase differences between the components, and the numbers of the values from 1 to 7 and from 9 to 15; the totals for the six occasions are given at the bottom of the table. There is a striking contrast between the data for the three pairs of components, the phase differences of most frequent occurrence being  $270^\circ$  between Z and N—S,  $90^\circ$  between Z and E—W and  $180^\circ$  between N—S and E—W. For Z and N—S, 82 of the differences are from 1 to 7 and 188 from 9 to 15, whilst for Z and E—W 217 are from 1 to 7 and 58 from 9 to 15. The N—S and E—W phase differences are more evenly distributed, the numbers in these groups being 126 and 131 respectively. The data for the separate days are examined in Section 5.

With each series containing only 50 measurements, irregularities in the distributions among the sixteen possible phase differences are inevitable and the values must be smoothed. The method adopted is to take overlapping groups of five values, giving double weight to the second and fourth, and treble weight to the third; thus, if  $F_n$  denotes the number of observations of any phase difference ( $n$ ), the smoothed frequency expressed as the percentage of the total number of values is

$$\{F_{n-2} + 2F_{n-1} + 3F_n + 2F_{n+1} + F_{n+2}\} \frac{100}{450}.$$

These smoothed frequencies for the six occasions are represented by ordinary graphs in fig. 3, and by vectorial diagrams in the insets to the weather maps, figs. 5–10. The figures on the axes of the vectorial diagrams represent frequencies of 5 and 10% of the total number of values per  $22\frac{1}{2}^\circ$ .

#### 4—RELATION BETWEEN THE PHASES OF THE OSCILLATIONS

In the curves of fig. 3 clearly defined maxima are shown in the region of  $270^\circ$  for the frequencies of the Z and N—S phase differences on 1930, January 11d 18h, 1934, January 18d 7h, January 23d 7h, and February 8d 7h, and of  $90^\circ$  for the Z and E—W differences of 1930, January 11d 18h, 1932, December 10d 7h, 1934, January 18d 7h, January 23d 7h, and February 8d 7h. There are maxima around  $180^\circ$  for the N—S and E—W

TABLE IV—NUMBER OF OCCURRENCES OF SPECIFIED PHASE DIFFERENCES BETWEEN THE COMPONENTS OF THE MICROSEISMS

Date	Components	Phase difference*																Number of values	
		0	1	2	3	4	5	6	7	8	9	10	11	12	13	14	15	1-7	9-15
1930, January 11d 18h ..	Z and N-S	1	0	1	1	2	2	1	0	2	6	7	8	3	6	2		7	40
	Z and E-W	3	4	7	12	7	5	4	3	1	1	1	1	0	1	0	0	42	4
	N-S and E-W	2	3	2	1	3	5	3	4	6	7	4	2	3	4	0	1	21	21
1932, December 10d 7h ..	Z and N-S	3	3	4	2	6	3	1	2	3	5	5	1	4	3	3	2	21	23
	Z and E-W	3	3	7	10	6	6	5	3	1	2	1	0	0	1	2	0	40	6
	N-S and E-W	2	2	3	2	5	4	4	2	5	2	3	3	0	6	4	3	22	21
1933, December 13d 7h ..	Z and N-S	4	4	5	2	6	5	0	4	1	2	3	1	3	3	5	2	26	19
	Z and E-W	2	4	7	4	2	2	2	4	4	1	3	1	3	4	4	3	25	19
	N-S and E-W	7	5	0	2	3	4	3	6	1	4	3	1	2	3	1	5	23	19
1934, January 18d 7h .....	Z and N-S	4	0	1	2	2	2	2	2	3	4	4	7	4	5	6	2	11	32
	Z and E-W	1	3	1	3	11	5	6	6	3	4	2	1	0	1	2	1	35	11
	N-S and E-W	4	3	2	1	3	1	2	4	5	2	3	5	2	6	5	2	16	25
1934, January 23d 7h .....	Z and N-S	2	0	2	1	3	0	1	2	2	5	6	6	6	3	6	5	9	37
	Z and E-W	4	5	2	9	8	4	3	6	1	3	1	0	0	0	2	2	37	8
	N-S and E-W	2	5	2	0	6	5	2	3	4	6	3	2	1	5	3	1	23	21
1934, February 8d 7h .....	Z and N-S	1	1	1	0	0	0	3	3	4	2	2	10	11	5	4	3	8	37
	Z and E-W	1	2	7	4	9	5	9	2	1	0	2	2	3	0	1	2	38	10
	N-S and E-W	1	3	3	2	2	3	3	5	4	2	5	6	2	3	3	3	21	24
Total for the six occasions	Z and N-S	15	8	14	8	19	12	8	12	15	24	27	33	36	22	30	16	82	188
	Z and E-W	14	21	31	42	48	27	29	24	11	11	10	5	6	7	11	8	217	58
	N-S and E-W	18	21	12	8	22	22	17	24	25	23	21	19	10	27	16	15	126	131

\* The unit in the scale of phase differences is  $\pi/8$ .

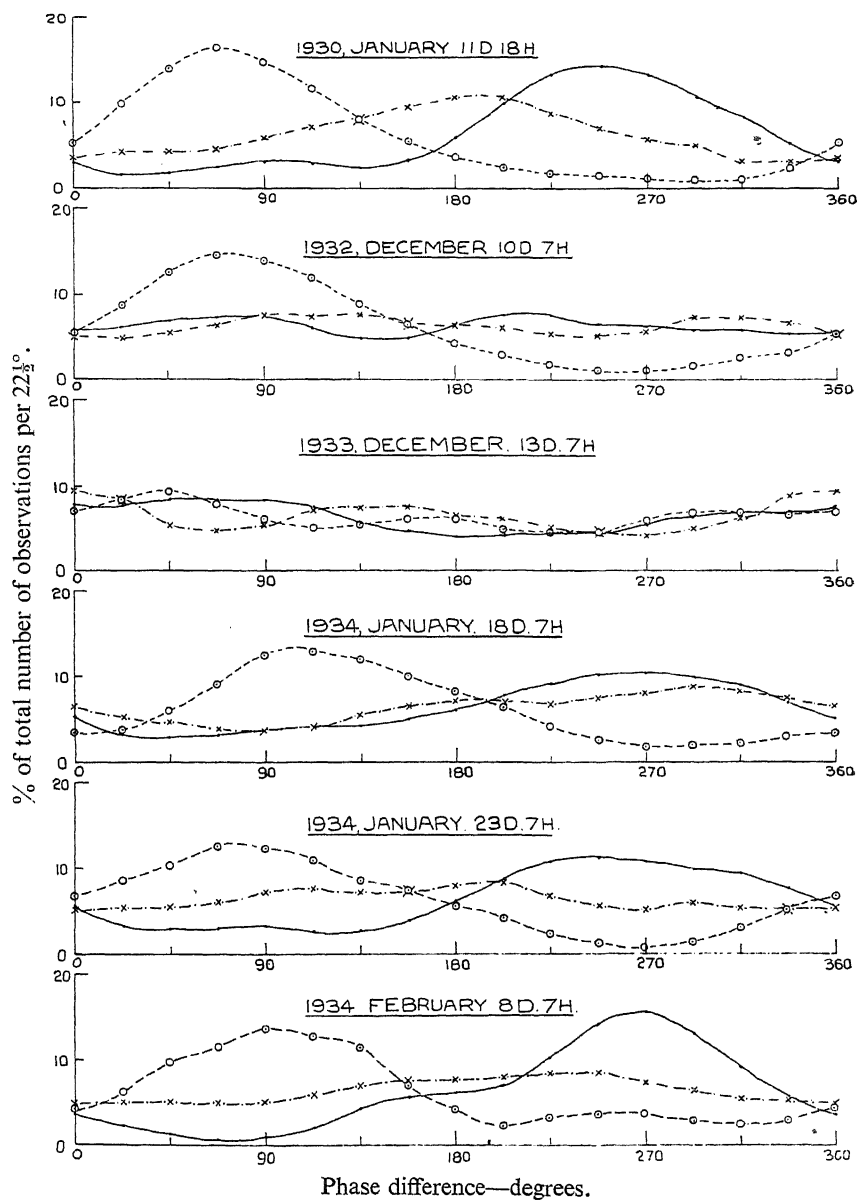


FIG. 3—Smoothed frequencies of specified phase differences between the components of the microseisms



differences on 1930, January 11d 18h, 1934, January 23d 7h, and February 8d 7h; on 1934, January 18d 7h differences between  $180^\circ$  and  $360^\circ$  predominated between these components. The variations shown in the three curves for 1933, December 13d 7h, and in two of the curves for 1932, December 10d 7h, (Z and N—S, N—S and E—W) are comparatively small.

The motion in Rayleigh waves is in the direction of propagation and in the vertical, and these components differ in phase by  $90^\circ$ , each earth particle moving in an elliptic orbit with the motion at the lowest point of the path in the direction of propagation of the waves. The movements for

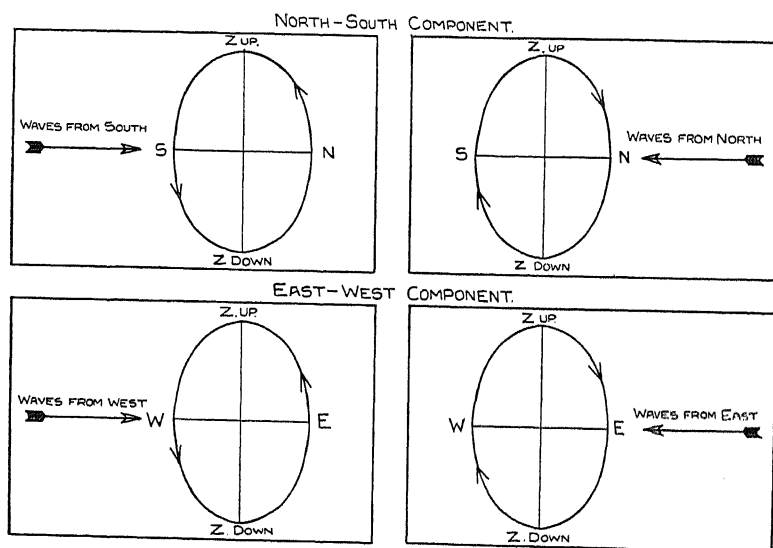


FIG. 4—Ground movements with Rayleigh waves from different directions

Rayleigh waves arriving from north, south, east and west would, therefore, be of the types shown in fig. 4.\* For the waves from south and from west the vertical movement lags by  $90^\circ$  behind the horizontal, and for waves from east and from north the vertical precedes the horizontal by  $90^\circ$ . It is shown in an appendix that when waves from adjacent directions interfere the most probable phase differences between the N—S, E—W, and Z components are those for waves travelling in an intermediate direction, but the differences may vary over a considerable range. Hence

\* The diagram illustrates the movement in simple Rayleigh waves on the surface of a homogeneous solid. The ratio of the amplitudes of horizontal and vertical microseismic movements varies from place to place according to the stratification of the underlying rocks. At Kew Observatory these amplitudes are nearly equal. (London, Meteorological Office, 'Geophysical Mem.,' No. 66 (*in the press*).)

the preponderance of phase differences of  $270^\circ$  between Z and N—S, of  $90^\circ$  between Z and E—W and of  $180^\circ$  between N—S and E—W, agrees with the theory that the microseisms are Rayleigh waves which are most frequently travelling from north-west to south-east.\*

### 5—COMPARISONS OF THE MICROSEISMIC PHASE DIFFERENCES WITH THE WEATHER MAPS

(a) 1930, January 11d 18h, fig. 5—The microseisms at this time were much larger and the periods were longer than on any of the other dates,

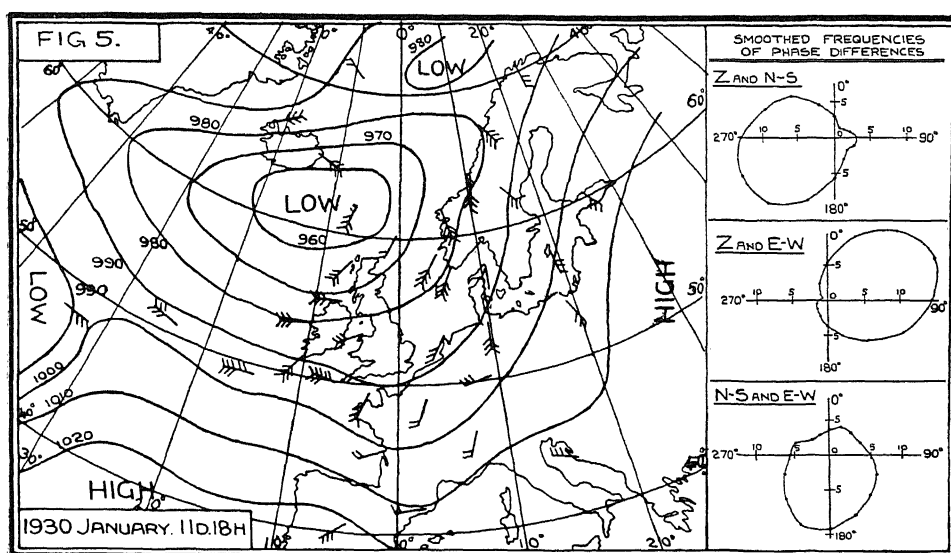


FIG. 5

the amplitude and period for the N—S component being  $10.0 \mu$  and 7.7 seconds.†

The distributions of the phase differences between the components are consistent with movements arriving from the north-west, indicating that

\* The conclusion reached by Don Leet (*loc. cit.*) was that the microseisms registered at the Harvard Observatory could not be Rayleigh waves, since the vertical component apparently agreed in phase with the dominant horizontal component. When allowance is made, however, for the difference between the types of seismograph at that observatory, the supposed anomaly disappears, and the phase differences are characteristic of Rayleigh waves reaching Harvard from the north-east and from the south-east.

† The amplitudes and periods are taken from the Observatories Year Books; the values for 6h G.M.T. are given in the comparisons with weather maps for 7h.

they were caused by the more northerly depression. If the depression near the Azores had been the more effective in generating the microseisms, the disturbances would have arrived at Kew from the west; the Z and E—W phases would tend to differ by  $90^\circ$ , but the N—S component would be affected by waves from the south as well as from the north of west, and its phases would be variable with little tendency to differ from those of Z by  $270^\circ$ , or from those of the E—W component by  $180^\circ$ .

The axes of the frequency distributions are not exactly on the  $90^\circ$  and  $270^\circ$  lines. No theoretical explanation of this discrepancy has been found, but it may possibly be due to the differences between the actual wave forms and the simple harmonic motion which has been assumed in computing the lag corrections of the seismographs.

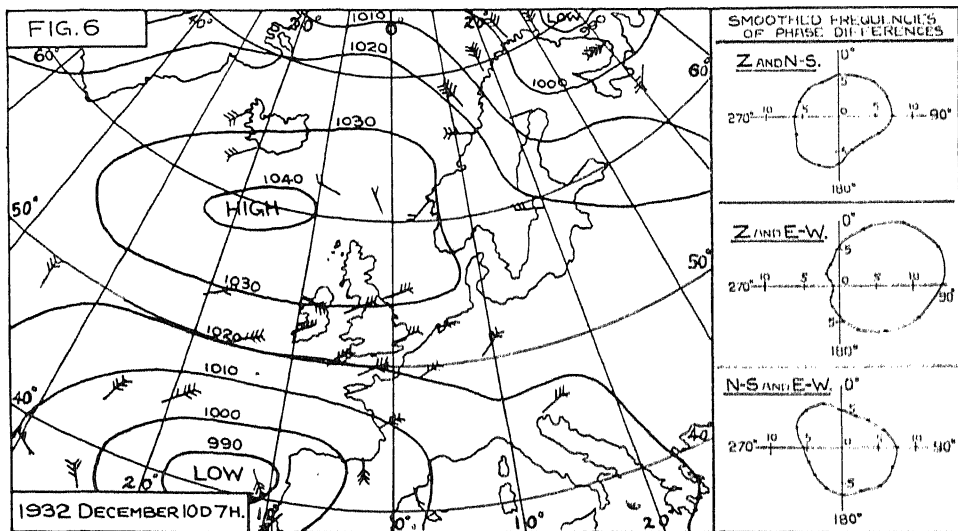


FIG. 6

(b) 1932, December 10d 7h, fig. 6—For a winter month the microseisms were small, the N—S tabulations giving an amplitude of  $1.6 \mu$  and period 6.7 seconds.

Two depressions appear in the weather map. The more southerly, off Portugal, gave strong winds over the Atlantic Ocean south-west of Britain, and around the English Channel, the Bay of Biscay and western Hibernia. Stormy conditions around the Norewegian coast were associated with the depression in the Barent's Sea; the wind reached gale force at Röst and very rough seas† were reported from Ingöy and Röst. Such conditions are very favourable for the generation of microseisms

† "New" International Code.

according to the German seismologists, who accept Wiechert's hypothesis that the oscillations are caused by surf breaking against rocky coasts. The small amplitude at this time does not support this hypothesis.

The distribution of the phase differences between Z and E—W corresponds with that on 1930, January 11, so the waves generally arrived at Kew from a westerly direction. There is no striking asymmetry in the other two diagrams, the inference being that the N—S component was affected by waves from south and north of west. It appears therefore that the Kew microseisms were generated from the northern sector of the Atlantic depression.

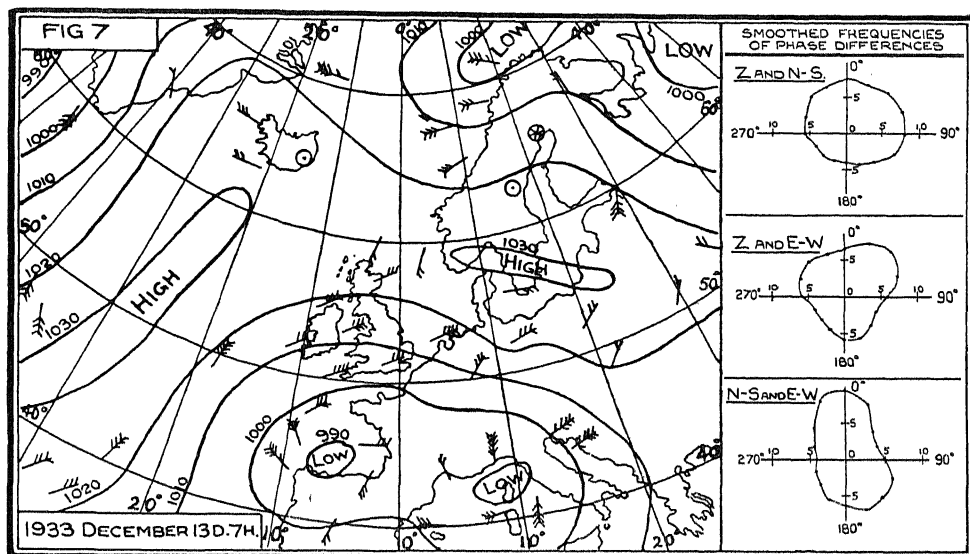


FIG. 7

(c) 1933, December 13d 7h, fig. 7—The amplitude ( $0.6 \mu$ ) was smaller and the period was shorter (4.0 seconds) than on either of the other five occasions.

A complex depression covered south-western Europe, with centres over the Bay of Biscay and the Ligurian Sea, and another depression was situated off Northern Norway. Winds were strong round the north of Norway, over the North Sea, southern Britain, the English Channel and the Bay of Biscay.

The phase differences between Z and N—S suggest that movements from southerly azimuths were more frequent than those from northerly azimuths, and the differences between Z and E—W suggest interference between waves from easterly and westerly sources.

(d) 1934, *January 18d 7h, fig. 8*—The microseisms, of amplitude  $3.6 \mu$  and period 6.0 seconds, are larger than the average for January.

The depression, centred between the Shetlands and Norway, raised gales over the North Sea and the south of Norway; sea disturbance was 5 (very rough) at Utsire and Bornholm, and 6 (high) at The Scaw and Blaavands Huk. A secondary depression west of Ireland was associated with stormy conditions on the Atlantic and from southern England to the Bay of Biscay.

The phase diagrams imply that the microseisms arrived at Kew from north-west. The axis of the Z and E—W diagram is skewed beyond the

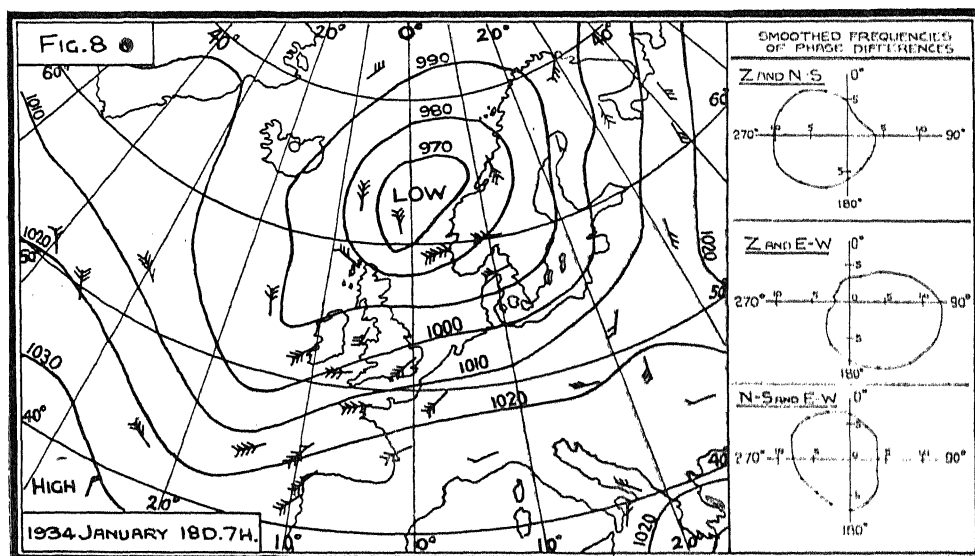


FIG. 8

90°, but the distribution strongly favours movements from the west rather than from the east of north.

(e) 1934, *January 23d 7h, fig. 9*—The microseisms (amplitude  $2.3 \mu$ , period 7.0 seconds) were about normal for January.

The map shows depressions over the Greenland Sea, and over the Atlantic west of Ireland. The depressions caused gales over the Atlantic and on the Norwegian coast; very rough seas were reported from Ingöy and Röst.

Movements from the west and from the north predominate in the phase diagrams, indicating that the Kew disturbances came chiefly from the north of west. With sea disturbances from south-west to north-west and from north to north-east of Britain, the absence of microseisms from

the east of north and from the south of west is notable; the inference is that the region most favourable for the generation of the microseisms was in the Atlantic north-west of Kew.

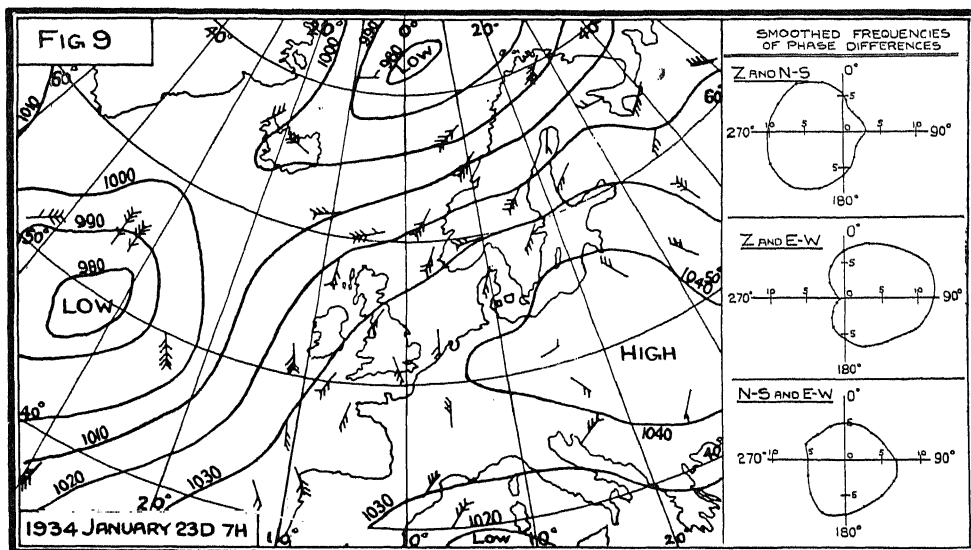


FIG. 9

(f) 1934, February 8d 7h, fig. 10—The microseisms were much larger than the average for February, the amplitude being  $4.8 \mu$  and the period 6.7 seconds.

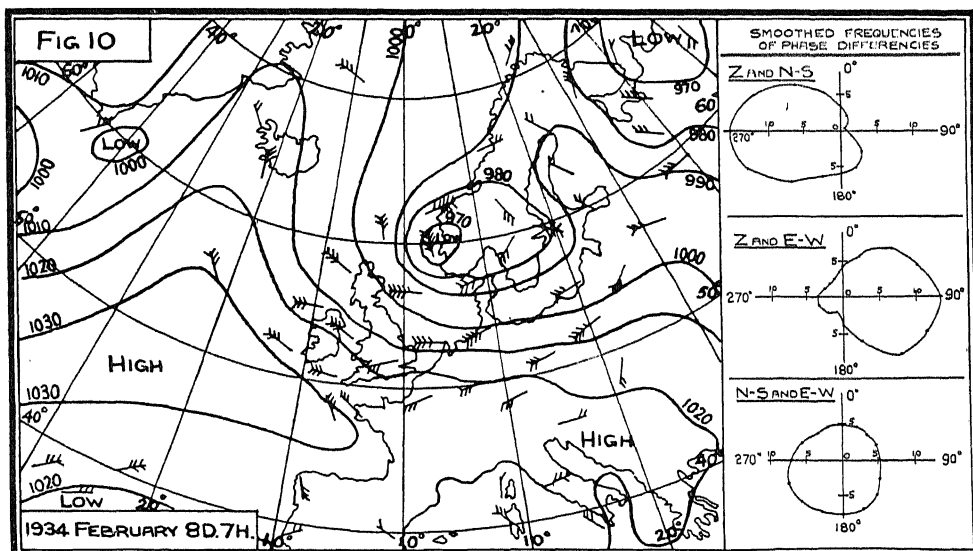


FIG. 10

A complex depression with centres over southern Norway and the Kanai Peninsula caused gales round the southern coasts of Norway and over the North Sea. The sea disturbance was high (6) at Ingöy, Utsire and The Scaw, very high (7) at Bornholm, and precipitous (8) at Blaavands Huk. Even under these conditions there is very little evidence of microseisms being produced north-east of Kew. Phase differences of  $270^\circ$  between Z and N—S, of  $90^\circ$  between Z and E—W, and to a lesser extent of  $180^\circ$  between N—S and E—W, predominate. It appears, therefore, that the microseisms must have arrived from north-west, having originated in regions well to the west where the wind and sea disturbance were less than near the centre of the depression.

### 6—CONCLUSIONS

The results of the comparisons of the microseismic phase differences and the weather maps are summarized in Table V.

TABLE V—COMPARISONS OF MICROSEISMIC PHASE DIFFERENCES AND THE WEATHER MAPS

Date	Figure	Centre of depression	Microseisms “Preponderance” of component
1930, January 11d 18h ..	5	N.W., W.	N., 0·7 ; W., 0·8
1932, December 10d 7h	6	S.W., N.N.E.	N.S., 0·0 ; W., 0·7
1933, December 13d 7h	7	S., N.N.E.	S., 0·1 ; W., 0·1
1934, January 18d 7h....	8	N.N.E.	N., 0·4 ; W., 0·5
1934, January 23d 7h....	9	N., W.	N., 0·6 ; W., 0·6
1934, February 8d 7h ....	10	N.N.E.	N., 0·6 ; W., 0·6

The figures for estimating the “preponderance” of the components of the microseisms have been computed from the numbers of phase differences from 1 to 7 and from 9 to 15, the difference between these numbers being expressed as a fraction of the total number. For example, of the 50 tabulated differences between Z and E—W for 1930, January 11d 18h, 42 are from 1 to 7 and 4 from 9 to 15, and the value is  $(42-4)/50$  or 0·8. The largest possible value (1·0) would occur with all 50 observations in one of the two groups, and the least (0·0) when the numbers in these groups were equal.

For two occasions, figs. 6 and 7, when depressions were centred to the south-west and south, the “preponderance” coefficients of the N—S component are very small, and the microseisms were generated over an area which included regions north and south of Kew. On the other

four occasions movements from the north-west predominate, and the regions in which the microseisms were produced are not affected by the position of the depressions. Figs. 8, 9 and 10 show stormy conditions around Norway, but the phases of the microseisms emphasize that the movements must have originated north-west of Kew. The results agree with the distributions of "standard" amplitudes in north-west Europe which were obtained from the "Survey of Microseismic Disturbances Recorded during January, 1930," these amplitudes being greatest north-west of Britain. Apparently the microseisms are generated in deep water. The directions of arrival are inconsistent with the theories that the oscillations are caused by the action of wind or waves on steep coasts, or by the motion of waves over shallow water.

The results have shown that although the phase differences between the components are variable, they are generally grouped around certain values, in accordance with the theory of Rayleigh waves approaching from neighbouring directions. The absence of Love waves (inferred from earlier investigations of the microseismic amplitudes\*) is confirmed, for if Love waves of appreciable magnitude had been superposed upon the Rayleigh waves, the phases of the horizontal movements would have been unrelated to those of the vertical movements.

It appears, therefore, that the microseisms are generated in regions where the water is deep, and the mechanism must be such that no shearing waves are developed.

In conclusion I wish to express my thanks to Dr. F. J. W. Whipple, Superintendent of Kew Observatory, who suggested a number of improvements which have been incorporated in this paper.

#### 7—SUMMARY

A new method has been developed for tabulation of the phases of the microseisms. It is found that the phase differences between the components are variable, but certain values predominate in accordance with the theory of Rayleigh waves approaching from adjacent directions; the distribution of the phase differences indicates the direction of arrival of the waves.

The phase differences between the N—S, E—W and Z components at Kew Observatory are compared with the weather maps for six occasions when depressions were located over different parts of the eastern Atlantic and western Europe. In two cases, with depressions to the south-west

\* 'Mon. Not. R. Astr. Soc.,' Geophys. Suppl. 3, p. 84 (1932).



and south, the microseisms were generated over an area which included regions north and south of Kew. On the other four occasions movements from the north-west predominate, and the regions in which the microseisms were produced are not affected by the position of the depressions. Apparently the microseisms are generated in deep water. There is no support for the theories that the oscillations are caused by the action of wind or waves on steep coasts, or by the motion of waves over shallow water.

The absence of Love waves is confirmed, showing that the mechanism by which the microseisms are generated must be such that no shearing waves are developed.

## APPENDIX

### *The Theory of Rayleigh Waves arriving from Adjacent Directions*

Since all the theories concerning the origin of microseisms agree that they are due to causes which operate over a large area, the motion must be due to trains of waves arriving from adjacent directions. The theoretical relations between the components of the motion are then more complicated than for a single train of Rayleigh waves. As an example we may combine two trains of simple Rayleigh waves (*i.e.*, waves in a homogeneous medium) differing slightly in period. The argument can be extended to cover any number of trains of waves of this type.

In these waves the movements are in vertical planes parallel to the direction of propagation. Let the constant ratio of the amplitudes of the vertical and horizontal movements be denoted by  $K$ , and let the bearings of the directions of propagation for the two trains of waves be  $\alpha$  and  $\beta$ , measured from north through east. If the time  $t = 0$  is chosen so that the waves are then in phase, the horizontal and vertical components of the displacements may be written:—

$$\begin{array}{ll} A \cos [(p + \delta p) t] & \text{and} \quad KA \sin [(p + \delta p) t] \\ B \cos [(p - \delta p) t] & \text{and} \quad KB \sin [(p - \delta p) t] \end{array}$$

The displacements of the ground to the north, to the east and upwards are:—

$$\begin{aligned} N &= A \cos \alpha \cos [(p + \delta p) t] + B \cos \beta \cos [(p - \delta p) t], \\ E &= A \sin \alpha \cos [(p + \delta p) t] + B \sin \beta \cos [(p - \delta p) t], \\ Z &= K \{ A \sin [(p + \delta p) t] + B \sin [(p - \delta p) t] \}. \end{aligned}$$

These equations may be rewritten in the form:—

$$N = A_N \cos (pt + \varepsilon_N),$$

$$E = A_E \cos (pt + \varepsilon_E),$$

$$Z = A_Z \sin (pt + \varepsilon_Z),$$

where

$$\left. \begin{aligned} A_N^2 &= A^2 \cos^2 \alpha + B^2 \cos^2 \beta + 2AB \cos \alpha \cos \beta \cos \\ A_E^2 &= A^2 \sin^2 \alpha + B^2 \sin^2 \beta + 2AB \sin \alpha \sin \beta \cos \\ A_Z^2 &= K^2 \{A^2 + B^2 + 2AB \cos \end{aligned} \right\} (2t \delta p),$$

$$\left. \begin{aligned} \tan \varepsilon_N &= \frac{A \cos \alpha - B \cos \beta}{A \cos \alpha + B \cos \beta} \tan \\ \tan \varepsilon_E &= \frac{A \sin \alpha - B \sin \beta}{A \sin \alpha + B \sin \beta} \tan \\ \tan \varepsilon_Z &= \frac{A - B}{A + B} \tan \end{aligned} \right\} (t \delta p).$$

The resultant motion shows a quasi-frequency  $p$ , which is the mean of the component frequencies. The motion differs from that with simple Rayleigh waves. The amplitudes of the ground movements in either component show beats, alternating between the sum and the difference of the component amplitudes. The values of  $\varepsilon_N$ ,  $\varepsilon_E$  and  $\varepsilon_Z$  pass through zero and through  $\pi/2$  together, but the differences between  $\varepsilon_N$ ,  $\varepsilon_E$  and  $\varepsilon_Z$  can oscillate through considerable ranges. The phase difference between the components depends upon  $t$  and the direction of propagation, but the dominant differences are those for a single train of waves from an intermediate direction. The two horizontal components are in phase, and the phase difference between these components and the vertical is  $90^\circ$ , if waves with the same frequency are arriving from adjacent directions, or if waves differing in frequency are travelling in the same direction.

With a greater number of sources, or when the waves are propagated through a stratified medium, other terms must be included in the equations for the motion and the interference phenomena are more complicated. The effects of interference are minimized in tabulations made according to the usual procedure, the amplitudes being measured from the largest oscillations during intervals of at least 10 minutes.

# The Transmutation of Heavy Hydrogen Investigated by the Cloud-Track Method

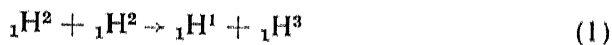
By P. I. DEE, M.A., Sidney Sussex College, and C. W. GILBERT, M.A.,  
Christ's College

(Communicated by Lord Rutherford, O.M., F.R.S.—Received February 8,  
1935)

[PLATES 4 AND 5]

## § 1—INTRODUCTION

One of the most important cases of artificial transmutation which have been investigated is that in which compounds containing heavy hydrogen are bombarded with high velocity  ${}_1\text{H}^2$  ions. It was first shown by Oliphant, Harteck and Lord Rutherford\* that such bombardment resulted in a copious emission of two proton groups of ranges 15.0 cm and 16.0 mm the relative numbers of particles in the two groups being equal within the errors of measurement. They postulated as a mechanism for the process involved the reaction



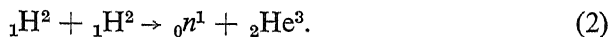
and showed that if one assumed the  ${}_1\text{H}^1$  particles to constitute the 15.0 cm group then the range of the  ${}_1\text{H}^3$  particles, calculated by the application of conservation of momentum to this process, was in approximate agreement with the shorter range. Expansion chamber photographs obtained by one of us† showed that in this bombardment the particles of 15.0 cm and 16.0 mm range were emitted in pairs in opposite directions, this result providing strong evidence in favour of the proposed reaction. In addition to this proton emission, however, it was shown by Oliphant, Harteck and Lord Rutherford\* that an intense neutron emission resulted from this bombardment and from an expansion chamber investigation by one of us‡ of helium nuclei recoiling from these neutrons it was shown that the neutrons were probably homogeneous and that their energy was  $1.8 \times 10^6$  electron volts. An investigation by Oliphant,

\* 'Proc. Roy. Soc.,' A, vol. 144, p. 692 (1934).

† Dee, 'Nature,' vol. 133, p. 564 (April 14, 1934).

‡ Dee, 'Proc. Roy. Soc.,' A, vol. 148, p. 628 (1935).

Harteck and Lord Rutherford using a linear counting chamber gave a maximum value for the neutron energy of about  $2 \times 10^6$  electron volts. The reaction proposed by Oliphant, Harteck and Lord Rutherford to account for these neutrons was



The mass of the  ${}_2\text{He}^3$  atom was obtained by them from the data for the disintegration of  ${}_3\text{Li}^6$  by protons,  $\{{}_3\text{Li}^6 + {}_1\text{H}^1 \rightarrow {}_2\text{He}^3 + {}_2\text{He}^4\}$ , and using the value thus derived (3.0166) and a neutron mass of 1.0067 they showed that the energy of the neutrons calculated from (2) was  $2.5 \times 10^6$  electron volts in approximate agreement with the observed value. Attempts were made by counting methods to detect the  ${}_2\text{He}^3$  nuclei which are to be expected according to the above reaction but were unsuccessful. The range to be expected from the above data is only 5 mm and the detection of particles of so short a range is very difficult and could not be expected under their experimental conditions. We first tried to detect these particles by passing a beam of  ${}_1\text{H}^2$  ions into an expansion chamber on to a solid target of heavy ammonium sulphate, but this experiment also failed probably on account of exchange of the heavy hydrogen in the target with the hydrogen of the water used in the chamber.

It was decided therefore to build a small sealed-off expansion chamber which could be filled with heavy hydrogen (the necessary saturation being produced by the addition of a drop of heavy water) and to bombard this gas with a beam of  ${}_1\text{H}^2$  ions admitted through a thin mica window. It was also decided to look for the  ${}_2\text{He}^3$  nuclei which may be ejected in the direction of the bombarding  ${}_1\text{H}^2$  ions since, as will be shown in what follows, their range in this direction is appreciably greater than for those emitted at right angles to the incident beam, and their detection thereby greatly facilitated.

## § 2—EXPERIMENTAL PROCEDURE

The application of the laws of conservation of energy and momentum to the proposed reaction (2) leads to a value for the velocity  $v_3$  of the  ${}_2\text{He}^3$  nucleus emitted at an angle  $\theta_3$  with the direction of the incident  ${}_1\text{H}^2$  ion of velocity  $v$  given by

$$v_3 = \frac{1}{2}v \cos \theta_3 + \sqrt{\frac{1}{4}v^2 \cos^2 \theta_3 + \frac{1}{6}(E - v^2)},$$

where  $E$  = the energy liberated in the reaction (ergs  $\div$  mass of proton).

Using values for  $E = 2.4$  and  $2.8 \times 10^6$  electron volts in approximate agreement with the data on the energy of the neutrons and taking  $\theta_3 = 0^\circ$ , the curves *c*, *d* of fig. 1 have been plotted giving the ranges to be expected for the  ${}^3_2\text{He}$  nuclei emitted in the forward direction for different energies of the incident  ${}^2_1\text{H}$  ion. The curves *a*, *b* show the ranges of  ${}^2_1\text{H}$  and  ${}^1_1\text{H}$  nuclei plotted against the accelerating voltage.

Now since in this work no magnetic analysis of the beam could easily be applied and since the beam contains both  ${}^2_1\text{H}$  and  ${}^1_1\text{H}$  nuclei it is evident that with  ${}^2_1\text{H}$  and  ${}^1_1\text{H}$  particles of 400 electron kv energy there

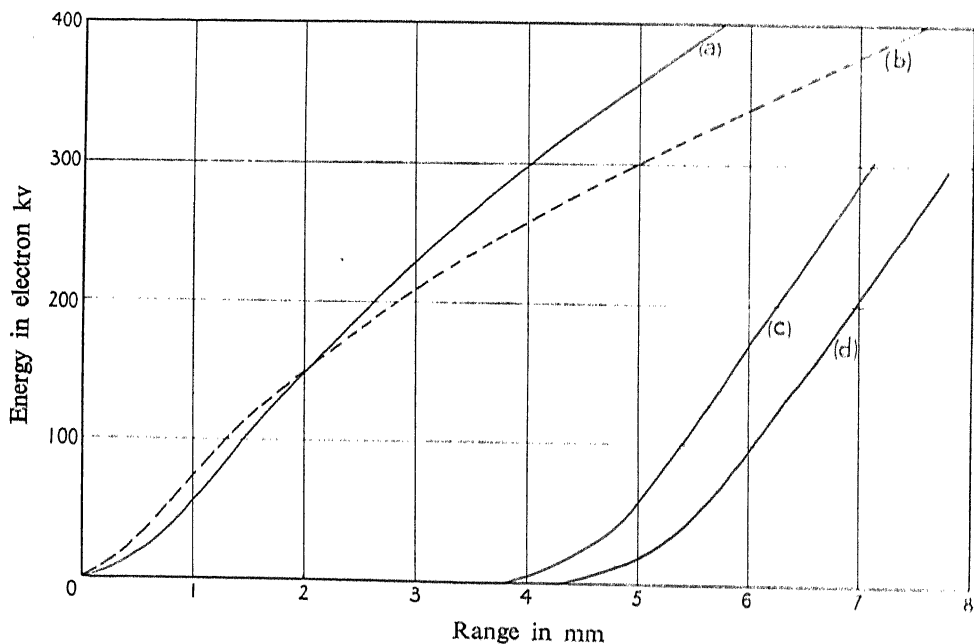


FIG. 1—(a)  ${}^2_1\text{H}$  ions; (b)  ${}^1_1\text{H}$  ions; (c)  $E = 2.4 \times 10^6$  e-volts; (d)  $E = 2.8 \times 10^6$  e-volts

is no hope of detecting the  ${}^3_2\text{He}$  particles since their range is then not greater than that of the bombarding beam. It also appears that up to 150 kv the *difference* between the ranges of the  ${}^3_2\text{He}$  particles and the  ${}^2_1\text{H}$  or  ${}^1_1\text{H}$  particles should not vary much and is equal to about 4 mm.

Above this voltage the excess range rapidly decreases. It was obviously important therefore that the energy of the  ${}^2_1\text{H}$  ions entering the chamber should be kept below this value. It is further obvious from this curve that the best results would be obtained by the use of the thinnest possible mica window between the accelerating tube and the chamber since the range of the  ${}^1_1\text{H}$  ions increases more rapidly than the range of the  ${}^2_1\text{H}$

for accelerating voltages  $> 150$  kv and since for a given energy of the  ${}_1\text{H}^2$  ions entering the chamber the proton range must be kept as small as possible. The great difficulty of detecting the  ${}_2\text{He}^3$  nuclei emitted at right angles to the direction of the bombarding beam is also apparent. In this direction the range of the  ${}_2\text{He}^3$  nucleus is only 3.8 mm for zero bombarding energy, and actually decreases as the energy of the incident particle is increased. Thus even if sufficient numbers of disintegrations

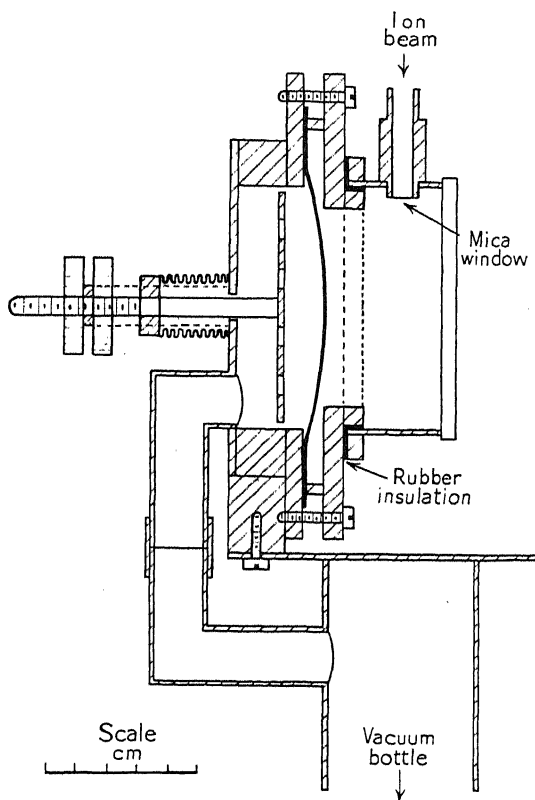


FIG. 2

could be obtained with  ${}_1\text{H}^2$  ions of 150 electron kv energy and range equal to 2 mm there would be an excess range of the  ${}_2\text{He}^3$  nucleus of less than 1.8 mm available for detection. The window finally used had an  $\alpha$ -particle stopping power of 2.8 mm and was supported upon the plane end of a cylindrical tube containing a large number of holes of diameter 0.33 mm.

A diagram of the expansion chamber is shown in fig. 2. A rubber diaphragm and wire gauzes were used in the manner recommended by

Professor C. T. R. Wilson.\* It was found convenient to make a gas-tight rubber seal by clamping the rubber between a flat circular brass plate and a circular brass ring of 2 mm wall thickness. The chamber proper was a separate unit made of brass with glass windows and carrying insulated wire gauzes. This unit was insulated from the brass rings clamping the rubber and made gas-tight with plasticene. The circular rubber sheet in its initial position made contact with a wire gauze and on expansion was drawn back against a perforated brass plate. The position of the latter plate could be readily adjusted, and determined the expansion ratio. An electric field of about 10 volt/cm was maintained between the gauze and the chamber. The expansion was made by the sudden evacuation of the space behind the rubber. The beam was admitted to the chamber at the completion of each expansion during an interval of 1/30 second by means of an electrically operated shutter contained in the evacuated tube connecting the accelerating tube to the expansion chamber. The procedure was as described in previous papers.

The expansion chamber was filled to a pressure of about 40 cm with a mixture of approximately 50% He, 25%  ${}^1_2\text{H}_2$ , 25% air and at the completion of a run the stopping power of the gas was determined by admitting  $\alpha$ -particles from a source of ThC through a small window in the base of the chamber. Under these conditions the track length photographed was about five times its length at N.T.P.

### § 3—EXPERIMENTAL RESULTS

A preliminary run of photographs at different accelerating voltages gave clear evidence of the existence of a group of tracks of about the range sought. Tracks which passed right across the chamber were also observed, their reduced range being  $> 15$  mm, and must doubtless be attributed to  ${}^1_1\text{H}^1$  and  ${}^1_1\text{H}^3$  nuclei produced according to reaction (1). Subsequent experiments were made keeping the bombarding energy as low as possible consistent with obtaining a few tracks per photograph. Typical photographs are shown in figs. 4–7, Plates 4 and 5. The plates were measured by replacing them in the cameras and reprojecting their images in space. For this purpose a dummy chamber was constructed with the same dimensions as the one actually employed but without the glass plates. By reprojecting the images of the illumination apertures on to this chamber it was possible to decide with precision whether an apparent short track actually ended within the illumination or whether it was to be attributed to one of the longer tracks passing out of the illuminating beam. Since under these conditions of use of an expansion

\* 'Proc. Roy. Soc.,' A, vol. 142, p. 88 (1933).

chamber dense condensation is produced throughout the whole chamber making the operation very critical only the best plates were measured. In a large number of cases it was obvious that tracks ended in the chamber from the small deflections visible at their ends, apart from the further test as to the position of this end relative to the illuminating beam. It was of course, impossible to observe the point of origin of any particular track within the sphere of ionization due to the entering beam. The "length" of each track was therefore determined by projecting its direction back to the mica window where the beam entered, and measuring from this point. The ranges thus obtained are therefore only true ranges for those tracks which actually originated at the window. Measure-

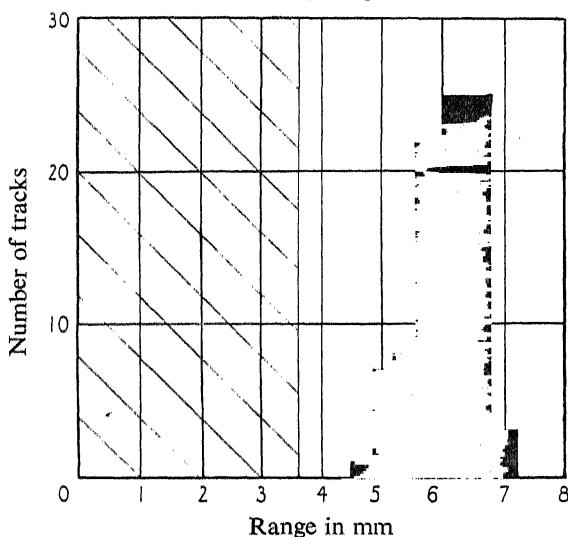


FIG. 3

ment of the tracks was confined to those emitted within  $30^\circ$  of the forward direction and as will be shown later it is easy to deduce the true range from the "range" distribution obtained in this manner. The "range" distribution measured directly in this manner is shown in fig. 3 where the abscissa scale has been adjusted to correct these ranges to air at N.T.P.

The reduced range corresponding to the edge of the beam was 3.6 mm. The mica window through which the beam passed had a stopping power of 2.8 mm whence the maximum range of the particles in the beam was 6.4 mm. These particles of range 6.4 mm were therefore protons of energy 355 electron kv. The accelerated  ${}_1\text{H}^2$  ions had therefore a total range of 4.9 mm and a range of 2.1 mm in the chamber.

The existence of a group of particles of maximum range 6.8 mm is clearly shown. Using the curves of fig. 1 and a range of the  ${}_1\text{H}^2$  ions



= 2.1 mm the expected range of the  ${}^3_2\text{He}$  particles would be 6.6 mm for an energy release in the reaction of  $2.8 \times 10^6$  electron volts. This mode of comparing the theoretical and experimental results is not obviously justifiable. It would be correct only if all the disintegration particles were produced at the mica window where the  ${}^1_1\text{H}^2$  ions entered. In order to obtain a more accurate value for the energy balance and to justify this comparison it is necessary to consider the range of  ${}^3_2\text{He}$  nuclei produced at all distances from this window up to the range of the entering  ${}^1_1\text{H}^2$  ions. This calculation is made in § 4.

No tracks having ranges between 6.8 mm and 1.5 cm were observed, and the fall in number on the short range side suggests also that the observed group is not continuous on the low energy side, since it would have been possible to detect tracks on these photographs up to within a reduced distance of 0.5 mm of the edge of the beam. The ratio of the numbers of tracks in this group to the numbers passing out of the chamber was  $0.41 \pm 0.06$  corresponding to a relative probability of the processes of disintegration into neutrons and  ${}^3_2\text{He}$  nuclei and disintegration into  ${}^1_1\text{H}^1$  and  ${}^1_1\text{H}^3$  particles of  $0.8 \pm 0.1$ . Two short control runs were taken with ordinary hydrogen in the chamber instead of heavy hydrogen the same proportions of air and helium being present. The first run showed several tracks of about the range of the  ${}^3_2\text{He}$  particles and also tracks going right across the chamber. The numbers were about a quarter of those obtained with heavy hydrogen in the chamber. In the second run, taken a day later, the number of tracks obtained per photograph was less than one-tenth of the number with heavy hydrogen in the chamber although the  ${}^1_1\text{H}^2$  ion beam was stronger than in previous runs. The high number obtained in the first run was almost certainly due to exchange occurring between the hydrogen introduced and heavy hydrogen from the heavy water which remained from the main experiments. This contamination effect was considerably reduced on allowing the chamber to stand overnight after introducing excess of ordinary water. It seems clear from these results that the short range group of particles is due to the bombardment of heavy hydrogen with its own ions.

#### § 4—THE ENERGY BALANCE IN THE REACTION

As we have shown in the above paragraph it is necessary to consider the fact that disintegration may occur at any distance from the mica window up to a value equal to the range of the  ${}^1_1\text{H}^2$  ions (*i.e.*, 2.1 mm), the “ranges” occurring in the distribution diagram being true ranges only for those  ${}^3_2\text{He}$  nuclei produced at the mica window. In Table I,

row 2 gives the actual ranges of the  ${}_2\text{He}^3$  nuclei obtained from the curves of fig. 1 using the value  $E = 2.4 \times 10^6$  e-volts and different energies of the  ${}_1\text{H}^2$  ions corresponding to the energies which these ions (of initial range 2.1 mm) would have at distances  $D$  from the plane of entry.

In row 4 the true range of row 2 has been added to the distance  $D$  giving the "ranges" as measured.

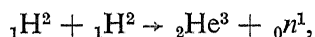
Rows 3 and 5 give the same data for an assumed value of  $E = 2.8 \times 10^6$  e.v.

TABLE I

	mm	mm	mm	mm
(1) $D$ .....	0	0.7	1.4	2.1
(2) Calculated range of ${}_2\text{He}^3$ nuclei for $E = 2.4 \times 10^6$ e.v. ....	5.9	5.3	4.7	3.8
(3) Calculated range of ${}_2\text{He}^3$ nuclei for $E = 2.8 \times 10^6$ e.v. ....	6.6	6.0	5.3	4.3
(4) Theoretical "range" as measured for $E = 2.4 \times 10^6$ e.v. ....	5.9	6.0	6.1	5.9
(5) Theoretical "range" as measured for $E = 2.8 \times 10^6$ e.v. ....	6.6	6.7	6.7	6.4

It is obvious that the ranges measured in the manner described are practically unaffected by changes in the point of origin, any increase in the distance of this point from the window being counterbalanced by the reduction in the effect of the energy of the bombarding  ${}_1\text{H}^2$  ion. The maximum observed range was 6.8 mm agreeing closely with the maximum value of row 5. Thus the value for the energy balance in the reaction is  $E = 2.8 \times 10^6$  e.v. The observed distribution is from 4.8 mm to 6.8 mm the main peak lying between 5.6 mm and 6.8 mm, whereas the theoretical width is from 6.4 to 6.7 mm. Part of this difference must be attributed to the fact that the tracks measured made angles up to  $30^\circ$  with the incident beam. For this angle the range of the  ${}_2\text{He}^3$  nucleus would be 6.1 mm. The remaining difference may be partly due to straggling of the  ${}_1\text{H}^2$  and  ${}_2\text{He}^3$  particles. The estimated error in the value of  $E$  is  $0.2 \times 10^6$  e-volts and lies mainly in the determination of the stopping power of the gas mixture used.

Thus from these experiments we obtain for the energy balance in the reaction



a value  $2.8 \pm 0.2 \times 10^6$  e-volts. It follows from the application of the law of conservation of momentum to this process that the neutron and

${}_2\text{He}^3$  nucleus are emitted in opposite directions for zero bombarding energy. In this case also the energy of the neutron would be

$$\frac{3}{4}(2.8 \pm 0.2 \times 10^6) \text{ e.v.} = 2.1 \pm 0.2 \times 10^6 \text{ e.v.}$$

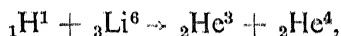
and the energy of the  ${}_2\text{He}^3$  nucleus  $\frac{1}{4}(2.8 \times 10^6) = 0.7 \times 10^6 \text{ e.v.}$  Thus the range of the  ${}_2\text{He}^3$  nucleus for zero bombarding energy would be 4.3 mm.

The investigation of the neutron emission\* using the expansion chamber gave a value for the energy of the neutrons  $= 1.8 \pm 0.2 \times 10^6 \text{ e-volts}$ , which agrees with the value deduced above within the limits of error. From the latter value we obtain for the energy release in the process a value  $\frac{1}{3}(1.8 \pm 0.2 \times 10^6) \text{ e.v.} = 2.4 \pm 0.3 \times 10^6 \text{ e.v.}$  Thus the mean value for the energy release from the two sets of experiments is  $2.6 \pm 0.2 \times 10^6 \text{ e-volts}$  or  $0.0028 \pm 0.0002 \text{ mass units}$ . For the reaction in question the only mass known with precision is that of  ${}_1\text{H}^2$  which, according to Bainbridge,† is  $2.0136 \pm 0.00007$ . Applying the conservation of energy to the process we obtain for the sum of the masses of  ${}_2\text{He}^3$  and  ${}_0n^1$  a value

$$2(2.0136 \pm 0.00007) - (0.0028 \pm 0.0002) = 4.0244 \pm 0.0003.$$

It is possible, however, to obtain the mass of  ${}_2\text{He}^3$  from another set of transmutation experiments.

In the disintegration of lithium by protons a group of particles of range  $< 2 \text{ cm}$  was detected by Cockcroft and Walton.‡ Subsequent work by Oliphant, Kinsey and Lord Rutherford§ showed these particles to consist of two groups one of range 11.5 mm and the other of range 6–8 mm. They proposed for the nuclear reaction



and expansion chamber photographs by one of us|| showed that these particles were emitted in opposite pairs as is required by the application of momentum considerations to the process assumed. Still further proof of the correctness of these views has been obtained by the bombardment of the separated isotopes of lithium when the short range products were shown to arise from the  ${}_3\text{Li}^6$  isotope.¶ It follows from the energies

\* Dee, 'Proc. Roy. Soc.,' A, vol 148, p. 628 (1935).

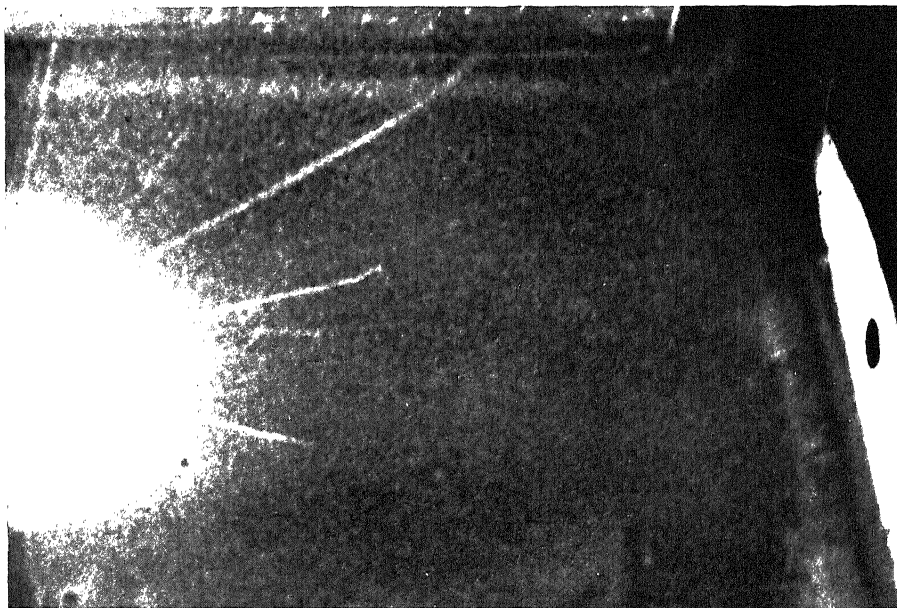
† 'Phys. Rev.,' vol. 44, p. 57 (July 1, 1933).

‡ 'Proc. Roy. Soc.,' A, vol. 137, p. 229 (1932).

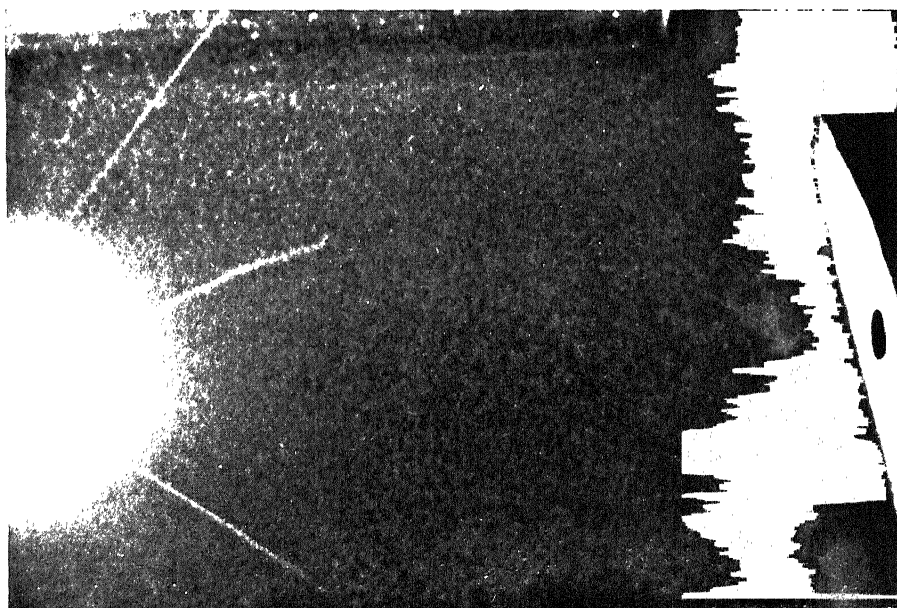
§ 'Proc. Roy. Soc.,' A, vol. 141, p. 722 (1933).

|| Dee, 'Nature,' vol. 132, p. 818 (1933).

¶ Oliphant, Shire and Crowther, 'Proc. Roy. Soc.,' A, vol. 146, p. 922 (1934).



Fig



Fig

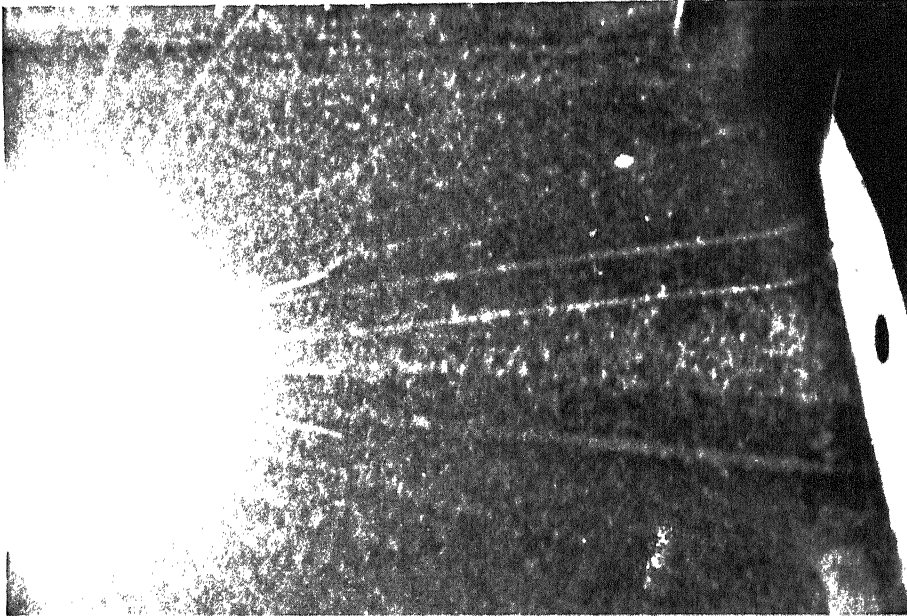


FIG. 7

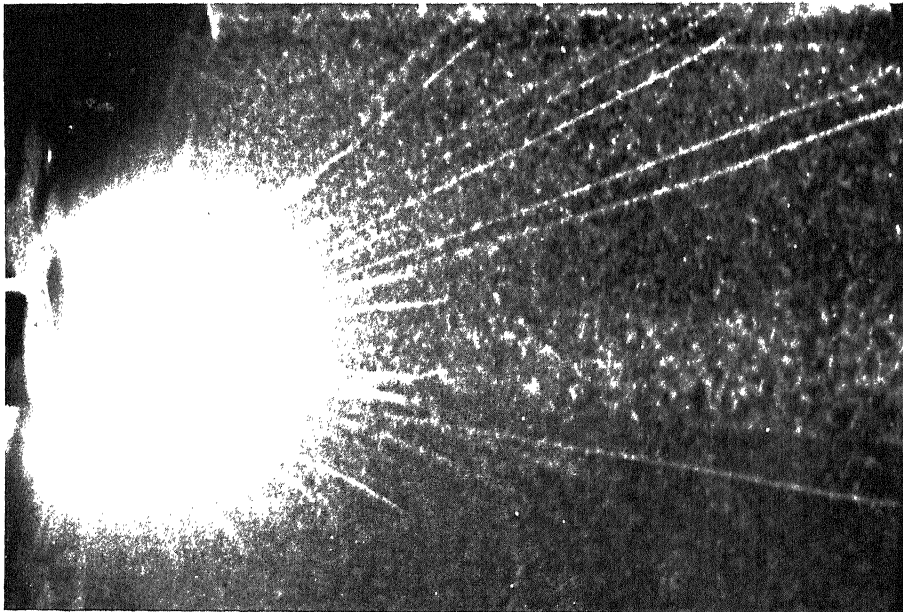


FIG. 6

of these short range particles that the mass of  ${}_2\text{He}^3$  is  $3.0164 \pm 0.0003$  and hence we obtain for the mass of the neutron, from the experiments of this paper, a value

$$(4.0244 \pm 0.0003) - (3.0164 \pm 0.0003) = 1.0080 \pm 0.0004,$$

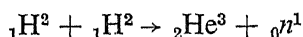
in good agreement with the value obtained by Chadwick and Goldhaber\* from the disintegration of heavy hydrogen by  $\gamma$ -rays.

We are indebted to Lord Rutherford for his interest and encouragement in this research.

One of us (C. W. G.) wishes to acknowledge a Senior Research Award by the Department of Scientific and Industrial Research. We wish to thank Mr. Birtwhistle for much technical assistance.

#### SUMMARY

The  ${}_2\text{He}^3$  nuclei produced in the reaction



have been detected in the expansion chamber by passing a beam of artificially accelerated  ${}_1\text{H}^2$  ions into a gas mixture containing heavy hydrogen.

The range of this group of particles has been measured and is  $4.3 \pm 0.2$  mm for zero bombarding energy. The neutrons produced in the same bombardment have an energy of  $1.8 \pm 0.2 \times 10^6$  e-volts, and it is shown that these results are in agreement with the application of the conservation of momentum to the process assumed. A value of  $1.0080 \pm 0.0004$  is thereby deduced for the mass of the neutron.

#### DESCRIPTION OF PLATES

The reproductions are 1.5 times natural size.

The length of a track in the gas is five times its range reduced to N.T.P.

The white fan at the top of each photograph is due to the intense ionization of the entering beam. Figs. 4, 5 show tracks of range about 6.8 mm, the small deflections often visible at their ends is evidence that they end in the gas. Some longer tracks passing out of the chamber are probably due to protons produced according to reaction (1).

Figs. 6, 7 taken with a more intense  ${}_1\text{H}^2$  ion beam show clearly the two groups of particles.

\* 'Nature,' vol. 134, p. 237 (1934).

## Results of Calculations of Atomic Wave Functions

## III—Results for Be, Ca and Hg

By D. R. HARTREE, F.R.S., and W. HARTREE

*(Received November 30, 1934)*

## § 1—INTRODUCTION

In two previous papers,\* results of calculations of approximate atomic fields and wave functions, carried out to a fairly high degree of numerical accuracy by the method of the “self-consistent field,”† have been presented. This paper gives similar results for the normal states of three other atoms, namely, Be, Ca, and Hg, both neutral and doubly ionized.

In all these cases, the “self-consistent field” calculation has been carried out both for the ion and for the neutral atom; it has not been assumed that the “core” formed by the doubly ionized atom is unperturbed by the addition of the two “valency” electrons, but the perturbation of the core on addition of the two valency electrons has been taken into account, as far as this is possible on the “self-consistent field” approximation to a many-electron atom. This perturbation is quite appreciable, especially for Hg, for which the outermost group,  $(5d)^{10}$ , of the core is very sensitive to perturbing influences; for Ca, for which the core is inert-gas-like and has its outermost group,  $(3p)^6$ , comparatively tightly bound, this perturbation was expected to be quite small; it was actually found to be a good deal larger than was expected.

It should be noted that this effect of the valency electrons on the core is not a “polarization” effect. It is a screening effect due to the penetration of the valency electrons into the core, and is a statistical effect depending on the average distribution of the valency electrons, whereas the polarization of the core by the valency electron may arise when the latter is outside the core, and depends on its position, not only on its average distribution.

Preliminary results for Hg, obtained at a earlier stage of the process of approximation to the self-consistent field, have already been published‡;

\* D. R. Hartree, ‘Proc. Roy. Soc.,’ A, vol. 141, p. 282 (1933); vol. 143, p. 506 (1934). These papers will be referred to as I and II.

† D. R. Hartree, ‘Proc. Camb. Phil. Soc.,’ vol. 24, pp. 89, 111 (1928).

‡ D. R. Hartree, ‘Phys. Rev.,’ vol. 46, p. 738 (1934). This paper will be referred to as III.

the approximation has been improved considerably since these results were obtained.

For Be and Ca the results are given in the same form as in the previous papers I and II, as follows:—

- (a) Table of the radial wave functions  $P(r)$ , unnormalized, and of  $P/r^{l+1}$  for small  $r$ ; also values of the normalization integral  $\int_0^\infty P^2 dr$  and of the energy parameter  $\varepsilon$  for each of the radial wave functions.
- (b) Table of contributions  $2(2l+1)[1 - Z_0(nl, nl|r)]$  to  $Z$  from each  $(nl)$  electron group and a corresponding number of positive charges on the nucleus. [ $Z = r^2 \times (\text{field at radius } r)$ ].
- (c) Table of total  $2Z_p$  and value of  $2v_0 = [d(2Z_p)/dr]_{r=0}$  for the whole atom. [ $Z_p = r \times (\text{potential at radius } r)$ ].

For Hg, a table of  $r^{-\frac{1}{2}}P$  is given in place of the table of  $P$ , and  $\log r$  is taken as the independent variable, for reasons explained in III; otherwise the results are in the standard form.

## § 2—RESULTS FOR Be AND Be<sup>++</sup>

The results for Be and Be<sup>++</sup> are given in Tables I and II. On account of the small atomic number, and in order to provide a reliable comparison with the results of calculation, now in progress, of the self-consistent field including exchange, by means of Fock's equations, the estimates of contributions to  $Z$  were made to three full decimals, instead of to two decimals and perhaps a 5 in the third decimal as has been done for heavier atoms, and the process of approximation to the self-consistent field carried on until the difference between estimated and calculated contributions to  $Z$  was nowhere greater than 0.001.

The results show the small, though appreciable, extent to which the  $(1s)^2$  group is affected by the addition of the  $(2s)^2$  group.

The main part of the work for Be<sup>++</sup> was carried out by Mrs. C. G. Darwin, whose assistance we are glad to acknowledge.

## § 3—RESULTS FOR Ca AND Ca<sup>++</sup>

The results for Ca and Ca<sup>++</sup> are given in Tables III, IV and V. The maximum difference between estimated and calculated  $Z$ , either for the neutral or ionized atom, is less than 0.01 in the aggregate and in the contribution from any one group.



TABLE I—Be AND Be<sup>++</sup>. TABLE OF RADIAL WAVE FUNCTIONS P

Be <sup>++</sup>				Be neutral			
$r$	(1s)	(1s)	(2s)	$r$	(1s)	(1s)	(2s)
0.00	0.000	0.000	0.000	1.6	0.103	0.108	-3.659
0.02	0.369	0.369	0.369	1.8	0.058	0.062	-3.966
0.04	0.682	0.682	0.682	2.0	0.033	0.035	-4.134
0.06	0.946	0.946	0.944	2.2	0.018	0.020	-4.190
0.08	1.166	1.166	1.162	2.4	0.010	0.011	-4.160
0.10	1.348	1.348	1.341	2.6	0.005 <sub>5</sub>	0.006	-4.063
0.12	1.496	1.496	1.484	2.8	0.003	0.003 <sub>5</sub>	-3.917
0.14	1.615	1.616	1.597	3.0	0.001 <sub>5</sub>	0.002	-3.738
0.16	1.709	1.710	1.683	3.2	0.001	0.001	-3.536
0.18	1.781	1.783	1.745	3.4	0.000 <sub>5</sub>	0.000 <sub>5</sub>	-3.321
0.20	1.833	1.836	1.785	3.6			-3.100
				3.8			-2.878
0.25	1.897	1.901	1.808	4.0			-2.660
0.30	1.887	1.893	1.742				
0.35	1.829	1.837	1.610	4.5			-2.147
0.40	1.740	1.748	1.429	5.0			-1.701
0.45	1.631	1.641	1.213	5.5			-1.327
0.50	1.512	1.523	0.971	6.0			-1.023
0.55	1.389	1.401	0.712	6.5			-0.781
0.60	1.266	1.279	0.442	7.0			-0.591
0.7	1.035	1.048	-0.113	8			0.331
0.8	0.831	0.844	-0.664	9			0.182
0.9	0.658	0.670	-1.192	10			0.098
1.0	0.515	0.527	-1.683				
1.1	0.400	0.410	-2.132	12			0.027 <sub>5</sub>
1.2	0.308	0.317	-2.532	14			0.007 <sub>5</sub>
1.3	0.236	0.244	-2.885	16			0.002
1.4	0.180	0.187	-3.189	18			0.000 <sub>5</sub>
Be <sup>++</sup>				Be neutral			
				(1s)	(1s)	(2s)	
$\epsilon$				11.344	9.499	0.5764	
$\int_0^\infty P^2 dr$				1.852 <sub>4</sub>	1.875 <sub>8</sub>	46.97	
$(P/r)_{r=0}$				20.00	20.00	20.00	

The perturbations of the wave functions of the K and L shells due to the addition of the (4s)<sup>2</sup> group are hardly appreciable to the accuracy to which the wave functions are tabulated (not more than three in the last decimal for the (2p) radial wave function), so results for Ca<sup>++</sup>, distinct from those for neutral Ca, are only given for the two outer groups (3s)<sup>2</sup>

TABLE II—Be AND Be<sup>++</sup>. TABLE OF CONTRIBUTIONS TO Z, AND TOTAL  $2Z_p$ 

$r$	Contributions to Z $2 [1 - Z_0(nl, nl r)]$			Total $2Z_p$	
	Be <sup>++</sup> (1s)	Be (1s)	Be (2s)	Be <sup>++</sup>	Be
0	2.000	2.000	2.000	8.000	8.000
0.02	1.999	1.999	2.000	7.707	7.667
0.04	1.993	1.993	2.000	7.419	7.339
0.06	1.978	1.978	1.999	7.140	7.021
0.08	1.954	1.955	1.998	6.874	6.718
0.10	1.919	1.920	1.997	6.623	6.429
0.12	1.876	1.877	1.995	6.388	6.155
0.14	1.823	1.825	1.993	6.169	5.898
0.16	1.765	1.767	1.991	5.966	5.659
0.18	1.698	1.701	1.988	5.778	5.434
0.20	1.627	1.631	1.986	5.605	5.226
0.25	1.438	1.444	1.979	5.236	4.769
0.30	1.244	1.251	1.972	4.945	4.391
0.35	1.057	1.065	1.966	4.718	4.080
0.40	0.884	0.893	1.961	4.543	3.820
0.45	0.731	0.740	1.957	4.409	3.603
0.50	0.597	0.606	1.955	4.307	3.420
0.55	0.483	0.492	1.953	4.230	3.261
0.60	0.388	0.397	1.953	4.172	3.122
0.7	0.245	0.252	1.952	4.095	2.884
0.8	0.151	0.157	1.951	4.052	2.680
0.9	0.091	0.096	1.948	4.028	2.495
1.0	0.054	0.057	1.939	4.014	2.324
1.1	0.032	0.034	1.923	4.007	2.161
1.2	0.019	0.020	1.900	4.004	2.005
1.3	0.011	0.011	1.869	4.002	1.855
1.4	0.006	0.006	1.830	4.001	1.712
1.6	0.002	0.002	1.729	4.000	1.445
1.8	0.000 <sub>5</sub>	0.000 <sub>5</sub>	1.604		1.208
2.0			1.463		1.000
2.2			1.315		0.822
2.4			1.166		0.670
2.6			1.022		0.544
2.8			0.886		0.438
3.0			0.761		0.351
3.2			0.649		0.281
3.4			0.548		0.224
3.6			0.460		0.177
3.8			0.384		0.140
4.0			0.319		0.110

TABLE II—(continued)

$r$	Contributions to $Z$ $2[1 - Z_0(nl, nl r)]$			Total $2Z_p$	
	Be <sup>++</sup> (1s)	Be (1s)	Be (2s)	Be <sup>++</sup>	Be
4.5			0.196		0.060
5.0			0.117		0.032
5.5			0.069		0.016
6.0			0.040		0.009
6.5			0.022		0.004 <sub>5</sub>
7.0			0.012		0.002 <sub>5</sub>
8			0.003 <sub>5</sub>		0.001
9			0.001		
10					

$$2v_0 = -14.8 \quad 2v_0 = -16.9$$

TABLE III—Ca AND Ca<sup>++</sup>. RADIAL WAVE FUNCTIONS. TABLE OF  $P/r^{l+1}$ 

$r$	Ca neutral						Ca <sup>++</sup>	
	(1s)	(2s)	(2p)	(3s)	(3p)	(4s)	(3s)	(3p)
0.000	100.00	100.00	1000.0	100.00	500.0	100.00	As for Ca neutral	
0.005	90.49	90.40	951.4	90.39	475.7	90.39		
0.010	81.90	81.56	905.6	81.52	452.6	81.52		
0.015	74.14	73.41	862.3	73.34	430.9	73.34		
0.020	67.12	65.90	821.3	65.80	410.3	65.79		
$r$	TABLE OF P Ca neutral						Ca <sup>++</sup>	
	(1s)	(2s)	(2p)	(3s)	(3p)	(4s)	(3s)	(3p)
0.00	0.000	0.000	0.000	0.000	0.000	0.000	0.000	0.000
0.01	0.819	0.816	0.091	0.815	0.045	0.815	0.815	0.045
0.02	1.342	1.318	0.329	1.316	0.164	1.316	1.316	0.164
0.03	1.651	1.579	0.672	1.572	0.335	1.572	1.572	0.335
0.04	1.807	1.655	1.086	1.642	0.541	1.641	1.642	0.541
0.05	1.854	1.592	1.545	1.570	0.768	1.568	1.570	0.768
0.06	1.828	1.427	2.028	1.394	1.006	1.391	1.394	1.006
0.07	1.753	1.188	2.519	1.142	1.247	1.138	1.142	1.247
0.08	1.648	0.899	3.006	0.839	1.482	0.835	0.839	1.482
0.10	1.395	0.238	3.929	0.153	1.921	0.146	0.153	1.921
0.12	1.135	-0.451	4.747	-0.554	2.294	-0.561	-0.554	2.294
0.14	0.899	-1.106	5.436	-1.214	2.588	-1.221	-1.214	2.588
0.16	0.698	-1.692	5.987	-1.787	2.799	-1.793	-1.787	2.799
0.18	0.535	-2.192	6.405	-2.252	2.926	-2.256	-2.252	2.926
0.20	0.405	-2.602	6.699	-2.604	2.975	-2.603	-2.604	2.975
0.22	0.304	-2.922	6.881	-2.842	2.953	-2.835	-2.842	2.953
0.24	0.227	-3.160	6.967	-2.974	2.867	-2.960	-2.973	2.866

TABLE III—(continued)

$r$	Ca neutral						Ca <sup>++</sup>	
	(1s)	(2s)	(2p)	(3s)	(3p)	(4s)	(3s)	(3p)
0.26	0.168	-3.323	6.969	-3.008	2.725	-2.984	-3.007	2.724
0.28	0.124	-3.422	6.902	-2.955	2.535	-2.921	-2.954	2.533
0.30	0.091	-3.465	6.778	-2.826	2.304	-2.780	-2.824	2.302
0.35	0.041	-3.386	6.289	-2.242	1.593	-2.164	-2.239	1.590
0.40	0.019	-3.133	5.650	-1.405	0.764	-1.295	-1.402	0.760
0.45	0.008	-2.792	4.956	-0.441	-0.113	-0.303	-0.438	-0.117
0.50	0.003 <sub>s</sub>	-2.421	4.268	+0.556	-0.985	+0.715	+0.560	-0.990
0.55	0.001 <sub>s</sub>	-2.055	3.622	1.522	-1.816	1.688	1.527	-1.821
0.60	0.000 <sub>s</sub>	-1.716	3.038	2.413	-2.582	2.571	2.418	-2.586
0.7		-1.153	2.077	3.880	-3.862	3.962	3.884	-3.895
0.8		-0.747	1.381	4.880	-4.785	4.803	4.883	-4.785
0.9		-0.471	0.899	5.451	-5.376	5.129	5.452	-5.372
1.0		-0.292	0.577	5.673	-5.688	5.026	5.672	-5.680
1.1		-0.179	0.366	5.636	-5.783	4.591	5.633	-5.770
1.2		-0.108	0.230	5.420	-5.716	3.912	5.414	-5.698
1.4		-0.039	0.090	4.694	-5.273	2.109	4.683	-5.246
1.6		-0.014	0.034	3.840	-4.630	0.044	3.825	-4.595
1.8		-0.005	0.013	3.030	-3.938	-2.034	3.013	-3.897
2.0		-0.001 <sub>s</sub>	0.005	2.332	-3.276	-3.986	2.315	-3.231
2.2		-0.000 <sub>s</sub>	0.002	1.763	-2.684	-5.74	1.745	-2.635
2.4			0.001	1.314	-2.169	-7.25	1.298	-2.120
2.6				0.969	-1.735	-8.52	0.954	-1.688
2.8				0.709	-1.377	-9.54	0.695	-1.331
3.0				0.514	-1.085	-10.33	0.502	-1.042
3.2				0.371	-0.851	-10.91	0.360	-0.810
3.4				0.266	-0.664	-11.30	0.257	-0.626
3.6				0.191	-0.515	-11.53	0.182	-0.481
3.8				0.136	-0.399	-11.61	0.128	-0.368
4.0				0.096	-0.308	-11.57	0.090	-0.280
4.5				0.041	-0.160	-11.06	0.037	-0.140
5.0				0.017	-0.082	-10.18	0.015	-0.068
5.5				0.007	-0.042	-9.12	0.006	-0.033
6.0				0.003	-0.021	-7.99	0.002	-0.016
6.5				0.001	-0.011	-6.90	0.001	-0.007
7.0					-0.005	-5.87		-0.003
8					-0.001	-4.13		-0.001
9						-2.81		
10						-1.86		
11						-1.21		
12						-0.78		
14						-0.31		
16						-0.12		
18						-0.04		
20						-0.01		

TABLE III—(continued)

	(1s)	(2s)	(2p)	(3s)	(3p)	(4s)
$\epsilon$ (Ca neutral) .....	298.4	30.70	25.59	3.537	2.156	0.3573
$\epsilon$ (Ca <sup>++</sup> ) .....	299.5	31.73	26.61	4.537	3.157	
$\int_0^\infty P^2 dr$ (Ca neutral) .... } 0.3267	4.103	17.280	{	31.66	39.78 <sub>0</sub>	506.7
$\int_0^\infty P^2 dr$ (Ca <sup>++</sup> ) .....				31.53	39.25 <sub>3</sub>	

and (3p)<sup>6</sup>. The perturbation of the (3s)<sup>2</sup> group is small, but that of the (3p)<sup>6</sup> group is quite appreciable.

It should be noted that the perturbation by the (4s)<sup>1</sup> electron of the singly ionized atom in its normal state will not be half the perturbation by the (4s)<sup>2</sup> group of the neutral atom, but will be greater than this since the charge distribution of an electron in the (4s) wave function of Ca<sup>+</sup> will be appreciably more compact than that of one of the (4s)<sup>2</sup> electrons of neutral Ca.

#### § 4—RESULTS FOR Hg AND Hg<sup>++</sup>

Mercury is the heaviest atom for which calculations of the self-consistent field have been carried out. As already mentioned in III, the numerical work involved is extensive, not only on account of the number of radial wave functions to be determined, and the small intervals of integration necessary on account of the large field, but also because of the extreme sensitiveness of the (5d)<sup>10</sup> group to the estimated field, which makes the process of approximation to the self-consistent field a slow one. In all, 18 steps of approximation have been made, for the ion and neutral atom together, and of these about half were concerned with the (5d)<sup>10</sup> group alone.

The results are given in Tables V, VI and VII. The maximum difference between estimated and calculated Z, either for the ion or neutral atom, is 0.02<sub>5</sub> in the aggregate, and 0.01 in the contribution from any one group; these maximum differences occur in a region where the total Z is comparatively large (about 60), so that they are small relative to the total Z, and are unimportant. It might seem superfluous to aim at this degree of approximation to the self-consistent field for such a heavy atom, for which relativity and spin effects must be appreciable, but it has seemed worth while to achieve, for one heavy atom, the same order of numerical accuracy as has been attained for light atoms, in order that the results, as far as they go, should be reliable for immediate applications and for comparison with any future work taking relativity and spin effects into account, and in order that differences between the ion and neutral atom should be significant.

The most interesting feature of the results is the considerable perturbation of the  $(5d)^{10}$  group by the addition of the  $(6s)^2$  group to  $\text{Hg}^{++}$  to give neutral Hg, as is shown most clearly by the table of contributions to  $Z$ , and, on the other hand, the surprisingly small perturbation of the  $(5p)^6$  group. The  $(5p)$  wave function is hardly affected, to the accuracy to which it is tabulated in Table V, and the maximum difference between the contributions of the  $(5p)^6$  group to  $Z$  for  $\text{Hg}^{++}$  and neutral Hg is 0.002, whereas for the  $(5d)^{10}$  group the corresponding maximum difference is 0.14.

This small perturbation of the  $(5p)^6$  group is partly due to the fact that this group is much less sensitive than the  $(5d)^{10}$  group to equal perturbing influences, but the main reason for it is that the perturbation of the  $(5d)^{10}$  group largely "shields" the inner group from the added  $(6s)^2$  group. The addition of the  $(6s)^2$  group alone would decrease  $Z$  at each radius, but the  $(5d)^{10}$  group expands and this increases  $Z$ , since it decreases the average number of electrons inside any given radius, and over the range where the  $(5p)$  wave function is appreciable, this decrease of  $Z$  due to the expansion of the  $(5d)^{10}$  group roughly compensates for the increase due to the charge density of the added  $(6s)^2$  group. It is interesting to note that over a small range ( $\rho = 7$  to  $7\frac{1}{2}$ ) the effect of the expansion of the  $(5d)^{10}$  group is the greater; for example the total charge of the  $(6s)^2$  group lying inside  $\rho = 7\frac{1}{2}$  is 0.05 electrons, but on account of the expansion of the  $(5d)^{10}$  group, the total charge of this group inside this radius is 0.10 electrons smaller for neutral Hg than for  $\text{Hg}^{++}$ , so the net effect of the addition of the  $(6s)^2$  group is to decrease the charge lying inside  $\rho = 7\frac{1}{2}$  by 0.05 electrons.

On account of the very small perturbation of the  $(5s)$  and  $(5p)$  wave functions (and, *a fortiori*, of those of the inner groups also), only the  $(5d)$  wave function and  $(5d)^{10}$  contribution to  $Z$  are tabulated for  $\text{Hg}^{++}$  as well as for neutral Hg.

If  $U(r)$  is the radial charge density (*i.e.*,  $U(r) dr$  is the charge lying in the spherical shell between radii  $r$  and  $r + dr$ ), for the whole atom,

$$rU(r) = -\frac{dZ}{d\rho} = \sum_n \left[ 2(2l+1) (r \cdot r^{-\frac{1}{2}} P_{nl})^2 \int_0^\infty P_{nl}^2 dr \right].$$

This quantity, for the neutral atom, is tabulated in Table IX as well as  $2Z_\rho$  for the neutral atom and ion; when, as here,  $\rho = \log r$  is taken as independent variable,  $rU(r)$  is probably a more convenient quantity to have tabulated than  $U(r)$  itself.

As this is the heaviest atom for which self-consistent field calculations have been carried out, it is interesting to compare the field with that

TABLE IV—Ca AND Ca<sup>++</sup> CONTRIBUTIONS TO  $Z$ , AND TOTAL  $2Z_p$ .  
Contributions to  $Z$ :  $2(2l+1)[1-Z_0(nl, nl|r)]$

$r$	Ca neutral						Ca <sup>++</sup>		Total $2Z_p$	
	(1s)	(2s)	(2p)	(3s)	(3p)	(4s)	(3s)	(3p)	Ca neutral	Ca <sup>++</sup>
0.000	2.000	2.000	6.000	2.000	6.000	2.000	2.000	6.000	40.000	40.000
0.005	1.998	2.000	6.000	2.000	6.000	2.000	2.000	6.000	39.215	39.215
0.010	1.985	1.999	6.000	2.000	6.000	2.000	2.000	6.000	38.433	38.443
0.015	1.955	1.997	6.000	2.000	6.000	2.000	2.000	6.000	37.678	37.694
0.020	1.910	1.993	6.000	1.999	6.000	2.000	1.999	6.000	36.950	36.971
0.025	1.846	1.988	6.000	1.998	6.000	2.000	1.999	6.000	36.252	36.278
0.030	1.769	1.983	5.999	1.997	6.000	2.000	1.998	6.000	35.583	35.614
0.04	1.584	1.969	5.996	1.996	6.000	2.000	1.996	6.000	34.337	34.379
0.05	1.377	1.956	5.990	1.994	5.999	2.000	1.994	5.999	33.201	33.253
0.06	1.168	1.946	5.979	1.993	5.998	2.000	1.993	5.998	32.159	32.221
0.07	0.971	1.937	5.961	1.992	5.996	2.000	1.992	5.996	31.192	21.265
0.08	0.794	1.932	5.934	1.991	5.993	2.000	1.991	5.993	30.290	30.373
0.10	0.509	1.928	5.850	1.991	5.984	2.000	1.991	5.984	28.631	28.735
0.12	0.312	1.927	5.718	1.991	5.971	2.000	1.991	5.970	27.118	27.243
0.14	0.185	1.921	5.537	1.990	5.952	2.000	1.990	5.952	25.717	25.863
0.16	0.107	1.901	5.310	1.987	5.930	2.000	1.987	5.930	24.414	24.581
0.18	0.061	1.864	5.042	1.982	5.906	1.999	1.982	5.905	23.200	23.388
0.20	0.034	1.808	4.743	1.974	5.879	1.999	1.974	5.878	22.078	22.286
0.22	0.019	1.733	4.422	1.965	5.853	1.998	1.965	5.851	21.042	21.270
0.24	0.010	1.642	4.089	1.954	5.827	1.998	1.954	5.826	20.090	20.338
0.26	0.005	1.539	3.751	1.943	5.803	1.997	1.942	5.802	19.216	19.485
0.28	0.003	1.428	3.417	1.931	5.782	1.996	1.931	5.781	18.417	18.706
0.30	0.001 <sub>5</sub>	1.312	3.091	1.921	5.765	1.995	1.921	5.763	17.685	17.994
0.35		1.022	2.346	1.900	5.735	1.994	1.900	5.733	16.115	16.474
0.40		0.762	1.725	1.889	5.724	1.994	1.889	5.722	14.830	15.240
0.45		0.547	1.236	1.886	5.723	1.994	1.886	5.721	13.748	14.208
0.50		0.381	0.866	1.886	5.720	1.993	1.886	5.717	12.806	13.317
0.55		0.259	0.596	1.882	5.705	1.993	1.882	5.701	11.961	12.522
0.60		0.172	0.403	1.869	5.668	1.992	1.869	5.664	11.184	11.795

0.7	0.072	0.178	1.804	5.506	1.988	1.804	5.500	9.768	10.479
0.8	0.029	0.075	1.681	5.220	1.980	1.679	5.209	8.512	8.322
0.9	0.011	0.031	1.510	4.826	1.970	1.507	4.810	7.403	8.313
1.0	0.004	0.012	1.313	4.361	1.960	1.309	4.340	6.445	7.453
1.1	0.001 <sub>5</sub>	0.005	1.110	3.862	1.951	1.105	3.836	5.629	6.735
1.2	0.000 <sub>5</sub>	0.002	0.916	3.362	1.944	0.911	3.332	4.944	6.146
1.4			0.588	2.441	1.936	0.585	2.408	3.900	5.293
1.6			0.357	1.698	1.935	0.354	1.663	3.177	4.762
1.8			0.208	1.141	1.934	0.205	1.111	2.667	4.442
2.0			0.117	0.749	1.926	0.115	0.723	2.290	4.254
2.2			0.065	0.481	1.907	0.063	0.459	1.994	4.144
2.4			0.035	0.304	1.874	0.034	0.288	1.751	4.081
2.6			0.018	0.190	1.824	0.017	0.177	1.543	4.045
2.8			0.010	0.117	1.760	0.009	0.108	1.360	4.025
3.0			0.005	0.071	1.681	0.005	0.064	1.197	4.013
3.2			0.003	0.043	1.592	0.003	0.038	1.051	4.007
3.4			0.001	0.026	1.494	0.001	0.022	0.919	4.004
3.6				0.016	1.391		0.013	0.800	4.002
3.8				0.009	1.285		0.007	0.695	4.001
4.0				0.005	1.179		0.004	0.600	4.000 <sub>4</sub>
4.5				0.001			0.001	0.412	4.000
5.0					0.701			0.277	4.000
5.5					0.517			0.184	
6.0					0.372			0.118	
6.5					0.262			0.076	
7.0					0.182			0.050	
8					0.083			0.018	
9					0.037			0.006	
10					0.015			0.002	
11					0.006			0.001	
12					0.002			0.000	

—158.6 —157.6

2*v*<sub>0</sub>



TABLE V—RADIAL WAVE FUNCTIONS,  
Hg

$\log_e(1000r)$ $= \rho$	$r$	(1s)	(2s)	(2p)	(3s)	(3p)	(3d)
0	0	80.00	80.00	2000	80.00	2000	10000
0	0.001	73.84	73.79	1921	73.78	1921	9740
$0\frac{1}{12}$	0.001396	71.54	71.44	1891	71.43	1891	9635
$0\frac{2}{12}$	0.001948	68.45	68.25	1850	68.23	1850	9495
1	0.002718	64.35	63.98	1794	63.93	1793	9305
$1\frac{1}{12}$	0.003794	59.05	58.36	1719	58.26	1717	9045
$1\frac{2}{12}$	0.005294	52.37	51.12	1620	50.94	1617	8690
2	0.007389	44.23	42.11	1491	41.78	1485	8230

TABLE OF  
Hg

$\log_e(1000r)$ $= \rho$	$r$	(1s)	(2s)	(2p)	(3s)	(3p)	(3d)
0	0.001	2.335	2.334	0.061	2.333	0.061	0.0003
$0\frac{1}{12}$	0.00140	2.673	2.669	0.099	2.668	0.099	0.0007
$0\frac{2}{12}$	0.00195	3.021	3.012	0.159	3.011	0.159	0.0016
1	0.00272	3.355	3.336	0.254	3.333	0.254	0.0036
$1\frac{1}{12}$	0.00379	3.637	3.595	0.402	3.589	0.401	0.0080
$1\frac{2}{12}$	0.00529	3.810	3.720	0.624	3.707	0.623	0.0177
2	0.00739	3.808	3.619	0.947	3.592	0.943	0.0385
$2\frac{1}{12}$	0.00873	3.720	3.451	1.153	3.412	1.147	0.0566
$2\frac{2}{12}$	0.01031	3.563	3.187	1.391	3.133	1.380	0.0823
$2\frac{3}{12}$	0.01218	3.337	2.818	1.660	2.744	1.641	0.1190
$2\frac{4}{12}$	0.01439	3.042	2.338	1.955	2.240	1.924	0.1706
$2\frac{5}{12}$	0.01700	2.686	1.751	2.267	1.624	2.216	0.2420
3	0.02009	2.285	1.070	2.581	0.913	2.498	0.339
$3\frac{1}{12}$	0.02373	1.860	0.325	2.878	0.141	2.744	0.469
$3\frac{2}{12}$	0.02803	1.437	-0.442	3.130	-0.642	2.918	0.639
$3\frac{3}{12}$	0.03312	1.044	-1.173	3.305	-1.363	2.979	0.855
$3\frac{4}{12}$	0.03912	0.706	-1.802	3.373	-1.935	2.881	1.118
$3\frac{5}{12}$	0.04622	0.438	-2.262	3.306	-2.270	2.587	1.427
4	0.0546	0.246	-2.503	3.092	-2.292	2.076	1.770
$4\frac{1}{12}$	0.0593	0.176	-2.531	2.931	-2.170	1.740	1.947
$4\frac{2}{12}$	0.0645	0.123	-2.499	2.738	-1.960	1.356	2.122
$4\frac{3}{12}$	0.0701	0.082	-2.409	2.516	-1.666	0.932	2.292
$4\frac{4}{12}$	0.0762	0.053	-2.268	2.273	-1.297	0.479	2.450
$4\frac{5}{12}$	0.0828	0.033	-2.084	2.015	-0.867	0.010	2.589
$4\frac{6}{12}$	0.0900	0.020	-1.868	1.751	-0.395	0.459	2.705
$4\frac{7}{12}$	0.0978	0.011	-1.631	1.488	+0.096	-0.912	2.789
$4\frac{8}{12}$	0.1063	0.006	-1.385	1.236	0.582	-1.329	2.837
$4\frac{9}{12}$	0.1156	0.003	-1.144	1.000	1.039	-1.693	2.844
$4\frac{10}{12}$	0.1256	0.001	-0.916	0.787	1.440	-1.989	2.807
$4\frac{11}{12}$	0.1365		-0.710	0.601	1.766	-2.204	2.724
5	0.1484		-0.532	0.445	2.001	-2.332	2.596

Hg AND Hg<sup>++</sup>. TABLE OF  $P/r^{l+1}$ 

neutral								Hg <sup>++</sup> (5d)
(4s)	(4p)	(4d)	(4f)	(5s)	(5p)	(5d)	(6s)	
80.00	2000	10000	12000	80.00	2000	10000	80.00	
73.78	1921	9740	11765	73.78	1921	9740	73.78	
71.43	1891	9635	11675	71.43	1891	9635	71.43	
68.23	1850	9495	11550	68.23	1850	9495	68.23	
53.92	1793	9365	11375	63.92	1793	9305	63.92	
58.23	1717	9045	11140	58.23	1717	9045	58.23	
50.89	1616	8690	10815	50.88	1616	8690	50.88	
41.70	1484	8225	10380	41.69	1484	8225	41.69	As for Hg neutral.

$r^{-\frac{1}{2}}P$ neutral								Hg <sup>++</sup> (5d)
(4s)	(4p)	(4d)	(4f)	(5s)	(5p)	(5d)	(6s)	
2.338	0.061	0.0003	0.00000	2.333	0.061	0.0003	2.333	
2.668	0.099	0.0007	0.00000	2.668	0.099	0.0007	2.668	
3.011	0.159	0.0016	0.00000	3.011	0.159	0.0016	3.011	
3.332	0.254	0.0036	0.00001	3.332	0.254	0.0036	3.332	
3.587	0.401	0.0080	0.00004	3.587	0.401	0.0080	3.587	
3.703	0.623	0.0177	0.00012	3.703	0.622	0.0177	3.703	
3.584	0.943	0.0385	0.00036	3.583	0.942	0.0385	3.583	
3.402	1.146	0.0565	0.00063	3.401	1.145	0.0565	3.400	
3.119	1.378	0.0822	0.00109	3.118	1.377	0.0822	3.117	
2.725	1.637	0.1189	0.0019	2.722	1.637	0.1189	2.722	
2.215	1.917	0.1702	0.0032	2.211	1.916	0.1702	2.210	
1.592	2.204	0.2413	0.0055	1.587	2.202	0.2413	1.586	
0.875	2.479	0.338	0.0094	0.868	2.476	0.338	0.866	
0.096	2.714	0.467	0.0157	0.088	2.708	0.466	0.086	
-0.689	2.871	0.634	0.0260	-0.698	2.862	0.633	-0.700	
-1.405	2.906	0.844	0.0424	-1.413	2.892	0.843	-1.415	
-1.962	2.774	1.099	0.0683	-1.966	2.753	1.096	-1.968	
-2.264	2.435	1.391	0.1080	-2.261	2.405	1.386	-2.263	
-2.231	1.869	1.705	0.1675	-2.217	1.830	1.695	-2.217	
-2.074	1.505	1.861	0.207	-2.054	1.460	1.847	-2.053	
-1.825	1.093	2.009	0.254	-1.796	1.044	1.992	-1.794	
-1.489	0.644	2.144	0.310	-1.451	0.591	2.121	-1.448	
-1.077	0.172	2.257	0.375	-1.031	0.116	2.228	-1.026	
-0.608	-0.307	2.341	0.451	-0.554	-0.364	2.304	-0.548	
-0.105	-0.772	2.388	0.540	-0.046	-0.827	2.342	-0.039	
+0.404	-1.202	2.390	0.637	+0.465	-1.251	2.332	+0.472	
0.887	-1.573	2.338	0.748	0.946	-1.610	2.267	0.953	
1.315	-1.862	2.227	0.869	1.362	-1.882	2.141	1.368	
1.649	-2.049	2.054	1.001	1.681	-2.046	1.950	1.686	
1.869	-2.118	1.816	1.141	1.875	-2.085	1.694	1.876	
1.953	-2.061	1.516	1.287	1.924	-1.990	1.376	1.921	1.376

As for Hg neutral, for  $\rho \leq 5$ .

TABLE OF  $r^{-1}P_{\infty}$   
Hg

$\log_e (1000r)$ $= \rho$	$r$	(1s)	(2s)	(2p)	(3s)	(3p)	(3d)
$5\frac{1}{12}$	0.1613		-0.384	0.318	2.136	-2.369	2.427
$5\frac{2}{12}$	0.1753		-0.266	0.219	2.170	-2.319	2.224
$5\frac{3}{12}$	0.1906		-0.177	0.145	2.110	-2.193	1.994
$5\frac{4}{12}$	0.2071		-0.112	0.092	1.969	-2.003	1.746
$5\frac{5}{12}$	0.2251		-0.068	0.056	1.766	-1.768	1.490
$5\frac{6}{12}$	0.2447		-0.039	0.032	1.522	-1.507	1.239
$5\frac{7}{12}$	0.2660		-0.021	0.017	1.260	-1.239	1.000
$5\frac{8}{12}$	0.2891		-0.011	0.009	1.002	-0.981	0.783
$5\frac{9}{12}$	0.3142		-0.005	0.004	0.764	-0.747	0.593
$5\frac{10}{12}$	0.3415		-0.002	0.002	0.557	-0.545	0.434
$5\frac{11}{12}$	0.3712		-0.001	0.001	0.388	-0.381	0.305
6	0.4034				0.257	-0.255	0.206
$6\frac{1}{12}$	0.4385				0.162	-0.163	0.134
$6\frac{2}{12}$	0.4766				0.097	-0.098	0.083
$6\frac{3}{12}$	0.518				0.055	-0.057	0.049
$6\frac{4}{12}$	0.563				0.029	-0.031	0.027
$6\frac{5}{12}$	0.612				0.015	-0.016	0.014
$6\frac{6}{12}$	0.665				0.007	-0.007	0.007
$6\frac{7}{12}$	0.723				0.003	-0.003	0.003
$6\frac{8}{12}$	0.786				0.001	-0.001	0.001
$6\frac{9}{12}$	0.854						
$6\frac{10}{12}$	0.928						
$6\frac{11}{12}$	1.009						
7	1.097						
$7\frac{1}{12}$	1.192						
$7\frac{2}{12}$	1.296						
$7\frac{3}{12}$	1.408						
$7\frac{4}{12}$	1.530						
$7\frac{5}{12}$	1.663						
$7\frac{6}{12}$	1.808						
$7\frac{7}{12}$	1.965						
$7\frac{8}{12}$	2.136						
$7\frac{9}{12}$	2.322						
$7\frac{10}{12}$	2.523						
$7\frac{11}{12}$	2.743						
8	2.981						
$8\frac{1}{12}$	3.240						
$8\frac{2}{12}$	3.522						
$8\frac{3}{12}$	3.828						
$8\frac{4}{12}$	4.160						
$8\frac{5}{12}$	4.522						

(continued)

neutral

(4s)	(4p)	(4d)	(4f)	(5s)	(5p)	(5d)	(6s)	Hg <sup>++</sup> (5d)
1.890	-1.874	1.160	1.436	1.817	-1.761	1.002	1.809	1.002
1.682	-1.567	0.759	1.581	1.559	-1.408	0.585	1.545	0.585
1.341	-1.155	0.327	1.723	1.166	-0.955	0.142	1.145	0.141
0.892	-0.664	-0.120	1.852	0.670	-0.427	-0.308	0.643	-0.309
0.372	-0.128	-0.562	1.963	0.112	+0.133	-0.742	0.080	-0.743
-0.179	+0.417	-0.976	2.051	-0.456	0.682	-1.136	-0.489	-1.137
-0.715	0.933	-1.345	2.112	-0.980	1.176	-1.464	-1.011	-1.465
-1.196	1.385	-1.649	2.141	-1.409	1.569	-1.707	-1.432	-1.708
-1.583	1.743	-1.875	2.135	-1.700	1.828	-1.848	-1.708	-1.848
-1.855	1.990	-2.015	2.095	-1.824	1.930	-1.877	-1.811	-1.877
-2.001	2.117	-2.068	2.022	-1.770	1.867	-1.791	-1.731	-1.791
-2.024	2.129	-2.040	1.920	-1.544	1.644	-1.597	-1.474	-1.596
-1.939	2.038	-1.940	1.793	-1.172	1.284	-1.308	-1.070	-1.306
-1.768	1.867	-1.784	1.646	-0.690	0.818	-0.941	-0.559	-0.939
-1.541	1.641	-1.587	1.486	-0.146	0.286	-0.521	+0.007	-0.518
-1.285	1.385	-1.368	1.318	+0.411	-0.268	-0.070	0.572	-0.067
-1.026	1.123	-1.141	1.148	0.934	-0.802	+0.384	1.083	+0.388
-0.784	0.875	-0.921	0.981	1.381	-1.278	0.818	1.492	0.821
-0.572	0.653	-0.718	0.821	1.722	-1.665	1.209	1.764	1.212
-0.399	0.467	-0.541	0.673	1.940	-1.942	1.540	1.876	1.543
-0.265	0.320	-0.392	0.539	2.031	-2.100	1.798	1.825	1.800
-0.167	0.209	-0.274	0.422	2.006	-2.143	1.977	1.621	1.978
-0.090	0.129	-0.183	0.322	1.882	-2.083	2.076	1.288	2.077
-0.056	0.076	-0.117	0.239	1.687	-1.939	2.102	0.857	2.101
-0.030	0.042	-0.072	0.173	1.452	-1.737	2.062	0.367	2.060
-0.015	0.022	-0.042	0.122	1.200	-1.500	1.970	-0.147	1.967
-0.007	0.011	-0.023	0.083	0.953	-1.251	1.837	-0.654	1.833
-0.003	0.005	-0.012	0.055	0.728	-1.009	1.676	-1.125	1.672
-0.001	0.002	-0.006	0.035	0.536	-0.787	1.500	-1.542	1.494
	0.001	-0.003	0.022	0.378	-0.593	1.317	-1.888	1.310
		-0.001	0.013	0.257	-0.432	1.136	-2.156	1.127
			0.007	0.167	-0.303	0.962	-2.344	0.950
			0.004	0.104	-0.205	0.801	-2.453	0.786
			0.002	0.062	-0.134	0.655	-2.487	0.637
			0.001	0.035	-0.084	0.526	-2.454	0.504
				0.018	-0.050	0.414	-2.363	0.389
				0.009	-0.029	0.320	-2.223	0.293
				0.004	-0.015	0.242	-2.044	0.214
				0.002	-0.008	0.179	-1.839	0.151
				0.001	-0.004	0.129	-1.617	0.103
					-0.002	0.090	-1.390	0.068

TABLE OF  $r^{-1} P$ —  
Hg

$\log_e (1000r)$ $= \rho$	$r$	(1s)	(2s)	(2p)	(3s)	(3p)	(3d)
$8\frac{6}{12}$	4.915						
$8\frac{7}{12}$	5.34						
$8\frac{8}{12}$	5.81						
$8\frac{9}{12}$	6.31						
$8\frac{10}{12}$	6.86						
$8\frac{11}{12}$	7.46						
9	8.10						
$9\frac{1}{12}$	8.81						
$9\frac{2}{12}$	9.57						
$9\frac{3}{12}$	10.40						
$9\frac{4}{12}$	11.31						
$9\frac{5}{12}$	12.29						
$9\frac{6}{12}$	13.36						
$9\frac{7}{12}$	14.52						
$9\frac{8}{12}$	15.78						
$9\frac{9}{12}$	17.15						

Hg neutral

	$\epsilon$	$24 \int_0^\infty P^2 dr$
1s	5553	0.07590
2s	925	0.6900
2p	892	0.8749
3s	216.9	3.109
3p	200.6	3.522
3d	170.5	3.803
4s	46.07	12.55 <sub>5</sub>
4p	38.89	14.56 <sub>5</sub>
4d	25.79	14.78 <sub>7</sub>
4f	8.39	16.64 <sub>4</sub>

TABLE VI—NEUTRAL Hg AND Hg<sup>++</sup>. CONTRIBUTIONSHg neutral and Hg<sup>++</sup>

$\rho$	(1s) <sup>2</sup>	(2s) <sup>2</sup>	(2p) <sup>6</sup>	(3s) <sup>2</sup>	(3p) <sup>6</sup>	(3d) <sup>10</sup>
0	2.00	2.00	6.00	2.00	6.00	10.00
$0\frac{2}{12}$	2.00	2.00	6.00	2.00	6.00	10.00
$0\frac{4}{12}$	1.99 <sub>5</sub>	2.00	6.00	2.00	6.00	10.00
$0\frac{6}{12}$	1.99 <sub>5</sub>	2.00	6.00	2.00	6.00	10.00
$0\frac{8}{12}$	1.99	2.00	6.00	2.00	6.00	10.00
$0\frac{10}{12}$	1.98 <sub>5</sub>	2.00	6.00	2.00	6.00	10.00
1	1.98	2.00	6.00	2.00	6.00	10.00
$1\frac{2}{12}$	1.97	1.99 <sub>5</sub>	6.00	2.00	6.00	10.00

(continued)

neutral

(4s)	(4p)	(4d)	(4f)	(5s)	(5p)	(5d)	(6s)	Hg <sup>++</sup> (5d)
					-0.001	0.062	-1.166	0.043
						0.041	-0.954	0.026
						0.026	-0.759	0.014
						0.016	-0.587	0.007
						0.010	-0.440	0.004
						0.005	-0.320	0.002
						0.003	-0.224	0.001
						0.002	-0.150	
						0.001	-0.097	
							-0.060	
							-0.035	
							-0.019	
							-0.010	
							-0.005	
							-0.002	
							-0.001	

Hg neutral

	$\epsilon$	$24 \int_0^\infty P^2 dr$
5s	6.93	62.99
5p	4.60	83.97
5d	0.920	161.7 <sub>8</sub>
6s	0.471	1196.0

Hg<sup>++</sup>

	$\epsilon$	$24 \int_0^\infty P^2 dr$
5s	8.11 <sub>6</sub>	
5p	5.77	
5d	2.095	158.3 <sub>8</sub>

TO Z. TABLE OF  $2(2l+1)[1 - Z_0(nl, nl|r)]$ 

Hg neutral and Hg <sup>++</sup>							Hg neutral			
ρ							ρ			Hg <sup>++</sup>
	(4s) <sup>2</sup>	(4p)	(4d) <sup>10</sup>	(4f) <sup>14</sup>	(5s) <sup>2</sup>	(5p) <sup>6</sup>		(5d) <sup>10</sup>	(6s) <sup>2</sup>	(5d) <sup>10</sup>
0	2.00	6.00	10.00	14.00	2.00	6.00	0	10.00	2.00	10.00
2	2.00	6.00	10.00	14.00	2.00	6.00	4	10.00	2.00	10.00
3	1.99 <sub>5</sub>	5.99 <sub>5</sub>	10.00	14.00	2.00	6.00	4 $\frac{4}{1\frac{1}{2}}$	9.99	2.00	9.99
3 $\frac{3}{1\frac{1}{2}}$	1.99 <sub>5</sub>	5.99	10.00	14.00	2.00	6.00	4 $\frac{3}{1\frac{1}{2}}$	9.97	2.00	9.97
3 $\frac{4}{1\frac{1}{2}}$	1.99 <sub>5</sub>	5.98	10.00	14.00	2.00	5.99 <sub>5</sub>	5	9.94	2.00	9.94
3 $\frac{5}{1\frac{1}{2}}$	1.99 <sub>5</sub>	5.96 <sub>5</sub>	10.00	14.00	2.00	5.99 <sub>5</sub>	5 $\frac{3}{1\frac{1}{2}}$	9.93	2.00	9.93
3 $\frac{6}{1\frac{1}{2}}$	1.99	5.95	9.99 <sub>5</sub>	14.00	2.00	5.99	5 $\frac{4}{1\frac{1}{2}}$	9.93	2.00	9.93
3 $\frac{7}{1\frac{1}{2}}$	1.98 <sub>5</sub>	5.93	9.98 <sub>5</sub>	14.00	1.99 <sub>5</sub>	5.99	5 $\frac{5}{1\frac{1}{2}}$	9.92 <sub>5</sub>	2.00	9.92

TABLE VI—

	Hg neutral and Hg <sup>++</sup>					
$\rho$	(1s) <sup>2</sup>	(2s) <sup>2</sup>	(2p) <sup>6</sup>	(3s) <sup>2</sup>	(3p) <sup>6</sup>	(3d) <sup>10</sup>
1 $\frac{1}{2}$	1.95 <sub>5</sub>	1.99 <sub>5</sub>	6.00	2.00	6.00	10.00
1 $\frac{0}{2}$	1.93	1.99	6.00	2.00	6.00	10.00
1 $\frac{8}{2}$	1.89	1.99	6.00	1.99 <sub>5</sub>	6.00	10.00
1 $\frac{7}{2}$	1.84	1.98 <sub>5</sub>	6.00	1.99 <sub>5</sub>	6.00	10.00
2	1.77	1.97 <sub>5</sub>	6.00	1.99 <sub>5</sub>	6.00	10.00
2 $\frac{9}{2}$	1.67	1.96 <sub>5</sub>	5.99 <sub>5</sub>	1.99 <sub>5</sub>	6.00	10.00
2 $\frac{8}{2}$	1.54 <sub>5</sub>	1.95 <sub>5</sub>	5.99	1.99	6.00	10.00
2 $\frac{6}{2}$	1.38 <sub>5</sub>	1.94	5.98 <sub>5</sub>	1.99	5.99 <sub>5</sub>	10.00
2 $\frac{5}{2}$	1.20	1.93	5.97	1.98 <sub>5</sub>	5.99	10.00
2 $\frac{4}{2}$	0.98 <sub>5</sub>	1.91 <sub>5</sub>	5.93 <sub>5</sub>	1.98 <sub>5</sub>	5.98 <sub>5</sub>	10.00
3	0.76 <sub>5</sub>	1.91	5.88	1.98	5.97	10.00
3 $\frac{2}{2}$	0.55	1.90 <sub>5</sub>	5.78	1.98	5.95	10.00
3 $\frac{1}{2}$	0.36	1.90 <sub>5</sub>	5.61 <sub>5</sub>	1.98	5.91	9.99 <sub>5</sub>
3 $\frac{0}{2}$	0.21	1.89 <sub>5</sub>	5.35	1.98	5.85 <sub>5</sub>	9.99
3 $\frac{8}{2}$	0.11	1.86	4.95	1.97	5.78	9.97 <sub>5</sub>
3 $\frac{7}{2}$	0.04 <sub>5</sub>	1.77	4.39	1.94 <sub>5</sub>	5.68 <sub>5</sub>	9.94 <sub>5</sub>
4	0.01 <sub>5</sub>	1.60	3.67 <sub>5</sub>	1.91	5.59	9.87 <sub>5</sub>
4 $\frac{1}{2}$	0.01	1.48	3.27	1.89	5.55	9.81 <sub>5</sub>
4 $\frac{2}{2}$	0.00 <sub>5</sub>	1.34	2.85	1.87	5.52	9.73 <sub>5</sub>
4 $\frac{3}{2}$		1.18	2.42	1.85	5.50	9.61 <sub>5</sub>
4 $\frac{4}{2}$		1.01 <sub>5</sub>	2.00	1.83 <sub>5</sub>	5.49	9.46
4 $\frac{5}{2}$		0.84	1.60	1.82 <sub>5</sub>	5.49	9.24 <sub>5</sub>
4 $\frac{6}{2}$		0.67	1.24	1.82	5.48 <sub>5</sub>	8.97
4 $\frac{7}{2}$		0.51 <sub>5</sub>	0.92 <sub>5</sub>	1.82	5.47	8.62
4 $\frac{8}{2}$		0.37 <sub>5</sub>	0.66	1.82	5.42 <sub>5</sub>	8.18
4 $\frac{9}{2}$		0.26 <sub>5</sub>	0.45	1.81	5.33	7.65 <sub>5</sub>
4 $\frac{10}{2}$		0.17 <sub>5</sub>	0.29	1.78	5.16	7.04 <sub>5</sub>
4 $\frac{11}{2}$		0.11	0.18	1.72	4.89	6.35 <sub>5</sub>
5		0.06 <sub>5</sub>	0.10 <sub>5</sub>	1.63	4.54	5.59 <sub>5</sub>
5 $\frac{1}{2}$		0.03 <sub>5</sub>	0.05 <sub>5</sub>	1.49 <sub>5</sub>	4.08 <sub>5</sub>	4.80
5 $\frac{2}{2}$		0.02	0.03	1.32 <sub>5</sub>	3.55 <sub>5</sub>	3.99 <sub>5</sub>
5 $\frac{3}{2}$		0.01	0.01 <sub>5</sub>	1.12 <sub>5</sub>	2.97	3.21 <sub>5</sub>
5 $\frac{4}{2}$		0.00 <sub>5</sub>	0.00 <sub>5</sub>	0.91 <sub>5</sub>	2.37 <sub>5</sub>	2.48 <sub>5</sub>
5 $\frac{5}{2}$				0.70 <sub>5</sub>	1.81	1.84 <sub>5</sub>
5 $\frac{6}{2}$				0.51	1.30 <sub>5</sub>	1.30 <sub>5</sub>
5 $\frac{7}{2}$				0.35	0.89	0.88
5 $\frac{8}{2}$				0.22 <sub>5</sub>	0.57	0.56
5 $\frac{9}{2}$				0.13	0.34	0.33 <sub>5</sub>
5 $\frac{10}{2}$				0.07 <sub>5</sub>	0.19	0.19
5 $\frac{11}{2}$				0.03 <sub>5</sub>	0.09 <sub>5</sub>	0.10
6				0.01 <sub>5</sub>	0.05 <sub>5</sub>	0.05
6 $\frac{1}{2}$				0.00 <sub>5</sub>	0.01 <sub>5</sub>	0.02
6 $\frac{0}{2}$					0.00 <sub>5</sub>	0.01
6 $\frac{3}{2}$						0.00 <sub>5</sub>

(continued)

Hg neutral and Hg <sup>++</sup>							Hg neutral			
$\rho$	(4s) <sup>2</sup>	(4p)	(4d) <sup>10</sup>	(4f) <sup>14</sup>	(5s) <sup>2</sup>	(5p) <sup>6</sup>	$\rho$	(5d) <sup>10</sup>	(6s) <sup>2</sup>	Hg <sup>++</sup> (5d) <sup>10</sup>
4	1.98	5.91	9.97	14.00	1.99 <sub>5</sub>	5.98 <sub>5</sub>	5 <sub>1/2</sub> <sup>8</sup>	9.88 <sub>5</sub>	2.00	9.88
4 <sub>1/2</sub> <sup>2</sup>	1.97	5.89 <sub>5</sub>	9.93 <sub>5</sub>	14.00	1.99 <sub>5</sub>	5.98 <sub>5</sub>	5 <sub>1/2</sub> <sup>10</sup>	9.80 <sub>5</sub>	1.99 <sub>5</sub>	9.80
4 <sub>1/2</sub> <sup>4</sup>	1.96	5.89 <sub>5</sub>	9.87 <sub>5</sub>	14.00	1.99 <sub>5</sub>	5.98	6	9.69 <sub>5</sub>	1.99 <sub>5</sub>	9.69
4 <sub>1/2</sub> <sup>6</sup>	1.96	5.89	9.77 <sub>5</sub>	13.99 <sub>5</sub>	1.99	5.98				
4 <sub>1/2</sub> <sup>8</sup>	1.96	5.86 <sub>5</sub>	9.62 <sub>5</sub>	13.98	1.99	5.97 <sub>5</sub>	6 <sub>1/2</sub> <sup>1/2</sup>	9.65	1.99	9.64
4 <sub>1/2</sub> <sup>10</sup>	1.94 <sub>5</sub>	5.79	9.45	13.94 <sub>5</sub>	1.99	5.96 <sub>5</sub>	6 <sub>1/2</sub> <sup>3/2</sup>	9.61 <sub>5</sub>	1.99	9.60 <sub>5</sub>
5	1.90	5.65 <sub>5</sub>	9.28 <sub>5</sub>	13.86	1.98	5.95	6 <sub>1/2</sub> <sup>5/2</sup>	9.60	1.99	9.59
							6 <sub>1/2</sub> <sup>7/2</sup>	9.59 <sub>5</sub>	1.99	9.58 <sub>5</sub>
5 <sub>1/2</sub> <sup>1/2</sup>	1.87 <sub>5</sub>	5.58	9.22 <sub>5</sub>	13.78 <sub>5</sub>	1.97 <sub>5</sub>	5.93	6 <sub>1/2</sub> <sup>9/2</sup>	9.59 <sub>5</sub>	1.99	9.58 <sub>5</sub>
5 <sub>1/2</sub> <sup>3/2</sup>	1.84 <sub>5</sub>	5.51	9.19	13.67 <sub>5</sub>	1.97	5.92	6 <sub>1/2</sub> <sup>11/2</sup>	9.57 <sub>5</sub>	1.99	9.56 <sub>5</sub>
5 <sub>1/2</sub> <sup>5/2</sup>	1.82	5.45 <sub>5</sub>	9.17 <sub>5</sub>	13.52 <sub>5</sub>	1.96 <sub>5</sub>	5.91 <sub>5</sub>	6 <sub>1/2</sub> <sup>13/2</sup>	9.51	1.98 <sub>5</sub>	9.50
5 <sub>1/2</sub> <sup>7/2</sup>	1.80 <sub>5</sub>	5.43	9.17 <sub>5</sub>	13.31	1.96 <sub>5</sub>	5.91	6 <sub>1/2</sub> <sup>15/2</sup>	9.37 <sub>5</sub>	1.98	9.36
5 <sub>1/2</sub> <sup>9/2</sup>	1.80	5.42	9.16 <sub>5</sub>	13.02	1.96 <sub>5</sub>	5.91	6 <sub>1/2</sub> <sup>17/2</sup>	9.14	1.97	9.12
5 <sub>1/2</sub> <sup>11/2</sup>	1.80	5.42	9.12	12.64 <sub>5</sub>	1.96 <sub>5</sub>	5.91	6 <sub>1/2</sub> <sup>19/2</sup>	8.79	1.96	8.76
5 <sub>1/2</sub> <sup>13/2</sup>	1.79 <sub>5</sub>	5.39 <sub>5</sub>	9.00	12.17	1.96	5.90	6 <sub>1/2</sub> <sup>21/2</sup>	8.31	1.95 <sub>5</sub>	8.27
5 <sub>1/2</sub> <sup>15/2</sup>	1.77	5.30 <sub>5</sub>	8.76	11.58 <sub>5</sub>	1.95 <sub>5</sub>	5.88	7	7.71	1.95	7.65 <sub>5</sub>
5 <sub>1/2</sub> <sup>17/2</sup>	1.71	5.12	8.37 <sub>5</sub>	10.88 <sub>5</sub>	1.94	5.84	7 <sub>1/2</sub> <sup>1/2</sup>	7.00 <sub>5</sub>	1.95	6.93 <sub>5</sub>
5 <sub>1/2</sub> <sup>19/2</sup>	1.61	4.80 <sub>5</sub>	7.82	10.07 <sub>5</sub>	1.92	5.78 <sub>5</sub>	7 <sub>1/2</sub> <sup>3/2</sup>	6.22 <sub>5</sub>	1.95	6.14
5 <sub>1/2</sub> <sup>21/2</sup>	1.47 <sub>5</sub>	4.36	7.10	9.16 <sub>5</sub>	1.89	5.72	7 <sub>1/2</sub> <sup>5/2</sup>	5.41	1.95	5.31
6	1.26	3.79 <sub>5</sub>	6.24	8.18 <sub>5</sub>	1.86 <sub>5</sub>	5.65	7 <sub>1/2</sub> <sup>7/2</sup>	4.58 <sub>5</sub>	1.94	4.47
6 <sub>1/2</sub> <sup>1/2</sup>	1.04	3.16	5.28 <sub>5</sub>	7.16	1.84 <sub>5</sub>	5.59 <sub>5</sub>	7 <sub>1/2</sub> <sup>9/2</sup>	3.79	1.92 <sub>5</sub>	3.67
6 <sub>1/2</sub> <sup>3/2</sup>	0.81	2.50	4.30 <sub>5</sub>	6.12	1.83	5.56 <sub>5</sub>	7 <sub>1/2</sub> <sup>11/2</sup>	3.05 <sub>5</sub>	1.89 <sub>5</sub>	2.92
6 <sub>1/2</sub> <sup>5/2</sup>	0.59	1.87	3.35	5.10	1.83	5.55	7 <sub>1/2</sub> <sup>13/2</sup>	2.39	1.84 <sub>5</sub>	2.25 <sub>5</sub>
6 <sub>1/2</sub> <sup>7/2</sup>	0.40 <sub>5</sub>	1.32	2.49	4.13 <sub>5</sub>	1.83	5.55	7 <sub>1/2</sub> <sup>15/2</sup>	1.82 <sub>5</sub>	1.77 <sub>5</sub>	1.68 <sub>5</sub>
6 <sub>1/2</sub> <sup>9/2</sup>	0.26	0.87 <sub>5</sub>	1.75 <sub>5</sub>	3.25 <sub>5</sub>	1.81 <sub>5</sub>	5.53 <sub>5</sub>	7 <sub>1/2</sub> <sup>17/2</sup>	1.35	1.68	1.21
6 <sub>1/2</sub> <sup>11/2</sup>	0.15 <sub>5</sub>	0.54	1.17 <sub>5</sub>	2.48	1.78	5.47	7 <sub>1/2</sub> <sup>19/2</sup>	0.97	1.56	0.84
6 <sub>1/2</sub> <sup>13/2</sup>	0.08 <sub>5</sub>	0.31	0.74	1.82 <sub>5</sub>	1.70 <sub>5</sub>	5.31 <sub>5</sub>	7 <sub>1/2</sub> <sup>21/2</sup>	0.67	1.41 <sub>5</sub>	0.55 <sub>5</sub>
6 <sub>1/2</sub> <sup>15/2</sup>	0.04 <sub>5</sub>	0.16 <sub>5</sub>	0.43 <sub>5</sub>	1.29 <sub>5</sub>	1.58 <sub>5</sub>	5.05	8	0.45	1.26	0.35
6 <sub>1/2</sub> <sup>17/2</sup>	0.02	0.08	0.24	0.88	1.41 <sub>5</sub>	4.65	8 <sub>1/2</sub> <sup>1/2</sup>	0.29	1.08 <sub>5</sub>	0.21
6 <sub>1/2</sub> <sup>19/2</sup>	0.01	0.03 <sub>5</sub>	0.12 <sub>5</sub>	0.57 <sub>5</sub>	1.20 <sub>5</sub>	4.13 <sub>5</sub>	8 <sub>1/2</sub> <sup>3/2</sup>	0.18	0.91 <sub>5</sub>	0.12
6 <sub>1/2</sub> <sup>21/2</sup>	0.00 <sub>5</sub>	0.01 <sub>5</sub>	0.06	0.36	0.98	3.53 <sub>5</sub>	8 <sub>1/2</sub> <sup>5/2</sup>	0.11	0.74 <sub>5</sub>	0.06 <sub>5</sub>
7		0.00 <sub>5</sub>	0.02 <sub>5</sub>	0.21 <sub>5</sub>	0.75 <sub>5</sub>	2.89	8 <sub>1/2</sub> <sup>7/2</sup>	0.06	0.58 <sub>5</sub>	0.03
7 <sub>1/2</sub> <sup>1/2</sup>			0.01	0.12	0.55	2.26	8 <sub>1/2</sub> <sup>9/2</sup>	0.03 <sub>5</sub>	0.44 <sub>5</sub>	0.01 <sub>5</sub>
7 <sub>1/2</sub> <sup>3/2</sup>			0.00 <sub>5</sub>	0.06 <sub>5</sub>	0.38	1.68	8 <sub>1/2</sub> <sup>11/2</sup>	0.01 <sub>5</sub>	0.32	0.00 <sub>5</sub>
7 <sub>1/2</sub> <sup>5/2</sup>				0.03 <sub>5</sub>	0.24 <sub>5</sub>	1.18 <sub>5</sub>	8 <sub>1/2</sub> <sup>13/2</sup>	0.01	0.22 <sub>5</sub>	
7 <sub>1/2</sub> <sup>7/2</sup>				0.01 <sub>5</sub>	0.15	0.79 <sub>5</sub>	8 <sub>1/2</sub> <sup>15/2</sup>	0.00 <sub>5</sub>	0.15	
7 <sub>1/2</sub> <sup>9/2</sup>				0.01	0.08 <sub>5</sub>	0.50 <sub>5</sub>	8 <sub>1/2</sub> <sup>17/2</sup>		0.09 <sub>5</sub>	
7 <sub>1/2</sub> <sup>11/2</sup>				0.00 <sub>5</sub>	0.04 <sub>5</sub>	0.30	8 <sub>1/2</sub> <sup>19/2</sup>		0.05 <sub>5</sub>	
7 <sub>1/2</sub> <sup>13/2</sup>					0.02	0.17	8 <sub>1/2</sub> <sup>21/2</sup>		0.03	
7 <sub>1/2</sub> <sup>15/2</sup>					0.01	0.09	9		0.01 <sub>5</sub>	
7 <sub>1/2</sub> <sup>17/2</sup>					0.00 <sub>5</sub>	0.04 <sub>5</sub>	9 <sub>1/2</sub> <sup>1/2</sup>		0.00 <sub>5</sub>	
7 <sub>1/2</sub> <sup>19/2</sup>						0.02				
7 <sub>1/2</sub> <sup>21/2</sup>						0.01				
8						0.00 <sub>5</sub>				



TABLE VII—Hg AND Hg<sup>++</sup>, TOTAL 2Z<sub>p</sub> AND Hg, CHARGE DISTRIBUTION

$\rho$	Total 2Z <sub>p</sub>		$-\frac{dz}{d\rho} = rU(r)$	$\rho$	Total 2Z <sub>p</sub>		$-\frac{dz}{d\rho} = rU(r)$
	Hg	Hg <sup>++</sup>			Hg	Hg <sup>++</sup>	
	neutral		neutral		neutral		Hg neutral
0	158.92	158.92	0.00	6	36.73	37.20	35.6
0 $\frac{2}{12}$	158.72	158.72	0.00	6 $\frac{1}{12}$	33.44	33.95	36.6
0 $\frac{4}{12}$	158.49	158.49	0.01	6 $\frac{2}{12}$	30.38	30.94	35.6
0 $\frac{6}{12}$	158.22	158.22	0.01	6 $\frac{3}{12}$	27.58	28.18	32.9
0 $\frac{8}{12}$	157.90	157.90	0.02	6 $\frac{4}{12}$	25.01	25.66	28.8
0 $\frac{10}{12}$	157.52	157.52	0.03	6 $\frac{5}{12}$	22.63	23.34	24.7
1	157.07	157.08	0.06	6 $\frac{6}{12}$	20.40	21.18	21.5
1 $\frac{2}{12}$	156.55	156.56	0.09	6 $\frac{7}{12}$	18.29	19.14	19.3
1 $\frac{4}{12}$	155.94	155.95	0.13	6 $\frac{8}{12}$	16.28	17.20	18.3
1 $\frac{6}{12}$	155.23	155.24	0.20	6 $\frac{9}{12}$	14.36	15.36	18.5
1 $\frac{8}{12}$	154.40	154.41	0.29	6 $\frac{10}{12}$	12.55	13.63	19.2
1 $\frac{10}{12}$	153.44	153.45	0.42	6 $\frac{11}{12}$	10.85	12.02	19.9
2	152.32	152.34	0.57	7	9.29	10.57	20.0
2 $\frac{2}{12}$	151.04	151.06	0.77	7 $\frac{1}{12}$	7.89	9.27	19.5
2 $\frac{4}{12}$	149.58	149.60	0.99	7 $\frac{2}{12}$	6.64	8.15	18.5
2 $\frac{6}{12}$	147.91	148.93	1.23	7 $\frac{3}{12}$	5.56	7.20	17.0
2 $\frac{8}{12}$	146.01	146.03	1.47	7 $\frac{4}{12}$	4.62	6.42	15.1
2 $\frac{10}{12}$	143.85	143.87	1.70	7 $\frac{5}{12}$	3.83	5.79	13.1
3	141.40	141.43	1.94	7 $\frac{6}{12}$	3.15	5.29	11.2
3 $\frac{2}{12}$	138.63	138.66	2.24	7 $\frac{7}{12}$	2.58	4.91	9.5
3 $\frac{4}{12}$	135.50	135.54	2.70	7 $\frac{8}{12}$	2.10	4.62	8.1
3 $\frac{6}{12}$	131.97	132.01	3.44	7 $\frac{9}{12}$	1.69 <sub>5</sub>	4.41	6.8
3 $\frac{8}{12}$	127.99	128.04	4.63	7 $\frac{10}{12}$	1.35 <sub>5</sub>	4.26	5.8
3 $\frac{10}{12}$	123.58	123.63	6.18	7 $\frac{11}{12}$	1.06 <sub>5</sub>	4.16	5.0
4	118.74	118.80	7.82	8	0.83	4.09 <sub>2</sub>	4.3
4 $\frac{1}{12}$	116.16	116.23	8.5	8 $\frac{1}{12}$	0.63	4.05 <sub>0</sub>	3.7
4 $\frac{2}{12}$	113.49	113.57	9.1	8 $\frac{2}{12}$	0.47	4.02 <sub>6</sub>	3.1
4 $\frac{3}{12}$	110.71	110.80	9.6	8 $\frac{3}{12}$	0.34 <sub>3</sub>	4.01 <sub>2</sub>	2.7
4 $\frac{4}{12}$	107.83	107.93	10.0	8 $\frac{4}{12}$	0.24 <sub>1</sub>	4.00 <sub>6</sub>	2.3 <sub>5</sub>
4 $\frac{5}{12}$	104.85	104.96	10.4	8 $\frac{5}{12}$	0.16 <sub>3</sub>	4.00 <sub>2</sub>	1.8 <sub>5</sub>
4 $\frac{6}{12}$	101.76	101.88	10.8	8 $\frac{6}{12}$	0.10 <sub>6</sub>	4.00 <sub>0</sub>	1.4 <sub>5</sub>
4 $\frac{7}{12}$	98.56	98.68	11.5	8 $\frac{7}{12}$	0.06 <sub>6</sub>		1.1 <sub>6</sub>
4 $\frac{8}{12}$	95.24	95.37	12.5	8 $\frac{8}{12}$	0.03 <sub>9</sub>		0.8 <sub>5</sub>
4 $\frac{9}{12}$	91.82	91.97	13.9	8 $\frac{9}{12}$	0.02 <sub>2</sub>		0.5 <sub>5</sub>
4 $\frac{10}{12}$	88.31	88.47	15.8	8 $\frac{10}{12}$	0.01 <sub>2</sub>		0.3 <sub>5</sub>
4 $\frac{11}{12}$	84.73	86.90	17.9	8 $\frac{11}{12}$	0.00 <sub>6</sub>		0.2
5	81.09	83.28	19.8	9	0.03 <sub>3</sub>		0.1
5 $\frac{1}{12}$	77.42	77.62	21.4	9 $\frac{1}{12}$	0.00 <sub>1</sub>		
5 $\frac{2}{12}$	73.74	73.96	22.1				
5 $\frac{3}{12}$	70.06	70.30	22.1				
5 $\frac{4}{12}$	66.38	66.64	21.3				
5 $\frac{5}{12}$	62.69	62.97	20.4				
5 $\frac{6}{12}$	58.97	59.27	19.8				
5 $\frac{7}{12}$	55.22	55.54	20.3				
5 $\frac{8}{12}$	51.43	51.77	22.1				
5 $\frac{9}{12}$	47.64	48.02	25.3				
5 $\frac{10}{12}$	43.89	44.29	29.2				
5 $\frac{11}{12}$	40.23	40.66	32.9				
6	36.73	37.20	35.6				

2v<sub>0</sub>

- 1085

(± 5)

- 1085

(± 5)

calculated by the method of Thomas\* and Fermi.† Such a comparison is made, for the neutral atom, in Table VIII. The values of  $Z$  for the Thomas-Fermi field given in this table were obtained, for  $\rho < 7$ , by multiplying the values for Cs given in Thomas' paper by 80/55, and interpolating, and for  $\rho > 7$  from the solution of Thomas' equation carried out to provide an estimate of the field for large  $r$  for the calculation

TABLE VIII—COMPARISON OF SELF-CONSISTENT FIELD AND THOMAS-FERMI FIELD FOR NEUTRAL Hg

$\rho$	$Z$ self-consistent field	$Z$ Thomas-Fermi field	$Z_{s.c.f.} - Z_{T.F.f.}$
0	80.0	80.0	0.0
1	80.0	80.0	0.0
2	79.7 <sub>5</sub>	80.0	-0.2 <sub>5</sub>
2½	79.3	79.6 <sub>5</sub>	-0.3 <sub>5</sub>
3	78.5	78.9 <sub>5</sub>	-0.4 <sub>5</sub>
3½	77.2	77.5 <sub>5</sub>	-0.3 <sub>5</sub>
4	74.5	74.8	-0.3
4¼	72.3	72.8	-0.5
4½	69.7 <sub>5</sub>	70.2	-0.4 <sub>5</sub>
4¾	66.7	66.8	-0.1
5	62.5	62.5 <sub>5</sub>	-0.0 <sub>5</sub>
5¼	57.1	57.6	-0.5
5½	51.9	51.9	0.0
5¾	46.5	45.5 <sub>5</sub>	+0.9 <sub>5</sub>
6	38.8	38.8	0.0
6¼	29.9	32.1 <sub>5</sub>	-2.1 <sub>5</sub>
6½	23.1	25.6	-2.5
6¾	18.4	19.7	-1.3
7	13.5 <sub>5</sub>	14.5	-0.9 <sub>5</sub>
7¼	8.8	10.3	-1.5
7½	5.3	7.0	-1.7
7¾	3.1	4.6	1.5
8	1.7	2.8	1.1
8¼	0.8 <sub>5</sub>	1.7	-0.8 <sub>5</sub>
8½	0.3	1.0	-0.7

of the first approximation to the self-consistent field (*cf.* III); these values are not certainly correct to 0.1, but are accurate enough for this comparison.

It will be seen that the Thomas-Fermi field is too large over nearly the whole range, but that the error is not serious for  $\rho < 6$  ( $r < 0.4$ ).

\* 'Proc. Camb. Phil. Soc.,' vol. 23, p. 542 (1927).

† 'Phys.,' vol. 48, p. 73 (1928).

Outside this radius, the difference is considerable, and towards the outside of the atom it is a considerable fraction of the whole field; the maximum error of the Thomas-Fermi field is about 2 units in  $Z$ , which is about the same as for Rb. This is worth noting, as though in Thomas' original paper the solution of the equation is not carried further than a radius corresponding to  $\rho = 7$  for Hg, on the ground that the equation is not an adequate representation of the facts beyond that radius, there is perhaps a tendency to assume that for a heavy atom the Thomas-Fermi field is a good approximation over the whole range of  $r$ .

On account of the sensitiveness of the  $(5d)^{10}$  group to the atomic field, and the bad approximation, for large  $r$ , given by the Thomas-Fermi field which was used as the first estimate of the field in the original self-consistent field calculation, the first approximation to the  $(5d)$  wave function, calculated from this field, was a very bad one, and this made the process of approximation to the self-consistent field in the early stages particularly slow and laborious. This experience shows that it is very desirable to begin calculations of the self-consistent field with an estimate of the field which is already better than that of Thomas-Fermi, if such can be obtained, and also shows that any results for the outer groups of a heavy atom, based on the Thomas-Fermi field, are of very doubtful significance.

The rather sharp variation of the difference between the self-consistent and Thomas-Fermi fields in the neighbourhood of  $\rho = 6$  arises from the rather considerable local concentration of charge at about this radius, due to the fact that the four groups of the N shell ( $n = 4$ ), which is complete for atoms as heavy as this and contains 36 electrons, all have their main maxima of radial charge density in this neighbourhood.

## § 5—SUMMARY

In continuance of the plan, outlined in an earlier paper, for making generally available the results of calculations of atomic wave functions by the method of the self-consistent field, results for the atoms Be, Ca and Hg, both neutral and doubly ionized, are here presented.

In calculating wave functions for the neutral atoms, the perturbation of the core by the two valency electrons has been taken into account as far as this is possible in the "self-consistent field" approximation; this perturbation is not large for Be and Ca, but is considerable for Hg on account of the sensitiveness of the  $(5d)^{10}$  group to the atomic field.

For neutral Hg, the self-consistent field is compared with the Thomas-Fermi field, and the differences between them are discussed.

The "standard calculations" (*cf.* I) for  $\text{Ca}^{++}$  were carried out professionally, with the assistance of a grant from the Government Grant Committee to one of us (D. R. H.), who wishes to acknowledge his thanks to the Committee for this assistance.

---

## The Interaction of Hydrogen with Micro-crystalline Charcoal—I

By RICHARD MALING BARRER and ERIC K. RIDEAL, F.R.S., Laboratory of Colloid Science, Cambridge

(Received November 3, 1934)

### PHYSICAL SORPTION PROCESSES

The interaction of hydrogen and carbon is one of the more important surface actions, but in the literature are found many discrepancies in the experimental data and conflicting views as to their interpretation. It seemed desirable to make a comprehensive examination of the system over a wide range of temperatures on the same specimens of carbon.

Both at high and at low temperatures the sorption of hydrogen by charcoal is a time process.\* The origin of these time processes has been a matter of dispute. Among the alternatives are activated diffusion† and activated adsorption.‡ Allmand§ suggested a slow increase of available area by dissociation and displacement of surface compounds. Some sorption processes may not be activated and yet may take time to reach equilibrium.

At 90° K Ubbelohde,|| and at 273° K Schuster¶ have described discontinuities in their adsorption isotherms which they claim cannot be accounted for by experimental error. The measurements were therefore

\* *Cf.* McBain, 'Phil. Mag.,' vol. 18, p. 910 (1909); 'Trans. Faraday Soc., Discussion,' 1932.

† Ward, 'Proc. Roy. Soc.,' A, vol. 133, p. 513 (1931).

‡ Taylor, 'J. Amer. Chem. Soc.,' vol. 53, p. 578 (1931).

§ 'Trans. Faraday Soc.,' vol. 28, p. 414 (1932).

|| 'Proc. Roy. Soc.,' A, vol. 134, p. 512 (1931).

¶ 'Trans. Faraday Soc.,' vol. 28, p. 423 (1932).

repeated using the static method. The hydrogen-charcoal system was employed by Taylor, Gould and Bleakney\* to separate the isotopes by fractional desorption. Eyring and Sherman† ascribed the separation obtained both to diffusion and to half quanta of vibrational energy due to the van der Waals forces between the gas and solid. By measuring equilibrium values of sorption the efficiency of the isotopic fractionation by evaporation alone may be obtained directly. Other problems of interest include the sorptive properties of the charcoal surface at very low pressures, and the structure and stability of charcoal adsorbents.

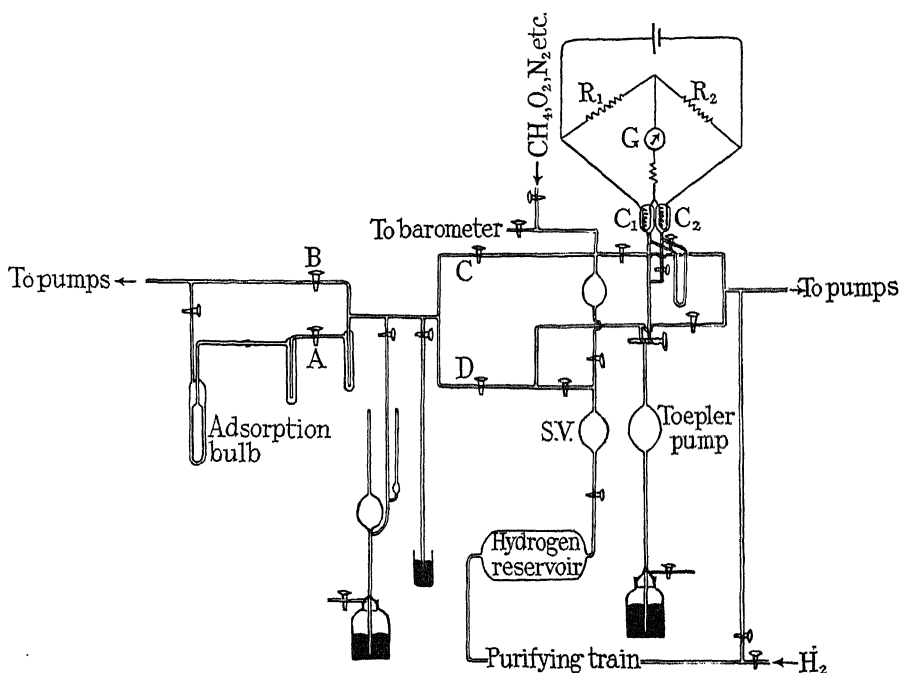


FIG. 1

## EXPERIMENTAL

The apparatus employed in the experiments is shown in fig. 1. Two McLeod gauges served for the determination of the pressures at low and intermediate values, and a barometer at high pressures. The adsorption bulb was made of silica with a double jacket of which the annular space could be continuously evacuated to eliminate penetration of atmospheric

\* 'Phys. Rev.', vol. 43, p. 496 (1933); 'J. Chem. Phys.', vol. 2, p. 351 (1934).

† 'J. Chem. Phys.', vol. 1, p. 345 (1933).

gases at elevated temperatures.\* Two mercury diffusion pumps were employed in evacuation. The furnace temperatures were measured by a platinum-platinum-rhodium thermocouple calibrated at the melting points of various metals, whilst standard alcohol thermometers were employed for mixtures of solid carbon dioxide and alcohol.

The volume relations of the apparatus were determined with the aid of the standard volume, S.V., fig. 1, and that of the adsorbent introduced from its known mass and assumed true density of 2.2 (equal to that of graphite). The ratio of the volume of the charcoal to that of the apparatus was *ca.* 1 : 100. Electrolytic hydrogen purified from oxygen was stored over phosphoric oxide. Charges of gas could be admitted and reduced to known pressure by manipulation of the taps A, B, C, D; and finally allowed to come into contact with the adsorbent.

The purity of the hydrogen desorbed was determined by means of a microthermal conductivity method. The apparatus for this consisted essentially of a Wheatstone bridge with two resistance arms  $R_1$ ,  $R_2$ , fig. 1, and two gas analysis cells,  $C_1$ ,  $C_2$ , containing similar thin platinum wires. The relative amounts of heat lost from the two platinum wires to the surrounding gas on passage of a current (0.1 ampere) could be determined from the relative changes in resistance. One cell contained pure hydrogen and the other the unknown mixture, both at the same constant pressure. The instrument was calibrated for methane hydrogen mixtures by admitting appropriate mixture to the comparison cell and constructing a calibration curve. The instrument could be used for mixtures with less than 1% methane and pressures of less than 1 mm in the sorption bulb.†

Deuterium was prepared from 0.1 cc of 80% heavy water by decomposing its vapour on a hot tungsten filament previously outgassed for an hour at 2000° C, and passing the resultant gas through liquid air and a palladium tube at 400° C.

#### CHARACTERISTICS OF THE CHARCOALS

Specimens of charcoals employed included the following:—

- (A) Acheson graphite (for comparison in X-ray reflection spectra).
- (B) Sugar charcoal formed at 670° K, briefly outgassed at 1200° K.
- (C) Same outgassed for some days at 1200° K.
- (D) Tartaric acid charcoal formed at 670° K.

\* Cf. Barrer, 'J. Chem. Soc.,' p. 378 (1934).

† Cf. Hurst and Rideal, 'J. Chem. Soc.,' vol. 125, p. 694 (1924).

- (E) Same outgassed for some days at 1200° K.
- (F) Sugar carbon of very small ash content (0.01%).
- (G) Gas carbon.

The charcoals B to E were prepared by charring at low temperatures in an electric furnace, the temperature being eventually raised to 678° K in a limited supply of air. Outgassing at 1200° K was then carried out.

The ash contents of the charcoals were found to be as follows:—

*Tartaric Acid Charcoal*—0.2% ash (77% SiO<sub>2</sub>, Al<sub>2</sub>O<sub>3</sub>, 23% K<sub>2</sub> CO<sub>3</sub>, Na<sub>2</sub> CO<sub>3</sub>, CaO, Fe<sub>2</sub>O<sub>3</sub>).

*Sugar Charcoal*—0.1% ash (80% insoluble in mineral acids, 20% soluble in mineral acids).

*Gas Carbon*—0.3% ash (35% SiO<sub>2</sub>, 28% Al<sub>2</sub>O<sub>3</sub>, 25% Fe<sub>2</sub>O<sub>3</sub>, 9% CaO, 3% MgO, etc.).

On continued extraction of both the sugar and tartaric acid charcoals by Soxhlet in hydrochloric acid metals of Groups I and II (Na, K, Mg, Ca) could be removed, but ignited iron oxide only with difficulty, and silica and alumina not at all.

All the specimens B to E gave X-ray reflection spectra\* showing certain of the characteristic spacings of the graphite lattice. These were obtained even with D, a product of a relatively low temperature distillation of tartaric acid, specially chosen as a non-benzenoid organic substance. The development of the graphite nuclei in C and E as compared with B and D was discernible in the increased clarity of the rings in the photograms of the former. The crystal sizes were obtained qualitatively by making a photometric examination† of the density of rings and employing the equation

$$B = 2 \sqrt{\frac{\log_e 2}{\pi}} \cdot \frac{\lambda}{D} \cdot \frac{1}{\cos \theta} + b,$$

where B is the angular half intensity width,  $\theta$  the half angle of reflection, D the crystallite diameter,  $\lambda$  the wave-length employed, and  $b$  a constant (the angular half intensity width for the Acheson graphite). In Table I approximate values of (B —  $b$ ) are given and a mean value of D thus calculated is employed in the subsequent calculations of the internal surface.

\* We are indebted to Dr. Astbury for his co-operation in taking the X-ray photograms.

† We express our thanks to Professor Stratton for having measured these curves on a high precision instrument.

TABLE I

Sugar carbon C			Tartaric acid charcoal E		
Planes	(B - b) radius	D in A°	Planes	(B - b) radius	D in A°
002	0.52	31	002	0.31	50
100	0.46	34	100	0.35	52

The crystallites are in each case about equal in diameter and thickness, but those from tartaric acid charcoal are somewhat larger than those from sugar charcoal. As the sequel showed, this resulted in a smaller adsorptive capacity for the former charcoal. The interplanar spacings were calculated from the expression

$$2d = \frac{n\lambda}{\sin \theta},$$

where  $n$  is the order of the spectrum, and  $d$  the required spacing. These are given in Table II.

TABLE II

Charcoal . . . . .	A	B	C	D	E
Spacing in A° ..	3.50	Not obtainable	4.20	4.65	4.25

As the crystallites developed (C and E) the mean interlaminar spacing decreased but in no case became less than the spacing for graphite. All carbons including soots\* show these crystalline properties in an X-ray or electron beam. The behaviour of graphite as a disperse laminar system in which alkali metals and oxygen may enter between the lattice layers with separations of 5.34 Å for C<sub>8</sub>K and >6 Å for graphitic anhydride C<sub>2</sub>O† suggests that the greater dispersion of the lattices obtained here may be due to interlaminar oxygen, hydrogen and metallic impurity. The micro-crystalline character of charcoals permits of a clearer picture of the adsorption processes.

#### THE STABILITY OF THE CHARCOALS

All the charcoals remained exceedingly stable in their low temperature adsorptive properties during a sequence of evacuations at 1200° K, in

\* Jenkins, 'Phil. Mag.,' vol. 17, p. 457 (1934); Berl, Andress, Reinhardt and Herbert, 'Z. phys. Chem.,' A, vol. 158, p. 273 (1932); Hofmann and Wilm, 'Z. phys. Chem.,' B, vol. 18, p. 401 (1932); Warren, 'Phys. Rev.,' vol. 45, p. 763 (1934).

† Hofmann and Frenzel, 'Kolloid Z.,' vol. 53, p. 7 (1932).



the double walled silica vessel. The initial slopes of the adsorption isotherms defined by  $k$  in the equation

$$x/m = kp,$$

are a relative measure of the surfaces involved in adsorption at various stages of the outgassing. These are given in Table III.

TABLE III—CHARCOAL B

Temperature °K	$k$ (cc at N.T.P. per gm per cm Hg)	Treatment
78	120	Outgassed for 4 hours at 1200° K.
	126	Washed daily for 3 weeks in hydrogen, and evacuated a number of times at 1200° K.
195	130	Further treatment as above.
	0.200	Washing in hydrogen, and 15 hours out- gassing at 1200° K.
	0.206	Washing in hydrogen and a further 15 hours outgassing at 1200° K.
	0.220	Washing in hydrogen and a further 15 hours outgassing at 1200° K.
273	0.085	As at 195° K.
	0.105	

After heating to 1270° K for several days and at 1370° K for some hours the surface as measured by the hydrogen adsorption decreased until  $k$  as defined above was only 4 at 78° K. During this time gases were continually evolved from a surface which had been stable at 1200° K. Graphitization is thus proceeding with a simultaneous break-down of very strongly bound surface compounds. Similar observations have been made by Langmuir,\* Lowry and Hulett,† Lowry,‡ and Norton and Marshall.§ The stability of surface compounds on charcoals may be interpreted as a limitation imposed by the inadequacy of ordinary vacuum technique and by the very large activation energy required before the thermal decomposition of surface compounds is initiated.|| The

\* 'J. Amer. Chem. Soc.,' vol. 38, p. 2276 (1916).

† 'J. Amer. Chem. Soc.,' vol. 47, p. 1408 (1920).

‡ 'J. Amer. Chem. Soc.,' vol. 46, p. 824 (1924); 'J. Phys. Chem.,' vol. 33, p. 1332 (1929).

§ 'Amer. Inst. of Min. Metallurg.,' (1932).

|| Frenkel ('Z. Physik,' vol. 26, p. 117 (1924)) gives the following expression for the density,  $n$ , of the sorption layer as a function of temperature and pressure:

$$\frac{s}{n} = \sigma_0 \left( 1 + \frac{\sqrt{2\pi mkT}}{p\sigma_0\tau_0} e^{-U_a/kT} \right),$$

where  $\tau_0$  = period of vibration of the adsorbate,  $S$  denotes the surface area,  $\sigma_0$  the

internal surface as calculated from the crystallite size and as measured in adsorption (Table IV) suggests that due to the interlocking of the crystallites only a small extent of the surface is accessible to hydrogen gas.

TABLE IV

Charcoal	Basal surfaces metres <sup>2</sup>	Prismatic surfaces metres <sup>2</sup>	Theoretical saturation value H <sub>2</sub> cc/gm	Observed saturation value H <sub>2</sub> cc/gm
Sugar (C) .....	330	670	360	57
Tartaric (E) .....	200	400	215	38
Gas carbon (G) .....	—	—	—	19

## THE EQUILIBRIUM AT LOW PRESSURES

In fig. 2 A and B, is shown a series of isotherms at low pressures and temperature. Since a wide pressure range was covered ( $10^{-5}$ –10 mm of mercury) a logarithmic scale is employed and  $\log x/mp$  is plotted against  $\log p$ . It will be noted that at low pressures enhancement of adsorption occurs (at 78° K on sugar charcoal at nearly  $10^{-5}$  mm pressure). Also at 78° K  $\log x/mp$  falls off at  $10^{-2}$  mm, whilst at 195° K and 273° K a linear isotherm was obtained up to the highest pressures measured. An analysis of each isotherm showed that the total adsorption can be expressed in the form

$$\frac{x}{m} = \frac{ap}{1 + bp} + \frac{a^1p}{1 + b^1p},$$

(see fig. 3, A and B).

area covered by an adsorbed molecule ( $\sim 10^{-15}$ ) and  $U_0$  the heat of adsorption. This surface density becomes pressure dependent where

$$\frac{\sqrt{2\pi mkT}}{p\sigma_0\tau_0} e^{-U_0/kT} \sim 1,$$

at which stage the surface is half covered. The values of  $U_0$  for hydrogen we have shown to be 50,000 cal/gm mol (Part II this paper) while for chemisorbed  $>CO$  the data of Shiels and Allmand ('Trans. Faraday Soc.', vol. 28, p. 225) suggest a similar value, *ca.* 53,000 cal/gm mol. For C—H, a wave number 2910 is assumed, and for C=O a wave number 1630. From these data we calculate the temperature of half decomposition at pressures of  $10^{-6}$  mm and 1 mm as *ca.* 800° K and 1350° K respectively for hydrogen and 840° K and 1500° K for carbon monoxide. In this way one can express quantitatively the degree of clean-up likely to be obtained under different conditions.

It is seen that a very small portion of the adsorbent possesses adsorptive characteristics quite distinct from those of the bulk of the material. The amount sorbed on this portion of charcoals C and E at saturation being

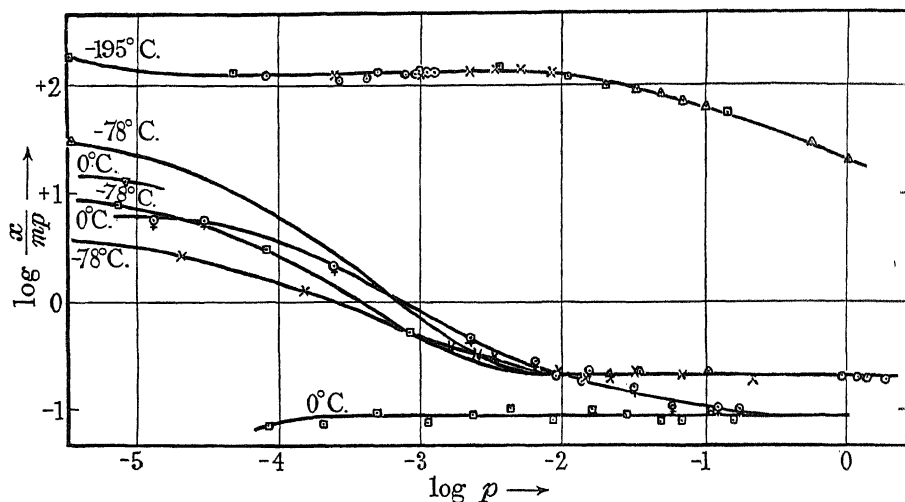


FIG. 2A—Hydrogen on sugar charcoal C, 0.1% ash, at low pressures

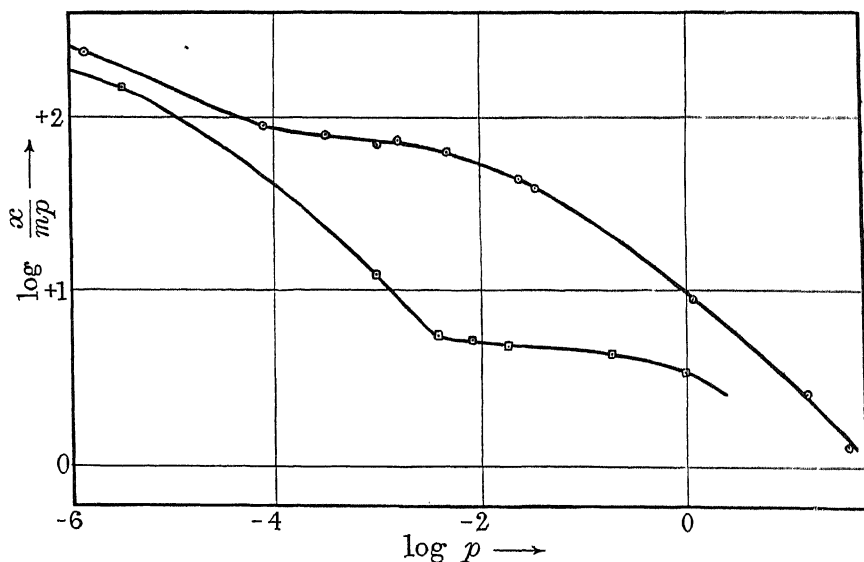


FIG. 2B—Hydrogen on tartaric acid charcoal E, 0.2% ash, at low pressures

only 0.005 and 0.02 cc respectively, at N.T.P. and for sorption at 78° K, in contrast to 57 and 38 cc on the rest of the surfaces of the two charcoals. It seemed possible that this strongly adsorptive portion was

due to metallic impurities (such as iron) of known high sorptive capacity for hydrogen. Progressive heating and evacuation of the charcoal rendered these centres more and more active. The rates of sorption of the gas by the active portion and by the normal portion of the charcoal

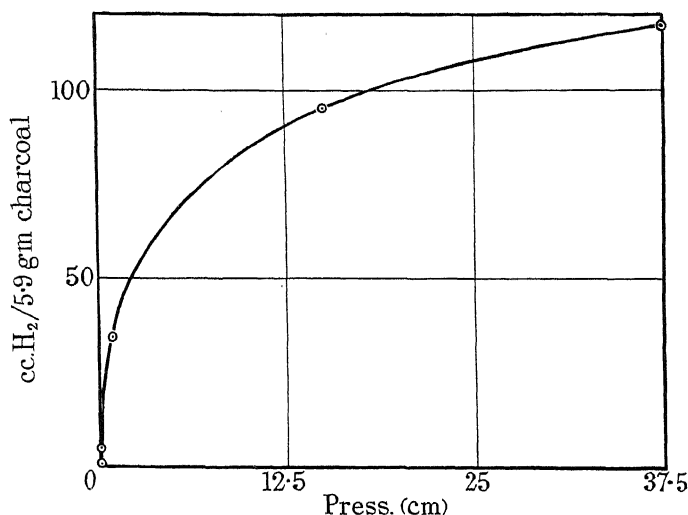


FIG. 3A—195° C. Isotherm on normal charcoal surface

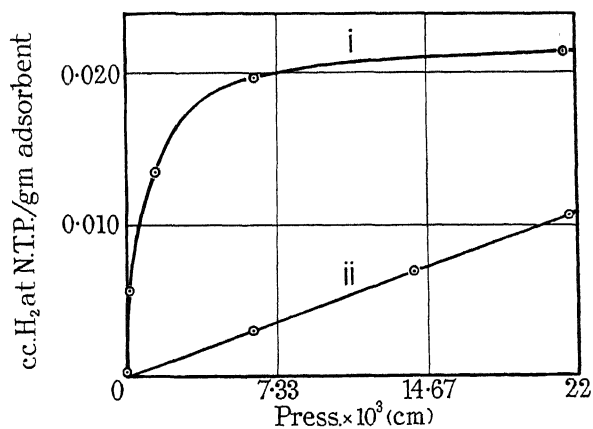


FIG. 3B—Curve I, -78° C. Isotherm on active centres; II, superposed normal sorption at -78° C on charcoal

surface were different. In this pressure region abnormalities were obtained with the para hydrogen conversion,\* and there seemed reason for ascribing these to the same cause. The initial Langmuir isotherm on the active

\* Bonhoeffer, Farkas and Rummel, 'Z. phys. Chem.,' B, vol. 21, p. 225 (1933); and Rummel, *Ibid.*, A, vol. 167, p. 221 (1934).

centres reached saturation at low pressures, so that thereafter a conversion on such centres would be a zero order reaction as was observed. A sample of the very pure charcoal (F)\* used by Bonhoeffer, Farkas and Rummel was used to test this point. The adsorption data, Table V, at 195° K showed no trace of abnormal adsorption. One must conclude that the anomalous conversion kinetics observed do not depend upon parallel anomalies in adsorption; and that when anomalous adsorption does occur it is due to active centres in the ash. Charcoal alone appears to show no enhanced activity due to edge atoms and special configurations of atoms at the lowest pressures.

TABLE V—4.105gm CHARCOAL F

Equilibrium pressure *cm $\times 10^4$	Amount sorbed cc at N.T.P. $\times 10^4$	Amount sorbed Equilibrium pressure
0.9	0.211	0.235
2.6	0.663	0.252
3.95	1.03	0.262
7.15	1.84	0.257
29.75	9.04	0.302
79.3	19.74	0.249
157.3	41.24	0.262

The normal sorption at the lowest pressures is slight, fig. 2, A and B, compared with the strong abnormal sorption which is also a much slower process. The kinetic process for the latter can be represented by the expression

$$C_t = Ap \cdot \sqrt{\frac{D \cdot t}{\pi}} + \alpha,$$

where  $A$ ,  $\alpha$ , are constants,  $D$  is the diffusion coefficient,  $t$  is the time, and  $C_t$  denotes the volume of gas sorbed at time  $t$ . From this expression

$$\frac{C_{t_1}^2 - C_{t_2}^2}{t_1 - t_2} = \text{constant.}$$

Some values of the constant are given in Table VI.

If the diffusion is regarded as activated the energy of activation lies between 2000–3000 cal. The quantities of gas adsorbed and the rates of adsorption in this region were so markedly dependent upon the number

\* Very kindly supplied by Professor Bonhoeffer, prepared according to the method of Bruns and Frumkin ('J. Phys. Chem.,' vol. 141, p. 145 (1929)) and containing 0.01% ash.

TABLE VI—CHARCOAL C

Temperature °K	Pressure range mm Hg $\times 10^4$	Time mins	$\frac{Ct_1^2 - Ct_2^2}{t_1 - t_2}$
195	2.78–1.82	1.3– 5.0	0.038
		3.5– 7.0	0.035
		7.0–13.0	0.030
		13.0–19.5	0.033
		19.5–29.0	0.031
273	6.025–3.18	1.0– 4.0	0.323
		4.0– 9.0	0.323
		9.0–16.5	0.245
		16.5–28.5	0.292

of pre-heatings as to preclude an accurate value of  $E$ , see fig. 2 A. The heat of adsorption on the active centres was small and positive.

For the normal adsorption at low pressures the heats of adsorption could readily be calculated from the isosteres by application of the expression

$$\frac{d \log K}{dt} = \frac{Q}{RT^2}.$$

These heats of adsorption are given for a range of surface concentrations for sugar and tartaric acid charcoal in Table VII.

TABLE VII

Sugar Charcoal (C)			Tartaric acid Charcoal (E)		
Temperatures 78° K and 195° K			Temperatures 78° K and 195° K		
$x/m$ cc at N.T.P.	$\log \frac{p_{195}}{p_{78}}$	$Q$ cals/gm mol	$x/m$ cc at N.T.P.	$\log \frac{p_{195}}{p_{78}}$	$Q$ cals/gm mol
0.00051	2.76	1650	0.00261	2.28	1420
0.0051	2.76	1650	0.0261	2.19	1360
0.051	2.76	1650	0.261	2.22	1380
0.161	2.76	1650	0.558	2.30	1430

It will be noted that there is a difference between the heats of adsorption on the two charcoals, the charcoal possessing the smallest crystallites (as shown by X-ray spectrograms) showing the largest heat of adsorption. The heat of adsorption is constant for any charcoal and independent of a several hundred-fold increase in the amount of gas adsorbed; by eliminating the abnormal adsorption by a preliminary sorption and desorption as was done to obtain the bottom curve (at 273° K) of fig.

2 A (since the abnormal sorption is only slowly reversible) it was possible to confirm the constancy of  $Q$  down to very low surface concentrations. The values are in good agreement with that obtained calorimetrically by Dewar,\* viz., 1600 cal/gm mol at 88° K and 760 mm pressure, and the value which can be calculated from Titoff's linear isotherms† between 195° K and 273° K, of 1700 cal/gm mol. Over the whole range the surface behaves for hydrogen as one of constant and uniform adsorption potential, similar to its behaviour with argon at higher temperatures.‡

#### THE KINETICS OF THE SORPTION OF OXYGEN, NITROGEN AND HYDROGEN

At 78° K on thoroughly outgassed charcoals C, F and G, sorption was not instantaneous. The observed velocities according to accepted theories are due to a displacement of surface impurity (Allmand, *loc. cit.*) to activated adsorption or to molecular flow or diffusion down pores or intercrystalline boundaries. Allmand's suggestion was shown to be untenable by the following observations:—

(a) Due to prolonged outgassing evolution of impurity had ceased at 1200° K. This evolution is itself a highly activated process; and cannot therefore be regarded as rapid or even measurable at 78° K.

(b) Sorption always involving the time process was repeated a very large number of times, with evacuation between each experiment. The amount of gas thus slowly sorbed was enough to increase the surface permanently many times if impurity were being displaced, yet no change in surface could be detected, Table III.

(c) Desorption was not instantaneous though rapid and gave rise to similar pressure-time curves to those for adsorption.

The results for these systems are likely to be of general applicability in low temperature persorption by porous solids like charcoal. If the time processes are due to diffusion and flow of the type described by Knudsen§ we should expect diffusion to obey the Fick law

$$\frac{\partial n}{\partial t} = D \cdot \frac{\partial^2 n}{\partial x^2},$$

and also a  $\sqrt{T/M}$  relation where  $T$  denotes the absolute temperature and  $M$  is the molecular mass. If time processes are due to activated diffusion,

\* 'Proc. Roy. Soc.,' vol. 74, p. 122 (1904).

† 'Z. phys. Chem.,' vol. 74, p. 651 (1910).

‡ Travers, 'Proc. Roy. Soc.,' A, vol. 137, p. 294 (1932).

§ 'Ann. Physik,' vol. 28, p. 75 (1909).

the equations given by Lennard-Jones,\* involving an activation energy and consequent large temperature coefficient would hold:

$$\frac{\partial n}{\partial t} = D \frac{d^2 n}{dx^2}; \quad \frac{\partial \log D}{\partial T} = \frac{E}{RT^2}.$$

There is also the more remote possibility of activated adsorption, which for the region where Henry's law is obeyed is described by the expression

$$\frac{\partial n}{\partial t} = k \cdot (p_t - p_e); \quad \frac{\partial \log k}{\partial T} = \frac{E}{RT^2}$$

( $p_t$ ,  $p_e$ , are gas pressures at time  $t$  and at equilibrium).

The conditions of diffusion in the sorption can be idealized as follows. At time  $t = 0$ , the space between the parallel planes  $x = 0$  and  $x = h$  is filled with gas at concentration  $C_0$  and the corresponding space between  $x = h$  and  $x = 1$  is occupied by the adsorbent, for simplicity supposed gas free. That is,

$$\begin{aligned} f(x) &= C_0 & \text{for } 0 \leq x < h \\ f(x) &= 0 & \text{for } h < x \leq 1, \end{aligned}$$

where  $f(x)$  denotes the distribution of gas with distance. Further  $\frac{\partial C}{\partial t} = 0$  at  $x = 1$  for all  $t$ , and  $\frac{\partial C}{\partial t} = D \frac{\partial^2 C}{\partial x^2}$ . Then the most general solution of the Fick law,  $e^{-K^{(1)}t}$  ( $A \cos kx + B \sin kx$ ) becomes for this case†

$$C = C_0 \left( \frac{h}{l} + \frac{2}{\pi} \sum_{n=1}^{\infty} \frac{1}{n} e^{-\left(\frac{n\pi}{l}\right)^2 Dt} \cdot \cos \frac{n\pi}{l} \cdot x \cdot \sin \frac{n\pi h}{l} \right)^* \quad (1)$$

The use of this formula could be simplified by choosing simple values of  $h/l$  although this is not possible in our experiments. If  $h/l = \frac{1}{2}$ , the quantity  $Q_t$  which penetrates into the solid is

$$\begin{aligned} Q_t &= - \int_0^t D \left( \frac{\partial C}{\partial x} \right) x = \frac{l}{2} \cdot \partial t \\ &= \frac{l C_0}{4} \left\{ 1 - \frac{8}{\pi^2} \sum_{m=1}^{\infty} \frac{1}{(2m-1)^2} e^{-\left(\frac{(2m-1)\pi}{l}\right)^2 Dt} \right\}, \end{aligned} \quad (2)$$

\* 'Trans. Faraday Soc.', vol. 28, p. 333 (1932).

† Williams and Cady, 'Chem. Rev.', vol. 14, p. 171 (1934); Stefan, 'S.B. Akad. Wiss. Wien.', vol. 79, p. 161 (1879).



where  $1C_0/4 = Q_e$  the amount sorbed at equilibrium. If there is an initial quantity  $Q_i$  of gas sorbed by the charcoal the solution is

$$\frac{Q_e - Q_t}{Q_e - Q_i} = \frac{8}{\pi^2} \sum_{m=1}^{m=\infty} \frac{1}{(2m-1)^2} e^{-(2m-1)^2 \frac{\pi^2}{l^2} t}. \quad (3)$$

The  $Q$ 's may readily be replaced by corresponding pressure or concentration terms. From the equations it may be shown that initially  $C_t^2 - C_i^2 = kt$ ; and finally for  $(C_t - C_i) > (C_e - C_i)$

$$\log \frac{C_e - C_t}{C_e - C_i} = kt.$$

The following data give the agreement between the complete diffusion expression ( $c$ -form) in Table VIII A and the sorption data for oxygen, hydrogen and nitrogen, and also the agreement for the unimolecular diffusion equation ( $p$ -form) in Table VIII B.

TABLE VIII A

Hydrogen on sugar carbon F at 78° K

$a = 0.261$ ;  $b(C_e - C_i) = 67.1 \times 10^{-3}$

Time, mins	$C_t$ (cc at N.T.P.) $\times 10^3$	$C_t$ (calc.) $\times 10^3$
0.167	13.93	12.7
1.50	40.15	37.1
3.00	54.07	52.0
4.50	62.20	62.0
6.00	68.03	69.1
7.50	72.25	73.25
9.50	76.14	76.5
13.50	78.63	80.7
$\infty$	82.7	82.7

Nitrogen on sugar carbon F at 195° K

$a = 0.115$ ;  $b(C_e - C_i) = 21.1 \times 10^{-3}$

Time, mins	$C_t$ (cc at N.T.P.) $\times 10^3$	$C_t$ (calc.) $\times 10^3$
0.167	5.32	2.96
1.50	11.92	7.80
3.00	13.30	11.05
5.50	16.08	14.90
7.50	17.63	17.24
10.00	19.35	19.43
13.00	21.07	21.34
16.00	22.35	22.72
19.00	23.37	23.70
$\infty$	26.05	26.05

TABLE VIII A—(continued)

Oxygen\* on sugar carbon F at 195° K  
 $a = 0.120$ ;  $b (C_e - C_i) = 55.5 \times 10^{-3}$

0.167	11.45	7.45
1.00	23.95	16.95
2.50	32.35	27.55
5.00	38.22	38.25
8.00	43.02	47.15
12.00	48.40	54.75
$\infty$	68.45	68.45

TABLE VIII B

Nitrogen on sugar carbon F at 195° K

Time, mins	cm pressure $\times 10^3$	$\frac{\Delta}{\Delta t} (\log (p_t - p_e)) = k$
1.50	26.2	—
3.0	25.6	0.050
5.5	24.9	0.045
7.5	24.5	0.034
10.0	24.1	0.034
13.0	23.7	0.036
16.0	23.4	0.044
19.0	23.1	0.041
$\infty$	22.35	—

Hydrogen on sugar carbon F at 78° K

1.50	9.94	—
3.0	7.27	0.113
4.5	5.65	0.098
6.0	4.50	0.098
7.5	3.70	0.095
9.5	2.91	0.105
$\infty$	1.64	—

Oxygen on sugar carbon F at 195° K

1.0	21.0	—
2.50	18.9	0.060
5.0	17.6	0.029
8.0	16.3	0.033
12.0	14.9	0.031
$\infty$	9.9	—

\* Oxygen at 195° K was not adsorbed in a completely reversible manner; to the normal diffusion a slow chemisorptive process was added which rendered the agreement less close.

Tables VIII A and B adequately support the diffusion equations. Only in the initial stages was there any deviation; which may in part at least be ascribed to instantaneous adsorption on external surfaces, and to the assumption that  $h/l = \frac{1}{2}$  in the derivation of these equations. It is noteworthy that the parabolic diffusion law does not hold for any appreciable time. So rapid is the initial sorption that the values of  $C_t$  for which it should hold are quickly passed.

The velocity constants defined by the equation  $\frac{\Delta}{\Delta t} \log (p_t - p_e) = k$  at different temperatures under comparable conditions for the different gases showed important relations.

TABLE IX

Gas	Temperature °K	Velocity constant
O <sub>2</sub>	78	—
	195	0.032
N <sub>2</sub>	78	0.041
	78	0.030
	183	0.056
	195	0.041
H <sub>2</sub>	78	0.102

The velocity constants for

$$\text{O}_2 : \text{N}_2 : \text{H}_2 = 1 : 1.1 : 3.2$$

whilst diffusion according to gas kinetic theory requires

$$\text{O}_2 : \text{N}_2 : \text{H}_2 = 1 : 1.1 : 4.$$

Further there is not any appreciable temperature coefficient, so that no activation energy of any sort is involved. Of the accepted theories only that of non-activated diffusion has any applicability.\*

#### THE INFLUENCE OF CHEMISORPTION ON VAN DER WAALS ADSORPTION

A decrease in surface available for physical sorption was observed after activated or chemisorption (Part II) which paralleled the amount of chemisorbed hydrogen. Thus, at low pressures the equation

$$\frac{x}{mp} = k,$$

gave the values in Table X for charcoal (C).

\* The possibility of the time process being the dissipation of heat evolved in sorption is ruled out by a simple calculation. For the experiments with hydrogen 0.01 cal would be generated. Since the specific heat of graphite is 0.025 at 78° K, 6 gm would be heated through 0.07° C.

The decrease in surface is a little greater than would be anticipated from the amount of hydrogen chemisorbed. The effect of chemisorption of hydrogen upon the kinetics of van der Waals sorption was not appreciable. These results are similar to those of Howard\* on the  $\text{Cr}_2\text{O}_3\text{-H}_2$

TABLE X

$k$	cc hydrogen at N.T.P. chemisorbed at 956° K/6.9 gm
= 120	0
= 104	25
= 85.3	39

system. On the other hand a pronounced retardation of the velocity was obtained when the charcoal was exposed for some days under vacuum wherein the vapour of tap-grease alone reached the sorbent. Here the equilibrium amounts were not noticeably altered. The hydrocarbon molecules occupy positions on the entrance to pores which hinder access of hydrogen to inner surfaces without themselves penetrating to those inner surfaces. Outgassing at 1200° K restored a poisoned charcoal to its original condition.

#### ON REPORTED DISCONTINUITIES IN THE ISOTHERMAL

Using a dynamic method of measurement Ubbelohde and Egerton (*loc. cit.*) observed a series of discontinuities at 90° K. One hundred and thirty points were measured on charcoal (C) between 6 cm and 0.2 mm pressure in an attempt to reproduce these discontinuities by a static method. The isotherm was measured in desorption, at 78° K. The adsorption bulb was immersed well below the surface of the liquid nitrogen and before making any pressure reading the level of the freezing agent was brought to a standard mark, by observing a glass float. A standard time interval was allowed for desorption equilibria to be established, such that true equilibrium was reached before taking any reading.

The results of a day's run are summarized in Table XI.

Each day's run gave a very smooth section of the isothermal. The values of  $\Delta v/\Delta p$  plotted against equilibrium pressures gave some minor fluctuations of an irregular nature most probably a result of errors in observation. No steps were found such as have been observed for many vapours and charcoal.† It is important to note that when diffusion controls the sorption, spurious irregularities are observed when standard

\* 'Trans. Faraday Soc.,' vol. 30, p. 278 (1934).

† Cf. Burrage, 'Tran. Faraday Soc.,' vol. 29, p. 458, 665 (1933).

TABLE XI

$\Delta v$ = cc desorbed (N.T.P.)	$\Delta P$ = pressure change	Equilibrium pressure, cm	$\frac{\Delta V}{\Delta p}$
0.222	—	0.0434	—
0.227	0.35	0.0399	0.61
0.210	0.31	0.0368	0.68
0.196	0.25	0.0343	0.78
0.187	0.20	0.0323	0.93
0.179	0.16	0.0307	1.12
0.173	0.12	0.0295	1.44
0.163	0.13	0.0282	1.25
0.158	0.10	0.0270	1.32
0.154	0.09	0.0261	1.71
0.148	0.10	0.0251	1.48
0.143	0.08	0.0243	1.79
0.138	0.08	0.0235	1.72
0.133	0.07	0.0228	1.90

conditions of experiment (especially a standard suitably long time interval) are departed from. We may conclude that we have been unable to produce evidence of any discontinuity which cannot be ascribed to experimental errors.

#### COMPARATIVE SORPTION OF HYDROGEN AND DEUTERIUM

The adsorption measurements were made in the dilute range wherein

$$x = kp.$$

Values of  $x/p$  as measured are given in Table XII.

TABLE XII—CHARCOAL F

Deuterium		Hydrogen	
$x$ (cc at N.T.P.)	$x/p$	$x$ (cc at N.T.P.)	$x/p$
0.174	283	—	—
0.316	249	—	—
0.057	285	—	—
0.166	294	0.132	220
0.337	313	0.302	245
0.229	275	0.487	235
0.370	290	0.646	241
Average 284		Average 235	

The distribution of gas between the adsorbed and gas phases is given by\*

$$p = \frac{\theta}{\alpha} \cdot A \cdot T^{3/2} \epsilon^{-b/T} \quad (4)$$

(where  $\alpha$ ,  $A$ , are constants,  $b \times R$  = heat of adsorption,  $\theta$  is the fraction of the surface covered).

For two different gases at two different temperatures we may write

$$\frac{\left(\frac{\theta}{p}\right)_1}{\left(\frac{\theta}{p}\right)_2} = \frac{\alpha_1}{\alpha_2} \left(\frac{T_2}{T_1}\right)^{3/2} \cdot e^{\left(\frac{b_1}{T_1} - \frac{b_2}{T_2}\right)} \quad (5)$$

If  $\alpha_1 = \alpha_2$  we may use the expression to calculate heats of adsorption. The latter assumption was tested by using the expression to determine heats (already known for calorimetric or other data) from collected data upon helium, neon, oxygen, nitrogen and hydrogen.

TABLE XIII

Gas	H (calculated) (cals/mol)	$\Delta H$ (observed) (cals/mol)
H <sub>2</sub>	1650*	1600
He	535†, 450‡, <700*	—
Ne	985‡	990
N <sub>2</sub>	3740‡, 3420*	3680
O <sub>2</sub>	3990*	3744

\* Barrer, unpublished results.

† Claude, 'C. R. Acad. Sci. Paris,' vol. 158, p. 861 (1914).

‡ Dewar, 'Proc. Roy. Inst. Gt. Brit.,' vol. 18, p. 183 (1905).

The agreement is close for different gases wherein different charcoals and different conditions were employed. For the hydrogen isotopes† it is therefore likely that  $\alpha_1 = \alpha_2$  and that in the dilute range, at the same temperature,

$$\frac{\left(\frac{x}{p}\right)_{D_2}}{\left(\frac{x}{p}\right)_{H_2}} = e^{\frac{Q_{D_2} - Q_{H_2}}{RT}}.$$

\* Cf. Langmuir, 'J. Amer. Chem. Soc.,' vol. 54, p. 1798 (1932).

† Statistical considerations may also be applied (cf. Dohse and Mark, "Adsorption of Gases by Solids," 1933).

A mixture was, however, employed of 80% D content. Data of Urey and Rittenberg\* indicate a composition before adsorption of 69% D<sub>2</sub>, 25% HD and 6% H<sub>2</sub>.

Let there be N<sub>i</sub> moles of mixture initially, and N<sub>f</sub> moles after adsorption. Then

$$\frac{N_i - N_f}{N_f} = k \cdot \frac{x}{p}. \quad (6)$$

Also

$$\left. \begin{aligned} N_i &= D_2 + HD + H_2 \\ N_f &= D'_2 + HD' + H'_2 \end{aligned} \right\}, \quad (7)$$

and

$$\left. \begin{aligned} \frac{D_2 - D'_2}{D'_2} &= \beta e^{\frac{Q_{D_2}}{RT}} \\ \frac{HD - HD'}{HD'} &= \beta e^{\frac{Q_{HD}}{RT}} \\ \frac{H_2 - H'_2}{H'_2} &= \beta e^{\frac{Q_{H_2}}{RT}} \end{aligned} \right\}. \quad (8)$$

From (6) and (7) the quantity measured,  $x/p$ , is given by

$$\frac{x}{p} = \frac{\beta}{k} \left( \frac{(D_2 - D'_2) + (HD - HD') + (H_2 - H'_2)}{D'_2 + HD' + H'_2} \right). \quad (9)$$

By substitution from (8) this reduces to

$$\frac{x}{p} = \frac{\beta}{k} \cdot e^{\frac{Q_{D_2}}{RT}} \left( \frac{D'_2 + HD'_2 e^{\frac{Q_{HD} - Q_{D_2}}{RT}} + H'_2 e^{\frac{Q_{H_2} - Q_{D_2}}{RT}}}{D'_2 + HD' + H'_2} \right). \quad (10)$$

When HD', H'\_2 are small, or when (Q<sub>HD</sub> - Q<sub>D<sub>2</sub></sub>) and (Q<sub>H<sub>2</sub></sub> - Q<sub>D<sub>2</sub></sub>) are small (10) reduces to

$$x/p \sim \frac{\beta}{k} \cdot e^{\frac{Q_{D_2}}{RT}}. \quad (11)$$

Since the actual adsorbabilities are not very different, the thermal differences must be small and therefore (11) may be used to determine (Q<sub>D<sub>2</sub></sub> - Q<sub>H<sub>2</sub></sub>) approximately, by comparison with  $x/p$  for pure hydrogen. The quantity (Q<sub>HD</sub> - Q<sub>H<sub>2</sub></sub>) may then be computed, if the hydrogen isotopes have identical force fields, and the different adsorbabilities are due to half quanta of vibrational energy for the van der Waals interaction with the surface. The following relationships will then hold:

$$E = \frac{1}{2\pi} \sqrt{\frac{K}{M}},$$

\* 'J. Chem. Phys.', vol. 1, p. 137 (1933).

where  $E$  = half quantum,  $M$  is reduced mass, and  $K$  is constant for  $H_2$ ,  $HD$ , and  $D_2$ , and  $\phi = E + Q$ , where  $\phi$  is the same for  $H_2$ ,  $HD$  and  $D_2$  and  $Q$  is the heat of adsorption.

Thus  $(E_{H_2} - E_{D_2}) = (Q_{D_2} - Q_{H_2})$ , etc., and it is seen that when  $(Q_{D_2} - Q_{H_2})$  is known  $E_{H_2}$ ,  $E_{HD}$ ,  $E_{D_2}$  and relative evaporation rates for the isotopes may be calculated.

Using the quantities obtained in the first approximation the equation (10) is then employed in a second approximation. From the evaporation rates for the first approximation it is found that the initial mixture

$$D_2 : HD : H_2 = 69 : 25 : 6$$

becomes

$$D'_2 : HD' : H'_2 = \frac{69}{1.20} : 25 \left( \frac{1.07}{1.20} \right) : 6,$$

after sorption and that

$$e^{\frac{Q_{H_2} - Q_{D_2}}{RT}} = \frac{1}{1.20}; \quad e^{\frac{Q_{HD} - Q_{D_2}}{RT}} = \frac{1}{1.07}.$$

Thus we obtain from equation (10) the data given in Table XIV.

TABLE XIV

Gas	Relative rate evaporation	Half-quantum vib. energy (cal/mol)	Heat of adsorption (cal/mol)
$H_2$ .....	1.25	121.5	1760
$HD$ .....	1.09	100	1782
$D_2$ .....	1.00	86	1796

$Q_{H_2}$  was measured by comparison of the sorption at 78° K and 195° K.

The relative desorption rates show the maximum separation which could be obtained by evaporation of the adsorbed gases from a plane surface. With a porous solid the first samples desorbed from external surfaces would show separations of this order. When the gas diffuses from the interior of the solid the molecules will undergo a number of resorptions before finally reaching the gas phase. This under ideal conditions would lead to  $(1.25)^n$ -fold concentration of  $H_2$  and  $D_2$  in the gas phase, where  $n$  is the number of times the gas molecules are resorbed on their passage to the surface. While it is not possible, owing to mixing of the gas and back diffusion, to idealize the separation in this way, it is reasonable to assume that hydrogen will reach the surface considerably faster than deuterium. The last sample retained by the charcoal would be much enriched in deuterium. In this way the van der Waals forces could markedly augment separation due to flow alone.



One of us (R. M. B.) wishes to acknowledge with gratitude the award of an exhibition by the 1851 Commissioners which has made this work possible.

#### SUMMARY

(1) The stability and crystallization of charcoal adsorbents has been examined by measurements of adsorption after outgassing at known temperatures, and by X-ray analysis. All the adsorbents were micro-crystalline but stable towards outgassing at 1200° K. Above 1270° K the adsorptive capacity diminished, owing to graphitization. Some graphite spacings appeared during preparation of charcoals even at 670° K. The calculated crystal sizes showed that only a small part of the internal surface was available to hydrogen at saturation.

(2) Sorption of hydrogen at 78, 195 and 273° K showed that the charcoal surface is composite. There are two different types of sorption with different rates, each obeying a Langmuir isotherm; the total sorption may be represented by

$$\frac{x}{m} = \frac{ap}{1 + bp} + \frac{a'p}{1 + b'p}.$$

Saturation for the first type of adsorption is reached at low pressures; and was shown to be caused by active centres due to the ash.

The second type of adsorption is ascribed to an ash-free carbon surface. From isobars heats of adsorption are obtained at low pressures, constant at all concentrations measured for the second type of adsorption, and agreeing with accepted values at one atmosphere pressure. There is no evidence of active centres due to a carbon surface alone, at the lowest pressures.

(3) The kinetics of sorption of hydrogen, nitrogen, and oxygen at low temperatures obey solutions of the Fick law. For hydrogen kinetic processes involving sorption by the ash can be described by the parabolic diffusion law. The sorption kinetics of all gases in ash-free charcoal can be described by the solutions

$$\frac{C_e - C_t}{C_e - C_i} = b(e^{-at} + \frac{1}{10}e^{-9at} + \frac{1}{25}e^{-25at} + \dots),$$

and over later stages of sorption

$$\log \frac{C_e - C_t}{C_e - C_i} = k.t.$$

The time processes have negligible temperature coefficients and obey a  $1/\sqrt{M}$  relation where  $M$  is the molecular mass.

(4) Chemisorption of hydrogen causes a decrease in the amount of van der Waals adsorption, without altering the velocity of adsorption.

(5) Deuterium is more strongly sorbed than hydrogen at 78° K. The relative rates of evaporation for the species  $H_2$ , HD and  $D_2$  are shown to be 1.25, 1.09 and 1.00 respectively.

(6) No evidence could be found for previously reported discontinuities in the isotherms.

---

## The Interaction of Hydrogen with Micro-Crystalline Charcoal

### II—Activated Sorption of Hydrogen and Methane by Carbon

By RICHARD MALING BARRER

(Communicated by E. K. Rideal, F.R.S.—Received November 3, 1934)

At high temperatures the reaction between hydrogen and charcoal is not simple. The work of Kingman,\* and Burstein and Frumkin† suggests that the process is one of activated adsorption. Burstein, Lewin and Petroff‡ regard the process as one involving activated diffusion of atoms from reaction centres. Burstein, Frumkin and Fedotov,§ in conformity with this idea, considered the sorbed hydrogen atoms as capable of being in equilibrium with protons, which can exchange with cations in solution. On the other hand if activated adsorption were a process of surface hydrogenation the C—H units should not behave in this manner. Broome and Travers|| suggest the formation of methane, and in fact Randall¶ reported a non-condensable gas which was not hydrogen, on desorption of chemisorbed hydrogen. Kingman (*loc. cit.*) on the other hand found the gas desorbed at 950° C to be pure hydrogen. On account of the fundamental importance of the hydrogen-carbon and methane-carbon systems in hydrogenation, it seemed desirable

\* 'Trans. Faraday Soc.,' vol. 28, p. 269 (1932).

† *Ibid.*, vol. 28, p. 275 (1932).

‡ 'Phys. Z. Sowjet.', vol. 4, p. 2 (1933).

§ 'J. Amer. Chem. Soc.,' vol. 55, p. 3052 (1933).

|| 'Proc. Roy. Soc.,' A, vol. 135, p. 512 (1932).

¶ 'Trans. Faraday Soc.,' vol. 28, p. 443 (1932).

to reinvestigate these systems and to obtain quantitative data on energies of activation and heats of reaction.

Measurements of the rates of sorption and the amounts of gas taken up, when equilibrium was established with the various charcoals, were conducted in a manner similar to that previously described in low temperature physical adsorption experiments. The process of adsorption was again found to be one involving time; at sufficiently elevated temperatures isothermals could be determined by approach from both sides of the equilibrium pressure.

In Table I are given some data for equilibrium at 956° K. It is seen that the equation proposed by Burstein, Lewin and Petroff (*loc. cit.*),

TABLE I—ISOTHERM WITH HYDROGEN  
MASS OF CHARCOAL 6.9 GM. TEMPERATURE 956° K

$p$ (cm)	$v$ (cc)	$v$ (calc. from $v = \frac{10p}{1 + 0.221p}$ )
1.95	13.63	[13.63]
5.27	25.56	22.4
10.10	30.54	31.0
19.71	36.68	43.33
24.18	38.21	48.00

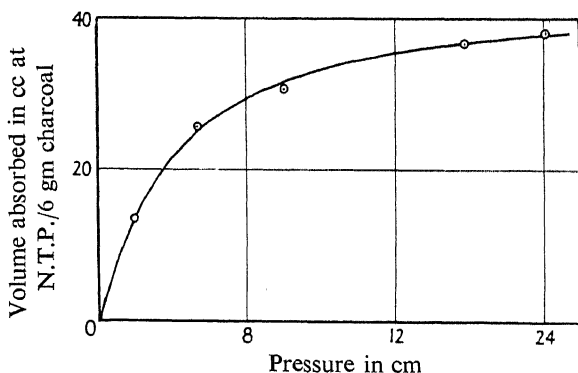


FIG. 1—Isotherm. Full curve from  $v = \frac{10p}{1 + 0.221p}$ . Temperature 956° K.

$v = Kp^{\frac{1}{2}}$ , is applicable only over a very limited range. On the other hand a simple Langmuir equation  $v = \frac{cp}{1 + bp}$ , where  $c = 10$ ,  $b = 0.221$ , holds with accuracy, as is shown in fig. 1.

Fig. 1 gives the experimental points and the curve derived from the Langmuir equation. This type of equation was obeyed wherever

equilibrium isotherms could be determined. It is the normal result of adsorptive and desorptive reactions in equilibrium. The saturation value for the above isothermal was 45.2 cc per 6.9 gm. The saturation value for the corresponding van der Waals isothermal was 262 cc per 6.9 gm as previously determined (Part I). Thus the activated process cannot be regarded as penetration of slip-planes not accessible to low temperature sorption. The result suggests a chemical origin for the activation energy. The isotherms became more and more rectangular as the temperature was lowered. The large amount sorbed at low pressure indicates the energetic nature of the sorption. When  $\log v/mp$

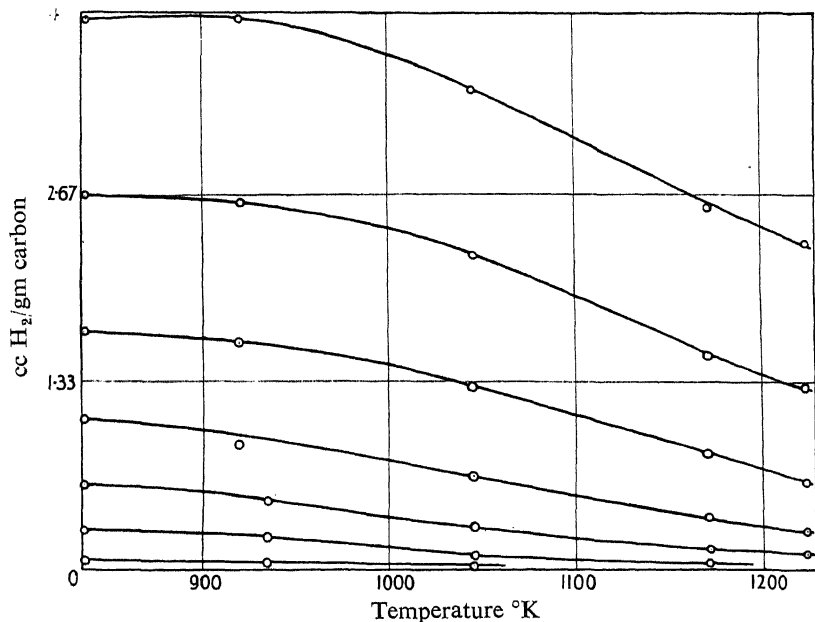


FIG. 2—Isobaric curves

is plotted against  $\log p$  no point of inflection is discovered, suggesting that, in contrast to the physical adsorption, activated sorption is not due to two simultaneous processes (here reduction of surface carbonyl as well as of carbon).

Fig. 2 shows the quantity/temperature curves at constant pressure for hydrogen on charcoal over the pressure range  $10^{-4}$  to 100 cm of mercury and between  $838^{\circ}\text{K}$  to  $1223^{\circ}\text{K}$ . The curve at 100 cm pressure involved a short extrapolation of the experimental data. At low temperatures and 100 cm pressure a distinct maximum appears—indicating that sorption is too slow for the establishment of equilibrium during the time of the experimental observations (two to three days per point). From our

results at higher temperature, where equilibrium from both sides can be established, it is possible to calculate the heat of adsorption from the equation

$$\frac{\partial \log p_1}{\partial T} = \frac{Q}{RT^2}.$$

where  $p_1$  denotes the equilibrium pressure at constant surface concentration.

Some results are given in Table II.

TABLE II  
TEMPERATURE RANGE 1171° K–1223° K

$v$ (cc at N.T.P. per 5.9 gm charcoal)	Temperature coefficient	$Q$ (cals/gm mol $H_2$ )
0.100	2.48	49,950
0.316	2.55	51,460
1.10	2.53	50,030
3.16	2.80	56,630

TEMPERATURE RANGE 1171° K–1045° K

0.100	12.70	49,400
0.130	11.9	48,100
0.316	10.5	45,700

Another independent set of experiments gave for 0.13 cc adsorbed :

Temperature range (° K) .....	1121–1223
$Q$ .....	55,000

As a mean value for the range of true equilibrium in the sorption isotherms we find  $50,000 \pm 5000$  cals/gm mol of hydrogen. This is independent of the amount of hydrogen sorbed as well as of the temperature.

#### KINETICS OF THE SORPTION

The equilibrium conditions reached in the previous section are the result of the reversibility of the surface reaction involved. This may be written

$$-\frac{dp}{dt} = K_1 p \cdot (1 - \theta) - K_2 \theta, \quad (1)$$

where  $-dp/dt$  is the rate of sorption,  $K_1$ ,  $K_2$  are constants,  $p$  is the hydrogen pressure and  $\theta$  is the fraction of the surface covered by sorbed

hydrogen. For small amounts adsorbed,  $(1 - \theta)$  may be taken as unity, and equation (1) reduces to

$$-\frac{dp}{dt} = k \cdot (p - p_e) \quad (1A)$$

(where  $p_e$  denotes the equilibrium pressure), as a limiting expression both for adsorption and desorption ( $p > p_e$ ).

If the rate of reaction is governed entirely by diffusion we have seen (Part I) that this is given by

$$\frac{C_e - C_t}{C_e - C_i} = \sum_{m=1}^{m=\infty} \frac{8}{(2m-1)^2} \frac{1}{\pi^2} e^{-\frac{D(2m-1)^2 \pi^2 t}{l^2}} \quad (2)$$

reducing to

$$C_t^2 - C_i^2 = kt \text{ for small values of } t \quad (2A)$$

and

$$\log(C_p - C_t) = k_1 t \text{ for large values of } t \quad (2B)$$

(where  $(C_t - C_i) > (C_e - C_t)$ ). It is clear that, if both activated adsorption and also diffusion processes are involved, the slower of the two will govern the reaction velocity. Since the rate of activated adsorption will be exponentially temperature dependent, and the diffusion process dependent only on  $\sqrt{T}$  ( $T$  = temperature) we should be able to resolve the two processes by experiments over a sufficiently wide range. In fig. 3  $\log(p_t - p_e) = \log \alpha (C_t - C_e)$  is plotted as a function of time for an initial pressure of *ca.*  $1.8 \times 10^{-2}$  cm. Above  $970^\circ$  K there is no temperature coefficient, but below  $970^\circ$  K a marked temperature dependence occurs. This reconciles the conflicting statements of Broome and Travers (*loc. cit.*) (above  $700^\circ$  C); and of Kingman (below  $530^\circ$  C).

In fig. 4 the experimental values of  $k$  in the equation

$$-\frac{dp}{dt} = k \cdot (p_t - p_e)$$

are plotted as a function of temperature, for such values of  $p$  that  $(C_t - C_i)$  is 0.095 cc at N.T.P. In the same figure are also given curves calculated from the expressions:

$$(a) \quad \text{for diffusion: } K_1 = a \sqrt{T}. \quad a = 0.107,$$

$$(b) \quad \text{for activated adsorption: } K_2 = b e^{-\frac{E}{RT}},$$

where  $E = 15,000$  cal/gm mol and  $b = 1440$ . In this manner it is shown that the process of sorption of hydrogen resolves itself into an activated adsorption and a non-activated diffusion such that the observed data agree closely with calculated data.

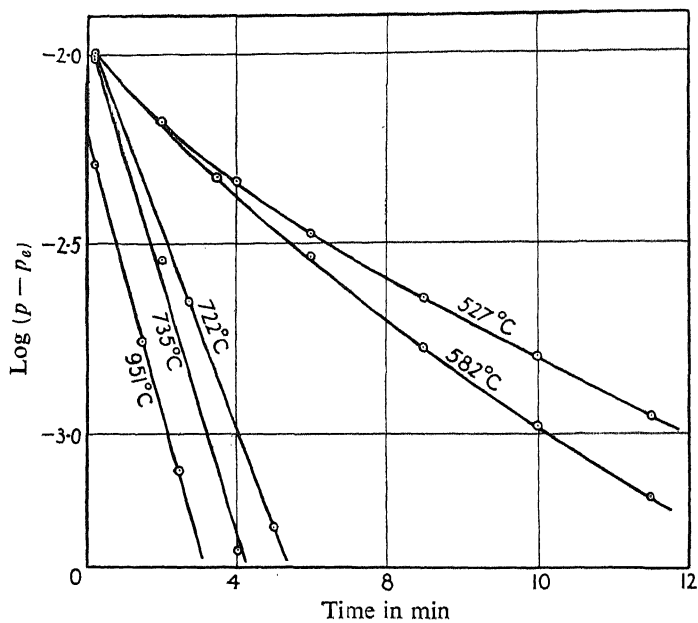


FIG. 3

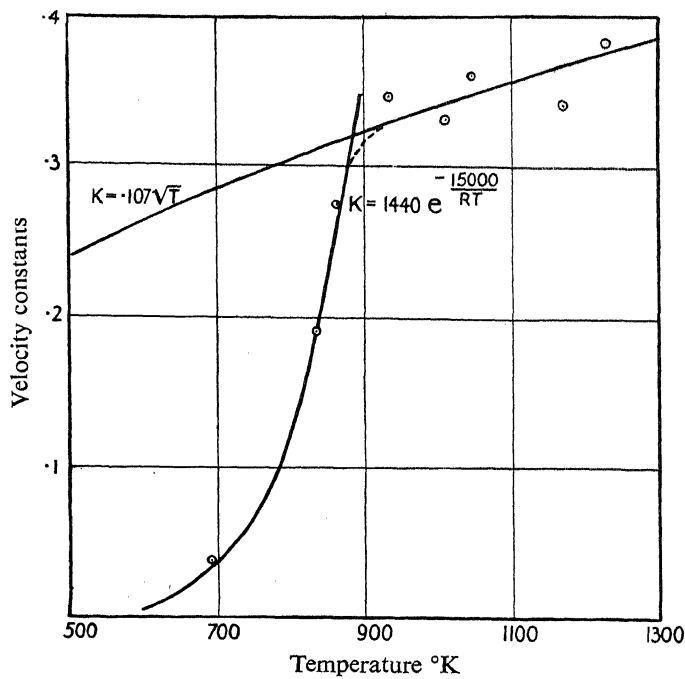


FIG. 4

For these experiments we have a formal parallel in the combustion of oxygen and charcoal, which at low pressures proceeds through intermediate formation of surface compounds\* and where† a  $\sqrt{T}$  diffusion process is approximated to at very high temperatures, displacing the lower temperature exponential temperature relation. In the oxygen carbon system the  $\sqrt{T}$  relation has been ascribed to a stationary gas film through which diffusion proceeds; so that our data wherein such a film is absent suggest an interesting alternative.

Further proof of the existence of diffusion processes was obtained by observation of desorption rate curves. These could be made to vary in form by varying the boundary conditions, while the total amount of sorbed gas was almost constant. A brief evacuation, by removal of surface gas, changed the form of the desorption velocity curves, so that the constant in the equation  $(C_i^2 - C_i^2) = kt$  instead of decreasing according to a characteristic function of time, actually increased as gas first diffused from internal to external surfaces instead of immediately into the gas phase. Under suitable conditions the parabolic law held during the early stages of adsorption as shown by Table III.

TABLE III  
TEMPERATURE 955° K. 6.9 GM CHARCOAL

$t$ (mins)	(cc gas sorbed at N.T.P.)	$k = \frac{C_t}{\sqrt{t}} (C_i = 0)$
6	5.75	0.60
9	6.80	0.62
14	7.85	0.61
32	8.98	0.51
46	9.30	0.45

#### THE ACTIVATION ENERGY FOR SORPTION

It has been shown that the high temperature adsorption of hydrogen by charcoal involves both a true activated adsorption and a diffusion, and that it is possible to separate these two processes. The activation energies for the adsorptive process may be determined by two different methods:

(a) From the curves of  $\log(p - p_e)$  against time, by drawing tangents at points of equal adsorption on the various isothermals whence

$$E = 2.303 R \cdot \frac{T_1 T_2}{T_2 - T_1} \log \frac{\tan \theta_{T_1}}{\tan \theta_{T_2}}.$$

\* Mayers, 'Chem. Rev.', vol. 14, p. 31 (1934).

† Tu, Davis and Hottel, 'J. industr. Engng. Chem.', vol. 26, p. 748 (1934).



(b) From the times required for equal adsorption at different temperatures\*

$$E = 2.303 R \cdot \frac{T_1 T_2}{T_2 - T_1} \log \frac{t_1}{t_2}.$$

The first method is more accurate and yields slightly higher energy values:—

Amount adsorbed, cc at

N.T.P. on 5.9 gm	....	0.175	0.225	0.257	0.281	0.300
Energy by method (a)	....	11,250	13,220	13,450	14,300	14,700
Energy by method (b)	....	10,150	11,400	12,000	12,700	13,100

Some values of E calculated by method (a) are given in Table IV.

TABLE IV

Temperature range ° K	Amount sorbed (cc at N.T.P. on 5.9 gm C)	Energy (cals/gm mol)
695–838	0.062	14,350
	0.077	15,000
838–935	0.085	13,900
	0.096	14,300
	0.100	17,700
860–695	0.062	13,600
	0.077	13,700
	0.087	14,700
860–630	0.077	9,800
	0.087	10,000
	0.175	11,250
	0.225	13,220
	0.257	13,450
	0.281	14,200
	0.300	14,700
864–630	0.175	11,700
	0.225	13,600
	0.257	14,000
	0.287	15,100

The unusual result was obtained that the energy of activation steadily increased with the charge of gas adsorbed. For small adsorptions of hydrogen Table IV establishes beyond doubt a small activation energy.

\* Taylor and Williamson, 'J. Amer. Chem. Soc.,' vol. 53, p. 2168 (1931).

For larger surface concentrations the following energies were measured (Table V).

TABLE V

TEMPERATURE RANGE 864–728° K	
cc sorbed at N.T.P. on 5.9 gm C	Energy (cals/gm mol)
1.01	22,000
1.44	23,300
1.88	25,900
2.31	26,200
2.75	28,100
3.18	29,000
3.61	29,700

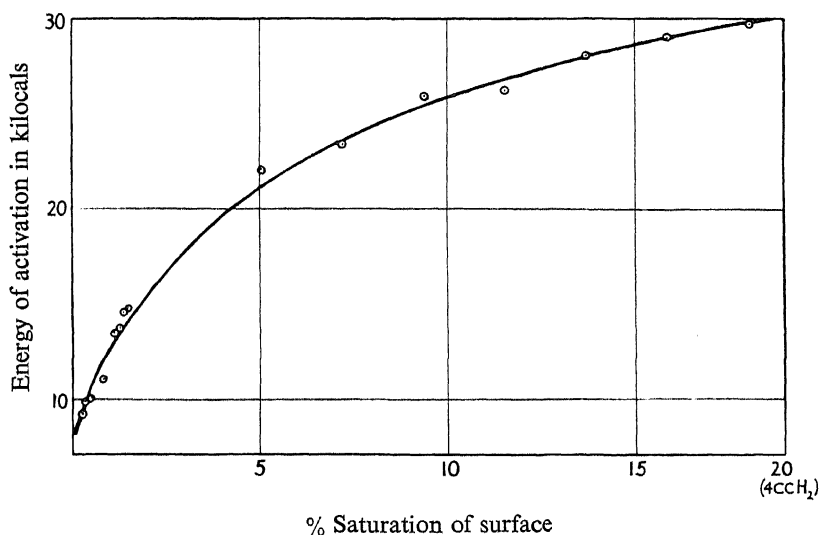


FIG. 5—Activation energy as function of gas sorbed

The final figure approaches the value obtained by Kingman (*loc. cit.*) of 30,000 cals/gm mol. Fig. 5 shows the activation energy as a function of the charge of gas. An extrapolation to saturation (*ca.* 20 cc on 5.9 gm C) gives 35,000 cals/gm mol as a limiting value. We have now the interesting case of a surface reaction of constant heat (50,000 cals/gm mol) and variable activation energy. Just two simultaneous reactions of the different activation energies, 11,000 and 30,000 cals/gm mol, might be expected to show a strong inflection in the  $\log x/mp$  against  $\log p$  curve, which, however, is not given by experiment (*cf.* Part I, fig. 2). There thus appears to be a number of processes leading to the

same chemical result with different probabilities of occurrence. We shall defer discussion of this phenomenon to a later section.

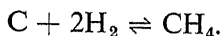
#### THE EQUILIBRIUM BETWEEN CHEMI-SORBED HYDROGEN, METHANE AND HYDROGEN GAS

The sorbed hydrogen regarded as a surface hydride is the first stage in the formation of methane. In view of the conflicting evidence as to the purity of hydrogen desorbed after chemisorption on charcoal, a number of measurements of the hydrogen content of the equilibrium gas were made with the following results.

TABLE VI

Experiment	Time allowed (hours)	Temperature ° K	Pressure (cm)	% hydrogen
1	10	715	57	100
2	15	953	57.4	91.4
3	24	848	15.5	91.1
4	40	848	15.5	90.9
5	2	848	3.4	100
6	18	848	3.4	98
7	20	848	44.6	95.7
8	20	848	35.8	100

It was always found that sorption was virtually completed before any foreign gas could be detected. The data are best interpreted as due to the slow establishment of a methane equilibrium:



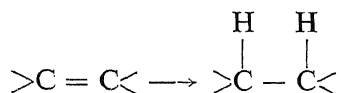
Experiments (2), (3), (4) and (6) agree very closely with the equilibrium concentrations as given by Mayer and Altmayer,\* Egloff, Schaad and Lowry, jnr.†

In some further experiments the charcoals covered with hydrogen at high temperatures were exposed to oxygen at room temperature, and finally re-evacuated and heated. Under these conditions the bulk of the hydrogen was obtained as such. The surface hydride is thus inert to oxygen at moderate temperatures, and sorption is best regarded as the formation of a very complex hydrocarbon of small hydrogen content. Since it has been shown (Part I) that traces of chemisorbed oxygen are

\* 'Ber. deuts. chem. Ges.,' vol. 40, p. 2134 (1907).

† 'J. Phys. Chem.,' p. 1611 (1930).

still present in the original carbon, this preparation, like coal, is not completely a hydrocarbon. There may also exist hydroxyl and carbonyl groups on the lattice layer. Provisionally we may write the specific chemical reaction involved in chemisorption as:



That methane may also react with a carbon surface is suggested by experiments on the cracking of hydrocarbons and by the experiments of Burstein, Lewin and Petroff (*loc. cit.*), although Kassel\* stated that the velocity of the homogeneous decomposition of methane was unaffected by the carbon deposited during the reaction. The following experiments show that a surface reaction readily proceeds on a clean carbon surface, but not upon the relatively inert surface of carbon covered with a layer of chemisorbed hydrogen. The measurements were carried out in the manner previously described, employing sugar charcoal and an initial pressure of methane of  $3.0 \times 10^{-2}$  cm. The reaction was found under conditions of low pressures of methane to be accurately unimolecular with respect to methane and to occur with a decrease in pressure in contrast to the homogeneous decompositions of Kassel (*loc. cit.*) and of Storch.† Two of the runs with constants given by  $\Delta/\Delta_t \log(p - p_e)$  are given below ( $p_e$  was small enough to be negligible):

TEMPERATURE 1078° K		TEMPERATURE 998° K	
Time (mins)	Constant	Time (mins)	Constant
1	0.0440	18	0.0053
3	0.0390	22	0.0053
5	0.0385	26	0.0056
7	0.0410	31	0.0054
9	0.0380	37	0.0053
11	0.0375	43	0.0052
13	0.0420	50	0.0055
15	0.0410	58	0.0059
17	0.0380	66	0.0050
23	0.0405	74	0.0056
		83	0.0048
Mean ....	0.0400	Mean ....	0.0054

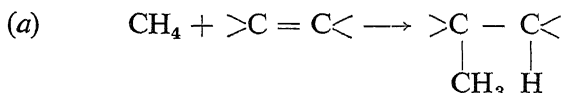
\* 'J. Amer. Chem. Soc.,' vol. 54, p. 3949 (1932).

† 'J. Amer. Chem. Soc.,' vol. 54, p. 4188 (1932).

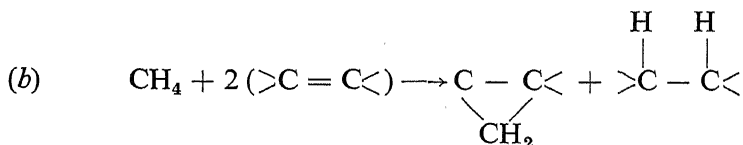
From a series of experiments the activation energy for this particular charcoal\* was calculated with the following results:—

Temperature range ° K	Energy in cal/gm mol
998–1078 .....	54,100
998–1079 .....	56,700
991–1079 .....	53,700
991–1113 .....	52,500
Mean .....	53,400

It is clear that the reaction measured is not identical with the homogeneous reaction for which  $E = 79,400$  cal/gm mol according to Kassel. The simplest interpretation is that the methane is chemisorbed to give a surface hydride according to equations such as



or



In this case as the reaction proceeds retardation should result due to the formation of inert surface hydride. The retarded reaction may be written

$$-\frac{dp}{dt} = K(1 - \theta)p_{\text{CH}_4},$$

where  $\theta$  represents the fraction of the surface covered with chemisorbed hydrogen, which will come into equilibrium with hydrogen (present at very low pressure) in the gas phase:

$$\theta^1 = \frac{K_1^1 p_{\text{H}_2}}{K_2^1 + K_1^1 p_{\text{H}_2}}.$$

i.e.,

$$-\frac{dp}{dt} = \frac{KK_2^1 p_{\text{CH}_4}}{K_2^1 + K_1^1 p_{\text{H}_2}}.$$

We apply the expression to a pressure range where

$$(p_{\text{CH}_4} + p_{\text{H}_2}) \simeq p_{\text{CH}_4} = p.$$

\* The decomposition of methane proceeded with a much greater velocity and a smaller energy of activation on a second charcoal, upon which rates and energies of activation for chemisorption of hydrogen were similar.

If the initial pressure is  $p_0$ , over a range of surface concentrations which is not too great one obtains:

$$p_{H_2} = K_3 x = K_4 (p_0 - p),$$

if  $x$  denotes the amount of methane decomposed. Hence

$$K = \frac{1 + p_0 b}{t} \log \frac{p_0}{p} - b \frac{(p_0 - p)}{t}.$$

Writing

$$\frac{1}{t} \log \frac{p_0}{p} = k_m; \frac{p_0 - p}{t} = v,$$

we obtain

$$K = (1 + p_0 b) K_m - b v,$$

or  $K_m$  is a linear function of  $v$  (*cf.* Hinshelwood, "Kinetics of Chemical Change"). Experiments were then conducted at higher pressures of methane, and the retardation was observed in close agreement with theory. The necessary data are summarized in Table VII, and fig. 6 shows the  $K_m - v$  curve.

TABLE VII

Pressure (cm)	Time (mins)	$1/t \log p_0/p$	$(p_0 - p)/t$
0.377	0	—	—
0.323	12	0.00570	0.00450
0.313	16	0.00507	0.00400
0.298	20	0.00510	0.00395
0.288	24	0.00492	0.00371
0.281	28	0.00457	0.00343
0.266	36	0.00422	0.00308
0.250	46	0.00390	0.00276
0.234	58	0.00359	0.00247
0.219	72	0.00329	0.00220
0.205	88	0.00301	0.00196
0.172	136	0.00251	0.00151
0.140	210	0.00204	0.00113

Finally, isotherms were measured at 1113° K and 1233° K with 0.4 cc methane adsorbed per 6 gm of charcoal.

From the isotherms the equilibrium pressures at equal surface concentrations could be obtained, giving a value of 48,000 cal/gm mol for the heat of adsorption, a value substantially that for the similar reaction between hydrogen and charcoal. Analysis of the gas showed it to be nearly pure hydrogen. Thus at these low pressures the surface hydride always comes to equilibrium with hydrogen, whether equilibrium is approached from the methane or hydrogen side.

1113° K		1233° K	
Equil. pressure	cc sorbed at	Equil. pressure	cc sorbed at
cm × 10 <sup>3</sup>	N.T.P.	cm × 10 <sup>3</sup>	N.T.P.
2.10	0.144	11.8	0.0995
6.75	0.451	40	0.332
83.5	1.79	339	0.724
2620	4.15		

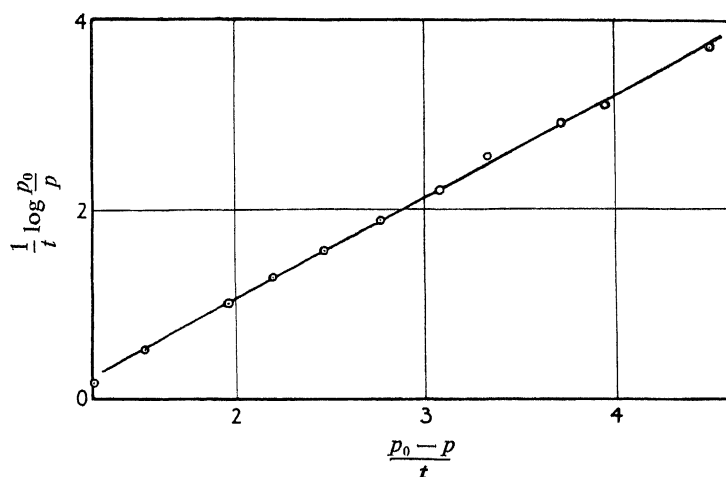
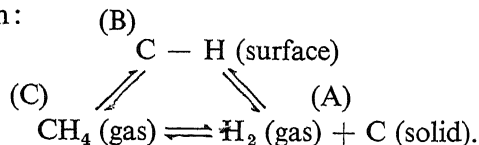


FIG. 6—Retardation in chemisorption of methane

## DISCUSSION

The relations in the system hydrogen-carbon-methane are shown by these investigations to be capable of representation by the following triple equilibrium:



We have seen that the chemisorption reaction (A)  $\longrightarrow$  (B) presents some interesting peculiarities which we must examine, whilst the reaction (B)  $\longrightarrow$  (C) which is certainly composite proceeds only slowly under ordinary conditions, but is certainly facilitated by hydrogenation catalysts.

The energies of the stages outlined above may be tabulated as follows:

Stage	Reaction
C $\longrightarrow$ B	.... $\text{CH}_4 \text{ (gas)} + 3\text{C (solid)} \longrightarrow 4 \text{ (CH) (surface)}$
	$\Delta H = 82,000 \text{ cal/gm mol methane (calculated from A} \longrightarrow \text{C and A} \longrightarrow \text{B)}$
	$E = 54,000 \text{ cal/gm mol methane (for the first step in the decomposition)}$

Stage	Reaction
A $\longrightarrow$ C . . . .	$2\text{H}_2 \text{ (gas)} + \text{C (solid)} \longrightarrow \text{CH}_4 \text{ (gas)}$ $\Delta\text{H} = 18,000 \text{ cal/gm mol methane}$
A $\longrightarrow$ B . . . .	$\text{H}_2 \text{ (gas)} + \text{C (solid)} \longrightarrow 2 \text{ (CH) (surface)}$ $\Delta\text{H} = 50,000 \text{ cal/gm mol hydrogen}$ $\text{E} = 10,000\text{--}30,000 \text{ cal/gm mol}$

hydrogen giving 60,000–80,000 cal/gm mol for the reverse reaction, *i.e.*, the elimination of a hydrogen molecule from the hydride surface. We have referred to the interesting peculiarity that the surface hydride formation is associated with a constant heat of formation, but a variable energy of activation which runs from 10,000 to 30,000 cal/gm mol as the surface becomes increasingly saturated. In Part I we noted that these charcoals were all microcrystalline as revealed by X-rays, consisting of crystallites wherein the lattice layers were separated by variable distances *e.g.*, a mean of 4.65 Å. in charcoal D, varying to 3.5 Å., the distance of closest approach which obtains in graphite. If chemisorption involves addition of hydrogen across the edges of two superposed lattices, the reaction involves dissociation of the molecule and formation of two CH links at varying distances apart (3.5 Å. to 4.65 Å.). Sherman and Eyring\* have calculated the energy of activation of such a process from quantum mechanical considerations. As the carbon-carbon distance varied from 3.6 Å. to 4.6 Å. the energy of activation increased from 8000 to 35,000 cal/gm mol, values which reproduce those actually obtained, though numerical agreement must be regarded as fortuitous.

We may compare the value obtained for the heat of the process  $\Delta\text{H} = 50,000$ ; and the activation energies 10,000–30,000; and 60,000–80,000 to the corresponding quantities for the reactions:

(a)  $\text{C}_2\text{H}_4 + \text{H}_2 \rightarrow \text{C}_2\text{H}_6$ ;  $\Delta\text{H} = 30,000 \text{ cal/gm mol}$ ,† and  $\text{E} = 43,150 \text{ cal/gm mol}$ ,‡ whilst Marek and McLuer§ gave 73,170 cal/gm mol for the activation energy for dissociation of ethane to ethylene.

(b)  $\text{C}_2\text{H}_2 + \text{H}_2 \rightarrow \text{C}_2\text{H}_4$ ;  $\Delta\text{H} = 48,000 \text{ cal/gm mol}$ .||

The heat of adsorption is equal to that for partial hydrogenation of a triple bond.

\* 'J. Amer. Chem. Soc.', vol. 54, p. 2661 (1932).

† Pease, 'J. Amer. Chem. Soc.', vol. 54, p. 187 (1931).

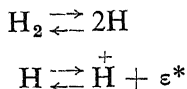
‡ Pease, *loc. cit.*

§ 'J. industr. Engng. Chem.', vol. 23, p. 878 (1931).

|| Kassel, *loc. cit.*



It is clear that this chemi-sorbed hydrogen is in all respects similar to the C—H linkage in a hydrocarbon. The thermal value of the bond is at least 75,000 cal/gm mol since the H—H bond has a thermal value 100,000 cal/gm mol and the thermal value of the process is 50,000 cal/gm mol. These C—H linkages cannot be involved in activated migration processes of the type pictured by Burstein, Lewin and Petroff (*loc. cit.*); nor is the hydrogen present in physically adsorbed atomic form, due to mechanisms such as



It is possible, however, that the electromotive behaviour, of carbon and hydrogen, and properties shown thereby in electrolyte adsorption may be due both to the presence of metallic impurities and to the presence of a certain amount of phenolic hydroxyl (formed by reduction of surface carbonyl) which can ionize and so impart a charge to the charcoal.

I wish to thank the Chemical Society for a grant which has helped to defray the cost of apparatus; and the 1851 Commissioners for the award of a scholarship, which has made the work possible.

#### SUMMARY

(1) Isotherms, isobars and kinetics of activated sorption of hydrogen by charcoal have been measured between 623° and 1223° K. Isotherms and kinetics of activated sorption of methane have also been studied.

(2) Measurements of the purity of the gas at equilibrium with carbon have shown that at small pressures a gas phase of hydrogen is obtained whether equilibrium is approached from the side of methane or hydrogen. At higher pressures small quantities of methane are very slowly formed, but are not detectable until activated sorption is virtually completed.

(3) Sorption of hydrogen is an activated chemi-sorption with further complication by diffusion. Non-activated diffusion limits the reaction rates above 970° K. The energy of activation varies from 10,000 cal/gm mol to 30,000 cal/gm mol at 20% saturation of the surface. The heat of the process is constant at  $50,000 \pm 5000$  cal/gm mol at high temperatures and from 0 to 20% saturation.

(4) At low pressures methane reacts with a carbon surface with diminution in pressure according to a unimolecular law. There is no

\* Frumkin, Burstein and Fedotov, 'J. Amer. Chem. Soc.', vol. 55, p. 3052 (1933).

variation in the energy of activation in this range. This energy is 53,400 cal/gm mol. At higher pressures of methane the surface reaction is retarded by the carbon hydride surface produced.

(5) Energy relations in the system chemisorbed hydrogen-hydrogen-methane have been discussed and compared with energetics of hydrogenations of double and triple bonds. A mechanism is proposed to explain variable activation energy for chemisorption of hydrogen. The presence of physically adsorbed ionizable hydrogen atoms as supposed by earlier workers is shown to be incompatible with the experimental data.

---

## The Nuclear Spin of Iodine

### I—Fine Structure in the First Spark Spectrum

By S. TOLANSKY, Ph.D., Manchester University

(Communicated by W. L. Bragg, F.R.S.—Received November 13, 1934)

#### INTRODUCTION

In an earlier paper on the fine structures of the visible lines in the arc spectra of bromine and iodine\* an attempt was made to estimate the nuclear spin of iodine, and a tentative value of  $9/2$  was proposed. The iodine arc lines were excited by a high frequency electrodeless discharge in pure iodine vapour and examined with a silvered Fabry-Perot interferometer. The fine structures in the arc lines are small, and as the patterns are highly complex and the individual components not very sharp, interpretation was difficult. It was concluded with certainty that the nuclear spin was at least equal to  $5/2$ , but one line in particular suggested a value of  $9/2$ . This was indefinite, and in view of the uncertainty a thorough examination of both the arc and spark spectra of iodine has been undertaken. A preliminary notice has already appeared.†

The first spark spectrum can be more easily studied than the arc spectrum, since the structures are on a very much bigger scale and more complete resolution can be attained. The present work is concerned with the spark lines excited in a hollow cathode discharge. Fine struc-

\* Tolansky, 'Proc. Roy. Soc.,' A, vol. 136, p. 585 (1932).

† Tolansky, 'Nature,' vol. 134, p. 851 (1934).

tures in iodine spark lines were first recorded long ago by Wood and Kimura\* who excited the lines in a Geissler tube and examined them with a transmission echelon. Murakawa† attempted to analyse the fine structure data, but as the source and instrument employed by Wood and Kimura were not able to give the high resolution attained here, the deductions made from these data, although generally correct, are uncertain and require further examination; for many of the line structures are much more complex than as reported by these earlier observers.

A partial analysis of the gross structure term multiplicity of the iodine spark spectrum has been made by Murakawa (*loc. cit.*) and his line classifications will be employed here. Unfortunately only a small number of the lines studied here for fine structure have been allocated, these transitions are shown in fig. 1. It is seen that a number of terms are involved more than once, so that the fine structure term analysis can be frequently checked. The important observed terms in the iodine spark spectrum are  $^5S$ ,  $^3S$  of the  $5s^2 5p^3 ns$  electron configuration, and  $^5P$ ,  $^3P$  of the  $5s^2 5p^3 6p$  configuration, and the line transitions studied for fine structure are between these S and P terms.

#### EXPERIMENTAL

The spark spectrum was excited in a water-cooled hollow cathode discharge. Helium was circulated continuously through the tube and when a current of 100 milliamperes was used, a brilliant spectrum was emitted, the lines being very much sharper than in the high frequency electrodeless discharge previously employed for the arc spectrum. By adjusting the pressure of the helium either the arc or spark spectrum could be excited at will with only a very small degree of intermingling. The lines were examined for fine structure by means of a large aperture silvered Fabry-Perot interferometer, crossed with a two-prism glass spectrograph. A succession of etalons between 2 and 25 mm was used to elucidate the structures. When using Ilford Hypersensitive plates exposure times varied from one second to half an hour.

Table I gives a complete list of the observed fine structures. The separations are given in units of  $\text{cm}^{-1} \times 10^{-3}$  and the visually estimated intensities of the components is shown below each in brackets. The line allocations, where known, are those given by Murakawa. Structures are classed as A, B, C, according to whether resolution is good, medium or bad. The observed components in the C class lines are blurred

\* 'Astrophys. J.', vol. 46, p. 182 (1917).

† 'Sci. Pap. Inst. phys. chem. Res. Tokyo,' vol. 20, p. 285 (1933).

patches arising from the crowding together of fine structure components which takes place when the structures in the upper and lower terms of a line are small and of a similar order. As the figures given in the table for these lines may appear misleading, the patterns are shown diagrammatically in fig. 5.

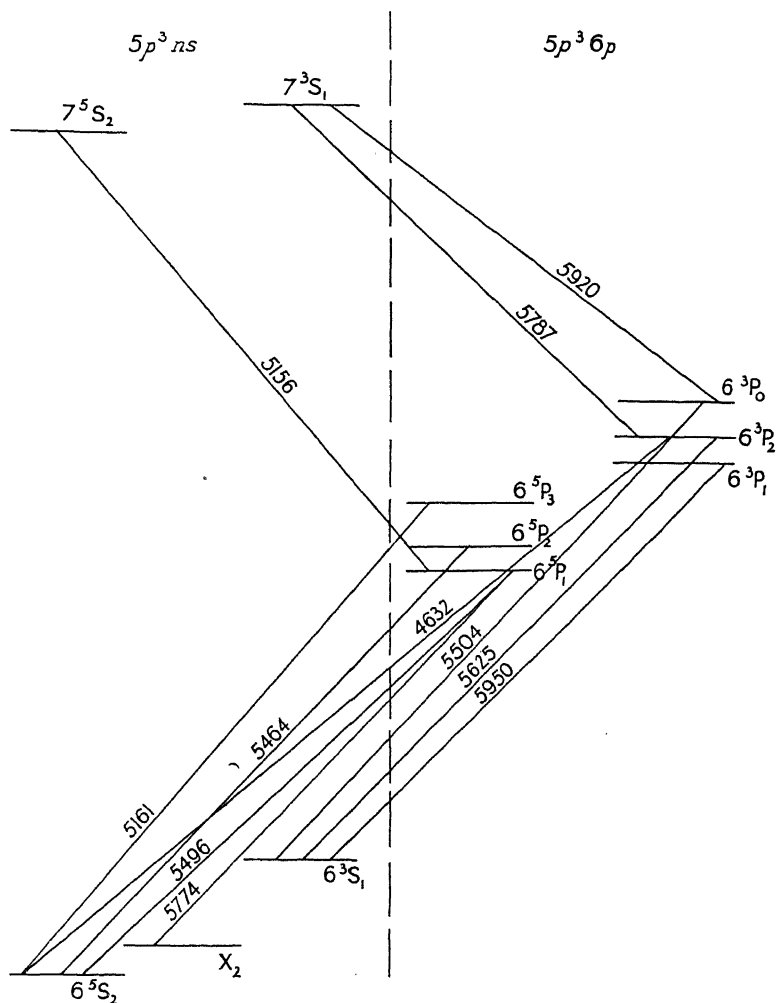


FIG. 1

## ANALYSIS

The three lines  $6^5S_2-6^5P_3$ ,  $6^5S_2-6^5P_1$ ,  $6^5S_2-6^3P_1$  all show very similar structures, namely, sharp quintets regularly degrading in intensity and intervals to the violet.  $X_2-6^5P_1$  exhibits a similar structure, but

TABLE I—FINE STRUCTURES IN THE IODINE SPARK SPECTRUM

Wave-length	Classification	Structure, $\text{cm}^{-1} \times 10^{-3}$										Class
		Red					Violet					
6585.0		0	47	178	256							A
		(2)	(6)	(3)	(2)							
6516.1		0	153	327	502	628	779	834	926	1053		A
		(1)	(3)	(12)	(2)	(4)	(5)	(4)	(4)	(3)		
6204.7		0	71	164	244	393						A
		(3)	(5)	(1)	(2)	(2)						
6161.9		0	579	949								A
		(4)	(3)	(2)								
6127.4		0	200	234	354	432	535	618	645			A
		(10)	(6)	(4)	(2)	(4)	(3)	(1)	(2)			
6068.8		0	35	126	251	308						A
		(2)	(3)	(10)	(4)	(15)						
5950.1	$6^3\text{S}_1-6^3\text{P}_1$	0	47	121	204							C
		(3)	(3)	(2)	(4)							
5920.7	$6^3\text{P}_0-7^3\text{S}_1$	Single										B
5890		0	57	150								C
		(4)	(3)	(2)								
5813		Single										A
5787.1	$6^3\text{P}_2-7^3\text{S}_1$	0	56	106	149							B
		(4)	(1)	(2)	(2)							
5774.7	$\text{X}_2-6^5\text{P}_1$	0	741	1291	1686	1913						A
		(5)	(4)	(3)	(2)	(1)						
5760.4		0	56	100	132	159						B
		(10)	(3)	(5)	(4)	(4)						
5679.0		0	86	173	238	293	424	482				A
		(1)	(3)	(10)	(4)	(3)	(3)	(6)				
5625.7	$6^3\text{S}_1-6^3\text{P}_2$	0	28	70								C
		(2)	(2)	(3)								
5598.5		0	395	618	813	1037						A
		(5)	(18)	(1)	(3)	(9)						
5593.1		0	26	80	121	151						B
		(7)	(10)	(2)	(4)	(4)						

TABLE I—(continued)

Wave-length	Classification	Structure, $\text{cm}^{-1} \times 10^{-3}$										Class
		Red								Violet		
5504.8	$6^3\text{S}_1-6^3\text{P}_0$	0 33 (1) (1)										C
5496.8	$6^3\text{S}_2-6^5\text{P}_1$	0 429 (5) (4)	756 (3)	991 (2)	1141 (1)							A
5464.8	$6^3\text{S}_2-6^5\text{P}_2$	0 89 ? (10) (1)	303 (1)	363 (4)	415 (2)	630 (3)	680 (3)	840 (2)	868 (3)	969 (3)		A
5407.3		0 182 (8) (4)	226 (3½)	363 (3)	423 (3)	528 (1)	572 (2)	659 (2)				A
5345.2		0 151 (1) (12)	305 (10)	419 (8)	507 (6)	536 (4)	605 (2)					A
5338.2		0 107 (1) (8)	236 (6)	348 (4)	429 (2)	461 (1)						B
5269.4		0 101 (8) (10)	216 (1)	353 (6)	490 (12)	623 (8)						B
5234.6		0 192 (7) (6)	355 (5)	502 (4)	622 (3)	701 (2)	732 ? (1)					A
5228.9		0 39 (1) (3)	84 (2)	176 (4)								C
5216.2		0 22 (3) (1)	79 (3)	122 (4)	199 (5)	283 (6)	366 (12)	441 (½)				B
5214.0		0 36 (2) (3)	83 (3)									C
5161.2	$6^5\text{S}_2-6^5\text{P}_3$	0 397 (5) (4)	695 (3)	905 (2)	1025 (1)							A
5156.4	$6^5\text{P}_1-7^5\text{S}_2$	0 75 (2) (3)	163 (4)	266 (5)	382 (6)							B
5125		0 70 (2) (2)	118 (5)	182 (1)								C
5124.6		0 52 (3) (2)										C
4987.0		0 38 (4) (3)										C
4806.4		0 53 (4) (5)	121 (5)	168 (6)	213 (6)	252 (12)	293 (2)					B

TABLE I—(continued)

Wave-length	Classifi- cation	Structure, $\text{cm}^{-1} \times 10^{-3}$						Class
		Red			Violet			
4675.5		0	150	295	365	508	673	B
		(6)	(2)	(5)	(10)	(2)	(1½)	
4666.5		Single						A
4632.4	$6^5\text{S}_2-6^3\text{P}_2$	0	399	695	928	1054		A
		(5)	(4)	(3)	(2)	(1)		
4561.0		0—————228						B
		(1)			(4)			
4544.3		0	240	373	685			C
		(3)	(2)	(5)	(1)			
4540.9		0	110	162				C
		(2)	(1)	(1)				
4488.8		0	117	162				B
		(2)	(1)	(1)				
4456.9		0	50					C
		(5)	(4)					

on almost twice the scale. Considering the first three lines, it is obvious that the structures in each must approximate closely to the structure of the common  $6^5\text{S}_2$  term. Since the term fine structure multiplicity is  $2I + J$  or  $2J + 1$ , according to which has the smaller value, the nuclear spin  $I$ , must be at least  $5/2$ . (A spin of  $3/2$  would only produce a quartet structure in a term with  $J = 2$ .) The differences in the fine structures of the lines are due to the small structures in the upper terms. In the line with the sharpest components,  $6^5\text{S}_2-6^5\text{P}_1$ , the upper term structure must be small, therefore the interval ratios within the line should approximate fairly closely to the interval ratios within the  $6^5\text{S}_2$  term, and thus the nuclear spin can be determined. As the interval between two fine structure levels with quantum numbers  $F$  and  $F + 1$  is equal to  $A(F + 1)$  where the constant  $A$  is the interval factor, Table II shows that the nuclear spin is  $5/2$ . This is proved by the fact that only this spin gives  $A$  a constant value.

TABLE II

Spin	Intervals of $6^5\text{S}_2-6^5\text{P}_1$ , in $\text{cm}^{-1} \times 10^{-3}$			
$5/2$	$9 \times 47\frac{1}{2}$	$7 \times 47$	$5 \times 47$	$3 \times 50$
$7/2$	$11 \times 39$	$9 \times 36$	$7 \times 33$	$5 \times 30$
$9/2$	$13 \times 33$	$11 \times 30$	$9 \times 26$	$7 \times 21$

The slight irregularities in the value of the interval constant for  $I = 5/2$  will be completely accounted for later, when the small upper term structure is taken fully into account.

Having determined the nuclear spin, the analysis of the classified lines can now be carried out. The Fisher-Goudsmit graphical method enables term structures to be calculated for lines exhibiting only partial resolution.\* Referring back to fig. 1, the analysis proceeds as follows.  $6^3S_1-6^3P_0$  has a very small structure, appearing with a 25 mm etalon as a slightly broadened patch whose total width is about 33 units. Since the upper term is single ( $J = 0$ ) it follows that  $6^3S_1$  has a very small structure with an interval factor of about  $5\frac{1}{2}$  units. From the structure of  $6^3S_1-6^3P_2$ , which is also a line with a narrow structure and only partially resolved, the small interval factor for  $6^3P_2$  can be calculated and is found to be 11 units. As the upper term has the wider structure the line pattern is degraded to the red.

From the known structure of the  $6^3P_2$  term, the structure of  $6^5S_2$  is obtained by means of the line  $6^5S_2-6^3P_2$ , the analysis of which is shown in fig. 2. If the lower interval factor is taken as 99 and the upper as 11 the agreement between the calculated and the observed values of the intervals is very good. The centres of gravity of the close unresolved groups have been determined by the Fisher-Goudsmit method and no ambiguity in the interpretation arises. A check on the values is given by a totally independent analysis of the  $6^5S_2$  term from the line  $6^5S_2-6^5P_1$ . This analysis is shown in fig. 3. No previous values have been assumed, and the interval factor found for the  $6^5S_2$  term from this independent analysis is 100. The  $6^5P_1$  term has an interval factor of 10 units. It is seen from the diagram that the agreement between the observed and calculated values is extremely good. The interval rule in the lower  $6^5S_2$  is strictly obeyed, and it is at once obvious how it is that small irregularities arise in the approximate values of the interval factor calculated from the line and not from the term. This then completely explains the deviations in Table II.

The value 100 for the  $6^5S_2$  term is more likely to be correct than 99, since for the same upper interval factor a  $\Delta J = 1 \rightarrow 2$  transition produces less spread of the non-diagonal wing components than a  $\Delta J = 2 \rightarrow 2$  transition. This appears in the diagrams, from which it is seen that in  $6^5S_2-6^5P_1$  the unresolved groups are narrower than in  $6^5S_2-6^3P_2$ , although the upper interval factors are practically identical. The nett effect is the production of sharper components in the first case and this

\* Fisher and Goudsmit, 'Phys. Rev.', vol. 37, p. 1059 (1931).



line must therefore be considered the more reliable for the determination of the interval factor. It is because of the relative displacements of components with differing intensities in the two  $\Delta J$  cases, that such

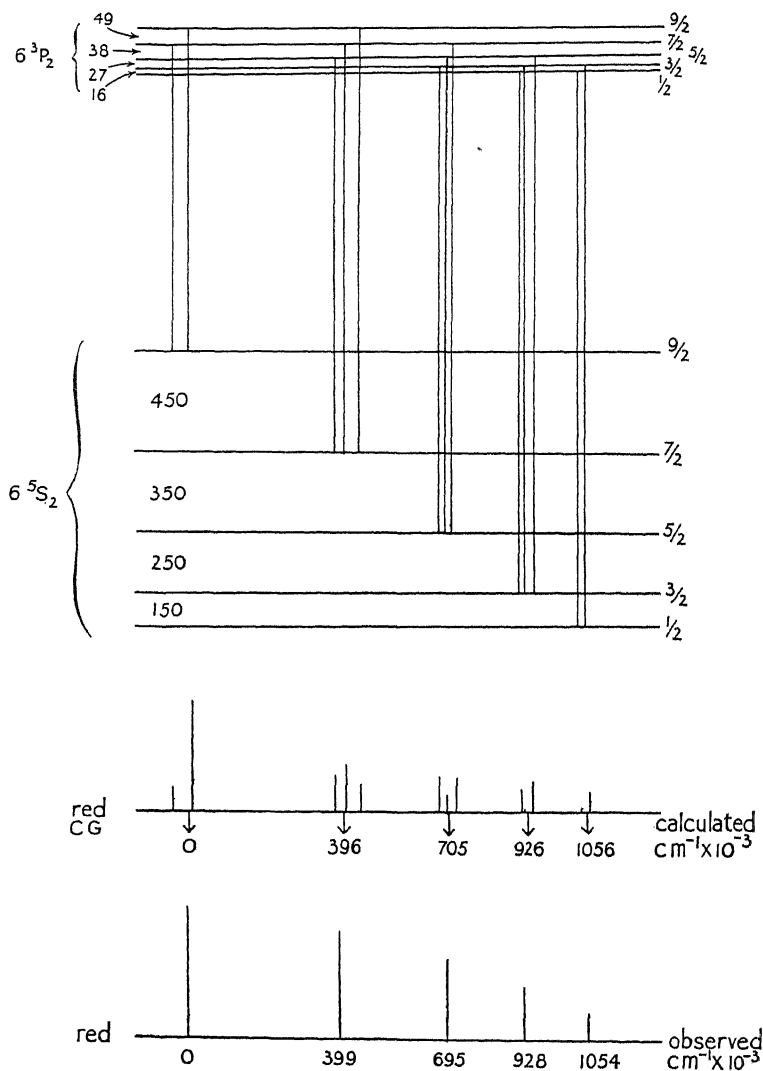


FIG. 2— $\lambda 4632.4$   $6^5S_2 - 6^3P_2$

appreciable differences occur in the intervals in the line structures, although the two sets of interval factors are virtually identical.

A further check on the analysis is given by comparing the observed and calculated structures of  $X_2 - 6^5P_1$  and  $6^5P_1 - 7^5S_2$ . Each line gives a value for  $6^5P_1$ , the values agreeing with that previously found. In

the two very wide terms, where the accuracy of determination is high, namely, in  $X_2$  and  $6\ ^5P_2$ , the interval ratios prove that the nuclear spin is  $5/2$ .

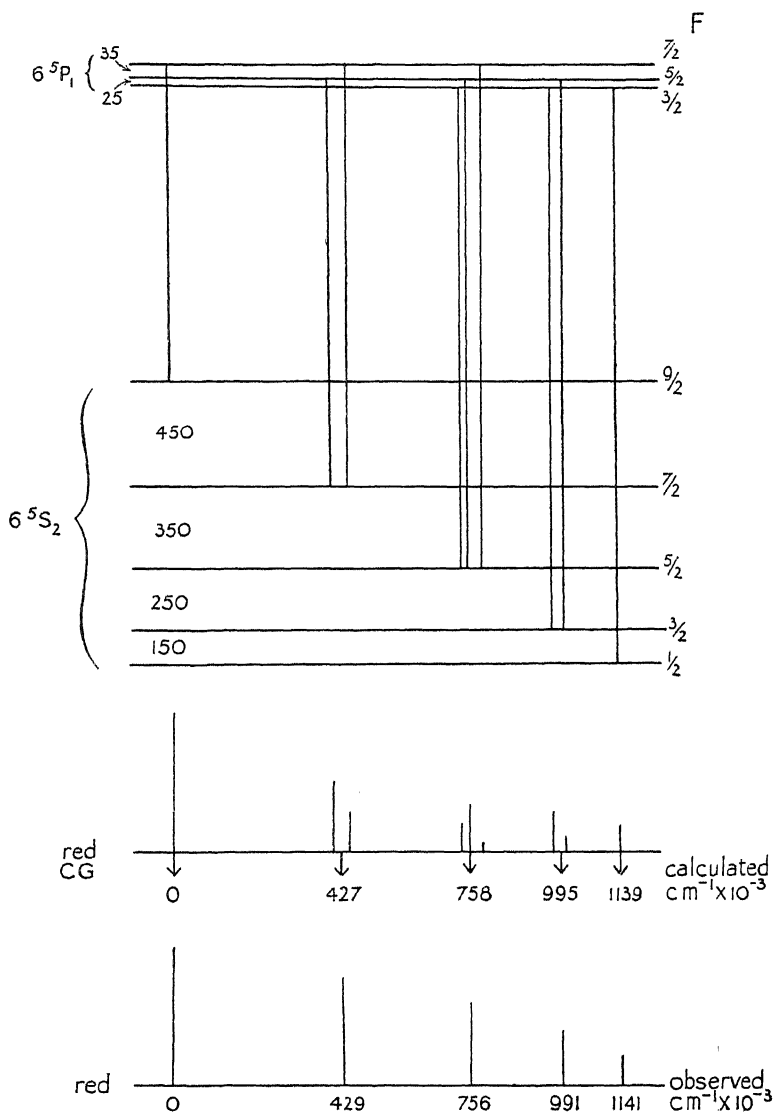


FIG. 3— $\lambda\ 5496.8\ 6\ ^5S_2 - 6\ ^5P_1$

The foregoing method of analysis, when extended to all the classified lines, gives the interval factors of all the terms involved. Table III shows the calculated interval factors. In more than half the terms, the interval factor can be independently calculated from more than one

line, and as illustrated in the previous examples, these values are in excellent agreement. Difficulty was experienced with the line  $6^5S_2-6^5P_2$ . An approximately close value to the interval factor of  $6^5P_2$  is 20, but it is possible that this term either exhibits perturbation or else

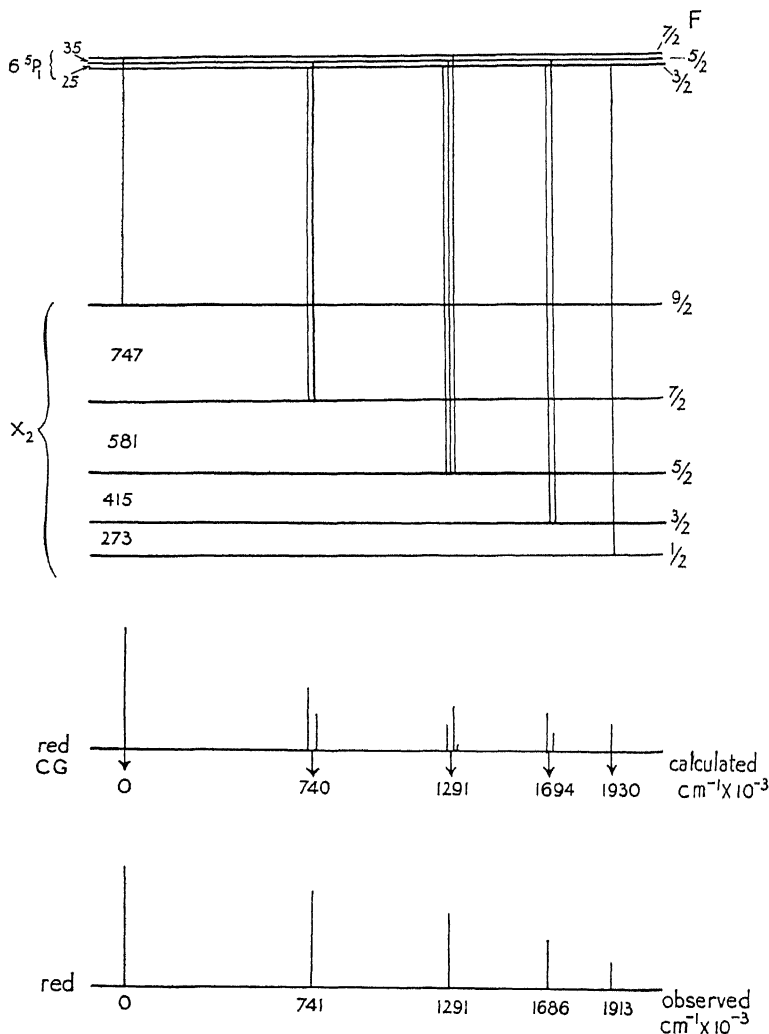


FIG. 4— $\lambda 5774.7$   $X_2-6^5P_1$

the line may be wrongly classified; for difficulty was encountered in trying to fit all the components into a fine structure term scheme.

#### DISCUSSION

Interval factors have been determined for terms based on three electron configurations, namely,  $5s^2 5p^3 6s$ ,  $5s^2 5p^3 7s$  and  $5s^2 5p^3 6p$ . The first

TABLE III—FINE STRUCTURE INTERVAL FACTORS,  $\text{cm}^{-1} \times 10^{-3}$ 

<i>ns</i>		<i>6p</i>	
$X_2$	166	$6^5P_1$	10
$6^5S_2$	100	$6^5P_2$	$\sim 20$
$7^5S_2$	26	$6^5P_3$	10
$6^3S_1$	$5\frac{1}{2}$	$6^3P_0$	0
$7^3S_1$	small	$6^3P_1$	$\sim 25$
		$6^3P_2$	11

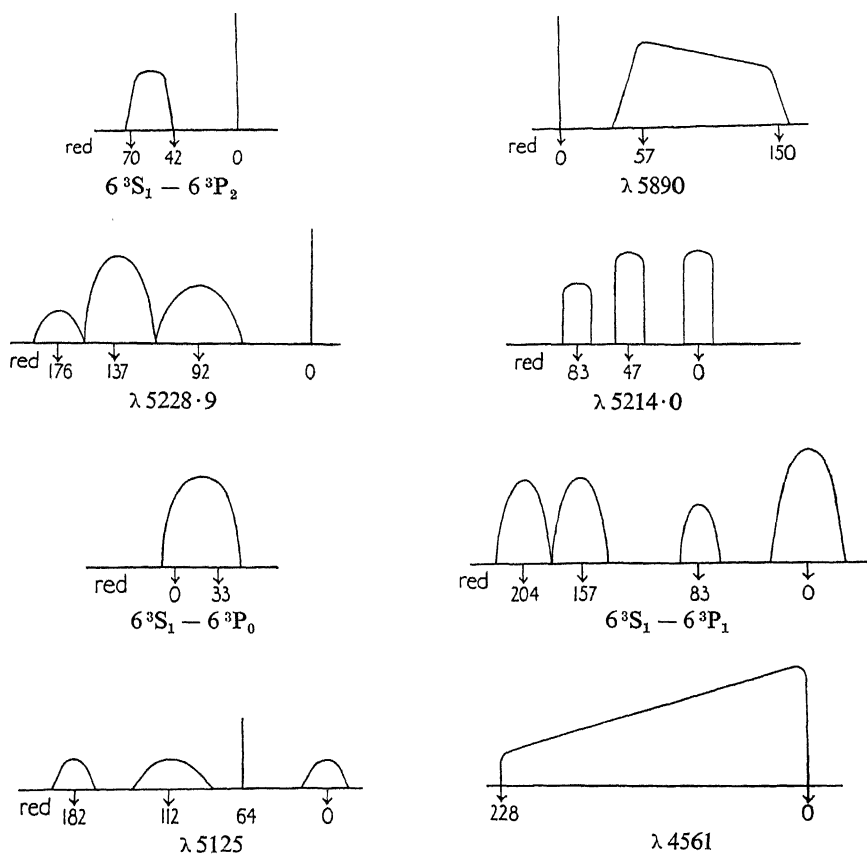


FIG. 5

configuration possesses a penetrating  $6s$  electron so that the coupling between the nucleus and the extra-nuclear system is large in the  $6^5S_2$  term. Therefore the interval factor should be large, as is indeed the case (see Table III). In the  $6^3S_1$  terms the coupling between the  $s$  electron and the  $5p^3$  group is not so favourable as in the  $6^5S_2$  term, for in this case

the spin of the  $s$  electron opposes the resultant  $j$  of the  $5p^3$  group. The interval factor should thus be small, and this is observed.

The  $7^3S_2$  term involves a much less penetrating  $s$  electron than the  $6^5S_2$  term and should therefore have a smaller interval factor than the latter. Actually it is about one-fourth as large. As the structure in  $6^3S_1$  is quite small, it is only to be expected that none can be detected in  $7^3S_1$ . Of interest is the fact that the  $6p$  terms have relatively quite large interval factors, although no  $s$  electron is involved. A similar case occurs in the bromine arc spectrum.\*

The line  $\lambda 6161.9$  is of particular interest. It consists of three extremely sharp components, none of which shows any trace of broadening. The structure is very wide and as the line is in the red, the separations of the components have been measured with a high degree of precision. The visually estimated intensities of the components are as 4:3:2, the intervals being 579 and 370. The interval ratio is thus 1.57:1. The structure, being a triplet, must arise from a term with  $J = 1$ , therefore a nuclear spin of  $5/2$  should result in an interval ratio of 1.40:1. This value is completely outside that determined; in fact, to produce a ratio of 1.40:1 the strongest component would need to be displaced by 52 units. The complete breakdown of the interval rule is not due to the same cause as that which produced the slight irregularities in the interval factors of previous lines, for a displacement of 52 units would only arise if the second term had a sufficiently large interval factor to enable its effect to be resolved. As the lines are very sharp, it must be concluded that a fine structure perturbation has taken place. It is known that when two terms perturb each other, the fine structure levels with the same  $F$  values suffer an apparent repulsion† and by this means the intervals can be distorted, particularly if the perturbing terms have different  $J$  values. The breakdown of the interval rule in the line  $\lambda 6161.9$  is therefore most probably due to perturbation. Perturbed terms may be expected in complex spectra like those of the halogens.

An analysis of the fine structures of the arc lines excited in the hollow cathode is now being carried out, and, as the nuclear spin is now known with certainty, approximately accurate interval constants are being obtained.

Fine structures are also being studied in the second spark spectrum excited by a high frequency electrodeless ring discharge. Details of these structures will be communicated at a later date.

\* Tolansky, 'Proc. Roy. Soc.,' A, vol. 136, p. 585 (1932).

† Schüler and Jones, 'Z. Physik,' vol. 77, p. 811 (1932).

[*Note added in proof: January 12, 1935*—After communicating this paper, a thesis was received from P. Lacroute (Faculty of Science, Paris University, November, 1934), which gives an extensive analysis of the gross structure multiplets in the iodine spark spectrum. Murakawa's classification is confirmed, the terms given by him going to the  $^4S$  series limit. Most of the unclassified lines given above go to the  $^2D$  limit, according to Lacroute who has classified them. The analysis of these lines is now being carried out. The term given above as  $X_2$  is given by Lacroute as  $5d\ ^3D_2$  ( $^4S$ ). It is remarkable that a  $d$  electron term should show such a large interval factor.]

#### SUMMARY

The fine structures of 42 lines of the first spark spectrum of iodine, in the region  $\lambda\lambda$  6600–4500, have been measured by means of a silvered Fabry-Perot interferometer. Eleven classified lines have been analysed, and it is proved that the nuclear spin of iodine is  $5/2$ . Fine structure interval factors have been calculated for 10 terms belonging to the  $5s^2\ 5p^3\ 6s$ ,  $5s^2\ 5p^3\ 7s$ ,  $5s^2\ 5p^3\ 6p$  electron configurations. A fine structure perturbation effect has been found in one unclassified line.

---

# X-Ray Study of the Inter-Diffusion of Copper and Zinc

By E. A. OWEN and LLEWELYN PICKUP, M.Sc. (Lond.), Ph.D. (Wales),  
University College of North Wales, Bangor

(Communicated by Sir William Bragg, O.M., F.R.S.—Received  
November 30, 1934)

Since the publication of Roberts-Austen's\* classical paper describing extensive investigations on the inter-diffusion of metals and alloys, several methods have been employed to study the phenomenon. A comprehensive survey of these has recently been published by Hevesy and Seith.† Only a few investigations have been recorded in which X-ray analysis has been applied to the problem, as it is only during the last few years that X-ray measurements and technique have attained the necessary precision to enable the phenomenon to be examined by this method. The present paper describes an attempt to develop the X-ray method for the investigation of the phenomenon of inter-diffusion in metals.

## METHOD

When a mixture of silver and zinc filings, or copper and zinc filings is heated *in vacuo*, inter-diffusion takes place. The heated mixture, when cool, can be broken up and then used to produce X-ray reflections in the precision camera.‡ In the photographs, the reflection lines from each phase present in the sample are usually well separated and can be studied independently, so that the composition of each phase can be determined from standard parameter-composition curves. The method therefore provides a means of studying any change which occurs in the composition of each phase with time and with change of temperature, and thus it differs from such methods as chemical analysis, zone measurements or electrical resistance, where usually a mean effect is measured. Since 0.01 mm of copper absorbs about 36% of the  $K\alpha$  radiation from copper, the reflected beams registered on the photographic film are produced by the surface layers of the particles, so that as diffusion proceeds, the photographs indicate the changing conditions in the outermost layers only.

\* Bakerian Lecture 1896, 'Proc. Roy. Soc.,' vol. 67, p. 101 (1900).

† 'Z. Electrochem.,' vol. 37, p. 528 (1931).

‡ 'Proc. Roy. Soc., A,' vol. 137, p. 397 (1932); vol. 140, p. 344 (1933).

The method is limited in its application when the metals form a complex phase system. During the very early stages of the diffusion process in such a system, the lattices of the transient phases, such as the  $\gamma$  and other zinc-rich phases in the copper-zinc system, are so distorted in their unstable condition that the reflection lines are not only unresolved, but often hardly show a distinct reflection band at the high reflecting angles covered by the short range of the precision camera. For this reason, measurements are confined in the present investigation to the lines of the  $\alpha$ -phase, although lines from other phases were sometimes recorded on the films.

#### EXPERIMENTAL PROCEDURE

Mixtures of copper and zinc filings were made up by weighing out, accurately, separate quantities of these metals so as to give the desired percentage composition in a 0.4 gramme sample. When thoroughly mixed, the sample was put into a glass tube (into Pyrex for heating at 600° C), and sealed after evacuating to a pressure of about 0.001 mm Hg. These sealed tubes were roughly 1.5 to 2.0 cm long and 0.5 cm in diameter, the mixture occupying about one-fourth of the enclosed volume. They were inserted in holes drilled in a steel block, which fitted closely into an electric furnace. This arrangement enabled a more steady and uniform temperature to be maintained throughout the heating operation. The mixtures "coked" somewhat after being heated, but only gentle crushing was required to powder them. These powders were then used to coat thin flexible sheets of aluminium to make suitable samples for the X-ray camera.

In a preliminary investigation two mixtures were prepared from ungraded filings, one containing 25% zinc with copper and the other 25% zinc with silver. After heating for 19 hours at 300° C the reflection lines obtained were found to be from copper and silver respectively with parameter values  $3.608_0$  Å and  $4.077_1$  Å, but they were relatively weaker in intensity than those from the pure metals. These two mixtures were further heated for 20 hours at about 355° C. On photographing no reflection lines from silver were produced by the silver-zinc mixture, while the reflection lines from copper in the copper-zinc mixture were very faint but in positions to indicate that no measurable change in the parameter value of copper had taken place. These changes in intensity of reflection lines after such comparatively low temperature treatment are indications of the type of diffusion, which finds practical application in commercial sherardizing, a process carried out below 400° C and occupying only a few hours.



On heating other similar mixtures for 18 hours at 435° C, distinct changes in the appearance of both mixtures were noted, that of the copper-zinc being most marked as it showed a yellow brass colour in place of the red copper colour. These mixtures were broken up, powdered in an agate mortar, and heated for 46 hours at 300° C. The object of this additional heating prior to photographing was to eliminate lattice distortion only, since previous work had shown that heating at such low temperatures did not promote any measurable diffusion effect in the times mentioned. The reflection lines from the silver-zinc mixture gave a parameter value of  $4.012_2$  Å, while the corresponding reflections from the copper-zinc mixture were ill-defined and were accompanied by lines reflected by the  $\beta$ -phase of this system. Approximate measurements of the latter photograph gave parameter values of  $3.69_2$  Å for the poor  $\alpha$ -phase lines and  $2.94_4$  Å for the  $\beta$ -phase lines.

This sample was again heated for 18 hours at 480° C, when only one very faint  $\beta$ -phase reflection (parameter value about 2.93 Å) was found to be present, with a strong well-defined reflection doublet from the  $\alpha$ -phase, giving a parameter value of  $3.677_9$  Å.

From such preliminary results two conclusions were drawn, namely, (1) that the diffusion of zinc into copper and into silver takes place in reasonable time under these conditions, only when the temperature is raised above the melting point of zinc, and (2) that during the diffusion process under the present experimental conditions, the phases in the surface layers of the copper particles are produced in order from the zinc-rich end, even when the composition of the mixture as a whole is in the pure  $\alpha$ -region. This second conclusion is based on the following observations: (a) the  $\alpha$ -phase on its first appearance together with some  $\beta$ -phase has a parameter value of about  $3.69_2$  Å, which is near the value of the zinc-saturated  $\alpha$ -phase lattice, 3.696 Å at 400–500° C,\* and (b) as the time of diffusion is increased, the  $\beta$ -phase reflections gradually disappear and the  $\alpha$ -phase parameter decreases until it reaches the value corresponding to the composition of the original mixture. These results were anticipated since the zinc was molten at the initial stages of the diffusion process. The results confirm the conclusions reached by Desch,† from a microscopical examination of the phenomenon. The presence of a phase is only assumed in the present work, when there is some indication of a reflected beam on the film. Owing to the high resolving power of the camera, the composition of a phase so indicated

\* Owen and Pickup, 'Proc. Roy. Soc.,' A, vol. 137, p. 397 (1932).

† See Desch's "Metallography," p. 222.

must necessarily be within fairly narrow limits, but on the other hand it may be possible for a phase to exist in such a distorted condition that no trace of it can be seen on the X-ray film. This, as already stated, is the reason why in this work attention is directed mainly to the  $\alpha$ -phase.

The investigation from this stage was continued with mixtures of copper and zinc because (1) accurate parameter measurements were available from alloys made by the usual melting process, and such data were essential for reference purposes, (2) the copper-zinc system has been subjected to extensive investigation by many workers, some of whom have studied the inter-diffusion of these two metals by different methods.

While it was recognized that numerous factors, such as temperature, time, external form and condition, and internal structure would have important effects on the rate, if not on the nature also, of the diffusion process, it was decided at this preliminary stage to proceed by diffusing an 80% copper of ungraded filings at 450° C for different times to trace, if possible, more closely the general nature of the diffusion process. It was necessary to diffuse for 68 hours before the  $\alpha$ -phase reflection doublet was resolved. After 4, 8, 18 and 30 hours' diffusion, an unresolved  $\alpha$ -doublet was registered, which after an attempt to produce its resolution by heating at 400° C for 4 hours showed little difference in appearance, the parameter also being unchanged in each sample. All subsequent samples were therefore gently broken up and then photographed without any further heat treatment.

It may be recorded here that while annealing at 400° C for 4 hours was found to eliminate the lattice distortion in the filings of an alloy ingot of uniform composition, this treatment did not appear to have any effect on the lattice distortion produced during the inter-diffusion process. It would appear either that two types of distortion exist, only one of which is eliminated by heat treatment, or that in the diffusion product a very great proportion of the mass is chaotic and devoid of uniform lattice formation.

The following table gives a summary of the data supplied by the 80% copper-zinc mixture, heated to 450° C for times ranging from 10 minutes to 120 hours.

Copper radiation was used throughout the investigation, and the reflecting planes responsible for the lines mentioned in the table were (420) for the  $\alpha$ -phase and (321) for the  $\beta$ -phase.

It will be noticed that the  $\beta$ -phase is formed after 10 minutes' diffusion and gives after 20, 35 and 60 minutes' diffusion a constant parameter of  $2.943_4$  Å, which is its value when saturated in the ( $\alpha + \beta$ ) region. When the  $\beta$ -phase disappears, the parameter of the  $\alpha$ -phase is about 3.69

(D. 12)—a value near that of the zinc-saturated  $\alpha$ -phase,  $3.694_7$  A at  $450^\circ$  C. As the time of diffusion is further increased, the  $\alpha$ -phase parameter becomes smaller, approaching ultimately the value  $3.650_0$  A, corresponding to the pure  $\alpha$ -phase alloy containing 80% copper.

TABLE I—80% COPPER MIXTURE DIFFUSED AT  $450^\circ$  C

Time of diffusion	Photo No.	Description and measurement
10 minutes	D. 13	Well defined Cu lines. Dark band due to $\beta$ -phase, with parameter about $2.947$ A.
20 minutes	D. 11	Cu lines as in D. 13. $\beta$ -phase lines just resolved, parameter = $2.943_7$ A.
35 minutes	D. 15	Faint Cu lines still present. $\beta$ -phase as D. 11, parameter = $2.943_2$ A.
1 hour	D. 9	Cu lines as in D. 15. $\beta$ -phase much fainter than in D. 15, parameter = $2.943_4$ A.
2 hours	D. 14	Cu lines fainter than in D. 15. No distinct $\beta$ -phase lines present.
4 hours	D. 12	No Cu or $\beta$ -phase lines. Dark band of saturated $\alpha$ -phase, parameter about $3.690$ A.
8 hours	D. 10	Dark band of $\alpha$ -phase reflection. No resolution, parameter = $3.667$ A.
18 hours	D. 16	Appearance as in D. 10, $\alpha$ -phase, parameter = $3.665$ A.
30 hours	D. 51	$\alpha$ -phase reflection, but not resolved, parameter = $3.658$ A.
68 hours	D. 17	$\alpha$ -phase reflection lines resolved, parameter = $3.658_1$ A.
120 hours	D. 53	$\alpha$ -phase reflection lines resolved, parameter = $3.654_7$ A.

Similar observations and measurements were made on mixtures containing 70 and 90% copper respectively. In the 90% mixture, traces of the pure copper lines could be found after 4 hours' diffusion, but these were absent after 4 hours in the other two mixtures. Though no  $\beta$ -phase reflections were observed in the 90% mixture, the  $\alpha$ -phase appeared with a parameter of  $3.639$  A after 8 hours. The 70 and 80% mixtures showed the transient presence of the  $\beta$ -phase, which had, on its first appearance in both these mixtures, a parameter of  $2.94_7$  A, and disappeared in both with the value  $2.94_3$  A. This phase persisted for about 1 hour in the 80% mixture, and for about 8 hours in the 70% mixture. The two limiting values are approximately those of the  $\beta$ -phase in the  $(\beta + \gamma)$  and  $(\alpha + \beta)$  regions,  $2.949_2$  A and  $2.943_3$  A respectively. The parameter value of

the  $\alpha$ -phase on its first appearance in the 70 and 80% mixtures is near its constant (saturated) value in the  $(\alpha + \beta)$  region.

Owing to the temporary production of the zinc-rich phases during the diffusion process, it is improbable that the same " mechanism " of diffusion exists when zinc diffuses out of a copper-zinc alloy, so that a clear distinction should be made between the experiments described here and those concerning the diffusion of zinc *out of* the  $\alpha$ -phase lattice.

At this stage a further series of photographs was taken to study the effect of temperature on the diffusion process. The temperatures chosen were 450°, 500° and 600° C. From a comparison of the data collected, the diffusion process is shown to be accelerated with increase in temperature, as was anticipated. The time during which the  $\beta$ -phase persists is so shortened with increasing temperature that, although a strong  $\beta$ -phase reflection is found after 2 hours at 500° C in the 70% mixture, no reflection of this phase is shown after 4 hours, while at 450° C its presence extended from after 10 minutes to about 4 hours, when its parameter was practically the same ( $2.943_{\frac{3}{4}}$  Å) as that after 2 hours at 500° C ( $2.942_{\frac{5}{8}}$  Å). At 600° C the  $\alpha$ -phase is formed and its reflection lines are almost resolved after 1 hour's diffusion, even in the 90% mixture. None of the mixtures heated at 600° C showed any distinct indications of the presence of the  $\beta$ -phase. Some typical results are shown in Table II.

It was found, from these preliminary measurements, that when  $\log(M - C)$  was plotted against time ( $t$ ), where  $M$  and  $C$  denote respectively the composition in weight per cent copper of the initial mixture and of the  $\alpha$ -phase after time ( $t$ ), an approximately linear relation was obtained. Assuming this linear relation the calculated curve showing the relation between time of inter-diffusion and composition, passed through the experimental points as well as might be expected (see fig. 1 where the calculated curves are shown for the diffusing temperature of 500° C). But there were irregularities observed at short times of diffusion. These are probably due to ill-defined reflection lines and to complications set up by the disappearance of the  $\beta$ -phase at the time when reflections from the  $\alpha$ -phase begin to appear. It was evident that more precise diffusing conditions were required before definite conclusions could be drawn concerning the laws governing the inter-diffusion of the two metals.

#### IMPROVEMENT IN EXPERIMENTAL PROCEDURE

The investigation was continued along the same lines as those already described, but with special attention paid to the elimination of small fluctuations in temperature during the periods of heating, and to the preparation

TABLE II

% copper in mixture (M)	Diffusing temperature 450° C			Diffusing temperature 500° C		
	Time of diffusion in hours (t)	Mean $\alpha$ -phase parameter in A	% copper in $\alpha$ -phase (C)*	Time of diffusion in hours (t)	Mean $\alpha$ -phase parameter in A	% copper in $\alpha$ -phase (C)*
70	4	3.69 <sub>5</sub>	62.1	1	3.689 <sub>1</sub>	64.4
	8	3.68 <sub>7</sub>	64.8	4	3.687 <sub>5</sub>	65.0
	12½	3.686 <sub>0</sub>	65.6	8	3.686 <sub>6</sub>	65.4
	18	3.684 <sub>5</sub>	66.1	14	3.684 <sub>5</sub>	66.2
	45	3.680 <sub>5</sub>	67.6	15½	3.681 <sub>7</sub>	67.2
	70	3.677 <sub>7</sub>	68.7	24	3.680 <sub>0</sub>	67.8
	140	3.674 <sub>8</sub>	69.8	40	3.675 <sub>1</sub>	69.7
80				70	3.674 <sub>4</sub>	70.0
	4	3.690	63.9	1	3.674 <sub>6</sub>	70.0
	8	3.666 <sub>8</sub>	73.2	2	3.676 <sub>7</sub>	69.0
	12½	3.660 <sub>3</sub>	75.6	4	3.670 <sub>0</sub>	71.5
	30	3.657 <sub>8</sub>	76.7	7	3.662 <sub>8</sub>	74.6
	65	3.655 <sub>1</sub>	77.8	12	3.661 <sub>5</sub>	75.2
	140	3.650 <sub>0</sub>	80.0	15	3.658 <sub>8</sub>	76.2
90				40	3.652 <sub>3</sub>	78.9
	8	3.639	84.7	70	3.650 <sub>0</sub>	79.9
	12½	3.637 <sub>5</sub>	85.4	14	3.636 <sub>6</sub>	85.8
	18	3.637 <sub>0</sub>	85.6	40	3.632 <sub>4</sub>	87.8
	43	3.631 <sub>2</sub>	88.3	70	3.630 <sub>0</sub>	89.0
	70	3.630 <sub>9</sub>	88.5			
	140	3.629 <sub>8</sub>	89.3			

\* These values of the compositions were obtained from the parameter values by means of a parameter-composition curve previously determined.

of particles of more uniform size. Temperatures were kept constant over prolonged periods by supplying the heating current to the electrical resistance furnaces from a 150-volt storage battery of large capacity, and maintaining a constant reading on an accurate ammeter connected in the circuit. Also the filings, after removing traces of iron, were graded by means of wire gauze sieves, the mean square side of the apertures in which were ascertained as accurately as possible with a Hilger travelling microscope. The mean values are given in Table III.

With these sieves, five different grades of particles were obtained as shown in Table IV, where the "grade value" for each is taken as the mean between the square side of the aperture which retains the filings.

TABLE III

Nominal number of apertures per inch	Mean square side of aperture in mm	Nominal number of apertures per inch	Mean square side of aperture in mm
100	0.15 <sub>0</sub>	160	0.09 <sub>0</sub>
120	0.12 <sub>8</sub>	180	0.08 <sub>0</sub>
140	0.10 <sub>0</sub>	200	0.06 <sub>8</sub>

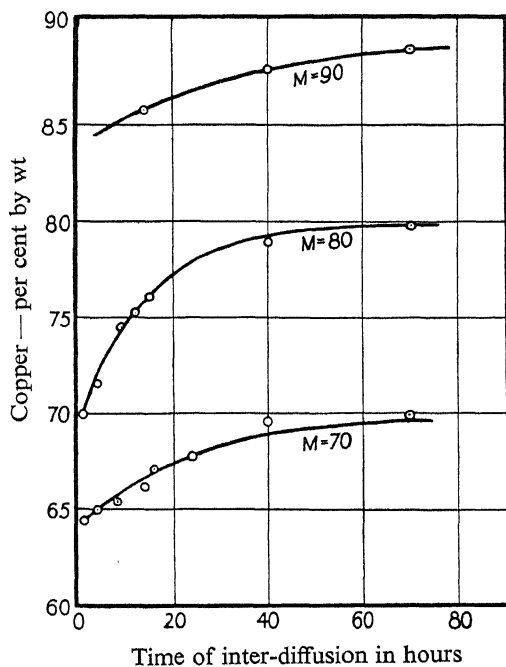


FIG. 1

and that of the next larger aperture which allows the particles to pass through. Two nests of these sieves were made, one for grading the copper filings, the other for the zinc filings.

TABLE IV

Through	Grade Retained by	Grade value
100	120	0.139
120	140	0.114
140	160	0.095
160	180	0.085
180	200	0.073

Apart from these two important precautions, information was desirable on other points such as the effect of possible contamination of the surfaces of the particles when exposed to the laboratory atmosphere. It was found that an exposure of the particles to the atmosphere for 3 days had no measurable effect on the diffusion process. An exposure of 40 days showed that contamination did have a marked effect. Precaution was taken, however, to enclose the mixtures in evacuated glass containers on the same day as that on which the filings were prepared, without undue exposure to the atmosphere.

Since Elam has shown that the diffusion of zinc into a single crystal of copper takes place slowly at comparatively low temperatures, graded copper filings were annealed at 500° C for 1½ hours before mixing them with the zinc. This annealing eliminated the lattice distortion produced by the filing, and tended to increase somewhat the grain size within the particles. To show the effect of this preliminary annealing on the rate of inter-diffusion, the results of experiments carried out on four samples diffused at 450° C for 15 hours are summarized in Table V.

TABLE V

Grade value	Condition of copper	$\alpha$ -phase parameter (A)
0.114 .....	{ Not annealed .....	3.665 <sub>3</sub>
	{ Annealed at 500° C for 1½ hours ..	3.665 <sub>9</sub>
Less than 0.066 .....	{ Not annealed .....	3.653 <sub>0</sub>
	{ Annealed at 500° C for 1½ hours ..	3.655 <sub>0</sub>

Only the small grade particles show a difference when the copper is annealed before mixing. Since the parameter values diminish as the diffusion proceeds, the above observations show that for small grade particles, the diffusion has not proceeded so far in the presence of annealed copper as it has in the presence of the unannealed material. Inter-diffusion thus takes place more readily with distorted (unannealed) crystals than with undistorted (annealed) crystals. This is in accordance with Elam's conclusions. No measurable effect was observed with the larger grade particles probably because the ratio of the amount of undistorted metal within the particles to the amount of distorted metal in the surface layers before annealing was greater in the large grade than in the small grade filings.

Owing to the unstable conditions of the structure, especially in the initial stages of the inter-diffusion, the reflection lines of the  $\alpha$ -phase, on

their first appearance, are ill-defined and unresolved. As inter-diffusion proceeds, these lines become more definite and are finally resolved.

In addition to the effect of the progress of diffusion on the appearance of the reflection lines, it was found that if the expansion of the mixture during the period of diffusion was hindered by the walls of the glass container, the definition of the reflection lines was impaired, although no difference in the value of the parameter was found from this cause. In order to obtain reflections as well defined as possible at each stage of the heating, the glass containers were therefore heated in a horizontal position in the furnace, with the mixture evenly distributed over the lower portion, so as to allow free expansion into the space above.

#### EFFECT OF PARTICLE SIZE ON INTER-DIFFUSION

Using five grades of particles, mixtures were prepared containing 80% copper. These were heated at 450° C in evacuated tubes for different times. Owing to the complex conditions which arise during the early stages of inter-diffusion when the zinc-rich phases consecutively but rapidly form and disappear, measurements were carried out as before on the  $\alpha$ -phase parameter.

The procedure of mixing particles of each grade of copper with particles of zinc of the same grade was still adopted as it was considered that a more intimate and uniform initial mixture could be obtained in this way. The experimental data which were obtained with these five grades of mixtures, for times ranging from 12½ to 185 hours, are collected in Table VI.

From these results the curves in fig. 2 were prepared. It is seen that (1) the extent of inter-diffusion in a given time is greater, the lower the grade value, (2) the relation between the parameter value and grade value is linear for each fixed time, and (3) the change in parameter value as the grade value increases becomes less as the time of inter-diffusion increases.

#### RELATION BETWEEN COMPOSITION AND THE TIME OF INTER-DIFFUSION AT CONSTANT TEMPERATURE

This relation can be derived for the temperature 450° C from the curves in fig. 2, by reading off the parameter values for the different times corresponding to each grade value. These readings are given in Table VII together with additional experimental data obtained later.

When the values of  $\log_{10} (80 - C)$  and  $t$  given in this table are plotted for each grade, a linear relation, in accordance with the results of the



TABLE VI—TEMPERATURE OF DIFFUSION 450° C

Time of diffusion hours	Grade value mm	$\alpha$ -phase parameter A	Time of diffusion hours	Grade value mm	$\alpha$ -phase parameter A
12½	0·073	3·662 <sub>2</sub>	48	0·073	3·653 <sub>4</sub>
	0·085	3·665 <sub>8</sub>		0·085	3·655 <sub>4</sub>
	0·095	3·668 <sub>4</sub>		0·167	3·665 <sub>3</sub>
	0·114	3·673 <sub>2</sub>			
	0·139	traces of $\beta$ -phase present			
15	0·073	3·658 <sub>8</sub>	82	0·073	3·653 <sub>0</sub>
	0·114	3·668 <sub>4</sub>		0·095	3·655 <sub>0</sub>
	0·139	3·674 <sub>3</sub>		0·114	3·656 <sub>4</sub>
				0·139	3·659 <sub>3</sub>
20	0·073	3·657 <sub>2</sub>	185	0·073	3·651 <sub>7</sub>
	0·085	3·659 <sub>5</sub>		0·085	3·652 <sub>5</sub>
	0·095	3·661 <sub>1</sub>		0·095	3·653 <sub>6</sub>
	0·114	3·664 <sub>1</sub>		0·114	3·654 <sub>0</sub>
	0·139	3·668 <sub>0</sub>		0·139	3·656 <sub>4</sub>

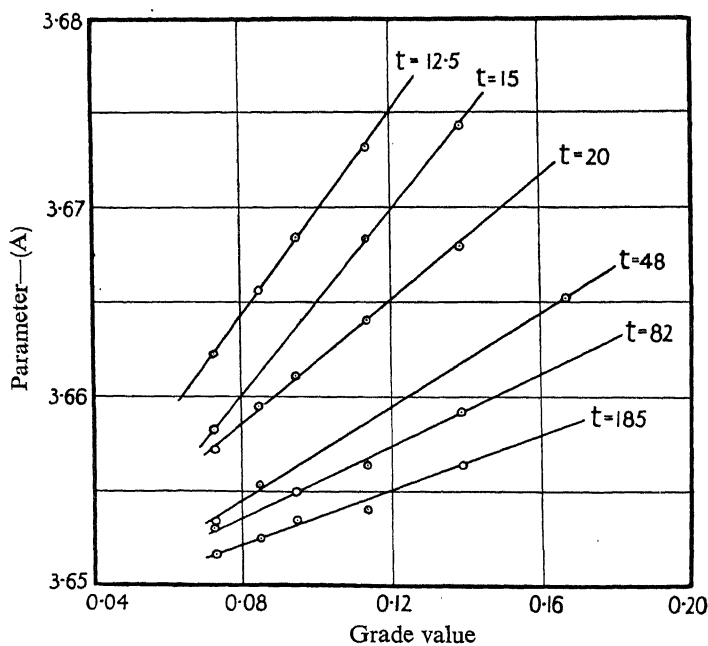


FIG. 2—Temperature of inter-diffusion 450° C, time (t) in hours

TABLE VII—TEMPERATURE OF DIFFUSION 450° C

Grade value mm	Time of diffusion hours	$\alpha$ -phase parameter A	Composition % copper by weight (C)	$\log_{10} (80 - C)$
0.073	12½	3.662 <sub>2</sub>	74.8	0.716
	15	3.658 <sub>3</sub>	76.4	0.556
	20	3.657 <sub>2</sub>	76.8	0.505
	48	3.653 <sub>6</sub>	78.4	0.204
	82	3.653 <sub>0</sub>	78.7	0.113
	185	3.651 <sub>6</sub>	79.2	1.903
0.085	12½	3.665 <sub>5</sub>	73.4	0.820
	15	3.661 <sub>2</sub>	75.2	0.681
	20	3.659 <sub>3</sub>	76.0	0.602
	48	3.655 <sub>2</sub>	77.8	0.340
	82	3.654 <sub>2</sub>	78.1	0.278
	185	3.652 <sub>4</sub>	78.8	0.079
0.095	12½	3.668 <sub>2</sub>	72.4	0.881
	15	3.663 <sub>7</sub>	74.2	0.763
	20	3.660 <sub>9</sub>	75.3	0.672
	30*	3.658 <sub>7</sub>	76.2	0.580
	40*	3.656 <sub>9</sub>	77.0	0.477
	48	3.656 <sub>4</sub>	77.4	0.415
	82	3.655 <sub>1</sub>	77.8	0.342
	185	3.653 <sub>1</sub>	78.6	0.146
0.114	12½	3.673 <sub>2</sub>	70.3	0.987
	15	3.668 <sub>3</sub>	72.4	0.881
	20	3.664 <sub>0</sub>	74.0	0.778
	48	3.658 <sub>8</sub>	76.4	0.556
	82	3.656 <sub>9</sub>	77.0	0.477
	185	3.654 <sub>5</sub>	78.0	0.301
0.139	12½	3.680 <sub>1</sub>	67.8	1.086
	15	3.674 <sub>4</sub>	70.0	1.000
	20	3.668 <sub>2</sub>	72.4	0.880
	30*	3.663 <sub>2</sub>	74.4	0.748
	40*	3.662 <sub>2</sub>	74.8	0.716
	48	3.661 <sub>9</sub>	75.2	0.681
	70*	3.659 <sub>2</sub>	76.0	0.602
	82	3.659 <sub>3</sub>	76.1	0.591
	120*	3.657 <sub>8</sub>	76.6	0.532
	185	3.656 <sub>4</sub>	77.2	0.447

\* Additional data obtained later.

preliminary investigation on ungraded particles, is found for times greater than about 70 hours. For shorter periods there is a marked deviation from this linear relation. The experimental data for short periods are less accurate than those for long periods of diffusion as the reflections are not well defined in the former case, but the deviations observed are well outside the limits of error of measurement. These deviations are no doubt due to the complicating influence of the  $\beta$  and other zinc-rich phases occurring at the initial stages. To investigate this, a detailed study was made of the data concerning grade value 0.139 in Table VII, for which several periods of diffusion were taken. The values of  $\log_{10} (80 - C)$  for this grade are plotted against time of

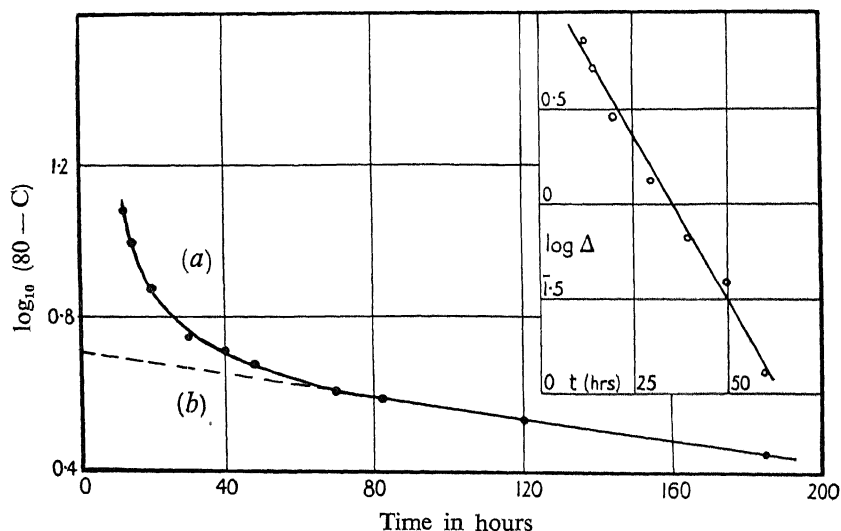


FIG. 3.

diffusion in fig. 3. This curve may be analysed into two components by continuing the straight portion along the dotted line (b) and taking the difference between its ordinates and those of curve (a). By plotting the logarithms of the difference in composition thus found against the corresponding times (fig. 3, inset), another approximately linear relation is obtained.

The influence of the  $\beta$ -phase operates strongly during the initial stages when the  $\alpha$ -phase composition is near its saturation value. This phase is disappearing quickly and as a result its lattice is so distorted when it breaks up that no regular reflection from it can be expected on the precision camera, but its temporary presence does affect the rate of diffusion as measured by the change of the  $\alpha$ -phase parameter.

Hence to account for the experimental curves we are led to the following relation between the  $\alpha$ -phase composition (C) and the time ( $t$ ) during which inter-diffusion has taken place at constant temperature,

$$M - C = K_1 e^{-m_1 t} + K_2 e^{-m_2 t} \quad (1)$$

where  $M$  is the composition of the undiffused mixture,  $K_1$ ,  $K_2$ ,  $m_1$  and  $m_2$  are constants,\* which are functions of the diffusing conditions (including temperature). The value of  $C$  cannot be less than that of the saturated composition of the  $\alpha$ -phase at the temperature of diffusion. It reaches this value some time after the heating process is commenced.

It does not appear possible to obtain a simpler relation between composition and time to represent the process of inter-diffusion when there are two or more phases present and the relation given, doubtless, does not represent the very initial stages of the diffusion process. When  $t$  is large,  $(M - C)$  is small and expression (1) takes the simpler form,

$$(M - C) = K e^{-m t} \quad (2)$$

When a mass of copper-zinc alloy consisting entirely of unsaturated  $\alpha$ -phase but with a heterogeneous composition is annealed at a constant temperature to produce a homogeneous composition, the process which brings about homogeneity conforms to expression (2). The rate of inter-diffusion ( $dC/dt$ ) at any instant under these conditions would therefore be proportional to the difference between the final composition after complete diffusion (the composition of the initial mixture) and the  $\alpha$ -phase composition at that instant.

It has been observed that the transitory production of one or more phases during the process of the inter-diffusion of two pure metals has a marked effect on the phenomenon; in fact the whole process is governed by the phases present in the thermal equilibrium diagram of the two metals. This point does not appear, in every case, to have received due attention when interpreting experimental work on the inter-diffusion of metals forming complicated systems.

#### EFFECT OF TEMPERATURE ON INTER-DIFFUSION

Since measurements are made on the  $\alpha$ -phase alone, the changes in its composition when saturated at different temperatures are to be taken into account when studying the influence of temperature on the rate of inter-diffusion.

\* For particles of grade value 0.139, diffused at 450° C, the following values of the constants were found:  $K_1 = 5.035$ ,  $m_1 = 0.0032$ ,  $K_2 = 17.38$ , and  $m_2 = 0.079$ .

In Table VIII, data on particles of two grade values are given for different temperatures and times of diffusion for 80% copper mixtures. These are illustrated in fig. 4. To interpret the curves, the effect of two factors are to be considered, (1) the change in the rate of inter-diffusion

TABLE VIII—80% COPPER MIXTURES

Time hours	Temperature °C				
	450	484	528	565	623
GRADE VALUE 0.114 MM					
12½	70.3	71.2	74.7	76.7	78.5
24	74.4	75.1	76.4	77.8	79.1
48	76.4	77.2	78.1	78.6	—
96	77.2	77.2	77.9	—	—
GRADE VALUE 0.085 MM					
12½	73.4	74.2	76.8	77.7	79.3
24	76.8	77.2	78.0	78.8	79.7
48	77.8	77.4	79.3	79.2	—
96	78.4	78.3	78.3	—	—

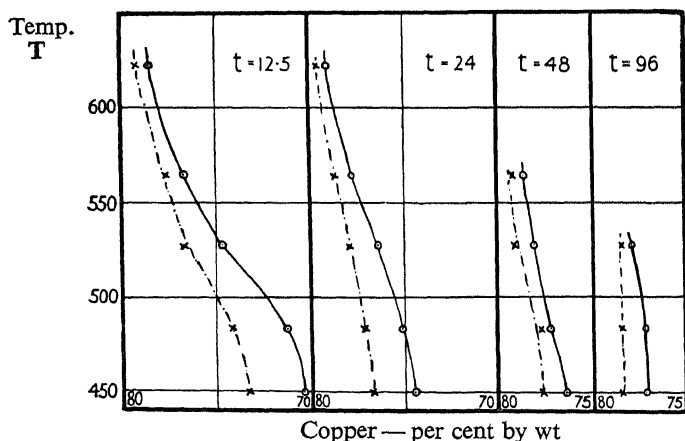


FIG. 4. —○—○— grade value 0.114 mm, —×—×— grade value 0.085 mm, time ( $t$ ) in hours

due to thermal agitation, which is considered here as the true temperature effect sought; and (2) the change just mentioned, in the solubility of zinc in the  $\alpha$ -phase which is represented by the form of the ( $\alpha$ ) — ( $\alpha + \beta$ ) boundary in the thermal equilibrium diagram of copper-zinc alloys. There is some similarity between the form of this boundary and the curves in fig. 4 for short times of inter-diffusion, when the composition

is near that of the boundary. While this effect of solubility on inter-diffusion cannot be definitely established from the present data, the results are sufficient to show that it may have an important bearing on the phenomenon of inter-diffusion in the case of complex systems.

To continue the investigation of the influence of temperature on inter-diffusion the difficulties which arise from the transient production of phases must, if possible, be eliminated. The work is being continued with this object in view.

We are much indebted to the Department of Scientific and Industrial Research for a grant which enabled us to carry out the investigation.

#### SUMMARY

An account is given of the application of X-ray analysis to the study of the inter-diffusion of copper and zinc in powder form. Mixtures of filings of these metals were heated for different times and at different temperatures in evacuated tubes. From the measured parameters of the  $\alpha$ -phase the composition of the surface of the particles was obtained by the aid of a standard parameter-composition curve.

From preliminary work done with ungraded particles it was found that copper-zinc alloys can be prepared in powder form by the inter-diffusion of filings at temperatures much below the melting point of copper, but that inter-diffusion takes place, in reasonable time, only when the temperature of diffusion is above the melting point of zinc. It was possible to detect on the photographs, in addition to the  $\alpha$ -phase, the production and disappearance of the  $\beta$ -phase from its reflection lines. The existence of the  $\gamma$ -phase was not revealed.

No effect on the rate of diffusion was observed when the particles were exposed to the atmosphere for short intervals but prolonged exposure produced a measurable effect.

Inter-diffusion takes place more readily between unannealed than between annealed particles, that is, more readily with distorted structures.

The results obtained with graded particles showed that the amount of inter-diffusion taking place in a given time is greater the smaller the size or the lower the grade value of the particle. The rate of change of parameter value or composition with increasing grade value or particle size diminishes as the time of inter-diffusion increases. A linear relation exists between the parameter value and the grade value for a given time of inter-diffusion.

The relation between  $\alpha$ -phase composition and time of inter-diffusion at constant temperature is given by

$$M - C = K_1 e^{-m_1 t} + K_2 e^{-m_2 t}$$

where  $M$  is the composition of the undiffused mixture,  $K_1$ ,  $K_2$ ,  $m_1$  and  $m_2$  are constants which are functions of the diffusing conditions including temperature. When  $t$  is large, this becomes

$$M - C = K_1 e^{-m_1 t}$$

The influence of temperature on inter-diffusion could not be satisfactorily studied owing to complications brought about by the change in the solubility of zinc atoms in the  $\alpha$ -phase solid solution with temperature.

In general, the trend of inter-diffusion between two metals as revealed by microscopical examination is confirmed in this X-ray investigation.

## The Diurnal Variation of Magnetic Disturbance in High Latitudes

By J. M. STAGG, M.A., B.Sc.

(*Communicated by G. C. Simpson, F.R.S.—Received November 30, 1934*)

1—The effect of natural disturbance on the earth's magnetic field at any one place is at least twofold:

- (i) to introduce a regular variation ( $S_d$ ) periodic within the day and additional to, as well as different in type from (except in a limited region round the magnetic axis pole), the variation associated with quiet days ( $S_q$ ); and
- (ii) to superpose on  $S_d$  irregular changes which may either be of the distinctive type peculiar to large storms especially in low latitudes and generally preceded by the particular type of perturbation known as a sudden commencement, or the changes in the field may be of the apparently nondescript class which comprises an unlimited variety of short-period irregular oscillations.

Of these effects of disturbance  $S_d$  is definitely a local time phenomenon: the sudden commencement with subsequent depression in the horizontal

component of the field as definitely follows universal time. For the irregular and unclassified oscillations which form such a common feature of magnetic records at observations in moderate and high latitudes a diurnal variation in their incidence has been shown to exist for a few isolated localities. But in the general view it is not known whether this aspect of disturbance is controlled by local or universal time. Nor is it known whether the form of the diurnal variation in disturbance (which variation we shall denote by  $D$ ) varies in any systematic way with latitude.

It is the object of this paper to summarize the results of an investigation of these aspects of irregular magnetic disturbance.

2—The observatories whose data will be used together with their geographical co-ordinates ( $\phi$ ,  $\lambda$ ), magnetic latitude ( $\phi_m$ ) computed with reference to the magnetic axis pole at  $78.5^\circ$  N,  $69.0^\circ$  W, the kind of disturbance index used, and the period covered by the data are given in Table I in descending order of  $\phi_m$ .

TABLE I

Observatory	$\phi$ °	$\lambda$ °	$\phi_m$ °	Period covered	Disturbance index used
Thule . . . . .	76.5 N	68.9 W	88.0	2 months	Hourly ranges ( $Zr_Z \cdot 10^{-4}$ )
Godhavn . . . . .	69.2 N	53.5 W	79.8	13 months	Hourly ranges ( $Hr_H + Zr_Z \cdot 10^{-4}$ )
Cape Evans . . . .	77.6 S	166.4 E	78.9	22 months	Character figures
Kingua Fjord . .	66.6 N	67.3 W	78.1	13 months	Frequency of disturbed hours
Gauss Land . .	66.0 S	89.6 E	76.1	10 months	Characters
Cape Denison	67.0 S	142.7 E	75.5	15 months	Characters and hourly ranges
Fort Rae . . . . .	62.8 N	116.1 W	69.0	13 months	Hourly ranges ( $Hr_H + Zr_Z \cdot 10^{-4}$ )
Sodankylä . . . .	67.4 N	26.6 E	63.8	14 years	Frequency of disturbed hours
Eskdalemuir . .	55.3 N	3.2 W	58.5	12 years	Character figures and hourly ranges
Wilhelmshaven	53.5 N	8.1 E	54.5	2½ years	Character figures

Disturbance measures for the two months January and June, 1933, will also be used in discussing the change of general irregular disturbance with approach to the axis pole. These will refer to all but the Antarctic and Kingua Fjord stations in the above list with the addition of Abisko, Sitka, and Lerwick.



It will be noted that the index of disturbance used in determining the form of  $D$  at the various stations is neither simple nor uniform throughout the list. The primary reason for this is that such investigations are seldom catered for in the published material from magnetic observatories. We must therefore use whatever indirect information is available in isolated publications. Except for the data from the First International Polar Year station (1882–83) at Kingua Fjord, where the measure of disturbance was assigned on the basis of three readings at intervals of 1 minute centred at each exact local hour, the unit of time has been the full hour. Allotted originally on a 0, 1, 2 scale either following the practice adopted internationally for whole days, or on the basis of arbitrary limits usually depending on the range of irregular disturbance within the hour, the character figures have been in the main restricted to the 2's, thus eliminating all but the most disturbed hours.

The use of the product of the mean value of the force element of the magnetic field ( $H$  or  $Z$ ) and the hourly range in that element ( $r_H$  or  $r_Z$ )

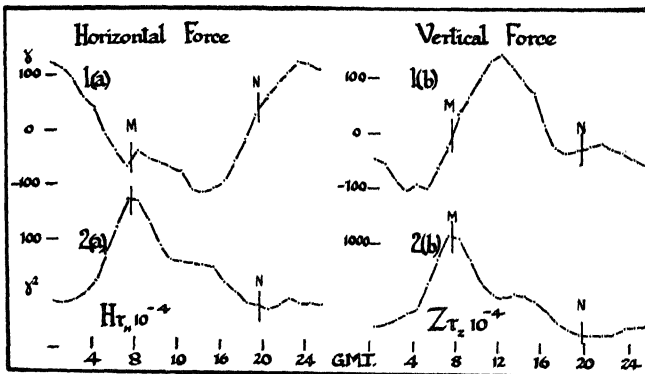


FIG. 1—Regular daily disturbance variation and incidence of irregular disturbance from hourly ranges: Fort Rae

imitates the procedure now undergoing international trial for the characterization of whole days. At observatories with  $\phi_m > 60^\circ$  the use of the combined products ( $Hr_H + Zr_Z$ ) in place of the product for the vertical force alone makes little or no difference to the form of  $D$ , since  $Z$  in such latitudes is of the order of 0.5 gauss and  $H$  falls steadily from 0.1 gauss at  $60^\circ$  to 0.04 gauss near the magnetic axis pole, the ranges in both components remaining of the same order.

3—Anticipating one of the results of the investigation it may be said that  $D$  is found to be controlled by local time over a range of  $\phi_m$  extending at least from  $55^\circ$  to the magnetic axis pole. Now the regular disturbance

variation  $S_d$  at a station in such a latitude as Fort Rae has a range exceeding 400  $\gamma$  in the average of five disturbed days per month in a magnetically quiet year. In such latitudes the contribution of the hourly rate of change of  $S_d$  to the hourly ranges used in typifying D might be considered overwhelming in comparison with the contribution of the irregular perturbations with whose daily variation we are here primarily concerned. If such were the case D might be expected *a priori* to be a local time phenomenon. Fig. 1 makes it clear that the facts are wholly otherwise. 1a and 1b represent  $S_d$  for H and Z respectively at Fort Rae on representative disturbed days. 2a and 2b are the corresponding D's for all days based on  $Hr_H$  and  $Zr_Z$ . Whereas 1a and 1b are completely dissimilar, 2a and 2b are almost identical, due regard being given to the scale which is 10 times greater for  $Zr_Z$  than for  $Hr_H$ . It may therefore be safely assumed that the hourly range data cannot be regarded simply as the time differentials of the corresponding  $S_d$ 's.

4—Fig. 2 shows D for the year as a whole at all the stations, in the same order of  $\phi_m$ , given in Table I. All the curves are arranged according to local time as nearly as the original time base of assignment of disturbance indices will allow. Where G.M.T. has been used in the original tabulations and when the nearest local whole hour differs appreciably from the Greenwich hour, the times of true local noon and midnight have been indicated on the curves. To show effectively the incidence of

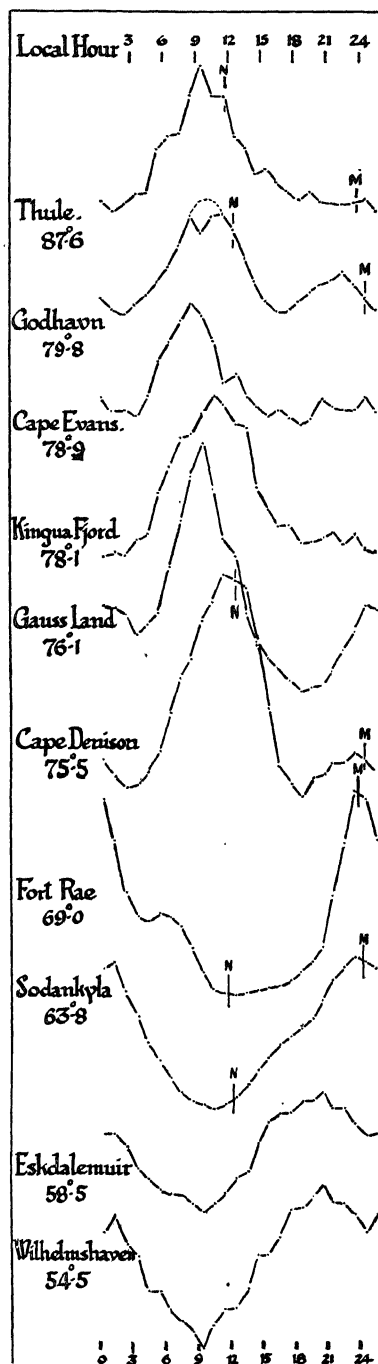


FIG. 2—Change of daily variation in incidence of disturbance with longitude and latitude

the late evening maximum the first two hours of each day have been repeated.

In fig. 2 the curves for Sodankylä, Eskdalemuir, and Rae make it clear that over a wide range of longitude the incidence of irregular disturbance has a very pronounced diurnal variation, and that, within an interval short compared with the local time difference between the two extreme stations ( $9\frac{1}{2}$  hours), the maximum in  $D$  occurs about the same local time in the evening at all three stations. Further, within the zone represented by these three stations ( $\phi_m$   $58^\circ$  to  $69^\circ$ ) the time of this maximum varies in a systematic way with  $\phi_m$ . At Eskdalemuir the time is  $21\frac{1}{2}$ h, Sodankylä 23h, and Fort Rae 24h. Wilhelmshaven ( $\phi_m = 55^\circ$ ) has its maximum slightly before 21h. We therefore conclude that up to  $69^\circ$   $D$  is controlled by local time, that  $D$  has its maximum invariably in the late evening hours and that there is a disposition for the time of the maximum to be delayed with increasing  $\phi_m$  at the rate of approximately 1 hour every  $5^\circ$ .

5—Extending the inquiry into the behaviour of  $D$  beyond  $70^\circ$ , the upper six curves of fig. 2 represent localities (in both hemispheres) up to within  $2^\circ$  of the magnetic axis pole. In the curve for Godhavn the dotted part indicates the probable course of the disturbance variation at 10–11h, had not the measurement of hourly ranges unavoidably suffered artificial reduction at the time of changing of the photographic record (see also fig. 3). Taken together these six representations of  $D$  show that above  $70^\circ$  (as below) disturbance is distributed during the day in a regular manner, and is controlled by local time right up to the axis pole. But in contrast to the state of affairs below  $70^\circ$  disturbance between  $75^\circ$  and the pole has its primary maximum invariably in the forenoon, taking the year as a whole. Again, and also in contrast to stations below  $70^\circ$ , there is strong evidence of a semidiurnal wave in  $D$  from  $75^\circ$  to  $80^\circ$  at least, producing a secondary maximum in the late evening. But beyond  $80^\circ$  this secondary maximum becomes vanishingly small till, within  $2^\circ$  of the axis pole, the hours before midnight are almost the quietest hours of the day.

6—Further insight into the remarkable change in  $D$  above  $70^\circ$  will now be sought by subdividing the whole year's data represented in fig. 2 into constituent seasons. Fig. 3 shows the separate seasonal curves for Godhavn and Fort Rae, for which two stations  $D$  is represented by the most strictly comparable and extensive data covering the identical months of the recent International Polar Year 1932–33. From these curves it is

obvious that the transition from winter through equinox to summer at Fort Rae entails no radical change in the type of D. The pronounced maximum at midnight remains steady except for a questionable retardation by about an hour in winter.

At Godhavn, on the other hand, there is a systematic change in the form of D from winter to summer. Even after making due allowance for the artificial depression it is clear that disturbance in winter at Godhavn

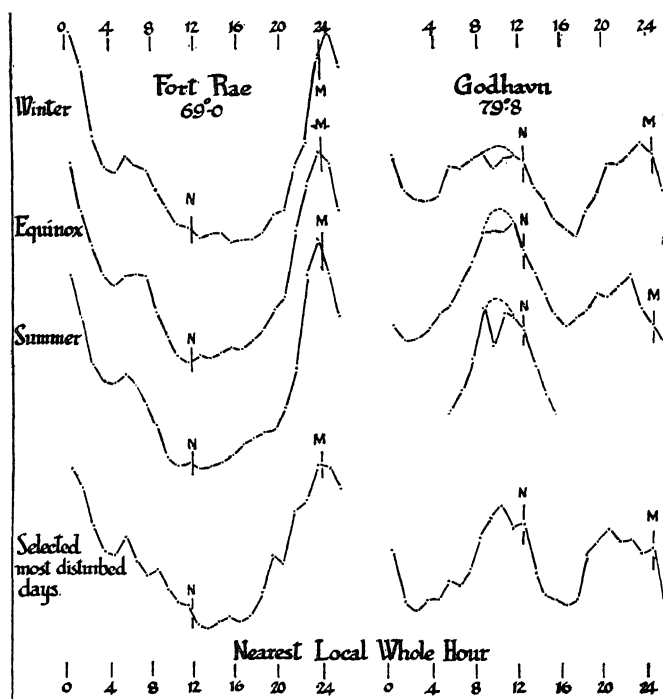


FIG. 3—Change of daily variation of disturbance at Fort Rae and Godhavn with season and disturbance

is as highly developed in the evening as in the forenoon hours; in summer the evening disturbance practically vanishes.

7—The evidence of the upper two curves in fig. 4 for the Antarctic station at Cape Denison ( $\phi_m = 75.5^\circ$ ) indicates that a precisely similar systematic seasonal change in the incidence of disturbance already prevails  $4^\circ$  below the latitude of Godhavn, *i.e.*, within  $6^\circ$  of Fort Rae. The two lower curves of the same figure showing the daily variation of disturbance in June, 1912, confirm that at mid-winter at  $\phi_m = 75^\circ$  the concentration of disturbance in the late evening hours (as in latitudes below  $70^\circ$ ) can be almost as great as in the forenoon hours, when, above

80°, D is most prominent. These two curves are also instructive in showing that even for such a short period as a month, the hourly range and character figure measures of disturbance are equally useful in portraying the main characteristics of D.

8—In addition to illustrating further the very pronounced seasonal change in the character of the daily variation of disturbance (D) at stations above 70°—including Kingua Fjord with its comparatively inadequate data—fig. 5 emphasizes another feature of D in the immediately circum (magnetic) polar regions of

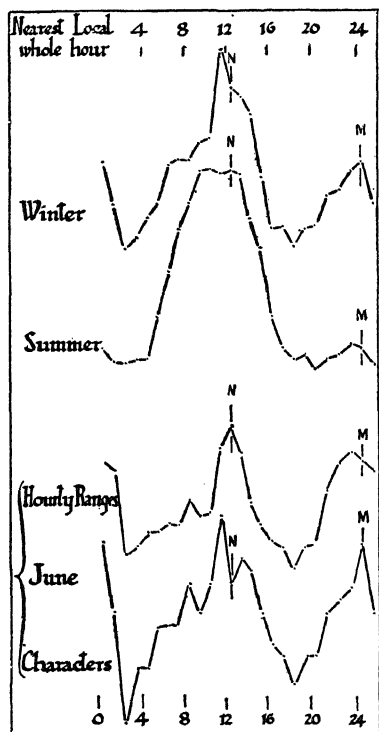


FIG. 4—Incidence of disturbance at Cape Denison. ( $\phi_m = 75.5$ )

and Rae, the stations with the most rigorously comparable basis of disturbance measure as well as representing the regions on the polar and equatorial sides of the belt of transition in the form of D. The amplitudes  $A_1$ ,  $A_2$  for the 24-hour and 12-hour waves at Godhavn and Fort Rae are in  $10^5 \gamma^2$  units and the corresponding phase angles are referred to Greenwich midnight as epoch; the equivalent local times of maximum in the two waves are given in adjacent columns.

For our present purpose the most significant deduction to be made

is that in winter the distribution of disturbance through the day is strikingly different from the distribution in the summer months, in that the very conspicuous single wave in D with maximum in the forenoon of the summer is replaced in winter by a feeble double wave having a maximum in the evening as well as the forenoon. The whole scale of D is also seriously reduced in winter as compared with summer to an extent which increases with approach to the axis pole. At Thule in June the range of D is 265% of the mean; in January it is only 61%. Indeed near the pole the only really characteristic feature of the daily disturbance variation in winter is the early morning minimum.

9—For further insight into the remarkable changes in D outlined in § 4–8 some of the data represented in figs. 1–5 have been analysed harmonically. Table II gives, primarily, the results for Godhavn

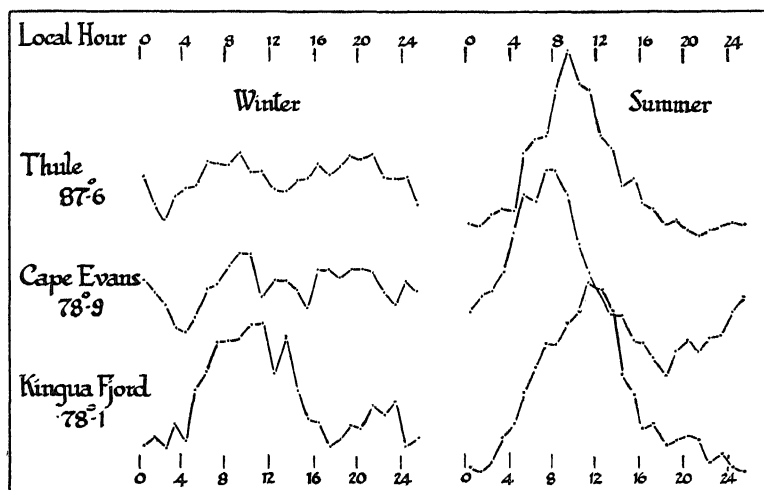


FIG. 5—Seasonal change in daily variation of disturbance at and above magnetic latitude  $78^{\circ}$

TABLE II—ALL DAYS

	$A_1$	$P_1$	Equivalent local time of maximum of $P_1$	$A_2$	$P_2$	Equivalent local time of maximum of $P_2$	$A_2/A_1$
			° h			° h	
Godhavn—							
Year .....	60	253	9.5	53	58	9.5	0.88
Winter .....	27	325	(4.7)	45	49	9.8	1.67
Equinox .....	64	242	10.3	62	64	9.3	0.97
Summer .....	111	245	10.0	55	60	9.4	0.50
Fort Rae—							
Year .....	187	312	1.5	62	218	0.0	0.33
Winter .....	160	302	2.2	65	203	0.5	0.41
Equinox .....	216	315	1.3	69	228	23.6	0.32
Summer .....	188	316	1.2	53	218	0.0	0.28
Sodankylä—							
Winter .....	300	144	22.1	30	166	11.3	0.10
Summer .....	245	127	23.4	87	101	13.4	0.36
Eskdalemuir—							
Year .....	109	149	20.0	12	306	4.8	0.11
Winter .....	136	152	19.9	30	238	7.7	0.22
Summer .....	81	145	20.3	29	15	2.5	0.36

from Table II is the predominance throughout the year at Rae of the 24-hour wave with its maximum just after midnight, compared with the steady decrease in the amplitude of this wave (maximum in the forenoon) from summer to winter at Godhavn  $10^\circ$  further north. At this station  $A_1$  in winter is only 24% of its value in summer; at Rae it is 85%.

This decrease is further reflected in the systematic change in the seasonal ratio  $A_2/A_1$  which at Godhavn rises from 0.50 in summer to 1.67 in winter; at Rae the corresponding figures are 0.28 and 0.41. It has to be noted that the artificial depression of the forenoon maximum, fig. 3, perhaps vitiates the values of the ratio at Godhavn especially in winter. But since the two waves are very nearly in phase both amplitudes suffer, so that the resultant ratio cannot be seriously affected. With a small winter amplitude for the 24-hour wave  $P_1$  probably suffers more from this cause.

Another feature of note in Table II is that for the year as a whole, and the seasons separately, the amplitude of the whole day wave at Godhavn is much smaller than at Rae. Except in winter the 12-hour wave amplitudes are very similar. This reduction in the scale of the constituent waves at Godhavn as compared with Rae is too great to be ascribed to the artificial depression of the maximum at the more northerly station (see § 13).

10—The results in Table II lead us to conclude that the mechanism responsible for replacing the late evening maximum in D below  $70^\circ$  by a forenoon maximum above  $75^\circ$  is also effective to a degree which increases progressively from summer to winter at, and probably below, the latitude at which the change in D first becomes apparent. How far below cannot at present be decided. Judging from the data for Eskdalemuir in Table II the effect is already reversed at  $\phi_m = 58.5^\circ$ ; it does not seem to penetrate so low even as Sodankylä ( $63.8^\circ$ ). The region of discontinuity must be sharply defined on the equatorial side. We further conclude that the whole day wave in D suffers serious damping with increase of  $\phi_m$  from  $69^\circ$  to  $80^\circ$ , and that this damping is very much exaggerated in the winter months.

11—These conclusions are confirmed in detail by the results given in Table III based on a similar analysis of the more heterogeneous material from Cape Evans, Kingua Fjord and Cape Denison. Taken in conjunction with the all-year values of the phases of both the whole and half-day waves in D at Godhavn, Table II, they give rise to the further suggestion that the times of the maxima of both waves in the daily variation

of disturbance advance steadily with increasing  $\phi_m$  up to  $80^\circ$ . This may be a reversed echo of the phenomenon obtaining below  $70^\circ$ . (§ 4.)

Though based on two months' data, the remaining results in Table III relating to Thule are exactly as might be anticipated from the deductions of the foregoing paragraphs. Notice is specially drawn to the seasonal

TABLE III—ALL DAYS

	$A_1$	$P_1$	Equivalent local time of maximum of $P_1$ h	$A_2$	$P_2$	Equivalent local time of maximum of $P_2$ h	$A_2/A_1$
Thule—							
January .....	7	148	16.5	17	52	8.7	2.43
June .....	65	225	11.4	23	8	10.1	0.35
Cape Evans—							
Year .....	37	132	8.3	23	155	8.9	0.62
Winter .....	13	28	15.2	16	144	9.3	1.23
Summer .....	76	145	7.4	19	184	8.0	0.25
Kingua Fjord—							
Year .....	112	298	10.1	45	158	9.7	0.40
Winter .....	44	303	9.8	27	162	9.6	0.61
Summer .....	73	292	10.5	21	151	10.0	0.29
Cape Denison—							
Year .....	83	72	10.7	40	39	11.2	0.48
Winter .....	48	71	10.8	42	39	11.2	0.88
Summer .....	97	72	10.7	37	52	10.8	0.38

change in the contributions to the complete D of the two constituent waves. In June  $A_1$  is about three times  $A_2$ ; in January  $A_1$  is insignificant. December data would probably have shown that around the winter solstice it completely vanishes. In both months the phase of the 12-hour wave at Thule is in close agreement with the phase of the same wave in lower latitudes and with the summer whole-day wave at the same station.

From these Thule results we deduce that the tendency to a forenoon maximum in D, already slightly operative below  $70^\circ$  (especially in winter), continues to have increasing effect right through the transition zone ( $70^\circ$ – $80^\circ$ ) into the region lying immediately round the magnetic axis pole. In this region the form of the daily variation is such that its forenoon maximum entirely supplants the late evening maximum obtaining on the equatorial side of the transition zone. Again, northwards of



75° to a degree increasing in severity with approach to the axis pole, the whole scale of  $D$  is much reduced in winter. At the pole itself the 24-hour wave probably vanishes at mid-winter; only a very feeble double wave of disturbance each day persists.

12—Another aspect of the changes now seen to be produced in  $D$  by varying latitude and season is illustrated by the results in Table IV and the two curves, one each for Rae and Godhavn, at the bottom of fig. 3. These are derived from the average daily variations of disturbance on days selected as being the most disturbed at the two stations during the recent International Polar Year, and are to be compared with the corresponding analysis and curves of  $D$  for the average of all days shown in Table II and the upper part of fig. 3. At Rae the only difference is one of scale. The ratio  $A_2/A_1$  is practically the same for all days and for the group of most disturbed days, but the separate amplitudes are about four times as great on disturbed days as on the average of all days of the year.

TABLE IV—DISTURBED DAYS

	$A_1$	$P_1$	Equivalent local time of maximum of $P_1$	$A_2$	$P_2$	Equivalent local time of maximum of $P_2$	$A_2/A_1$
	$10^5 \gamma^2$	°	h	$10^5 \gamma^2$	°	h	
Godhavn .....	46	226	11.3	303	61	9.4	6.59
Rae .....	746	312	1.5	238	240	23.3	0.32

At Godhavn, on the other hand, though the phases remain very comparable, great disturbance effects a very great increase in  $A_2$  relative to  $A_1$ . For all days  $A_2/A_1$  is 0.88; for the selected disturbed days it is 6.59. Now of the 27 days at Rae and 30 at Godhavn which contributed to the disturbed day results, 7 were from winter and 9 from summer at Rae, and 8 from winter and 12 from summer at Godhavn. It is therefore clear that the dominating influence of the 12-hour wave during the most disturbed conditions at this latter station is not simply an indirect result of the seasonal change which we now know to have the same effect there. It must be concluded that at  $\phi_m = 80^\circ$  the distribution of disturbance through the day is altered during great disturbance—irrespective of season—in the same way as, but to a much more impressive extent than, it is altered in the transition from summer to winter.

13—In addition to the change in form which  $D$  undergoes as  $\phi_m$  is increased above  $70^\circ$ , the marked damping in the range of  $D$  in winter in

the immediate neighbourhood of the magnetic axis pole has already been commented on (§ 8). Table IV shows that while the amplitude of the 12-hour wave increases by only 27% in the  $10^\circ$  increase of  $\phi_m$  above Rae, the 24-hour wave amplitude falls from 746 to 46 units of  $10^5 \gamma^2$ . The general scale of disturbance must fall rapidly above  $70^\circ$  long before the immediately circum-polar region is reached.

14—Further light on this feature of general disturbance is given by Table V which on the left side contains the average values of the hourly range product ( $Zr_Z \cdot 10^{-4}$ ) from all hours of the two months, January and June, 1933, and on the right hand the average values of the daily range product ( $ZR_Z \cdot 10^{-4}$ ) for the same months at stations arranged in order of  $\phi_m$ . Within each compartment the data are strictly comparable. That the vertical force component alone can be used as a sufficient criterion of disturbance in high latitudes has been noted in § 2. At Rae the contribution of  $Hr_H$  to the combined product ( $Hr_H + Zr_Z$ ) is only 13%; at Godhavn 11%.

TABLE V

Station	$\phi_m$	Average $Zr_Z \cdot 10^{-4}$		Average $ZR_Z \cdot 10^{-4}$		
		January	June	January	June	Mean
Thule .....	88	80	234	351	1271	811
Godhavn .....	80	316	384	1619	2006	1813
Fort Rae .....	69	413	434	2304	2760	2532
Abisko .....	66	—	—	1098	1056	1072
Sodankylä ....	64	—	—	987	872	930
Lerwick .....	63	—	—	367	399	383
Sitka .....	60	—	—	464	605	535
Eskdalemuir ..	58	—	—	128	177	153

The striking features of Table V are the very steep falls in general disturbance both to the north and south of  $69^\circ$  and the very large reduction in the scale of the disturbance in winter as compared with summer with increasing approach to the axis pole above  $70^\circ$ . It is easy to infer that there exists both in summer and winter a very intense and highly localized disturbance field along the lower (equatorial) edge of the zone in which the diurnal variation of disturbance has been shown to change character so conspicuously.

15—Fig. 6 summarizes diagrammatically some of the main features in the paper. It will be recognized that the general trend in winter is for

the conditions producing irregular disturbance below  $70^\circ$  to invade the transition zone and extend up to the vicinity of the magnetic axis pole itself. The reverse process occurs in summer. This seasonal advance and retreat of disturbance phenomena around the axis pole is well supported by other evidence based on the regular disturbance variation ( $S_d$ ) to be published shortly.

Fig. 6 assists appreciation of a peculiarity of the region lying within  $12^\circ$  of the magnetic axis pole which usually escapes attention. Since the latitude of the magnetic axis pole is itself  $78.5^\circ$  relative to the rotation axis pole of the earth, this region is the only part of the earth's surface

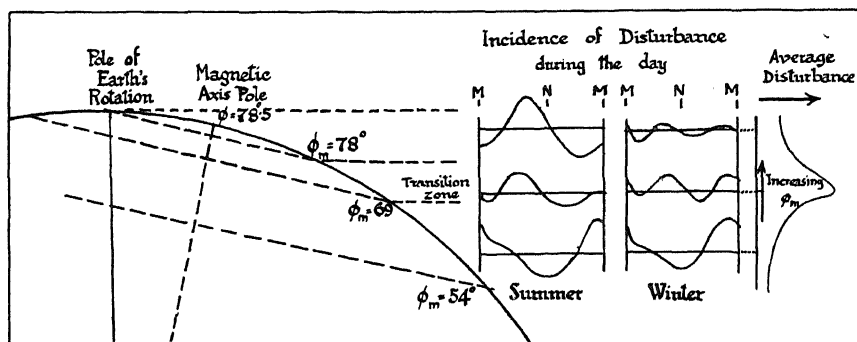


FIG. 6

which is continually in sunlight during the summer months. In winter it is the only part continually turned away from direct sunlight. In the equinoctial months the whole zone is exposed to the sun at noon and turned away at midnight. In these respects it is the only all-or-none region of the earth's surface. There is therefore a strong temptation to connect the remarkable phenomena of the magnetic disturbance field outlined in this paper with this unique feature (as regards the incidence of direct solar radiation) of the area lying immediately around the axis pole, and to interpret the phenomena in terms of changes in conductivity in the responsible layer of the ionosphere consequent upon the seasonal shift in the areas wholly or partially exposed to the sun.

I thank the National Polar Year Committee for permission to use unpublished data for Fort Rae, and also Dr. D. la Cour, Director of the Meteorological Office, Copenhagen, for data from the Greenland magnetic observatory at Godhavn and the Danish Polar Year station at Thule.

## SUMMARY

16—Using observational material from ten stations in moderate and high latitudes in both hemispheres, it is found that the daily variation of irregular disturbance in  $D$  is controlled by local time over the whole region extending to at least  $35^\circ$  from the magnetic axis pole. The form of  $D$  varies with latitude and with season (above  $\phi_m = 70^\circ$ ) and with the state of general disturbance.

Below  $70^\circ$   $D$  is primarily governed by a 24-hour wave with the maximum (invariably in the evening) becoming later at the rate of one hour per  $5^\circ$  increase of  $\phi_m$  till it falls at midnight at  $70^\circ$ . Up to this latitude neither varying seasonal conditions nor great disturbance have important effects on the form of  $D$ . Only its scale is changed.

Above  $80^\circ$   $D$  has again one dominant maximum but now invariably in the forenoon. The transition from summer to winter in this region involves both a change of form and scale. A semidiurnal wave of disturbance which, being in phase with the whole day wave, serves only to enhance the forenoon maximum in summer, becomes in winter the dominating feature of the daily variation, so that  $D$  then has a maximum in the late evening as well as in the forenoon. But in the vicinity of the axis pole the whole scale of the variation is so reduced in winter that the early morning minimum is the only really characteristic feature.

In the transition zone ( $70^\circ$ – $80^\circ$ ) the form of  $D$  depends entirely on the season and on the amount of general disturbance. In this zone the changes are such as would arise from an advance of the conditions normally obtaining below  $70^\circ$  right through the zone (and, indeed, up to the axis pole) in winter with the additional effect that the advance is accompanied by a very high degree of damping not only in the range of the diurnal variation of disturbance but also in the scale of irregular disturbance in general. At  $80^\circ$  and probably elsewhere within the transition zone the effect of great disturbance on  $D$  is to change its form and scale in a similar way to, but to a much greater extent than, that affected by the transition from summer to winter conditions there.

On the equatorial side of the transition zone, *i.e.*, *ca.*  $\phi_m = 70^\circ$ , general disturbance probably reaches greater proportions than elsewhere on the earth. It is also highly localized there. That the region of  $\phi_m > 78^\circ$ , where the disturbance field undergoes such radical change, is also unique in its summer and winter receipt of direct solar radiation is probably more than coincidence.

---

## The Behaviour of Three Single Crystals of Aluminium in Fatigue under Complex Stresses

By H. L. COX, B.A., and W. J. CLENSHAW, B.Sc., A.Inst.P.

(Communicated by H. J. Gough, F.R.S.—Received November 30, 1934)

[PLATES 6–7]

### INTRODUCTION

In the ordinary type of Wöhler machine used for testing materials in fatigue under reversed bending stresses, the load system is stationary in space, and variation of the stress system with respect to the test piece is obtained by rotating the test piece. It is, of course, essential to the success of the test that the system of displacements caused by the application of the load system to the test piece should remain stationary in space; but, since the test piece rotates, this requirement can only be fulfilled if the material of the test piece is isotropic. Thus, if an attempt were made to test a single crystal in a Wöhler machine it might be anticipated that either actual elastic anisotropy or the virtual anisotropy due to restricted slip movement would cause the deformation to vary with the orientation of the stress system relative to the axes of the crystal and that “whipping” of the specimen would occur. Three such attempts have indeed been made: but in spite of great care exercised in setting up the specimens and in applying the loads, only in one case, in which the orientation of the crystal was such as to provide effective symmetry about the axis of the specimen, was the test successful.

A new type of testing machine recently developed at the N.P.L. for testing specimens in fatigue under systems of combined bending and torsional stresses, differs in principle from the Wöhler machine in that the variation of stress is produced by actual variation of load. In this machine both the test piece and the orientation of the stress system remain stationary, only the magnitude of the stresses being varied. The deformation of the test piece is therefore only that due to one type of stress system fixed in relation to the orientation of the test piece and varying only in magnitude. Moreover, the construction of the machine is such that the strain of the test piece is not required to be of the same type as the stress system applied, *e.g.*, the application of pure bending moment does not restrict the test piece to pure bending strain and the

test piece remains free to twist also if necessary. These conditions render this type of machine perfectly suitable for tests on single crystals. Accordingly, tests have been carried out in this machine on three single crystals of aluminium; the first was tested under reversed flexural stresses, the second under reversed torsional stresses and the third under a combination of reversed flexural and reversed torsional stresses.

#### DETAILS OF TESTING MACHINE AND METHOD OF CALIBRATION

The machine used for the present tests is described in the Annual Report of the National Physical Laboratory for 1933, p. 149. The only modification made to this machine for the tests on single crystals was to provide support for the stressing arm,\* so that its weight should not be borne by the specimen. This support was provided by suspending the stressing arm by rubber bands from a point about 6 feet above the machine. The elasticity of the bands was such that the variation of load due to the amplitude of motion of the point of attachment of the bands to the stressing arm was quite inappreciable.

#### DETAILS OF SPECIMENS

All three specimens used in the present tests were cut from the same bar. This bar had been converted to the single crystal form by the strain and heat treatment method devised by Carpenter and Elam. None of the specimens was entirely single, each containing one or two small stranger crystals. The traces of the boundaries of these stranger crystals on the surfaces of the specimens are shown in figs. 4, 5 and 6. In the test in simple bending, the specimen was oriented so that the stranger crystals lay near the neutral axis, and it is improbable that they affected the behaviour of the specimen in any way. In the other two tests, in simple torsion and in combined bending and torsion, it was impossible to arrange that the stranger crystals should occupy positions of low stress, and they may, therefore, have had some effect on the distortion; but all the stranger crystals were small and, except perhaps in the cracking stage, their influence on the behaviour of the main crystal is not likely to have been serious.

The three specimens machined from the bar were all of the same form; they were marked CHJIE1, CHJIE2, and CHJIE3. The test portion of each specimen was 0.3 inch in diameter and 0.5 inch long and was joined to the enlarged ends, 3/8 inch in diameter and 1.0 inch long, by

\* A in fig. 29, 'Ann. Rep., Nat. Phys. Lab.,' 1933.

fillets of 1.0 inch radius. Reference marks were scribed on the enlarged ends of each specimen. After machining and etching to remove the surface distortion due to machining, each specimen was X-rayed independently with respect to its own axis and one of the reference marks on the enlarged ends. The results showed that the change of orientation caused by machining was in each case quite inappreciable, the only differences being constant differences in the  $\psi$  values of the same planes in the three specimens due to the arbitrary positions of the reference marks. The spherical co-ordinates of the slip planes as obtained by correction of the original X-ray readings are given in Table I, and a stereographic diagram giving the positions of all the principal planes and directions is shown in fig. 1. The  $\psi$  co-ordinates given in Table I refer to the reference marks scribed on the individual specimens, and the positions of these reference marks are shown in fig. 1.

TABLE I—SPHERICAL CO-ORDINATES OF SLIP PLANES

Plane	$\theta$		$\psi$ (CHJIE1)		$\psi$ (CHJIE2)		$\psi$ (CHJIE3)	
0 (111)	$^{\circ}$ 37	$'$ 55	$^{\circ}$ 127	$'$ 8	$^{\circ}$ 333	$'$ 41	$^{\circ}$ 21	$'$ 49
1 ( $\bar{1}\bar{1}\bar{1}$ )	74	13	285	3	131	36	179	44
2 ( $\bar{1}\bar{1}\bar{1}$ )	70	23	210	19	56	52	105	0
3 ( $\bar{1}\bar{1}\bar{1}$ )	43	31	2	54	209	27	257	35

#### DETAILS OF TESTS

In order to enable the specimen to be gripped in the testing machine, the enlarged ends were fitted with mild steel collars made to fit the square section chucks of the machine. Apart from the possibility of a  $90^{\circ}$  rotation, the fixing of these collars determined the orientation of the specimen relative to the plane of the bending moment applied by the machine.

The first specimen (reference mark CHJIE1) was tested under reversed flexural stresses, the specimen being so oriented that the plane of bending was very nearly perpendicular to the slip plane 3( $\bar{1}\bar{1}\bar{1}$ ). The second specimen (reference mark CHJIE2) was tested at practically the same orientation under simultaneous cycles of equal shear stresses due to flexure and torsion. The third specimen (reference mark CHJIE3) was also tested at approximately the same orientation; but, since this specimen was tested under reversed torsional stresses only, the orientation of the specimen in the machine did not affect the distribution of stress. The actual positions of the planes of bending relative to the crystal structure of the two specimens CHJIE1 and CHJIE2 are shown in fig. 1.

The ratios of the ranges of shear stress resolved along the three possible slip directions on each of the four possible slip planes to the range of nominal maximum shear stress are shown for each of the three specimens in figs. 2*a*, *b* and *c*. In this figure, the diagrams have been arranged one below the other so that the central vertical (dotted) line represents in each case the axial plane of the specimen containing the normal to the slip plane 3( $\bar{1}\bar{1}1$ ). The actual positions of the planes of bending in the

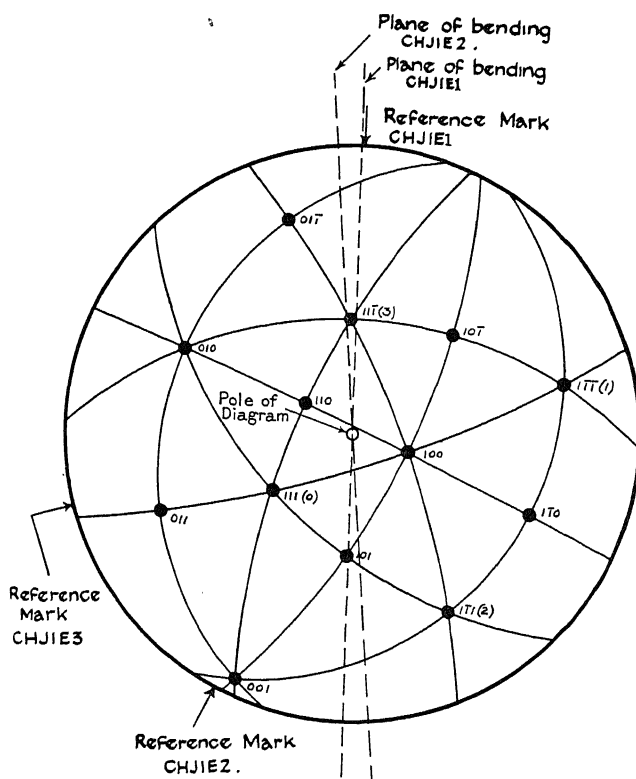


FIG. 1—Stereographic projection of principal planes

cases of the specimens CHJIE1 and CHJIE2 are shown to left and right of this common line respectively. The difference between figs. 2*a* and 2*b* should be remarked; the addition to a simple bending moment of a torsion moment sufficient to produce the same shear stress has altered the stress distribution entirely. The plane 3, which in simple flexure was the only operative slip plane, becomes under combined stresses the only slip plane *not* operative.

The range of nominal maximum shear stress ( $\pm q$ ) is determined simply by the loads on the disc of the testing machine and is independent of the



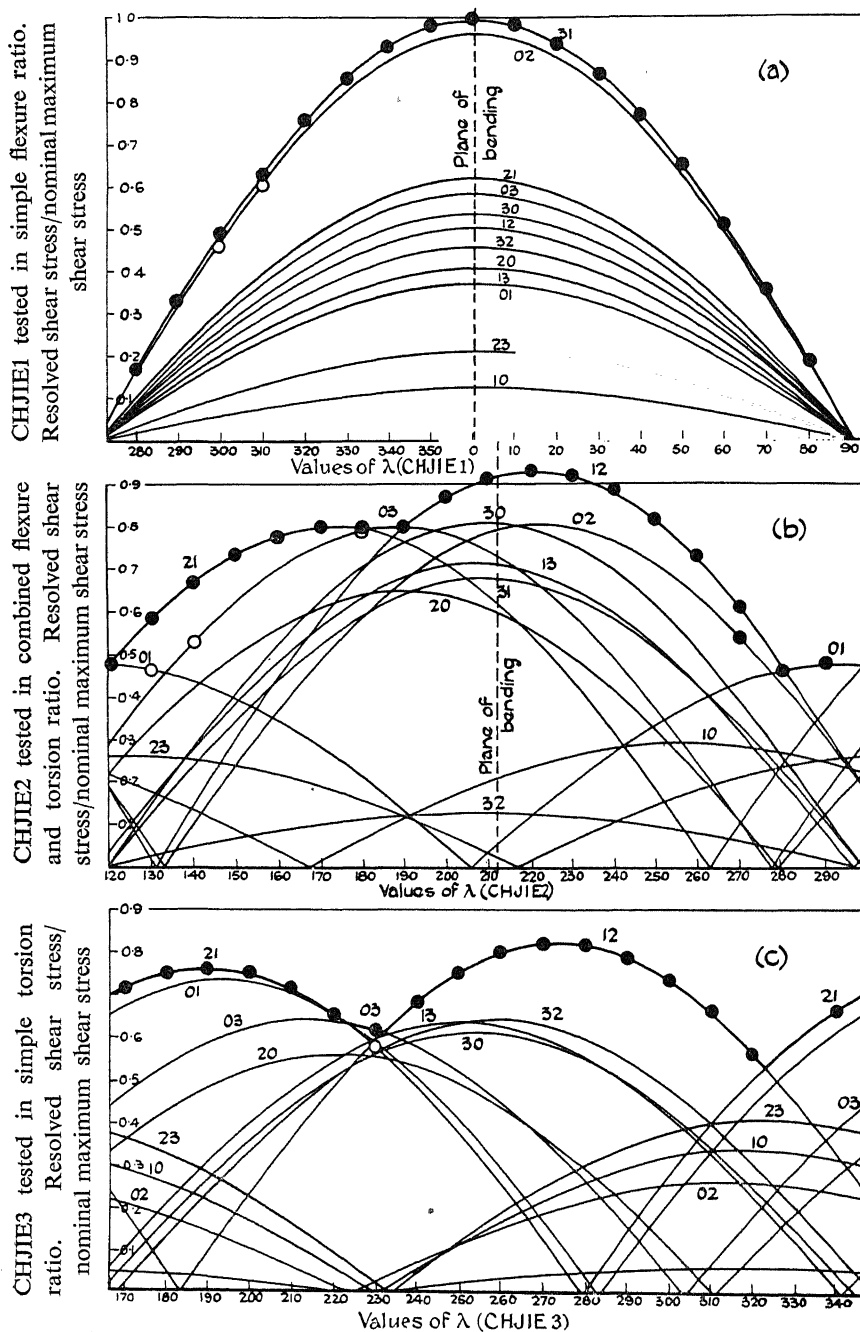


FIG. 2—Distribution of resolved shear stress and records of slip bands observed

angle  $\alpha$  between the plane of the applied moment and the axis of the specimen. The range of shear stress due to flexure is  $\pm q \cos \alpha$  and the range of shear stress due to torsion is  $\pm q \sin \alpha$ . The stress conditions are most easily stated in terms of  $q$  and  $\alpha$ .

Details of all the tests made on the three specimens are given in Table II. From fig. 2 it will be seen that the differences between the maximum stress factors for the three specimens were fairly large, and for this reason in Table II the values of both the nominal maximum shear stress and of the actual maximum resolved shear stress are given; the symbols in brackets after the latter values denote the plane and direction on and in which the maximum resolved shear stress was developed (*cf.* fig. 2).

TABLE II—DETAILS OF TESTS

Specimen Marked	Test No.	Angle ( $\alpha$ )	Range of nominal	Range of actual	Number of reversals	Remarks
			shear stress (tons/ sq in)	maximum resolved shear stress (tons/sq in)		
		°				
CHJIE1 ....	1	0	$\pm 0.6$	$\pm 0.60$ (31)	270,000	—
	2a	0	$\pm 1.1$	$\pm 1.10$ (31)	251,000	—
	2b	0	$\pm 1.1$	$\pm 1.10$ (31)	<226,000*	Broken
CHJIE2 ....	1a	45	$\pm 0.6$	$\pm 0.56$ (12)	261,000	—
	1b	45	$\pm 0.6$	$\pm 0.56$ (12)	943,000	—
	2a	45	$\pm 1.1$	$\pm 1.02$ (12)	209,000	—
	2b	45	$\pm 1.1$	$\pm 1.02$ (12)	408,000	Broken
CHJIE3 ....	1a	90	$\pm 0.6$	$\pm 0.49$ (12)	252,000	—
	1b	90	$\pm 0.6$	$\pm 0.49$ (12)	900,000	—
	2a	90	$\pm 1.1$	$\pm 0.90$ (12)	275,000	—
	2b	90	$\pm 1.1$	$\pm 0.90$ (12)	730,000	—
	3	90	$\pm 1.4$	$\pm 1.15$ (12)	67,000	Broken

\* The failure of this specimen did not cause sufficient increase in amplitude of the stressing arm to operate the trip gear to stop the machine. The number of reversals to fracture was not greater than the number given but was probably more than 200,000.

#### GENERAL RESULTS OF TESTS

*Endurance of Specimens*—The general scheme of the tests was to subject each specimen to a small number of reversals of a nominal stress fairly well below the probable fatigue range and then to test each specimen to fracture at a range of nominal stress slightly above the safe limit. The

object of the preliminary run was to exhaust "settling down" slip; but it was intended to impose only a small number of reversals of this lower range in the hope that, if hardening under this range could be avoided, the endurances of the three specimens at the higher range would give some indication of their relative strengths. The first tests on the specimens CHJIE2 and CHJIE3 caused so little slip that further runs at the same stress were imposed in order to be sure that slipping under this range should be exhausted. The only other departure from the general scheme was in the last test on the specimen CHJIE3. For this specimen the maximum stress factor was rather low (0.82) and after the specimen had endured a million reversals of the range of nominal stress that caused failure of the specimens CHJIE1 and CHJIE2, the range was increased to bring the value of the maximum *resolved* shear stress up to a value comparable with that which caused failure of the other two specimens.

The loads required to stress the relatively weak single crystals in the present tests were very much below the normal capacity of the testing machine. In spite of the fact that the machine was specially calibrated at low loads, the accuracy with which the range of stress developed could be estimated was therefore probably not much better than  $\pm 5\%$ . For this reason, a close comparison of the endurances of the three specimens is not justified; but, from the results set out in Table II it is probably safe to conclude that it is the value of the maximum *resolved* shear stress that determines failure by fatigue.

*Distribution of Slip Bands*—After each test, the surface of the specimen tested was examined and the distribution of slip bands and cracks was compared with the distribution of stress. Apart from irregular "settling down" slip in the first tests, the distribution of slip was in every case closely in accordance with that anticipated on the basis of the resolved shear stress law. The distribution of slip bands after the tests 2a are shown in fig. 2. The planes upon which slip occurred were, of course, identified by comparison of the slope of the slip bands with the calculated slopes of traces of the slip planes, the agreement in all cases being very good; but in fig. 2 slip bands have been recorded (at the appropriate values of  $\lambda$ ) on the highest of the three stress curves corresponding to the plane of which they represented the trace. General systems of slip are recorded by full circles and occasional bands by open circles. In view of the large amount of evidence already obtained of the general applicability of the resolved shear stress law, the good agreement illustrated by fig. 2 is of interest chiefly on account of the unusual nature of the stress cycles applied to the specimens CHJIE1 and CHJIE2.

*Spacing of Slip Bands*—Referring again to fig. 2, it will be seen that in the specimen CHJIE1 slip was confined entirely to one plane and occurred on that plane at values of the resolved shear stress from zero (or the slip limit, if it exists) up to a maximum of  $\pm 1 \cdot 10$  tons/sq inch. A panoramic photograph of the surface of this specimen from  $\lambda = 270^\circ$  to  $\lambda = 90^\circ$  was taken after the test 2a. Individual photographs taken from this panorama are shown in figs. 7, 8, Plate 6. Even these photographs suggest some correlation between value of resolved shear stress and spacing of slip bands, and from the panorama itself it is quite obvious that some correlation exists. Accordingly an attempt was made to determine the mean spacing of slip bands at intervals of  $10^\circ \lambda$  and to compare the values obtained with the corresponding values of the resolved shear stress. In the first instance counts of the number of bands in the full width of the panorama (3.7 inches corresponding to about 1 mm on the specimen) were made independently by two observers.

In the regions where the range of resolved shear stress had been less than about  $\pm 0.9$  tons/sq inch, the two counts agreed almost exactly; but in the regions where the range of resolved shear stress had been greater than  $\pm 0.9$  tons/sq inch, the estimates differed considerably. Comparison of the two methods of counting showed that this difference was due to the difficulty experienced in counting the number of bands in areas of "massed" slip. A typical area of "massed" slip is shown in fig. 8, Plate 6; it will be seen that individual slip lines are not in every case resolved. Better resolution could, of course, be obtained by using a higher power objective (compare for instance, fig. 9, Plate 6); but counts of slip lines cannot conveniently be made except from panoramas, and the use of a higher power objective for the preparation of panoramas is normally impracticable.

The results of counts of slip bands depend so much on personal error that when once disagreement between two observers has been registered, it is not safe to try to reconcile the results. On the other hand, it is reasonable to adopt the *lower* estimate of the number of bands and to regard this number as a minimum estimate. For the purpose of comparison of slip band spacing at different values of resolved shear stress, this minimum estimate may be sufficient. In fig. 3, the number of slip bands on the specimen CHJIE1 after the test 2a per mm normal to the slip plane has been plotted against the value of the resolved shear stress. For values of resolved shear stress up to and including 0.84 tons/sq inch the number of slip bands may be regarded as exact; above that stress value the number plotted represents the minimum number, and the arrows indicate the amount by which these estimates may be in default of the true number of bands.

It will be seen that, even allowing for a considerable measure of uncertainty at the higher stress values, marked correlation between the value of the resolved shear stress and the spacing of slip bands is shown; moreover, the stress at which "massed" bands first appear is marked by a fairly well defined "knee."

A similar comparison of slip-band spacing with range of resolved shear stress for the specimen CHJIE2 was also made; the counts were made on

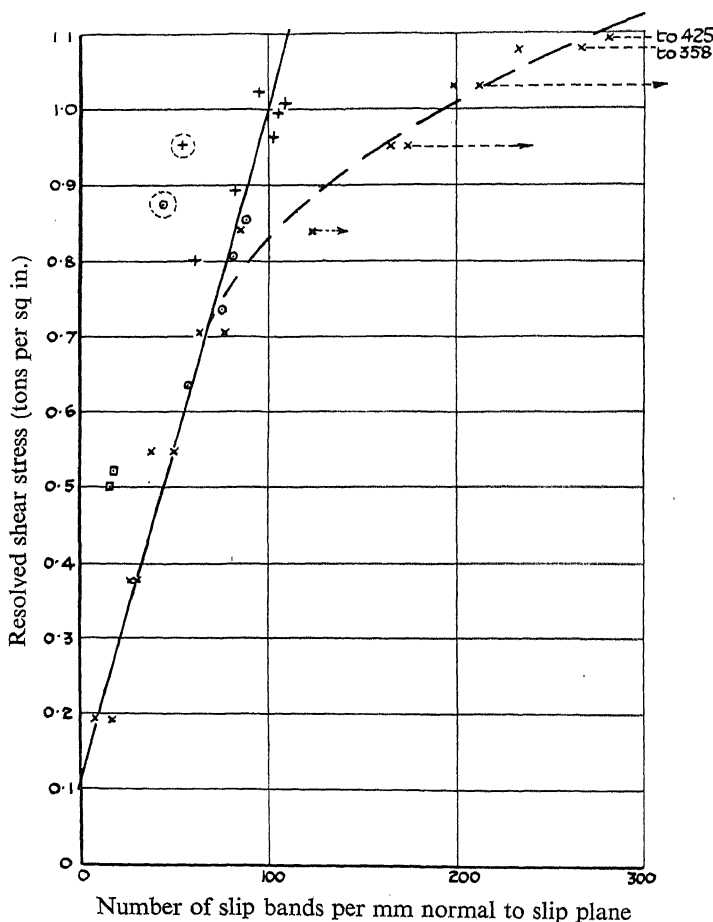


FIG. 3—Slip band spacing in relation to range of resolved shear stress

- × CHJIE1 tested in simple flexure (plane 3)
- CHJIE2 tested in combined flexure and torsion (plane 2)
- + CHJIE2 tested in combined flexure and torsion (plane 1)
- CHJIE2 tested in combined flexure and torsion (plane 0)

Readings enclosed in dotted circles may be in error due to the proximity of cracks reducing the effective range of resolved shear stress

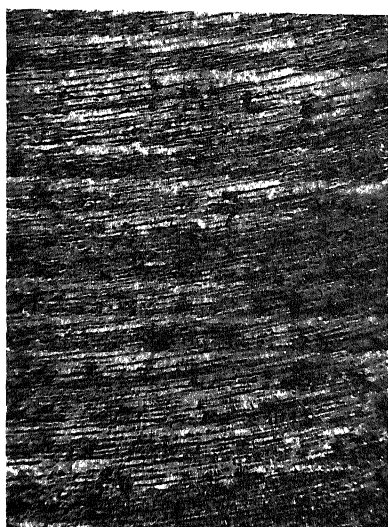


FIG. 8—CHJIE1  $\lambda = 10$   $d = 0.14$   $\times 97$



FIG. 10—CHJIE1  $\lambda = 159$   $d = 8.26$   $\times 97$

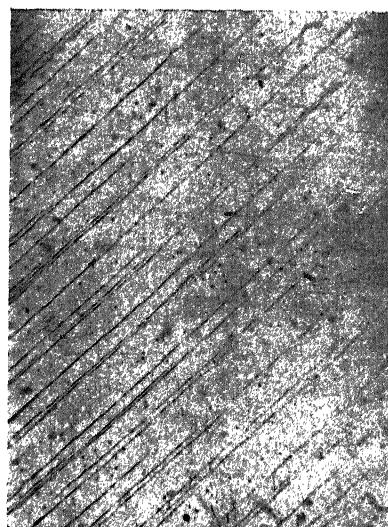


FIG. 7—CHJIE1  $\lambda = 70$   $d = 0.14$   $\times 97$



FIG. 9—CHJIE1  $\lambda = 180$   $d = 0.26$   $\times 328$



Fig. 12—CHJIE2  $\lambda = 47.2$   $d = -0.015$   $\times 180$



Fig. 14—CHJIE3  $\lambda = 69$   $d = -0.10$   $\times 97$



Fig. 11—CHJIE1  $\lambda = 154$   $d = -0.09$   $\times 180$



Fig. 13—CHJIE2  $\lambda = 23$   $d = 0.01$   $\times 97$

a panorama taken after the test 2*b*. In this case, there was very little "massed" slip anywhere on the panorama and the two independent counts agreed fairly closely at all points at which they were made. The number of slip bands per mm normal to the slip plane is shown plotted against the value of the resolved shear stress in fig. 3.

In this specimen, there were three operative slip planes and the variation of stress on any one of them was not very great. On the other hand, the panorama was taken after failure and included portions of at least three cracks, each of which followed the direction of the operative slip plane in its neighbourhood; one of these cracks is shown in fig. 13, Plate 7. The presence of these cracks must, of course, have affected the stress distribution, since the edges of the cracks must have been free from shear stress. If the cracks were formed at an early stage the reduction of stress due to their presence would be expected to be reflected in a spacing of slip bands in their neighbourhood wider than the calculated range of resolved shear stress would indicate. In fig. 3 readings that may be expected to be affected by the proximity of cracks are enclosed in dotted circles.

The results of the measurements of slip-band spacing made on the specimen CHJIE2 were generally consistent with the results of the measurements made on the specimen CHJIE1; but in this case the number of slip bands was more or less in proportion to the range of stress over the whole range, and there was no apparent "knee." This difference is certainly to be ascribed to the virtual absence of "massed" slip in the panorama of CHJIE2 from which the slip-band spacing was estimated. The panorama of CHJIE1 was therefore re-examined in order to determine whether, if areas of "massed" slip were ignored, the mean slip-band spacing in other areas was more or less in proportion to the stress range according to the straight line drawn in fig. 3. It will be appreciated that the conditions, under which these latter counts were made, were too vague to permit definite figures to be quoted; but, although the results were far from conclusive they were at least consistent with the view that the marked decrease in mean spacing of slip bands might possibly be due entirely to the occurrence of "massed" slip.

The final tests on the specimen CHJIE3 unfortunately caused too much distortion of the actual surface of the specimen to permit counts of slip-bands to be made.

*Distribution of Cracks*—In all three specimens failure commenced by the formation of a large number of fine cracks in regions of high resolved shear stress, where previously heavy slip had occurred, and these cracks



showed a marked tendency to extend along the operative slip planes, fig. 10, Plate 6, and figs. 11 and 12, Plate 7. In the specimen CHJIE1 one main crack developed and finally resulted in complete severance of the specimen into two pieces; the other cracks, though very numerous, remained small. In the specimen CHJIE2 again there was one main crack; but the test was stopped just before it could cause complete fracture of the specimen. The other cracks were again very numerous and some few developed to a considerable size. In the specimen CHJIE3 also the main crack

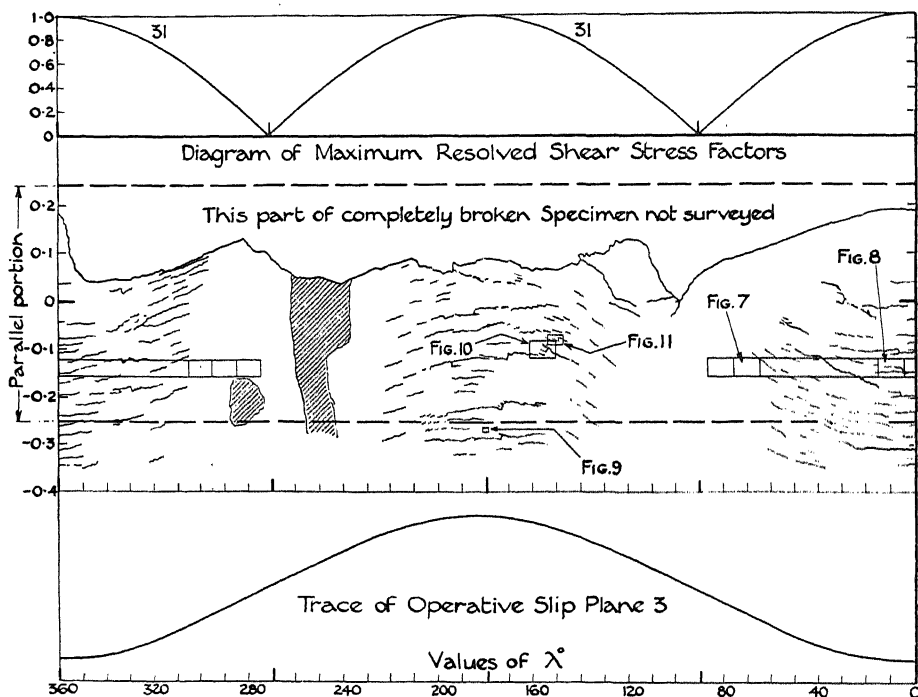


FIG. 4—Specimen CHJIE1 tested in simple flexure. Survey of cracks after fracture

developed right round the specimen causing complete severance; but, although the number of subsidiary cracks was less than in the other two specimens, several were very large.

The distribution of the cracks observed on the surface of each specimen after fracture is shown in figs. 4, 5 and 6. The tendency of the cracks to follow the directions of the operative slip planes is well illustrated by these diagrams and further illustration of this tendency is afforded by figs. 10, Plate 6, and figs. 11, 12 and 13, Plate 7. Figs. 4, 5 and 6 also illustrate the tendency of cracks to develop in the areas immediately adjacent to inter-crystalline boundaries; a photograph of such a crack is shown in fig. 14,

Plate 7. This tendency has already been noted in a test on another specimen\*; but in that case it was felt that the result might have been accidental. In fig. 6, however, is shown a crack, that developed in the specimen CHJIE3, which runs for practically its whole length within a few hundredths of a millimetre of the boundary. In places indeed this crack appears to run actually along the boundary. This crack is almost parallel to the axis of the specimen and, although of course this direction is a direction of maximum shear stress, long cracks in this direction are

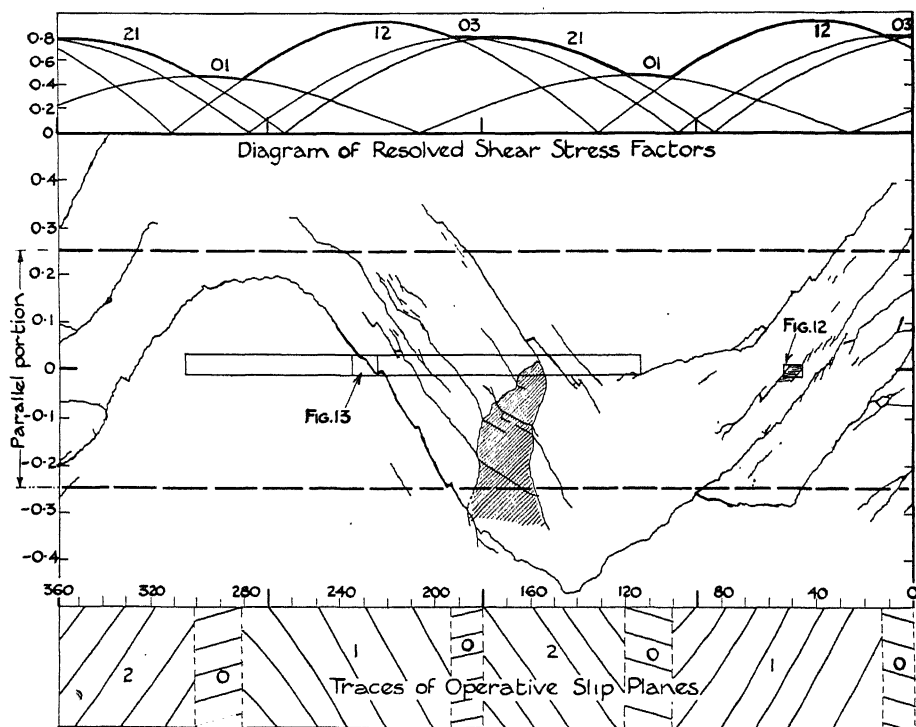


FIG. 5—Specimen CHJIE2 tested in combined flexure and torsion. Survey of cracks after fracture

rather rare, propagation in the circumferential direction being far more usual. Moreover, the main crack in the specimen CHJIE3 was circumferential and therefore, unless the axial crack were developed very early, much of its development must have occurred under rather altered stress conditions.

In view of the very similar crack observed in a previous test,† it seems reasonable to conclude that cracks are more liable to occur near boundaries

\* 'J. Inst. Met.,' vol. 54, No. 1, p. 213 (1934).

† 'J. Inst. Met.,' *loc. cit.*

than elsewhere. Of course, this conclusion does not mean that the presence of a boundary can have only a weakening effect. The presence of boundaries may quite well have a general strengthening effect and may yet introduce additional stresses which may cause cracks to be formed more readily in the vicinity of the boundary than elsewhere.

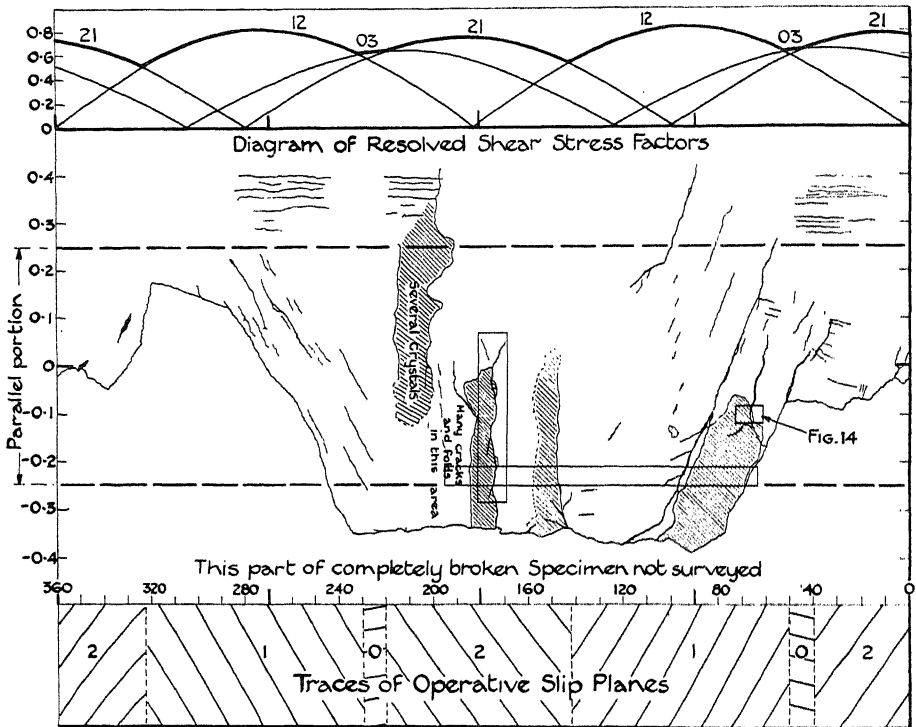


FIG. 6—Specimen CHJIE3 tested in simple torsion. Survey of cracks after fracture

### GENERAL CONCLUSIONS

The chief results of the tests may be briefly summarized as follows:—

1—In each specimen the distribution of slip bands was closely in accordance with that anticipated on the basis of the resolved shear stress law.

2—The slip-band spacing was directly related to the range of resolved shear stress on the slip plane, the spacing being close where the stress was high and wide where the stress was low.

3—Failure was determined by the value of the maximum resolved shear stress and not by that of the nominal maximum shear stress.

4—Cracks were formed first in regions subjected to high stress, where heavy slip had previously occurred, and tended to develop along the traces of the operative slip planes.

5—The total number of cracks formed was larger than usual, the specimens tested in flexure and in combined flexure and torsion in particular developing a very large number.

6—There was a definite tendency for cracks to develop in the vicinity of boundaries.

#### REMARKS ON GENERAL CONCLUSIONS

The first, third and fourth conclusions need little comment. So many other tests have led to the same conclusions that, in the present case, they are remarkable only on account of the unusual nature of the stress conditions imposed.

The second conclusion might reasonably be stated in more definite terms; but it is recognized that the number of measurements made in the present tests are far too few to justify anything more than a general statement of the nature of the results.

The fifth conclusion probably points a real difference between the test conditions in flexure and in torsion; but it is possible that the greater number of cracks may be due merely to the fact that in the combined stress machine (with the very small loads used in the present tests) increase of strain may lead to reduction of load, whereas in the Stromeier machine (in which tests on single crystal specimens have hitherto usually been made) it leads to an increase of load.

The sixth conclusion is indicated fairly clearly by the results of the present tests and is in accordance with the result of a previous test; but it is not necessary to infer from it that the presence of boundaries should have only a weakening effect.

The experiments described form a part of a general research into the characteristics of fatigue financed by the Department of Scientific and Industrial Research and supervised by the Executive Committee of the National Physical Laboratory; the authors desire to record their appreciation of the opportunities afforded for carrying out the research. They also wish to express their thanks to their colleagues in the Physics and Metallurgical Departments of the N.P.L. for assistance kindly rendered in connection with X-ray analysis and preparation of specimens, and particularly to Dr. H. J. Gough, F.R.S., for the interest he has taken in the work.

## SUMMARY

The recent development at the National Physical Laboratory of a new type of combined flexural and torsional fatigue testing machine has made it possible to carry out tests under alternating flexural stresses on single crystal specimens.

Three single crystal specimens all of the same orientation have been tested, one under alternating flexural, one under alternating torsional and the other under a combination of alternating flexural and alternating torsional stresses. The distribution of slip bands on each specimen was entirely in accordance with that predicted from the calculated values of the shear stresses according to the resolved shear stress law, and the results thus afford evidence of the validity of this law in cases where the stress distribution is not simple. Measurements of the mean slip band spacing have been made and the relation between mean slip band spacing and the value of the resolved stress has been examined. The fracture of the specimens has been shown to occur in the normal manner by the development of cracks formed on the site of previous heavy slip, and the dependence of failure on the value of the *resolved* shear stress has been demonstrated.

---

## Investigations of Raman Spectra

### Part I—The Raman Spectra of Sulphuric, Nitric, and Nitrosylsulphuric Acids

By W. ROGIE ANGUS and ALAN H. LECKIE, Sir William Ramsay  
Laboratories of Inorganic and Physical Chemistry, University College,  
London

(Communicated by F. G. Donnan, F.R.S.—Received December 6, 1934)

#### 1—INTRODUCTION

Apart from the large amount of research undertaken to prove the existence of nitrosylsulphuric acid as an intermediate product in the manufacture of sulphuric acid by the lead chamber process, many researches have been made to determine the composition and constitution of the molecule. Whilst it is universally agreed that the empirical formula is  $\text{HNSO}_5$ \* there is diversity of opinion on the molecular configuration and four different molecular structures are to be found in the literature.

The present work was undertaken in an endeavour to clarify the position and in the hope that, by correlating the results obtained by Raman spectroscopy with the large amount of existing chemical data, more definite conclusions could be drawn regarding the molecular structure.

The Raman spectra of nitrosylsulphuric acid in the solid state and of solutions of nitrosylsulphuric acid in sulphuric acid have therefore been examined. The range of concentrations of sulphuric acid in which nitrosylsulphuric acid is incompletely hydrolysed has also been investigated. Spectra of commercial 100% sulphuric acid and of pure 100% nitric acid have been studied in order to trace any relationships between these acids and nitrosylsulphuric acid and to help in the assignment of displacements.

#### 2—PREPARATION OF MATERIALS

*Sulphuric Acid*—This was the 100% A.R. acid supplied by Messrs. Spencer, Chapman and Messel and was used without further purification. On analysis by dilution and titration with standard sodium hydroxide, it was found to be 98%  $\text{H}_2\text{SO}_4$ .

\* Weber, 'Pogg. Ann.,' vol. 123, p. 341 (1864).

*Nitric Acid*—The nitric acid was prepared by mixing one volume of pure concentrated nitric acid with two volumes of 100% A.R. sulphuric acid and distilling *in vacuo*. The distillate was analysed by diluting and titrating with standard sodium hydroxide and was found to contain 99.90%  $\text{HNO}_3$ .

*Nitrosylsulphuric Acid*—Nitrosylsulphuric acid was prepared by a method similar to that given by Biltz, Hall and Blanchard.\* Dry sulphur dioxide at 0° C was bubbled into a mixture of three volumes of fuming nitric acid and one volume of glacial acetic acid. The magma thus produced was filtered off, washed with cold glacial acetic acid and carbon tetrachloride, and dried in a vacuum desiccator over concentrated sulphuric acid. Perfectly dry and colourless crystals were obtained which melted with slight decomposition at 73 to 76° C (*cf.* de Claubry†, 120 to 130° C; Weltzein,‡ 73° C; Tilden,§ 85 to 87° C; Elliot, Kleist, Wilkins and Webb,|| 73.5° C). No other method of preparation was tried since Elliot and his co-workers (*loc. cit.*) found that samples obtained by different methods of preparation always had the same crystalline form and the same melting point.

### 3—EXPERIMENTAL ARRANGEMENT

The source of exciting radiation was an air-cooled mercury arc. For liquids light from the arc was directed on a tube essentially the same as Wood¶ has described; whilst for solid nitrosylsulphuric acid a triangular vessel similar to that used by Krishnamurti\*\* was employed. The scattered light was examined by a Hilger E439 glass spectrograph having a mean dispersion of approximately 70 Å per mm at 4600 Å. Since the temperature variation of the laboratory was not more than 1° C in 24 hours it was unnecessary to place the spectrograph in a thermostat, the error arising from temperature variation being only of the order of 0.5 Å.††

Various filters were tried. To reduce the intensity of the 4047 Å mercury line a solution of *p*-nitrotoluene in alcohol‡‡ was found to be as

\* "Laboratory Methods of Inorganic Chemistry," p. 204 (1909).

† 'Ann. Chim. Phys.,' vol. 45, p. 284 (1832).

‡ 'Liebig's Ann.,' vol. 115, p. 213 (1860).

§ 'J. Chem. Soc.,' vol. 27, p. 630 (1874).

|| 'J. Chem. Soc.,' p. 1219 (1926).

¶ 'Phil. Mag.,' vol. 6, p. 729 (1928).

\*\* 'Ind. J. Phys.,' vol. 5, p. 1 (1930).

†† Merton, 'Proc. Roy. Soc.,' A, vol. 113, p. 704 (1927).

‡‡ West and Farnsworth, 'J. Chem. Phys.,' vol. 1, p. 402 (1933).

satisfactory as a saturated aqueous solution of sodium nitrite,\* and had the added advantages of maintaining its efficiency over a longer period of time and of reducing the intensity of the 4358 Å line to a much less extent. The region beyond 4600 Å was satisfactorily reduced by a solution of copper sulphate in ammonia† approximately N/30 with respect to copper; if this concentration is exceeded the 4358 Å mercury line is diminished in intensity. Although a solution of didymium chloride does remove the continuous spectrum in certain regions, it gives absorption bands and was accordingly not used in these investigations.

For short exposures Ilford Double X-Press plates were found to be most suitable in combining speed and fineness of grain. With the longer exposures necessary to bring out weak Raman lines, the undisplaced mercury lines were very strong and these plates tended to become slightly fogged. Wellington Anti-Screen plates were found to be slightly more satisfactory under these conditions.

The Raman spectra were photographed between a mercury arc spectrum, over-exposed to approximately the same extent as in the Raman spectrum, and a silver arc spectrum. The 4668 Å silver line was used as a standard since the undisplaced mercury lines were too broad for accurate measurement; wave-lengths of the Raman lines were obtained by Hartmann interpolation from this standard.

The function of the mercury arc spectrum was to distinguish Raman lines from lines of the mercury spectrum, especially weak lines between 4358 Å and 4916 Å. In this connection it is noteworthy that although Kohlrausch‡ gives only three weak mercury lines between 4358 Å and 4916 Å there are in reality seven such lines which appear in the spectrum of pure mercury and in Raman spectra. The frequencies of the four not given by Kohlrausch are approximately 20520, 21010, 21130, and 21230  $\text{cm}^{-1}$ , the last being very faint indeed. All these lines are easily confused with Raman lines and confusion has arisen in some cases.

#### 4—EXPERIMENTAL RESULTS

*Sulphuric Acid*—Ilford Double X-Press plates and *p*-nitrotoluene filters were used and exposures of 2 and 6 hours were given. The displacements, in  $\text{cm}^{-1}$ , are given in Table I (A. & L.) where they are compared with existing data on concentrated sulphuric acid. Estimated intensities are given in parenthesis.

\* Pfund, 'Phys. Rev.,' vol. 42, p. 581 (1932).

† Bowen, 'J. Chem. Soc.,' p. 2236 (1932).

‡ "Der Smekal-Raman Effekt," p. 18 (1931).



TABLE I

A. & L.	G. & V.	N.	T.	B. & F.	W.	M.	R.	W. & H.	B. & J.
385-434 (4 <i>b</i> )	—	414	404	405	396	$\left\{ \begin{array}{l} 395 \\ 437 \end{array} \right.$	416	$\left\{ \begin{array}{l} 381 \\ 417 \end{array} \right.$	363
564 (5 <i>b</i> )	564	564	557	567	561	560	562	555	556
—	—	740	—	—	—	—	742	—	—
916 (8)	909	911	923	921	908	917	910	910	905
—	—	—	—	—	—	972	—	978	—
1045 (0)	1044	1043	—	1015	—	—	—	—	—
1140 (4)	1149	1170	1133	1128	1143	1135	1171	$\left\{ \begin{array}{l} 1121 \\ 1195 \end{array} \right.$	1123
1364 (1)	—	1366	1326	—	1359	1373	1365	—	—
—	—	1517	—	—	—	—	—	—	—

G. & V. = Ganesan and Venkateswaran, 'Ind. J. Phys.,' vol. 4, p. 196 (1929).

N. = Nisi, 'Jap. J. Phys.,' vol. 5, p. 119 (1929).

T. = Taylor, 'Trans. Faraday Soc.,' vol. 25, p. 781 (1929).

B. & F. = Bell and Frederickson, 'Phys. Rev.,' vol. 37, p. 1562 (1931).

W. = Woodward, 'Phys. Z.,' vol. 32, p. 777 (1931).

M. = Medard, 'C. R. Acad. Sci. Paris,' vol. 197, p. 582 (1933).

R. = Rao, 'Ind. J. Phys.,' vol. 8, p. 123 (1933).

W. & H. = Woodward and Horner, 'Proc. Roy. Soc.,' A, vol. 144, p. 129 (1934).

B. & J. = Bell and Jeppeson, 'J. Chem. Phys.,' vol. 2, p. 711 (1934).

Since the results obtained are in good agreement with the results of other investigators it is not necessary to discuss them in great detail. The weak line at 1364  $\text{cm}^{-1}$  was brought out only on the longer exposure. Undoubtedly the fact that our acid was not absolutely 100%  $\text{H}_2\text{SO}_4$  accounts for the appearance of the extremely faint displacement of 1045  $\text{cm}^{-1}$  which has been assigned to  $\text{HSO}_4'$ . It was difficult to estimate accurately the position of the band maximum in the region 385-434  $\text{cm}^{-1}$  and we have therefore given the breadth of the band in preference to the approximate band maximum of 405  $\text{cm}^{-1}$ . It is interesting to note that Medard gives two displacements of 395 and 437  $\text{cm}^{-1}$ , attributing them to the "bonded  $\text{SO}_4$  ion." Their origin is much more probably the  $> \text{SO}_2$  group since both chlorsulphonic acid and sulphuryl chloride show strong, but diffuse, displacements in this region. For chlorsulphonic acid Nisi\* gives 419  $\text{cm}^{-1}$  and Matossi and Aderhold†

\* 'Jap. J. Phys.,' vol. 5, p. 119 (1929).

† 'Z. Physik,' vol. 68, p. 683 (1931).

give  $414\text{ cm}^{-1}$ ; whilst for sulphuryl chloride Nisi\* gives  $410\text{ cm}^{-1}$ . No trace of the displacements at 740, 975 and  $1517\text{ cm}^{-1}$  was obtained; but these displacements have not been universally encountered previously and, except in the case of the  $975\text{ cm}^{-1}$  displacement, may arise from an impurity. The  $975\text{ cm}^{-1}$  displacement is assumed by Woodward and Horner, and by Medard, to be characteristic of the  $\text{H}_2\text{SO}_4$  molecule and appears only in acid containing 100%  $\text{H}_2\text{SO}_4$ . It is doubtful, however, if this assumption is correct since this frequency was not detected by Bell and Jeppeson who used highly purified  $\text{H}_2\text{SO}_4$  (f.p. =  $10.3^\circ\text{C}$ ).

In addition to the displacements given in column 2 of Table I Ganesan and Venkateswaran give displacements of 2043, 2178, and  $2372\text{ cm}^{-1}$ , which is approximately where the weak mercury lines discussed earlier in the paper would appear. Actually  $2043\text{ cm}^{-1}$  is exactly the frequency difference between 4358 Å ( $\nu = 22938\text{ cm}^{-1}$ ) and the weak mercury line  $\nu = 20897\text{ cm}^{-1}$ ; whilst the other two displacements are given approximately by the differences between the 4358 Å line and the weak mercury lines of frequencies 20742 and  $20520\text{ cm}^{-1}$  respectively.

TABLE II

A. & L.	D. & K.	M. & V.	A. & W.
608 (3)	607	613	607
679 (4)	667	675	667
924 (6)	916	923	916
1064 (2)	—	1048	—
1126 (0)	—	1103	—
1297 (8b)	1292	1295	1291
1407 (1)	—	—	—
1516 (1)	—	1537	—
1611 (0)	1665	—	1665
1699 (4)	1687	1679	1687
—	3420	—	—

A. & L. = this investigation.

D. & K. = Dadiou and Kohlrausch, 'Naturwiss.,' vol. 19, p. 690 (1931).

M. & V. = Medard and Volkringer, 'C. R. Acad. Sci. Paris,' vol. 197, p. 833 (1933).

A. & W. = Aderhold and Weiss, 'Z. Physik,' vol. 88, p. 83 (1934).

*Nitric Acid*—The spectra were obtained using Wellington Anti-Screen plates and *p*-nitrotoluene filters. An exposure time of 3 to 4 hours brought out all the strong lines, but about 16 hours' exposure was necessary to bring out the weaker lines, including one corresponding with a displacement of  $1407\text{ cm}^{-1}$  not hitherto reported. A comparison is given in Table II and the agreement with recorded values is good.

\* 'Jap. J. Phys.,' vol. 6, p. 1 (1930).

*Nitrosylsulphuric Acid*—A large number of spectrograms of nitrosylsulphuric acid in sulphuric acid were taken using the two kinds of plates and appropriate filters. The exposure times were varied between 5 hours and 24 hours, and with the longer exposures all the displacements recorded in the first column of Table III were obtained. The striking feature of all these spectra, as we have already pointed out,\* is the persistence and intensity of the displacement of  $2338\text{ cm}^{-1}$ . To determine if this displacement was really due to nitrosylsulphuric acid the spectrum of solid nitrosylsulphuric acid was then examined and the displacements are recorded in the second column of Table III. Included in this table are the values obtained for sulphuric and nitric acids in the present investigation.

TABLE III

HNSO <sub>5</sub> in 98% H <sub>2</sub> SO <sub>4</sub>	HNSO <sub>5</sub> (solid)	H <sub>2</sub> SO <sub>4</sub>	HNO <sub>3</sub>
422 (5)	428 (1)	405 (4b)	—
561 (5)	560–608 (3, band)	564 (5b)	607 (3)
—	—	—	679 (4)
726 (2)	720 (4)	—	—
810 (1)	811 (1)	—	—
915 (7)	922 (4)	916 (8)	924 (6)
975 (5)	992 (0)	—	—
1045 (4)	1041 (4)	1045 (0)	1064 (2)
1170 (5)	1164 (3)	1140 (4)	1126 (0)
1292 (1)	1286 (4)	—	1297 (8b)
1377 (2)	1392 (1)	1364 (1)	1407 (1)
1497 (5)	1485 (3)	—	1516 (1)
1605 (5)	1592 (0)	—	1611 (0)
1690 (5)	1687 (0)	—	1699 (4)
2338 (9)	2311 (9)	—	—

It will be noticed that similar frequencies were obtained for the solution and for the solid and that under both sets of experimental conditions the frequency displacement of about  $2340\text{ cm}^{-1}$  is most pronounced. In comparing nitrosylsulphuric acid with sulphuric and nitric acids there is marked agreement indicating that nitrosylsulphuric acid contains some of the groups which, in the simpler acids, give rise to these displacements. It is difficult, however, to say definitely in the case of some frequencies exhibited by nitrosylsulphuric acid whether they are due to groups contained in sulphuric acid or to groups contained in nitric acid. It was hoped that examination of the spectrum of nitrosylsulphuric acid in

\* 'Nature,' vol. 134, p. 572 (1934).

nitric acid would shed light on this point but, unfortunately, solution of nitrosylsulphuric acid in 99.90% nitric acid is accompanied by decomposition. The resulting solution absorbs in the blue region of the spectrum and thereby precludes the observation of a Raman effect. Further, certain frequencies occur in nitrosylsulphuric acid which are totally different from the frequencies associated with either of the other two acids and must therefore be due to the molecule of nitrosylsulphuric acid itself. These points of similarity and dissimilarity in the spectra will be discussed more fully in the next section.

One method of demonstrating the characteristic nature of the displacement of  $2340\text{ cm}^{-1}$  was to find out if it occurred in solutions of nitrosylsulphuric acid in various concentrations of sulphuric acid. This would, at the same time, give an indication of the range of concentration of sulphuric acid in which nitrosylsulphuric acid was incompletely hydrolysed. Accordingly solutions of the acid in sulphuric acid containing 90%, 80%, 75%, 65%, 60% and 55%  $\text{H}_2\text{SO}_4$  by weight were examined. On making up these solutions it was observed that only a negligible decomposition was visible for the 90% and 80% solutions. With 75% and 65%  $\text{H}_2\text{SO}_4$  the solutions were perceptibly yellow; whilst at the two lowest concentrations solution was accompanied by considerable effervescence and the formation of a greenish-blue solution. For the more concentrated solutions exposures of 10 to 15 hours were sufficient to produce good spectra, but 22 to 24 hours were required for the weaker solutions. The results are collected in Table IV and compared with those for a solution in 98%  $\text{H}_2\text{SO}_4$ .

TABLE IV

98%	90%	80%	75%	65%	60%	55%
422 (5)	430 (3b)	432 (3b)	424 (2)	—	—	—
561 (5)	586* (3b)	598* (3b)	595 (2)	—	—	—
726 (2)	690 (1)	696 (1)	—	—	—	—
810 (1)	794 (1)	790 (1)	780 (1)	—	—	—
915 (7)	913 (5b)	910 (4b)	901 (2)	Sulphuric acid Raman lines were unobservable on account of absorption.		
975 (3)	—	—	—			
1045 (4)	1041 (5b)	1041 (5b)	1036 (5)			
1170 (5)	1176 (2b)	—	1168 (0)			
1292 (1)	1278 (1)	1214 (1)	1262 (1)	—	—	—
1377 (2)	1381 (1)	1349 (3b)	1365 (1)	—	—	—
1497 (3)	1465 (0)	1490 (0)	—	—	—	—
1605 (3)	1610* (1)	—	—	—	—	—
1690 (3)	—	—	—	—	—	—
2338 (9)	2330 (5)	2317 (5)	2315 (8)	2309 (2)	2305 (3)	? trace

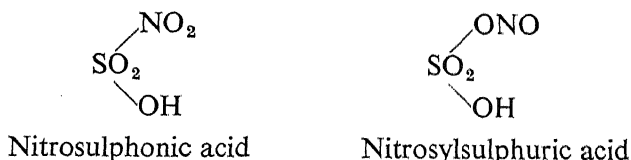
\* Indicates a band centre.

The existence of the strong frequency  $2340\text{ cm}^{-1}$  as characteristic of the nitrosylsulphuric acid molecule was definitely established; it persisted in solutions containing 60%  $\text{H}_2\text{SO}_4$  or more, which agrees very well with the conclusions of Reynolds and Taylor\* from a study of the production of nitrosylsulphuric acid by evaporation of solutions of potassium nitrite in sulphuric acid. Schlesinger and Salathe† from absorption spectra measurements have already confirmed this view, which is contradictory to the view of Raschig that nitrosylsulphuric acid cannot exist *per se* in solutions of sulphuric acid containing less than 80%  $\text{H}_2\text{SO}_4$  by weight.

Further proof that the frequency  $2340\text{ cm}^{-1}$  was associated in some way with nitrosylsulphuric acid was obtained from examining mixtures of concentrated nitric and sulphuric acids. Absolutely no trace of this frequency could be found and the spectra obtained for all the mixtures examined consisted entirely of the frequencies due to the two component acids of the mixture.

#### 5—STRUCTURE OF NITROSYLSULPHURIC ACID

In considering the structure of this substance it will be necessary first of all to discuss briefly the different structures which have been assigned to it. Up to 1926 controversy raged between the two structures:—



Michaelis and Schumann‡ concluded from the reaction between nitrosylsulphuric acid and phosphorus pentachloride that it had the *nitro* structure. Its formation by bubbling sulphur dioxide into well-cooled nitric acid led Raschig, after very extensive chemical research on the substance and its reduction products, to state that “the composition is  $\text{HNSO}_5$  or constitutionally  $\text{O}_2\text{N} \cdot \text{SO}_2 \cdot \text{OH}$ , nitrosulphonic acid,”§ a view which was also shared by Wentzki.||

On the other hand, the nitroso formula was suggested by the following observations. Tilden¶ observed that the appropriate nitrosyl halide was

\* ‘J. Soc. Chem. Industr.’ vol. 31, p. 367 (1912).

† ‘J. Amer. Chem. Soc.’ vol. 45, p. 1863 (1923).

‡ ‘Ber. deuts. chem. Ges.’ vol. 7, p. 1075 (1874).

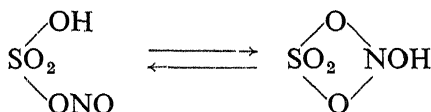
§ ‘J. Soc. Chem. Industr.’ vol. 30, p. 166 (1911).

|| ‘Z. angew. Chem.’ vol. 24, p. 392 (1911).

¶ ‘J. Chem. Soc.’ vol. 27, p. 630 (1874).

obtained when nitrosylsulphuric acid was distilled with sodium chloride or sodium bromide. This was confirmed by Girard and Pabst.\* Lunge† from studying the reaction between nitrogen peroxide and sulphuric acid also favoured this form. Additional evidence in favour of this structure was the formation of nitrosylsulphuric acid from acid silver sulphate and nitrosyl chloride,‡ and from acid silver sulphate and nitrosyl bromide.§

In 1916 Biehringer and Borsum|| studied the reaction between nitrosylsulphuric acid and dimethylaniline. They found that both *p*-nitro- and *p*-nitroso-dimethylaniline were formed, the relative amounts of both products depending on the temperature at which the reaction took place. They suggested therefore that the substance  $\text{HNSO}_5$  consists of the two forms given above. This work was repeated 10 years later¶ and only *p*-nitrosodimethylaniline was obtained. Hantzsch and Berger\*\* state that Sperling†† using 100%  $\text{H}_2\text{SO}_4$  repeated this work and never succeeded in obtaining even a trace of *p*-nitrodimethylaniline. This, then, would seem to indicate that  $\text{HNSO}_5$  exists only in the nitroso form. Elliot and his co-workers state that “whilst the acid may be tautomeric the existence of non-dynamic isomerides is improbable.” They put forward the view that the substance is present as an equilibrium mixture of the two forms:



basing their view on observations on the products obtained in reactions between  $\text{HNSO}_5$  and benzoyl chloride, acetyl chloride, acetic anhydride, and diethyl ether.

A fourth structure has been put forward by Hantzsch and Berger (*loc. cit.*) following observations of the molecular weight in absolute sulphuric acid and by analogy with nitrosyl perchlorate,  $\text{NOClO}_4$ . They suggest that it is nitrosacidium sulphate and has the salt-like formula  $[\text{HOSO}_3]^{+}[\text{NO}]^{-}$ .

\* ‘Bull. Soc. Chim. Franc.’, vol. 30, p. 531 (1878).

† ‘Ber. deuts. chem. Ges.’, vol. 12, p. 1058 (1879).

‡ Berl, ‘Z. angew. Chem.’, vol. 23, p. 2250 (1910).

§ Berl, Becker and Begerow, ‘Z. anorg. Chem.’, vol. 209, p. 264 (1932).

|| ‘Ber. deuts. chem. Ges.’, vol. 49, p. 1402 (1916).

¶ Elliot, Kleist, Wilkins and Webb, ‘J. Chem. Soc.’, p. 1219 (1926).

\*\* ‘Z. anorg. Chem.’, vol. 190, p. 321 (1930).

†† ‘Dissertation,’ Leipzig, 1925.

So far only chemical evidence has been considered. The absorption spectrum has been investigated by Baly and Desch,\* and by Schlesinger and Salathe.† The earlier workers found that solutions of  $\text{HNSO}_5$  in  $\text{H}_2\text{SO}_4$  gave continuous absorption and refer to it as nitrosulphonic acid. Schlesinger and Salathe (*loc. cit.*) found from their measurements that nitrosylsulphuric acid was not completely hydrolysed until the concentration of sulphuric acid had been lowered to 40%. They found also that nitrosylsulphuric acid in 39.6%  $\text{H}_2\text{SO}_4$  and potassium nitrite in sulphuric acid of the same concentration gave exactly the same absorption spectra indicating the complete hydrolysis to  $\text{HNO}_2$  at this concentration. Berl and Winnacker‡ have confirmed this by observing that an 0.2 mol solution of  $\text{HNSO}_5$  in 40%  $\text{H}_2\text{SO}_4$  gave a spectrum similar to the spectrum of  $\text{N}_2\text{O}_3$  in water. With more concentrated sulphuric acid Schlesinger and Salathe found that the spectra of  $\text{HNSO}_5$  and  $\text{HNO}_2$  were not similar. From the fact that there is strong evidence for considering  $\text{HNO}_2$  to have the structure  $\text{HONO}$ , they conclude that  $\text{HNSO}_5$  contains the  $\text{NO}_2$  group. The reason for our being unable to obtain Raman displacements with  $\text{HNSO}_5$  in solutions containing less than 60%  $\text{H}_2\text{SO}_4$  may be that, with the long exposures we have given, complete hydrolysis is accomplished during the exposure.

Returning now to our experimental data, we would repeat the close similarity between the spectra of nitrosylsulphuric acid and the two simple acids, which is readily observed by reference to Table III. The outstanding difficulty is, certainly, the origin of the strong Raman frequency of  $2340\text{ cm}^{-1}$  which is absent in the spectra of the simple acids. A careful search of the literature on nitro-paraffins and nitro-aromatic compounds revealed only a very slight similarity between the spectrum under consideration and their spectra. Moreover, the recent results of Medard§ on alkyl nitrates exhibit no displacement near to  $2340\text{ cm}^{-1}$  and there is no close agreement between his results and ours. If  $\text{HNSO}_5$  has the configuration  $\text{OH} \cdot \text{SO}_2 \cdot \text{ONO}$ , it would be expected that the spectrum obtained for it would be similar, in many respects, to the spectra of alkyl nitrites. Whilst there is, with this type of compound, a much closer agreement with our results than existed for the other types mentioned, Dadieu, Jele and Kohlrausch|| record no displacement near to

\* 'J. Chem. Soc.,' vol. 93, p. 1747 (1908).

† 'J. Amer. Chem. Soc.,' vol. 45, p. 1863 (1923).

‡ 'Z. anorg. Chem.,' vol. 212, p. 113 (1933).

§ 'J. Chim. Phys.,' vol. 31, p. 281 (1934).

|| 'S. B. Akad. Wiss. Wien.,' vol. 140, p. 293 (1931).

2340  $\text{cm}^{-1}$ . This frequency, as will be shown later, plays a very important rôle in deciding the structure of the molecule.

The observed displacements for nitrosylsulphuric acid can be divided conveniently into four groups.

(a) *Displacements observed for both Sulphuric Acid and Nitric Acid*—The displacements in this group are 915, 1045, 1170 and 1377  $\text{cm}^{-1}$  and it will be shown later that their origin is much more likely to be in the groups of  $\text{H}_2\text{SO}_4$  than in the groups of  $\text{HNO}_3$ .

(b) *Displacements observed for Nitric Acid only*—There are four displacements in this group at 1292, 1497, 1605 and 1690  $\text{cm}^{-1}$ . The last three correspond with weak Raman lines of nitric acid, whereas 1292  $\text{cm}^{-1}$  corresponds with the strongest Raman line of  $\text{HNO}_3$  at 1297  $\text{cm}^{-1}$ . In nitrosylsulphuric acid 1292  $\text{cm}^{-1}$  is a weak line, but in alkyl nitrates a strong line is reported by Medard (*loc. cit.*) in this region. These facts, and the complete absence of any trace of the strong  $\text{HNO}_3$  displacement of 679  $\text{cm}^{-1}$ , indicate the improbability of  $\text{HNSO}_5$  having the nitrosulphonic acid structure.

(c) *Displacements observed for Sulphuric Acid*—Two displacements at 422 and 561  $\text{cm}^{-1}$  appear in this group and their origin is undoubtedly the  $>\text{SO}_2$  group. By reference to Table IV it will be seen that the intensities of the displacements 422, 561, 915, 1170 and 1377  $\text{cm}^{-1}$  are diminished considerably in the less concentrated solutions of sulphuric acid; this is proof that these displacements have their origin in an  $>\text{SO}_2$  or OH

an  $>\text{SO}_2$  group.\* The frequency, 1045  $\text{cm}^{-1}$ , on the other hand, shows slightly enhanced intensity in the more dilute solutions. In 98%  $\text{H}_2\text{SO}_4$  this frequency is very weak and has been attributed to  $\text{HSO}_4'$ . But in a solution of nitrosylsulphuric acid in 98%  $\text{H}_2\text{SO}_4$  and also in solid nitrosylsulphuric acid it is one of the strongest frequencies observed. Clearly, then, this indicates the presence of the  $\text{HSO}_4'$  group in  $\text{HNSO}_5$  and supports the formulation of Hantzsch and Berger (*loc. cit.*).

(d) *Displacements observed in  $\text{HNSO}_5$  only*—Of the four displacements, 726, 810, 975 and 2340  $\text{cm}^{-1}$ , peculiar to  $\text{HNSO}_5$ , the first three are weak. The persistence and prominence of the 2340  $\text{cm}^{-1}$  displacement has already been commented on. It occurs in a region (2000–2800  $\text{cm}^{-1}$ ) in which

\* Cf. Raman effect data on  $\text{H}_2\text{SO}_4$  and sulphates.



very few groups give characteristic Raman frequencies, the most important being—

$C \equiv C$	.....	1980–2240 $\text{cm}^{-1}$
$C \equiv N$	.....	2050–2270 $\text{cm}^{-1}$
$C \equiv O$	.....	2155 $\text{cm}^{-1}$
$N \equiv N$	.....	2330 $\text{cm}^{-1}$
$S - H$	.....	2570 $\text{cm}^{-1}$

Of these, only  $N \equiv N$  and  $S - H$  need be considered. It is unlikely that it arises from  $N \equiv N$  as it is inconceivable how this link could be incorporated even in a polymerized molecule. The  $S - H$  link is ruled out because of the similarity between  $\text{HNSO}_5$  and concentrated sulphuric acid, which is  $\text{HO} \cdot \text{SO}_2 \cdot \text{OH}$ .

A possible reason is that this very strong displacement is due to  $S - N$ , but very little data is available on this link and no record of Raman measurements on substances containing this link could be found in the literature. The only available spectroscopic evidence is from the band spectrum observed by Fowler and Bakker\* on photographing the spectrum produced by passing a condensed discharge through a mixture of nitrogen and sulphur vapour. Bands corresponding with the  $\beta$  and  $\gamma$  bands of  $\text{NO}$  were observed and vibrational analysis gave the characteristic frequency of  $1220 \text{ cm}^{-1}$ . This evidence makes it unlikely that the  $N - S$  link is the origin of the  $2340 \text{ cm}^{-1}$  displacement. Since it is only in nitrosulphonic acid that an  $N - S$  link would appear, this formulation cannot be accepted.

It has been suggested in the previous section that the correct formulation of  $\text{HNSO}_5$  is  $[\text{HOSO}_3][\text{NO}]^+$ , nitrosacidium sulphate. It is highly probable, therefore, that the  $2340 \text{ cm}^{-1}$  displacement is associated with the positive ion of this formulation. Direct comparison with Raman effect data for  $\text{NO}$  is not possible since Rasetti† observed only rotational Raman bands but no vibrational Raman bands; but even if this evidence were available the comparison would not be legitimate because of the difference in the electronic configurations of  $\text{NO}$  and  $\text{NO}^+$ . Whilst band spectra (*vide* Jevons, "Report of Band Spectra of Diatomic Molecules," 1932) give information on the characteristic frequencies of  $\text{NO}$  in the ground state and in excited states, corresponding data for  $\text{NO}^+$  are not available. To prove that the  $2340 \text{ cm}^{-1}$  displacement has its origin in the  $\text{NO}^+$  group we have used the following process of reasoning by analogy from recorded band spectra data.

\* 'Proc. Roy. Soc.,' A, vol. 136, p. 28 (1932).

† 'Nuovo Cim.,' vol. 7, p. 261 (1930).

In the ground state the  $\text{O}_2^+$  molecule has a characteristic frequency ( $\omega_e$ ) of  $1876\text{ cm}^{-1}$  and an internuclear separation ( $r_e$ ) of  $1.14\text{ \AA}$ .  $\text{O}_2^+$  has 15 electrons and is isoelectronic with NO, for the ground state of which  $\omega_e$  is  $1906\text{ cm}^{-1}$  and  $r_e$  is  $1.15\text{ \AA}$ . When NO loses an electron to give  $\text{NO}^+$  the resultant molecule is isoelectronic with  $\text{N}_2$ . For  $\text{N}_2$  the Raman frequency is  $2330\text{ cm}^{-1}$ . The agreement between this frequency and our observed frequency of  $2340\text{ cm}^{-1}$  is as close as the agreement between the frequencies of the isoelectronic pair of molecules, NO and  $\text{O}_2^+$ .

This not only confirms the belief that the  $2340\text{ cm}^{-1}$  displacement arises from  $\text{NO}^+$  but explains why this displacement is not exhibited by alkyl nitrates or nitrites. The absence of this strong frequency in the Raman spectra of these alkyl derivatives precludes the assignment of a nitro or nitroso structure to  $\text{HNSO}_5$ . From our experimental results we are led to the conclusion that the molecule,  $\text{HNSO}_5$ , contains the  $\text{HSO}_4^-$  group and the  $\text{NO}^+$  group—a conclusion which supports the salt-like configuration  $[\text{HOSO}_3]^+[\text{NO}]^+$ .

In Table V are summarized the variations in the value of the strong displacements of  $2340\text{ cm}^{-1}$  in different strengths of sulphuric acid.

TABLE V

% $\text{H}_2\text{SO}_4$ by weight . . . . .	98	90	80	75	65	60
$\Delta\nu$ . . . . .	2338	2330	2317	2315	2309	2305

The corresponding displacement for the solid is  $2311\text{ cm}^{-1}$ . If these displacements in Table V are plotted against the concentration of  $\text{H}_2\text{SO}_4$  an almost linear relationship is obtained. The significance of this is not clear, and it must be assumed that the  $\text{NO}^+$  ion is affected in some way by the acid strength.

In conclusion, we agree with Hantzsch and Berger that the correct formulation is  $[\text{HOSO}_3]^+[\text{NO}]^+$  and that it is in full agreement with chemical evidence. Also, it explains the dissimilarity between the spectra of  $\text{HNSO}_5$  and  $\text{HNO}_2$  reported by Schlesinger and Salathe. We feel that nitrosyl sulphate is the most suitable designation for the substance, particularly since "nitrosylsulphuric acid" does not give metallic derivatives and cannot therefore be regarded as a true acid.

Our thanks are due to Professor F. G. Donnan for his kind interest and encouragement, to Dr. E. Teller for helpful criticism, to Mr. Olaf Bloch, of Messrs. Ilford, Ltd., for valuable advice regarding plates, and to Mr. G. A. Benford for advice regarding the preparation of 100% nitric acid.

## SUMMARY

Raman spectra are recorded for concentrated sulphuric and nitric acids, for solutions of  $\text{HNSO}_5$  in sulphuric acid and for solid  $\text{HNSO}_5$ . By observing the spectra of  $\text{HNSO}_5$  in various concentrations of  $\text{H}_2\text{SO}_4$  it is concluded that in solutions of  $\text{HNSO}_5$  in sulphuric acid containing more than 60%  $\text{H}_2\text{SO}_4$  the hydrolysis of  $\text{HNSO}_5$  is incomplete. The spectra of  $\text{HNSO}_5$ , both in solution and in the solid state, are characterized by a prominent displacement of  $1045\text{ cm}^{-1}$  which is assigned to the  $\text{HSO}_4^-$  ion. Another very prominent displacement of  $2340\text{ cm}^{-1}$  for solutions and  $2311\text{ cm}^{-1}$  for the solid state is shown, by analogy from band spectral data for isoelectronic groups, to arise from the group  $\text{NO}^+$ . Of the different molecular structures reviewed, only  $[\text{HOSO}_3]'$   $[\text{NO}]'$ , nitrosyl sulphate, is in accord with observed data.

---

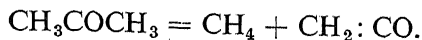
The Thermal Decomposition of Acetone Vapour

By C. A. WINKLER and C. N. HINSHELWOOD, F.R.S.

(Received December 18, 1934)

## INTRODUCTION

The decomposition of acetone first aroused interest as an example of a unimolecular gas reaction at a time when few suitable for kinetic investigation were known. The rate of decomposition in the earlier work\* was inferred from the rate of pressure increase, a method which is only reliable when certain conditions are fulfilled. Whether they are fulfilled by the acetone decomposition has been questioned from time to time. The main reaction is followed by a slow decomposition of unsaturated hydrocarbons which it produces, and the correction of the "end-point" for the subsequent pressure changes is subject to some uncertainty.\* Further, ketene is known to be a possible decomposition product of acetone, and the suggestion has even been made that the rate actually measured was that of the decomposition of ketene,† produced almost instantaneously from acetone by the reaction



\* Hinshelwood and Hutchison, 'Proc. Roy. Soc.,' A, vol. 111, p. 245 (1926).

† Taylor, 'J. Phys. Chem.,' vol. 30, p. 1433 (1926); cf. Rice and Wollrath, 'Proc. Nat. Acad. Sci. Wash.,' vol. 15, p. 702 (1929).

For these reasons the reaction has been re-investigated by an analytical method which measures directly the rate of disappearance of acetone without any assumptions about the products or about their subsequent decompositions. In addition the nature of the products has been more fully studied.

It has recently been suggested\* that acetone decomposes by a mechanism involving long chains. One important criterion of such reactions is the influence of the surface area and the dimensions of the vessel. Therefore in the present work these factors have been carefully re-examined.

Interest has lately been directed towards the shape of the curves connecting reaction rate and initial pressure, especially in the region of lower pressures.† These curves have been determined for acetaldehyde,‡ propionic aldehyde§ and nitrous oxide,|| but the original investigation gave no clue to the behaviour of acetone below about 100 mm. The range from 100 mm down to 2.5 mm has now been included.

#### EXPERIMENTAL METHOD

The principle of the method used for following the course of the reaction was to withdraw samples from the vessel into an evacuated pipette, dissolve out the residual acetone in water and estimate it by the iodoform method, which was found by blank tests on undecomposed acetone to be applicable over the whole range of acetone pressures employed. While it would be possible to plot directly the analyses against the corresponding reaction times, a better procedure is first to construct a set of calibration curves giving analysis against pressure change in the reaction vessel, then to determine a set of pressure increase-time curves, and to translate these into analysis-time curves by means of the calibration curves. The advantage of this method lies in the fact that, since the accuracy with which the points lie on the final curve depends above all on the exactness of the temperature control, an expeditious method of making the actual rate measurements is desirable. Slight temperature variations during the construction of a calibration curve are

\* Rice and Herzfeld, 'J. Amer. Chem. Soc.', vol. 56, p. 284 (1934).

† Hinshelwood, 'Proc. Roy. Soc.,' A, vol. 146, p. 239 (1934); Hinshelwood, Fletcher, Verhoek and Winkler, *ibid.*, p. 327.

‡ Fletcher and Hinshelwood, *ibid.*, vol. 141, p. 41 (1933).

§ Winkler, Fletcher and Hinshelwood, *ibid.*, vol. 146, p. 345 (1934).

|| Musgrave and Hinshelwood, *ibid.*, vol. 135, p. 23 (1932); Hunter, *ibid.*, vol. 144, p. 386 (1934).

unimportant since they affect the pressure change measurement and the analysis to almost exactly the same extent.

The apparatus was in all essential respects the same as that used recently in the study of the reaction with propionic aldehyde.\* Calibration curves of pressure increase  $(p - p_0)$ , against the amount of acetone in millimetres which had disappeared from the reaction vessel were constructed for initial pressures of acetone of 300, 200, 100, 50 and 15 mm. For the latter the McLeod gauge technique previously described was used. In all these determinations the pressure of the acetone vapour in the reaction bulb had to be calculated from the weight found analytically in a measured fraction of the total content of the bulb. A correction was applied for the volume of the tubing connecting the sampling pipette and the reaction vessel. A further correction was applied for the capillary tube of the manometer, containing acetone which cannot decompose except in experiments so prolonged that diffusion occurs. This dead-space is about 1–2% of the total volume, but is effectively greater on account of the difference in temperature between it and the reaction vessel. The effective value was determined by taking samples of pure acetone vapour from the bulb at room temperature and at 270°. From the weight (by analysis), the pressure and the temperature, the effective volume of the whole system was calculated. Deducting from this the true volume of the reaction vessel itself, the effective volume of the dead-space at the two temperatures is found. Extrapolation gives the appropriate correction for other temperatures. The total weight of acetone,  $w$ , in the bulb plus dead-space is given by

$$w = \frac{273M}{760 \times 22,400T} \{pV + p_0v\},$$

where  $M$  is the molecular weight,  $T$  the temperature of the reaction bulb,  $p$  the partial pressure of acetone when the sample is taken,  $p_0$  the initial pressure,  $V$  the true volume of the reaction bulb at  $T$  and  $v$  the effective volume of the dead-space. The use of  $p_0$  assumes that the original acetone in the dead-space simply remains there unchanged, which is obviously only an approximation, but one justified by the fact that what is calculated is itself only a correction amounting to a few per cent.

The calibration curves are shown in fig. 1, all plotted on the same scale to show the variation with pressure, though naturally for practical use separate large scale versions were available. Other initial pressures could be provided for by interpolation.

\* Winkler, Fletcher and Hinshelwood, 'Proc. Roy. Soc.,' A, vol. 146, p. 345 (1934).

## THE REACTION-TIME CURVES

Fig. 2 shows the relation between the pressure increase and the time at 595° C (curve A), and the translation of this curve into terms of the actual acetone which has reacted (curve B). For comparison is plotted a curve (C) showing the rate of disappearance of acetone as inferred from the pressure increase by the approximate method previously used. Fig. 3 shows the two typical experiments at two different initial pressures at 602° C.

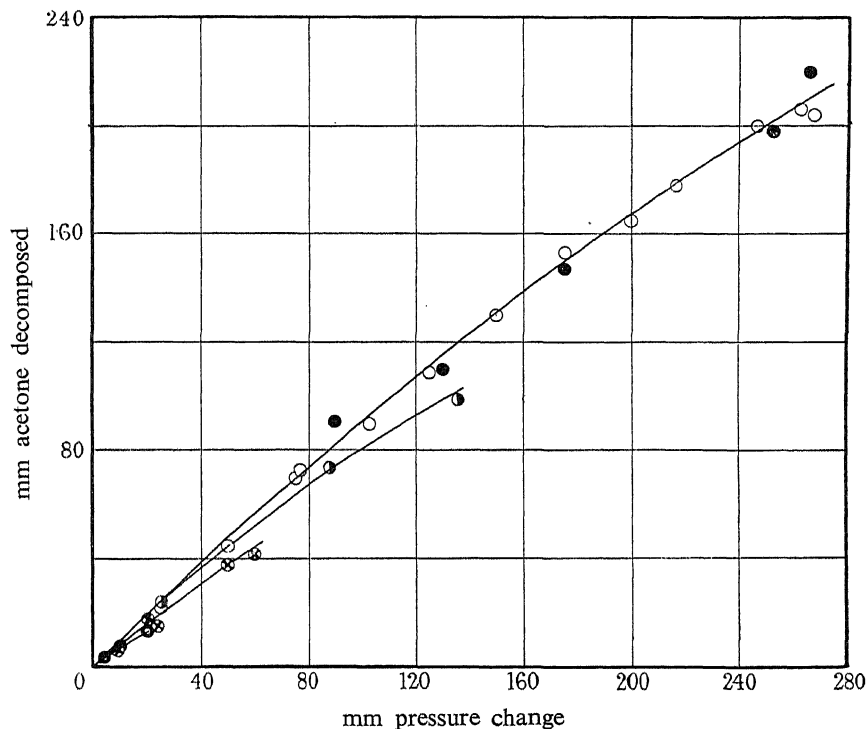


FIG. 1—Relation between pressure change and acetone decomposed. Initial pressure ● = 300 mm, ○ = 200 mm, ● = 100 mm, ⊗ = 50 mm, ⊙ = 15 mm

The curves B and C in fig. 2 are so plotted that they reach the same end-point. Curve B does not deviate widely from C until the reaction is about half over, after which the divergence becomes fairly marked, and in the sense that acetone disappears less rapidly than would have been inferred from the pressure change alone. The time of half change,  $t_{\frac{1}{2}}$ , inferred from B is 150 seconds while that from C is 134 seconds. From C the ratio  $t_{\frac{1}{2}}/t_{\frac{1}{4}}$  is 2.16, while from B it is 2.69. The latter figure is quite close to the mean value for this ratio at 200 mm in a number

of other experiments. For an ideally unimolecular reaction the ratio is 2.00. Thus a first order velocity constant calculated for curve B shows, as the reaction proceeds, a diminution which is much more marked than for curve C. On the other hand, the influence of the initial pressure on  $t_{\frac{1}{2}}$  between 112 and 212 mm is negligible, the values read off from the curves in fig. 3 being 100 seconds and 101 seconds for the two pressures respectively.

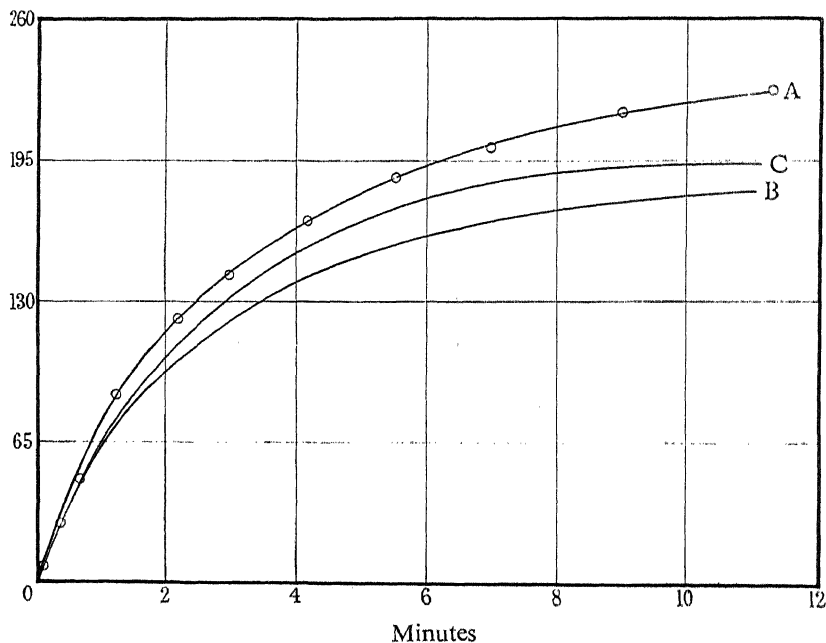


FIG. 2—Decomposition of acetone at 595° C and 218 mm initial pressure. A, pressure increase; B, acetone decomposed (new method); C, acetone decomposed (old method)

#### THE INTERMEDIATE PRODUCTION OF KETENE

The amount of ketene produced at different stages of the reaction at 595° C was determined by withdrawing samples in a gas pipette, dissolving in water and titrating with dilute alkali using cresol red as indicator. If the solution was warmed before titration no difficulty was found with the end-point.

The results are shown in fig. 4. The amount of ketene present reaches a maximum and then decreases in the way characteristic of an intermediate product. If we assume

$$-d[\text{CH}_3\text{COCH}_3]/dt = k_1[\text{CH}_3\text{COCH}_3]$$

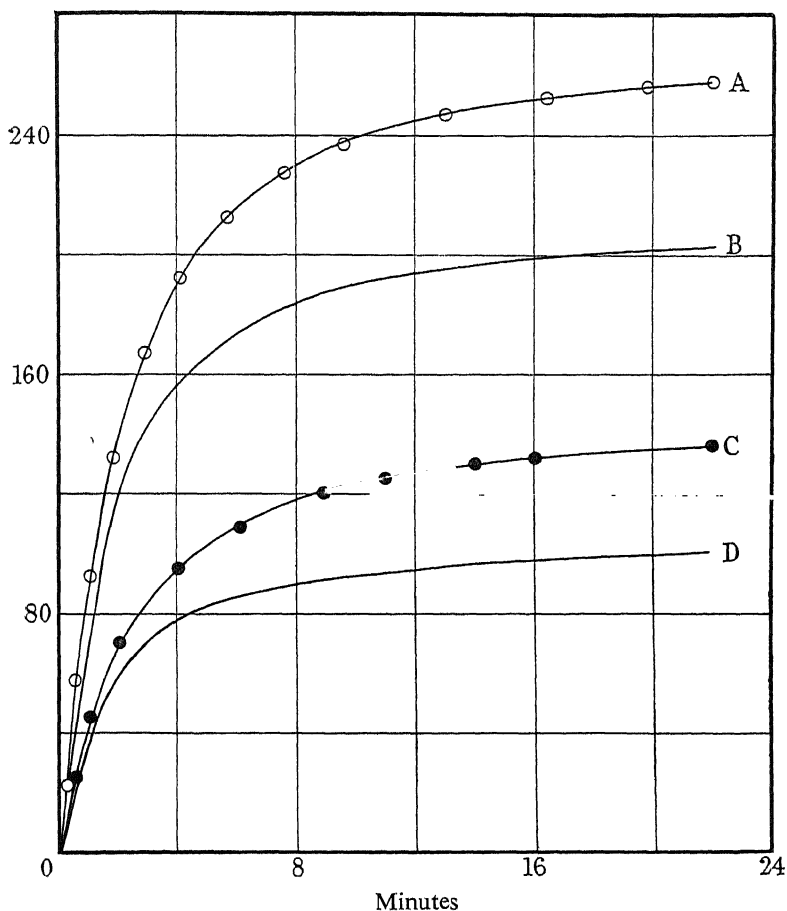


FIG. 3—Decomposition of acetone at two different initial pressures at 602° C. A, pressure increase,  $p_0 = 212$ ; B, acetone decomposed,  $p_0 = 212$ ; C, pressure increase,  $p_0 = 112$ ; D, acetone decomposed,  $p_0 = 112$

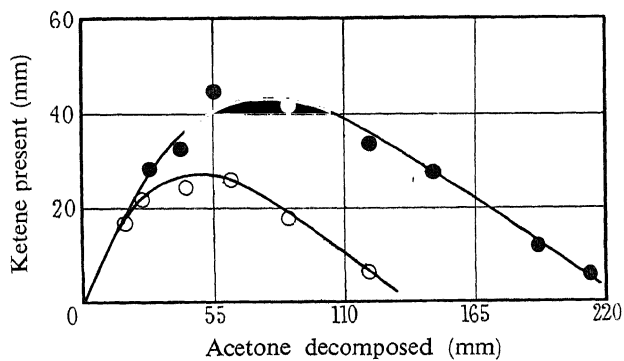


FIG. 4—Intermediate formation of ketene from acetone at 595° C. ●,  $p_0 = 200$ ; ○,  $p_0 = 100$



and

$$-d[\text{CH}_2:\text{CO}]/dt = k_2 [\text{CH}_2:\text{CO}]$$

realizing that  $k_2$  may prove to be a function of concentration, and if  $(a - x)$  is the concentration of acetone at time  $t$  and  $y$  that of ketene, then  $dy/dt = k_1(a - x) - k_2y$  whence  $y_{\text{max}} = (k_1/k_2) \cdot a \cdot e^{-k_1 t_{\text{max}}}$ . Thus from the position and magnitude of the maximum the ratio of the two velocity constants can be found. At  $595^\circ$  for 200 mm initial pressure of acetone,  $y_{\text{max}} = 44$  and occurs when 72.5 mm of acetone have reacted. At this temperature and initial pressure  $t_{\frac{1}{2}}$  for acetone is 132 seconds, whence  $k_1 = 5.25 \times 10^{-3}$ .  $t_{\text{max}}$  is 85.6 seconds, whence  $k_2/k_1 = 2.9$ . For 100 mm initial pressure the corresponding calculation gives 1.9. For the higher initial pressure, therefore, the ketene decomposes three times as fast as the acetone. For the smaller initial pressure the ratio is lower, indicating that the rate of decomposition of ketene falls off more rapidly than that of acetone. The decomposition of ketene is thus of a higher order than that of acetone, which is of the first order over this pressure range. This conclusion agrees with the direct experiments of Williamson\* on the decomposition of ketene.

#### ANALYSIS OF THE GASEOUS REACTION PRODUCTS

Samples were withdrawn at various stages of the reaction, and analysed, after the unchanged acetone and the ketene had been dissolved out in water. The results are given in Table I.

TABLE I—PRODUCTS FROM DECOMPOSITION OF ACETONE AT  $600^\circ \text{C}$

Initial pressure	% acetone decomposed	CO <sub>2</sub>	Unsat.	CO	H <sub>2</sub>	CH <sub>4</sub>	C <sub>2</sub> H <sub>6</sub>
200	12	1.5	8.6	21.5	2.5	66.1	0.0
200	25	3.1	10.1	29.4	1.4	54.5	0.0
200	50	3.6	11.6	33.6	3.0	49.0	0.0
50	50	3.6	11.4	31.9	2.5	48.4	0.0
200	75	2.7	10.1	38.3	1.3	48.0	0.0
200	98	4.7	8.0	42.0	2.1	42.4	1.5
200	38 hours after completion	4.1	2.8	38.4	7.8	45.8	0.0

The fall in the proportion of methane and the parallel increase in that of carbon monoxide is consistent with the assumption that the primary reaction gives methane and ketene, and is followed by the decomposition

\* 'J. Amer. Chem. Soc.,' vol. 56, p. 2216 (1934).

of the latter yielding carbon monoxide. If ketene gave  $\text{CO} + \frac{1}{2}\text{C}_2\text{H}_4$ , the proportion of unsaturated compounds should reach a higher value than it does. This indicates either a more complex method of decomposition of ketene, or a decomposition of some of the acetone by a mechanism independent of ketene. At 98% reaction, the methane and carbon monoxide are equivalent, as required. As has been stated, there is a long slow pressure increase subsequent to the main reaction. Inspection of the table shows that some at least of this is due to the slow decomposition of the unsaturated hydrocarbons. The relative rates of the acetone decomposition itself and this subsequent reaction of the products is indicated by the fact that the "98%" analysis in the table was taken after about 2 hours.

#### THE INFLUENCE OF THE SURFACE AND DIMENSIONS OF THE REACTION VESSEL

Three reaction vessels were used. The first was an unpacked silica bulb of 300 cc capacity and diameter 7 cm. The second was a similar bulb packed with lengths of silica tubing of internal diameter 1 cm, of the same origin as the bulbs themselves. The third was a bulb packed with small silica spheres. The surface/volume ratios of these bulbs were 1:5:16, so that a heterogeneous reaction would be very much favoured in the third. A reaction depending upon chains which can be broken at the vessel wall would be greatly retarded in the packed bulbs because of the diminished free space. In them the rate of the hydrogen-oxygen reaction had actually been found to be a small fraction only of the rate in the unpacked bulb. The reaction being very sensitive to temperature, all the experiments were made in an uninterrupted series, each bulb being placed carefully in the same position in the furnace. The results of one typical series of experiments are shown graphically in figs. 5 and 6. For the present purpose pressure increases have been plotted directly.

It is obvious that there is no increase in rate proportional to increased surface/volume ratio, nor any diminution in rate with diminished free space at all comparable with that found in such chain reactions as the oxidation of hydrogen or of methyl alcohol. Nevertheless, there appears at first sight from fig. 5 to be a definite small retardation of the reaction in the packed bulbs, such as would indicate the existence of short chains. This, however, is probably illusory. In the packed vessels the end-point of the reaction is somewhat disturbed, the total pressure increase being smaller than in the unpacked vessels, as is obvious from fig. 5. Even in an unpacked vessel a small amount of acetone is lost in a side reaction

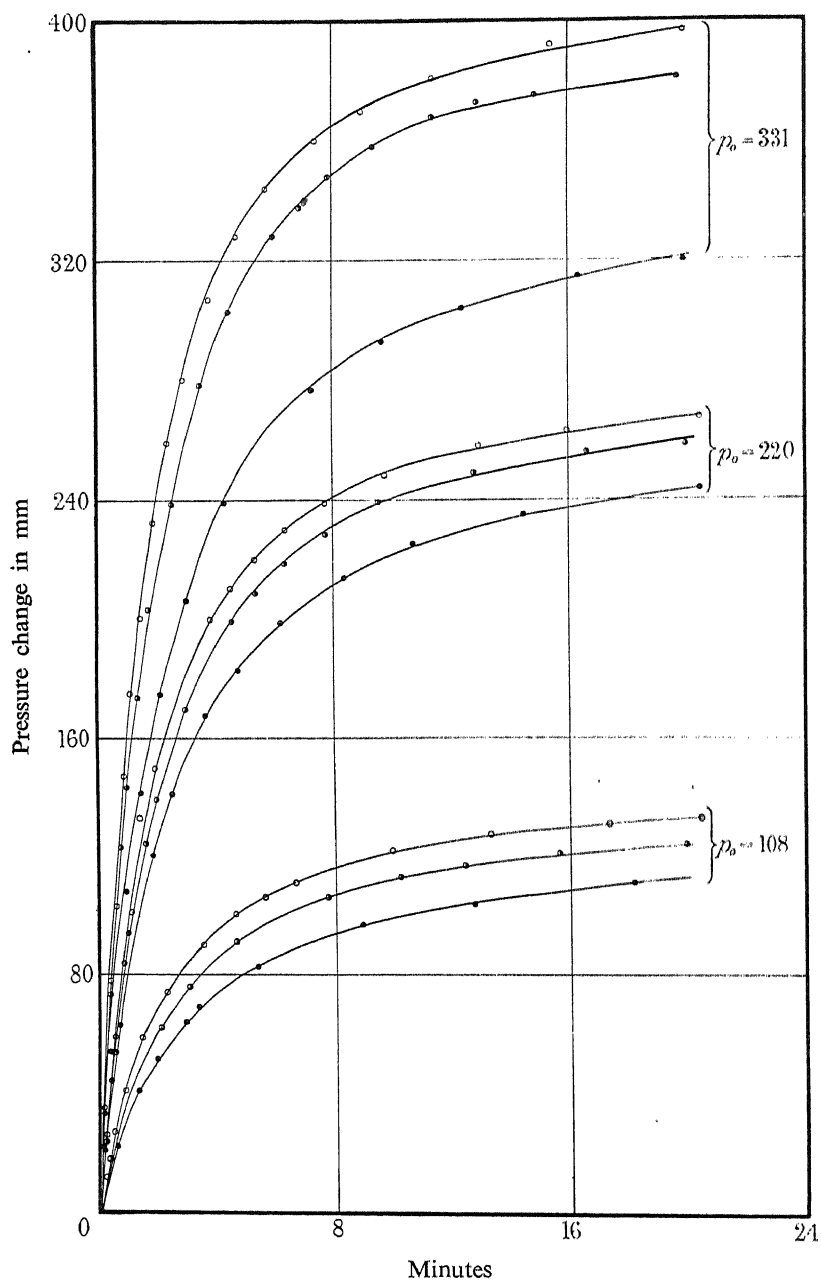


FIG. 5—Influence of surface and vessel size. For each initial pressure the upper curve refers to the unpacked vessel, the middle curve to the tube-packed vessel, and the lower to the sphere-packed vessel

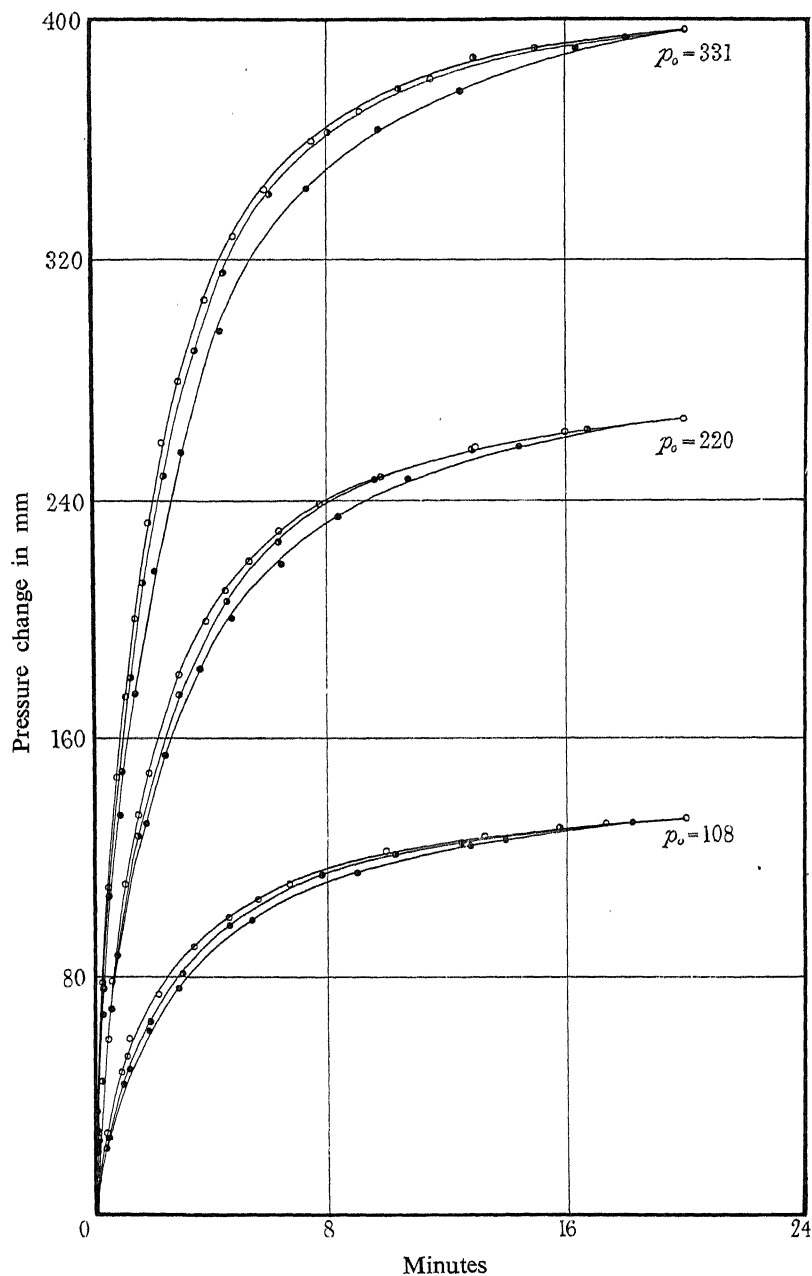


FIG. 6—Influence of surface and vessel size. For each initial pressure, upper, middle and lower curves refer respectively to unpacked, tube-packed and sphere-packed vessels

giving high boiling condensation products. The condensation reactions are probably heterogeneous, and therefore become more serious as the surface is increased. The curves in fig. 5 are thus not directly comparable. A truer picture is obtained if the disturbance due to the condensation reaction in the packed bulb is corrected for. The simplest way of making the correction is to plot the curves on such a scale that they reach the same end-point, a method depending on the assumption that the increased condensation occurs uniformly throughout the course of the reaction. The corrected curves are shown in fig. 6, and are seen to be much more nearly coincident. How far the small differences which remain are real is difficult to say.

In general the initial rates for the three bulbs are nearly identical. This suggests that the small differences in  $t_{\frac{1}{2}}$  may not be real, but due to the approximate nature of the correction for the condensation reactions in the packed bulbs. The following are some of the numerical results:—

Bulb	108 mm		220 mm		330 mm	
	initial pressure		initial pressure		initial pressure	
	Initial rate	$t_{\frac{1}{2}}$ sec	Initial rate	$t_{\frac{1}{2}}$ sec	Initial rate	$t_{\frac{1}{2}}$ sec
Unpacked . . . .	1.00	72	1.00	69	1.00	66
Tube-packed . .	0.90	90	1.00	78	1.00	66
Sphere-packed . .	0.90	93	1.00	84	1.00	84

These results leave no doubt that the reaction is almost entirely homogeneous. (In the unpacked vessel the condensation reaction is very small at the pressures used, though it might become of great importance at high pressures—to prove which would not affect any of the conclusions of this paper.)

With regard to the question of the occurrence of chains, either there are none, or they must be very short, or they must be capable of reflection from the walls. Since chains would probably involve radicles such as methyl, it is difficult to believe that recombination would not occur on the wall with interruption of the chain. Thus it seems that chains are entirely absent or very short, a conclusion which is not inconsistent with the fact that an acceleration of the reaction by the introduction of free methyl radicles cannot be demonstrated.\*

#### INFLUENCE OF TEMPERATURE

The temperature coefficient was redetermined using the new method of measuring the reaction rate.

\* Rice, Rodowskas and Lewis, 'J. Amer. Chem. Soc.,' vol. 56, p. 2497 (1934).

Temperature ° C	$k$ sec <sup>-1</sup>
622	0.0182
612	0.0116
602	0.00730
582	0.00301
562	0.00116
552	0.000693
542	0.000415

These results are summarized by the formula

$$\ln k = 34.34 - 68,000/RT. \quad (1)$$

The earlier investigation gave

$$\ln k = 34.95 - 68,500/RT. \quad (2A)$$

The method then used for finding  $k$  gave values which need to be multiplied by 134/150 (ratio of  $t_{\frac{1}{2}}$  values by old and new method) to be brought into comparison with the present values. The corrected values are given by

$$\ln k = 34.84 - 68,500/RT. \quad (2B)$$

As far as the purely experimental agreement goes, equations (1) and (2B) correspond to a shift of the temperature scale by one degree.

#### RELATION BETWEEN REACTION RATE AND INITIAL PRESSURE OF ACETONE

For initial pressures above 100 mm the reaction is of the first order, as was shown in the earlier experiments and confirmed in the present series. Table II shows some typical figures found at 602° C.  $t_{\frac{1}{2}}$  is the time of half decomposition of the acetone as determined by the analytical method. Below 100 mm the value of  $t_{\frac{1}{2}}$  increases steadily. The last four values were found by the McLeod gauge method. In fig. 7  $1/t_{\frac{1}{2}}$  is plotted against the initial pressure. The curve resembles the corresponding curves for acetaldehyde, propionic aldehyde and nitrous oxide in showing definite evidence of a composite form. The significance of this is discussed in a later section. It may be mentioned that two quite independent series of experiments gave curves of identical form.

The energy of activation determined at 50 mm pressure over an 80° range is 62,200 calories, which would become 63,100 if the rates at

TABLE II

Initial pressure	$t_{\frac{1}{2}}$	Initial pressure	$t_{\frac{1}{2}}$
mm	sec	mm	sec
311	89	93	102
232	90	87	102
212	96	77	107
207	95	64	120
182	95	55	131
155	95	49	142
142	96	40	147
129	97	30	162
121	97.5	26	167
113	95	15.5	186
110	98	8.0	230
106	99	5.0	276
99	99	2.5	298

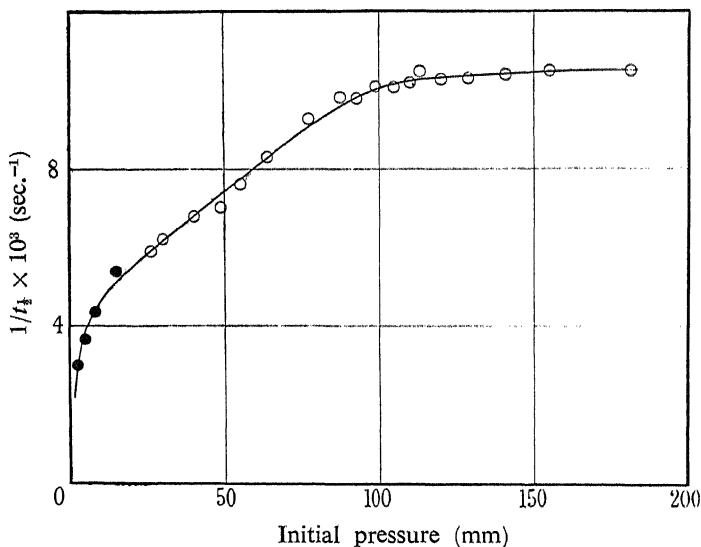


FIG. 7—Influence of initial pressure on time of half change of acetone at 602° C  
different temperatures were measured not at a constant pressure, but at a constant concentration of acetone.

#### INFLUENCE OF HYDROGEN ON THE REACTION

An attempt was made to find whether hydrogen would prevent the fall in  $1/t_{\frac{1}{2}}$  at the lower pressures, but the hydrogen reacted chemically with the acetone. The rate of reaction could be increased, by the addition of excess hydrogen, to a value far beyond the limiting rate for acetone

itself at the higher pressures, the end-point was changed and the products of reaction were different. At  $600^{\circ}$  with 160 mm acetone and 209 mm hydrogen the products had the following composition:—

Unsat. 2·8, CO 28·0,  $H_2$  20·3,  $CH_4$  46·0%. From the original amount of hydrogen and the final pressure in the reaction vessel it is calculated that if no hydrogen had reacted there should have been 40·1% in the products.

#### DISCUSSION

The method of following the course of gaseous reactions by pressure measurements is simple and convenient: without its aid it would hardly be possible to investigate a wide enough range of conditions to give a coherent picture of the whole subject. When, however, owing to the existence of complications in the reaction mechanism the pressure measurements can only be interpreted with the aid of assumptions about the exact way in which they are related to the amount of chemical change, then an independent confirmation is advantageous. It is interesting therefore to enquire in what respects the present investigation confirms or modifies the earlier conclusions which were based essentially upon pressure measurements.

In the first place, the general conclusion that the reaction is of the first order above 100 mm is unchanged, though the actual values of the half times need correction by 10–12%. The values of the energy of activation are almost identical. The most marked difference is in the trend shown by the first order velocity constant during the course of the reaction. With the old method the constant showed only a slight fall: with the new, a more pronounced fall is revealed. This is consistent with the falling off in the values of  $1/t_{\frac{1}{2}}$  now found by extending the experiments to initial pressures below 100 mm.

The results obtained in the lower pressure region are of interest in that a definitely composite appearance of the  $1/t_{\frac{1}{2}}$ ,  $p_0$  curve is once more revealed. The interpretation suggested of the similar curves for nitrous oxide and for the aldehydes is based upon the hypothesis of the existence of different activated states. The objection to this is that acetaldehyde can tautomerize into vinyl alcohol, and that without this possibility the characteristic composite curves would not be found. Such a suggestion could hardly apply to nitrous oxide, which shows the effect as clearly as the aldehydes. Additional examples, however, are evidently desirable. The more common the behaviour in question proves to be, the less probable a specific chemical explanation becomes and the more probable a general physical explanation. The possible tautomer of



acetone—the enolic form—has not been isolated, and only exists in minute concentration in equilibrium with acetone. At present, therefore, there is no reason against extending to acetone the hypothesis of the various activated states already suggested for the other substances.

We are indebted to Imperial Chemical Industries, Ltd., for a grant by means of which apparatus for the investigation was obtained.

#### SUMMARY

The kinetics of the decomposition of acetone have been reinvestigated by a method depending upon direct analysis of the unchanged acetone. In confirmation of the earlier work, the reaction is found to be of the first order for initial pressures greater than 100 mm. The velocity constants calculated by the method previously used need to be reduced by 10–12%. The new value for the energy of activation agrees with the old within 500 calories. The new velocity constants for initial pressures greater than 100 mm are given by the equation

$$\ln k = 34.34 - 68,000/RT.$$

The products of reaction at various stages have been analysed, and the intermediate formation of ketene studied quantitatively.

Measurements have now been made in the range 100–2.5 mm. The curve of  $1/t_k$  against initial pressure shows a composite form similar to that shown by the curves for nitrous oxide and various aldehydes. The energy of activation falls slightly at lower pressure. The hypothesis of the existence of various activated states seems applicable to acetone.

A detailed study of the influence of surface and vessel size shows that the reaction is almost entirely homogeneous, and that reaction chains are either entirely absent or very short, unless improbable assumptions about their reflection from the walls are made.

---

# The Thermal Decomposition of Acetaldehyde

By C. A. WINKLER and C. N. HINSHELWOOD, F.R.S.

(Received December 18, 1934)

This paper contains a more detailed study than has hitherto been made of the effect of surface and vessel size on the thermal decomposition of acetaldehyde. This was desirable in view of the suggestion\* recently made that the reaction might take place by a chain mechanism, and also because the validity of the previous evidence that the reaction is homogeneous has been called in question.†

In an unpacked silica bulb between 500° and 600° the reaction is attended by a pressure increase which is about 98% of that corresponding to the equation  $\text{CH}_3\text{CHO} = \text{CH}_4 + \text{CO}$ , and the gaseous products consist of equal parts of carbon monoxide and methane. When a packed vessel with very large surface is used the pressure increase is rather less than the theoretical, indicating that some condensation reaction occurs which is probably heterogeneous in contrast with the principal decomposition.

For the new experiments the three reaction vessels described in the preceding paper were used, and reaction rates were measured at 562°. The temperature was very carefully controlled, the bulbs were all placed in exactly the same position in the furnace, and no air was allowed access to the silica surface.‡

In fig. 1 pressure increase is plotted against time. Curve A refers to the unpacked bulb, B to the bulb packed with silica tubes (of the same origin as the bulb) and C to the bulb packed with silica spheres. The surface/volume ratios of the three vessels were 1:5:16. In all the experiments the initial pressure was 240 mm. The lower end-point in C is especially evident. If the time of half-change were read off from

\* Rice and Herzfeld, 'J. Amer. Chem. Soc.,' vol. 56, p. 284 (1934).

† Travers, 'Proc. Roy. Soc.,' A, vol. 146, p. 284 (1934); 'Nature,' vol. 134, p. 569 (1934).

‡ In the earlier experiments of Hinshelwood and Hutchison ('Proc. Roy. Soc.,' A, vol. 111, p. 380 (1926)), at rather lower temperatures, a packing of silica powder, which was known to increase the rate of decomposition of ammonia some 20 times, caused an acceleration of about one-third. A simple calculation shows that in the unpacked vessel, therefore, not more than about 2% would be heterogeneous reaction. As a matter of fact even some of this acceleration was probably due to adsorbed air, the effect of which was not fully realized at the time.

these curves there would be an apparent retardation of the reaction in the packed bulbs, unless the changes end-point were taken into account. When, however, the curves are re-plotted so as to reach the same end-point, as in fig. 2, no definite acceleration or retardation of the reaction appears. Some numerical data read from the curves are given below.

Bulb	Initial rate (relative)	$t_{\frac{1}{2}}$ sec	$t_{\frac{3}{4}}$ sec
Unpacked .....	1.0	108	300
Tube-packed .....	1.0	114	330
Sphere-packed .....	1.0	114	366

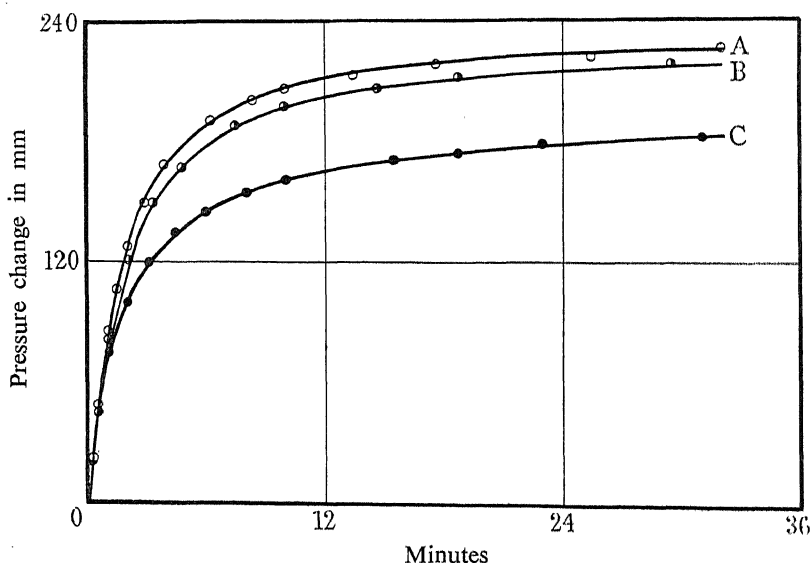


FIG. 1

That the condensation reaction which lowers the end-point in the packed bulb is heterogeneous is proved by an observation made by Dr. Verhoek that a normal end-point in the acetaldehyde decomposition can be obtained even in the sphere-packed bulb if the surface is "poisoned" by decomposing certain organic compounds at higher temperatures. In fig. 3, curve 4 represents the reaction in the clean sphere-packed bulb, curve 3 that in the same bulb after treatment with acetone vapour at 600°, and curve 2 the reaction after the sphere-packed bulb had been treated with acetic acid vapour at 600°. Curve 1, which is identical with curve 2, refers to the clean unpacked bulb. It is seen that, the end-points having become identical owing to the suppression of the condensation reaction, the curves are superposable over their entire course.

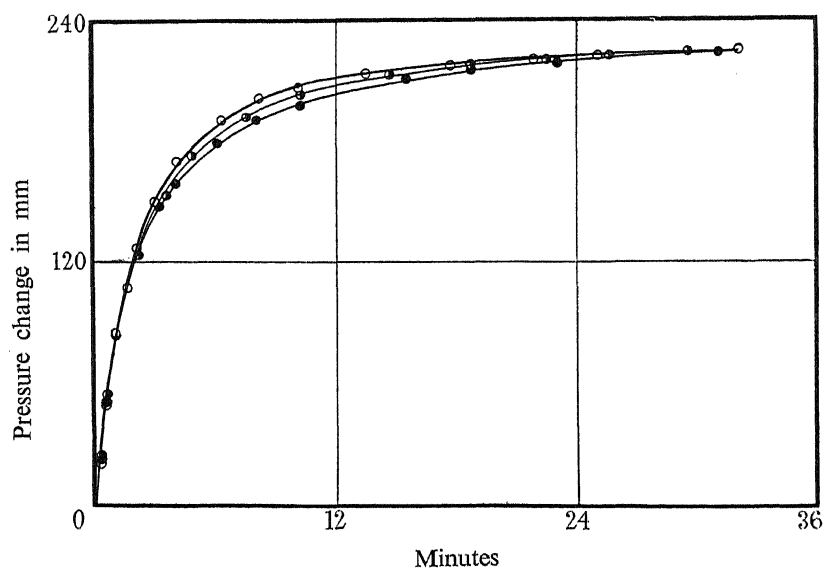


FIG. 2—○, unpacked; ◐, tube-packed; ●, sphere-packed

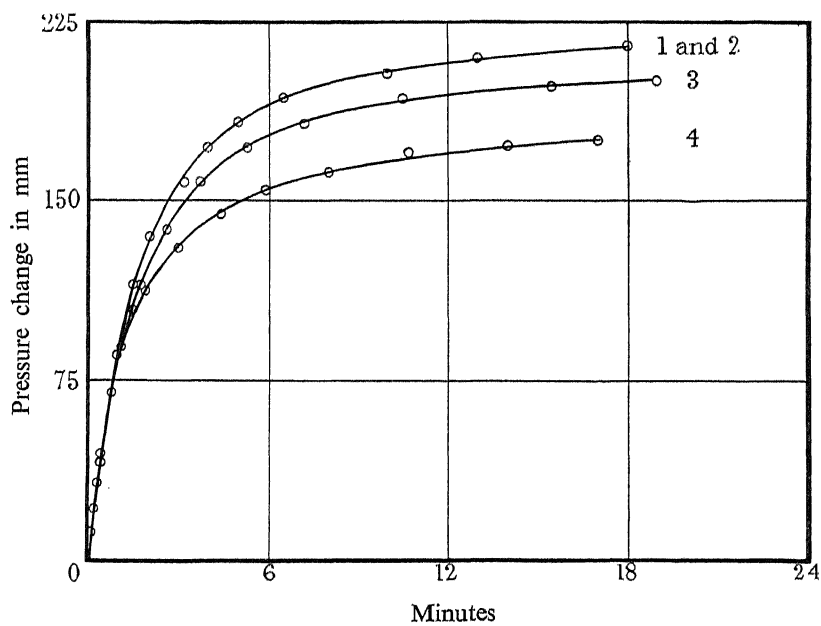
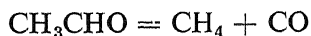


FIG. 3

It is important that the poisoning treatment be carried out without admitting air to the bulb.

These results provide no evidence either that the reaction



is appreciably heterogeneous, or that it depends upon a chain mechanism.

Although the reaction in the unpacked bulb takes place at least to the extent of 98% in accordance with the equation given, under the conditions which have been prescribed in all work from this laboratory, the

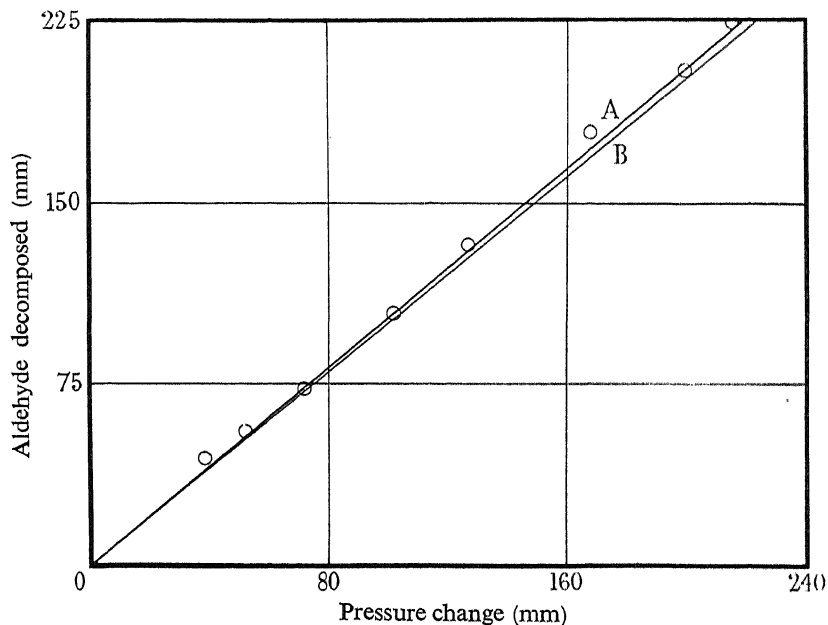


FIG. 4

validity of the assumption that pressure changes can be used to follow the course of the reaction has been questioned.\* To remove all possible doubt about this, an analytical method, similar in principle to that described in the previous paper, has been used to verify the previous conclusions. Direct analyses of acetaldehyde were made by withdrawing samples and estimating by the bisulphite method of Friedmann, Cotonio and Shaffer.† The reliability of the method was tested by blank experiments at temperatures below the reaction temperature, the calculations and corrections being made as described in the previous paper.

\* Travers, *loc. cit.*

† 'J. Biol. Chem.,' vol. 73, p. 342 (1927).

In fig. 4, curve A, is the experimental relation between pressure change and aldehyde decomposed, while B is that based on the assumption that each millimetre of aldehyde decomposed gives one millimetre pressure increase.

It should be pointed out that these conclusions refer to the range of conditions under which previous work from this laboratory has been done, and do not necessarily apply to high pressures or quite low temperatures. That under extreme conditions other reactions than the decomposition into methane and carbon monoxide may predominate is irrelevant to the present issue.

#### SUMMARY

A detailed study of the influence of surface and vessel size yields no evidence that the reaction  $\text{CH}_3\text{CHO} = \text{CH}_4 + \text{CO}$  is appreciably heterogeneous, or that it depends upon a chain mechanism.

Direct chemical analysis proves that the rate of pressure increase gives a reliable measure of the rate of reaction of the aldehyde.

---

## Adsorption on Measured Surfaces of Vitreous Silica

By W. G. PALMER, Fellow of St. John's College, Cambridge, and  
R. E. D. CLARK, St. John's College, Cambridge

(Communicated by Sir William Pope, F.R.S.—Received October 31, 1934)

### INTRODUCTION

The theoretical treatment of the phenomena of adsorption has been very largely based upon the results of experiments with charcoal, a material which is not chemically homogeneous, and about whose undoubtedly very complex physical structure little is known. The uncertainties thus arising are not rendered less formidable by the various empirical methods of "activation" to which the charcoal is usually subjected. Vitreous silica, on the contrary, has properties which seem to provide a nearly ideal foundation for adsorption experiments of theoretical significance. It is chemically inert and homogeneous, and its structure has been the subject of detailed and successful investigation.\* In common with that of charcoal the surface of powdered silica undergoes little change by sintering even on prolonged exposure to red heat. The low retentivity (adsorption/pressure) of this form of silica, while destroying its value as a practical adsorbent, proves a great advantage for theoretical development in that the early portions of isothermals are accessible at external pressures easily measurable by simple manometric means. Also a low retentivity obviously minimizes the difficulty of preparing a bare surface. There is lastly the advantage, by no means the least important, that an apparently trustworthy method has been devised for evaluating the surface of the powdered material independently of the adsorption experiments.

### THE PREPARATION OF POWDERED FUSED SILICA FOR ADSORPTION EXPERIMENTS

A coarsely crushed fused quartz was narrowly graded by sieving until the material consisted of particles of average diameter (calculated as spheres) of 0.8 mm. After thorough cleaning in acid bichromate and washing in distilled water the silica was dried and then formed the starting point for all subsequent preparations of adsorbent. The superficial

\* Jeffreys, 'Proc. Camb. Phil. Soc.,' vol. 24, p. 19 (1928).

area of 1 gm of the silica at this stage was estimated by the method described later as very nearly 100 cm<sup>2</sup>.

To prepare a charge for the adsorption apparatus 15 gm of the coarse silica were ignited to bright redness, cooled in a desiccator, and then finely ground in 3 or 4 portions in an agate mortar under pure benzene dried over sodium. The mixture of silica and benzene was drawn by suction into the detached adsorption tube, A, fig. 1. After centrifuging, the greater part of the supernatant benzene was withdrawn from the tube by similar means, and the ground silica washed thrice with further dry benzene, so that finally all but about 1% of the original grinding

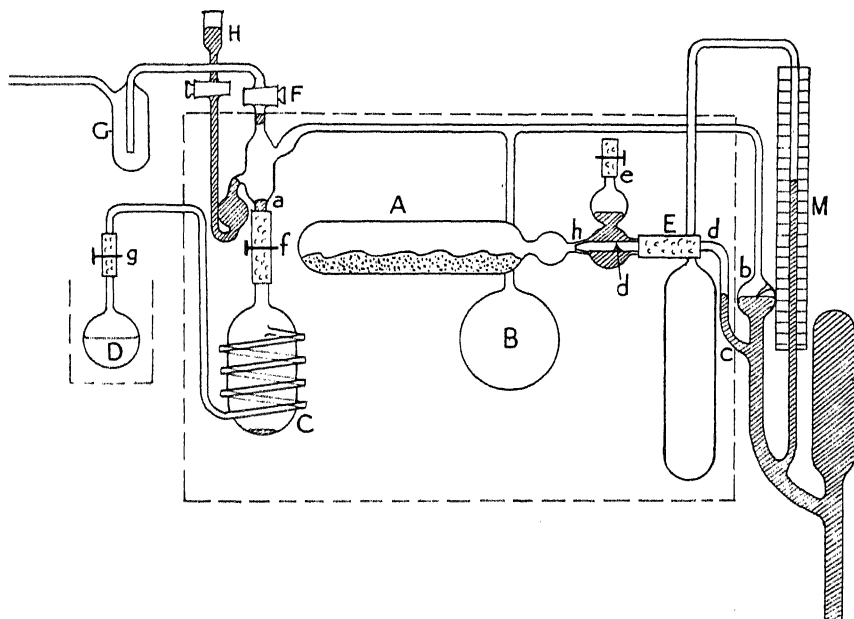


FIG. 1

liquid was displaced from the silica. The residual benzene was now removed by distillation *in vacuo*, the receiver being cooled first in ice, and finally in liquid air for 4 hours while the powdered silica was heated to 200° C. Direct experimental evidence that the final silica surface was not contaminated with benzene was obtained as follows: the adsorption isothermals for benzene at 25° C were determined (1) on a sample of silica prepared as described above, (2) after detaching the adsorption tube *in vacuo*, heating to only 50° C *in vacuo* with a receiver cooled in liquid air, and then reassembling in the apparatus. The two isothermals coincided throughout their course, thus proving that the second and less drastic treatment produced the same surface as the first, which is hardly



credible unless the surface was bare in both cases. A more complete proof was obtained in the study of the adsorption of cyclo-pentane, to which reference will be made later (p. 378). The grinding process increased the surface per gram from 100 cm<sup>2</sup> to approximately 5000 cm<sup>2</sup>, so that practically the whole of the adsorption surface could be formed under fully controlled conditions.

#### THE MEASUREMENT OF ADSORPTION

The specific adsorption of the "permanent" gases on the prepared silica is very small at moderate external pressures and room temperature, so that it was thought more profitable to examine in the first instance the adsorption of vapours below their critical temperatures. A temperature of 25° C was chosen for all the experiments. Measurements of the amount of adsorption were obtained by the ordinary method operated as follows. A quantity of vapour was admitted to a part of the apparatus of known capacity  $V$ , between the mercury trap at  $a$ , fig. 1, and the manometer bulb  $b$ , including the bulb  $B$ . After setting the mercury to the glass point in  $b$  in the usual way, the pressure  $p_0$  was read on the scale  $M$  to the nearest 0.1 mm. It is essential that the cross-section of the bulb  $b$  should be sufficiently large to eliminate the effects of changing capillarity of the mercury under increasing pressures of vapour. The sample of vapour was then allowed to expand into the adsorption tube  $A$  by temporarily lowering the mercury to open the trap  $c$ . The final equilibrium pressure  $p_1$  was read as before. To secure a specimen of vapour whose behaviour approximated sufficiently closely to the gas laws—that is, a "dry" vapour—it was found necessary not only to expand it twice after withdrawal from over the supply of liquid in the bulb  $D$  and before pressure measurements were made, but also to superheat it by arranging that the temperature of the liquid in  $D$  was always at least 5° lower than that of the thermostat. If  $r$  is the expansion ratio, or ratio of initial and final pressures in the absence of adsorption, and  $n_0$  and  $n_1$  the gm mols of vapour in the vapour phase—

$$\text{gm mols of vapour adsorbed} = n_0 - n_1 = (p_0 - rp_1) \cdot V/kT.$$

To prepare for adsorption measurements the evacuated adsorption tube containing the prepared silica was first attached by means of its rubber projection  $E$  to the tube  $d$ , but a screw-clip on  $E$  was not released until the rest of the apparatus had been exhausted through the tap  $F$  and the liquid air trap  $G$ . The screw-clip was then opened and the rubber  $E$

slipped forwards along the tube *d* until the ground-glass joint at *h* was closed; the joint was finally sealed with mercury from *e*. The whole process of preparing the silica and final connection to the main apparatus was thus carried out *in vacuo*. It will be noticed that the mode of attachment of the adsorption tube allowed it to be freely turned about its long axis and the contained powder thus stirred. Although advantage was frequently taken of this during the adsorption experiments, no consequent alteration of pressure ever occurred. At the conclusion of the operations needed to determine an isothermal the mercury was allowed to flow from the joint *h* by turning the tube A so that the bulb *e* pointed downwards, the tube and its rubber connection were slipped back on the tube *d* until the screw-clip could be closed and the adsorption tube was detached. It could then be connected to the receiver in liquid air, the adsorbed substance removed from the silica by heating *in vacuo*, and the tube re-connected to the apparatus as above described. Thus an extended series of adsorption measurements could be accomplished, throughout which the silica was *in vacuo* when not in contact with the vapour being adsorbed.

The supply of pure liquid in the bulb D was carefully freed from dissolved gases by boiling *in vacuo* followed by exhaustion after solidification in liquid air. The temperature of the bath surrounding D was chosen in relation to the vapour pressure of the liquid at 25°. In the early parts of serial measurements with a volatile liquid such as chloroform the temperature of this bath could be kept as low as -10° C and allowed to rise gradually to 20° C as higher pressures were required in the apparatus. In admitting vapour to the measuring apparatus the screw-clip *f* was first kept closed, and the rubber of the connection sealed at *a* with mercury from the reservoir H. On now opening the clip *g* the vessel C, of capacity about 20 cc, became filled with vapour at saturation pressure corresponding with the temperature of D, but superheated to 25°. It was found that the coiling of the inlet tube to C, as shown in fig. 1, greatly increased the efficiency of the superheating. The clip *g* being now closed and *f* opened, the mercury of the seal *a* fell into C, allowing a free passage to the vapour into the section *aBb* (capacity 22.5 cc). The sudden rush of vapour caused a bead of mercury to be thrown into the capillary below the tap F, by which simple means the tap with its lubricant became sealed from the space *aBb* during the subsequent adsorption measurements. After again flooding the joint at *a* with a small measured quantity of mercury from H, the initial pressure was read. Finally the vapour was admitted to the adsorption tube. By following this procedure the vapour to be adsorbed could

only come into contact with clean glass and small surfaces of mercury in addition to the silica surface.

With all the substances examined equilibrium must have been attained within the space of 1 minute, the time necessary for taking a reading on the manometer, for the pressures never showed a further change even when they had been first recorded as rapidly as possible after alterations in the amount of vapour. Readings were, however, always continued for at least 10 minutes; in some lengthy series of experiments interruptions of several hours were unavoidable, and on several occasions the measurements were resumed overnight, but in no case was any change of pressure detectable after the first reading. The necessity for superheating the vapour prevented the isothermals from being followed beyond values of the relative pressure  $\left[ \frac{\text{equilibrium pressure}}{\text{saturation pressure}} \right]$  equal to approximately 0.6, but as the adsorption film even at that stage generally contains more material than would correspond to a unimolecular layer (p. 382), it is doubtful if much information is lost by this restriction.

#### THE DETERMINATION OF THE EXPANSION RATIO

The empty adsorption tube was connected to a receiver cooled in liquid air, the whole exhausted and the tube then kept at 200° C for 2 3 hours. After the tube had been connected to the adsorption apparatus in the manner previously described, the measurements recorded in the following table were made under the same conditions and by the same means as an adsorption measurement with silica present. In Table I  $p_0$  = total pressure of vapour admitted from the beginning,  $p_1$  = final pressure after expansion,  $r_0$  = expansion ratio =  $p_0/p_1$ . Pressures are all in millimetres of mercury.

TABLE I  
ADSORPTION TUBE NO. 1, CAPACITY 41 CC

(a) Air		
$p_0$	$p_1$	$r_0$
80.4	28.7	2.80
143.4	51.6	2.78
190.3	68.3	2.79
(b) Benzene		
92.7	33.1	2.80
145.2	52.9	2.75
177.1	66.0	2.73

TABLE I—(continued)  
 ADSORPTION TUBE NO. 2, CAPACITY 49 CC

(a) Air.  $r_0 = 3.18$

(b) Ethyl Alcohol

21.7	6.9	3.15
41.7	13.1	3.19
62.8	19.7	3.19

(c) Cyclopentane

15.8	5.0	3.16
36.2	11.4	3.17
71.1	22.4	3.17
104.2	32.4	3.20
140.0	43.8	3.20

These determinations demonstrate that if there is any adsorption on the glass or mercury of the apparatus the amount adsorbed is independent of both the pressure and the substance used. The most natural conclusion is that such adsorption is negligible, but, in any case, if, in the subsequent experiments with silica in the tube, the expansion ratio  $r$  is calculated as shown below from the values of  $r_0$  in the above tables the results will clearly give the adsorption on the silica alone. The specific gravity of the silica, determined before powdering, was found to be 2.21; the capacity of the part of the apparatus *aBb*, fig. 1, was 22.5 cc. Then if  $X$  is the "dead space" in the adsorption tube containing  $m$  gm of silica,

$$\frac{(X + m/2.21)}{22.5} + 1 = r_0,$$

and hence

$$r = r_0 - m/(2.21 \times 22.5).$$

## THE SPECIFIC SURFACE OF THE POWDERED SILICA

### *The Lower Limit of Particle Size*

A small specimen of the powder was shaken with dry ligroin and the mixture then centrifuged under an acceleration of 80 g. The minimum time required for the intensity of the Tyndall effect in a layer 1 cm deep to diminish to that in a blank tube without silica was 5 minutes. Calculations on the basis of Stokes' law for spherical particles indicates a diameter  $1.8 \times 10^{-5}$  cm for the smallest particles.

*The Rate of Dissolution of the Powder in Dilute Hydrofluoric Acid*

It has been shown\* that the rate of dissolution of coarse fused silica in hydrofluoric acid is exceptional in being independent of the rate of stirring, provided this suffices to keep the acid homogeneous, and in that the whole surface undergoes uniform attack without local etching, every particle apparently preserving its original geometrical form through a long period. Moreover, the great disparity in the degrees of ionization of the product of the reaction, hydrofluosilicic acid, and the reagent acid renders measurement of electrolytic conductivity a very sensitive and convenient method of determining the rate of dissolution, especially in the important initial stages. Thus 1 mg of silica dissolved in 50 cc of decimolar acid at 25° C produces the easily measurable decrease of 25 ohms in the original resistance of 750 ohms. For the purpose of the present work it was necessary to devise a conductivity cell that could be dipped into the reaction liquid from time to time and the accuracy of which would not be impaired by the presence of suspended powder. The cell adopted, of which sections are drawn in fig. 2, was constructed entirely of ebonite and bakelite, except the electrodes, and was the outcome of close attention to details of design. Resistance measurements with this cell were reproducible with an accuracy of  $\pm 0.5$  ohm in 500 ohms.

We first standardized the reaction by determining the rate of dissolution of several lengths of clear fused quartz rod of easily ascertained geometrical surface, using different acid concentrations round M/10. Two ebonite tubes containing equal quantities, approximately 60 gm, of acid were arranged in a thermostat at 25° C in such a manner that they could be slowly rotated by mechanical means in a plane containing their long axes. Four rods of clear fused quartz each of approximately 0.5 cm diameter supported in a rubber bung were set in one tube, where they were nearly covered by the acid, and the spare tube was closed. After rotating for 20–40 minutes the rods were quickly transferred to the second tube, and the conductivity of the acid in the first tube measured with the cell described. This measurement was easily completed in at the most 2 minutes. Rotation was then resumed and the operations repeated. In this way two sets of readings A and B could be obtained correlating conductivity with the duration of the dissolution.

On plotting data in Table II an accurately linear relation is disclosed between conductivity and the time of contact of the acid with the silica

\* Palmer, 'J. Chem. Soc.,' p. 1656 (1930).

TABLE II—CONCENTRATION OF ACID 0.078 M. TEMPERATURE 25°

Tube A		Tube B	
Time (mins)	$(1/R) \times 10^3$	Time (mins)	$(1/R) \times 10^3$
0	1.174	0	1.171
29	1.182	33	1.184
58	1.192	63	1.193
86	1.200	94	1.202
116	1.208	127	1.211

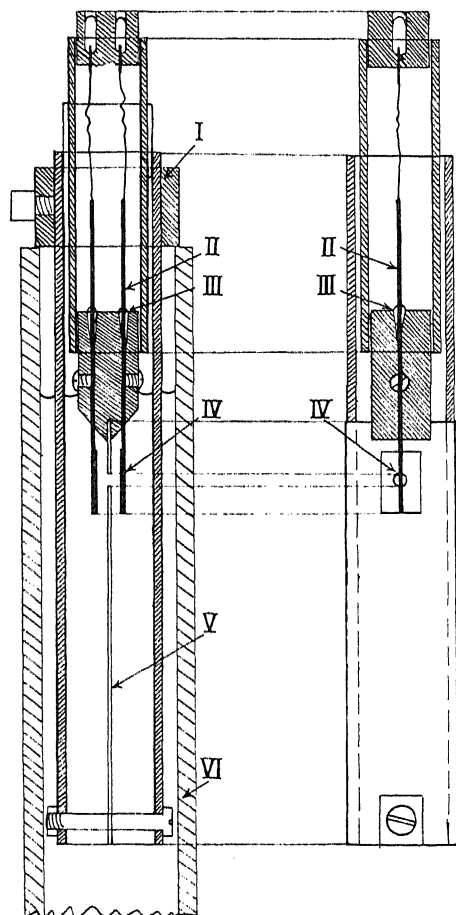


FIG. 2—(i) Collar for depth adjustment; (ii) heavy platinum leads; (iii) wax joint; (iv) platinum electrodes; (v) bakelite partition; (vi) tube containing acid and silica

surface; in addition, the slope of the lines is proportional to the concentration of the acid over the short range used, fig. 3. As neither the extent of the dissolving surface nor the acid concentration had appreciably

changed during the experiments, we can associate a particular slope, at  $25^{\circ}$ , with (a) a definite acid concentration, and (b) a definite geometrical surface of attack. The experiments also proved, as might have been expected, that the change of conductivity is proportional to the uptake of silica (while this remains small), and is independent of the acid concentration. Thus by measuring the conductivity of a few standard solutions of silica in M/10 acid, conductivity and silica content of the acid could be finally correlated for our conditions of experiment, fig. 4.

In proceeding to study the rate of dissolution of powdered material used in the adsorption experiments it was important to realize that there must exist an optimum ratio between the quantity of acid used (at

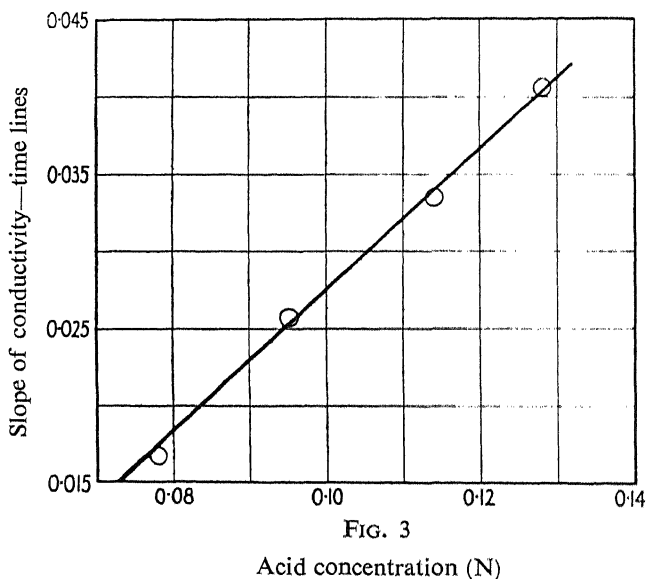


FIG. 3

Acid concentration (N)

a given concentration) and the weight of powder taken. Since at a given temperature the rate of attack is regulated solely by the extent of the surface, and therefore by the weight, of the powder, it is obvious that if the bulk of the acid is deficient its concentration will rapidly diminish, and it will become necessary to evaluate the initial rate of reaction by some extrapolation. On the other hand, if the bulk of the acid is too large the dilution of the hydrofluosilicic acid is too great for accurate measurements of the change of conductivity. It was found by trial that for a 50 cc portion of M/10 acid a sample of powder from 0.5 to 1.0 gm was suitable.

A circular stirrer of thin ebonite rod was attached to one end of a lever whose fulcrum was supported by a rubber strip. At the other end

the lever was oscillated mechanically about 200 times a minute. At the bottom of the stroke the head of the stirrer touched the base of the ebonite tube containing the acid and then rose to within a few millimetres of the liquid surface. Vigorous stirring was thus secured without splash, and, as a test showed, without raising the temperature of the acid. When this type of stirrer was used the conductivity cell could be inserted into the reaction tube over the head of the moving stirrer, whose action was taken up by the elastic fulcrum of the lever, and the stirring resumed automatically when the cell was removed. Trial runs showed the

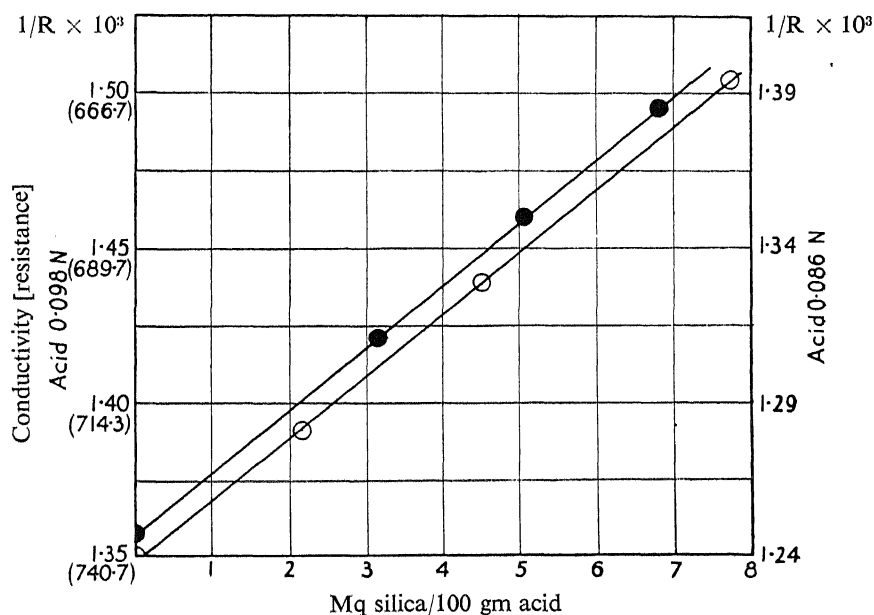


FIG. 4—○ acid 0.086 N; ● acid 0.098 N

approximate setting required on the conductivity bridge at different intervals, so that in observing conductivities for the final results the stirring was not interrupted for more than a few seconds at a time. The sample of powder was usually ignited to 400–500° C in air in a silica tube for a short time immediately before mixing with the acid. Control experiments proved that this treatment caused no appreciable sintering of the powder. It was thought to be necessary in order to remove non-volatile contamination accumulated during the unavoidable exposure to air in removal from the adsorption tube and subsequent preservation, but experiments on powder transferred directly from the tube to acid gave the same final results as those on ignited powder.



Table III shows a typical set of results. Time intervals were recorded electrically on a moving drum.

TABLE III—TEMPERATURE 25° C. 0.400 gm OF POWDER AND 58.3 gm OF 0.0908 M ACID

Time (mins)	Resistance	(1/R) $\times 10^3$
0	727.7	1.374
2.56	717.6	1.393
4.35	709.2	1.410
6.96	698.0	1.433
8.88	688.3	1.453
11.76	676.0	1.479
14.20	666.0	1.502
17.20	657.1	1.522
20.40	643.9	1.553

The graph of conductivity against time is again a straight line apparently passing accurately through the origin of conductivity for the acid before the introduction of the powder, thus suggesting that a direct comparison of the slopes of the lines derived from Tables II and III would lead to a true ratio of surfaces. It is, however, necessary to be confident that there is not a rapid change of slope at the beginning of the experiments with powder, owing to the complete dissolution of the smallest particles before the first observation of conductivity can be made. The direct comparison mentioned combined with measurement of the geometrical area of the silica rods (71.2 cm<sup>2</sup>) gives a minimum specific area of 5000 cm<sup>2</sup> for the powder. The centrifuging test (p. 365) proved that the minimum diameter of a particle in the powder was of the order  $2.0 \times 10^{-5}$  cm. For uniform spherical particles of this diameter 100 cm<sup>2</sup> or only 2% of the minimum estimate of the surface would correspond to 0.7 mg of silica. Reference to fig. 4 shows that this weight of silica, if dissolved in the first few seconds of the experiment, would cause the very easily detectable lateral displacement of the line from Table III by 0.04 unit of conductivity. It therefore seems safe to conclude that a direct comparison of the data in Tables II and III will give an estimate of the surface of the powder in terms of the geometrical surface of the rods to at least an accuracy of one part in fifty, and this is well within the limits of discrepancy between different experiments on the same powder as shown in Table IV.

TABLE IV—POWDER PREPARATION NO. 15

Weight of powder	Weight of acid	Concentration of acid normal	Specific surface cm <sup>2</sup> per gm
0.710	59.50	0.1033	4700
0.744	64.15	0.1007	4750
0.693	56.45	0.1000	5060
0.354	56.40	0.0996	4660
0.596	52.35	0.0975	4740
Mean			4690

## ADSORPTION ISOTHERMALS AT 25° C

The preparation of the powdered silica and the method of experiment have already been described. When in the following tables it is indicated that the same specimen of adsorbent has been used for more than one isothermal it is to be understood that between experiments the adsorption tube has been detached *in vacuo*, connected to the receiver cooled in liquid air, and the silica heated to 200° *in vacuo* for some hours. A typical series of actual readings is given in full for acetone, but for other vapours only the final results are included. In fig. 5, which shows the isothermals graphically, the curves have been made comparative by calculating the adsorptions for a standard apparent surface of 1 sq metre. To avoid confusion in the curves it proved necessary to raise the adsorption axis for acetone and methyl alcohol.

Fig. 6 shows the equilibrium pressure  $p_1$  plotted against  $p_1/x$  for acetone and methyl acetate. The points for relative pressures up to 0.1 are seen to lie on a straight line, an indication that in this range of pressure the isothermals conform to Langmuir's formula. The slopes of the lines are found to be 0.019 for acetone, and 0.021 for methyl acetate,  $x$  being reckoned (as in the tables) in micromols. The apparent specific area was determined as 4690 cm<sup>2</sup>, the same silica being used (14.6 gm) for both compounds. The apparent area occupied on the silica surface by one molecule of the adsorbed substance is

$$\frac{4690 \times 14.6}{6.06 \times 10^{23}} \times (\text{slope} \times 10^6),$$

giving for acetone  $21.5 \times 10^{-16}$  and for methyl acetate  $23.5 \times 10^{-16}$  cm<sup>2</sup>. These values agree closely with the figures  $20.5 \times 10^{-16}$  and  $23.5 \times 10^{-16}$  cm<sup>2</sup> obtained by Adam for close-packed films on water of long-chain compounds terminating in the CO—CH<sub>3</sub> and COO—CH<sub>3</sub> groups.\*

\* Adam, "The Physics and Chemistry of Surfaces," Oxf. Univ. Press, p. 50.

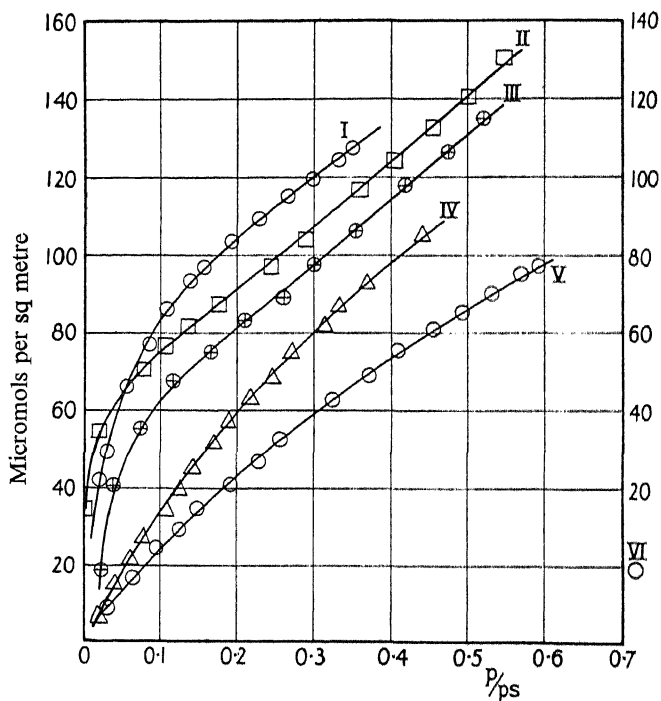


FIG. 5—Curve I, methyl alcohol; II, acetone; III, acetonitrile; IV, chloroform; V, benzene; VI, methyl alcohol and acetone

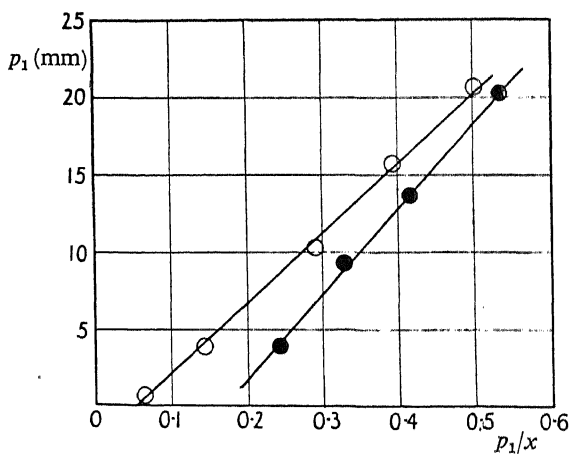


FIG. 6—○ methyl acetate; ● acetone

The apparent area thus calculated is based ultimately on the geometrical area of the standard rods of silica used in the reaction with hydrofluoric acid, but in view of the above agreement we have felt some confidence in identifying the geometrical with the actual area of the rods. This assumption is in harmony with the close relation of vitreous substances to liquids.

*The General Form of the Isothermals*

Graphical treatment of the data in the tables of isothermals shows that, except for acetone and methyl acetate, Langmuir's simple principle is not generally applicable even at low relative pressures, but we believe that we have been able to establish a new general formula for the isothermals

TABLE V—ACETONE

Adsorption tube No. 2,  $r_0 = 3.15$ . Weight of silica = 14.67 gm  
 $r = 3.15 - 14.67 / (2.21 \times 22.5) = 2.85$ .

Temperature 25° C. In formula  $n_0 - n_1 = (p_0 - rp_1) \cdot V/kT = x$ ,  $V/kT = 1.22 \times 10^{-6}$ , the adsorbed amount  $x$  is expressed in micromols (gm mols  $\times 10^{-6}$ ). Saturation pressure ( $p_s$ ) = 221 mm. Specific surface of silica = 4690 cm<sup>2</sup>. (The suffixes to  $p$  have the same significance as in Table I.)

$p_0$	$p_1$	$x$	Relative pressure $p_1/p_s$
24.3	3.9	16.1	0.0176
36.8	6.3	22.9	0.0285
49.4	9.3	28.4	0.042
65.9	13.6	32.7	0.063
88.7	20.2	38.0	0.093
108.2	25.7	42.6	0.116
124.8	30.4	46.6	0.138
143.2	36.1	49.0	0.163
167.1	43.1	53.7	0.195
191.0	50.3	58.5	0.229
212.7	57.0	61.2	0.258
240.0	65.3	66.0	0.273
275.5	75.9	72.5	0.344
307.9	85.8	77.9	0.388
335.4	94.0	82.7	0.425
360.5	101.2	88.3	0.457
389.0	109.5	94.0	0.495
405.0	114.3	97.3	0.515
419.9	118.4	101.0	0.535

TABLE V—(continued)

METHYL ACETATE			ACETONITRILE		
(Same specimen as for acetone)			Silica 14.6 gm Sp surface		
$p_s = 210$ mm			5250 sq cm		
			$r = 2.86, p_s = 86.7$ mm		
$p_1$	$p_1/p_s$	$x$	$p_1$	$p_1/p_s$	$x$
0.7	0.0033	10.98	1.9	0.022	14.1
3.9	0.0186	27.5	3.3	0.038	31.3
10.3	0.049	35.5	6.3	0.073	42.5
15.7	0.075	40.0	10.0	0.115	51.8
22.4	0.107	45.0	14.3	0.165	57.5
28.3	0.135	48.9	18.2	0.210	63.7
36.7	0.175	53.4	22.5	0.260	67.8
43.2	0.206	55.9	26.5	0.305	74.7
51.7	0.246	61.0	30.7	0.354	81.3
61.0	0.290	66.3	36.2	0.418	90.0
70.2	0.335	70.5	41.1	0.474	96.7
75.3	0.359	76.3	45.0	0.520	103.3
86.7	0.408	82.0			
95.9	0.456	88.9			
105.0	0.500	95.0			
115.7	0.550	102.5			

TABLE V—(continued)

METHYL ALCOHOL			ETHYL ALCOHOL		
Silica 15.0 gm Sp surface			Silica 14.6 gm Sp surface		
5410 sq cm			5000 sq cm		
$r = 2.87 \quad p_s = 125$ mm			$r = 2.86 \quad p_s = 59.0$ mm		
$p_1$	$p_1/p_s$	$x$	$p_1$	$p_1/p_s$	$x$
2.5	0.020	17.8	3.3	0.056	10.7
3.7	0.029	23.8	5.3	0.090	22.9
6.9	0.055	37.5	6.4	0.108	28.0
10.4	0.083	46.5	8.9	0.151	37.9
13.8	0.112	54.4	11.6	0.197	47.1
17.7	0.142	60.3	14.3	0.243	53.7
19.9	0.159	63.0	16.6	0.282	57.0
23.7	0.190	68.9	20.7	0.352	63.3
28.7	0.230	73.0	24.2	0.410	67.5
33.2	0.266	77.9	26.8	0.455	71.0
37.5	0.300	81.5	29.7	0.505	73.9
41.2	0.330	85.9	33.2	0.562	75.0
43.5	0.349	87.5			
51.7	0.414	92.4			
58.4	0.468	99.3			
63.2	0.506	104.1			
66.7	0.534	108.0			

TABLE V—(continued)

BENZENE			CHLOROFORM		
Silica 14.6 gm Sp surface			(Same specimen as for benzene)		
5250 sq cm			$p_s = 195$ mm		
$r = 2.86$ $p_s = 94$ mm					
$p_1$	$p_1/p_s$	$x$	$p_1$	$p_1/p_s$	$x$
2.9	0.031	6.8	3.8	0.019	5.5
5.9	0.063	12.8	7.9	0.041	11.7
8.9	0.095	18.8	11.9	0.061	16.8
11.6	0.124	22.6	15.0	0.077	21.0
13.9	0.148	26.5	19.9	0.110	26.6
17.8	0.190	31.2	24.4	0.125	30.5
20.4	0.217	36.0	27.8	0.142	34.8
23.9	0.255	40.1	32.9	0.169	39.6
27.9	0.297	44.8	36.9	0.189	43.9
30.4	0.324	48.2	42.0	0.215	48.7
34.9	0.371	53.0	47.6	0.245	52.6
38.4	0.409	57.9	52.9	0.271	57.8
42.6	0.454	61.9	61.4	0.315	62.8
46.2	0.492	65.2	66.7	0.343	67.0
49.9	0.531	68.9	71.9	0.369	71.0
53.4	0.568	72.4	79.9	0.410	73.5
55.6	0.591	74.4	86.1	0.442	80.4

by considering the adsorptions from the point of view of the adsorption potential  $\epsilon = RT \log p_s/p_1$  advocated by Polanyi and others. When the potential  $\epsilon$  is plotted against the adsorbed amount we obtain accurately logarithmic curves for all the compounds examined, except the two alcohols. The logarithmic character is clearly shown in fig. 7, where  $\log \epsilon$  is plotted against amount adsorbed per square metre, and a family of nearly parallel straight lines is obtained. The measured slopes in fig. 7, reckoned arbitrarily as tangents of the inclination to the  $x$  axis are given in Table VI.

TABLE VI

Acetone .....	1.5	Acetonitrile ..	1.6	Chloroform ..	1.5
Methyl acetate ..	1.6	Benzene .....	1.6		

The isothermals of methyl and ethyl alcohols yield curves and not straight lines for the graph of  $\log \epsilon$  against  $x$ , fig. 8. For all the isothermals represented in fig. 7 we may make the generalization  $d \log \epsilon / dx = k$ , or more shortly  $d\epsilon / dx = k\epsilon$ , for relative pressures up to *ca.* 0.5. The absolute value of  $\epsilon$  must depend on both the nature of the surface and the structure of the adsorbed molecule, but the nearly fixed value of  $k$

suggests that this constant relates only to the surface; it may be considered as a distribution factor for points of varying potential over the surface.

It has now to be considered whether the above rule is valid down to the lowest pressures and adsorptions. If this were so, a projection of the line to cut the ordinate in figs. 7 and 8 would give for each compound a sharply defined value of  $\varepsilon = \varepsilon_{\max}$  corresponding to zero adsorption. This would mean that adsorption begins not at zero pressure, but at a

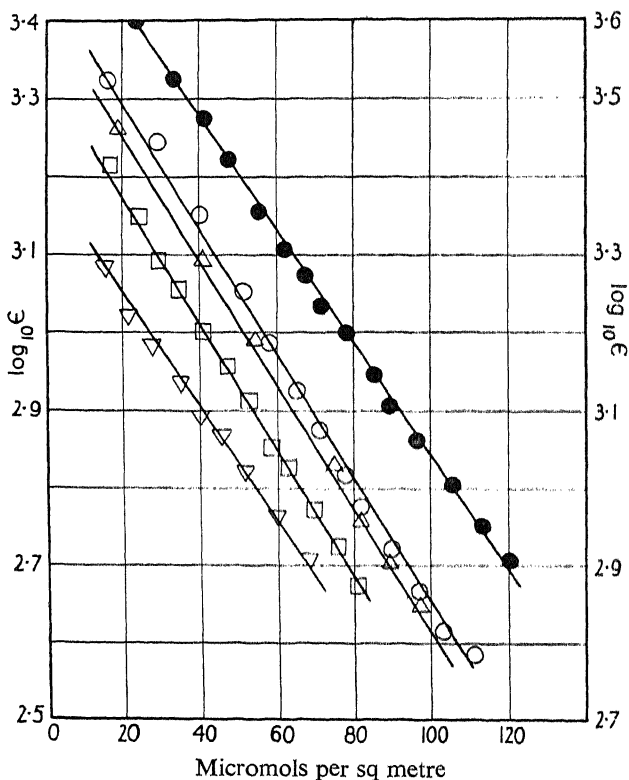


FIG. 7—Δ acetonitrile; ○ methyl acetate; ▽ chloroform; ● acetone; □ benzene

finite critical pressure  $p_L$ , defined by  $\log p_L = \log p_s - \varepsilon_{\max}/RT$ , a conclusion which might receive some encouragement from experiments on the condensation of metallic and other vapours on glass surfaces.\* Also if we adopt the view of a finite minimum pressure it can be shown as follows that for pressures near the minimum the rule  $d\varepsilon/dx = k\varepsilon$  reduces to Langmuir's formula. Using the rule in its integrated form  $\log(\varepsilon_{\max}/\varepsilon) = kx$ , we see that when  $x$  is small and therefore  $\varepsilon$  differs

\* E.g., Chariton and Semenoff, 'Z. Physik,' vol. 25, p. 287 (1924).

little from  $\epsilon_{\max}$ , the left-hand member will approximate to  $1 - \epsilon/\epsilon_{\max}$ , giving on simplification  $\log(p_x/p_L) = \epsilon_{\max} kx$ . In this  $p_x$  is the actual equilibrium pressure corresponding with an adsorption  $x$ . If we now reckon the pressure from  $p_L$  as zero,  $p_x = p_L + p$ , and

$$\log [(p_L + p)/p_L] = \epsilon_{\max} kx.$$

Approximating in the same way as above for small values of  $p$ , we find

$$p/(p_L + p) = (\text{constant}) \cdot x.$$

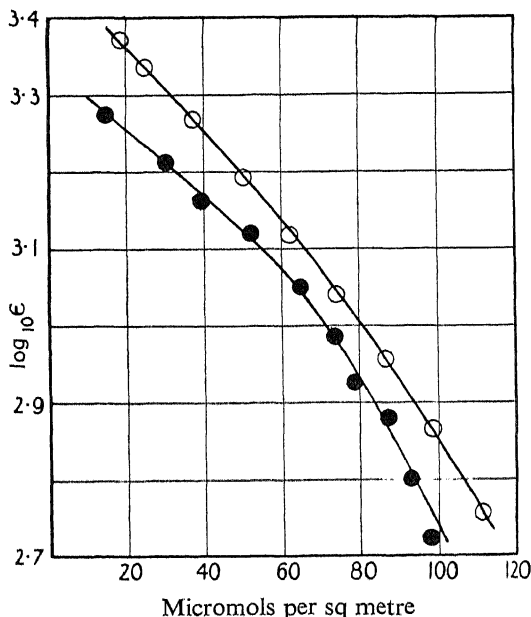


FIG. 8—○ methyl alcohol; ● ethyl alcohol

Since  $p_L$  is a fixed critical pressure for a given substance adsorbed, this relation is obviously in the form of Langmuir's expression.

We have attempted to elucidate the general course of isothermals at low adsorptions experimentally. It may be inferred from the foregoing discussion that the part of an isothermal for low adsorption will be most easily accessible (without resorting to very low pressures) for an adsorptive of high vapour pressure and low adsorptive power. The hydrocarbon cyclo-pentane with a vapour pressure at 25° of 303 mm well satisfied these requirements, and the low retentivity of the adsorbent greatly facilitated the investigation. A supply of the hydrocarbon had been isolated and purified for use in a previous research, and the specimen had been standing over sodium for some months before being distilled



for our present purpose. Two determinations of the isothermal were made by the methods already explained, the silica being subjected to heat treatment *in vacuo* between the two series of experiments. Fig. 9 shows the (smoothed) curve obtained, and the points in the two determinations; there is inevitably some "spread" in these points owing to the decreased accuracy inherent in measuring the low adsorptions concerned. The early part of the isothermal for benzene is also shown in fig. 9 on the scale of this figure.

The isothermal for cyclo-pentane can be divided into two parts: one convex to the pressure axis and the other of the "normal" concave form.

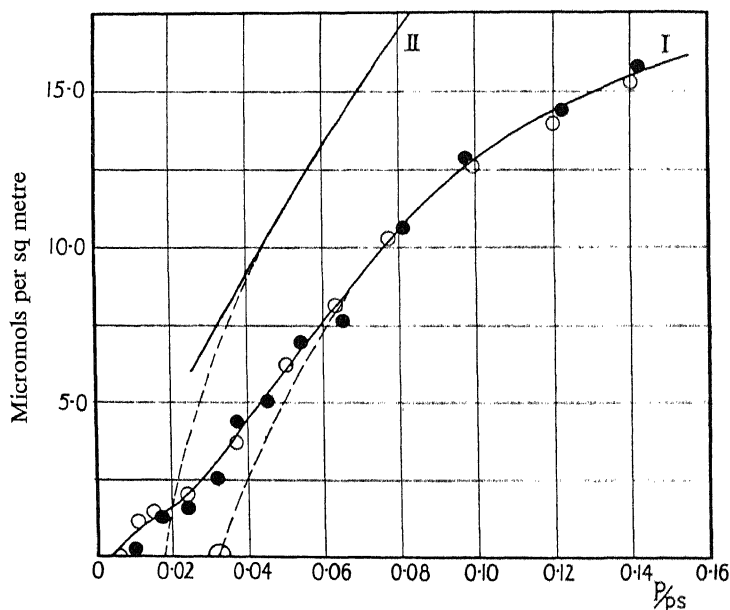


FIG. 9—I, Cyclopentane; ○ experiment 1; ● experiment 2. II, benzene

Polanyi predicted,\* from his own adsorption theory, that such should be the general form of isothermals, and the type of curve has since been realized experimentally, notably by Patrick† (carbon dioxide on silica gel at 78° C), Polanyi and Welke‡ (sulphur dioxide on charcoal) and Coolidge§ (water on charcoal). Experimentally such a form should be found if the adsorbent surface were initially contaminated by a sub-

\* 'Verh. deuts. phys. Ges.,' vol. 18, p. 55 (1916).

† 'Dissertation, Göttingen' (1914); quoted and discussed by Berenyi, 'Z. phys. Chem.,' vol. 94, pp. 628, 661 (1920).

‡ 'Z. phys. Chem.,' vol. 132, p. 371 (1928).

§ 'J. Amer. Chem. Soc.,' vol. 46, p. 623 (1924).

stance of higher adsorptive power; in our case it might be alleged that in the preparation of the silica the benzene was not completely removed but was gradually displaced subsequently by the cyclo-pentane. If this were true, it is certain that the second determination of the isothermal would have disclosed a curve of more "normal" course than the first, but within the limits of experimental error the two determinations are identical. A part of an isothermal convex to the pressure axis has often been taken to indicate the progressive development of the film beyond unimolecular thickness. A fully-packed film of cyclo-pentane of unimolecular thickness over an area of  $5000 \times 14.8 \text{ cm}^2$  requires the adsorption of 24 micromols if the area of the molecule lying flat is taken as  $50 \times 10^{-16} \text{ cm}^2$ . The maximum adsorption shown in the isothermal ( $p = 42.5 \text{ mm}$ ) is 20 micromols, and at the point of inflexion ( $p = 17 \text{ mm}$ ) the adsorption is

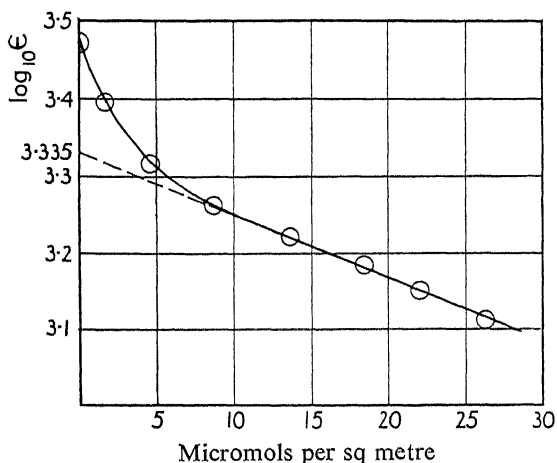


FIG. 10

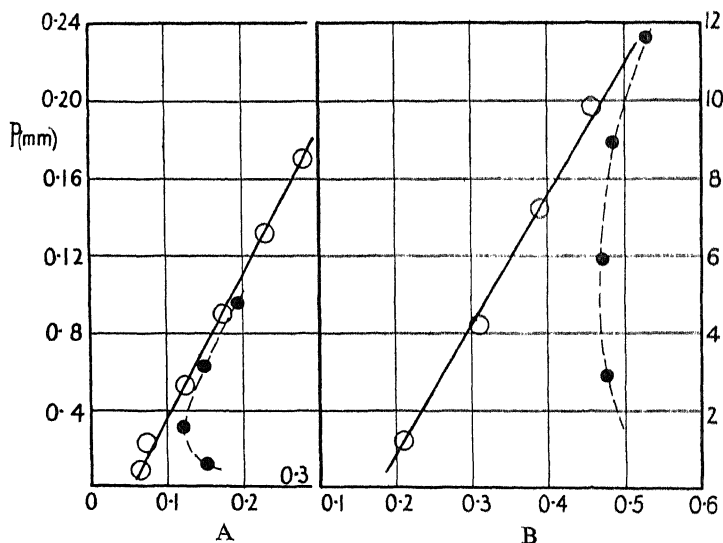
8 micromols or only one-third of the amount for a unimolecular film, even in the unlikely event that all the hydrocarbon molecules remained flat on the surface in the saturated film.

A graph of  $\log \epsilon$  against  $x$  (micromols per square metre) for cyclopentane is drawn in fig. 10. The slope of the straight part of the line is 1.6, on the scale of fig. 7, agreeing exactly with the previous values from that figure. There is also a finite  $\epsilon_{\max}$  of 3020 calories, corresponding with a critical pressure of 2 mm. If the straight part of the line is projected to cut the  $\log \epsilon$  axis, a value of  $\epsilon$  is given ( $\log \epsilon = 3.335$ ) corresponding with a pressure of 11 mm ( $p/p_s = 0.033$ ), allowing the "normal" part of the isothermal to be continued hypothetically as in the broken line of fig. 9. This (apparent) critical pressure has already been given

the symbol  $p_L$  (p. 376), the suffix being intended to signify that this pressure is the zero of pressure for Langmuir's formula. A summary of the values of  $p_L$  is given in Table VII, all the values being obtained from the backward projection of the lines in figs. 7 and 8.

TABLE VII

Adsorbed substance	Apparent critical pressure	
	$p_L$ , mm	
Methyl acetate	0.10	from fig. 7
Acetone	0.42	"
Acetonitrile	1.00	"
Benzene	1.70	"
Chloroform	3.40	"
Cyclo-pentane	11.0	"
Methyl alcohol	0.71	from fig. 8
Ethyl alcohol	1.50	"

FIG. 11—A, acetonitrile,  $p_L = 1.0$  mm; B, benzene,  $p_L = 1.7$  mm

Thus only with methyl acetate and possibly acetone can  $p_L$  be regarded as negligible, and in these two cases alone a direct plot of  $p/x$  against  $p$  gives a straight line and the correct area per molecule on the surface (p. 371). If for the other substances the pressure is corrected by deducting the value of  $p_L$ , a procedure suggested by the calculation on p. 376, we find that Langmuir's principle applies accurately to the low pressure part of the isothermal, since graphs of  $p_{\text{corr}}/x$  against  $p$  give straight lines (fig. 11, a, b in which the broken lines show the result obtained with

uncorrected pressure). From our knowledge of the area exposed by the silica the values given in Table VIII are found for the areas occupied by the molecules (*cf.* p. 371).

TABLE VIII

Acetone .....	$21.5 \times 10^{-16} \text{ cm}^2$	—COCH <sub>3</sub>	$20.5 \times 10^{-16} \text{ cm}^2$
Methyl acetate ....	23.5	—COOCH <sub>3</sub>	23.5
Acetonitrile .....	22.0	—CN	27.0
Benzene .....	36.0	—C <sub>6</sub> H <sub>5</sub>	24.0
Cyclo-pentane .....	35.0		
Ethyl alcohol .....	10.0	—OH	20.5

In the last column are seen the values recorded by Adam (*loc. cit.*) for films on water. While the values we attribute to acetone, methyl acetate, and the hydrocarbons are reasonable, the area for alcohol is apparently only half that for closest packing, and that for the nitrile is somewhat too small. These discrepancies can be easily explained (and indeed predicted) when the polar nature of these molecules is taken into account.\* At low pressures, molecules of the alcohol, as of other substances, condense first on the points of highest potential, but the polar structure of the condensed molecule then enhances the surface potential in its immediate neighbourhood, so that a second molecule will tend to condense next to the first, although the normal potential of the surface might have been too low to permit this at the given pressure with non-polar molecules. Langmuir's theory can easily be modified to take account of behaviour of this kind, without any change of principle. If  $\theta$  is the fraction of the surface unoccupied by adsorbed molecules, then the rate of condensation on this portion will consist of two terms: first, the usual term,  $k_1 p (1 - \theta)$  and, second, a term  $k_2 p \theta$ , showing the special condensation due to the polar nature of the molecules. The rate of evaporation remains as before  $k_3 \theta$ . We thus have for equilibrium

$$k_1 p (1 - \theta) + k_2 p \theta = k_3 \theta.$$

Writing  $a$  for  $k_1/k_3$  and  $b$  for  $k_2/k_3$  we finally obtain

$$\frac{ap}{1 + (a - b)p} = \theta = x/x_{\max}.$$

From this it follows that the slope of the graph of  $p/x$  against  $p$  will give not the true area of the molecules but the fraction  $(a-b)/a$  of the area. The same theory will apply to acetonitrile, but the discrepancy

\* *Cf.* McBain, "The Sorption of Gases by Solids," Routledge, 1932, p. 149.

between the calculated and the true area will be less since this compound shows less tendency to association.

Another aspect of the same matter comes to light in fig. 8, where curves replace the normal straight lines, fig. 7. The general slope of the initial nearly straight portions of the curves in fig. 8 is 1.0 and 1.3 respectively, instead of the constant normal value 1.55, Table VI. It has been suggested above that the presence of polar molecules on the surface must increase the normal number of points of high potential, or, in other words, as adsorption increases with increasing pressure, points of high potential are used up less rapidly than normally, with the result that the distribution factor  $k$  is diminished. It can be seen from fig. 8 that as the amount of adsorbed alcohol becomes considerable the value of  $k$  gradually rises to the normal level.

#### THE NATURE OF THE ADSORPTION FILM

Table IX shows that for relative pressures 0.5–0.6 the adsorption films all contain approximately enough of the adsorbed substance to produce two complete unimolecular layers. However, neither the isothermals nor the  $\log \epsilon, x$  lines exhibit any break in continuity such as might be expected if the first unimolecular layer were completely formed before the appearance of the second layer.

TABLE IX

	Area per molecule on the surface $\text{cm}^2 \times 10^{-16}$	Micromols per sq metre for unimolecular thickness	Actual micromols for greatest adsorption determined	Relative pressure at greatest adsorption
Acetone .....	21.5	7.87	14.6	0.535
Methyl acetate ....	23.5	7.04	14.8	0.550
Acetonitrile .....	27.0*	6.13	13.5	0.520
Methyl alcohol ....	20.5*	8.06	14.8	0.534
Benzene .....	36.0	4.50	9.7	0.591

\* Adam's values.

#### *The Application of Langmuir's Theory*

The fundamental premise of this theory may be stated thus: if the rate of evaporation from a saturated film is  $k$ , then the rate from a film covering a fraction  $\theta$  of the surface will be  $k\theta$ . This statement implies that the intrinsic properties of the unsaturated film—for instance, the specific volatility—are identical with those of the saturated film; the only operative variable assumed is that of area. Bearing in mind the inevitable

heterogeneity of actual surfaces we have concluded that the only type of film structure to which the theory can apply is one in which the unsaturated film consists of "islands" of liquid, ultimately coalescing to a continuous film as adsorption increases. If the islands each cover an area on the surface sufficient to be considered a fair sample of the whole (heterogeneous) surface, then clearly area is the only variable influencing the rate of evaporation from the whole surface. There will exist, associated with some definite equilibrium pressure, a lower limit to the size of the islands, below which they cease to be miniatures of the surface as a whole, but contain predominantly points of high adsorption potential. We think that the pressure we have called the apparent critical pressure ( $p_c$ , Table VII) corresponds at least approximately to this limit, which we have taken as representing zero pressure for the "normal" or liquid-island section of the isothermal. Below this limit of pressure adsorption can only occur on the (small) areas of highest potential, and the molecules so adsorbed will be so firmly held that lateral translatory motion is prohibited. In this part of the isothermal decreasing area of film and increasing potential are the variables jointly controlling evaporation, and it is the introduction of the latter factor that, by diminishing the rate of change of the adsorption with pressure, causes the first or low pressure part of the isothermal to take a form convex to the pressure axis. Suppose that at a low pressure  $p_1$  a fractional area  $\theta_1$  is occupied, and at a less pressure  $p_2$ ,  $\theta_2$  is the area covered, Langmuir's principle demands that  $p_1$  and  $p_2$  are related by the expression  $p_2 = p_1 \cdot \theta_2/\theta_1$ , but actually  $p_2$  has a less value since the fractional area  $\theta_2$  contains a greater proportion of points of high potential than  $\theta_1$ . At pressures above  $p_c$ , points of lower potential come to be occupied, from which lateral translatory motion is possible and results in the ultimate formation of the liquid islands. The data in Table IX above show that in the later stages a second layer of molecules can be retained on the then large unimolecular islands. This development will set an upper limit of pressure to the application of Langmuir's theory in its simplest form, but it appears from the earlier discussion that the rule  $d\varepsilon/dx = k\varepsilon$  is applicable to the whole course of the liquid island part of the isothermal up to at least the adsorption corresponding with a relative pressure 0.5.

#### SUMMARY

A study has been made of the adsorption of vapours on powdered vitreous silica, prepared by a method that excludes fortuitous contamination of the surface.

The absolute surface available for adsorption has been determined from measurements of the initial rate of dissolution of the powder in dilute hydrofluoric acid. The areas covered by molecules on the surface have been calculated and found to agree with values from other sources.

A general expression has been proposed connecting adsorption potential with amount adsorbed, leading to a new theoretical isothermal.

The restricted applicability of Langmuir's formula to parts of the isothermals is interpreted theoretically.

Special experiments were made on the form of the adsorption isothermal at low adsorptions.

---

## On Gauss' Theorem and the concept of Mass in General Relativity

By E. T. WHITTAKER, F.R.S.

(Received January 7, 1935)

### § 1—INTRODUCTION

The present communication is concerned with the extension to General Relativity theory of the well-known theorem of Gauss on the Newtonian potential, viz., that the total flux of gravitational force through a simple closed surface is equal to  $(-4\pi)x$  the total gravitating mass contained within the surface: and to various questions which arise in connection with this. In the extended theorem, which is found in § 2, the Newtonian concept of "gravitating mass" is naturally replaced by that of the energy-tensor, which does not in general consist solely of the "material" energy-tensor, and need not involve any "matter" at all. This new feature is illustrated in § 3 by an example in which the "gravitating mass" is simply an electrostatic field. In § 4 a theorem of "energy" is obtained which is required later, and which enables us to make precise the concept of the "potential energy" of an infinitesimal particle in a statical field in general relativity; this "potential energy" is shown to be the product of two factors, one depending on the particle alone (which may be called its "potential mass") and the other depending solely on its position. It is shown in § 5 that the definition of "potential mass" introduced in § 4 enables us to express the generalized Gauss' theorem of

§ 2, in the case when the energy-tensor is due to actual masses, by a simple statement practically identical with the original Gauss' theorem of Newtonian theory. Finally in § 6 it is shown that the electrostatical form of Gauss' theorem in Newtonian physics, viz., that the total strength of the tubes of force issuing from a closed surface is equal to the total electric charge within the surface, can also be extended to General Relativity, but that this extension is different in character from the gravitational theorem of § 2.

## § 2—THE EXTENDED GAUSS' THEOREM FOR THE GRAVITATIONAL FIELD

We shall first consider the extension to General Relativity of Gauss' theorem

$$\iint_S \frac{\partial V}{\partial \nu} dS = 4\pi M, \quad (2.1)$$

where  $V$  denotes the gravitational potential,  $S$  a simple closed surface of which  $dS$  is an element of area,  $d\nu$  the element of inwards-drawn normal to  $dS$ , and  $M$  the total gravitating mass contained within the surface  $S$ .

In attempting to generalize this, we must remember that in General Relativity the gravitational force, as measured by any observer, depends not only on the observer's position but also on his velocity and acceleration, being in fact represented by the four-vector

$$g^i = - \left\{ \frac{d^2 x^i}{d\tau^2} + \sum_{h,k} \left\{ \begin{matrix} hk \\ i \end{matrix} \right\} \frac{dx^h}{d\tau} \frac{dx^k}{d\tau} \right\}, \quad (2.2)$$

where  $d\tau$  denotes the element of proper-time of the observer. In speaking of an integral involving gravitational force we must, therefore, specify at every point an observer with respect to whom the force is measured: this can be done in a natural way only for worlds whose metric can be defined by an equation of the type

$$d\tau^2 = U dt^2 - \frac{1}{c^2} \sum_{p,q=1}^3 a_{pq} dx^p dx^q, \quad (2.3)$$

where  $U$  may involve all four co-ordinates and where the coefficients  $a_{pq}$  depend only on the co-ordinates  $(x_1, x_2, x_3)$ .<sup>\*</sup> In this world we can

<sup>\*</sup> The variable  $t$  may obviously be replaced by any constant multiple  $\lambda t$ , provided  $U$  is replaced by  $U/\lambda^2$ ; we may take advantage of this to normalize  $t$  and  $U$  so that at infinity  $U \rightarrow 1$ ; for  $U$  must in any case tend to a constant value at infinity, since the metric tends to a Galilean metric there.



suppose at every point an observer who is "at rest," *i.e.*, whose co-ordinates  $(x_1, x_2, x_3)$  are constant, his co-ordinate  $t$  alone varying, and we can define gravitational force to be that measured by these observers. Now for such an observer we have

$$\frac{dt}{d\tau} = U^{-\frac{1}{2}}, \quad \frac{dx^1}{d\tau} = 0, \quad \frac{dx^2}{d\tau} = 0, \quad \frac{dx^3}{d\tau} = 0,$$

and thus equation (2.2) gives for  $i = 1, 2, 3$ ,

$$g^i = - \begin{Bmatrix} 0 & 0 \\ i & j \end{Bmatrix} \left( \frac{dt}{d\tau} \right)^2 = - \frac{1}{U} \begin{Bmatrix} 0 & 0 \\ i & j \end{Bmatrix} = \frac{1}{2} \sum_k \frac{g^{ik}}{U} \frac{\partial U}{\partial x^k},$$

so

$$g^i = - \frac{c^2}{2} \sum_k \frac{a^{ik}}{U} \frac{\partial U}{\partial x^k} \quad \text{for } i = 1, 2, 3, \quad (2.4)$$

and

$$g^0 = - \left[ \frac{dU^{-\frac{1}{2}}}{d\tau} + \begin{Bmatrix} 0 & 0 \\ 0 & j \end{Bmatrix} U^{-1} \right] = 0.$$

It is therefore natural to consider, as a possible generalization of the integral on the left-hand side of (2.1), some constant multiple of the integral

$$\iint \left\{ g^1 \frac{\partial (x^2, x^3)}{\partial (u, v)} + g^2 \frac{\partial (x^3, x^1)}{\partial (u, v)} + g^3 \frac{\partial (x^1, x^2)}{\partial (u, v)} \right\} \sqrt{-g} \, du \, dv, \quad (2.5)$$

where  $(g^1, g^2, g^3)$  is the three-vector in the space  $(x^1, x^2, x^3)$  (which is the "instantaneous space" of the observer) given by (2.4), which represents the gravitational force as measured by the observer, and where the integration is taken over any simple closed surface  $S$  on the space of  $(x^1, x^2, x^3)$ ;  $u$  and  $v$  are any two parameters which specify the position of points in this surface; and  $g$  denotes as usual the determinant of the coefficients of the metric (2.3), so that

$$\sqrt{-g} = c^{-3} U^{\frac{1}{2}} \sqrt{a},$$

where  $a$  is the determinant of the coefficients of the form  $\sum a_{\mu\nu} dx^\mu dx^\nu$ .

To find what the constant multiplier of the integral (2.5) should be, let us calculate the integral (2.5) for the case of the field of a single gravitating mass, for which the metric is given by Schwarzschild's formula

$$ds^2 = \left( 1 - \frac{\alpha}{R} \right) dt^2 - \frac{1}{c^2} \left( \frac{dR^2}{1 - \frac{\alpha}{R}} + R^2 d\theta^2 + R^2 \sin^2 \theta d\phi^2 \right),$$

where  $\alpha = \frac{2\beta M}{c^2}$ , and  $\beta$  denotes the Newtonian constant of gravitation,

while  $M$  is the mass of the gravitating central body. Here the integral (2.5), taken over a sphere of radius  $R$ , becomes

$$-\frac{\beta M}{c^3} \iint \sin \theta \, d\theta \, d\phi \quad \text{or} \quad -\frac{4\pi\beta M}{c^3}.$$

Since we want such a multiple of the integral (2.5) as will give  $4\pi\beta M$ , we see that the required multiplier must be  $-c^3$ ; and thus we shall study the quantity

$$I = -c^3 \iint \left\{ g^1 \frac{\partial(x^2, x^3)}{\partial(u, v)} + g^2 \frac{\partial(x^3, x^1)}{\partial(u, v)} + g^3 \frac{\partial(x^1, x^2)}{\partial(u, v)} \right\} \sqrt{-g} \, du \, dv. \quad (2.6)$$

Substituting from (2.4) in (2.6), we have

$$I = \frac{1}{2}c^2 \iint \sum_k \left\{ a^{1k} \frac{\partial U}{\partial x^k} \frac{\partial(x^2, x^3)}{\partial(u, v)} + a^{2k} \frac{\partial U}{\partial x^k} \frac{\partial(x^3, x^1)}{\partial(u, v)} + a^{3k} \frac{\partial U}{\partial x^k} \frac{\partial(x^1, x^2)}{\partial(u, v)} \right\} a^{\frac{1}{2}} U^{-\frac{1}{2}} \, du \, dv.$$

Converting this surface-integral into a volume-integral, it becomes

$$I = \frac{1}{2}c^2 \iiint \sum_{h,k} \frac{\partial}{\partial x^h} \left( \frac{a^{hk} \cdot a^{\frac{1}{2}}}{U^{\frac{1}{2}}} \frac{\partial U}{\partial x^k} \right) dx^1 dx^2 dx^3,$$

integrated over the three-dimensional region  $R$  contained by the surface  $S$  in the space  $(x^1, x^2, x^3)$ .

Since Beltrami's differential parameter of the second order with respect to the quadratic form  $\Sigma a_{pq} dx^p dx^q$  is defined by the equation

$$\Delta_2 V = \frac{1}{\sqrt{a}} \sum_{h,k} \frac{\partial}{\partial x^h} \left( a^{\frac{1}{2}} a^{hk} \frac{\partial V}{\partial x^k} \right),$$

the preceding equation may be written

$$I = c^2 \iiint \Delta_2 U^{\frac{1}{2}} \cdot a^{\frac{1}{2}} dx^1 dx^2 dx^3. \quad (2.7)$$

Now denoting the contracted Riemann tensor of the metric (2.3) by  $K_{pq}$ , we find, on substituting the coefficients of this metric in the ordinary formula for  $K_{pq}$ , that

$$K_{00} = -c^2 U^{\frac{1}{2}} \cdot \Delta_2 U^{\frac{1}{2}}, \quad \text{so} \quad K_0^0 = -c^2 U^{-\frac{1}{2}} \cdot \Delta_2 U^{\frac{1}{2}}.$$

Thus (2.7) becomes

$$I = - \iiint K_0^0 \cdot U^{\frac{1}{2}} a^{\frac{1}{2}} dx^1 dx^2 dx^3. \quad (2.8)$$

But the field-equations of gravitation give

$$K_0^0 = -\frac{8\pi\beta}{c^5} (T_0^0 - \frac{1}{2}T),$$

where  $\beta$  denotes the Newtonian constant of gravitation, and  $T_p^q$  is the energy-tensor, and thus (2.8) becomes

$$I = \frac{8\pi\beta}{c^5} \iiint (T_0^0 - \frac{1}{2}T) \cdot U^{\frac{1}{2}} a^{\frac{1}{2}} dx^1 dx^2 dx^3, \quad (2.9)$$

or

$$\begin{aligned} & -c^3 \iint \left\{ g^1 \frac{\partial(x^2, x^3)}{\partial(u, v)} + g^2 \frac{\partial(x^3, x^1)}{\partial(u, v)} + g^3 \frac{\partial(x^1, x^2)}{\partial(u, v)} \right\} \sqrt{-g} du dv \\ & = \frac{8\pi\beta}{c^2} \iiint (T_0^0 - \frac{1}{2}T) \sqrt{-g} dx^1 dx^2 dx^3. \quad (I) \end{aligned}$$

*This is the theorem in General Relativity which corresponds to Gauss' theorem in Newtonian potential theory*—The left-hand side is the surface-integral of the gravitational force over an arbitrary simple closed surface, and the right-hand side is the volume-integral, taken over the space enclosed by the surface, of a quantity that depends only on the energy-tensor, which in General Relativity plays the part that is taken by matter in Newtonian physics.

### § 3—AN ELECTROSTATIC EXAMPLE

The theorem (I) is naturally much wider in its physical significance than the original Gauss' theorem, since the energy-tensor  $T_p^q$  is not, in general, constituted solely of the "material" energy-tensor, but includes the electrical energy-tensor, etc. Let us take, as an example, a system in which there is no material energy-tensor, namely, an electrostatic system such as a condenser formed of two massless concentric spherical surfaces carrying equal and opposite charges. Let  $E_p^q$  denote the electric energy-tensor due to the electrostatic field between the surfaces, so that  $E_0^0$  represents the density of electrostatic energy: the energy-fluxes  $E_0^q$  are zero, the components of electromagnetic momentum  $-E_p^0$  are also zero, and the remaining components  $E_p^q$  ( $p, q = 1, 2, 3$ ) represent the Maxwell stresses. The condenser will not, however, be in equilibrium unless there is also a system of mechanical stresses keeping the surface-elements of the two spherical surfaces in position by antagonizing the mechanical forces exerted on these by the electric field. The simplest arrangement, in theory, is to have stresses represented by an energy-tensor  $R_p^q$  such that the components  $R_p^q$  for  $p, q = 1, 2, 3$  exactly

neutralize the Maxwell stresses  $E_p^q$ , that is,  $R_p^q + E_p^q = 0$  for  $p, q = 1, 2, 3$ . Since the system is statical, the energy-fluxes  $R_0^q$  and the momentum components  $-R_p^0$  will be null. Thus the total energy-tensor  $T_p^q = E_p^q + R_p^q$  will have all its components null except  $T_0^0$ ; and therefore  $T = \sum_p T_p^p = T_0^0$ , and so

$$\iiint (T_0^0 - \frac{1}{2}T) \sqrt{-g} dx^1 dx^2 dx^3 = \frac{1}{2} \iiint T_0^0 \sqrt{-g} dx^1 dx^2 dx^3 \\ = \frac{1}{2} \times (\text{energy of system}).$$

Now the mass  $M$  of the system is  $1/c^2 \times$  its energy. Thus

$$\iiint (T_0^0 - \frac{1}{2}T) \sqrt{-g} dx^1 dx^2 dx^3 = \frac{1}{2}c^2 M,$$

and thus the theorem (I) becomes in this case

$$-c^3 \iiint \left\{ g^1 \frac{\partial (x^2, x^3)}{\partial (u, v)} + g^2 \frac{\partial (x^3, x^1)}{\partial (u, v)} + g^3 \frac{\partial (x^1, x^2)}{\partial (u, v)} \right\} \sqrt{-g} du dv = 4\pi \beta M,$$

the analogy of which with the Newtonian Gauss' theorem is evident.

#### § 4—THE INTEGRAL OF ENERGY FOR A PARTICLE IN A STATICAL FIELD

In order to express our extended Gauss' theorem (I), in the case when the energy-tensor is purely "material," in a form more closely analogous to the original Gauss' theorem, we shall need to enquire more closely what is to be understood by "mass" in this connection. Light will be thrown on this question by studying the energy-relations, in a statical gravitational field, of a "test-particle," *i.e.*, a particle so small that it does not sensibly disturb the field, although it is acted on by it.

Let the metric of space-time be specified by

$$d\tau^2 = U dt^2 - \frac{1}{c^2} dl^2 = U dt^2 - \frac{1}{c^2} \sum_{p,q=1}^3 a_{pq} dx^p dx^q,$$

where  $d\tau$  is the element of proper-time and where  $U$  and the  $a_{pq}$  are functions of  $(x^1, x^2, x^3)$  only. Then if  $d\sigma$  denotes the element of time as measured by an observer  $P$  at rest in  $(x^1, x^2, x^3)$ , we have  $d\sigma^2 = U dt^2$ . The kinetic energy of a small particle of proper-mass  $m$ , momentarily at  $P$ , as measured by this observer, is

$$mc^2 \left\{ 1 - \frac{1}{c^2} \left( \frac{dl}{d\sigma} \right)^2 \right\}^{-\frac{1}{2}}, \text{ or } mc^2 \left\{ 1 - \frac{1}{c^2 U} \left( \frac{dl}{dt} \right)^2 \right\}^{-\frac{1}{2}}, \text{ or } mc^2 U^{\frac{1}{2}} \frac{dt}{d\tau}. \quad (4.1)$$

Now writing

$$T = \frac{1}{2}U\dot{t}'^2 - \frac{1}{2c^2}\dot{l}'^2,$$

where the accents denote differentiations with respect to  $\tau$ , one of the equations of motion of the particle is

$$\frac{d}{d\tau} \left( \frac{\partial T}{\partial \dot{t}'} \right) - \frac{\partial T}{\partial t} = 0,$$

which gives

$$\frac{\partial T}{\partial \dot{t}'} = \text{constant},$$

or

$$U \frac{dt}{d\tau} = \varepsilon, \quad (4.2)$$

where  $\varepsilon$  denotes a constant. From (4.1) and (4.2), the kinetic energy is

$$mc^2 \varepsilon U^{-\frac{1}{2}}. \quad (4.3)$$

Now at infinity, *i.e.*, where the influence of the gravitational field vanishes and space-time is Galilean, let the velocity of the particle be  $w$ . In this region,  $U \rightarrow 1$ , so by (4.1) the kinetic energy tends to  $mc^2 \left(1 - \frac{w^2}{c^2}\right)^{-\frac{1}{2}}$ , and by (4.3) it tends to  $mc^2 \varepsilon$ . Equating these two values, we have

$$\varepsilon = \left(1 - \frac{w^2}{c^2}\right)^{-\frac{1}{2}}. \quad (4.4)$$

From (4.1), (4.3), and (4.4), we have

$$\frac{mc^2}{\left\{1 - \frac{1}{c^2 U} \left(\frac{dl}{dt}\right)^2\right\}^{\frac{1}{2}}} = \frac{mc^2}{\left(1 - \frac{w^2}{c^2}\right)^{\frac{1}{2}}} \cdot U^{\frac{1}{2}}, \quad (II)$$

and *this is the equation of conservation of energy for the particle*. The expression on the left is the kinetic energy, and the expression on the right may be called the *lost potential energy*. The *lost potential energy*

*corresponds to that of a particle of mass  $\frac{m}{\left(1 - \frac{w^2}{c^2}\right)^{\frac{1}{2}}}$  in a field of force  $c^2/U^{\frac{1}{2}}$ .*

We are now in a position to see the difference between Newtonian dynamics and the dynamics of General Relativity, in the matter of potential

energy. In Newtonian dynamics the equation of conservation of energy for a single particle is

$$(\text{kinetic energy}) + (\text{potential energy}) = C, \quad (4.5)$$

where the potential energy is the product of the mass—a fixed quantity—into a function which depends only on the position of the particle, and where  $C$  is a constant which depends on the type of motion, *i.e.*, on the initial circumstances of projection. In General Relativity with statical fields, on the other hand, the equation of conservation of energy for a single small particle of proper-mass  $m$  is (as we see from (II)) of the form

$$(\text{kinetic energy}) = (\text{lost potential energy}), \quad (4.6)$$

where now the lost potential energy is the product of  $m \left(1 - \frac{w^2}{c^2}\right)^{-\frac{1}{2}}$  into a function which depends only on the position of the particle: *here  $w$  denotes the velocity which the particle would have after escaping from the gravitational field and arriving at the Galilean space-time at infinity*; the constant  $w$  in (4.6) corresponds to the constant  $C$  in (4.5), since it characterizes the various types of motion, but it enters in a wholly different manner into the equation, since in (II) or (4.6) its effect is to modify the effective mass. We shall call  $m \left(1 - \frac{w^2}{c^2}\right)^{-\frac{1}{2}}$  the *potential mass*, since it is the coefficient which plays the part of mass in the expression for the potential energy. It is, of course, equal to  $1/c^2 \times$  the energy of the particle when it has escaped to infinity out of the influence of the gravitational field.

We may remark that the constant  $w^2$  is not necessarily positive; it will, in fact, be negative if the particle has not sufficient energy to carry it out of the gravitational field into the Galilean field at infinity.

We may remark in passing that equation (II) leads immediately to the formula for the shift to the red of a spectral line which is emitted in a strong gravitational field, when measured by an observer outside the field. For we have only to pass to the limiting case when the material particle becomes a light-quant, so that its kinetic energy is now  $h\nu$ , where  $\nu$  is the frequency and  $h$  is Planck's constant. Equation (II) now becomes

$$h\nu = \frac{h\nu_0}{U^{\frac{1}{2}}} \quad \text{or} \quad \nu_0 = \nu U^{\frac{1}{2}},$$

where  $\nu$  is the frequency at the place of emission (*e.g.*, on the sun) and  $\nu_0$  is the frequency as observed outside the gravitational field (*e.g.*, on the earth). This is the well-known formula for the shift to the red of spectral lines emitted in a strong gravitational field.

§ 5—INTERPRETATION OF THE EXTENDED GAUSS' THEOREM FOR  
PURELY MATERIAL FIELDS

We shall now show that the conception of "potential mass," introduced in § 4, furnishes a physical interpretation of the extended Gauss' theorem (I) of § 2, for purely material statical fields.

When the field is purely material (*i.e.*, there are no electromagnetic phenomena) and incoherent, the energy-tensor is simply

$$T^{pq} = c^2 \sigma_0 \frac{d\xi^p}{d\tau} \frac{d\xi^q}{d\tau},$$

where ( $\xi^0 \dots \xi^3$ ) are the co-ordinates of a particle when its proper-time is  $\tau$ , and  $\sigma_0$  is the proper-density of matter, defined by the invariant condition that

$$\int \sigma_0 \sqrt{-g} dx^0 dx^1 dx^2 dx^3 \quad (5.1)$$

integrated over any region of space-time, is equal to the sum of the lengths of the world-lines of material particles in this region, each multiplied by the proper-mass of the particle to which it belongs.

Since the field is statical, we shall suppose the material particles to be at rest in the space ( $x^1, x^2, x^3$ ),\* so that  $d\xi^p/d\tau = 0$  for  $p = 1, 2, 3$ . Thus the only non-zero constituent of  $T^{pq}$  is

$$T^{00} = c^2 \sigma_0 \left( \frac{d\xi^0}{d\tau} \right)^2 = \frac{c^2 \sigma_0}{U},$$

whence  $T_0^0 = c^2 \sigma_0$  and  $T = \sum_p T_p^p = T_0^0$ . Thus (2.9) becomes

$$I = \frac{4\pi\beta}{c^3} \iiint \sigma_0 U^{\frac{1}{2}} a^{\frac{1}{2}} dx^1 dx^2 dx^3 = 4\pi\beta \iiint \sigma_0 \sqrt{-g} dx^1 dx^2 dx^3.$$

Thus if  $\delta t$  denotes a small increment of the variable  $t$ , we have

$$I\delta t = 4\pi\beta \iiint \sigma_0 \sqrt{-g} \delta t dx^1 dx^2 dx^3. \quad (5.2)$$

Let  $Q$  denote the region of space-time obtained by multiplying the three-dimensional region  $R$  (*viz.*, the space inside the surface  $S$  in the space of  $x^1, x^2, x^3$ ), by  $\delta t$ . Then, by (5.1), equation (5.2) is equivalent to the statement that—

$I\delta t = 4\pi\beta \times$  the sum of the lengths of the world-lines of the material particles in the region  $Q$ , each multiplied by the proper-mass of the particle to which it belongs.

\* This, of course, requires that they should be situated at places for which  $U$  has maximum or minimum values.

Dividing both sides of this equation by  $\delta t$ , and making  $\delta t \rightarrow 0$ , we obtain

$I = 4\pi\beta \times$  the sum of the proper-masses of the material particles in the three-dimensional region  $R$ , each multiplied by the value of  $d\tau/dt$  for the particle in question,

or

$I = 4\pi\beta \times$  the sum of the proper-masses of the material particles in the region  $R$ , each multiplied by the value of  $U^{\frac{1}{2}}$  at the particle. (5.3)

Now the equation of energy (II) of § 4, for one of these particles at rest in the space  $(x^1, x^2, x^3)$ , is

$$mc^2 = \frac{mc^2}{\left(1 - \frac{w^2}{c^2}\right)^{\frac{1}{2}}} \cdot U^{\frac{1}{2}}$$

so

$$U^{\frac{1}{2}} = \left(1 - \frac{w^2}{c^2}\right)^{-\frac{1}{2}} \quad (5.4)$$

so (5.3) becomes

$I = 4\pi\beta \times$  the sum of the proper-masses of the material particles in the region  $R$ , each multiplied by the value of  $(1 - w^2/c^2)^{-\frac{1}{2}}$  belonging to it,

or

$I = 4\pi\beta \times$  the sum of the "potential masses" of the material particles in the region  $R$ .

Thus finally we have the result that *when the statical gravitational field is due solely to material particles, the extended Gauss' theorem of § 2 takes the form*

$$-c^3 \iint \left\{ g^1 \frac{\partial(x^2, x^3)}{\partial(u, v)} + g^2 \frac{\partial(x^3, x^1)}{\partial(u, v)} + g^3 \frac{\partial(x^1, x^2)}{\partial(u, v)} \right\} \sqrt{-g} du dv = 4\pi\beta M, \quad (\text{III})$$

where the integration is taken over any simple closed surface in the space of  $(x^1, x^2, x^3)$ , and  $M$  denotes the sum of the "potential masses" of those material particles that are inside this surface.

The close analogy between this and the original Gauss' theorem of Newtonian potential-theory is obvious. The remarkable feature is that it is the "potential masses," and not the proper masses, of the particles which occur in the right-hand side of the equation.



## § 6—THE EXTENDED GAUSS' THEOREM FOR THE ELECTRIC POTENTIAL.

In Newtonian physics, Gauss' theorem is applicable not only to the gravitational potential but also to the electrostatic potential, taking the form (in suitable units)

$$\iint_S \frac{\partial V}{\partial \nu} dS = \text{Total electric charge inside the surface } S,$$

where  $V$  denotes the electrostatic potential. This theorem can be extended to electromagnetic fields of any kind, in gravitational fields of any kind in general relativity, as follows:

Let  $M$  be any three-dimensional multipoint in space-time, whose frontier is a closed surface  $S$ . Denote by  $J^\mu$  the electric current-vector whose components are  $(\rho, \rho v_x, \rho v_y, \rho v_z)$ , where  $\rho$  is the density of electric charge and  $(v_x, v_y, v_z)$  is its velocity. Then the total quantity of electricity belonging to those world-lines of electric charge which intersect the multipoint  $M$  is

$$\iiint_M \left\{ J^0 \frac{\partial (x^1, x^2, x^3)}{\partial (p, q, r)} + J^1 \frac{\partial (x^2, x^3, x^0)}{\partial (p, q, r)} + J^2 \frac{\partial (x^3, x^0, x^1)}{\partial (p, q, r)} + J^3 \frac{\partial (x^0, x^1, x^2)}{\partial (p, q, r)} \right\} \sqrt{-g} dp dq dr, \quad (6.1)$$

where  $(p, q, r)$  are any parameters specifying position in  $M$ .

Now the fundamental equations of the electromagnetic field (Maxwell's equations extended to general relativity) are

$$\frac{1}{\sqrt{-g}} \sum_a \frac{\partial (\sqrt{-g} X^{pa})}{\partial x^a} = J^p \quad (p = 0, 1, 2, 3) \quad (6.2)$$

where

$$X_{rs} = \frac{\partial \phi_r}{\partial x^s} - \frac{\partial \phi_s}{\partial x^r} \quad (6.3)$$

$(\phi_0, \phi_1, \phi_2, \phi_3)$  being the electromagnetic potential-vector, so  $X_{rs}$  is the six-vector of which three components represent the electric force and the other three represent the magnetic vector.

Substituting from (6.2) in (6.1), and transforming into a surface-integral, we obtain the result that *the total electric charge, belonging to*

particles whose world-lines intersect a three-dimensional multipoint whose frontier is a simple closed surface  $S$ , is

$$\iint_S \left\{ X^{23} \frac{\partial (x^0, x^1)}{\partial (u, v)} + X^{31} \frac{\partial (x^0, x^2)}{\partial (u, v)} + X^{12} \frac{\partial (x^0, x^3)}{\partial (u, v)} + X^{03} \frac{\partial (x^1, x^2)}{\partial (u, v)} \right. \\ \left. + X^{02} \frac{\partial (x^3, x^1)}{\partial (u, v)} + X^{01} \frac{\partial (x^2, x^3)}{\partial (u, v)} \right\} \sqrt{-g} \, du \, dv. \quad (\text{III})$$

This is the extension, to the most general electromagnetic field in any gravitational field, of Gauss' theorem on the electrostatic potential. Evidently it differs greatly from the extension of Gauss' theorem on the gravitational potential, which was the subject of §§ 2-5.

#### SUMMARY

The well-known theorem of Gauss on the Newtonian potential, viz., that the total flux of gravitational force through a simple closed surface is equal to  $(-4\pi) \times$  the total gravitating mass contained within the surface, is extended to General Relativity. In the extended theorem, the Newtonian concept of "gravitating mass" is naturally replaced by that of the energy-tensor, which does not in general consist solely of the "material" energy-tensor, and need not involve any matter at all. It is shown that in order to provide a simple physical interpretation of the formulæ obtained, a new concept must be introduced, to which the name "potential mass" is given. The electrostatic form of Gauss' theorem is also extended to General Relativity.

---

# The Isotopic Constitution and Atomic Weights of Hafnium, Thorium, Rhodium, Titanium, Zirconium, Calcium, Gallium, Silver, Carbon, Nickel, Cadmium, Iron and Indium

By F. W. ASTON, F.R.S.

(Received January 24, 1935)

An account of experiments has already been given\* by which the analyses of the rare earth elements were completed with the aid of a particularly favourable arrangement of the anode ray apparatus. This paper contains a description of analyses of other elements made with the same setting and also of some others subsequently made to obtain more accurate and complete data on elements whose constitution had already been provisionally settled.

## RESULTS

(72) *Hafnium*—Many previous attempts to obtain the mass spectra of this element had failed. For the most similar element, zirconium, the only successful results had been obtained from the fluoride. A pure sample of hafnium fluoride had been kindly provided by Professor G. v. Hevesy, one of the discoverers of the element, and this was incorporated into the anode mixture. The first trial was a failure; but after the work on zirconium described below a second attempt was made, this time with success. As with the complex rare earths the lines were not clearly resolved, so that only rough estimates of abundance could be obtained. These were as follows:—

Mass numbers . . . . .	176	177	178	179	180
% abundance . . . . .	5	19	28	18	30

These give a mean mass number 178.5. Applying the same correction as with the rare earths we get

$$\text{atomic weight of hafnium} = 178.4 \pm 0.2$$

in fair agreement with the International value 178.6.

(90) *Thorium*—Thorium fluoride was prepared by the action of hydrofluoric acid on the pure oxide. This was incorporated into the anode

\* Aston, 'Proc. Roy. Soc.,' A, vol. 146, p. 46 (1934).

and a long exposure on a particularly sensitive plate was given. The expected line at 232 appeared. This was of considerable strength and photometry showed no indication of a higher isotope suggested by the chemical atomic weight 232·15.

(45) *Rhodium*—This element, the lightest which had defeated all previous attacks, was examined by means of the compound rhodium sodium chloride, a pure sample of which was kindly supplied by Dr. F. G. Mann. Positive results were at last obtained, but they were extremely feeble. It was just possible to detect a line at the expected position 103. The chemical atomic weight is 102·9, and as from the curve it may be expected to have a large negative packing fraction it is probable that rhodium is simple.

(22) *Titanium*—Although positive results had been obtained with this element years ago which indicated that its principal isotope was of mass number 48 they were regarded as highly unsatisfactory owing to the presence of lines due to compounds of silicon and fluorine. Quite recently experiments with the ordinary discharge in titanium bromide, prepared specially for the purpose, were equally inconclusive owing to the maze of lines due to adventitious compounds. The remarkable freedom from such lines in the setting of the apparatus available gave a unique opportunity to examine this element. The titanium fluoride used in the original experiments was used and gave immediate and conclusive spectra. The strong line 48 was found flanked by weak symmetrical pairs of satellites 46, 47, 49, 50, the whole forming a group of striking appearance. Photometry gave the following abundances:—

Mass number	....	46	47	48	49	50
% abundance	....	8·5	7·8	78·3	5·5	6·9

These correspond to a mean mass number 47·94<sub>5</sub>. The packing fraction of titanium 48 has not yet been determined, but if we take it to lie on the curve and correct to the chemical scale

$$\text{atomic weight of titanium} = 47\cdot91 \pm 0\cdot01$$

in good agreement with the International value 47·90.

(40) *Zirconium*—The only mass-spectra of this element had been obtained with the greatest difficulty during the early work with anode rays and were very feeble. Now by the use of the same sample of zirconium fluoride very much better results were obtained. Not only was the faint and doubtful isotope 96 confirmed, but a new and fairly

abundant one, 91, was discovered, which had been overlooked owing to the inferior resolution in the early plates. Photometry gave relative abundances roughly as follows:—

Mass numbers	....	90	91	92	94	96
% abundance	....	48	11.5	22	17	1.5

These give a mean mass number 91.32 which, corrected for most probable packing fraction and change of scale, gives

$$\text{atomic weight of zirconium} = 91.24 \pm 0.05$$

in good agreement with the International value 91.22.

It is of interest to note that zirconium of mass number 96 forms with molybdenum and ruthenium the lightest known isobaric triplet.

(20) *Calcium*—The isotopic constitution of this element, first investigated by Dempster, has a particular interest in connection with theories of the radioactivity of potassium.\* In the earlier work with anode rays it had given feeble results only sufficient to show that its principal isotope obeyed the whole number rule. The fact that the lines of potassium were always present in considerable strength eliminated any hope of showing whether calcium contained the expected isotope 41 or not. A setting which gave unprecedented freedom from the lines of any elements except those present in the anode mixture offered an opportunity not to be missed of obtaining data on this point. Calcium fluoride was used, and the first spectra showed lines 41, 42, 43 in addition to 40 and 44 originally announced by Dempster. Of these 42 and 43 were certainly new isotopes of calcium. Line 39 due to potassium was, however, present and the difficulties of photometry in the neighbourhood of the enormously strong line 40 made quantitative measurements too uncertain to decide if the line 41 could be entirely ascribed to potassium or not. The utmost pains were now taken to exclude potassium entirely. Calcium chloride of the highest chemical purity was used mixed with pure graphite instead of the commercial article previously found most effective in the anode. At the loss of some intensity in the beam mass spectra were now obtained from which line 41 had disappeared entirely, and it is safe to conclude that this mass number does not occur in calcium to the extent of 1 part in 1000. Photometry gave the following constitution:—

Mass number	....	40	42	43	44
% abundance	....	96.76	0.77	0.17	2.30

\* For a recent discussion on this problem the reader is referred to Klemperer, 'Proc. Roy. Soc.' A, vol. 148, p. 638 (1935).

which corresponds to a mean mass number 40·112. If we give Ca 40 the same packing fraction as its isobar in argon and correct for change of scale we get

$$\text{atomic weight of calcium} = 40\cdot076 \pm 0\cdot006$$

in excellent agreement with 40·08 obtained by chemical means. It will be noted that the abundance of Ca 44 is considerably higher than that originally estimated by Dempster\* and in better accord with the chemical atomic weight.

The original and simple view of the radioactivity of potassium was that it consisted of an ordinary beta ray disintegration of one of its isotopes, which resulted in a calcium of the same mass number. The beautiful experiments of Hevesy,† who found that the radioactivity followed the heavier fraction in free distillation, showed that the isotope responsible must be 41 or some other unknown heavy one. On the first view mass number 41 should have accumulated in considerable quantity in calcium associated with old potassium minerals.

The writer was kindly supplied with compounds of calcium extracted from the oldest micas, having a high ratio of potassium to calcium, by Professor v. Hevesy, and of those extracted from pegmatites from Rhiconich and Portsoy by Professor J. Kendall. On analysis the mass spectra of these showed no appreciable difference from that of ordinary calcium, so that the abnormally high atomic weights reported by Kendall‡ cannot be ascribed to the presence of Ca 41. It also seems probable that the final stable product of the disintegration of potassium may not be calcium at all.

(31) *Gallium*—A repetition of the anode ray analyses of this element were made in order to obtain values for the relative abundance of its two isotopes 69 and 71. The fluoride was used as before, and very much more satisfactory spectra were obtained. Photometry gave for the abundances 61·5 and 38·5 respectively, corresponding to a mean mass number 69·77 which, corrected for probable packing fraction and scale, gives

$$\text{atomic weight of gallium} = 69\cdot71 \pm 0\cdot02$$

virtually identical with the International value 69·72.

(47) *Silver*—The analysis of this element, as with gallium, was made to obtain definite numerical data for the relative abundance of its almost

\* 'Phys. Rev.', vol. 20, p. 633 (1922).

† 'Nature,' vol. 120, p. 838 (1927).

‡ 'Nature,' vol. 131, p. 688 (1933).

equally strong isotopes 107 and 109. Excellent results were obtained with fused silver chloride in the anode paste. Photometry gave 52·5 and 47·5 for the most probable percentages corresponding to a mean mass number 107·95. This corrected for probable packing fraction and change of scale gives

$$\text{atomic weight of silver} = 107\cdot87 \pm 0\cdot02$$

in excellent agreement with the exceptionally well-established chemical value 107·880.

(6) *Carbon*—Much interest has been recently attached to the atomic weight of carbon; the values obtained by chemical methods and by density determinations varying from 12·00, the present International value, to 12·01 or even more. The isotopic weight of the main constituent 12 is known with great certainty, so that to check the atomic weight by purely physical means only the percentage abundance of the rare isotope 13 is needed. For this the figures so far obtained have varied over wide limits. The original estimate by the discoverers was 1 in 400; but 1% or more has been suggested in more recent publications. The direct method of mass spectrum photometry cannot be applied to this problem in the case of the first order lines of carbon owing to the presence of compounds; but the second order lines of the element 6 and 6·5\* are very unlikely to be contaminated in this way, so that direct comparison of the intensities of these should give the abundance required.

For this purpose the anode ray generator was replaced by an ordinary discharge bulb, wide slits being retained in the collimator. Carbon monoxide was used in the discharge, which was maintained as constant as possible, the object being to vary the length of the exposure so as to obtain roughly equal intensity. With alternating exposures of 15 minutes for line 6·5 against 5 seconds for line 6, consistent results were obtained; but, unfortunately, three corrections due to the position of the lines on the plate, the different photographic efficiency of the two particles and a background effect were all large and uncertain. When these had been estimated and applied the most probable value ratio of abundance worked out at  $140 \pm 14$ . Allowing for a packing fraction of 3·0 and correcting for change of scale we get

$$\text{atomic weight of carbon} = 12\cdot0080 \pm 0\cdot0005.$$

\* It is of interest to note that this line was observed very early in the work on mass spectra and noted as a "line of unknown origin" (Aston, 'Phil. Mag.', vol. 40, p. 632 (1920)).

This value lies between two of the latest obtained from density determinations 12·011 by Woodhead and Whytlaw-Gray\* and 12·0065 by Moles and Salazar.†

(28) *Nickel*—The improved means of detecting faint isotopes warranted a further examination of this element in which only two mass numbers 58 and 60 had been previously detected. As before the carbonyl was used. The liquid was cooled to  $-20^{\circ}\text{C}$  and the pure vapour allowed to pass continuously into the discharge tube. Several new lines were detected of which 61 and 62 are new isotopes with reasonable certainty. Lines at 56 and 64 showed a steady decrease in intensity as the experiments proceeded, indicating that they were largely, if not entirely, due to adventitious compounds. They never quite disappeared so the existence of these isotopes is not excluded; but the abundance of neither can be so high as 1%. Photometry of the nickel group gave the following figures:—

Mass numbers	.....	58	60	61	62
% abundance	.....	67·5	27·0	1·7	3·8

These give a mean mass number 58·74. The packing fraction of Ni 58 is  $-10$ , so that with correction to scale

$$\text{atomic weight of nickel} = 58\cdot68 \pm 0\cdot02,$$

virtually identical with the International value 58·69.

(48) *Cadmium*—The data on this element had been obtained before by anode rays but were dependent on a single mass spectrum. A complete failure, after many attempts, to obtain its mass rays by the discharge in cadmium methyl was reported a few years ago.‡ After the experiments with calcium it was clear that the useful life of the anode ray setting, after a record yield of results, was near its end. It was considered this might be most advantageously employed in repeating the original analysis of cadmium. The fluoride was used as before, but this time the discharge failed to give any sign of cadmium lines and only resulted in forming so much deposit on the walls of the discharge tube that further work with it became impossible. The ordinary gas discharge was now reinstated and, after this had produced good results with carbon and nickel, cadmium methyl was again tried, though with little hope of success. The same

\* 'J. Chem. Soc.', p. 846 (1933).

† 'Ann. Soc. esp. Fis. Quim.', vol. 32, p. 954 (1934).

‡ Aston, 'Proc. Roy. Soc.', A, vol. 130, p. 302 (1931).



small sample of the liquid was used as in the previous abortive investigation; but now faint lines in the expected place were soon seen and, as the experiments progressed, the discharge settled down to give fairly good spectra. The failure of the methyls to give metallic ions, particularly at the first trial, has been the subject of much conjecture, and at one time it was supposed that the presence of mercury might be the deciding factor. The new results suggest that even when considered pure in the chemical sense the methyls are apt to contain traces of some unknown volatile compound, probably organic, which has a disturbing effect on the discharge suppressing the formation of the metallic ions. As the sample is used this "poison" ultimately disappears by fractionation and the residue of the methyl behaves satisfactorily. This explanation covers all the known effects observed for zinc, cadmium and various lead methyls. As was hoped, the new spectra revealed three more isotopes, 106, 108, 115, and enabled photometric estimates of the constitution of this very complex element to be made as follows:—

Mass numbers ..	106	108	110	111	112
% abundance ....	1.5	1.0	15.2	15.2	21.8
Mass numbers ..	113	114	115	116	
% abundance....	14.9	23.7	0.8	5.9	

These figures give cadmium the very high isotopic moment of 1.47 and a mean mass number 112.30. Applying the usual corrections

$$\text{atomic weight of cadmium} = 112.2 \pm 0.1,$$

suggesting that the present value 112.41 may be too high; but owing to the somewhat unsatisfactory conditions under which the abundances were measured the difference is not of great significance.

(26) *Iron*—For the further examination of this element a particularly pure sample of the carbonyl had been kindly prepared by Dr. v. Grosse. In addition to the strong isotope 56 and a weak one, 54, previously known, a third, 57 was revealed. Line 58 was present but weakened as the work proceeded and was most probably due to traces of nickel still left in the tube. The best values obtained for the relative abundance were:—

Mass numbers .....	54	56	57
% abundance .....	6.5	90.7	2.8

giving a mean mass number 55.90. The packing fraction of iron has

not yet been measured but is probably  $-10$ . Correcting for this and change of scale

$$\text{atomic weight of iron} = 55.84 \pm 0.02,$$

a value identical with the present International one.

(49) *Indium*—The first mass spectra of this element obtained by anode rays, showed only one line 115, but were too faint to exclude the possible presence of a lighter constituent suggested by the chemical atomic weight. During the work on the rare earths the discovery of a rare isotope 113 was announced by Wehrli,\* who deduced its presence from optical spectra and estimated its abundance as one-fourteenth of the main constituent.

An attempt was made, after the work on calcium, to obtain indium rays of sufficient strength to confirm this by introducing indium fluoride into the anode, but, contrary to expectations, this was completely unsuccessful. Recently, however, the preparation of indium trimethyl† held out possibilities of treatment by the more powerful and convenient gas discharge. Through the kindness of Professor L. M. Dennis, a small quantity of this crystalline solid was made available. Beyond the fact that it has a vapour pressure of about 3 mm at ordinary temperature and is therefore sufficiently volatile for the purpose in view, the compound has little to recommend it, for it is spontaneously and explosively inflammable on exposure to air at room temperature. This objection was overcome by manipulating it at the temperature of liquid nitrogen during the short period during which such exposure was unavoidable. As its vapour pressure is much lower than that of most of the compounds previously used, it was necessary to improvise a suitably coarse leak for its flow into the discharge tube by means of a capillary stopcock. The first trials were by no means hopeful and only resulted in deposition of metallic indium on the walls which upset the discharge. After washing this off and resetting the apparatus the main line 115 appeared, and ultimately, by means of long exposures, line 113 was definitely confirmed. The discharge was troublesome and very unsteady so that it was impossible to measure its abundance with accuracy. The final estimate of  $4.5 \pm 1\%$ , which is less than that of Wehrli, gives a mean mass number 114.91, which with the usual corrections gives

$$\text{atomic weight of indium} = 114.80 \pm 0.05.$$

This appears to support the older value for the chemical atomic weight

\* 'Naturw.', vol. 22, p. 289 (1934); 'Helv. Phys. Acta.', vol. 7, p. 611 (1934).

† Dennis, Work and Rochow, 'J. Amer. Chem. Soc.', vol. 56, p. 1047 (1934).

114·8 rather than the new International value 114·76; but since the packing fraction is unknown the discrepancy is not serious.

#### EXPERIMENTS WITH NEGATIVE RESULTS

In addition to those giving results of definite value many experiments were made which failed in this respect. Thus iridium, palladium, and gold introduced into the anode paste, either as finely divided metals or in compounds, gave no detectable effects. Even more surprising it was found impossible to repeat the analysis of copper although the identical salts used before were available. After the measurement of the abundance of C 13 an attempt was made to do the same with the corresponding rare isotope of nitrogen N15. The second order line 7·5 could just be detected, but was so faint in comparison with the background that no useful measurement was possible. The only conclusion to be drawn was that this rare isotope is much less abundant than that of carbon.

Owing to the great theoretical interest in the possibility of isomeric isotopes discussed at the recent congress on nuclear physics, many efforts were made to confirm the existence of Pb 210. A line ascribed to this had been detected and estimated at 0·08% in ordinary lead,\* but only in spectra of quite extraordinary intensity. The same discharge tube was set up, but it was found impracticable to get intensities of the same order, and after much time had been expended the experiments had to be abandoned without any further data being obtained.

A final attack was made on palladium by the use of the compound "Dichloro-*bis* (tri-*n* amyl phosphine) palladium," first prepared by Dr. F. G. Mann, who kindly supplied a very pure sample. This crystalline solid was introduced into the discharge tube and proved volatile enough to maintain the discharge; but even with long exposures and the most sensitive plates no trace of lines attributable to palladium could be detected. A similar compound of gold from the same laboratory was also tried with equally disappointing results.

#### CONCLUDING SURVEY

Since a previous survey of "elements yet to be analysed" was made 10 years ago† great progress has been made. In all some 247 stable isotopes have been detected and, of the ordinary elements, only four, palladium, iridium, platinum and gold, remain devoid of any mass spectrum data. The chemical properties of these recalcitrant elements

\* Aston, 'Proc. Roy. Soc.,' A, vol. 140, p. 535 (1933).

† Aston, 'Phil. Mag.,' vol. 49, p. 1200 (1925).

seem particularly unfavourable, and it is not easy to see at present how these difficulties are to be overcome. One of the most astonishing facts disclosed in the work is that stable elementary atoms are found for practically every natural number up to 210. In many cases they are doubly, and in three—96, 124, 203—triply filled with isobares. Of numbers not filled there is no evidence yet of a stable atom of mass 5. Recent disintegration experiments show that Be 8 must be capable of existence though its stability is not certain. Palladium will doubtless supply 105 and iridium and platinum the other four, 191, 193, 194, 195.

The method, worked out in 1929, of determining atomic weights by the photometry of mass spectra has now been applied to the large majority of elements. The agreement with accepted chemical values is very satisfactory on the whole, though a fair number of serious discrepancies has appeared. In connection with these it may be noted in support of the intrinsic reliability of the method that with every one of the six elements, Kr, Xe, Se, Cs, Nb,\* Ta,\* in which revision by ordinary methods has since been undertaken, the mass spectrum values have been confirmed.

In conclusion, the author desires to express his most cordial thanks to the chemists mentioned who prepared and supplied material otherwise unavailable and to Dr. Olaf Bloch of the Ilford Company for his generous co-operation in connection with research on the plates used.

#### SUMMARY

The mass spectrum analyses of 13 elements are described, some by the use of the very favourable setting of an anode ray generator already used for the rare earths, others by the ordinary discharge with improved technique.

In the course of the experiments some 20 new isotopes were discovered, those of hafnium, thorium, and rhodium being detected for the first time.

With cadmium success was attained in an unexpected manner and gave interesting information on the peculiar behaviour of the discharge in methyl compounds.

The values of the chemical atomic weights calculated from photometric measurements are in general in good accord with the International ones.

The general situation with regard to the discovery of isotopes and determination of atomic weights is briefly surveyed.

\* Aston, 'Nature,' vol. 130, p. 130 (1932).

---

## The Accurate Determination of the Energy Released in Certain Nuclear Transformations

By M. L. E. OLIPHANT, Messel Research Fellow of the Royal Society,  
A. R. KEMPTON, and Lord RUTHERFORD, O.M., F.R.S.

*(Received February 25, 1935)*

During the last few years, very definite information has been obtained on the various modes of transformation of certain elements, particularly of lithium, when bombarded by protons and heavy hydrogen. The nature of these transformations has received strong confirmation by examining the effects produced when each of the isotopes of lithium of mass 6 and 7 is separately bombarded. Sufficient quantity of these two isotopes—of the order of a microgram—has been obtained to settle the groups of liberated particles to be ascribed to each isotope under the two types of bombardment.\* In the pioneer experiments on these transformations, the range in air of the emitted  $\alpha$ -particles or protons was approximately determined by finding the thickness of mica required to stop the particles. In general, no special precautions were taken to measure the ranges in air with accuracy. The counting chamber and the first valve of the linear amplifier were usually mounted on rubber sponge to avoid disturbances due to vibration, so that the position of the counting chamber relative to the source was difficult to fix with certainty. In addition, even in the most favourable cases, the range of the particles is difficult to measure with the same accuracy as the range of a group of  $\alpha$ -particles emitted from a clean radioactive source. Apart from the probability variations dependent on the number of particles counted, the intensity of the bombarding source is liable to vary capriciously during the time required for a complete experiment. Moreover, the straggling of the particles is more pronounced than in the usual radioactive case, partly on account of the difficulty of preserving a smooth radiating surface under intense bombardment, and partly also on account of the sensible depth of penetration of the bombarding ions. The actual stopping power of mica relative to air for the fast particles is not known with the certainty desired, introducing a serious difficulty in accurate measurements.

\* Oliphant, Shire and Crowther, 'Proc. Roy. Soc.,' A, vol. 146, p. 922 (1934).

In order to test whether the conservation of energy holds in these transformations, it is necessary to know the energy of the emitted particles with considerable precision. With this information, we are able to deduce the relative mass numbers of the isotopes involved, and thus obtain a check on the values obtained by direct measurements with various types of mass spectrograph. When there is clear evidence of the mechanism of transformation, the measurement of the energy changes allows us to deduce with considerable certainty the masses of new isotopes which in some cases are produced during transformations.

#### THE METHOD OF DETERMINING THE RANGES OF GROUPS OF PARTICLES

In order to measure ranges with certainty, it is essential to use narrow beams of particles and to absorb the particles as far as possible by their passage through air and not through mica. For this purpose, we arranged that the rays under examination passed through a brass tube 12 cm long and 2 cm in diameter, closed at each end by mica screens, each of stopping power about 1.06 cm of air. One end of this tube was fixed rigidly to the bombarding chamber, while the counter was fixed permanently at the far end of the tube. The absorption of the rays was examined by altering the pressure of dry air in the chamber. When a complete absorption curve of the particles had been obtained from a photographic record of the particles in the usual way, the target was removed and a clean source of  $\text{Th}(\text{C} + \text{C}')$  substituted, and the absorption curve of these particles was determined under the same conditions as before. In this way the maximum range of the particles in the two cases can be directly compared. Since the maximum range of the  $\text{Th}(\text{C} + \text{C}')$  particles is known with accuracy, no sensible correction is required for the stopping power of the mica screens at the two ends of the tube, which is the same in both experiments.

In illustration of this method, fig. 1 gives the absorption curves obtained for the  $\alpha$ -particles arising from  $\text{Li}^7$  bombarded by protons (curve A), and the corresponding curve B for the  $\alpha$ -particles from the thorium source of range about 8.6 cm. It is seen that not only is the range of the  $\alpha$ -particles from lithium sensibly shorter than from  $\text{ThC}'$ , but the straggling, shown by the slope of the absorption curve, is much greater. This, as already pointed out, is mainly due to imperfections of the surface of the lithium target, and also in part to the depth of penetration of the target by the bombarding protons. If the linear slopes of the curves are continued to cut the axis of the abscissæ, it is seen that the difference between the

extrapolated ranges is 2.2 mm. For a perfect target and zero bombarding potential it can be deduced from these data that the disintegration particles possess a mean range of  $8.29 \pm 0.03$  cm. In deriving this range from the observed extrapolated range of 8.40 cm relative to the ThC' particles, corrections have to be applied for temperature and for barometric height, but as the difference between the known ThC' range and

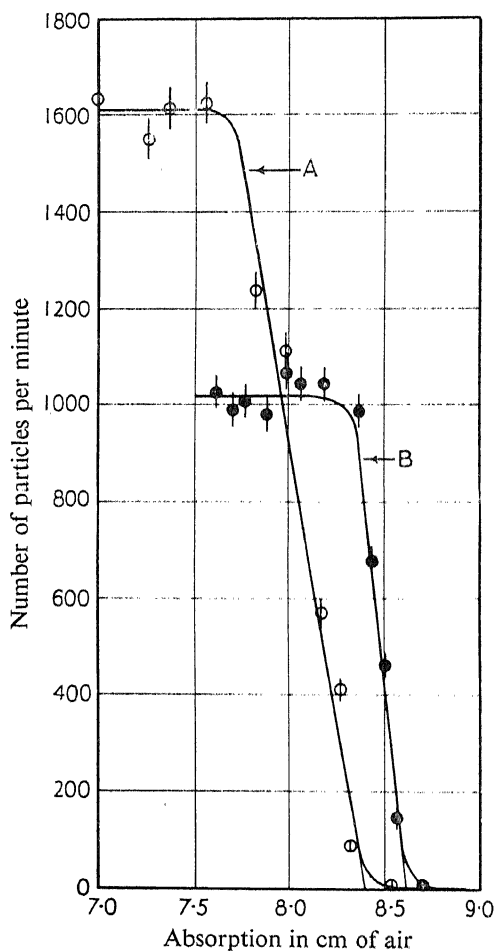
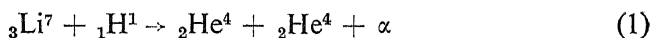


FIG. 1

the lithium range is so small, these corrections are negligible. A more important correction is that for bombarding potential. The energy of the bombarding protons must appear as part of the energy of the disintegration particles, and it is possible to calculate the correction required to transform the observed range to that for zero bombarding energy by application of the laws of the conservation of energy and

momentum. Fortunately the fact that observations are made exclusively at right angles to the bombarding beam simplifies such considerations for then the whole of the forward momentum of the bombarding particle must be carried by the other product or products of the transformation.

We believe that the  $\alpha$ -particles under consideration arise from the nuclear transformation



where  $\alpha$  is the energy released in the transformation. If the particles observed leave the target at right angles to the path of the bombarding beam, the opposing group will be expelled at such an angle with the beam that momentum and energy are conserved. If  $M_1$  and  $E_1$  are the mass and energy of the bombarding particle, and  $M_2, M_3, E_2, E_3$  the masses and energies of the products of the transformation, and if  $M_3$  is observed at right angles to  $M_1$ , then

$$E_3 = \left[ E + E_1 \left( 1 - \frac{M_1}{M_2} \right) \right] / \left( 1 + \frac{M_3}{M_2} \right), \quad (2)$$

where  $E$  is the energy released in the transformation. In the present case, it is seen that the fraction of the bombarding energy appearing in the energy of the observed particles is  $3/8$ .

The range of  $8.29 \pm 0.03$  cm under standard conditions, which we have found for the  $\alpha$ -particles resulting from the bombardment of  $\text{Li}^7$  by protons, corresponds with an energy of  $8.53 \pm 0.03 \times 10^6$  e-volts. The relation between energy and range used to obtain this value is a curve which has been drawn from all the empirical data of Rutherford and his collaborators,\* the short range portion being derived from the data of Mano,† Briggs‡ and Blackett,§ and the curve extrapolated to ranges greater than 12 cm by use of a formula given by Duncanson.|| The total energy  $\alpha$  released in the reaction is thus  $17.06 \pm 0.06 \times 10^6$  e-volts. The mass of  $\text{Li}^7$  calculated from equation (1) by substitution of the masses of  $\text{He}^4$  and of the proton given by Aston is then  $7.0148 \pm 0.0002$ . This agrees remarkably well with the measurement of Bainbridge¶ who gives for  $\text{Li}^7$  a mass of  $7.0146 \pm 0.0006$ . It is therefore clear that energy, in the wider relativistic sense, is strictly conserved in the reaction,

\* Rutherford and others, 'Proc. Roy. Soc.,' A, vol. 139, p. 617 (1933).

† 'Ann. Physique,' vol. 11, p. 407 (1934).

‡ 'Proc. Roy. Soc.,' A, vol. 114, p. 341 (1927).

§ 'Proc. Roy. Soc.,' A, vol. 134, p. 658 (1931).

|| 'Proc. Camb. Phil. Soc.,' vol. 30, p. 102 (1934).

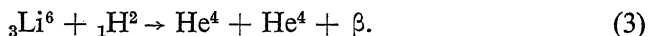
¶ 'Phys. Rev.,' vol. 44, p. 56 (1933).



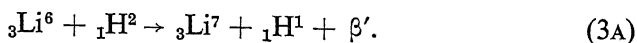
or alternatively that the mass determination of Bainbridge is well within the limits of error given by him.

#### BOMBARDMENT OF $\text{Li}^6$ BY HEAVY HYDROGEN

The transformation of  $\text{Li}^6$  by bombardment with heavy hydrogen\* is in many respects similar to that of  $\text{Li}^7$  by protons



It is found that the range of the  $\alpha$ -particles emitted at right angles to the bombarding beam is  $12.70 \pm 0.05$  cm under standard conditions at a bombarding potential of 190 kv. In this case the corrections for temperature and pressure are appreciable, as the difference between the standard range of 8.62 cm and the observed range is about 4 cm. Here the  $\alpha$ -particles observed carry  $\frac{1}{4}$  of the energy of the bombarding  $\text{H}^2$  particles, and  $\beta$  becomes  $22.06 \pm 0.07 \times 10^6$  e-volts. The mass of  $\text{Li}^6$  can be shown to be  $6.0143 \pm 0.0002$  if the mass of  $\text{H}^2$  is assumed to be  $2.01363 \pm 0.00007$  as found by Bainbridge.† The mass of  $\text{Li}^6$  according to Bainbridge is  $6.0145 \pm 0.0003$ , so that the present measurements afford convincing proof of the correctness of his values of the masses of both  $\text{Li}^6$  and  $\text{H}^2$ . It is worth noticing here that the difference between the masses of the isotopes of lithium given by Bainbridge is in accord with an observation of Cockcroft and Walton.‡ They observed the emission of a group of protons of range  $30.5 \pm 1.0$  cm when lithium was bombarded with heavy hydrogen ions at a potential of 500,000 volts. The nuclear transformation was assumed to be



The proton, observed at right angles to the bombarding beam, carried  $\frac{5}{8}$  of the bombarding energy, and making the appropriate correction for the straggling of the range, we find that  $\beta'$  is  $5.0 \pm 0.05 \times 10^6$  e-volts. The energy calculated by substituting Bainbridge's masses is  $5.3 \pm 0.08 \times 10^6$  e-volts, while that calculated from the masses which we have obtained from transformations (1) and (3) is  $5.1 \pm 0.1 \times 10^6$  e-volts. The range of the protons was measured by absorption in mica,§ and in addition it is by no means certain that Duncanson's curve gives

\* Oliphant, Shire and Crowther, *loc. cit.*

† 'Phys. Rev.', vol. 44, p. 57 (1933).

‡ 'Proc. Roy. Soc., A', vol. 144, p. 704 (1934).

§ Cf. Mano, 'J. Phys.', vol. 5, p. 628 (1934).

the correct ranges for high energy protons. The agreement must therefore be regarded as very satisfactory.

#### BOMBARDMENT OF HEAVY HYDROGEN BY HEAVY HYDROGEN

We were able to show\* that when the isotope of hydrogen of mass 2 was used as both projectile and target, protons and  $\text{H}^3$  particles were emitted, the nuclear transformation concerned being

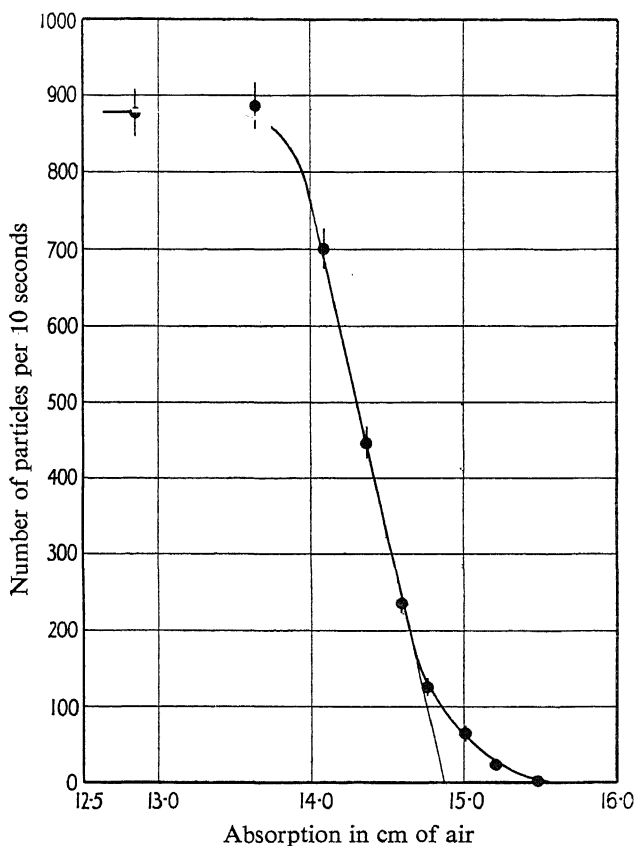


FIG. 2

Measurement of the range of the protons led to an energy release  $\gamma$  of  $4 \times 10^6$  e-volts, and a mass for  $\text{H}^3$  of 3.0151. We have now measured the range of the protons with greater precision by the method of comparison with  $\text{ThC}'$   $\alpha$ -particles. Fig. 2 shows the curve which has been obtained. It is seen that the apparent extrapolated number-range is

\* Oliphant, Harteck and Rutherford, 'Proc. Roy. Soc.,' A, vol. 144, p. 692 (1934).

$14.87 \pm 0.05$  cm at 200 kv. When this is corrected for temperature and pressure the extrapolated range under standard conditions becomes  $14.70 \pm 0.05$  cm. The question now arises as to what energy this represents. The energy-range curve for protons used by us is one calculated by Duncanson (*loc. cit.*) from the empirical  $\alpha$ -particle curve, and gives mean ranges. In order to transform from our observed extrapolated range to the actual mean range we must know something of the straggling of protons of this energy.

The straggling of a group of homogeneous particles is the result of fluctuations in the number of inelastic collisions made by the particles in their passage through matter. It is known that the inelastic collisions made by a swift  $\alpha$ -particle and proton of the same velocity are similar in type, but are four times more numerous for the  $\alpha$ -particle than the proton. As a consequence the range of a swift  $\alpha$ -particle is nearly the same as for a proton of equal speed, the slightly greater range of the  $\alpha$ -particle resulting from the reduction of its average charge near the end of its range. Neglecting this small correction, it can be shown from simple considerations or from calculations based on the general theory of straggling given by Bohr,\* that the straggling of a group of homogeneous protons is twice that of a group of  $\alpha$ -particles of the same initial speed, *i.e.*, of the same range. The straggling of the observed groups of protons of extrapolated range 14.7 cm should thus be twice that of a group of  $\alpha$ -particles of equal range. The magnitude of the straggling of  $\alpha$ -particles of this range can be deduced from the measured straggling of  $\alpha$ -particles of known range by extrapolation, using Bohr's theory. In this way it is found that the straggling of  $\alpha$ -particles of 14.7 cm range is such that the difference between the extrapolated and mean ranges is 1.8 mm. The corresponding difference for the group of protons should be twice this amount, *i.e.*, 3.6 mm. Applying this result to the observed range, and remembering that according to equation (2) the proton carries  $\frac{1}{4}$  of the energy of the bombarding particle, we find

$$\gamma = 4/3 (2.98 \pm 0.01 \times 10^6 \text{ e-volts}) = 3.97 \pm 0.02 \times 10^6 \text{ e-volts.}$$

The mass of  $\text{H}^3$ , in terms of Bainbridge's mass of  $\text{H}^2$  and of Aston's mass of  $\text{H}^1$ , is then  $3.0152 \pm 0.0002$ .

#### TRANSFORMATIONS IN WHICH THREE PARTICLES ARE LIBERATED

So far we have dealt with transformations in which two particles are expelled in nearly opposite directions. In the types of transformation

\* 'Phil. Mag.', vol. 30, p. 531 (1915).

in which three particles may be emitted as the result of a single explosion, *e.g.*, in the reactions  $\text{Li}^7 + \text{H}^2$ ,  $\text{B}^{11} + \text{H}^1$ , there is much more difficulty in interpretation and in deducing with accuracy the energy released as the result of the transformation. In these cases, the particles do not show in general any well-marked range, but are expelled with widely different speeds. The end of the range corresponding to the swiftest particles can usually be fixed with some certainty, but it is not easy to be sure of the angular distribution of the particles which give rise to this maximum range. In the absence of any detailed information of the mechanism of these atomic explosions, it is natural to assume that all angular distributions are possible which are consistent with the conservation of momentum and energy in the reaction. It may happen, however, that the angular distribution of particles, which should theoretically give the maximum range, has a very low or even zero probability. A study of the tracks of particles due to individual explosions by means of the cloud-chamber should give us more definite information on a number of these points.

In all types of reaction it is essential to examine whether energy is emitted in the form of  $\gamma$ -rays. This in general is not easy unless the  $\gamma$ -rays are of a penetrating type, for the bombardment of the target always gives rise to a fairly strong X-radiation of a softer kind, while X-rays produced by the secondary electrons in the main accelerating tube possess a penetrating power which varies widely with the potentials applied.

#### THE TRANSFORMATION OF $\text{Li}^7$ BY $\text{H}^2$ PARTICLES

When  $\text{Li}^7$  is bombarded by heavy hydrogen, both  $\alpha$ -particles and neutrons are produced.\* The  $\alpha$ -particles are very heterogeneous, having all ranges up to about 7.8 cm in air. An absorption curve obtained with the air absorption chamber is given in fig. 3. The form of the end of the group was obtained by using a target of  $\text{Li}^7$  free from  $\text{Li}^6$  in a separate experiment, and the two curves were fitted at 6.0 cm.

It is seen that over the greater part of its length the number-range relation is very accurately linear, a peculiarity which is borne out by the differential curve shown in the figure, obtained by counting only those deflections of the oscillograph greater than 1 cm. The end of the group straggles out to between 7.6 and 7.8 cm. More careful experiments with thicker targets of  $\text{Li}^7$  or with a differential counting chamber will be necessary to determine the end of this group with precision.

\* Oliphant, Shire and Crowther, *loc. cit.*

We have already pointed out that for various reasons the  $\alpha$ -particles emitted suffer considerable straggling. This is most easily seen with a pure range such as that of the 8.4 cm particles in fig. 1, where the "straight" dropping portion of the curve extends over about 6 mm as compared with about 2 mm for the particles from an absolutely clean source of ThC'. It is evident that particles, which in the absence of straggling would all

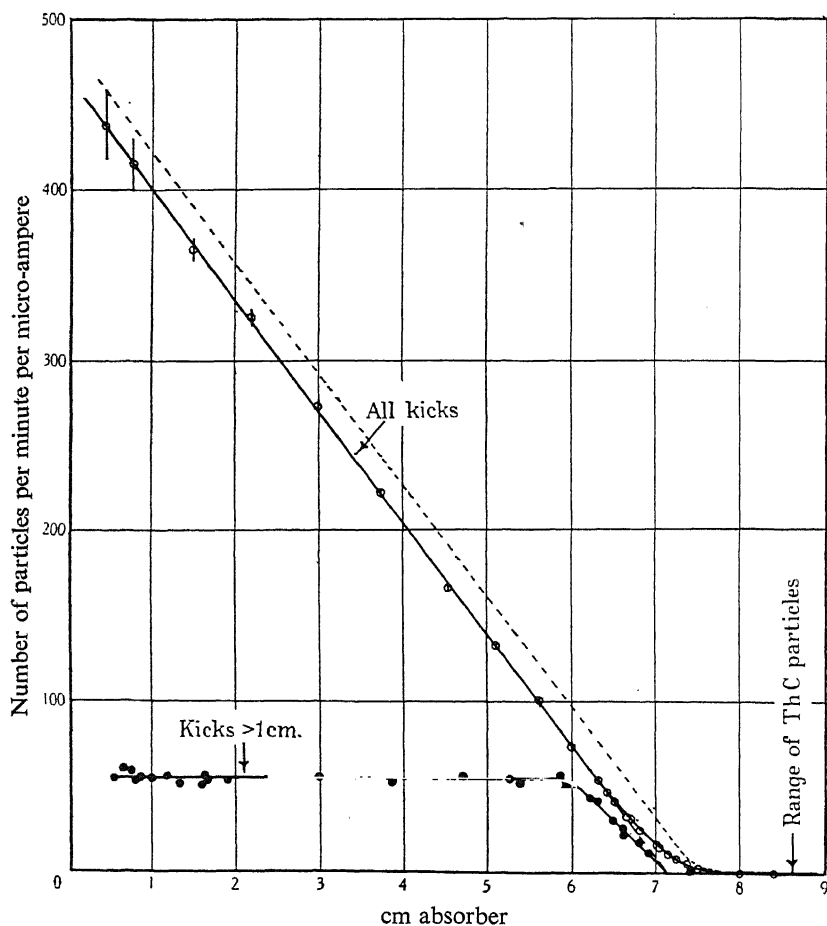
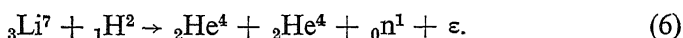


FIG. 3

possess the same range, begin to fail to be counted under the conditions of the experiment some 6 mm from the real end of the extrapolated range. In a distributed group of particles as in fig. 3, it is then clear that the actual range-number curve will lie to the right of the observed curve except at the end, where the two curves must coalesce. If all the particles failed to be counted 6 mm from the end of the range the curve

would be displaced 6 mm to the right. However, it is evident that as the straggling is roughly linear the real curve will, in fact, be displaced about half that distance. A curve corrected in this way is dotted in the figure.

The bombardment of  $\text{Li}^7$  with heavy hydrogen gives rise to a copious emission of neutrons. Observation of the magnitude of the ionization produced by recoil nuclei in pure helium at a pressure of 8 atmospheres, leads to the conclusion that neutrons are present with energies at least as high as  $6 \times 10^6$  e-volts, but the actual maximum energy and the distribution of energy among them have not yet been determined. We assume that the neutrons and  $\alpha$ -particles arise from the same reaction:



The distribution of energy among the particles will be determined by unknown conditions operative during the actual disruption, and it is possible to satisfy the conservation of energy and momentum in an infinite number of ways. An  $\alpha$ -particle with the greatest possible energy, corresponding with the end part of the tail of the absorption curve in fig. 3, may be produced when a single  $\alpha$ -particle escapes opposite an  $\alpha$ -particle and neutron moving together parallel to one another. The absorption curve suggests that this is a rare event, but assuming this case, the  $\alpha$ -particles of maximum energy will possess  $\frac{8}{9}$  of the total energy  $\epsilon$ , whence we find

$$\epsilon \geq 14.60 \pm 0.25 \times 10^6 \text{ e-volts.}$$

The value calculated from equation (6) using the data of Aston and Bainbridge for  $\text{H}^2$  and  $\text{He}^4$ , and with the mass of the neutron given by Chadwick and Goldhaber,\* is

$$\epsilon = 14.9 \pm 0.8 \times 10^6 \text{ e-volts.}$$

The agreement is satisfactory.

#### CONCLUSION

The data which we have presented afford strong evidence of the validity of the laws of conservation of mass-energy, and of momentum, in some atomic transmutations in which  $\text{H}^1$ ,  $\text{H}^2$ ,  $\text{H}^3$ ,  $\text{He}^4$ ,  $\text{Li}^6$ ,  $\text{Li}^7$  and the neutron are involved, and at the same time give very convincing support to the mass measurements of Aston and of Bainbridge. It should be emphasized, however, that these elements form a group in which the masses have been measured against one another, and are only referred

\* 'Nature,' vol. 134, p. 237 (1934).

to oxygen, the standard of mass, through the  $\text{He}^4\text{—O}^{16}$  ratio of Aston. Any change which may be made in this ratio will leave the mass differences unaltered except for a second order correction. It will be shown in a later paper that with beryllium and boron, there occur serious discrepancies between the energies observed in some transformations and the energies calculated from mass data. For the present we must conclude that the mass differences between hydrogen, helium and lithium are given correctly by the mass data available.

One of us (A. R. K.) is indebted to the Department of Scientific and Industrial Research for a grant. We have to thank Mr. C. H. Westcott and Mr. G. R. Crowe for help with some of these experiments.

#### SUMMARY

Experiments have been made to determine accurately the ranges and energies of the swift particles emitted in certain transformations. It is found that when changes of mass are taken into account the law of conservation of energy holds closely for the transformations of the isotopes of lithium when bombarded by ions of ordinary and of heavy hydrogen. The masses of  $\text{Li}^6$  and  $\text{Li}^7$  are found to be  $6.0143 \pm 0.0002$  and  $7.0148 \pm 0.0002$  respectively, in good agreement with the mass spectroscopic values  $6.0145 \pm 0.0003$  and  $7.0146 \pm 0.0006$  found by Bainbridge. By application of the laws of conservation of momentum and energy the mass of the hydrogen isotope of mass 3 is found to be  $3.0152 \pm 0.0002$ . Attention is drawn to the factors involved in determining the mean ranges of expelled particles and to the difficulties of interpretation when more than two particles are emitted in a single transformation.

---

# Ship Waves: The Relative Efficiency of Bow and Stern

By T. H. HAVELOCK, F.R.S.

(Received January 11, 1935)

1. It seems fairly certain that one of the main causes of differences between theoretical and experimental results is the neglect of fluid friction in the calculation of ship waves, and further that the influence of fluid friction may be regarded chiefly as one which makes the rear portion of the ship less effective in generating waves than the front portion. The process may be pictured, possibly, in terms of a friction belt or boundary layer whose more important effect is equivalent to smoothing the lines of the model towards the rear. Some calculations were made from this point of view in a previous paper,\* the purpose then being to show how such an asymmetry, fore and aft, reduced the magnitude of interference effects between bow and stern waves. We may also describe the frictional effect as a diminution in the effective relative velocity of the model and the surrounding water as we pass from bow to stern. This is not very satisfactory from a theoretical point of view; but, on the other hand, it leads to a comparatively simple modification of expressions for the waves produced by the model. From a formal point of view, we may regard the modification as an empirical introduction of a reducing factor to allow for decrease in efficiency of the elements of the ship's surface as we pass from bow to stern.

There are now available experimental results, for wave profiles as well as for wave resistance, which make it possible to attempt such a comparison. The following work is limited to a few simple cases, and the assumptions are made in as simple a form as possible for the purpose of the calculations; these deal with the wave profile and wave resistance of a model of symmetrical form, and also with the difference between motion bow first and motion stern first for a simple asymmetrical model.

2. Take the origin  $O$  in the undisturbed free surface of the water, with  $Ox$  horizontal and  $Oz$  vertically upwards; and let the origin  $O$  be moving with uniform velocity  $c$  in the direction  $Ox$ . We suppose that there is a given distribution of sources and sinks over the  $zx$ -plane, or, alternatively, that the normal fluid velocity is given over this plane; let it be  $F(h, f)$  at

\* 'Proc. Roy. Soc.,' A, vol. 110, p. 233 (1925).



the point  $(h, 0, -f)$ . Then the surface elevation  $\zeta$  due to this travelling distribution is given by

$$\zeta = -\frac{i}{2\pi^2 c} \int_{-\infty}^{\infty} \int_0^{\infty} F(h, f) dh df \int_{-\pi}^{\pi} \sec \theta d\theta \int_0^{\infty} \frac{\kappa e^{-\kappa f + i\kappa \varpi} d\kappa}{\kappa - \kappa_0 \sec^2 \theta + i\mu \sec \theta}, \quad (1)$$

where  $\varpi = (x - h) \cos \theta + y \sin \theta$ , and the limiting value is to be taken as the positive quantity  $\mu$  tends to zero.

If the form of the ship is given by  $y$  as a function of  $h$  and  $f$ , the usual approximation is to take  $F(h, f)$  as equal to  $c \partial y / \partial h$ . We modify this now by supposing that the effective value of  $c$  in this expression for  $F(h, f)$  diminishes from bow to stern; we introduce what may be called a reducing factor  $f(h)$ , so that we shall use in (1)

$$F(h, f) = cf(h) \frac{\partial y}{\partial h}. \quad (2)$$

We have assumed that the reducing factor is independent of the depth. It will, no doubt, depend upon the velocity and form of the model, and in particular upon the value of the Reynolds number; but, meantime, we shall neglect any such considerations. It may even be that, in certain circumstances, the factor should allow for an increase of apparent efficiency near the bow of the model. However, it appears from such experimental evidence as is available that the wave profile near the bow agrees fairly well, for simple models, with calculations made without any allowance for frictional effects; so that the chief effect of the latter appears to be a reduction in efficiency over the rear portion of the model. In view of these considerations, and also to lighten the numerical calculations, very simple expressions have been used in the following work. Calculations are made for two cases, and in both we assume the reducing factor to be constant and less than unity over the rear portion; in one case the factor is taken as constant and equal to unity over the front portion, while in the other, to avoid possible discontinuities, it is assumed to diminish uniformly from the bow to the value which it has for the rear portion.

We shall consider only models of great draught and of uniform horizontal section; for such, (1) and (2) give for the surface elevation

$$\zeta = -\frac{i}{2\pi^2} \int_{-\infty}^{\infty} f(h) \frac{\partial y}{\partial h} dh \int_{-\pi}^{\pi} \sec \theta d\theta \int_0^{\infty} \frac{e^{i\kappa \varpi} d\kappa}{\kappa - \kappa_0 \sec^2 \theta + i\mu \sec \theta}. \quad (3)$$

3. We consider a model of length  $2l$  and beam  $2b$ , and of symmetrical parabolic lines given by

$$y = b(1 - h^2/l^2). \quad (4)$$

The reduction factor  $f(h)$  is to mean a diminution of effective velocity from the value  $c$  at the bow to a smaller value  $\beta c$  at the stern. In order to allow the calculations to be made in terms of known functions, we shall suppose the diminution to take place uniformly over the front half of the model; thus we assume

$$\begin{aligned} f(h) &= \beta + (1 - \beta) h/l, & 0 < h < l \\ &= \beta, & -l < h < 0. \end{aligned} \quad (5)$$

Using (5) and (4) in (3) and carrying out the integration with respect to  $h$ , we obtain

$$\zeta = \frac{b}{\pi^2 l^3} \int_{-\pi}^{\pi} \sec^2 \theta \, d\theta \int_0^{\infty} \frac{A d\kappa}{\kappa^3 (\kappa - \kappa_0 \sec^2 \theta + i\mu \sec \theta)}, \quad (6)$$

where

$$\begin{aligned} A &= \{2(1 - \beta) \sec^2 \theta + (2 - \beta) i\kappa l \sec \theta - \kappa^2 l^2\} e^{i\kappa [(x-l) \cos \theta + y \sin \theta]} \\ &\quad - 2(1 - \beta) \sec^2 \theta e^{i\kappa (x \cos \theta + y \sin \theta)} \\ &\quad - (i\beta \kappa l \sec \theta + \beta \kappa^2 l^2) e^{i\kappa [(x+l) \cos \theta + y \sin \theta]}. \end{aligned} \quad (7)$$

This expression gives finite and continuous values for the surface elevation. It is convenient, for purposes of calculation, to separate it into finite and continuous expressions associated respectively with the bow ( $x = l$ ), amidships ( $x = 0$ ), and the stern ( $x = -l$ ). Further, for points on the central line  $y = 0$ , we can express these in terms of known functions.

Writing

$$G(q) = i \int_{-\pi}^{\pi} \sec \theta \, d\theta \int_0^{\infty} \frac{e^{i\kappa q \cos \theta} d\kappa}{\kappa - \kappa_0 \sec^2 \theta + i\mu \sec \theta}, \quad (8)$$

$$G_0(q) = \int_0^q G(q) \, dq, \quad G_1(q) = \int_0^q G_0(q) \, dq, \quad (9)$$

and so on, it can readily be shown that (6) gives, for the wave profile along  $y = 0$ ,

$$\begin{aligned} \zeta &= -\frac{b}{\pi^2 l^3} \{l^2 G_0(x-l) + (2 - \beta) l G_1(x-l) + 2(1 - \beta) G_2(x-l) \\ &\quad - 2(1 - \beta) G_2(x) + \beta l^2 G_0(x+l) - \beta l G_1(x+l)\}. \end{aligned} \quad (10)$$

In the limit, when we take  $\mu$  zero, we have\*

$$\begin{aligned} G(q) &= \pi^2 \{H_0(q) - Y_0(q)\}, & q > 0 \\ &= -\pi^2 \{H_0(-q) - Y_0(-q)\} - 4\pi^2 Y_0(-q), & q < 0 \end{aligned} \quad (11)$$

\* 'Proc. Roy. Soc.,' A, vol. 135, p. 5 (1932).

In the notation used in previous work, we have

$$\left. \begin{aligned} Q_0(u) &= \frac{\pi}{2} \int_0^u \{H_0(u) - Y_0(u)\} du, \\ Q_1(u) &= \int_0^u Q_0(u) du, \quad Q_2(u) = \int_0^u Q_1(u) du, \\ P_0(u) &= -\frac{\pi}{2} \int_0^u Y_0(u) du, \\ P_0^{-1}(u) &= \int_0^u P_0(u) du = 1 + P_1(u), \\ P_0^{-2}(u) &= \int_0^u P_0^{-1}(u) du = u + P_2(u). \end{aligned} \right\} \quad (12)$$

Summing up these results, we obtain finally for the wave profile

$$\begin{aligned} \zeta = -\frac{2b}{\pi} \left\{ \frac{1}{p} F_0(\kappa_0 q_1) + \frac{2-\beta}{p^2} F_1(\kappa_0 q_1) + \frac{2(1-\beta)}{p^3} F_2(\kappa_0 q_1) \right. \\ \left. - \frac{2(1-\beta)}{p^3} F_2(\kappa_0 q_2) + \frac{\beta}{p} F_0(\kappa_0 q_3) - \frac{\beta}{p^2} F_1(\kappa_0 q_3) \right\}, \end{aligned} \quad (13)$$

with  $\kappa_0 = g/c^2$ ,  $p = \kappa_0 l$ ,  $q_1 = x - l$ ,  $q_2 = x$ ,  $q_3 = x + l$ . Also we have

$$\left. \begin{aligned} F_0(u) &= Q_0(u), \quad u > 0 \\ &= Q_0(-u) - 4P_0(-u), \quad u < 0, \\ F_1(u) &= Q_1(u), \quad u > 0 \\ &= -Q_1(-u) + 4P_0^{-1}(-u), \quad u < 0, \\ F_2(u) &= Q_2(u), \quad u > 0 \\ &= Q_2(-u) - 4P_0^{-2}(-u), \quad u < 0. \end{aligned} \right\} \quad (14)$$

Using tables and graphs of the various P and Q functions, the wave profile can now be found, for any speed, for any assigned value of  $\beta$ . We have chosen the value  $\beta = 0.6$ , and calculations have been made for a sufficient number of values of  $x$  to give the wave profile for two different speeds; the speeds are those for which  $\kappa_0 l = 6$  and  $\kappa_0 l = 3$ , or for  $c/\sqrt{gl}$  equal to 0.408 and 0.577 respectively. The wave profile has also been calculated at these speeds for the value  $\beta = 1$ , that is for the usual theory without any allowance for frictional effects. The four curves are shown in fig. 1, the full curves being for  $\beta = 1$  and the dotted curves for  $\beta = 0.6$ .

These curves may be compared with some given recently by Wigley\* in a comparison of experimental and calculated wave profiles.

\* 'Proc. Roy. Soc.,' A, vol. 144, p. 144 (1934).

In fig. 2 of that paper, the full curves are calculated from the usual theory, that is, for  $\beta = 1$  in the notation of the present paper; while the dotted curves are observed values. It may be concluded that the value  $\beta = 0.6$  is of the right order of magnitude to bring the calculated values into better agreement with observed values, at least for medium values of  $c/\sqrt{(gl)}$ . It should be noted that Wigley's model is slightly different from that of the present calculation, in that it has a certain amount of parallel middle body inserted between the parabolic ends.

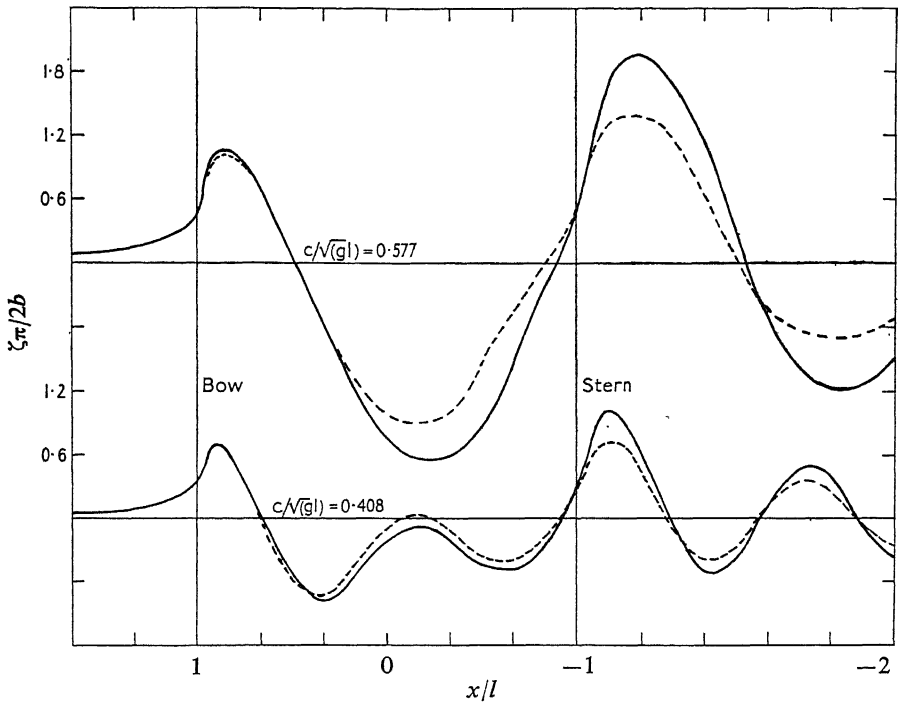


FIG. 1

For that, and other obvious reasons, it is not worth while attempting any closer comparison of the results meantime.

4. It is of interest to examine the corresponding change in the wave resistance for this model. It can easily be deduced from (6) that the wave pattern at a great distance to the rear of the model approximates to

$$\begin{aligned} \zeta = & -\frac{4b}{\pi p^3} \int_{-\pi/2}^{\pi/2} \{p^2 \sin(x-l, y) - (2-\beta)p \cos \theta \cos(x-l, y) \\ & - 2(1-\beta) \cos^2 \theta \sin(x-l, y) + 2(1-\beta) \cos^2 \theta \sin(x, y) \\ & + \beta p^2 \sin(x+l, y) + \beta p \cos \theta \cos(x+l, y)\} d\theta, \end{aligned} \quad (15)$$

where we have used the abbreviation

$$(q, y) = \kappa_0 \sec^2 \theta (q \cos \theta + y \sin \theta).$$

In (15) the wave pattern is analysed into simple constituents associated with the bow, amidships, and the stern; putting the expression into the form

$$\zeta = \int_0^{\pi/2} \{A_1 \sin(\kappa_0 x \sec \theta) + A_2 \cos(\kappa_0 x \sec \theta)\} \cos(\kappa_0 y \sin \theta \sec^2 \theta) d\theta, \quad (16)$$

the wave resistance is given by\*

$$R = \frac{1}{4} \rho c^2 \int_0^{\pi/2} (A_1^2 + A_2^2) \cos^3 \theta d\theta. \quad (17)$$

Carrying out the reduction we obtain

$$\begin{aligned} R = \frac{16\rho b^2 c^2}{\pi} & \left\{ \frac{2(1+\beta^2)}{3p^2} + \frac{16\beta^2}{15p^4} + \frac{128(1-\beta)^2}{35p^6} + \frac{2\beta}{p^2} P_3(2p) \right. \\ & + \frac{2\beta(\beta-3)}{p^3} P_4(2p) - \frac{2\beta(3\beta-4)}{p^4} P_5(2p) - \frac{4\beta(1-\beta)}{p^5} P_6(2p) \\ & \left. - \frac{4(1-\beta^2)}{p^4} P_5(p) + \frac{8(1-\beta)}{p^5} P_6(p) - \frac{8(1-\beta)^2}{p^6} P_7(p) \right\}. \quad (18) \end{aligned}$$

In terms of P functions which have been tabulated this becomes, for the particular case  $\beta = 0.6$ ,

$$\begin{aligned} R = \frac{16\rho b^2 c^2}{\pi} & \left\{ \frac{2.72}{3p^2} + \frac{0.384}{p^4} + \frac{20.48}{35p^6} + \left( \frac{1.2}{p^2} - \frac{0.32}{p^4} \right) P_3(2p) \right. \\ & - \left( \frac{2.88}{p^3} - \frac{0.8}{p^5} \right) P_4(2p) + \frac{2.32}{p^4} P_5(2p) + \frac{3.52}{7p^4} P_3(p) \\ & \left. - \frac{18.88}{7p^5} P_4(p) - \left( \frac{14.4}{7p^4} - \frac{7.68}{7p^6} \right) P_5(p) \right\}. \quad (19) \end{aligned}$$

This is to be compared with the value for the same model without any reducing factor, that is, with (18) when  $\beta = 1$ , or

$$R = \frac{16\rho b^2 c^2}{\pi} \left\{ \frac{4}{3p^2} + \frac{16}{15p^4} + \frac{2}{p^3} P_3(2p) - \frac{4}{p^3} P_4(2p) + \frac{2}{p^4} P_5(2p) \right\}. \quad (20)$$

The curves are given in fig. 2, and show the variation of  $R/c^2$  with the quantity  $c/\sqrt{gl}$ ; in addition to the smaller value of the resistance from (19) compared with (20), there is also a relative decrease in interference effects.

\* 'Proc. Roy. Soc.,' A, vol. 144, p. 519 (1934).

5. The wave resistance of a ship model in a frictionless liquid is the same whether it is moving bow first or stern first, even when the model is not symmetrical fore and aft. If, however, we introduce a reducing factor to represent the effect of fluid friction, it is clear that we shall obtain a difference between the two cases, and it is also easy to foresee the general character of the result. Suppose that the bow is finer than the stern, and assume that the reducing factor is the same whether going ahead or astern. Then it is obvious that the resistance will be less when going bow first than when going stern first; and further, that interference effects between bow and stern waves will be relatively more marked in the former case than in the latter.

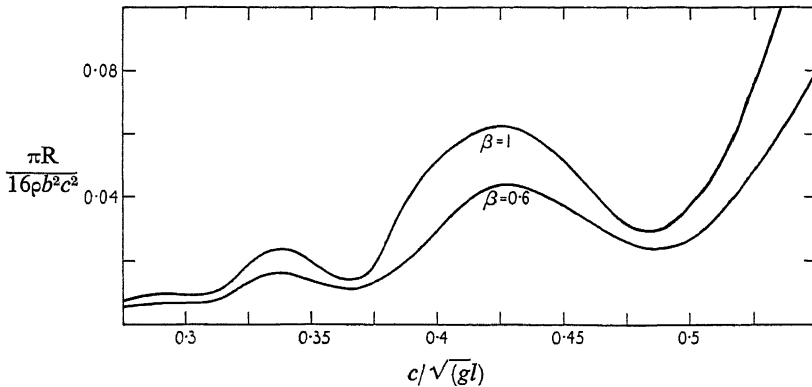


FIG. 2

We shall now work out a particular case, a model of great draught with parabolic ends and with some parallel middle body. The lines of the horizontal section are given by

$$\begin{aligned}
 y &= b(1 - h^2/l^2), & 0 < h < l \\
 &= b, & -\tfrac{1}{2}l < h < 0 \\
 &= -\frac{4b}{l^2}(h^2 + lh), & -l < h < -\tfrac{1}{2}l.
 \end{aligned} \tag{21}$$

In this model the change of gradient at the stern is twice that at the bow.

In order to simplify the calculations, we shall assume that the reducing factor is constant and equal to unity over the front half of the model, and has a constant value  $\beta$  over the rear half; there will be only a small difference between the results so obtained and those with a more natural form of reducing factor, because in any case the middle portion of this

model does not contribute much to the wave-making. We shall not examine the wave profile in this case. For the wave resistance we have

$$R = (4\rho/\pi) \int_0^{\pi/2} (A^2 + B^2) \cos \theta \, d\theta, \quad (22)$$

where

$$\begin{aligned} A - iB = & -\frac{4\beta bc}{l^2} \int_{-l}^{-l/2} (2h + l) e^{-i\kappa_0 h \sec \theta} \, dh \\ & - \frac{2bc}{l} \int_0^l h e^{-i\kappa_0 h \sec \theta} \, dh. \end{aligned} \quad (23)$$

This leads to the result

$$\begin{aligned} R = \frac{16\rho b^2 c^2}{\pi} & \left\{ \frac{2(1 + 4\beta^2)}{3p^2} + \frac{16(1 + 16\beta^2)}{15p^4} + \frac{4\beta}{p^2} P_3(2p) \right. \\ & - \frac{12\beta}{p^3} P_4(2p) + \frac{8\beta}{p^4} P_5(2p) + \frac{8\beta}{p^3} P_4\left(\frac{3}{2}p\right) - \frac{8\beta}{p^4} P_5\left(\frac{3}{2}p\right) \\ & - \frac{2(1 - 2\beta)}{p^3} P_4(p) + \frac{2(1 - 4\beta)}{p^4} P_5(p) - \frac{16\beta^2}{p^3} P_4\left(\frac{1}{2}p\right) \\ & \left. + \frac{8\beta(1 + 4\beta)}{p^4} P_5\left(\frac{1}{2}p\right) \right\}. \end{aligned} \quad (24)$$

This expression may be written as

$$R = R_0 + \beta R_1 + \beta^2 R_2. \quad (25)$$

The form (25), with  $\beta$  a positive quantity less than unity, applies to the model when going bow first. It is easily seen that the corresponding result for motion stern first, assuming the same reduction factor  $\beta$ , is

$$R = \beta^2 R_0 + \beta R_1 + R_2. \quad (26)$$

Numerical calculations have been made from these expressions for  $\beta = 0.6$ , and from these curves have been drawn showing the variation of  $R/c^2$  with speed, on a base of  $c/\sqrt{gl}$ ; these are given in fig. 3.

The curve A in fig. 3 is for motion bow first, the curve B for motion stern first. The curve C is for (24) with  $\beta = 1$ , that is, it is the resistance curve for motion in either direction when no allowance is made for frictional effects. There are few experimental data available for comparison; but in any case it should be noted that, apart from other simplifying assumptions, the preceding calculations are for a model of very great draught. However, reference should be made to some experimental curves given by Wigley;\* in fig. 3 of his paper there are three resistance

\* 'Trans. Inst. Nav. Arch.', vol. 72, p. 216 (1930).

curves which correspond to curves A, B and C of fig. 3 below, and the mutual relations of the three curves in the two cases have much in common.

6. In the preceding work, the reducing factor has been given specially simple forms in order that the calculations might be made in terms of functions which have already been tabulated. However, for the wave resistance of a model of ordinary form and draught, the calculations are usually made by numerical and graphical methods for the particular case; the introduction of a reducing factor of suitable form would not

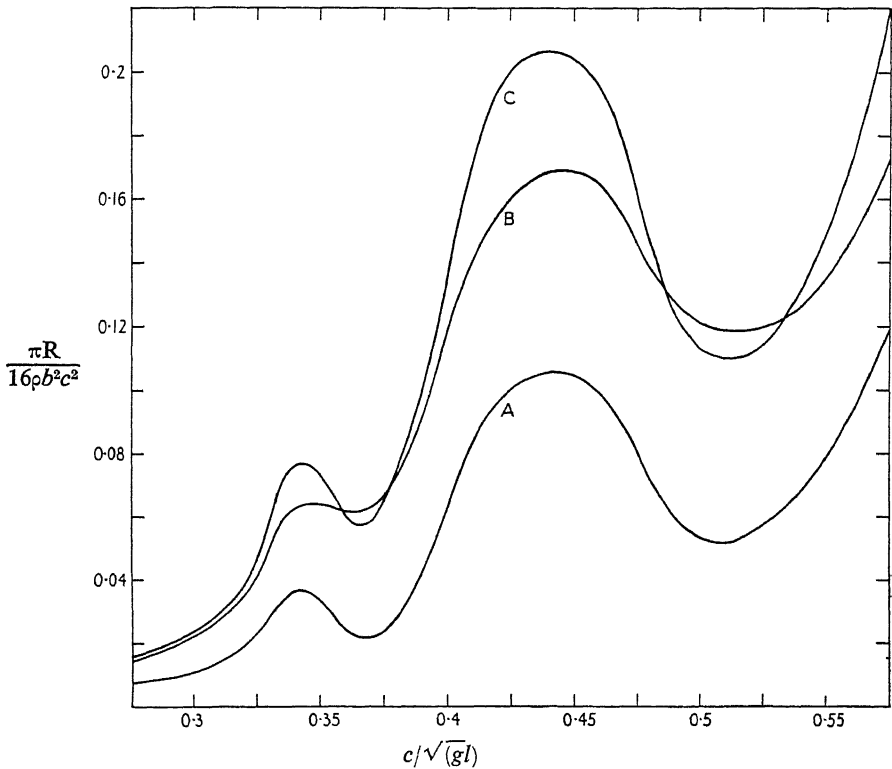


FIG. 3

add any great complication. The usefulness of such a factor would depend largely upon whether it proved to be sufficiently independent of speed and of variation of form of the model.

#### SUMMARY

The main effect of fluid friction in regard to the production of waves by a ship may be described as a decreasing efficiency of elements of the ship's surface with increasing distance from the bow. A reducing factor,



of a semi-empirical nature, is introduced into the theory of ship waves to represent this effect. With certain assumptions, calculations are made for the wave profile for a simple model, and curves are also given; these are compared with available experimental data. It appears that, as a rough estimate for such forms at moderate speeds, the efficiency of the stern is of the order of 60% of that of the bow. Curves are also drawn to show the corresponding change in the wave resistance. The introduction of the reducing factor leads to different wave resistances for a model going ahead and going astern, when the model is not symmetrical fore and aft; this is illustrated by calculations and curves for a particular case.

---

## The Variation of the Mobility of Gaseous Ions with Temperature

### I—Positive Ions in their own Gas

By A. M. TYNDALL, F.R.S., and A. F. PEARCE, H. H. Wills Physical Laboratory, University of Bristol

(Received January 24, 1935)

Recent work in this laboratory\* on the mobility of gaseous ions has shown that the results of early investigators were all influenced by the effect of polar impurities in the gas, which led to the formation of clustered ions. When precautions are taken to exclude them, the higher values of mobility which are obtained indicate that, as at low pressures, the positive ions are normally singly charged atoms or molecules. The negative carriers are electrons in all the purified gases in which these experiments have been carried out, namely helium, neon, argon, krypton, xenon, nitrogen and hydrogen.

In view of its possible theoretical interest, it seemed desirable to repeat another early investigation,† that of the variation of mobility with temperature. The following account records experiments on the positive

\* Tyndall and Powell, 'Proc. Roy. Soc.,' A, vol. 134, p. 125 (1931); vol. 136, p. 146 (1932); Powell and Brata, 'Proc. Roy. Soc.,' A, vol. 138, p. 117 (1932), etc.

† Phillips, 'Proc. Roy. Soc.,' A, vol. 78, p. 167 (1906); Kovarik, 'Phys. Rev.,' vol. 30, p. 415 (1910); Erikson, 'Phys. Rev.,' vol. 6, p. 345 (1915).

ions of helium in helium and of nitrogen in nitrogen, and discusses the results obtained.

### APPARATUS

The apparatus was designed to allow the use of liquid baths of hydrogen, nitrogen, oxygen and ethylene, boiling under reduced pressure if required. Liquid hydrogen could not, of course, be employed in the work in nitrogen. Fig. 1 is a  $2/5$  scale diagram of the main Pyrex glass apparatus with its Dewar flask for these baths. The inlet T was used for filling the flask. For temperatures above that of the room the flask was removed and replaced by an electrically heated enclosure. The method of measurement has been described elsewhere in detail (*loc. cit.*), but the dimensions of the mobility tube were reduced to secure economy in liquid hydrogen.

Fig. 2 shows the plates of the mobility tube M drawn to full scale, together with a diagrammatical sketch of the electrical connections. The grids CD and EF, to which an alternating potential of variable frequency  $n$  is applied, act like shutters in transmitting a thin layer of ions to the electrometer at a critical value of  $n$ , when the time taken by an ion to pass from C to E is  $1/n$ . D, D, are diode voltmeters for measuring this potential. On plotting the electrometer current with frequency a peaked curve is obtained, the frequency at the peak being proportional to the mobility. If the two shutters work in phase the peak (diminished in height) should repeat itself at frequencies  $2n$ ,  $3n$ , etc. In this work the "second order" peaks at frequency  $2n$  were used, and some typical curves for helium are shown in fig. 3.\* Only two of the pinches used for the insertion of the tungsten leads to the measuring tube are shown in fig. 1, but they were actually five in number. From these pinches the leads continued in

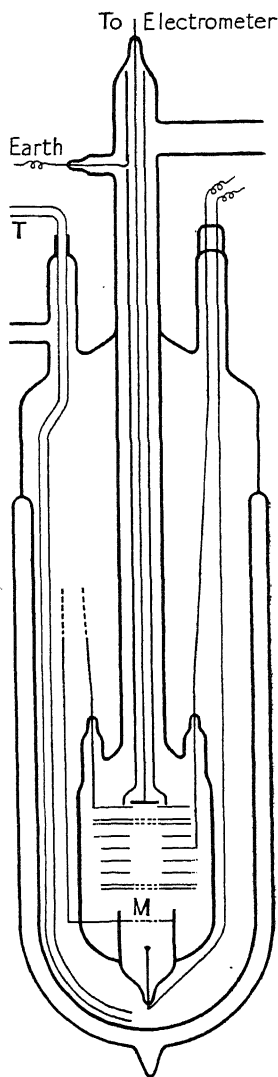


FIG. 1

\* The abscissæ are shown as the product of frequency and pressure in order to reduce the results obtained at different temperatures to a common pressure, the field being kept constant.

fine wire to other pinches in a glass canopy to which the Dewar flask was attached. The purpose of this arrangement was to minimize thermal conduction between the plates and the outside air and to avoid the deposition of moisture or frost around the pinches of the measuring tube itself. The shield for the electrometer lead was a glass tube

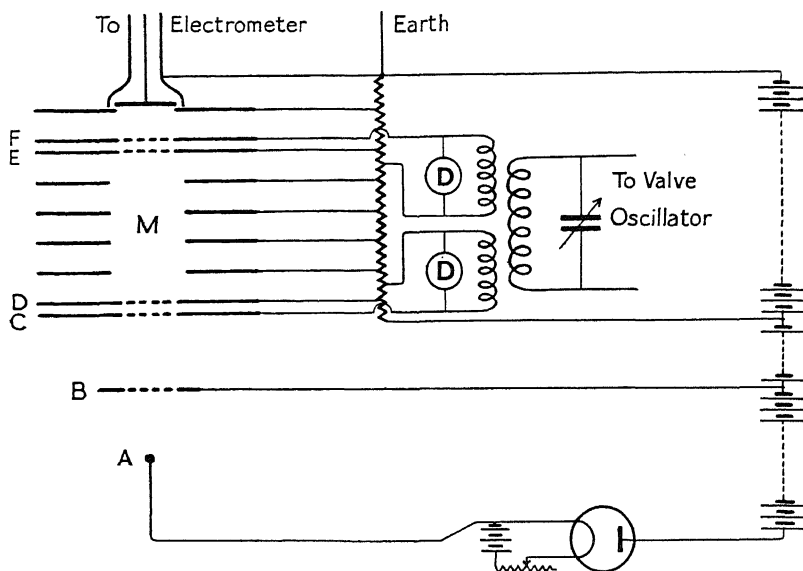


FIG. 2

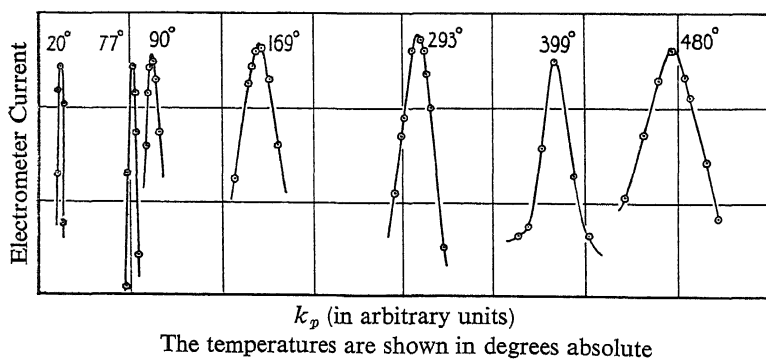


FIG. 3

coated with platinum paint and earthed. The range of temperature used in helium was 20° K to 480° K and in nitrogen 65° K (nitrogen boiling at 15 cm pressure) to 590° K. A platinum-platinum-rhodium couple, not shown in the figure, was inserted into M, fig. 1, through a seal. This was used to determine temperatures above that of the room. While

this is not a suitable thermocouple for use at low temperatures, it served to show when the liquid bath had reduced the temperature of the gas to a steady value, then assumed to be the boiling point of the liquid.

As in previous investigations, the helium was produced from thorianite, and the nitrogen from sodium azide, the procedure of final purification being that previously described. The vessel and connecting tubes were previously subjected to a rigorous bake-out. A liquid oxygen trap was inserted between the last stop-cock and the main tube. Charcoal was placed in this trap in the experiments on helium. With helium the main field used was 32 volts/cm, and the pressures 7 to 27 mm. With nitrogen the field was 64 volts/cm, and the pressures 5 to 20 mm; the frequencies ranged from 3 to 30 kilocycles per second.

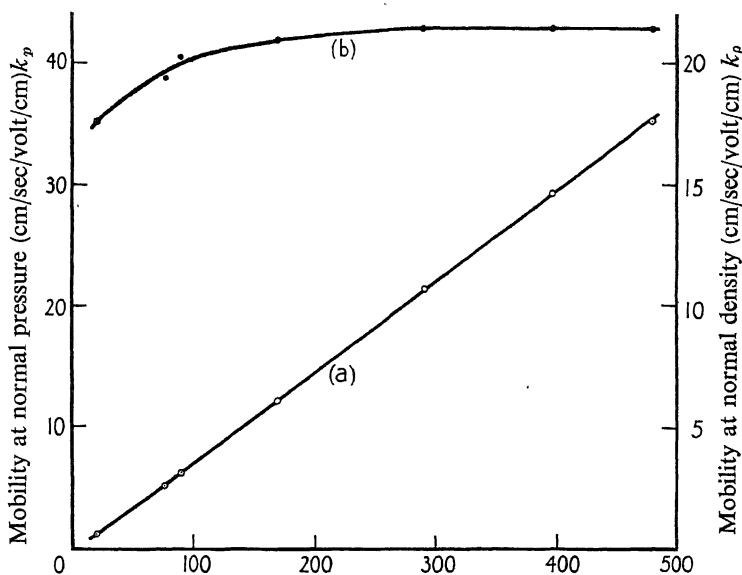


FIG. 4—Helium ions in helium. (a),  $\odot$   $k_p$ ; (b),  $\bullet$   $k_p$

## RESULTS

*Helium*—The results for helium ions in helium are shown in Table I, and they are plotted in fig. 4. The results are given in two forms. The mobility of an ion in a gas at any temperature is usually defined as the speed of the ion in centimetres per second in a field of 1 volt per cm, the gas pressure being 760 mm of mercury. We call this quantity  $k_p$ , the mobility at normal pressure. The results can also be expressed in terms of a quantity  $k_p$ , the mobility of the ions in centimetres per second in a

TABLE I—HELIUM

Temp ° K	$k_p$	$k_\rho$
480	35.3	21.4
399	29.3	21.4
291	21.4	21.4
169	12.2	21.0
90	6.26	20.3
77	5.10	19.3
20	1.21	17.6

field of 1 volt per cm and in gas at constant density. We arbitrarily chose this density to be that of the gas at a pressure of 760 mm of mercury and at a temperature 18° C. At any temperature  $T^\circ$  K there is, therefore, the following relationship between  $k_p$  and  $k_\rho$

$$k_p = k_\rho \times \frac{291}{T}.$$

The quantity  $k_\rho$  we call the mobility at normal density. The variation of the quantities  $k_p$  and  $k_\rho$  with temperature for helium ions in helium are shown in fig. 4. It will be seen that the mobility at constant density is practically independent of temperature from 480° K down to about 300° K and then decreases.

*Nitrogen*—Table II and fig. 5 show the corresponding results for nitrogen ions in nitrogen. In this case, however, the decrease in mobility at constant density with decrease in temperature is continuous over the

TABLE II—NITROGEN

Temp ° K	$k_p$	$k_\rho$
587	6.45	3.19
500	5.35	3.11
407	4.11	2.94
292	2.67	2.67
169	1.25	2.15
90	0.501	1.62
77	0.412	1.56
65	0.327	1.46

whole range. For theoretical reasons discussed below, it would have been interesting to have extended the temperature range upwards to see if the complete curve rose to a maximum and fell beyond it. But in practice the range was limited by the fact that the ions drawn from a glow discharge are very sensitive to traces of impurity and, despite a previous bake-out it is difficult to avoid some minute contamination

at higher temperatures long before the softening point of Pyrex glass is reached.

## DISCUSSION

Lennard-Jones\* has used the variation of certain physical quantities with temperature to determine an expression for the force between neutral atoms. He also pointed out that similarly the variation of mobility with temperature might give us information on the field of force between a neutral atom and an ion moving in a weak electric field.

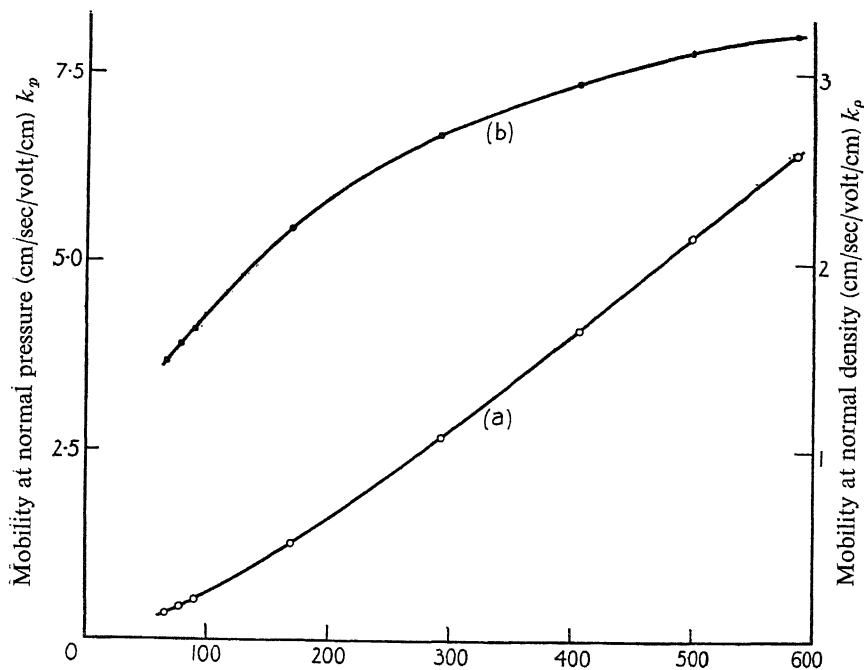


FIG. 5—Nitrogen ions in nitrogen. (a),  $\circ$   $k_p$ ; (b),  $\bullet$   $k_p$

The writers have recently had the benefit of discussions with Professors Hassé and Mott on this problem, and the position may be summarized as follows.

Langevin's theory† of elastic spheres of least distance of approach  $\sigma$  with an attractive field of the form  $\mu r^{-5}$  due to polarization of the gas molecules in the field of the ion leads to the following expression for the mobility  $k$

$$k = \frac{A}{\sqrt{\rho(K-1)}} \left(1 + \frac{m}{M}\right)^{\frac{1}{2}},$$

\* 'Proc. Phys. Soc.', vol. 43, p. 461 (1931).

† 'Ann. Chim. Phys.', vol. 5, p. 245 (1905).

where  $\rho$  is the density of the gas,  $K$  its dielectric constant and  $m$  and  $M$  the masses of gaseous molecule and ion respectively.  $A$  is a function of a parameter  $\lambda$  where  $\lambda^2 = 8\pi p\sigma^4/(K-1)e^2$ ;  $p$  being the pressure of the gas.  $\lambda$  may therefore be regarded as a measure of the relative importance of the finite radii of the atoms and polarization forces in determining the path of an ion. At constant density  $\lambda$  is proportional to  $T^{1/2}$ . Langevin, and also Hassé\* have calculated the values of  $A$  for different values of  $\lambda$ , and hence it is possible to express the mobility at constant density  $k_p$  as a function of temperature. It may thus be shown that  $k_p$  should have a maximum value at a temperature which depends upon the value of  $\lambda$ . When  $\lambda$  is large the curve rises and falls steeply about a maximum which occurs at a relatively low temperature. As the value of  $\lambda$  is decreased, *i.e.*, as  $\sigma$  is decreased or  $(K-1)$  increased, the temperature at the maximum rises and the curve flattens.

Hassé and Cook† have also deduced an expression on a model of point centres of repulsive and attractive fields of the form  $\alpha r^{-3} - \mu r^{-5}$ . In this case in place of  $\lambda$  we have a parameter  $s$  where  $s^2 = 2RT\alpha/\mu^2$ .  $s$  is therefore also proportional to  $T^{1/2}$  and a similar relationship between  $k$  and temperature is obtained where  $s$  plays the same role as  $\lambda$  in determining the shape of the curve and position of its maximum.

But if in order to compare the results with experiment accepted values of, let us say,  $\lambda$  and  $K$  are taken, it is found that the two temperature curves deviate from one another quite markedly. It is of course possible that by regarding  $\lambda$  and  $K$  as arbitrary constants one might find values for them which would give a mobility temperature variation in agreement with experiment. But it is unnecessary to make the attempt because there is a very good reason for not expecting quantitative agreement in the case of positive ions moving in their own gas. The classical theory takes no account of electron exchange, a phenomenon for which, apart from theoretical considerations, there is experimental evidence from the mobility determinations of Mitchell and Ridler‡ for nitrogen ions in nitrogen.

A wave mechanical treatment is therefore necessary.

The only attempt made so far to apply the wave mechanics to the problem of mobility has been that of Massey and Mohr,§ who use an interaction energy due to Majorana and Pauling for helium ions in helium. This unfortunately is quantitatively even less satisfactory since

\* 'Phil. Mag.', vol. 1, p. 139 (1926).

† 'Phil. Mag.', vol. 12, p. 554 (1931).

‡ 'Proc. Roy. Soc.', A, vol. 146, p. 911 (1934).

§ 'Proc. Roy. Soc.', A, vol. 144, p. 188 (1934).

they deduced a value of 12 at room temperature and pressure instead of the experimental value 21.4. Professor Mott has, however, suggested to us that Massey and Mohr may have over-estimated the effect of exchange forces by their assumption that the mean period of electron exchange is small compared with the time of passage of the ion past the atom. An over-estimation of the effect of exchange forces would lead to a value of mobility which was too low, though there should be a closer agreement between theory and experiment at very low temperatures because of the reduced relative velocity of the two colliding particles.

While the full interpretation of the above results must, therefore, await further theoretical calculations, it is interesting to note that exchange forces would not arise with foreign ions such as those of the alkalis moving, for instance, in an inert gas. A slow-moving positive ion can only capture an electron from an atom of lower ionization potential, and the ionization potentials of the inert gases are all much higher than those of the alkalis. It would, therefore, be interesting to repeat the experiments using ions of this type, because in the absence of exchange forces, we should not expect the values calculated on a classical model and a wave mechanical model to differ much from one another. The problem presents certain additional experimental difficulties, but we propose to make an attempt to obtain the data.

We are indebted to the Colston Research Society of the University of Bristol for a grant in aid of the investigation. We also wish to acknowledge that the construction of the mobility tube would not have been possible without the skill of the laboratory glassblower, Mr. J. H. Burrow, B.Sc.

#### SUMMARY

A method has been developed for determining the effect of temperature on the mobility of positive ions in pure gases. It has been applied to the positive ion of helium in helium and to the nitrogen molecular ion in nitrogen over a temperature range from 20° K to 480° K in helium, and from 65° K to 590° K in nitrogen.

If the results are expressed at normal density instead of, as commonly, normal pressure, the mobility in helium is practically independent of temperature from 480° K down to about room temperature, below which there is a marked decrease. In nitrogen the decrease in mobility with decrease in temperature is continuous over the whole range.



Owing to lack of knowledge of the precise effect of electron exchange on the mobility of ions, it is not possible at present to use these results to deduce the forces between the ions and the gas atoms or molecules with which they are colliding. It is therefore proposed to extend the experiments to alkali ions in inert gases, since exchange processes do not then occur.

---

## Electronic Spectra of Polyatomic Molecules I—Saturated Aldehydes

By E. EASTWOOD and C. P. SNOW, Laboratory of Physical Chemistry,  
Cambridge

(Communicated by T. M. Lowry, F.R.S.—Received July 14, Revised  
November 27, 1934)

[PLATE 8]

### INTRODUCTION

Of the two methods which are now available to describe the electronic structures of polyatomic molecules, only the more recent—the *orbital* method—can at present be applied to the excited levels of molecules, and so any interpretation of the spectra of polyatomic molecules must be done in its terms. This method, which was suggested by Lennard-Jones for diatomic molecules and applied to polyatomic molecules by Hund, Mulliken, and Lennard-Jones, starts on the assumption of the symmetry of the nuclear framework; the electrons are then added one by one to orbitals characteristic of the molecule as a whole and not of any particular atom-pair. In this last feature, the method differs from the earlier one developed by Pauling and Slater on the lines of the Heitler-London treatment of the hydrogen molecule, where the electron-pair bond between two atoms is generally assumed.

For some purposes the electron-pair method has advantages over the orbital method (an example of the use of the electron-pair method where the other would be inapplicable is given by Penney's recent work on benzene); the advantages and disadvantages of each have been discussed in various papers, and it is probable that they will both be necessary

complements of each other for some time in the elucidation of any particular problem.

The assignment of energy levels and spectroscopic transitions fall within the scope of the orbital method alone, and these papers accordingly will employ its language and ideas. The orbital method, beginning from a knowledge of the geometrical symmetry of the nuclei of a molecule, can describe the symmetry of the possible electronic states and give selection rules which govern the transition between them. For molecules of high symmetry (*e.g.*,  $\text{CH}_4$ ,  $\text{C}_2\text{H}_4$ ,  $\text{SF}_6$ ) this method will provide detailed accounts of the individual electronic configurations in the ground state and in a number of upper states; in general the order of the upper states will not be accurately predictable. If, however, the spectra resulting from transitions from the ground state to the upper states are known with sufficient accuracy, certain characteristics of the rotational structure can decide unequivocally between the upper states, and thus the combination of the theoretical and spectroscopic data can give unambiguous assignments in fortunate cases. Actually, however, such data as exist on the spectra of polyatomic molecules have been obtained at random and under comparatively small dispersion; so that there are almost no precise measurements upon molecules which can be treated by the theory.

These papers will, therefore, attempt to give spectroscopic observations of such molecules as are amenable to the orbital theory, and in some cases we hope to obtain knowledge of the electronic structures of ground and upper states which may be compared with those derived from chemical theories of valency. For the present work, the saturated aldehydes were chosen as satisfying the criteria of theoretical utility and chemical interest, first, because their spectra have already been fairly widely investigated in solution; secondly, because the key molecule of the series, formaldehyde, has been subjected by Dieke and Kistiakowsky\* to the only satisfactory analysis that has yet been reached in the electronic spectra of polyatomic molecules; thirdly, because the absorption band due to  $>\text{C}=\text{O}$  has figured a great deal in qualitative chemical investigations. This band, with its maximum at approximately  $\lambda$  2900 Å, is possessed by all saturated aldehydes and ketones, and for years it has been considered to possess a similar electronic origin in all these cases. The details of our results confirm this view. It has also been usual on chemical grounds to consider the electronic transition as taking place in an electron or electrons of the  $>\text{C}=\text{O}$  double bond, but the orbital theory in conjunction with the experimental results suggests that this is not a valid assumption.

\* 'Phys. Rev.', vol. 45, p. 4 (1934).

Mulliken has built up an orbital structure of the  $C=C$  double bond in ethylene, and has assigned the bands of ethylene at  $\lambda$  1900 Å to an electronic transition localized in the double bond and corresponding to a change of electric moment parallel to the axis of the molecule. (Owing to the absence of fine structure in the ethylene bands, this hypothesis, though very probable, is not definitely established.) In correspondence with us he has also suggested a structure for the  $>C=O$  double bond in formaldehyde, which is quoted later in this paper. For this molecule the precise analysis of Dieke and Kistiakowsky shows definitely that the change of electric moment must be perpendicular to the axis of the molecule. The number of possible upper states of formaldehyde is accordingly limited: and further arguments, and an application of Dieke and Kistiakowsky's complete analysis, give a unique choice of upper states and a transition which is not localized in the double bond.

Although the change in symmetry in passing from formaldehyde to acetaldehyde and the higher aldehydes implies, according to the formal scheme of molecular orbitals, a complete alteration in the description of the states, this alteration is formal and not real; it is confirmed in this paper that the electronic transition in acetaldehyde, propionaldehyde, etc., is similar to that in formaldehyde, and in all these molecules is not localized in the double bond. (In all  $>C=C<$  molecules it is probable that the transition is similar to that in ethylene and is localized in the double bond).

#### EXPERIMENTAL

The apparatus consisted of an absorption tube of length 1 metre, constructed wholly from fused silica. To this was attached a pumping system, a McLeod gauge for measurement of pressure, and two small side tubes or reservoirs joined in series. Each substance was carefully purified and only the appropriate fraction of the final distillation was employed; this was introduced into the first of the reservoirs immediately before the experiment, solidified with liquid air and the apparatus evacuated. Thus contact with the air was reduced to a minimum, whilst a further distillation was then performed *in vacuo* using the two reservoirs and liquid air. A hydrogen discharge tube was employed as a source of ultra-violet radiation and the spectra were photographed upon a small Hilger quartz E.37 spectrograph and also upon a large Hilger E.1 spectrograph, a series of pressures for each substance from zero to saturation being employed. For heptaldehyde, with boiling point  $155^{\circ}C$ , the saturation vapour pressure was too small to yield any appreciable absorp-

tion, so that it was necessary to investigate the absorption spectrum of a solution of heptaldehyde in cyclohexane.

## RESULTS

As already mentioned in the introduction, it is known that all the aliphatic aldehydes and ketones possess an ultra-violet absorption band in the region  $\lambda$  3500–2500 Å, and we may, with considerable probability, interpret this fact as indicating an excited state of the  $>\text{C}=\text{O}$  part of the molecule situated  $28600\text{ cm}^{-1}$  above the ground state. Further, by Raman and infra-red investigations it has been established that a vibration frequency of  $1700\text{ cm}^{-1}$  is characteristic of the carbonyl group in its ground state. That this frequency appears for all aldehydes and ketones demonstrates that it is in large measure a property of the  $>\text{C}=\text{O}$  group and independent of the rest of the molecule (at least in the aliphatic series, with which only we are concerned here). The magnitude of the frequency will be dependent upon the nature of the potential field binding the carbon and the oxygen atoms; the constancy of this frequency therefore suggests that the electronic structure of  $>\text{C}=\text{O}$  in all these compounds, in the ground state, is very nearly identical. The presence of a constant electric moment of  $2.7 \times 10^{-18}$ , attributable to the carbonyl group in these compounds, supports this conclusion as noted by Almasy.\*

The investigations on formaldehyde by Henri and Schou,† Herzberg,‡ and finally that of Dieke and Kistiakowsky, have yielded an electronic band system which may be represented in terms of two fundamental vibrational frequencies of the excited state of  $1187$  and  $830\text{ cm}^{-1}$ , the first of which is regarded as essentially a carbon-oxygen valency vibration and thus corresponds to the frequency of  $1700\text{ cm}^{-1}$  of the ground state. The energy level system of formaldehyde in its excited state consists of a series of vibrational energy levels with a separation of  $1187\text{ cm}^{-1}$  and upon each of these major levels is built a succession of subsidiary vibrational levels, or combination levels, due to the second frequency of  $830\text{ cm}^{-1}$ . The spectrum itself consists of a series of strong bands separated by  $1187\text{ cm}^{-1}$  which corresponds to transitions from the ground state to the above major levels. With each of these major strong bands is associated a subsidiary series of weaker bands with a separation of  $830\text{ cm}^{-1}$ , which are thus combination bands corresponding to transitions from the ground

\* 'J. Chim. Phys.,' vol. 30, p. 528 (1933).

† 'Z. Physik,' vol. 49, p. 774 (1928).

‡ 'Trans. Faraday Soc.,' vol. 27, p. 378 (1931).

state to the combination levels. These series tend to overlap and so it may be said that the  $1187\text{ cm}^{-1}$  frequency determines the broad features of the formaldehyde spectrum, the major bands and their associated subsidiary series imposing a definite periodicity of intensity on the spectrum.

Since the carbonyl group in the aliphatic aldehydes and ketones possesses essentially the same ground state and requires the same energy to raise it to its first stable excited state, we may conclude, with a fair degree of certainty, that this excited state itself will also be very nearly identical in these compounds. If this is so, then a  $>\text{C}=\text{O}$  valency vibration would be expected in the excited state analogous to that which has been established for formaldehyde, and its existence should be shown in the absorption spectrum in its broad outline at least, being similar to that of formaldehyde in the periodicity of intensity. It is most likely that, in view of the increasing complexity of the molecule as we pass up the homologous series, the ultimate structure of the spectrum will tend to fuse together, for additional subsidiary frequencies will be introduced and the increasing moments of inertia will render the component bands continuous. The periodic variation of intensity across the main region of absorption should, however, persist. The spectra which we have obtained fulfil these expectations.

For all the substances examined, at pressures above 25 mm the usual broad, continuous, ketonic band was obtained. The variation of absorption with pressure was observed to be identical for each substance, which is to be expected since, for a given pressure, by Avogadro's Law, we have the same number of molecules per unit volume, *i.e.*, the same number of potential absorbing centres. For a pressure of 18 mm, when the main absorption was very weak, this major band was observed to be clearly resolved into a series of small diffuse bands. These are readily visible upon the spectrograms which have been reproduced, fig. 1, Plate 8. It will be observed that the bands become increasingly more difficult to distinguish as we pass from acetaldehyde up the series. With acetone and methyl-ethyl ketone the bands were so weak as to prevent reproduction and permitted only a very rough estimate of their separations. Since acetone has been the subject of many investigations and no such structure has been reported, it was subjected to very careful scrutiny, and the spectra of samples prepared by the use of sodium iodide and the bisulphite compound respectively, were investigated; confirmation of the structure was obtained. These spectrograms were obtained upon the E.37 instrument. When taken upon the large dispersion E.1 spectrograph the periodic variations of intensity becomes extremely difficult to distinguish

even for acetaldehyde and propionaldehyde; it is only when the spectrum is compressed within a short space that the structure is readily visible. No evidence for the further resolution of these broad bands into the real ultimate bands was obtained, except for propionaldehyde and acetone when the commencement of the region of absorption became partially resolved with the E.1 spectrograph. With acetaldehyde, however, the

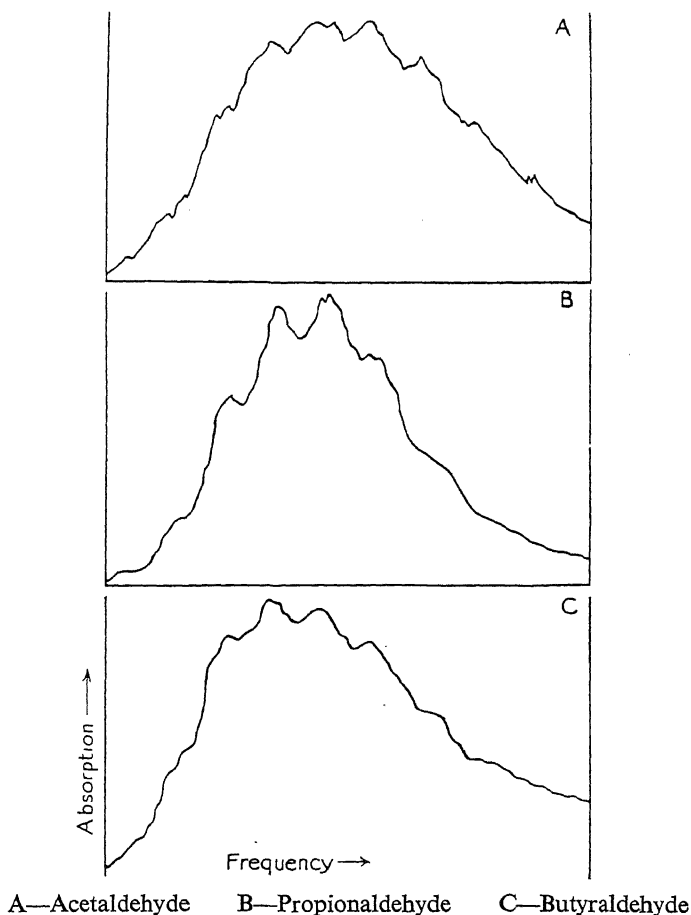


FIG. 2

band system was clearly resolved up to 2825 Å as Schou had already reported.

Microphotometric records of the plates were taken. The reproduction, fig. 2, shows those of acetaldehyde, propionaldehyde and butyraldehyde. These curves clearly illustrate the general form of the absorption—the main broad region with the periodicity imposed by the  $>\text{C}=\text{O}$  vibration

and the structure becoming progressively smoothed out as the molecule increases in complexity.

In the measurement of the plates the approximate centres of the bands have been measured since these are the only measurable features. The wave-lengths of these centre points, the wave numbers and frequency separations are exhibited in Table I. The measurements were repeated many times and the means taken; but no great accuracy is claimed

TABLE I

Wave-length in air in Å	Frequency <i>in vacuo</i> in $\text{cm}^{-1}$	Frequency separation
Acetaldehyde		
3206	31182	
3092	32332	1150
2992	33413	1081
2897	34508	1095
2813	35539	1031
2734	36566	1027
2662	37555	989
2590	38599	1044
2524	39608	1009
Mean frequency difference = $1053 \text{ cm}^{-1}$		
Propionaldehyde		
3223	31018	
3116	32083	1065
3020	33103	1020
2931	34108	1005
2845	35139	1031
2767	36130	991
2690	37164	1034
2618	38186	1022
2550	39204	1018
Mean frequency difference = $1023 \text{ cm}^{-1}$		
Butyraldehyde		
3350	29842	
3233	30922	1080
3128	31960	1038
3028	33016	1056
2937	34038	1022
2852	35053	1015
2773	36051	998
2700	37026	975
2627	38055	1029
Mean frequency difference = $1027 \text{ cm}^{-1}$		

TABLE I—(continued)

Wave-length in air in Å	Frequency <i>in vacuo</i> in $\text{cm}^{-1}$	Frequency separation
Isobutyraldehyde		
3242	30836	
3132	31919	1083
3032	32972	1053
2942	33981	1009
2857	34991	1010
2776	36012	1021
2703	36985	973
2629	38026	1041
Mean frequency difference = $1027 \text{ cm}^{-1}$		
Isovaleraldehyde		
3361	29744	
3252	30741	997
3142	31818	1077
3042	32864	1056
2952	33865	1001
2868	34857	992
2787	35870	1013
Mean frequency difference = $1023 \text{ cm}^{-1}$		
Heptaldehyde		
3228	30970	
3123	32011	1041
3025	33048	1037
2934	34073	1025
2849	35090	1017
2770	36090	1000
2695	37095	1005
Mean frequency difference = $1021 \text{ cm}^{-1}$		
Acetone ?		
2804	35653	
2720	36754	1101
2640	37867	1113
Mean frequency difference = $1107 ? \text{ cm}^{-1}$		

for them in view of the widths of the bands (approximately  $400 \text{ cm}^{-1}$ ) and the vagueness attached to the selection of the centre points as the points defining the bands. The table is thus intended to be suggestive only, to indicate the great probability of the existence of the  $>\text{C}=\text{O}$  valency vibration in the excited state with the approximate values given.



The mean frequency separations are collected together for comparison, in Table II.

TABLE II

Substance		Mean frequency separations of "bands"
Acetaldehyde	$\text{CH}_3\text{CHO}$	1053 $\text{cm}^{-1}$
Propionaldehyde	$\text{C}_2\text{H}_5\text{CHO}$	1023
Butyraldehyde	$\text{C}_3\text{H}_7\text{CHO}$	1027
Isobutyraldehyde	$\text{C}_3\text{H}_7\text{CHO}$	1027
Isovaleraldehyde	$\text{C}_4\text{H}_9\text{CHO}$	1023
Heptaldehyde	$\text{C}_6\text{H}_{13}\text{CHO}$	1021
Acetone	$\text{CH}_3 \cdot \text{CO} \cdot \text{CH}_3$	1107 ?
Methyl-ethyl ketone	$\text{CH}_3 \cdot \text{CO} \cdot \text{C}_2\text{H}_5$	Too faint to estimate

It is evident from Tables I and II that, as with the ground state, for the excited state also we have a  $>\text{C}=\text{O}$  vibration which remains remarkably constant throughout the aliphatic aldehyde series. For acetaldehyde a slightly larger frequency of 1053  $\text{cm}^{-1}$  is indicated. Thus in passing from formaldehyde to acetaldehyde there is quite a large change in frequency viz., 1187 to 1053  $\text{cm}^{-1}$ , and again a change, although this time much smaller, in passing to propionaldehyde, 1023  $\text{cm}^{-1}$ , after which it remains constant. This result is not surprising for in formaldehyde the carbonyl group is not so much an appendage of the molecule as its major part. The change to acetaldehyde is thus comparatively a radical one calculated to modify the perturbing forces upon the carbonyl group and so produce the marked change in the frequency, while in the succeeding homologues the atoms immediately adjacent to the  $>\text{C}=\text{O}$  group remain unchanged. Again, the evidence, though slight, suggests a larger frequency of acetone of the order 1100  $\text{cm}^{-1}$ , *i.e.*, more analogous to that of formaldehyde. This seems reasonable in view of the fact that the symmetry of acetone with respect to the  $>\text{C}=\text{O}$  double bond approximates much more closely to that of formaldehyde than does acetaldehyde.

The approximate nature of the measurements precludes any deductions from the variation of the frequency separations across the spectrum, but from the tables as a whole, the values of the separation seem to show a tendency to diminish as we pass to shorter wave-lengths. Especially interesting is the presence of such comparatively large progressions of  $>\text{C}=\text{O}$  bands. This was commented upon by Herzberg and Franz\* for formaldehyde, for which long progressions were obtained in both the absorption and fluorescent spectra. According to the Franck-Condon Principle, this would be related to a modification in the form and position

\* 'Z. Physik,' vol. 76, p. 720 (1932).

of the potential energy curves for the  $>\text{C}=\text{O}$  group, and would indicate a pronounced bond-loosening, as the diminution in the  $>\text{C}=\text{O}$  frequency also suggests. There is no passage into a region of continuous absorption corresponding to dissociation of the  $>\text{C}=\text{O}$  group.

In the investigation of Schou\* upon acetaldehyde a series of sixty bands was measured and explained by assuming a doublet excited state, with a separation of  $147\text{ cm}^{-1}$  and two fundamental frequencies, one for the ground state and one for the excited state, their magnitudes being  $825$  and  $517\text{ cm}^{-1}$  respectively. There are serious difficulties in the way of this interpretation of which the most obvious is that transitions from even the seventh level of the ground state are admitted; this is directly opposed to the Maxwell-Boltzmann Law. The previous work having suggested a  $>\text{C}=\text{O}$  frequency for acetaldehyde of  $1053\text{ cm}^{-1}$  which found no place in Schou's scheme, it seemed desirable to investigate the spectrum afresh.

We have now photographed the spectrum in the first and second orders of a 21-foot concave grating (dispersion  $1.2\text{ Å/mm}$ ) and from the first order plate have measured seventy bands. Even under this dispersion the first strong bands of the system (Schou's "*g*" and "*h*" bands, here reproduced in fig. 3, Plate, 8) are not completely resolved and thus Schou's rotational analysis is rendered rather meaningless. It will be observed that the "lines" are very broad indeed and would very probably be resolved under still higher dispersion. It was hoped that by achieving some approximation to the ultimate rotational structure, similarities could be traced in the general appearances of the bands which would permit certain bands to be classed together unambiguously as forming a progression, and which would thus furnish a definite frequency. With acrolein (Part II) this procedure was followed but for acetaldehyde the hope could not be fulfilled, and until a satisfactory rotational analysis of the acetaldehyde bands has been made it will not be possible to perform a rigorous vibrational analysis of the spectrum. We find, however, that the frequency  $1053\text{ cm}^{-1}$  can be fitted to the spectrum quite convincingly.

#### ELECTRONIC STATES OF ALDEHYDE MOLECULES

The results of the vibrational analysis in this paper suggest strongly that the electronic transition is effectively the same in all the molecules considered. That is, the electronic structure of the  $>\text{C}=\text{O}$  group in acetaldehyde must be similar to that of the  $>\text{C}=\text{O}$  group in the higher

\* 'J. Chim. Phys.,' vol. 26, pp. 1, 69 (1929)

aldehydes, both in the ground and upper states. In the same way, the observed states of acetaldehyde must be similar to those of formaldehyde. (Formally the change from higher to lower symmetry may introduce a greater number of permitted transitions; but as expected, this does not occur in the more favourable case of ethylenic molecules and in general the possibility may be dismissed.)\* And so if the electronic structure of C=O in formaldehyde is known, we can now assign similar orbital structures to any of the molecules investigated, and by implication, to any saturated aldehyde and, probably, to any saturated ketone.

In a private communication Professor Mulliken has derived structures for the ground states and the first excited state of formaldehyde which appear definite in the light of Dieke and Kistiakowsky's analysis and which also, even before that analysis was known, seemed probable on the basis of chemical and other evidence. Mulliken writes, for the ground state of formaldehyde, omitting  $s$  and  $[s]$  electrons†:—

$$[y + y]^2 [x + x]^2 [z + z]^2 [y - y]^2 \quad ({}^1A).$$

From this structure there arise the possible upper states:—

$$[y + y]^2 [x + x]^2 [z + z]^2 [y - y]^2 \quad {}^1A \text{ [ground state]}$$

$$[y + y]^2 [x + x]^2 \frac{[z + z]}{[x - x]} [y - y]^2 \quad {}^3B_1, {}^1B_1$$

$$[y + y]^2 [x + x]^2 [z + z]^2 \frac{[y - y]}{[z - z]} \quad {}^3B_2, {}^1B_2.$$

From Dieke and Kistiakowsky's preliminary results it was shown that the rotational bands were of the perpendicular type, *i.e.*, transitions corresponding to a change of electric moment along the axis of symmetry

\* Snow and Alsopp, 'Trans. Faraday Soc.', vol. 20, p. 93 (1934).

† In the same notation as in his paper on ethylene (Mulliken, 'Phys. Rev.', vol. 41, p. 751 (1932)) of which the orbital structure is:

$$[y + y]^2 [x + x]^2 [z + z]^2 [y - y]^2,$$

$[y + y]^2$  means two electrons of type  $[y + y]$  (*cf.*  $s^2$ , etc., in atoms).  $[y + y]$  means: const.  $[y]_A + \text{const. } [y]_B$  and refers to an orbital wave function formed by the overlapping of two single electron wave functions from atom A and atom B. For formaldehyde,  $z$  is the direction of the C=O axis,  $y$  is perpendicular to  $z$  and in the plane of the H's,  $x$  is perpendicular to  $y$  and  $z$ .

$[y + y]^2$  for two atoms A and B means: const.  $[y]_A + \text{const. } [y]_B$ . Reference should be made to the above paper or for a short summary to the paper by Snow and Alsopp already quoted.

could be ruled out at once. In ethylene the lowest transition is assumed to be  $[x + x]^2 \rightarrow [x + x] [x - x]$ , which corresponds to such a change in electric moment. This possibility does not exist for formaldehyde, and the excitation must be either of a  $[z + z]$  or  $[y - y]$  electron. The transition  ${}^1A \rightarrow {}^1B_1$ ,  $[z + z]^2 \rightarrow [z + z] [x - x]$  corresponds to a change of electric moment along the  $x$ -axis  ${}^1A \rightarrow {}^1B_2$ ,  $[y - y]^2 \rightarrow [y - y] [z - z]$  corresponds to a change of electric moment along the  $y$ -axis (in the plane of the hydrogens). The  ${}^1A \rightarrow {}^1B_1$  transition would be confined to the double bond: the  ${}^1A \rightarrow {}^1B_2$  transition would affect the CH binding to some extent, and would alter somewhat in going from formaldehyde to acetaldehyde, etc. The photochemical decompositions studied by Norrish and his collaborators, have proved that the excitation of  $R_1 R_2 > C=O$  molecules by this transition results in a decomposition into  $R_1$ ,  $R_2$  and CO, *i.e.*, that the excitation affects the  $CR_1$  and  $CR_2$  bindings. From this fact and from the spectroscopic data it would appear that the  ${}^1A \rightarrow {}^1B_2$  transition was the more probable. Dieke and Kistiakowsky's final analysis, which has shown unambiguously that the change in electric moment is along the  $y$ -axis, distinguishes definitely between the two levels; and so Mulliken writes the formaldehyde transition:—

$$\begin{array}{ll} [y + y]^2 [x + x]^2 [z + z]^2 [y - y]^2 & {}^1A \\ [y + y] [x + x]^2 [z + z]^2 [y - y] [z - z] & {}^1B_2. \end{array}$$

The formaldehyde  $\alpha$ -band may correspond to a singlet-triplet transition  ${}^1A \rightarrow {}^3B_2$ .

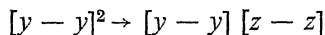
We tentatively assign the same transition  $[y - y]^2 \rightarrow [y - y] [z - z]$  to the 2900 Å band in aldehydes and ketones. We propose to postpone a discussion of the chemical implication of these electronic structures until the second band in aldehydes, at approximately 1900 Å due to  $>C=O$  and corresponding to a transition from the ground state to a second upper level has been further investigated.

We are grateful to Professor R. S. Mulliken for a great deal of advice, and in particular for the suggestion of the electronic structure of formaldehyde; to Professor J. E. Lennard-Jones for helpful conversations on the orbital theory; and to Professor T. M. Lowry for showing us the relation of this work to chemical problems and for constant interest, criticism and advice throughout this and the subsequent work. Also to the Commissioners of the Exhibition of 1851 for a Senior Studentship during the tenure of which this work was begun; and to the Department of Scientific and Industrial Research for a grant which made its continuance possible.

## SUMMARY

The absorption spectra of the vapours of six saturated aldehydes and two ketones have been studied. The vibrational analysis of the spectra suggests a common ground state and first excited state for these molecules, these states being a property of the electronic structure of  $>\text{C}=\text{O}$ .

The electronic structures of  $>\text{C}=\text{O}$  in these molecules is regarded as essentially similar to that of  $>\text{C}=\text{O}$  in formaldehyde: so that the transition responsible for the band at 2900 Å in all cases is



in the sense defined above. This transition is *not* localized in the double bond, and will affect the atoms adjacent to the C atom of the double bond.

## Electronic Spectra of Polyatomic Molecules

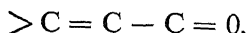
## II—Acrolein

By E. EASTWOOD and C. P. SNOW, Laboratory of Physical Chemistry,  
Cambridge

(Communicated by T. M. Lowry, F.R.S.—Received July 14, Revised  
November 28, 1934)

[PLATES 9 and 10]

In the Introduction to Part I we discussed the orbital structure of the  $>\text{C}=\text{C}$  and  $>\text{C}=\text{O}$  double bonds and the difference between these structures in their excited states. With so much spectroscopic evidence upon these *isolated* double bonds, and at least a provisional theoretical description of each of them, it seemed natural to investigate the effect of double bonds upon each other in conjugated systems such as



These systems occupy an important place in chemical theories of valency. Another reason for investigating such molecules was that measurements under low dispersion by Lüthy\* upon the simplest conjugated aldehyde  $\text{CH}_2=\text{CH}\cdot\text{C}=\text{O}$  showed a spectrum which gave promise of unusual



features.

\* 'Z. phys. Chem.,' B, vol. 107, p. 285 (1923).

This promise was more than borne out by observations under high dispersion, and in fact the spectrum of acrolein reveals a fine structure which so far as we know is unique in molecular spectra at present recorded.

Nine bands have been resolved into what appears to be series of rotational lines; each series can be perfectly expressed by a single parabolic formula as though it were an isolated R-branch. The non-appearance of a related P branch is very strange, although a possible explanation is later suggested; but more curious still is the failure of the various formulæ to yield the same value of the moment of inertia of the ground state. No satisfactory explanation of this fine structure has been found; but it was remarkable enough in itself, and other portions of the interpretation of the spectrum were sufficiently definite, to lead us to put it forward here.

#### EXPERIMENTAL

The apparatus was the same as in Part I for the preliminary work, the spectrum being photographed on a Hilger E.37 and also upon a large Hilger E.1. In the subsequent detailed investigation the spectrum was photographed in the second order of a 21-foot Rowland concave grating giving a dispersion of 1.2 Å/mm, and for this purpose a powerful electric lamp was used as source, no interference resulting from the glass since the spectrum lies in the region  $\lambda$  3900–3250 Å. The iron arc was used as comparison spectrum. The acrolein was purified and only the appropriate fraction of the final distillate was used (with b.p. 52.4° C).

#### RESULTS

Even when observed upon the plates of the small spectrograph the spectrum is remarkable for its sharpness. This is illustrated upon the spectrogram reproduced, fig. 1, Plate 9, when the pressure of the absorbing gas is 12 mm. As Lüthy has also observed, the first strong region of absorption extends from  $\lambda$  4133 to 3260 Å, while a second very intense region extends from a sharp limit at  $\lambda$  2500 towards the violet. This second region was carefully investigated but no traces of structure were obtained; its presence, however, establishes an excited electronic level of the acrolein molecule 40,000  $\text{cm}^{-1}$  above the ground state.

The first region of absorption may be correlated tentatively with the usual aldehyde band (with the absorption maximum situated at  $\lambda$  2900 Å in saturated aldehydes). The assignment of both regions to particular electronic transitions is discussed briefly later.

## VIBRATIONAL LEVELS

A microphotogram of fig. 1, Plate 9 (the acrolein spectrum under low dispersion) was taken and clearly indicates, fig. 2, the general nature of the absorption with its outstanding features of the series of strong main bands and the subsidiary series of weaker bands.

The four strong bands were measured by Lüthy who deduced a constant frequency separation of  $1260\text{ cm}^{-1}$ . By measurements of these maxima of absorption we have confirmed this result and find in addition that the satellite bands, which are not indicated in Lüthy's curve nor

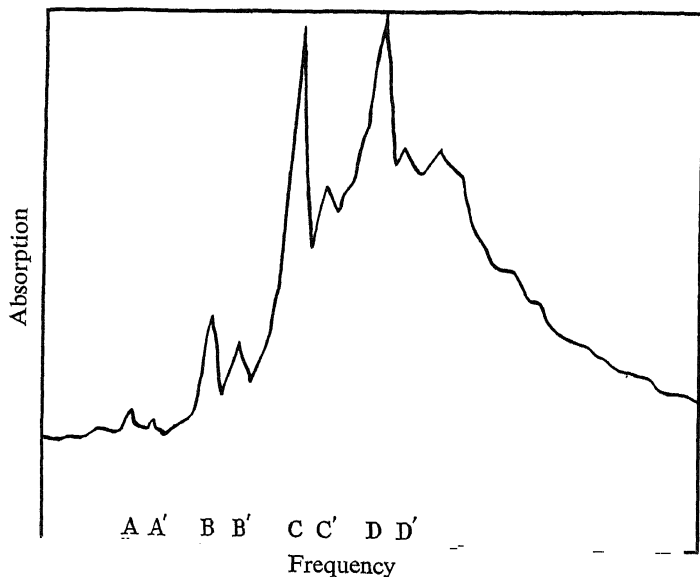


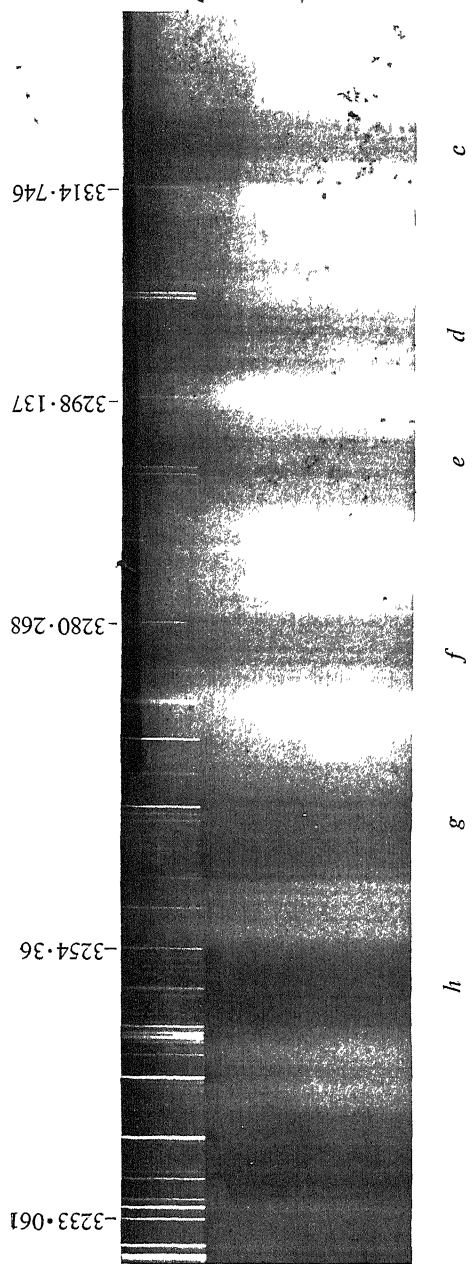
FIG. 2

mentioned by him, are equidistant from their primaries with a separation of  $500\text{ cm}^{-1}$ .

For a molecule of as little symmetry as  $\text{CH}_2 = \text{CH} \cdot \text{CH} = \text{O}$  it is not yet possible to predict what type of vibration will accompany the electronic transition; these observations, however, suggest two fundamental vibrational frequencies of the excited state or  $1260\text{ cm}^{-1}$  and  $500\text{ cm}^{-1}$ . It seems obvious to attribute the frequency of  $1260\text{ cm}^{-1}$  to a

vibration of the type  $\text{CH}_2 = \text{HC} \begin{array}{c} \swarrow \quad \searrow \\ \text{H} \quad \text{C} \end{array} \rightarrow \leftarrow \text{O}$  similar to the frequency at

$1180\text{ cm}^{-1}$  in the excited state of formaldehyde  $\text{H} \begin{array}{c} \swarrow \quad \searrow \\ \text{H} \quad \text{C} \end{array} \rightarrow \leftarrow \text{O}$  and at



Schou's band letters

Fig. 3—Acetaldehyde—second order grating

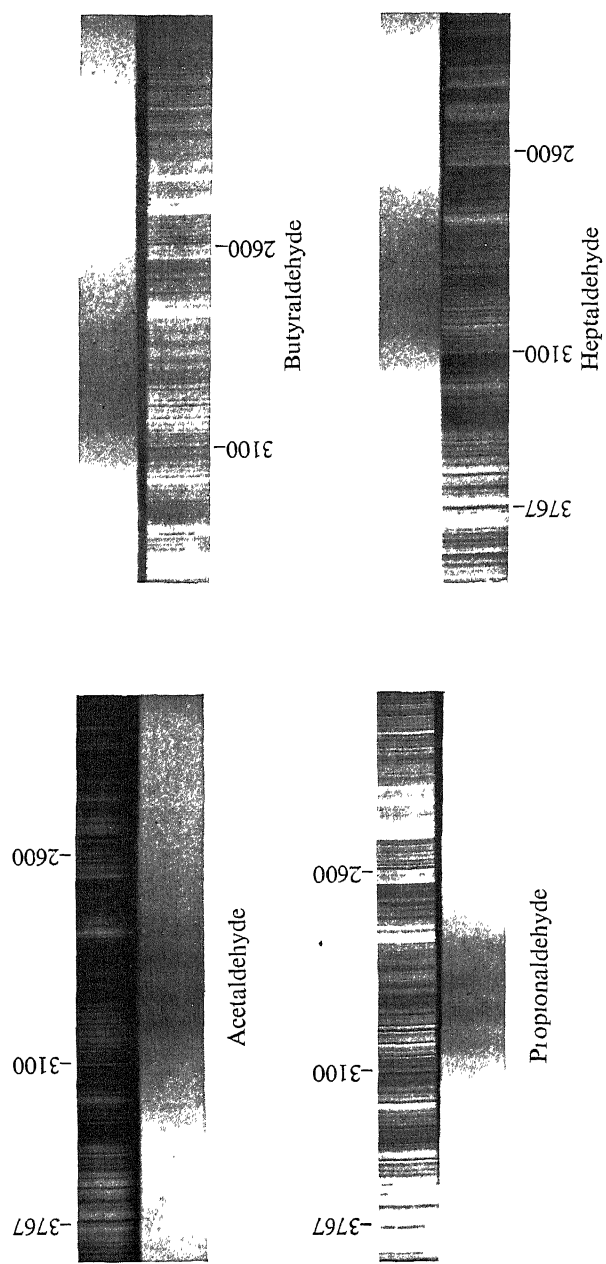


Fig. 1





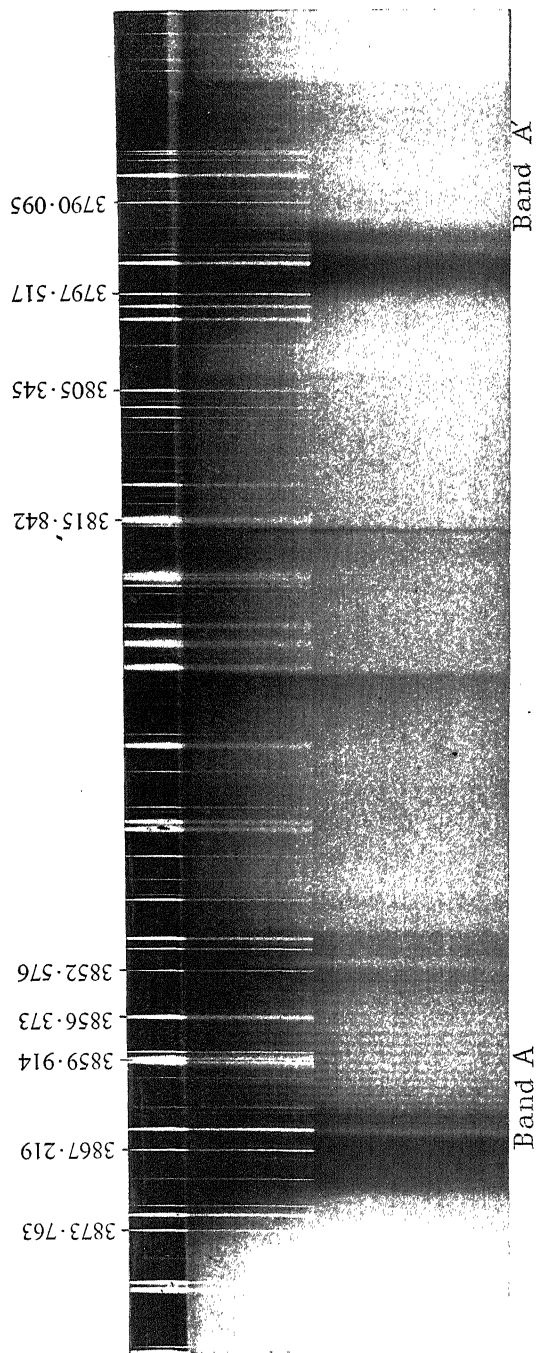


FIG. 3

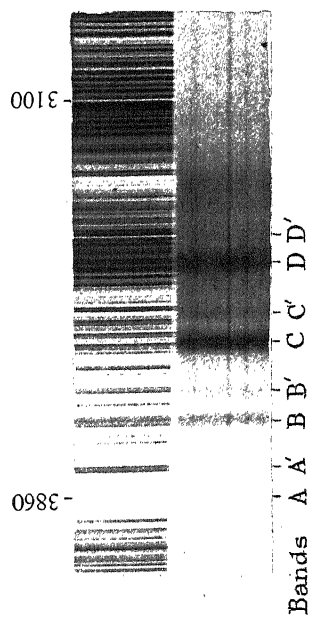


FIG. 1—Acrolein

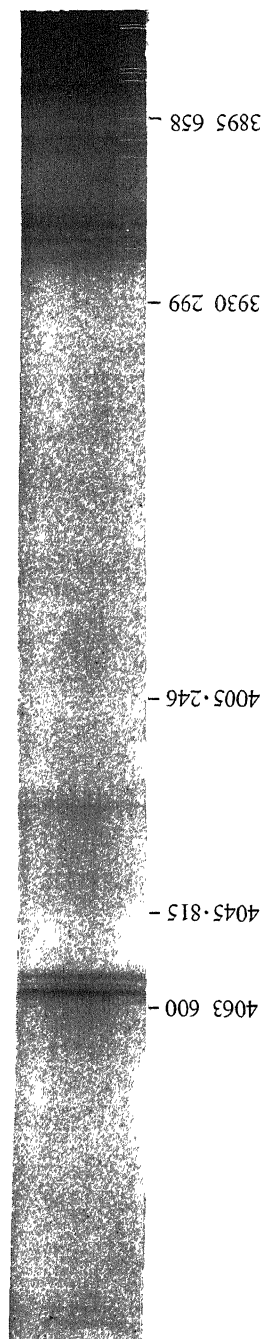


Fig. 5—Acrolein

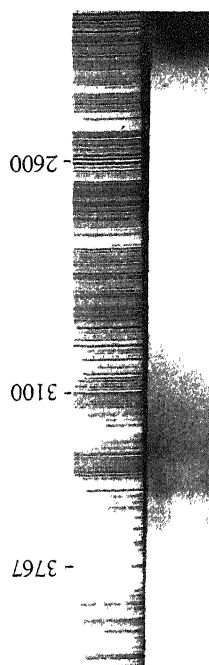


Fig. 7—Citononaldehyde

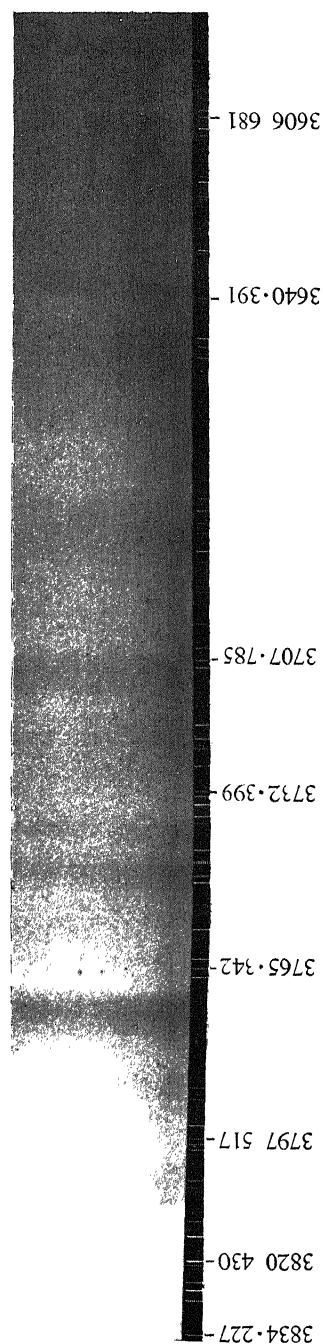


Fig. 9—Citononaldehyde (from second order of grating)

1050  $\text{cm}^{-1}$  in the excited state of acetaldehyde and the other aldehydes (see Part I).

If this were true the difference between the value of this frequency of the excited state for the saturated and unsaturated aldehyde (omitting formaldehyde, where the small mass of the hydrogens may make the result anomalous) would be expected in view of the difference in the upper states which is demonstrated by other features of the spectrum.

However, the assignment of 1260  $\text{cm}^{-1}$  and 500  $\text{cm}^{-1}$  as frequencies of the excited state of acrolein has to be given with reserve; for, as is shown later, measurements under high dispersion reveal curious anomalies and only partially subscribe to this apparently simple and satisfying scheme. Some of the important features of the spectrum under high dispersion are to be seen in the reproduction, fig. 3, Plate 9, which is taken from a second order plate and extends over the wave-length region  $\lambda\lambda$  3880 to 3760 Å. On it is shown the first strong band A and its satellite A', which correspond to the bands similarly named on the small dispersion spectrogram. At the most cursory inspection of the band A it is at once apparent that the spectrum is of an entirely novel type. There is, first, the region of intense absorption extending over 5 Å terminated to short wave-lengths by a very sharp edge but shading out through two pronounced discontinuities of intensity to the red. This region of absorption yields no sign of structure whatever, even for the smallest pressure at which the band could be observed (2 mm  $1\frac{1}{2}$  m tube). From the above sharp edge a series of 20 lines degrade towards short wave-lengths. The first line of the series is weak, the two following very strong, whilst the succeeding lines, although much less intense than these two latter, show first a slight rise in intensity and then a diminution towards the last of the series. The intensity distribution is clearly shown on the microphotogram of the band in fig. 4. At this point a second broad band of continuous absorption becomes superposed. This is very faint, as is also the band series proceeding from it, but when the pressure is increased this second band rapidly increases in intensity.

The satellite band A', which is also present in this reproduction, presents a structure similar to that possessed by A; but on closer examination it will be seen that the first lines of the series, which are difficult to observe, are very curiously spaced; the band also degrades much more rapidly. As in the A band there is a much weaker band towards shorter wave-lengths and also some slight evidence of a third band still further displaced.

Proceeding through 1264  $\text{cm}^{-1}$  from A, we have the next band B of the main series. This presents a very similar structure to the band A,

with the difference that the lines of the series are much more closely spaced.

In this region there are definitely three bands of this same general appearance but only two have proved capable of measurement. The third and fourth bands of the main series, that is C and D, have not yet been resolved into their fine structure, for the general absorption is very intense in this region. However, the bands are again superficially similar, that is, the very strong wide continuous portion separated from the less intense discontinuous lines by a narrow region of complete transmission. This appearance is due to the intense second and third lines fusing together and isolating the remaining band lines. In addition

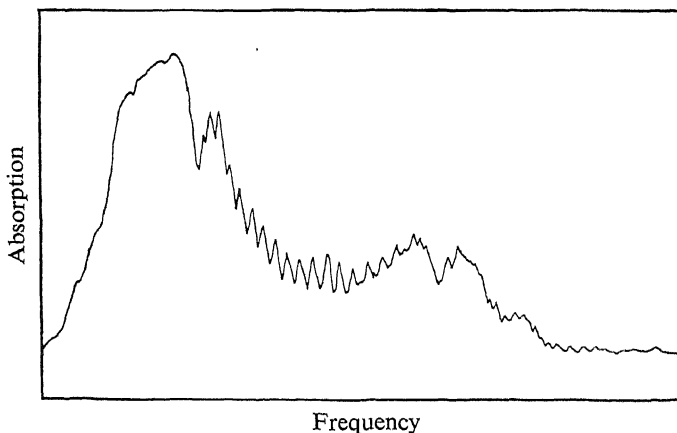


FIG. 4

to the bands of the two main series (A B C D), (A' B' C' D') there are obviously a large number of other bands of an essentially different type consisting for the most part of successive regions of continuous absorption which possess sharp heads to short wave-lengths and shade out to the red. With these continuous bands the present paper makes no attempt to deal. In a further investigation of the spectrum an absorbing column of 6 m and saturated acrolein vapour were employed. By this means three additional bands were obtained (later designated as "a," "b" and "c"). All of these possess the characteristic single line series and are situated on the long wave-length side of the band A. These high pressure bands are extremely faint and diffuse, and therefore difficult to distinguish and measure. Finally, at a distance of  $1230\text{ cm}^{-1}$  to the red side of the first band A, an extremely weak band has been observed, which appears to possess no trace of structure (being very narrow—3 Å) and is in no way comparable to the bands of the main series. Lüthy

also registered absorption in this region and correlated it with his band series previously mentioned, since it possesses roughly the same separation from A; its lack of the characteristic features seems definitely to rule out this possibility. In the subsequent investigation additional information was obtained of the absorption in this region. As shown in the reproduction, fig. 5, Plate 10, the "bands" consist of two narrow regions of absorption sharp on their inner edges, and fading out to the long and short wave-length sides respectively. They are separated by a region of partial transmission, the centre of which is crossed by a fine line. From the point  $\lambda 4059.2 \text{ \AA}$  a series of at least four such bands has been observed extending towards larger wave-lengths with rapidly diminishing intensity and separations of  $33 \text{ cm}^{-1}$ . Thus, these bands are definitely distinct from those of the main region of absorption and we therefore tentatively ascribe the band system to a different electronic transition; it is interesting to remember that the  $\alpha$ -band of formaldehyde is definitely attributable to an electronic transition different from that which results in the main region of absorption, that is, the aldehyde band. It is convenient to represent the vibrational bands whose fine structure has been observed upon a frequency scale, the height of the line being an approximate measure of its intensity.

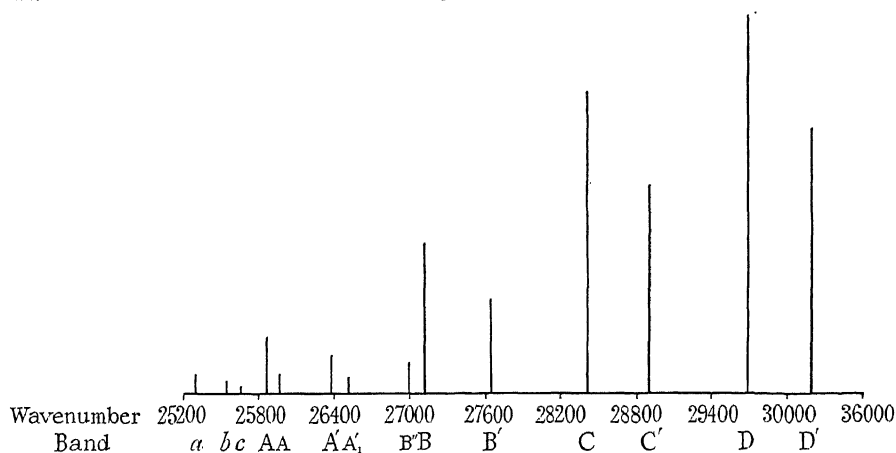


FIG. 6

The actual wave-lengths and wave numbers of the bands are indicated in Table I together with the frequency intervals separating them.

In most spectra due to polyatomic molecules there occur diffuse bands of comparatively large width of, say,  $5 \text{ \AA}$  or  $50$  wave numbers. In general, no definite measurable feature is present in the band and usually the approximate limits of absorption have to be measured. Then in

order to identify the fundamental vibration frequencies to which the band system may be attributed, points within the various bands can be selected arbitrarily as their origins in order to give the best fit to the probable frequencies. In the present series of bands, however, this rather convenient latitude is not present. Each band is defined by the sharp edge of the strong continuum which precedes the line series and

TABLE I

Main series			Subsidiary series	
A.	3865.9 A	25860 cm <sup>-1</sup> (508) (1264)	A'.	3791.4 A 26368 cm <sup>-1</sup>
B.	3685.7	27124 (516) (1280)	B'.	3617.0 27639
C.	3519.7	28403 (490) (1284)	C'.	3460 28893
D.	3367.5	29687 (488)	D'.	3313 30175

the above values are thus accurate, even for the last diffuse pair D and D', to within two wave numbers. The anomalies, then, in the frequency separations can be taken as real. There is no systematic diminution in the separations. This point is considered later.

#### ROTATIONAL STRUCTURE OF THE BANDS

Nine of these associated series of lines have been measured and are included. These may not be the only series in the spectrum, for it may here be emphasized, as has already been mentioned in Part I, that the apparent diffuseness and lack of structure in a band, as for example in C and D, does not justify the immediate conclusion that these are regions of predissociation. The sharpness of the bands is very sensitive to variations of pressure, and it was actually observed that when the pressure had been so adjusted that band B was well developed, and the structure in A was also clearly visible, there was complete diffuseness in A'.

In each case we find only one series of lines proceeding from the continuum and degrading towards shorter wave-lengths. These lines are quite sharp and high accuracy is attainable in their measurement. Apart from any theoretical considerations whatever, we find that employing a method of least squares the lines of a given series may be accurately represented by a simple quadratic formula. For this purpose the lines have been designated by successive integral numbers commencing with unity for the line immediately following the continuum, *i.e.*, the series is representable by the formula

$$\nu_m = A + 2Bm + Cm^2,$$

where  $m$  is the frequency of the  $m$ th line and A, B, and C, are constants for a given series. For the bands A, B'', B, the numbering carried out in this fashion is quite unambiguous, for the end of the strong continuum and the first lines of the series are clearly discernible. For the bands A and A' which are very weak indeed (as is also B'') and exceedingly difficult to measure, shift of the numbering by one unit is possible, whilst for the bands A',  $a$ ,  $b$ , and  $c$  in which the first lines are very diffuse, a change of one or even two units is quite possible. Such changing of the numbering does not, of course, affect the accuracy of the representation nor the value of the constant C, but merely changes the constants A and B.

All the nine bands can in this way be represented by quadratic formulæ, as though they were single R-branches in the spectrum of diatomic molecules. This is, however, misleadingly simple. There are only two known modes by which a discontinuous absorption or emission spectrum can be produced, namely, by transitions between quantized rotational or vibrational energy levels. The possibility of attributing the fine structure

TABLE II

## BAND A

$\nu_0 = 25858.97$		$\nu_m = 25860.48 + 3.028m + 0.0898m^2$		
Number of line $m$	Intensity	Wave-length in air in A	Frequency ( $\text{cm}^{-1}$ in vacuo)	
			Observed	Calculated
1	0	3865.33	25863.7	25863.6
2	4	3864.86	25866.9	25866.9
3	4	3864.30	25870.6	25870.4
4	1	3863.79	25974.0	25874.0
5	2	3863.24	25877.7	25877.9
6	2	3862.64	25881.7	25881.9
7	2	3862.02	25885.9	25886.1
8	2	3861.36	25890.3	25890.4
9	2	3860.70	25894.7	25895.0
10	2	3860.00	25899.4	25899.7
11	3	3859.22	25904.6	25904.6
12	3	3858.44	25909.9	25909.8
13	3	3857.66	25915.1	25915.0
14	2	3856.87	29520.4	25920.5
15	2	3856.00	25926.3	25926.1
16	1	3855.14	25932.1	25931.9
17	1	3854.26	25938.0	25937.9
18	1	3853.32	25944.3	25944.1
19	0	3852.40	25950.5	25950.4
20	0	3851.52	25956.4	25956.9



TABLE II—(continued)

BAND A<sub>1</sub>

$$\nu_0 = 25955.44 \quad \nu_m = 25956.20 + 1.524m + 0.0876m^2$$

Number of line <i>m</i>	Intensity	Wave-length in air in Å	Frequency (cm <sup>-1</sup> <i>in vacuo</i> )	
			Observed	Calculated
1	The centre of a single broad diffuse line measured	3851.28	25958.1	25957.8
2				25959.6
3	1	3850.76	25961.6	25961.6
4	1	3850.43	25963.8	25963.7
5	1	3850.09	25966.1	25966.0
6	1	3849.76	25968.3	25968.5
7	1	3849.37	25970.9	25971.2
8	0	3848.94	25973.8	25974.0
9	1	3848.48	25977.0	25977.0
10	0	3847.99	25980.3	25980.2
11	1	3847.48	25983.7	25983.6
12	1	3846.96	25987.2	25987.1
13	1	3846.43	25990.8	25990.8
14	1	3845.82	25994.9	25994.7
15	0	3845.25	25998.8	25998.8
16	0	3844.51	25903.8	25903.0
17	0	3843.90	25907.9	25907.4

## BAND A'

$$\nu_0 = 26369.39 \quad \nu_m = 26370.07 + 1.366m + 0.1747m^2$$

Number of line <i>m</i>	Intensity	Wave-length in air in Å	Frequency (cm <sup>-1</sup> <i>in vacuo</i> )	
			Observed	Calculated
1	Very weak and practically continuous	3790.76	26372.5	26371.6
2		3790.60	26373.6	26373.5
3		3790.20	26376.4	26375.7
4		3789.93	26378.2	26378.3
5	0	3789.50	26381.3	26381.3
6	0	3789.04	26384.4	26384.6
7	0	3788.52	26388.1	26388.2
8	0	3787.94	26392.1	26392.2
9	0	3787.34	26396.3	26396.5
10	1	3786.66	26401.0	26401.2
11	1	3785.90	26406.3	26406.2
12	1	3785.12	26411.8	26411.6
13	1	3784.27	26417.7	26417.3
14	0	3783.44	26423.5	26423.4
15	0	3782.53	26429.8	26429.8

TABLE II—(continued)

## BAND B'

$$\nu_0 = 26509.88 \quad \nu_m = 26511.49 + 3.216m + 0.0956m^2$$

Number of line <i>m</i>	Intensity	Wave-length in air in Å	Frequency (cm <sup>-1</sup> <i>in vacuo</i> )	
			Observed	Calculated
1	1	3770.39	26514.9	26514.8
2	2	3769.91	26518.3	26518.3
3	2	3769.26	26522.8	26522.0
4	0	3768.79	26526.1	26525.9
5	0	3768.24	26530.0	26530.0
6	1	3767.64	26534.2	26534.2
7	1	3766.98	26538.9	26538.7
8	1	3766.33	26543.5	26543.3
9	1	3765.70	26547.9	26548.2
10	1	3765.00	26552.8	26553.2
11	1	3764.20	26558.5	26558.4
12	1	3763.43	26563.9	26563.9

## BAND B''

$$\nu_0 = 26994.10 \quad \nu_m = 26995.57 + 3.006m + 0.0227m^2$$

Number of line <i>m</i>	Intensity	Wave-length in air in Å	Frequency (cm <sup>-1</sup> <i>in vacuo</i> )	
			Observed	Calculated
1	0	3702.85	26998.6	26998.6
2	1	3702.45	27001.5	27001.7
3	1	3701.99	27004.8	27004.8
4	1	3701.57	27007.9	27007.9
5	1	3701.14	27011.0	27011.2
6	1	3700.69	27014.3	27014.4
7	1	3700.21	27017.8	27017.7
8	1	3699.79	27020.9	27021.1
9	1	3699.30	27024.5	27024.5
10	1	3698.80	27028.1	27027.9
11	1	3698.33	27031.6	27031.4
12	0	3697.88	27034.8	27034.9
13	0	3697.31	27039.0	27038.5

TABLE II—(continued)

## BAND B

$$\nu_0 = 27122.90 \quad \nu_m = 27124.50 + 3.192m + 0.0665m^2$$

Number of line $m$	Intensity	Wave-length in air in Å	Frequency ( $\text{cm}^{-1}$ in <i>vacuo</i> )	
			Observed	Calculated
1	0	3685.21	27127.8	27127.8
2	1	3684.79	27130.9	27131.1
3	1	3684.25	27134.9	27134.7
4	0	3683.77	27138.4	27138.3
5	0	3683.28	27142.0	27142.1
6	1	3682.75	27145.9	27146.0
7	1	3682.20	27150.0	27150.1
8	1	3681.63	27154.2	27154.3
9	1	3681.03	27158.6	27158.6
10	2	3680.45	27162.9	27163.1
11	2	3679.79	26167.8	27167.7
12	1	3679.13	27172.6	27172.4
13	1	3678.49	27177.3	27177.2
14	1	3677.80	27182.5	27182.2
15	1	3677.14	27187.3	27187.3
	1*	3676.64	27191.0	2192.6
16	00*	3676.16	27194.5	
17	1	3675.49	27199.5	27198.0
18	1	3674.79	27104.7	27103.5
19	0	3674.11	27109.7	27109.2
20	0	3673.51	27114.2	27114.9

\* Perturbation ?

of these bands to a vibration seems to be definitely ruled out by the smallness of the frequency in question  $3 \text{ cm}^{-1}$  (*i.e.*, the separation of the lines); also the fact that the lines diverge towards shorter wave-lengths, that is, the coefficient  $C$  is positive, while the bands arising from an anharmonic vibration would have negative  $C$  and would thus converge towards shorter wave-lengths. As another possibility we might invoke transitions.

The following three high pressure bands (Table III) are extremely diffuse and tend to merge into the general background, hence any visual estimate of the relative intensities of successive lines of the series is precluded between vibration levels of the ground state and the excited state, the change in associated quantum number remaining constant for each line like a band sequence in a diatomic molecule. Each of the lines in the fine structure would thus appear as a band in itself, with rotational structure superposed, and would thus cause the band structure as a

TABLE III

BAND *a*

$$\nu_0 = 25295 \cdot 15 \quad \nu_m = 25296 \cdot 50 + 2 \cdot 702m + 0 \cdot 1123m^2$$

Number of line <i>m</i>	Wave-length in air in Å	Frequency (cm <sup>-1</sup> <i>in vacuo</i> )	
		Observed	Calculated
1	3951·56	25299·3	25299·3
2	3951·12	25302·1	25302·3
3	3950·58	25305·6	25305·6
4	3950·03	25309·1	25309·1
5	3949·46	25312·8	25312·8
6	3948·81	25316·9	25316·7
7	3948·19	25320·9	25320·9
8	3947·49	25325·4	25325·3
9	3946·85	25329·5	25329·9
10	3946·04	25334·7	25334·7
11	3945·18	25340·2	25339·8
12	3944·37	25345·4	25345·1
13	3943·65	25350·1	25350·6
14	3942·67	25356·4	25356·3
15	3941·75	25362·3	25362·3

BAND *b*

$$\nu_0 = 25540 \cdot 54 \quad \nu_m = 25542 \cdot 22 + 3 \cdot 360m + 0 \cdot 0457m^2$$

Number of line <i>m</i>	Wave-length in air in Å	Frequency (cm <sup>-1</sup> <i>in vacuo</i> )	
		Observed	Calculated
1	3913·46	25545·6	25545·6
2	3912·89	25549·3	25549·1
3	3912·42	25552·4	25552·7
4	3911·86	25556·1	25556·4
5	3911·24	25560·1	25560·2
6	3910·57	25564·5	25564·0
7	3910·05	25567·9	25568·0
8	3909·53	25571·3	25572·0
9	3908·84	25575·8	25576·2
10	3908·13	25580·5	25580·4
11	3907·40	25585·2	25584·7
12	3906·74	25589·6	25589·1
13	3906·12	25593·6	25593·6

TABLE III—(continued)

BAND *c*

$$\nu_0 = 25646.64 \quad \nu_m = 25647.88 + 2.480m + 0.1287m^2$$

Number of line <i>m</i>	Wave-length in air in Å	Frequency (cm. <sup>-1</sup> <i>in vacuo</i> )	
		Observed	Calculated
1	3897.46	25650.5	25650.5
2	3897.02	25653.4	25653.4
3	3896.55	25656.5	25656.5
4	3896.07	25659.6	25659.9
5	3895.59	25662.8	25663.5
6	3894.97	25666.9	25667.4
7	3894.30	25671.3	25671.5
8	3893.58	25677.0	25676.0
9	3892.81	25681.1	25680.6
10	3892.14	25685.5	25685.5

whole to become diffuse and continuous; for this and other reasons the hypothesis is untenable.

It will appear strange at first sight why such remote possibilities have received sufficient consideration to be registered here, when a rotational effect seems obviously responsible for the fine structure. Actually these explanations were introduced because the hypothesis of a rotational effect involves immediate difficulties of its own. If the assumption is made that the fine structure is due to rotational transitions, without reference, for the present, as to the nature of the rotational motion executed whether by the molecule as a whole or of one portion relative to another, the series of lines will now appear as an R-branch, and if we consider the first band A, then the equation to the branch is—

$$\nu_m = 25860.48 + 3.028m + 0.0898m^2.$$

But no traces of an associated P-branch have been observed either in this or in any of the bands. This is the first serious difficulty. It can perhaps be plausibly removed by the consideration that from the above formula the calculated position of the P-head will be at 25834.8 cm<sup>-1</sup>, which is well within the continuum the limits of which are 25803.6 and 25860.4 cm<sup>-1</sup>. Also  $M_{P\text{-head}} = 17$  and therefore from the intensities of the R-lines, this line would already be very weak and the returning lines of the P-branch would occur in the R-branch region and could not be expected to be observed.

The second difficulty is more considerable. If each of these series is to be attributed to the same rotational mechanism, it should be possible

to find some correlation between the moments of inertia of the various ground states of the bands, in other words between the values of the  $B$ 's occurring in the formulæ. (The application of the combination relations cannot of course, be made since we have only one branch.) Then in the formula for the branch of a band due to a diatomic molecule or for a band of the perpendicular type due to a polyatomic molecule, *i.e.*, the distribution of the sub-bands,

$$\nu_m = A + 2Bm + cm^2.$$

It is well known that  $C = B' - B''$ ,  $B'$  referring to the upper state and  $B''$  to the lower,  $B$  being defined by the relation  $B = h/8\pi^2 Ic$ , where  $I$  is the moment of inertia,  $h$  Planck's constant and  $c$  the velocity of light, and finally  $A = \nu_0 + B'$ , where  $\nu_0$  is the true origin of the band. From the empirical formulæ which have already been given we may easily derive the values of  $\nu_0$ ,  $B'$  and  $B''$ . These values\* are represented in Table IV.

In the light of Table IV it is necessary to raise the question of the vibrational analysis of the principal bands again. As was mentioned previously the bands fall quite obviously into two main series but show anomalous frequency separations which are neither constant nor give systematic uniform increase or decrease. In spite of this the explanation that  $A$  is the (0.0) band and  $B$ ,  $C$ ,  $D$  its harmonics seems very probable. But now from Table IV the bands  $A$  and  $B$ , which show identical appearances and in which the numbers allotted to the lines of the associated series are quite certain, give values of the  $B$ 's of the ground states as 1.424 and 1.534. These values are quite far apart in spite of the fact that both bands must arise from the same ground state of the molecule. In the same way it has been found impossible to correlate the  $B$  values of either upper or lower states of the bands so far analysed.

A number of possible rotational mechanisms have been considered in order to explain the continuous bands and the regular series. None, however, removes the major difficulties, which seem to arise in any rotational explanation, simple or complex. Dieke and Kistiakowsky†

\* [Note added in proof March 2, 1935.—If we use the term  $B_E m^2$ , this being the principal part of the rotational energy term appropriate to the symmetrical top molecule with small  $C$ , where  $B_E = \frac{h}{8\pi^2 c} \left( \frac{1}{C} - \frac{1}{A} \right)$ ,  $C$  and  $A$  being the moments of inertia about, and perpendicular to, the symmetry axis, then the true R-branch formulation would number the lines commencing with  $m = 0$ . Following this procedure the constants  $B'$ ;  $B''$  and  $\nu_0$  would be changed slightly, thus the values of  $B''$  for the bands  $A$  and  $B$  become 1.514 and 1.596 respectively.]

† 'Phys. Rev.', vol. 45, p. 4 (1934).

have recently tabulated the rotational fine structure to be expected for the electronic bands of a symmetrical rotator; but no use of such selection rules seem capable of interpreting even the grosser features of the fine structure. Unless we consider the rotation to be executed by part of the

molecule (*e.g.*, the  $\text{—C} \begin{array}{c} \text{H} \\ \diagup \\ \text{O} \end{array}$  rotating against the comparatively rigid double bond) it is improbable that they can be due to a symmetrical rotator. The molecule as a whole will probably have to be considered as an

TABLE IV

Designation of band	Origin point $\nu_0$ $\text{cm}^{-1}$	$B' - B''$	$B'$	$B''$	Remarks
A	25858.97	0.0898	1.514	1.424	Values quite definite. Numbering is unambiguous
$A_1$	25955.44	0.0875	0.762	0.674	Very probable but not absolutely certain to change of 1 unit
A'	26369.39	0.1747	0.683	0.508	Numbering slightly uncertain
$A'_1$	26509.88	0.0956	1.608	1.512	Numbering very probable
* $B''$	26994.10	0.0227	1.503	1.480	Numbering quite definite
B	27122.90	0.0665	1.596	1.530	Numbering quite definite
<i>a</i>	25295.15	0.1123	1.351	1.239	Numbering very probable
<i>b</i>	25540.54	0.0457	1.680	1.634	Numbering slightly uncertain
<i>c</i>	25646.64	0.1287	1.240	1.111	Numbering slightly uncertain

asymmetric rotator, with two large moments of inertia and a third which is considerably smaller. The rotational energy of an asymmetric top has been investigated by Kramers and Ittman, Wang, Klein, and is conveniently summarized by Dennison.\* The energy levels prove to be functions of the principal moments of inertia and a quantum number  $J$ , there being  $(2J + 1)$  levels for each value of  $J$ . These energy levels are not all expressible by a single general formula as for the diatomic molecule or the symmetrical top rotator, but must be determined by solving the secular determinant appropriate to the problem. The result-

\* 'Rev. of Mod. Phys.,' vol. 3, p. 280 (1931).

ing spectrum is in general exceedingly complex. The acetaldehyde molecule probably acts as an asymmetric rotator and in Part I we have included a spectrogram of its principal bands taken with the same dispersion as that used for the acrolein spectrum. This shows the general type of spectrum to be expected and offers a sharp contrast to the bands of acrolein. Though changes in the relative magnitude of the three moments of inertia may produce profound changes in the character of the fine structure, it does not appear probable that the acrolein line series can be explained in this manner; and in all these considerations of an origin due to some rotational effect the failure of the various bands to yield the same  $B''$  value for the ground state remains a fundamental difficulty.

#### EVIDENCE FROM THE SPECTRUM OF CROTONALDEHYDE

In the endeavour to trace the origin of the line series the possibility for a free rotation of the aldehyde group about the C—C single bond offered a possible mode of attack. It is the only internal rotation possible since no free rotation of the methylene may occur about the C=C double bond.

Now in crotonaldehyde we have simply a methyl group substituted for a hydrogen of the  $\text{CH}_2$  of acrolein, the rest of the molecule remaining as for acrolein. This substance was also investigated by Lüthy (*loc. cit.*), and absorption obtained over approximately the same region as for acrolein. The spectrum consisted of a series of diffuse bands which appeared to be arranged in groups. We have therefore made a detailed examination of the absorption spectrum of crotonaldehyde, under both low and high dispersion, employing methods and instruments identical with those used for acrolein.

The spectrograms from the E.37, fig. 7, Plate 10, show clearly the grouping observed by Lüthy, which is seen to be quite analogous to that observed in the previous paper on the aldehydes. No such band series are present as in acrolein, and the spectrum as a whole is diffuse. The sharp contrast between the spectra of acrolein and crotonaldehyde is clearly shown by comparing fig. 2 and fig. 8, the microphotogram of the crotonaldehyde spectrum.

The curve is smooth and no band series are indicated but we do have the intensity periodicity as for the aldehydes, demonstrating the dominating effect of the C=O vibration. The period is of the order  $1200\text{ cm}^{-1}$  and so comparable with that of acrolein. This result, together with the fact that both acrolein and crotonaldehyde absorb in the same region, indicates



that the condition of the  $=\text{CH} \cdot \text{CHO} \cdot$  is nearly identical in the two molecules.

For crotonaldehyde, the subsidiary series of bands has disappeared, and this effect may be correlated with the substitution of the methyl group in the  $\text{CH}_2$  portion of the molecule. It seems that the subsidiary frequency of  $500 \text{ cm}^{-1}$  which appeared in the acrolein spectrum may be allotted to a vibration of the methylene group about the  $\text{C}=\text{C}$  double bond.

In fig. 9, Plate 10, is reproduced the relevant portion of the crotonaldehyde spectrum from a second order grating plate. The bands are practically continuous and show no trace of the acrolein line series.

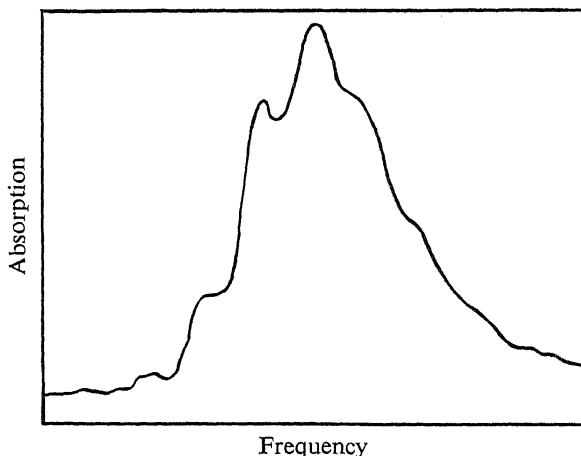


FIG. 8

In the light of these observations it is probable that the acrolein line structure is not adequately explained by a free rotation of the  $\text{CHO}$  group. But there remains the possibility that this motion may occur in acrolein but be suppressed in crotonaldehyde by the interaction of the oxygen atom and the substituted methyl group.

Of the intense continuous region preceding the line series of the individual bands of acrolein little has been said, but it must be emphasized that this region is intimately related to the lines themselves, and that their juxtaposition is not a mere coincidence. Each band consists of continuum plus line series. The band A has been closely examined in the fourth order of the grating (dispersion  $0.6 \text{ \AA/mm}$  and correspondingly increased resolving power) with an extremely narrow slit and conditions of absorption most favourable for the development of the band. The continuum still showed none of the signs of structure which might be

produced, for example, by a partial fusion of the rotational lines of an asymmetric rotator with large moments of inertia. Again, if one assumes some internal mechanism in the molecule to be responsible for the line series, it must be remembered that the molecule is capable of rotating as a whole and that the lines would not be expected to be sharp; for upon each transition of the mechanism resulting in a line would be superposed the energy due to this rotational motion.

#### ELECTRONIC STATES OF ACROLEIN

Analysis of the rotational levels of a molecular spectrum is the only reliable method of determining its electronic states; it was mentioned in Part I how from the character of the levels of a polyatomic molecule, *e.g.*, whether in a symmetric rotator they are parallel or perpendicular, some of the symmetry properties of the upper state can be inferred and accordingly a choice made between the possible upper states permitted by the orbital theory. Obviously the unique rotational structure of the acrolein bands precludes any such process at present.

It is not possible to say whether the displacement of electric moment is along the axis of the double bonds or perpendicular to them. Whatever the origin of the structure, however, there is an indisputable difference between these bands and those of acetaldehyde. It is just conceivable that this is due to a mere geometrical difference between the molecules (such as the capacity of the  $\text{—CO}$  group in acrolein to rotate relative to

H

the  $\text{C}=\text{C}$  double bond) and that there is no profound difference in the electronic transitions involved. This is very improbable, and it seems a more reasonable hypothesis to suppose that orbitals different in kind from those of  $\text{>C=O}$  in acetaldehyde have to be written for acrolein probably in the ground state, certainly in the upper state. The chemical character of conjugated double bonds suggests some difference of this kind, and the spectroscopic evidence, both of accumulated experience of past work in molecules with conjugated double bonds\* and also of this research seem fairly decisive. That is, the electronic systems of  $(\text{C}=\text{C}=\text{O})$  in acrolein is definitely not similar to the system of  $(\text{C}=\text{C}=\text{O})$

H

H

in acetaldehyde in the sense that the system of  $(\text{C}=\text{C}=\text{O})$  in all the

H

saturated aldehydes examined is similar to that existing in acetaldehyde.

\* Lowry and French, 'J. Chem. Soc.,' vol. 125, p. 1921 (1924).

This conclusion is supported by all the data in the present paper, *e.g.*—

- (1) The difference in rotational structure of acrolein and acetaldehyde.
- (2) The difference in the vibrational frequencies of the upper states of those molecules (which were seen to remain remarkably constant through the series of saturated aldehydes).
- (3) The change in position and intensity of the electronic band system, the point of maximum intensity being situated at  $35263\text{ cm}^{-1}$  for acetaldehyde but displaced to  $29976\text{ cm}^{-1}$  for acrolein. The investigation of the saturated aldehydes has shown how little sensitive the ordinary "aldehyde" transition is to considerable changes in the molecule. This seems generally true of transitions due to many kinds of electronic groups in molecules; and is correlative with the persistence through a series of molecules of chemical properties attributable to a common group. A change of the order of  $5300\text{ cm}^{-1}$  in such transitions as the "aldehyde" (*i.e.*, " $\text{C}=\text{O}$ ") must apparently be regarded as a very drastic one corresponding to a real difference of the upper states, ground states, or both.
- (4) The change in position and intensity of the short wave-length absorption region from that of ordinary "ethylenic" molecules. (This region is markedly different from that of  $\text{>C}=\text{C}<$  molecules already studied,\* in the same way as the long wave-length system is different from the normal bands of  $\text{>C}=\text{O}$ ).†

From these facts, the difference in kind of upper state between acrolein and the saturated aldehydes seems almost certain. The difference between the ground states, though probable, is not established by our results; we hope to revert to this point in a later paper.

We wish to express our thanks to Professor W. L. Bragg for permission to use the grating installation of the Manchester University Physical Laboratory, to Mr. A. Baxter for the microphotograms, and to the Department of Scientific and Industrial Research for a grant which made the work possible.

#### SUMMARY

The absorption spectrum of acrolein vapour has been measured under high dispersion. A vibrational analysis gives probable values of fre-

\* Snow and Allsopp, 'Trans. Faraday Soc.', vol. 30, p. 93 (1934).

† (3) and (4) may possibly be due to the quantum mechanical repulsion of two energy curves  $\text{>C}=\text{C}<$  and  $\text{>C}=\text{O}$  lying close together.

quencies of the upper state as  $1270\text{ cm}^{-1}$  and  $500\text{ cm}^{-1}$ . By comparison with the spectrum of crotonaldehyde which has been similarly examined, the frequency of  $500\text{ cm}^{-1}$  is attributed to an oscillation of the methylene group about the  $\text{C}=\text{C}$  double bond.

The upper state is different in kind from that of the saturated aldehydes.

A fine structure, probably of rotational origin, is found in nine bands of acrolein (but not for crotonaldehyde); each series is single and can be represented, like the R-branch of a diatomic molecule, by a parabolic formula. The constants of the formulæ, however, give divergent results for the moment of inertia of the ground state of the molecule.

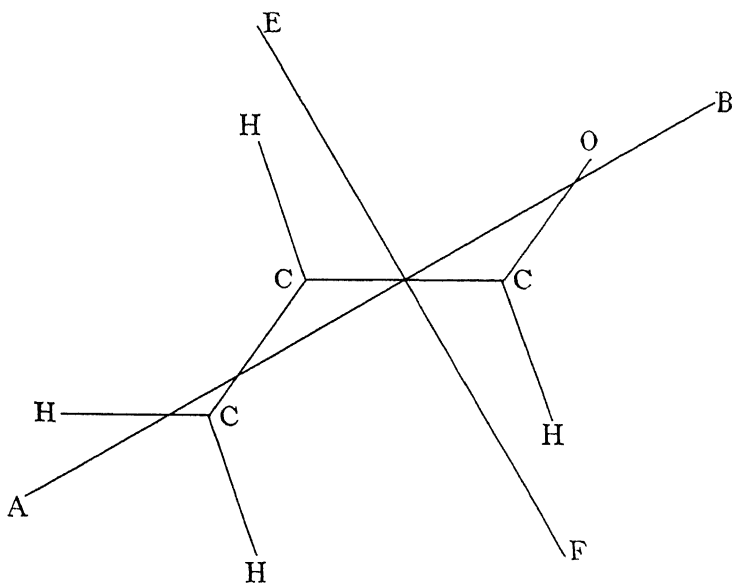


FIG. 10

[*Note added in proof, March 27, 1935*—We have recently carried out a high dispersion investigation of the absorption spectrum of monomeric glyoxal vapour, the complete results of which will be published later. The spectrum, however, is extremely sharp and possesses many features in common with that of acrolein. This is very suggestive in view of the fact that acrolein may be considered as arising from glyoxal by the substitution of an iso-electronic  $\text{CH}_2$  group for one of the oxygen atoms of the latter molecule. Consideration of the various bond directions indicates that both molecules are very probably plane, and by use of known interatomic distances the centre of gravity of acrolein proves to be situated almost exactly at the mid-point of the  $\text{C}-\text{C}$  bond, *i.e.*, coinciding with that of glyoxal. The principal axes of inertia through

this point are likewise almost superposed. From the values of the principal moments of inertia the asymmetry factor in both cases comes out to be about 0.003, indicating probable small departure from symmetrical top behaviour, whilst the value of  $B''_x$  for acrolein proves to be 1.46, thus agreeing closely with the value 1.514 deduced from the band A. Similar agreement has been found for glyoxal, whilst the bands for this substance appear to be of the true symmetrical top type suggested by the smallness of the estimated asymmetry factor. It therefore seems feasible that a rotational motion about the indicated axis of least inertia AB, fig. 10, is responsible for the acrolein fine structure, the sub-bands possessing Q-branches only which, due to the large moment of inertia about EF and its constancy during electronic transition, appear as single, rather diffuse lines as actually observed. Further, in such a complex molecule as this, the configurations of the vibrational upper states corresponding to the various bands will certainly be different. Since, however, the ground level of given symmetry combining with a given upper level must possess the same symmetry as this upper level, it follows that the ground states from which the various bands originate cannot be identical nor yield absolutely the same  $B''$  values. For ground state configurations widely divergent from that indicated, the resulting large moments of inertia and molecular asymmetry would very probably render the structure quite continuous, and it may well be that to this effect the continuum must be ascribed, which completely masks the P-branch.]

---

# Statistical Error in Counting Experiments

By R. PEIERLS, University of Manchester

(Communicated by R. H. Fowler, F.R.S.—Received November 27, 1934)

## 1—INTRODUCTION

Experiments in which single particles are studied with the aid of counters would, in principle, lead to an exact determination of the statistical laws governing the behaviour of these particles if the number of counted particles were infinitely large. With a finite number of counts, however, a finite statistical error will always remain.

This error depends upon the number of counts and upon the way in which one makes use of the counter readings to calculate the parameters entering into the statistical laws. The purpose of the following investigation is to show for some typical cases which way of calculating has to be adopted in order to make the error a minimum.

## 2—GENERAL REMARKS ABOUT STATISTICAL ERRORS

The properties of the statistical fluctuations leading to such errors are well known, but, in view of their importance for discussing experimental results, it might be worth while to repeat the principal facts.

In most cases where errors are due to limited accuracy of observations, the arrangement allows errors up to a certain upper limit and all values below this limit are nearly equally probable. The exact magnitude of this maximal error is often difficult to estimate. One then makes several independent observations and takes the range of variation of their results as an estimate for the error. The result obtained by combining these various observations will then have the same relative error as each single observation, unless one has reasons to believe that there is no systematic error which might affect all observations in the same way.

If, however, the error is entirely due to statistical fluctuations, the probability that it should have a value between  $\delta$  and  $\delta + d\delta$  is

$$p(\delta) d\delta = \text{const } e^{-\delta^2/2\delta_0^2} d\delta, \quad (1)$$

where  $\delta_0$  is the mean error. This mean error is frequently quoted in experimental papers, but it must be kept in mind that it represents by no means an upper limit, since the probability that  $\delta$  exceeds  $\delta_0$  is about 0.32.

In this case any two series may be combined to form a bigger series and the error of the result will then be correspondingly smaller.

On the other hand nothing can be gained by considering parts of the observations as separate series and comparing their results. Such comparison can only be useful to make sure that there are no other sources of error besides the fluctuations and an indication of such a source would be given if the differences between various results would be much larger than the mean statistical error.

If, however, the results differ by less than the mean statistical error, this cannot, of course, mean that each series is more accurate than the fluctuations would allow. The difference is itself subject to fluctuations and if in a particular instance it is less than the average, no conclusion can be drawn that just in this instance the results were very near to the true value. If the variation of the results comes out too small, this must be taken as an indication of a fault in the method of counting.

### 3—GENERAL FORMULÆ

This section contains a repetition of well-known statistical laws of which use will be made in the following.

If of a great number  $N$  of independent events each one has a probability  $w_i$ , to occur in the  $i$ th of  $k$  time intervals the probability that exactly  $n_1, n_2, \dots, n_k$  will occur in the first, second,  $\dots$ ,  $k$ th interval respectively is

$$P = \frac{N!}{n_1! n_2! \dots n_k! (N - m)!} w_1^{n_1} w_2^{n_2} \dots w_k^{n_k} (1 - w)^{N-m}. \quad (2)$$

Here  $m = n_1 + n_2 + \dots + n_k =$  total number of observed events,  $w = w_1 + w_2 + \dots + w_k =$  probability for one event to happen in any one of the intervals, and therefore  $1 - w$  the probability for it to happen in none of them.

From (2) one derives readily the average of  $n_i$ ,

$$\overline{n_i} = Nw_i, \quad (3)$$

and the mean value of the products of the fluctuations  $\delta n_i = n_i - \overline{n_i}$ ,

$$\overline{\delta n_\mu \delta n_\nu} \equiv \overline{n_\mu n_\nu} - \overline{n_\mu} \cdot \overline{n_\nu} = \begin{cases} Nw_\mu (1 - w_\mu) & \mu = \nu \\ -Nw_\mu w_\nu & \mu \neq \nu \end{cases}. \quad (4)$$

If  $t_\nu$  is the centre of the  $\nu$ th interval, we will later require the following expression,

$$s = \sum t_\nu n_\nu / m. \quad (5)$$

For its average value and mean square error we have from (3), (4)

$$\bar{s} = \Sigma t_\nu w_\nu / w \quad \overline{\delta s^2} = \Sigma (t_\nu^2 - \bar{s}^2) w_\nu / mw.$$

In the limit of infinitely short intervals,  $s$  becomes the centroid of the distribution of events,

$$s = (t_{\nu_1} + t_{\nu_2} + t_{\nu_3} \dots) / m \quad (5')$$

(where  $t_{\nu_1}, t_{\nu_2}, \dots$ , are the exact times at which the events occurred) and we have

$$\bar{s} = \frac{\int_0^{t_k} t(w)(t) dt}{\int_0^{t_k} w(t) dt} \quad \overline{\delta s^2} = \frac{\int_0^{t_k} (t^2 - \bar{s}^2) w(t) dt}{m \int_0^{t_k} w(t) dt}. \quad (6')$$

#### 4—DETERMINATION OF DECAY CONSTANT. DISCUSSION OF USUAL METHODS

One typical case of the application of counting methods is the following. The particles emitted by a radioactive source are registered as a function of time.\* The source is assumed to decay according to an exponential law so that the average intensity

$$Nw(t) dt = \frac{N}{\tau} e^{-t/\tau} dt. \quad (7)$$

The mean life  $\tau$  is to be determined.

We first treat an idealized case in which the counter has no natural effect and in which we suppose the counting to be continued for a very long time so that practically  $w = 1$  and  $m = N$ .

The following simple ways of determining  $\tau$  are frequently used:—

*a*—One counts the particles emitted during short periods and plots the logarithm of their number against time. One then fits a straight line through the points. The inclination of this line determines  $\tau$ . This method is often useful for qualitative purposes, *i.e.*, to show that the particles are likely to follow a simple exponential law of the form (7). But as with most graphical methods using logarithmic scales it is very difficult to estimate the error. The inclination of the line is greatly influenced by the position of the points corresponding to late times, *i.e.*, small counted numbers. For these the fluctuations lead to a high relative error and their logarithm therefore shows a high absolute error.

\* In practice the counter never registers all particles, but only those emitted into a certain solid angle. Since, however, the number of the latter also follows the law (7) with only a smaller constant  $N$ , this makes no difference to the results.



*b*—The total number  $n_2$  of counts after a suitably chosen time  $l$  is compared with the total number  $N$  of counts. Their ratio ought to be

$$r_0 = e^{-l/\tau}.$$

If the observed ratio is  $r$ , one therefore has approximately

$$\tau = -l/\log r.$$

Here the intervals of counting are 0 to  $l$  and  $l$  to  $\infty$ ; therefore  $w_1 = 1 - e^{-l/\tau}$ ,  $w_2 = e^{-l/\tau}$ . According to (4)

$$\overline{\delta r^2} = \left(\frac{dr}{dn_2}\right)^2 \overline{\delta n_2^2} = \frac{1}{N} w_2 (1 - w_2)$$

and

$$\overline{\delta \tau^2} = \left(\frac{d\tau}{dr}\right)^2 \overline{\delta r^2} = \frac{l^2}{r^2 (\log r)^4} \frac{1}{N} w_2 (1 - w_2).$$

If the error is small we may insert  $r_0 = w_2$  instead of  $r$ ,

$$\overline{\delta \tau^2} = \frac{\tau^2}{N} \left(\frac{\tau}{l}\right)^2 (e^{l/\tau} - 1). \quad (8)$$

The relative error is thus proportional to

$$(e^\xi - 1)/\xi^2$$

(with  $\xi = l/\tau$ ) and becomes a minimum for  $l/\tau = 1.6$ . This minimum is

$$\frac{1}{\tau^2} \overline{\delta \tau^2} = \frac{1}{N} 1.54.$$

The corresponding value of  $n_2/N = e^{-l/\tau}$  is 0.20.

*c*—Another method frequently in use is the following: counts are made for equal time intervals of length  $l$ . If their results are  $n_1, n_2, \dots$ , the following expression is calculated,

$$r = \frac{n_1 + n_3 + \dots}{n_2 + n_4 + \dots}. \quad (9)$$

The statistical average of  $r$  is  $e^{l/\tau}$  so that approximately

$$\tau = l/\log r. \quad (9A)$$

The individual probabilities are in this case

$$w_\nu = e^{-(\nu-1)l/\tau} - e^{-\nu l/\tau} \quad \nu = 1, 2, 3, \dots,$$

and since

$$\overline{\delta r^2} = \sum_{\mu, \nu} \frac{\partial^2 r}{\partial n_\mu \partial n_\nu} \overline{\delta n_\mu \delta n_\nu},$$

we have (cf. (4) )

$$\overline{\delta r^2} = \frac{1}{N} e^{l/\tau} (1 + e^{l/\tau})^2,$$

and

$$\overline{\delta \tau^2} = \frac{l^2}{(\log r)^4} \frac{1}{r^2} \frac{1}{N} e^{l/\tau} (1 + e^{l/\tau})^2,$$

or, inserting  $e^{l/\tau}$  for  $r$ ,

$$\frac{1}{\tau^2} \overline{\delta \tau^2} = \frac{1}{N} \left( \frac{\tau}{l} \right)^2 \frac{(1 + e^{l/\tau})^2}{e^{l/\tau}}. \quad (10)$$

If again  $\xi = l/\tau$  we have to find the minimum of  $(1 + e^\xi)^2/\xi^2 e^\xi$  which is 2.27 at  $\xi = 2.4$ , so that

$$\frac{1}{\tau^2} \overline{\delta \tau^2} = \frac{1}{N} \cdot 2.27,$$

while the number of particles in the second interval compared with that in the first is  $e^{-l/\tau} = 0.09$ .

Method *c* is less efficient than *b* although more complicated.

## 5—DETERMINATION OF DECAY CONSTANT. RIGOROUS TREATMENT

In this section we shall determine the probability that with given counts,  $\tau$  has a certain value. The value for which this probability is a maximum obviously yields the best possible approximation for  $\tau$ .

To avoid later repetition we treat the problem more generally than before by assuming that counts are taken only up to a finite time  $T$ .

We may consider the source to be one of a big number of sources having various "intensities"  $N$  and decay constants  $1/\tau$ . We then select from these sources the group of those which give a certain set of counts. The number of sources in this group that have definite  $N$  and  $\tau$  is proportional to the probability we want to determine.

This number is given by the total number of sources which gives  $N$  and  $\tau$  which we assume to be independent of  $N$  and  $\tau$  over a certain range of values,\* multiplied by the fraction (2) of them that give counts  $n_1 n_2 \dots$

The quantities entering into (2) are now

$$w_\nu = \int_{t_\nu}^{t_{\nu+1}} w(t) dt \quad w(t) = \frac{N}{\tau} e^{-t/\tau}$$

$$w = \int_0^T w(t) dt \quad n = \sum_{\nu=1}^k n_\nu.$$

\* This assumption about the *a priori* probability does not actually matter as long as the mean relative error in  $\tau$  is small compared with unity.

If we assume the intervals to be of a very short length  $dt$  so that all  $n_v$  are either 0 or 1, we have

$$w_v = w(t_v) dt,$$

and, inserting into (2),

$$p = \frac{N!}{(N-m)!} \left(\frac{dt}{\tau}\right)^m \cdot e^{-\sum t_v/\tau} (1-w)^{N-m}. \quad (11)$$

We are not interested in  $N$  and therefore sum the expression with respect to  $N$ :

$$P(\tau) = \sum_N p(N, \tau) = \frac{m!}{w^{m+1}} e^{-\sum t_v/\tau} \left(\frac{dt}{\tau}\right)^m.$$

Dropping the factors  $m!$  and  $(dt)^m$  which do not depend upon  $\tau$

$$P(\tau) = \text{const.} \frac{1}{w} \left[ \frac{1}{w\tau} e^{-s/\tau} \right]^m = \text{const.} \frac{1}{w} [f(\tau)]^m.$$

Here  $s = \sum t_v/m$  denotes the arithmetic mean of the individual times of counting, and  $f$  is the function

$$f = \frac{e^{-s/\tau}}{\tau(1 - e^{-T/\tau})}. \quad (12)$$

Neglecting the slowly varying factor  $w$ , we may determine the maximum of  $f$  instead of that of  $P$ . Since  $m$ , the total number of counts, is large, only values of  $f$  very near to the maximum matter. We may therefore write

$$f = f_0 - \frac{1}{2}(\delta\tau)^2 |f''|$$

and

$$\begin{aligned} P &= \text{const} (1 - \frac{1}{2}\delta\tau^2 |f''/f_0|)^m \\ &= \text{const} e^{-\frac{1}{2}m|f''/f_0|(\delta\tau)^2}. \end{aligned} \quad (13)$$

The mean square error in  $(\tau)$  is therefore  $|f/mf''|$ , taken at the place  $\tau = \tau_0$ .

Equation (12) takes a particularly simple form if, as in the preceding section,  $T$  is very large. We may then neglect  $e^{-T/\tau}$  and have

$$f = e^{-s/\tau}/\tau.$$

This function is a maximum for  $\tau = s$  and  $\frac{f''(s)}{f(s)} = -\frac{1}{s^2}$ . In this particular case we therefore come to the conclusion:

The best approximation to the life time  $\tau$  is the arithmetic mean of the individual times at which particles have been observed and the mean relative error is

$$\frac{1}{\tau^2} \overline{\delta \tau^2} = \frac{1}{N},$$

where  $N$  is the total number of counts (in this case,  $N = m$ ). This result has to be compared with those of 4b and 4c.

If  $T$  is finite, the connection between  $s$  and  $\tau$  is more complicated. The condition  $df/d\tau = 0$  yields

$$\tau - s = \frac{T}{e^{T/\tau} - 1}. \quad (14)$$

TABLE I

$T/\tau$	$T/s$	$\tau/s$	$\sigma$
1.0	2.39	2.392	12.5
1.2	2.48	2.071	9.09
1.4	2.58	1.846	6.71
1.6	2.69	1.680	5.29
1.8	2.80	1.554	4.31
2.0	2.91	1.456	3.63
2.2	3.03	1.378	3.12
2.4	3.16	1.315	2.72
2.6	3.29	1.263	2.41
2.8	3.42	1.221	2.17
3.0	3.56	1.186	1.98
3.5	3.93	1.122	1.65
4.0	4.32	1.081	1.44
4.5	4.74	1.053	1.30
5.0	5.18	1.035	1.21
6	6.09	1.015	1.10
7	7.04	1.006	1.05
8	8.02	1.003	1.02

Equation (14) determines  $\tau$  as a function of  $s$  and  $T$ . For the numerical treatment it is convenient to write the equation in the form

$$1 - \frac{s}{\tau} = \frac{T/\tau}{e^{T/\tau} - 1}$$

and tabulate  $s/\tau$  as a function of  $T/\tau$ . In this way Table I has been obtained. The second and third column of Table I give the connection between the measured  $s$  and the unknown  $\tau$  for any  $T$ .

From (12) we obtain the second derivative at the point  $\tau_0$ ,

$$f'' = -\frac{f}{\tau^2} \left[ 1 - \frac{(\tau - s)(T - s + \tau)}{\tau^2} \right]. \quad (15)$$

The expression

$$\sigma = \frac{m}{\tau^2} \overline{\delta\tau^2} = -\frac{f}{f''} \quad (15')$$

from (15) is given in the last column of Table I.

We note also that according to (14) and (15')

$$d\tau/ds = \sigma. \quad (15'')$$

The formulæ given above allow us to express the life time in terms of the arithmetic mean  $s = \Sigma t_\nu/m$ . In order to determine  $s$  it is not really necessary to know all  $t_\nu$  separately, but it is sufficient to count the number of particles emitted during intervals that are sufficiently short compared with  $\tau$ .

If  $n_\nu$  is again the number of counts during the  $\nu$ th interval

$$(t_\nu < t < t_\nu + d)$$

and  $s_\nu$  the actual centroid of the times of counting during this interval, we have

$$s = \frac{\Sigma n_\nu s_\nu}{\Sigma n_\nu} = \frac{1}{m} \Sigma n_\nu s_\nu, \quad (16)$$

$s_\nu$  is not known since we do not know the distribution of counts over each interval. We may, however, replace it by its average value, which we obtain by applying (6') to the series of counts within this interval:

$$\bar{s}_\nu = t_\nu + \frac{\int_{t_\nu}^{t_\nu+d} twdt}{\int_{t_\nu}^{t_\nu+d} wdt} = t_\nu + \tau - \frac{d}{e^{d/\tau} - 1}.$$

If  $d \ll \tau$ ,

$$\bar{s}_\nu = t_\nu + \frac{1}{2}d - \frac{1}{12}\frac{d^2}{\tau} + \frac{23}{360}\frac{d^4}{\tau^3}.$$

We therefore have

$$s = \frac{1}{m} \Sigma_\nu n_\nu (t_\nu + \frac{1}{2}d) - \frac{1}{12}\frac{d^2}{\tau} + \frac{23}{360}\frac{d^4}{\tau^3}. \quad (17)$$

For  $d < 0.3\tau$  the last term is practically negligible, the second may be considered as a correction.

The error involved by inserting the average value  $\bar{s}_v$  instead of  $s_v$  is according to (6')

$$\overline{\delta s_v^2} = \frac{1}{n_v} \frac{\int w (t^2 - \bar{s}_v^2) dt}{\int w dt} = \frac{d^2}{12n_v}.$$

Correspondingly

$$\overline{\delta s^2} = \frac{d^2}{12m^2} \Sigma n_v = \frac{d^2}{12m}. \quad (18)$$

This error will result in an error in  $\tau$ :

$$\overline{\delta \tau^2} = \left( \frac{d\tau}{ds} \right)^2 \frac{d^2}{12m},$$

$d\tau/ds$  is of order unity unless  $T$  is very small. Since the statistical error is always at least  $\tau^2/m$  the increase of this error due to the finite length of the intervals will in all practical cases be negligible. In spite of this one should avoid making the intervals much longer than  $0.3\tau$ , since then the evaluation of  $\tau$  from the results becomes more complicated.

In general the procedure of determining  $\tau$  would be as follows: divide the total time  $T$  available into intervals of length  $d < 0.3\tau$ ,\* and count the particles during each of them. If the counts are  $n_1, n_2, \dots$ , and their sum  $m$ , form

$$s_0 = (n_1 + 3n_2 + 5n_3 + \dots) d/2m$$

as a first approximation for  $s$ . Insert the corresponding value of  $T/s$  into Table I and determine  $\tau/s$  and from this  $\tau$ . With this value obtain (if necessary) a second approximation for  $s$  from

$$s_1 = -\frac{1}{12} \frac{d^2}{\tau},$$

and correspondingly the correction for  $\tau$  (cf. (15'')),

$$\tau_1 = \frac{d\tau}{ds} s_1 = \sigma s_1,$$

taking  $\sigma$  from Table I. The error of this method consists of the pure statistical error (15') (cf. Table I) and of the error of the evaluation which is less than 1%.

\* If the number of counts is small so that the error is anyhow large, longer intervals may be taken.

## 6—MOST EFFICIENT LENGTH OF SERIES\*

In practice the following problem is of interest. An artificial radioactive source can be reproduced *ad libitum*. Its decay constant is to be determined. Each source is, for this purpose, subject to measurements during a time  $T$ , then it is activated again or replaced by a new source. What is the value of  $T$  that leads to the highest accuracy in a given time?

We neglect the time necessary for replacing the source.

If in each single series  $m$  particles are counted the mean square relative error of each series will be (cf. (15'))

$$\sigma/m,$$

where  $\sigma$  is the quantity tabulated in Table I. Correspondingly if  $z$  series are made the error will be

$$\sigma/mz.$$

Here  $m$  may be expressed as

$$m = N(1 - e^{-T/\tau}),$$

where  $N$  depends no longer upon  $T$  but only upon the intensity of activation.

TABLE II

$T/\tau$	$\frac{\sigma T/\tau}{1 - e^{-T/\tau}}$
1.0	19.8
2.0	8.40
3.0	6.25
3.5	5.96
4.0	5.87
4.5	5.91
5.0	6.09
6	6.61
7	7.36

If we now keep  $zT$ , the total time of measuring, constant, the error will be proportional

$$\frac{T\sigma}{1 - e^{-T/\tau}},$$

and we have to choose  $T$  so as to make this a minimum. According to Table II this means  $T \sim 4\tau$  so that the fraction of particles we miss is

\* I am indebted to W. Ehrenberg for pointing out this problem.

only about 2% of the total. For such small intensities the natural effect of the counter will already be of importance.

# 7—NATURAL EFFECT. APPROXIMATE TREATMENT

Apart from counts due to the particles under investigation every counter shows a certain natural effect. Let  $\alpha$  be the average number of these "blind" counts per unit time, and denote by  $m_c$  and  $s_c$  the total number of actual counts and their centroid. If then  $m_n$  and  $s_n$  denote the (unknown) number and centroid for the "blind" counts, the centroid of the true counts will obviously be

$$s = \frac{m_c s_c - m_n s_n}{m_c - m_n}. \quad (19)$$

Approximately we may insert instead of the unknown quantities  $m_n$  and  $s_n$  their statistical expectation values  $\alpha T$  and  $\frac{1}{2}T$

$$s = \frac{m_c s_c - \frac{1}{2}\alpha T^2}{m_c - \alpha T}. \quad (20)$$

If we denote by  $\delta m_n$  and  $\delta m_n s_n$  the deviations of  $m_n$  and  $m_n s_n$  from their statistical expectation, the error in (20) will be

$$\delta s = \frac{\partial s}{\partial m_n} \delta m_n + \frac{\partial s}{\partial (m_n s_n)} \delta (m_n s_n) = \frac{-\delta (m_n s_n) + s \delta m_n}{m_c - \alpha T},$$

and its mean square

$$\overline{\delta s^2} = \frac{\overline{\delta (m_n s_n)^2} - 2s \overline{\delta m_n \delta m_n s_n} + s^2 \overline{\delta m_n^2}}{(m_c - \alpha T)^2}. \quad (21)$$

The values of  $\overline{\delta m_n^2}$  and  $\overline{\delta s_n^2}$  may be obtained from (4) and (6) by letting  $N \rightarrow \infty$  and  $wN \rightarrow \alpha dt$ :

$$\overline{\delta m_n^2} = \alpha T$$

$$\overline{\delta s_n^2} = \frac{1}{3m_n^2} [(T - s_n)^3 + s_n^3]/T.$$

Since  $m_n$  and  $s_n$  are statistically independent, we have therefore

$$\overline{\delta s^2} = \frac{\alpha T \left[ \frac{1}{3} \frac{(T - s_n)^3 + s_n^3}{T} + (s - s_n)^2 \right]}{(m_c - \alpha T)^2},$$



or, by inserting  $s_n = T/2$

$$\overline{\delta s^2} = \frac{\alpha [(T-s)^3 + s^3]}{3m^2}. \quad (22)$$

The mean square of the error in  $\tau$  is the sum of the squares of the ordinary statistical error given in Table I and the error due to the fluctuations of  $s$  according to (22). We therefore have

$$\frac{1}{\tau^2} \overline{\delta \tau^2} = \frac{\sigma}{m} + \frac{1}{\tau^2} \left( \frac{d\tau}{ds} \right)^2 \overline{\delta s^2}.$$

Noting (22) and (15'')

$$\frac{m}{\tau^2} \overline{\delta \tau^2} = \sigma + \frac{\alpha T}{3m} \sigma^2 \left[ \frac{(T-s)^3 + s^3}{\tau^3} \right]. \quad (23)$$

Here  $m$ , the total number of true counts, depends upon the time of observation  $T$ :

$$m = N(1 - e^{-T/\tau}).$$

We therefore have

$$\frac{N}{\tau^2} \overline{\delta \tau^2} = \frac{\sigma}{1 - e^{-T/\tau}} + \frac{1}{3\lambda} \left( \frac{\sigma}{1 - e^{-T/\tau}} \right)^2 \left[ \frac{(T-s)^3 + s^3}{\tau^3} \right] \equiv A + \frac{1}{\lambda} B, \quad (24)$$

where now  $N$  is independent of  $T$ .  $\lambda = N/\alpha\tau$  is the ratio of the intensity at  $t = 0$  to the natural effect. One will in general try to make  $\lambda$  as large as the counter permits. The largest value of  $\lambda$  for which the counter works satisfactorily is called the resolving power.

Equation (24) is evidently large for small  $T$ , and it increases again for large  $T$ , since increasing  $T$  more and more does not increase the number of "true" counts but only makes the natural effect more and more important. The best choice of  $T$  depends upon  $\tau$  and  $\lambda$ . Table III gives numerical values of  $A$  and  $B$  and Table IV gives the error (24) as function of  $T/\tau$  for various  $\lambda$ .

Table V contains the most suitable values of  $T/\tau$  and the corresponding minimum values of the mean square error as function of  $\lambda$ .

The actual procedure of measuring a decay constant is then the same as that described at the end of section 5, with the addition that the length  $T$  of the series is not arbitrary but has to be determined from Table V according to the ratio  $\lambda$  of initial intensity and natural effect and that from the actual counter readings one must subtract the average natural effect. The error is then given in the third column of Table V or, for intermediate values of  $\lambda$  may be calculated from (24) and Table III.

TABLE III

$T/\tau$	A	B
1.0	19.8	14.1
1.2	13.0	13.4
1.4	8.90	11.9
1.6	6.63	11.4
1.8	5.16	11.2
2.0	4.20	11.4
2.2	3.51	11.6
2.4	2.99	11.9
2.6	2.60	12.4
2.8	2.31	13.1
3.0	2.08	13.9
3.5	1.70	16.7
4.0	1.47	20.6
4.5	1.38	25.7
5.0	1.22	32.5
6	1.10	51.3
7	1.05	80
8	1.02	119

TABLE IV

$\lambda = 2$		$\lambda = 10$		$\lambda = 30$		$\lambda = 100$	
$T/\tau$	$N\delta\tau^2/\tau^2$	$T/\tau$	$N\delta\tau^2/\tau^2$	$T/\tau$	$N\delta\tau^2/\tau^2$	$T/\tau$	$N\delta\tau^2/\tau^2$
2.0	9.9	2.4	4.18	2.8	2.75	3.5	1.87
2.2	9.3	2.6	3.84	3.0	2.54	4.0	1.68
2.4	8.9	2.8	3.62	3.5	2.26	4.5	1.57
2.6	8.8	3.0	3.47	4.0	2.16	5	1.54
2.8	8.9	3.5	3.37	4.5	2.17	6	1.61
3.0	9.0	4.0	3.53	5.0	2.30	7	1.85
3.50	10.1	4.5	3.83	6.0	2.80	8	2.21

TABLE V

$\lambda$	$T/\tau$	$N\delta\tau^2/\tau^2$	
		§ 7	§ 8
2	2.6	8.8	6.41
10	3.5	3.37	2.7
30	4.0	2.16	—
100	5	1.54	1.39

## 8—NATURAL EFFECT. RIGOROUS TREATMENT

Instead of subtracting the average natural effect one can, more rigorously, put the problem of finding the most probable mean life, provided the actual counts (including the natural effect) and the average natural effect are known. This problem can be treated by a method analogous to that of section 3. The method will be developed in this section and it will turn out that the increase in accuracy as compared with the preceding section does not outweigh the increase in complication.

Suppose  $M$  particles have been observed at the individual times  $t_1, t_2, \dots, t_m$  between 0 and  $T$ . For each individual particle the probability that it would be emitted between  $t$  and  $t + dt$  was

$$w dt = \text{const} \left( \alpha + \frac{N}{\tau} e^{-t/\tau} \right) dt,$$

where  $\alpha$  is again the mean intensity of the natural effect, and  $N$  the (unknown) total number of "true" counts.

The constant has to be so chosen that

$$\int w dt = 1.$$

Therefore

$$w dt = \frac{w_0(t)}{a_0} dt,$$

with

$$w_0(t) = \alpha + (N/\tau) e^{-t/\tau}, \quad (25)$$

and

$$a_0 = \int_0^T w_0(t) dt = \alpha T + N.$$

In the last equation  $e^{-T/\tau}$  has been neglected compared with unity and throughout this section we shall assume that  $T$  is very large.

Consequently (2) yields

$$p = M! w_0(t_1) w_0(t_2) \dots w_0(t_M) (dt/a_0)^M,$$

after dropping factors that do not depend upon either  $N$  or  $\tau$  we have

$$p = \text{const} e^{\sum_{v=1}^M \log w_0(t_v) - M \log a_0}. \quad (26)$$

We have now to determine the most probable value of  $\tau$  and the intensity  $N$  of the source. For this purpose we must choose that pair of values for which  $p$ , or, more conveniently,  $\log p$  is a maximum.

$$\frac{\partial \log p}{\partial N} = \frac{\partial \log p}{\partial \tau} = 0.$$

This leads to

$$\sum_{\nu} \left( 1 + \frac{\alpha\tau}{N} e^{t_{\nu}/\tau} \right)^{-1} = MN/(\alpha\tau + N)$$

$$\sum_{\nu} (t_{\nu} - \tau) \left( 1 + \frac{\alpha\tau}{N} e^{t_{\nu}/\tau} \right)^{-1} = 0.$$

If  $T$  is sufficiently large we may neglect the fluctuations of the total number of particles,  $M$ , and assume it to be equal to its expectation value,  $\alpha T + N$ . We have then the two equations,

$$\left. \begin{aligned} N &= \sum_{\nu=1}^M \left( 1 + \frac{\alpha\tau}{N} e^{t_{\nu}/\tau} \right) \\ N\tau &= \sum_{\nu=1}^M t_{\nu} \left( 1 + \frac{\alpha\tau}{N} e^{t_{\nu}/\tau} \right)^{-1} \end{aligned} \right\}, \quad (27)$$

for the simultaneous determination of  $N$  and  $\tau$ .

Equations (27) have a simple meaning:  $\frac{\alpha\tau}{N} e^{t_{\nu}/\tau}$  would be the ratio between "blind" and "true" counts if they were distributed according to statistical expectation. According to (27) the correct procedure does not consist in replacing the number of "blind" counts by its statistical average, as we did in the preceding section, but rather in doing so with the ratio between "blind" and "true" counts. So if in a certain interval of time the number of counts is much greater than it ought to be in the average, we must not ascribe all the excess counts to the "true" particles, but must assume that both the "blind" and the "true" counts exceed their expectation values by the same relative amount. That this makes the error less can be seen, *e.g.*, from the fact that this procedure entirely cuts out the very late particles which are certainly due to natural effect, since the source has already decayed, while with the first method we would go on ascribing all (positive and negative) fluctuations to the "true" particles.

The handling of the simultaneous equations (27) is extremely difficult. They simplify considerably if  $\lambda = N/\alpha\tau$  is very large. In this case  $(1 + e^{t/\tau}/\lambda)^{-1}$  is practically unity up to a certain time  $t_0$  and vanishes for  $t > t_0$  while it passes the intermediate values rapidly in the neighbourhood of  $t_0$ .  $t_0$  is defined as

$$t_0 = \tau \log tN/\alpha\tau.$$

We may then replace (27) by

$$\left. \begin{aligned} \alpha\tau e^{-t/\tau} &= N(t_0) \\ \tau N(t_0) &= \sum_{t_{\nu} < t_0} t_{\nu} \end{aligned} \right\}, \quad (27')$$

where the symbol  $N(t_0)$  means the total number of counts before  $t = t_0$ . (27') are much easier to handle than (27) but they are a sufficiently good approximation only for extremely high values of  $\lambda$ , which are of little practical importance.

The mean square error of  $\tau$ , if  $\tau$  is determined from (27), becomes

$$\overline{\delta\tau^2} = p_0 \left( \frac{d^2 p}{d\tau^2} \right)_0^{-1} = \left( \frac{d^2 \log p}{d\tau^2} \right)^{-1}.$$

Here the suffix 0 indicates the value at the maximum and in taking the derivative  $n$  has to be considered a function of  $\tau$ . The result is

$$\frac{N}{\tau^2} \overline{\delta\tau^2} = \left\{ 1 - \frac{1}{N} \sum_v \frac{(1 - t_v/\tau)^2}{(1 + e^{t_v/\tau}/\lambda)(1 + \lambda e^{-t_v/\tau})} - \frac{\left[ \frac{1}{\lambda} \sum_v \frac{(1 - t_v/\tau)}{(1 + e^{t_v/\tau}/\lambda)(1 + \lambda e^{-t_v/\tau})} \right]^2}{1 - \sum_v \frac{1}{(1 + e^{t_v/\tau}/\lambda)(1 + \lambda e^{-t_v/\tau})}} \right\}^{-1}.$$

In evaluating this error we may assume that the counts are distributed according to statistical expectation, *i.e.*, that the number of counts per unit time is

$$\frac{N}{\tau} e^{-t/\tau} + \alpha.$$

We have then

$$\frac{N}{\tau^2} \overline{\delta\tau^2} = \left\{ 1 - \frac{1}{\lambda} \int_0^\infty \frac{(1-u)^2 du}{1 + e^u/\lambda} - \frac{\left[ \frac{1}{\lambda} \int_0^\infty \frac{(1-u) du}{1 + e^u/\lambda} \right]^2}{1 - \frac{1}{\lambda} \int_0^\infty \frac{du}{1 + e^u/\lambda}} \right\}^{-1}, \quad (28)$$

where again  $\lambda = N/\alpha\tau$ .

For extremely large values of  $\lambda$  (28) simplifies by the same method that led to (27'). For  $\lambda \sim 100$  this approximation is, however, insufficient and we have therefore computed the integrals in (28) numerically for  $\lambda = 2, 10$  and  $100$ . The third column of Table IV gives the results, while the second column contains the mean square error of the method of section 7. One sees that the error of section 7 is not much greater than (28). Since (28) has been obtained with the method of inverse probabilities and therefore gives the least possible error, we may conclude that the primitive method of section 7 is a satisfactory approximation.

#### 9—DETERMINATION OF ABSORPTION COEFFICIENT

Another important application of counting methods is the determination of absorption coefficients.

Suppose that a particle, striking an absorption screen, has a probability  $1 - q$  of being retained and  $q$  of getting through. Then of  $n$ -particles in the average

$$\bar{v} = qn \quad (29)$$

will pass, while the fluctuations of this number will be

$$\overline{\delta v^2} = q(1 - q)n. \quad (30)$$

The number  $n$  of particles falling on the screen is in general not known, but has to be determined by observing the source without screen during a time interval  $t_1$  and with screen during an interval  $t_2$ . If  $n_1$  and  $n_2$  are the numbers emitted during these periods, and  $v_2$  the number that passed the screen, we obviously have

$$q = \frac{v_2}{n_2} = \frac{v_2}{n_1} \cdot \frac{n_1}{n_2} \quad (31)$$

with an error

$$\overline{\delta q^2} = \left( \frac{\partial q}{\partial v_2} \right)^2 \overline{\delta v_2^2} = \frac{q(1 - q)}{n_2}. \quad (32)$$

If we now replace  $n_1/n_2$  in (31) by the average ratio of particles emitted during the corresponding intervals:

$$q = \frac{v_2}{n_1} \frac{w_1}{w_2}, \quad (33)$$

we introduce a new source of error:

$$\overline{\delta \left( \frac{n_1}{n_2} \right)^2} = \frac{1}{n_2^2} \overline{\delta n_1^2} + \frac{n_1^2}{n_2^4} \overline{\delta n_2^2} - 2 \frac{n_1}{n_2} \overline{\delta n_1 \delta n_2},$$

or, according to (4)

$$\overline{\delta (n_1/n_2)^2} = \frac{1}{n_2} \left( \frac{w_1}{w_2} + \frac{w_1^2}{w_2^2} \right).$$

This gives rise to a new error in  $q$ :

$$\overline{\delta q^2} = \left( \frac{v_2}{n_1} \right)^2 \cdot \frac{1}{n_2} \left( \frac{w_1}{w_2} + \frac{w_1^2}{w_2^2} \right). \quad (34)$$

This has to be added to (32). Introducing the total number of particles emitted during the experiment,  $m = n_1 + n_2$ , and writing  $w_1/w_2 = x$  the total error becomes

$$\overline{\delta q^2} = \frac{q}{m} (1 + x) \left( 1 + \frac{q}{x} \right). \quad (35)$$

In order to make this a minimum, we must choose

$$x = \sqrt{q} \quad (36)$$

and inserting this, we have

$$\overline{\delta q^2} = \frac{1}{m} q (1 + \sqrt{q})^2.$$

Equation (36) means that  $n_1^2 = n_2 v_2$ . *The number of particles observed without screen must be the geometric mean of the number falling on the screen and the number transmitted.*

For this result the detailed distribution of the particles does not matter, it is not important whether  $t_2$  is a short interval during which the source is strong or a longer one nearer to the end of its life. We also have not made use of the fact that the two intervals are continuous, they may consist of many parts so that one counts during short intervals alternatingly with and without screen. The above formulæ then still apply if  $n_2$  and  $n_1$  denote the total number of particles emitted while the screen was on and off respectively and  $v_2$  the total number counted behind the screen.

This latter procedure is advisable to make the result as much as possible independent of the decay curve of the source (which enters into  $w_1$  and  $w_2$ ) if the decay constant of the latter is not accurately known.

If the counter has a natural effect, one obtains  $v_2$  and  $n_1$  as differences between the actually counted figures and the average natural effect. If  $\alpha$  denotes again the average number of "blind" counts per unit time, the additional error introduced by the natural effect is

$$\left. \begin{aligned} \overline{\delta v_2^2} &= \alpha t_2 & \overline{\delta n_1^2} &= \alpha t_1 \\ \overline{\delta q^2} &= \alpha \left( \frac{t_2}{n_2^2} + q^2 \frac{t_1}{n_1^2} \right) \end{aligned} \right\}, \quad (37)$$

so that the total error in  $q$  becomes

$$\overline{\delta q^2} = \frac{q}{m} (1 + x) \left( 1 + \frac{q}{x} \right) + \alpha \left( \frac{t_2}{n_2^2} + q^2 \frac{t_1}{n_1^2} \right). \quad (38)$$

The simplest case is that in which the decay of the source during the measurement may be neglected. In this case

$$t_1/t_2 = w_1/w_2 = n_1/n_2 = x.$$

Introducing the ratio of intensity to natural effect  $\kappa = n_1/\alpha t_1$ :

$$m \overline{\delta q^2} = (1 + x) \left[ q (1 + q/x) + \frac{1}{\kappa} (1 + q^2/x) \right], \quad (39)$$

which becomes a minimum for

$$x = q \sqrt{\frac{1 + 1/\kappa}{q + 1/\kappa}}. \quad (40)$$

When determining the transmission coefficient  $q$  of a screen one must make the ratio of the times of counting with and without screen equal to (40), where  $\kappa$  is the ratio between the intensity without screen and the natural effect. Numerical values of (40) are given in Table VI while

TABLE VI

	$k = \infty$	30	10	3	1
$q = 0$	0.0	0	0	0	0
0.1	0.31	0.28	0.23	0.18	0.13
0.2	0.45	0.42	0.38	0.32	0.26
0.3	0.55	0.53	0.51	0.44	0.37
0.4	0.63	0.62	0.59	0.54	0.48
0.5	0.71	0.69	0.67	0.63	0.57
0.6	0.77	0.77	0.75	0.72	0.67
0.7	0.84	0.83	0.82	0.80	0.76
0.8	0.89	0.89	0.88	0.87	0.84
0.9	0.95	0.95	0.94	0.94	0.92
1.0	1.00	1.0	1.0	1.0	1.0

TABLE VII

	$k = \infty$	30	10	3	1
$q = 0$	0	0.03	0.10	0.33	1.00
0.1	0.15	0.20	0.30	0.60	1.42
0.2	0.42	0.47	0.57	0.92	1.90
0.3	0.72	0.78	0.90	1.30	2.45
0.4	1.06	1.13	1.27	1.74	3.06
0.5	1.46	1.53	1.69	2.22	3.73
0.6	1.88	1.98	2.15	2.75	4.47
0.7	2.37	2.46	2.65	3.33	5.26
0.8	2.86	2.96	3.20	3.95	6.12
0.9	3.42	3.54	3.76	4.62	7.03
1.0	4.00	4.14	4.40	5.33	8.00

Table VII contains the corresponding values of the mean square error in  $q$ , multiplied by the total number of particles which would have been observed if the screen had been off all the time.\* The value of  $q$  is to be obtained by dividing the numbers of particles per unit time with and without screen after subtracting from both the average natural effect.

\* If  $M$  is the total number of particles that have been counted,  $m = M \frac{1 + x}{q + x}$ .



If one takes the decay of the source into account, the error is, according to (38),\* no longer a function of  $n_1$  and  $n_2$ , but depends also upon the arrangement of the intervals. It is obvious that in order to make the error which is due to natural effect as small as possible, one has to observe with screen while the source is strong and without screen while it has already become weaker. In this way the ratio of true counts and natural effect is kept as large as possible throughout the measurement. A complete treatment of (38) is, however, somewhat lengthy, and probably useless since in all cases where the source can be re-activated, the highest accuracy in a given time can be obtained by using the source after each activation only for such a short time that its decay may be neglected.

The author wishes to express his thanks to Dr. C. D. Ellis and to Dr. O. R. Frisch for interesting discussions. The hospitality of Manchester University enabled the calculations to be done.

#### SUMMARY

Various methods of determining the mean life of a source from the counter readings are discussed (section 4) and the method leading to the least error is described (section 5). It is found that the most probable mean life depends only upon the arithmetic mean of the times at which particles have been recorded. If the measurements are continued by re-activating the source over and over again the accuracy reached in the whole series is greatest if one each time lets the source decay to about 2% of its initial intensity before re-activating (section 6). A simple method is given to take the natural effect of the counter into account (section 7). It is shown that this method sufficiently accurately approximates the most probable value of the life time. The formula for the latter is derived in section 8, but it is too complicated for practical use. The determination of an absorption coefficient is discussed (section 9).

\* Here again the error could, in principle, be made less than (38) by applying a method analogous to that of section 8; but this method would be just as difficult to handle as that described in section 8.

---

# On the Spectrum of the Normal Frequencies of a Polar Crystal Lattice

## I.—General Theory

By J. H. C. THOMPSON, Fellow of Merton College, Oxford

(Communicated by E. A. Milne, F.R.S.—Received December 6, 1934)

### INTRODUCTION

In a previous joint paper with M. Born\* the importance of the lattice frequency spectrum in problems concerning the physical properties of the solid state was discussed; and a possible method for its determination was suggested and briefly outlined. This previous note provides a suitable introduction to the present paper, as the method, suggested there, is here used to build up the general theory required for the numerical determination of the lattice frequency spectrum.

The development of the general theory is most easily understood after an examination of the problem in the case of the one-dimensional crystal model.† There, on account of the simplicity of the model, all the mathematical difficulties of the general theory are avoided, and the significance of each step is always apparent.

In the present investigation, the most general type of crystal lattice is considered, but the assumptions of Born's original theory are made concerning the forces between the ions in the crystal. Thus the ions are regarded as charged *particles*, and their interactions are supposed to be *central* forces. The force between any two ions is conveniently resolved into the sum of two terms, the first being the Coulomb electrical interaction of the point charges, while the additional term is a repulsive force (decreasing rapidly with the distance) owing to the internal structure of the ions.

In § 1 certain formulæ are given for the displacement of the lattice particles in a normal mode of vibration.‡ An expression for the electrical charge density of the particles, when displaced in this manner, is obtained

\* 'Proc. Roy. Soc.,' A, vol. 147, p. 594 (1934).

† No account of this simple theory is given here, as one is already available—see Born and Göppert-Mayer, 'Handb. der Physik,' vol. 24 (2), p. 638 (1934).

‡ The results of this section are not new. They are given, in effect, by Born in "Atomtheorie des festen Zustandes," 'Enc. Math. Wiss.,' vol. 5, p. 587.

in § 2; and, from this, an expression for the electrical potential is derived in § 3. In § 4 this expression is transformed into another one, whose second order partial derivatives are sufficiently rapidly convergent for purposes of numerical calculation. Finally, in § 5 the equations of motion of the particles are constructed. From these the "frequency equation" is deduced, with its elements expressed in a form suitable for calculation.\*

### § 1—THE CYCLIC LATTICE: ITS DISPLACEMENT IN A NORMAL MODE OF VIBRATION

We consider a finite piece of crystal of any shape. The sides of the crystal cell are denoted by the vectors  $\mathbf{a}_1$ ,  $\mathbf{a}_2$ ,  $\mathbf{a}_3$ . There are  $s$  particles in each cell, the  $k$ th particle having a charge  $e_k$ .

There are two obvious initial difficulties in determining the motion of the charged particles in this piece of crystal. The first difficulty is the treatment of boundary conditions, while the second lies in the fact that it does not appear possible to determine the total electrical interaction of all the particles acting on one particle, when the particles are displaced from their equilibrium positions in a completely random manner. Both difficulties are overcome by the use of the "cyclic lattice," introduced by Born (*loc. cit.*).

Weyl has shown that the vibrations which determine the inner thermal state of a crystal are almost independent of its shape and boundary conditions,† if the crystal is big enough to contain a large number of elementary cells ( $N$ , say). We accordingly replace the actual boundary conditions by *fictitious* boundary conditions, which are easier to handle mathematically. Using the method of the cyclic lattice, we suppose the shape of our crystal to be the same as the shape of the elementary crystal cell, but with sides  $n\mathbf{a}_1$ ,  $n\mathbf{a}_2$ ,  $n\mathbf{a}_3$ , where  $n^3 = N$  approximately. Thus the number of particles in this "crystal block" is the same as in the original piece of crystal. The fictitious boundary conditions are obtained by supposing this block to be part of an infinite crystal lattice which can be regarded as built up from blocks of this shape and size. The crystal block has  $3sn^2 (= 3sN)$  degrees of freedom just as the original crystal had.

\* The numerical determination of the spectrum for some of the alkali halides has been started. Mallock's calculating machine is used for some of the calculations, and the author is indebted to the Government Grant Committee of the Royal Society for a grant to defray the expenses of these calculations.

† 'Math. Ann.' vol. 71, p. 441 (1911); 'J. reine angew. Math.,' vol. 141, p. 163 (1912) and vol. 143, p. 177 (1914); 'R.C. Circ. mat. Palermo,' vol. 39, p. 1 (1915).

Now, purely from considerations of the geometry of the lattice block, we shall find certain formulæ for the displacement of the particles in a normal mode of vibration. Thus, when constructing the equations of motion of the particles, it will only be necessary to determine the forces acting in this ordered displacement, thus avoiding the difficulty of calculating the forces for a completely random displacement.

Suppose that the particles are vibrating in such a way that the displacement of the  $k$ th particle in the  $l$ th cell ( $l \equiv l_1, l_2, l_3$ , which are whole numbers) is given by\*

$$\mathbf{r}_k^l = \mathbf{r}_k^{0l} + \mathbf{u}_k \exp \{iq\mathbf{s} \cdot (\mathbf{r}_k^{0l} - \mathbf{r}_k^0)\}, \quad (k = 1, 2, \dots s). \quad (1.1)$$

Here  $\mathbf{r}_k^0$  is the vector co-ordinate of the  $k$ th particle in the origin cell in the equilibrium configuration; and the cells are numbered in such a way that the co-ordinate of the  $k$ th particle in the  $l$ th cell in the equilibrium configuration is given by

$$\mathbf{r}_k^{0l} = l_1 \mathbf{a}_1 + l_2 \mathbf{a}_2 + l_3 \mathbf{a}_3 + \mathbf{r}_k^0. \quad (1.2)$$

The vector  $\mathbf{r}_k^l$  is the value of this co-ordinate in the displaced configuration. The equation (1.1) represents a wave-like displacement, with a wave number  $q/2\pi$  and a wave-length  $\lambda = 2\pi/q$ , a maximum displacement of  $\mathbf{u}_k$ , and with the wave normal in a direction represented by the unit vector  $\mathbf{s}$ . Let us restrict (1.1) so that the displacements of corresponding particles in all the blocks of the infinite lattice are the same. This requires

$$\exp \{iq(\mathbf{s} \cdot \mathbf{r}_k^{0l'})\} = \exp \{iq(\mathbf{s} \cdot \mathbf{r}_k^{0l})\},$$

where  $l'$  indicates the cell, which is in the same position in any block as the  $l$ th cell in the given block.

Thus

$$l'_1 = l_1 + m_1 n, \quad l'_2 = l_2 + m_2 n, \quad l'_3 = l_3 + m_3 n,$$

where  $m_1, m_2, m_3$  are whole numbers. From (1.2)

$$\mathbf{r}_k^{0l'} = \mathbf{r}_k^{0l} + m_1 n \mathbf{a}_1 + m_2 n \mathbf{a}_2 + m_3 n \mathbf{a}_3,$$

so that the condition becomes

$$\exp \{iq\mathbf{s} \cdot (m_1 n \mathbf{a}_1 + m_2 n \mathbf{a}_2 + m_3 n \mathbf{a}_3)\} = 1.$$

This is always satisfied if  $nq(\mathbf{s} \cdot \mathbf{a}_1)$ ,  $nq(\mathbf{s} \cdot \mathbf{a}_2)$ ,  $nq(\mathbf{s} \cdot \mathbf{a}_3)$  are multiples of  $2\pi$ , *i.e.*, if

$$q\mathbf{s} = \mathbf{b}_1 \phi_1 + \mathbf{b}_2 \phi_2 + \mathbf{b}_3 \phi_3, \quad (1.3)$$

\* Owing to the complicated formulæ it is not always convenient to put brackets round the vectors in a scalar product, but this does not give rise to any confusion in this paper.

where  $\mathbf{b}_1, \mathbf{b}_2, \mathbf{b}_3$  are the inverse lattice vectors, determined by

$$(\mathbf{a}_i \cdot \mathbf{b}_j) = \delta_{ij},$$

and  $\phi_1, \phi_2, \phi_3$  are multiples of  $2\pi/n$ .

Now it is readily seen that a vibration in which the particles are displaced according to (1.1) and (1.3) is not a vibration in all the  $3n^3$  normal modes, but in  $3s$  modes only. Consider the equations of motion of the  $k$ th particle in the  $l$ th cell, and of the  $k$ th particle in any other cell, the  $m$ th, say. The equations of motion are linear in the displacement components, higher powers being neglected on the assumption that the displacements of the particles are small. Since the lattice is infinite, we see from (1.1) that the circumstances of the  $k$ th particle in the  $m$ th cell differ from those of the  $k$ th particle in the  $l$ th cell only in the fact that the displacement is multiplied by the constant factor  $\exp \{iqs (\mathbf{r}_k^{0m} - \mathbf{r}_k^{0l})\}$ . The two sets of three equations of motion will thus be identical. Of the  $3n^3$  equations of motion of particles of the  $k$ th kind only 3 will be distinct; and of the  $3n^3$  equations of motion of the particles in the block only  $3s$  will be distinct. Thus (1.1) represents a motion of the lattice particles in  $3s$  normal modes only.

Now (1.1) has been restricted by the conditions of the cyclic lattice, *i.e.*,  $\phi_1, \phi_2, \phi_3$  (related to  $qs$  by (1.3)) must be multiples of  $2\pi/n$ . It is easily seen that the increase of  $\phi_1, \phi_2$ , or  $\phi_3$  by a multiple of  $2\pi$  does not cause any change in (1.1). Thus  $\phi_1, \phi_2, \phi_3$  can be confined to a range of  $2\pi$ , and we have

$$\left. \begin{aligned} \phi_1 &= \frac{2\pi r}{n}, & \phi_2 &= \frac{2\pi s}{n}, & \phi_3 &= \frac{2\pi t}{n}, & (r, s, t \text{ integers}), \\ \text{where} & & & & & & \\ & & & & & & -\pi < \phi_1, \phi_2, \phi_3 \leq \pi. \end{aligned} \right\} \quad (1.4)$$

Hence there are just  $n^3$  variations of (1.1), subject to the conditions imposed.

The problem of determining the  $3n^3$  normal frequencies of the block has thus been reduced to  $n^3$  similar problems of finding  $3s$  normal frequencies. We now attempt to determine a typical set of  $3s$  normal frequencies,  $\omega_1, \omega_2, \dots, \omega_{3s}$ , namely, those of the motion represented by (1.1), subject to (1.3) and (1.4). Each  $\omega$  depends on the values of  $\phi_1, \phi_2, \phi_3$ ; and the aggregate of frequencies, regarded as functions of  $\phi_1, \phi_2, \phi_3$ , constitute a discrete spectrum, which we call the "frequency spectrum of the crystal."

## § 2—THE CHARGE DISTRIBUTION IN THE DISPLACED LATTICE

In constructing the equations of motion of the particles in this displaced lattice, the first step is to calculate the resultant force on one particle owing to the action of all the other particles. The sum of the "repulsive forces" is not difficult to calculate directly, since they decrease rapidly with increasing distance. Any assumptions as to the nature of these repulsive forces are most suitably left to the discussion of individual crystals, and have no place in the general theory. But the Coulomb forces decrease so slowly that, even for restricted displacement under consideration, it has not been found possible to calculate their contribution to the resultant force by direct summation. Instead we seek an expression for the charge density of the lattice in such a form that we can obtain a solution of the electromagnetic equation for the Coulomb electric potential.

A suitable expression has already been obtained by Ewald\* in the case when the lattice is in its equilibrium configuration. We derive an expression for the charge density in the displaced configuration from that for the equilibrium configuration in the following manner.

It is necessary to consider the simple lattices composed of each kind of particle separately. We consider an "image space" (denoted by the co-ordinate  $\mathbf{r}'$ ) related to the *real* space of the lattice composed of particles of the  $k$ th kind (denoted by the co-ordinate  $\mathbf{r}$ ) according to

$$\mathbf{r} = \mathbf{r}' + \mathbf{u}_k \exp \{i\mathbf{q}\mathbf{s} \cdot (\mathbf{r}' - \mathbf{r}_k^0)\}. \quad (2.1)$$

Comparison of (2.1) with (1.1) shows that, when  $\mathbf{r} = \mathbf{r}_k^l$ ,  $\mathbf{r}' = \mathbf{r}_k^{0l}$ , i.e., the displaced lattice in real space has as image an undisplaced lattice in the image space.

For the undisplaced lattice Ewald (*loc. cit.*) expanded the charge density in a three-dimensional Fourier series of the type† where

$$\rho'_k = \sum_l \rho'_k{}^l \exp \{i\mathbf{q}^l \cdot (\mathbf{r}' - \mathbf{r}_k^0)\}, \quad (2.21)$$

where

$$\mathbf{q}^l = 2\pi (l_1 \mathbf{b}_1 + l_2 \mathbf{b}_2 + l_3 \mathbf{b}_3), \quad (2.22)$$

and  $\sum_l$  denotes summation for all values of the integers  $l_1, l_2, l_3$ , from

\* 'Ann. Phys.,' vol. 64, p. 253 (1921).

† As in Ewald's paper no attempt is made here at mathematical rigour. We give only a formal derivation of the various formulæ.

$-\infty$  to  $+\infty$ . The orthogonal property of the series for integrals extending over the origin cell is easily verified, so that

$$\rho'_k{}^i = \frac{1}{\Delta} \iiint \rho'_k \exp \{-iq^i \cdot (\mathbf{r}' - \mathbf{r}_k^0)\} dx' dy' dz'.$$

Here the integration extends over the origin cell, and  $\Delta$  denotes the *volume of a cell in the equilibrium configuration*. The only charge is a point charge  $e_k$  at  $\mathbf{r}' = \mathbf{r}_k^0$ , so that

$$\rho'_k{}^i = \frac{e_k}{\Delta}. \quad (2.23)$$

The charge density  $\rho_k$  in the real space is connected with the charge density  $\rho'_k$  of the image space by the equation expressing the conservation of charge in the space transformation. This is

$$\begin{aligned} \rho_k(dx dy dz) &= \rho'_k(dx' dy' dz'), \\ \text{i.e.,} \quad \rho_k &= \rho'_k J \left( \frac{x', y', z'}{x, y, z} \right), \end{aligned} \quad (2.31)$$

since

$$dx' dy' dz' = J \left( \frac{x', y', z'}{x, y, z} \right) dx dy dz.$$

It is sufficient for our purposes to calculate the Jacobian to the first order in  $u_k$ . From (2.1)

$$x = x' + u_{kx} \exp \{iq \cdot \sum_x s_x (x' - x_k^0)\}.$$

Thus

$$\frac{\partial x}{\partial x'} = 1 + iqs_x u_{kx} \exp \{iq \cdot \sum_{x'} s_x (x' - x_k^0)\},$$

and

$$\frac{\partial x}{\partial y'} = iqs_y u_{ky} \exp \{iq \cdot \sum_x s_x (x' - x_k^0)\}.$$

Hence, to the first order in  $u_k$ ,

$$\begin{aligned} J \left( \frac{x, y, z}{x', y', z'} \right) &= 1 + \sum_x iqs_x u_{kx} \exp \{iq \cdot \sum_x s_x (x' - x_k^0)\} \\ &= 1 + iqs \cdot \mathbf{u}_k \exp \{iqs \cdot (\mathbf{r}' - \mathbf{r}_k^0)\}, \end{aligned}$$

so that

$$J \left( \frac{x', y', z'}{x, y, z} \right) = 1 - iqs \cdot \mathbf{u}_k \exp \{iqs \cdot (\mathbf{r}' - \mathbf{r}_k^0)\}. \quad (2.32)$$

From (2.31) and (2.32) we obtain

$$\begin{aligned}\rho_k &= \rho'_k (1 - iqs \cdot \mathbf{u}_k \exp \{iqs \cdot (\mathbf{r}' - \mathbf{r}_k^0)\}) \\ &= \sum_i \frac{e_k}{\Delta} (1 - iqs \cdot \mathbf{u}_k \exp \{iqs \cdot (\mathbf{r}' - \mathbf{r}_k^0)\}) \exp \{iq^l \cdot (\mathbf{r}' - \mathbf{r}_k^0)\}.\end{aligned}$$

In this expression we express  $\mathbf{r}'$  in terms of  $\mathbf{r}$  according to (2.1), retaining only first order terms in  $\mathbf{u}_k$ . Thus

$$\begin{aligned}\rho_k &= \frac{e_k}{\Delta} \sum_i (1 - iqs \cdot \mathbf{u}_k \exp \{iqs \cdot (\mathbf{r}' - \mathbf{r}_k^0)\}) \exp \{iq^l \cdot (\mathbf{r}' - \mathbf{r}_k^0)\} \\ &\quad \times (1 - iq^l \cdot \mathbf{u}_k \exp \{iqs \cdot (\mathbf{r}' - \mathbf{r}_k^0)\}) \\ &= \frac{e_k}{\Delta} \sum_i \exp \{iq^l \cdot (\mathbf{r} - \mathbf{r}_k^0)\} \\ &\quad - \frac{e_k}{\Delta} i \sum_i (\mathbf{q}^l + qs) \cdot \mathbf{u}_k \exp \{i(\mathbf{q}^l + qs) \cdot (\mathbf{r} - \mathbf{r}_k^0)\}.\end{aligned}\quad (2.4)$$

The total charge density of the displaced lattice is obtained from (2.4) by summation over all  $k$ . Here we make use of the fact that the algebraic sum of the charges in a cell is zero, *i.e.*,  $\sum_k e_k = 0$ . The origin term ( $l \equiv 0, 0, 0$ ) of the first series in (2.4) is 1, thus yielding a term  $e_k/\Delta$  to  $\rho_k$ . On summation over  $k$  this gives  $\frac{1}{\Delta} \sum_k e_k = 0$ . Hence

$$\begin{aligned}\rho &= \sum_k \rho_k \\ &= \sum_k \bar{\rho}_k,\end{aligned}\quad (2.51)$$

where

$$\begin{aligned}\bar{\rho}_k &= \frac{e_k}{\Delta} \sum_i \exp \{iq^l \cdot (\mathbf{r} - \mathbf{r}_k^0)\} - \frac{e_k}{\Delta} i \sum_i (\mathbf{q}^l + qs) \cdot \mathbf{u}_k \exp \{i(\mathbf{q}^l + qs) \cdot (\mathbf{r} - \mathbf{r}_k^0)\} \\ &= e_k \rho \{(\mathbf{r} - \mathbf{r}_k^0), \mathbf{u}_k\}.\end{aligned}\quad (2.52)$$

Here

$$\begin{aligned}\rho(\mathbf{r}, \mathbf{u}) &= \frac{1}{\Delta} \sum_i \exp \{iq^l \cdot \mathbf{r}\} - \frac{i}{\Delta} \sum_i (\mathbf{q}^l + qs) \cdot \mathbf{u}_k \exp \{i(\mathbf{q}^l + qs) \cdot \mathbf{r}\} \\ &= \frac{1}{\Delta} \sum_i \exp \{iq^l \cdot \mathbf{r}\} - \frac{\mathbf{u}_k}{\Delta} \cdot \sum_i \mathbf{grad} \exp \{i(\mathbf{q}^l + qs) \cdot \mathbf{r}\}.\end{aligned}\quad (2.53)$$

( $\sum_i$  is used to denote summation over all  $l_1, l_2, l_3$  except the origin term  $0, 0, 0$ ).

The quantity  $\bar{\rho}_k$  is not the charge distribution of the lattice particles of the  $k$ th kind, but is this charge distribution together with a uniform



charge distribution of the same total amount but of opposite sign:  $\rho(\mathbf{r}, \mathbf{u})$  is its value when the charges are unit charges at the corners of the lattice cells. It is an essential step in the argument to get rid of the constant term in  $\rho_k$  since there is no suitable solution of Poisson's equation (or any electromagnetic extension) for a constant density.

### § 3—THE ELECTRIC POTENTIAL

When the charge in a field is stationary, the electric potential (*i.e.*, the potential energy of a charge of 1 e.s.u. in the field) is determined by Poisson's equation,

$$\nabla^2 \Psi = -4\pi\rho.$$

When the charges are moving, however, a correction term must be added to take account of the fact that the interaction of the charges is not instantaneous, but transmitted only with the speed of light.\* Here we neglect magnetic interactions compared with the electric interactions, and the appropriate equation for the electric potential, derived from the electromagnetic theory is†

$$\nabla^2 \Psi - \frac{1}{c^2} \frac{\partial^2 \Psi}{\partial t^2} = -4\pi\rho. \quad (3.11)$$

We suppose that the particles are moving in a normal mode of vibration with frequency  $\omega$ . Thus all displacement components are proportional to  $\exp(i\omega t)$ , so that

$$\frac{\partial}{\partial t} \equiv i\omega.$$

Thus (3.11) reduces to

$$\left( \nabla^2 + \frac{\omega^2}{c^2} \right) \Psi = -4\pi\rho \quad (3.12)$$

$$= -4\pi \sum_k \bar{\rho}_k, \quad (3.13)$$

using the equation (2.51) for  $\rho$ .

Hence

$$\Psi = \sum_k \psi_k, \quad (3.21)$$

where  $\psi_k$  is the solution of

$$\left( \nabla^2 + \frac{\omega^2}{c^2} \right) \psi_k = -4\pi\bar{\rho}_k.$$

\* This might be thought to have only a negligible effect on the vibrations of the particles. We shall see later that, though this is the case in general, the finite speed of transmission is of great importance for modes of vibration where  $q$  is very small, but the normal frequency of vibration is not small.

† See, for instance, Jeans' "Electricity and Magnetism" (5th ed., 1927), p. 570.

From (2.52)

$$\bar{\rho}_k = e_k \rho \{(\mathbf{r} - \mathbf{r}_k^0), \mathbf{u}_k\},$$

so that

$$\psi_k = e_k \psi \{(\mathbf{r} - \mathbf{r}_k^0), \mathbf{u}_k\}, \quad (3.23)$$

where  $\psi(\mathbf{r}, \mathbf{u})$  is the solution of

$$\left(\nabla^2 + \frac{\omega^2}{c^2}\right)\psi = -4\pi\rho(\mathbf{r}, \mathbf{u}), \quad (3.31)$$

$\rho(\mathbf{r}, \mathbf{u})$  being defined by (2.53).

The potential is thus

$$\Psi = \sum_k e_k \psi \{(\mathbf{r} - \mathbf{r}_k^0), \mathbf{u}_k\}, \quad (3.32)$$

and now we require only  $\psi(\mathbf{r}, \mathbf{u})$ , the solution of (3.31).

The solution of (3.31) becomes trivial when we note the effect of the Laplacian operator on an exponential function of the form occurring in (2.53). If  $\mathbf{a}$  is any vector,

$$\nabla^2 \exp(i\mathbf{a} \cdot \mathbf{r}) = \sum_x (ia_x)^2 \exp(i\mathbf{a} \cdot \mathbf{r}) = -|\mathbf{a}|^2 \exp(i\mathbf{a} \cdot \mathbf{r}).$$

Thus

$$\nabla^2 \exp(i\mathbf{q}^l \cdot \mathbf{r}) = -|\mathbf{q}^l|^2 \exp(i\mathbf{q}^l \cdot \mathbf{r}),$$

and

$$\nabla^2 \exp\{i(\mathbf{q}^l + \mathbf{qs}) \cdot \mathbf{r}\} = -|\mathbf{q}^l + \mathbf{qs}|^2 \exp\{i(\mathbf{q}^l + \mathbf{qs}) \cdot \mathbf{r}\}.$$

Hence the solution of (3.31) will be

$$\psi(\mathbf{r}, \mathbf{u}) = \psi_0(\mathbf{r}) - \mathbf{u} \cdot \text{grad } \psi_1(\mathbf{r}), \quad (3.41)$$

where

$$\psi_0(\mathbf{r}) = \frac{4\pi}{\Delta} \sum_i \frac{\exp(i\mathbf{q}^l \cdot \mathbf{r})}{|\mathbf{q}^l|^2 - \frac{\omega^2}{c^2}}, \quad (3.42)$$

and\*

$$\psi_1(\mathbf{r}) = \frac{4\pi}{\Delta} \sum_i \frac{\exp\{i(\mathbf{q}^l + \mathbf{qs}) \cdot \mathbf{r}\}}{|\mathbf{q}^l + \mathbf{qs}|^2 - \frac{\omega^2}{c^2}}. \quad (3.43)$$

\* On account of the conditions previously imposed this solution for  $\Psi$  must be periodic in  $\phi_1, \phi_2, \phi_3$  with period  $2\pi$ . Now  $\phi_1, \phi_2, \phi_3$  only occur in  $\psi_1$ , and there in the form  $\mathbf{q}^l + \mathbf{qs}$ . From (1.3) and (2.22)

$$\mathbf{q}^l + \mathbf{qs} = 2\pi \left\{ \mathbf{b}_1 \left( l_1 + \frac{\phi_1}{2\pi} \right) + \mathbf{b}_2 \left( l_2 + \frac{\phi_2}{2\pi} \right) + \mathbf{b}_3 \left( l_3 + \frac{\phi_3}{2\pi} \right) \right\}.$$

Thus the effect of increasing  $\phi_1, \phi_2$ , or  $\phi_3$  by a multiple of  $2\pi$  is the same as that of increasing  $l_1, l_2$ , or  $l_3$  by an integer. This is simply a shift of the terms in the sum representing  $\psi_1$ . This leaves the value of the sum unchanged, since it is a triple sum extending from  $-\infty, -\infty, -\infty$  to  $+\infty, +\infty, +\infty$  and has no terms missing.

In the construction of the equations of motion of a particle (of the  $k$ th particle in the origin cell, say) we shall need, not the potential of the whole lattice, but the potential of the whole lattice minus this particular particle. If  $\bar{\Psi}^k$  is this potential, then

$$\bar{\Psi}^k = \Psi - \frac{e_k}{|\mathbf{r} - \mathbf{r}_k|}, \quad (3.51)$$

where  $\mathbf{r}_k$  is the co-ordinate of the (displaced) position of the  $k$ th particle and is obtained from (1.1) by putting  $l \equiv 0, 0, 0$ . Thus, to the first order in  $\mathbf{u}_k$ ,

$$\mathbf{r}_k = \mathbf{r}_k^0 + \mathbf{u}_k. \quad (3.52)$$

The expression (3.51) will be unsuitable in its present form as we shall require its value when  $\mathbf{r} = \mathbf{r}_k$ , in which case the additional term has a zero denominator. But the potential  $\psi_k$  must also become infinite at any point occupied by one of its lattice particles; so we take the additional term with  $\psi_k$ , and evaluate the resultant before proceeding to the limit.

Substituting for  $\Psi$  in (3.51) according to (3.21), we obtain

$$\bar{\Psi}^k = \sum_{k' \neq k} \psi_{k'} + \bar{\psi}_k, \quad (3.53)$$

where

$$\bar{\psi}_k = \psi_k - \frac{e_k}{|\mathbf{r} - \mathbf{r}_k|}.$$

Now

$$\frac{1}{|\mathbf{r} - \mathbf{r}_k|} = \frac{1}{|(\mathbf{r} - \mathbf{r}_k^0) - \mathbf{u}_k|} = \frac{1}{|\mathbf{r} - \mathbf{r}_k^0|} - \mathbf{u}_k \cdot \text{grad} \frac{1}{|\mathbf{r} - \mathbf{r}_k^0|},$$

to the first order in  $\mathbf{u}_k$ . Using (3.23) for  $\psi_k$ , we see that

$$\bar{\psi}_k = e_k \bar{\psi} \{(\mathbf{r} - \mathbf{r}_k^0), \mathbf{u}_k\}, \quad (3.54)$$

where

$$\bar{\psi}(\mathbf{r}, \mathbf{u}) = \bar{\psi}_0(\mathbf{r}) - \mathbf{u} \cdot \text{grad} \bar{\psi}_1(\mathbf{r}). \quad (3.61)$$

Here

$$\bar{\psi}_0(\mathbf{r}) = \psi_0(\mathbf{r}) - \frac{1}{|\mathbf{r}|}, \quad (3.62)$$

and

$$\bar{\psi}_1(\mathbf{r}) = \psi_1(\mathbf{r}) - \frac{1}{|\mathbf{r}|}. \quad (3.63)$$

#### § 4—TRANSFORMATION OF THE POTENTIAL FUNCTIONS

The expressions obtained for the various potential functions are all too slowly convergent for purposes of calculation, and their second order

derivations, which we shall require, are actually divergent when obtained by term by term differentiation. Before differentiation it is therefore necessary to transform them into more rapidly convergent series, and also to obtain suitable expressions for  $\bar{\Psi}_0(\mathbf{r})$  and  $\bar{\Psi}_1(\mathbf{r})$ .

In his calculation of the electrostatic energy of the crystal lattice, Ewald (*loc. cit.*) obtained a potential expression which was the same as  $\psi_0(\mathbf{r})$ , except that  $\omega^2/c^2$  was missing from the denominators of the terms. He transformed his series into a rapidly convergent form by means of a certain three-dimensional  $\vartheta$ -series transformation. Here we follow closely the methods adopted by Ewald, making this  $\vartheta$ -series transformation the basis of our transformations.

By consideration of the numerical magnitude of  $\omega^2/c^2$ , we shall see that it can be omitted from the series (3.42) for  $\psi_0(\mathbf{r})$ , and also from the series (3.43) for  $\psi_1(\mathbf{r})$  except for the origin term. From experimental data it is known that  $\omega$  cannot exceed its value for the "residual rays," which is of the order of magnitude  $10^{13}$ . Thus  $\omega^2/c^2 < 10^3$ . From (2.22)

$$\mathbf{q}^l = 2\pi (l_1 \mathbf{b}_1 + l_2 \mathbf{b}_2 + l_3 \mathbf{b}_3).$$

The vectors  $\mathbf{b}_1, \mathbf{b}_2, \mathbf{b}_3$  are of the order of magnitude  $1/\sqrt[3]{\Delta}$ , i.e.,  $10^7$  at least.\* Thus  $|\mathbf{q}^l|^2 > 10^{15}$ , unless  $l_1 = l_2 = l_3 = 0$ ; and  $\omega^2/c^2$  is negligible in each term of (3.42) in comparison with  $|\mathbf{q}^l|^2$ , the origin term being absent from the summation. Hence

$$\psi_0(\mathbf{r}) = \frac{4\pi}{\Delta} \mathbf{S}' \frac{\exp(i\mathbf{q}^l \cdot \mathbf{r})}{|\mathbf{q}^l|^2}. \quad (4.11)$$

In dealing with  $\omega^2/c^2$  in the series (3.43) for  $\psi_1(\mathbf{r})$  we need to compare the order of magnitude of  $\omega^2/c^2$  with that of  $|\dot{\mathbf{q}}^l + \mathbf{q}\mathbf{s}|^2$ . Using (1.31) and (2.22) it is readily seen that  $|\mathbf{q}^l + \mathbf{q}\mathbf{s}|^2$  is of the same order of magnitude as  $|\mathbf{q}^l|^2$ , if  $\mathbf{q}^l \neq 0$ , the restriction (1.4) being placed on the values of  $\phi_1, \phi_2, \phi_3$ . Thus, when  $l \neq 0, 0, 0$ ,  $\omega^2/c^2$  can be neglected in comparison with  $|\mathbf{q}^l + \mathbf{q}\mathbf{s}|^2$ . When  $l \equiv 0, 0, 0$ ,  $\mathbf{q}^l = 0$ , and from (1.31) it is seen that  $|\mathbf{q}\mathbf{s}|^2 (= q^2)$  can be made indefinitely small by making  $\phi_1, \phi_2, \phi_3$  indefinitely small. Thus  $\omega^2/c^2$  may be as great as  $q^2$ , and, in the actual limit  $q = 0$  ( $\phi_1 = \phi_2 = \phi_3 = 0$ ), will clearly play a dominant role. When  $S_1, S_2, S_3$  are not all small, we see from (1.3) that  $q$  is of the order of magnitude of  $\mathbf{b}_2$ , i.e.  $10^7$ ; and  $\omega^2/c^2$ , i.e.  $10^6$ , can

\* The frequency of the residual rays is generally expressed in terms of the corresponding wave-length in a vacuum, which is equal to  $2\pi c/\omega$ . For NaCl, this wave-length is  $61\mu$ . The linear dimensions of the lattice cells are of the order  $10^{-8}$  cm.

be neglected in comparison with  $q^2$ , *i.e.*  $10^{14}$ . Hence from (3.43), we have\*

$$\psi_1(\mathbf{r}) = \frac{4\pi}{\Delta} \mathbf{S}'_i \left[ \frac{\exp \{i(\mathbf{q}^i + \mathbf{q}\mathbf{s}) \cdot \mathbf{r}\}}{|\mathbf{q}^i + \mathbf{q}\mathbf{s}|^2} + \frac{\exp(i\mathbf{q}\mathbf{s} \cdot \mathbf{r})}{q^2 - q_0^2} \right], \quad (4.12)$$

where  $q_0 = \omega/c$ .

The expression (4.11) for  $\psi_0(\mathbf{r})$  is now exactly the same as one obtained by Ewald, and its transformation has already been effected by him. Here we transform the series expression (4.12) for  $\psi_1(\mathbf{r})$ , and derive the transformation of  $\psi_0(\mathbf{r})$  as a special case of our more general transformation.

Replacing the denominators of the terms in (4.12) according to

$$\frac{1}{a} = \int_0^\infty \exp(-a\xi) d\xi,$$

we can write

$$\frac{4\pi}{\Delta} \mathbf{S}'_i \frac{\exp \{i(\mathbf{q}^i + \mathbf{q}\mathbf{s}) \cdot \mathbf{r}\}}{|\mathbf{q}^i + \mathbf{q}\mathbf{s}|^2} = \frac{4\pi}{\Delta} \int_0^\infty \mathbf{S}'_i \exp \{-|\mathbf{q}^i + \mathbf{q}\mathbf{s}|^2 \xi + i(\mathbf{q}^i + \mathbf{q}\mathbf{s}) \cdot \mathbf{r}\} d\xi.$$

We now split up the range of integration from 0 to  $\eta$  and  $\eta$  to  $\infty$ . The value of the integral over the range  $\eta$  to  $\infty$  is

$$\frac{4\pi}{\Delta} \mathbf{S}'_i \frac{\exp \{-\eta |\mathbf{q}^i + \mathbf{q}\mathbf{s}|^2 + i(\mathbf{q}^i + \mathbf{q}\mathbf{s}) \cdot \mathbf{r}\}}{|\mathbf{q}^i + \mathbf{q}\mathbf{s}|^2}.$$

We write

$$\psi_1(\mathbf{r}) = \psi'_1(\mathbf{r}) + \psi''_1(\mathbf{r}), \quad (4.21)$$

where  $\psi'_1(\mathbf{r})$  is the sum of the above integral from  $\eta$  to  $\infty$  and the extra term in (4.12), while  $\psi''_1(\mathbf{r})$  is simply the integral over the range 0 to  $\eta$ . Thus

$$\psi'_1(\mathbf{r}) = \frac{4\pi}{\Delta} \left[ \mathbf{S}'_i \frac{\exp \{-\eta |\mathbf{q}^i + \mathbf{q}\mathbf{s}|^2 + i(\mathbf{q}^i + \mathbf{q}\mathbf{s}) \cdot \mathbf{r}\}}{|\mathbf{q}^i + \mathbf{q}\mathbf{s}|^2} + \frac{\exp(i\mathbf{q}\mathbf{s} \cdot \mathbf{r})}{q^2 - q_0^2} \right], \quad (4.22)$$

\* In point of fact the subsequent transformations can be made if the series are kept in their original forms (3.42) and (3.43), but the mathematical complications which result are not justified by any physical interest.

It is important to remember that  $\omega$  is a variable which we shall eventually determine as a solution of the frequency equation. The omission of  $\omega^2/c^2$  from terms in the potential functions will thus cause an omission of roots in the frequency equation. It can be shown, however, that, concerning order of magnitude, these roots would be given by  $\omega^2/c^2 \sim |\mathbf{q}^i|^2$ , or  $\omega \sim 10^{18}$  at least. So high a frequency has already been excluded from the theory on account of the various limitations imposed, and is thus of no real physical interest.

and

$$\psi''_1(\mathbf{r}) = \frac{4\pi}{\Delta} \int_0^\eta \mathbf{S}' \exp \{ - |\mathbf{q}^l + q\mathbf{s}|^2 \xi + i(\mathbf{q}^l + q\mathbf{s}) \cdot \mathbf{r} \} d\xi. \quad (4.23)$$

We now employ the  $\vartheta$ -series transformation\*

$$\mathbf{S}_i \exp \{ - |\mathbf{G}_i|^2 + i(\mathbf{G}_i \cdot \mathbf{V}) \} = \frac{\pi^{3/2}}{[\alpha_1 \alpha_2 \alpha_3]} \mathbf{S}_i \exp \{ - |\mathbf{Q}_i + \frac{1}{2}\mathbf{V}|^2 - 2i(\mathbf{Q}_i \cdot \boldsymbol{\alpha}) \}, \quad (4.31)$$

where

$$\mathbf{G}_i = \alpha + l_1 \alpha_1 + l_2 \alpha_2 + l_3 \alpha_3, \quad (4.32)$$

and†

$$\mathbf{Q}_i = \frac{\pi}{[\alpha_1 \alpha_2 \alpha_3]} \{ l_1 (\alpha_2 \wedge \alpha_3) + l_2 (\alpha_3 \wedge \alpha_1) + l_3 (\alpha_1 \wedge \alpha_2) \}. \quad (4.33)$$

Putting

$$\alpha_1 = \frac{\mathbf{a}_1}{2\sqrt{\xi}}, \quad \alpha_2 = \frac{\mathbf{a}_2}{2\sqrt{\xi}}, \quad \alpha_3 = \frac{\mathbf{a}_3}{2\sqrt{\xi}},$$

we have

$$[\alpha_1 \alpha_2 \alpha_3] = \frac{1}{8\xi^{3/2}} [\mathbf{a}_1 \mathbf{a}_2 \mathbf{a}_3] = \frac{\Delta}{8\xi^{3/2}},$$

and

$$\frac{(\alpha \wedge \alpha_3)}{[\alpha_1 \alpha_2 \alpha_3]} = 2\sqrt{\xi} \frac{(\mathbf{a}_2 \wedge \mathbf{a}_3)}{[\mathbf{a}_1 \mathbf{a}_2 \mathbf{a}_3]} = 2\sqrt{\xi} \cdot \mathbf{b}_1.$$

Thus

$$\mathbf{Q}_i = 2\pi\sqrt{\xi} (l_1 \mathbf{b}_1 + l_2 \mathbf{b}_2 + l_3 \mathbf{b}_3) = \sqrt{\xi} \mathbf{q}^i.$$

Putting

$$\alpha = -\mathbf{r}/2\sqrt{\xi},$$

we have also

$$\mathbf{G}_i = \frac{1}{2\sqrt{\xi}} (\mathbf{r}^i - \mathbf{r}),$$

\* This is the transformation used by Ewald. It is a special case of a more general transformation occurring in the theory of theta functions (see Krazer, "Lehrbuch der Thetafunktionen" (Liepzig, 1903), p. 108). Ewald gave an independent derivation of the formula, which is both simple and interesting. He found two solutions of the equation of heat conduction which were periodic in the crystal lattice with the cell as period. One was the d'Alembert solution, and the other the solution in Fourier series. The transformation formula is obtained by equating the two results.

†  $[\alpha_1, \alpha_2, \alpha_3]$  denotes the triple scalar product of the vectors  $\alpha_1, \alpha_2, \alpha_3$ , and is equal to the volume of the parallelepiped whose sides are represented by these vectors. The vectors,  $\beta_1, \beta_2, \beta_3$ , inverse to  $\alpha_1, \alpha_2, \alpha_3$ , are defined by

$$(\alpha_i \cdot \beta_j) = \delta_{ij},$$

from which it follows that

$$\beta_1 = \frac{(\alpha_2 \wedge \alpha_3)}{[\alpha_1 \alpha_2 \alpha_3]}, \text{ etc.,}$$

where

$$\mathbf{r}^l = l_1 \mathbf{a}_1 + l_2 \mathbf{a}_2 + l_3 \mathbf{a}_3,$$

and is the vectorial distance between two particles of the same kind in the origin cell and the  $l$ th cell respectively.

Finally, we make  $\mathbf{V} = 2 \sqrt{\xi} q \mathbf{s}$ , and substitute these expressions in (4.31) to obtain

$$\begin{aligned} \mathbf{S}_l \exp \left\{ -\frac{1}{4\xi} |\mathbf{r}^l - \mathbf{r}|^2 + i q \mathbf{s} \cdot (\mathbf{r}^l - \mathbf{r}) \right\} \\ \text{Thus} \quad &= \frac{\Delta}{8\pi^{3/2} \xi^{3/2}} \mathbf{S}_l \exp \{ -|\mathbf{q}^l + q \mathbf{s}|^2 \xi + i (\mathbf{q}^l \cdot \mathbf{r}) \}. \\ \mathbf{S}_l' \exp \{ -|\mathbf{q}^l + q \mathbf{s}|^2 \xi + i (\mathbf{q}^l + q \mathbf{s}) \cdot \mathbf{r} \} \\ &= \frac{\Delta}{8\pi^{3/2} \xi^{3/2}} \mathbf{S}_l \exp \left\{ -\frac{1}{4\xi} |\mathbf{r}^l - \mathbf{r}|^2 + i q (\mathbf{s} \cdot \mathbf{r}^l) \right\} - 1. \end{aligned}$$

We now integrate from 0 to  $\eta$  for the variable  $\xi$ , and, using (4.23), we obtain

$$\begin{aligned} \psi''_1(\mathbf{r}) &= \frac{4\pi}{\Delta} \int_0^\eta \mathbf{S}_l' \exp \{ -|\mathbf{q}^l + q \mathbf{s}|^2 \xi + i (\mathbf{q}^l + q \mathbf{s}) \cdot \mathbf{r} \} d\xi \\ &= \frac{1}{\sqrt{\pi}} \mathbf{S}_l \exp \{ i q (\mathbf{s} \cdot \mathbf{r}^l) \} \int_0^\eta \frac{1}{2\xi^{3/2}} \exp \left\{ -\frac{1}{4\xi} |\mathbf{r}^l - \mathbf{r}|^2 \right\} d\xi - \frac{4\pi}{\Delta} \eta. \end{aligned}$$

In these integrals we put  $a = 1/2 \sqrt{\xi}$ , and  $\epsilon = 1/2 \sqrt{\eta}$ . Hence

$$\psi''_1(\mathbf{r}) = \frac{2}{\sqrt{\pi}} \mathbf{S}_l \exp \{ i q (\mathbf{s} \cdot \mathbf{r}^l) \} \int_\epsilon^\infty \exp \{ -a^2 |\mathbf{r}^l - \mathbf{r}|^2 \} da - \frac{\pi}{\Delta \epsilon^2}.$$

We now introduce Gauss's error function (which is available in numerical tables).

$$F(x) = \frac{2}{\sqrt{\pi}} \int_0^x e^{-a^2} da,$$

and

$$G(x) = 1 - F(x) = \frac{2}{\sqrt{\pi}} \int_x^\infty e^{-a^2} da.$$

Thus

$$\psi''_1(\mathbf{r}) = \mathbf{S}_l \frac{G(\epsilon |\mathbf{r}^l - \mathbf{r}|)}{|\mathbf{r}^l - \mathbf{r}|} \exp \{ i q (\mathbf{s} \cdot \mathbf{r}^l) \} - \frac{\pi}{\Delta \epsilon^2}. \quad (4.34)$$

Putting  $\eta = 1/4\epsilon^2$  in (4.22), we have

$$\psi'_1(\mathbf{r}) = \frac{4\pi}{\Delta} \left[ \mathbf{S}_l' \frac{\exp \left\{ -\frac{1}{4\epsilon^2} |\mathbf{q}^l + q \mathbf{s}|^2 + i (\mathbf{q}^l + q \mathbf{s}) \cdot \mathbf{r} \right\}}{|\mathbf{q}^l + q \mathbf{s}|^2} + \frac{\exp \{ i q (\mathbf{s} \cdot \mathbf{r}) \}}{q^2 - q_0^2} \right]. \quad (4.35)$$

We have thus split up  $\psi_1(\mathbf{r})$  into two expressions (4.34) and (4.35), containing an adjustable parameter  $\varepsilon$ . It is readily seen that (4.35) is most rapidly convergent for small  $\varepsilon$ , and (4.34) for large  $\varepsilon$ . In calculating the values of these series or their derivatives, it is necessary to compromise in choosing the value of  $\varepsilon$ , choosing a value which makes both series just about as rapidly convergent as each other. A suitable value is generally found to be  $\varepsilon = 1/\sqrt[3]{\Delta}$ .

By putting  $qs = 0$ , and omitting the extra term in (4.12), we obtain Ewald's transformation of  $\psi_0(\mathbf{r})$ , namely,

$$\psi_0(\mathbf{r}) = \psi'_0(\mathbf{r}) + \psi''_0(\mathbf{r}), \quad (4.41)$$

where

$$\psi'_0(\mathbf{r}) = \frac{4\pi}{\Delta} \mathbf{S}'_i \frac{\exp \left\{ -\frac{1}{4\varepsilon^2} |\mathbf{q}^i|^2 + i(\mathbf{q}^i \cdot \mathbf{r}) \right\}}{|\mathbf{q}^i|^2}, \quad (4.42)$$

and

$$\psi''_0(\mathbf{r}) = \mathbf{S}_i \frac{G(\varepsilon |\mathbf{r}^i - \mathbf{r}|)}{|\mathbf{r}^i - \mathbf{r}|} - \frac{\pi}{\Delta \varepsilon^2}. \quad (4.43)$$

To obtain  $\bar{\psi}_0(\mathbf{r})$  and  $\bar{\psi}_1(\mathbf{r})$  (given by (3.62) and (3.63)), we write

$$\frac{1}{|\mathbf{r}|} = \frac{F(\varepsilon |\mathbf{r}|)}{|\mathbf{r}|} + \frac{G(\varepsilon |\mathbf{r}|)}{|\mathbf{r}|}.$$

Thus, since

$$\bar{\psi}_0(\mathbf{r}) = \psi_0(\mathbf{r}) - \frac{1}{|\mathbf{r}|},$$

it follows that

$$\bar{\psi}_0(\mathbf{r}) = \bar{\psi}'_0(\mathbf{r}) + \bar{\psi}''_0(\mathbf{r}), \quad (4.51)$$

where

$$\begin{aligned} \bar{\psi}'_0(\mathbf{r}) &= \psi'_0(\mathbf{r}) - \frac{F(\varepsilon |\mathbf{r}|)}{|\mathbf{r}|} \\ &= \frac{4\pi}{\Delta} \mathbf{S}'_i \frac{\exp \left\{ -\frac{1}{4\varepsilon^2} |\mathbf{q}^i|^2 + i(\mathbf{q}^i \cdot \mathbf{r}) \right\}}{|\mathbf{q}^i|^2} - \frac{F(\varepsilon |\mathbf{r}|)}{|\mathbf{r}|}, \end{aligned} \quad (4.52)$$

and

$$\begin{aligned} \bar{\psi}''_0(\mathbf{r}) &= \psi''_0(\mathbf{r}) - \frac{G(\varepsilon |\mathbf{r}|)}{|\mathbf{r}|} \\ &= \mathbf{S}'_i \frac{G(\varepsilon |\mathbf{r}^i - \mathbf{r}|)}{|\mathbf{r}^i - \mathbf{r}|} - \frac{\pi}{\Delta \varepsilon^2} \end{aligned} \quad (4.53)$$

$\left( \frac{1}{|\mathbf{r}|} G(\varepsilon |\mathbf{r}|) \right)$  being precisely the origin term of the series in (4.43).



Similarly,

$$\bar{\psi}_1(\mathbf{r}) = \bar{\psi}'_1(\mathbf{r}) + \bar{\psi}''_1(\mathbf{r}), \quad (4.61)$$

where

$$\bar{\psi}'_1(\mathbf{r}) = \frac{4\pi}{\Delta} \left[ \sum_i' \frac{\exp \left\{ -\frac{1}{4\epsilon^2} |\mathbf{q}^i + \mathbf{q}\mathbf{s}|^2 + i(\mathbf{q}^i + \mathbf{q}\mathbf{s}) \cdot \mathbf{r} \right\}}{|\mathbf{q}^i + \mathbf{q}\mathbf{s}|^2} + \frac{\exp \{iq(\mathbf{s} \cdot \mathbf{r})\}}{q^2 - q_0^2} \right] - \frac{F(\epsilon|\mathbf{r}|)}{|\mathbf{r}|} \quad (4.62)$$

and

$$\bar{\psi}''_1(\mathbf{r}) = \sum_i' \frac{G(\epsilon|\mathbf{r}^i - \mathbf{r}|)}{|\mathbf{r}^i - \mathbf{r}|} \exp \{iq(\mathbf{s} \cdot \mathbf{r}^i)\} - \frac{\pi}{\Delta\epsilon^2}. \quad (4.63)$$

### § 5—DERIVATION OF THE FREQUENCY EQUATION

We are now in a position to construct the equations of motion of the particles. The potential energy of a unit charge at the point occupied by the  $k$ th particle in the origin cell in the field of the electric interactions of all the other particles has been denoted by  $\bar{\Psi}^k(\mathbf{r})$ : we denote its potential energy in the field of the repulsive forces of all the other particles by\*  $\bar{\Phi}^k(\mathbf{r})$ . It has been shown that the equations of motion of all particles of the same kind are identical (p. 490). For convenience we construct the equations of motion of the particles in the origin cell. The motion of the  $k$ th particle is determined by the vector equation

$$m_k \frac{\partial^2}{\partial t^2}(\mathbf{r}_k) = -e_k \mathbf{grad} [\bar{\Psi}^k(\mathbf{r}) + \bar{\Phi}^k(\mathbf{r})]_{\mathbf{r}=\mathbf{r}_k}, \quad (5.11)$$

where  $m_k$  is the mass of the  $k$ th particle. Here

$$\mathbf{r}_k = \mathbf{r}_k^0 + \mathbf{u}_k,$$

by (3.52), and

$$\frac{\partial}{\partial t} \equiv i\omega,$$

since

$$\mathbf{u}_k \propto \exp(i\omega t).$$

Hence the equation of motion becomes

$$m_k \omega^2 \mathbf{u}_k = e_k \mathbf{grad} [\bar{\Psi}^k(\mathbf{r}) + \bar{\Phi}^k(\mathbf{r})],$$

\* The function  $\bar{\Phi}^k(\mathbf{r})$  is not evaluated here, this being left to the consideration of particular crystals (see p. 491).

which is equivalent to three component equations

$$m_k \omega^2 u_{kx} = e_k \frac{\partial}{\partial x} [\bar{\Psi}^k(\mathbf{r}) + \bar{\Phi}^k(\mathbf{r})]. \quad (5.12)$$

Now

$$\begin{aligned} \bar{\Psi}^k(\mathbf{r}) &= \sum_{k \neq k'} \psi_{k'}(\mathbf{r}) + \bar{\psi}_k(\mathbf{r}) \quad (\text{by (3.53)}) \\ &= \sum_{k \neq k'} e_{k'} [\psi_0(\mathbf{r} - \mathbf{r}_{k'}^0) - \mathbf{u}_{k'} \cdot \mathbf{grad} \psi_1(\mathbf{r} - \mathbf{r}_{k'}^0)] \\ &\quad + e_k [\bar{\psi}_0(\mathbf{r} - \mathbf{r}_k^0) - \mathbf{u}_k \cdot \mathbf{grad} \bar{\psi}_1(\mathbf{r} - \mathbf{r}_k^0)], \end{aligned} \quad (5.21)$$

by (3.23), (3.41), and (3.54), (3.61).

We expand the right-hand side of (5.12) in powers of the displacement components. Since the particle is in equilibrium when the lattice is undisplaced, there will be no constant term; and we neglect all powers of the displacement components, higher than the first, on the assumption that these are small. We shall thus obtain an equation of the form

$$m_k \omega^2 u_{kx} = \sum_{k'} \sum_y A_{xy}^{kk'} u_{k'y}, \quad (5.22)$$

where

$$A_{xy}^{kk'} = B_{xy}^{kk'} + C_{xy}^{kk'}. \quad (5.23)$$

Here  $B_{xy}^{kk'}$  denotes the contribution of the electric forces,  $C_{xy}^{kk'}$  that of the repulsive forces. In expanding  $\frac{\partial}{\partial x} (\bar{\Psi}^k(\mathbf{r}))$  (given by (5.21)) by the generalized Taylor expansion to the first order in the displacement components the  $\psi_1$  terms can be replaced by their undisplaced values, since they only occur as multiples of the displacement components.

Thus

$$\begin{aligned} \frac{\partial}{\partial x} [\bar{\Psi}^k(\mathbf{r})]_{\mathbf{r}=\mathbf{r}_k^0+\mathbf{u}_k} &= \sum_{k \neq k'} e_{k'} \left[ \frac{\partial \psi_0(\mathbf{r} - \mathbf{r}_{k'}^0)}{\partial x} - \mathbf{u}_{k'} \cdot \mathbf{grad} \frac{\partial \psi_1(\mathbf{r} - \mathbf{r}_{k'}^0)}{\partial x} \right]_{\mathbf{r}=\mathbf{r}_k^0+\mathbf{u}_k} \\ &\quad + e_k \left[ \frac{\partial \bar{\psi}_0(\mathbf{r} - \mathbf{r}_k^0)}{\partial x} - \mathbf{u}_k \cdot \mathbf{grad} \frac{\partial \bar{\psi}_1(\mathbf{r} - \mathbf{r}_k^0)}{\partial x} \right]_{\mathbf{r}=\mathbf{r}_k^0+\mathbf{u}_k} \\ &= \text{constant} + \sum_{k \neq k'} e_{k'} \sum_y \left[ u_{ky} \frac{\partial^2 \psi_0(\mathbf{r} - \mathbf{r}_{k'}^0)}{\partial y \partial x} - u_{k'y} \frac{\partial^2 \psi_1(\mathbf{r} - \mathbf{r}_{k'}^0)}{\partial y \partial x} \right]_{\mathbf{r}=\mathbf{r}_k^0} \\ &\quad + e_k \sum_y u_{ky} \left\{ \frac{\partial^2 \bar{\psi}_0(\mathbf{r} - \mathbf{r}_k^0)}{\partial y \partial x} - \frac{\partial^2 \bar{\psi}_1(\mathbf{r} - \mathbf{r}_k^0)}{\partial y \partial x} \right\}_{\mathbf{r}=\mathbf{r}_k^0} \\ &= \text{constant} - \sum_{k \neq k'} e_{k'} \sum_y u_{k'y} \left( \frac{\partial^2 \psi_1(\mathbf{r})}{\partial y \partial x} \right)_{\mathbf{r}=\mathbf{r}_k^0-\mathbf{r}_{k'}^0} \\ &\quad + \sum_y u_{ky} \left\{ e_k \left[ \frac{\partial^2 \bar{\psi}_0(\mathbf{r})}{\partial y \partial x} - \frac{\partial^2 \bar{\psi}_1(\mathbf{r})}{\partial y \partial x} \right]_{\mathbf{r}=\mathbf{0}} + \sum_{k \neq k'} e_{k'} \left[ \frac{\partial^2 \psi_0(\mathbf{r})}{\partial y \partial x} \right]_{\mathbf{r}=\mathbf{r}_k^0-\mathbf{r}_{k'}^0} \right\}. \end{aligned}$$

Hence, if  $k \neq k'$ ,

$$B_{xy}{}^{kk'} = -e_k e_{k'} \left( \frac{\partial^2 \psi_1(\mathbf{r})}{\partial y \partial x} \right)_{\mathbf{r}=\mathbf{r}_k^0 - \mathbf{r}_{k'}^0} \quad (5.24)$$

and\*

$$B_{xy}{}^{kk} = e_k^2 \left( \frac{\partial^2 \bar{\psi}_0(\mathbf{r})}{\partial y \partial x} - \frac{\partial^2 \bar{\psi}_1(\mathbf{r})}{\partial y \partial x} \right)_{\mathbf{r}=0} + \sum_{k \neq k'} e_k e_{k'} \left( \frac{\partial^2 \psi_0(\mathbf{r})}{\partial y \partial x} \right)_{\mathbf{r}=\mathbf{r}_k^0 - \mathbf{r}_{k'}^0}. \quad (5.25)$$

These coefficients can easily be evaluated, using the expressions for  $\psi_0(\mathbf{r})$ ,  $\psi_1(\mathbf{r})$ ,  $\bar{\psi}_0(\mathbf{r})$ ,  $\bar{\psi}_1(\mathbf{r})$ , obtained in the last section, and the resulting series are sufficiently rapidly convergent for purposes of calculation.

There are  $3s$  equations of the type (5.22) (obtained by changing  $x$  and  $k$ ), all linear in the  $3s$  displacement components  $u_{ky}$ . By elimination of the displacement components a determinantal frequency equation of the  $3s$ th order for  $\omega^2$  is obtained.† To describe the dynamics of the crystal block completely it is necessary to solve the  $n^3$  frequency equations, obtained by giving  $\phi_1$ ,  $\phi_2$ ,  $\phi_3$  the values (1.4). Though  $\phi_1$ ,  $\phi_2$ ,  $\phi_3$  can only have discrete values it is convenient to regard them as continuous variables, and we then have the  $3s$  normal frequencies as functions of three variables, *i.e.*,

$$\omega_1(\phi_1, \phi_2, \phi_3), \omega_2(\phi_1, \phi_2, \phi_3), \dots, \omega_{3s}(\phi_1, \phi_2, \phi_3).$$

The actual normal frequencies of the crystal block are given by the intersections of the planes

$$\phi_1 = \frac{2\pi r}{n}, \quad \phi_2 = \frac{2\pi s}{n}, \quad \phi_3 = \frac{2\pi t}{n},$$

with the four-dimensional frequency surfaces. The number  $n$  is large and depends on the size of the block, and it is the continuous four-dimen-

\* With the approximation that the displacement is small the force of the displaced lattice on a displaced particle is approximately the sum of the force of the displaced lattice on the undisplaced particle and the force of the undisplaced lattice on the displaced particle. The recent approximations and the form of the coefficients in (5.24) and (5.25) are now more apparent, the  $\psi_1$  terms representing forces of the former kind,  $\psi_0$  terms forces of the latter kind.

† It is found that the determinant is of Hermitic form. We find  $B_{xy}{}^{kk} = B_{yx}{}^{kk}$ , and both are real; while  $B_{xy}{}^{kk'} = B_{yx}^{*kk'}$ . Similar relations hold for the repulsive force coefficients. It is convenient to normalize the displacement components according to

$$\mathbf{u}_k = \frac{1}{\sqrt{m_k}} \cdot \mathbf{v}_k \exp \{iq(\mathbf{s} \cdot \mathbf{r}_k^0)\}.$$

sional frequency surfaces (extending over  $-\pi < \phi_1, \phi_2, \phi_3 \leq \pi$ ) which are of interest.\*

The most convenient method of visualizing the frequency spectrum seems to be by means of 3s "three-dimensional contour maps." The plane contour map in cartography represents three dimensions in two dimensions. By using contour surfaces instead of contour lines we can represent four dimensions in three dimensions (the ordinary spatial dimensions representing  $\phi_1, \phi_2, \phi_3$ , and the contours being surfaces  $\omega = \text{constant}$ ). This is particularly useful, as the volume between two successive contours is a measure of the number of frequencies lying between two definite frequencies—a quantity of essential importance in the calculation of specific heats.

I wish to acknowledge my indebtedness to Professor M. Born for much valuable advice.

### SUMMARY

The dynamical theory of the vibrations of the particles in a polar crystal lattice is worked out. A determinantal frequency equation, for the determination of a typical set of points of the "frequency spectrum," is obtained in a form in which the coefficients can be calculated.

\* It is of interest to examine the effect of  $q_0 = \omega/c$ , which occurs in the coefficients. We have seen (§ 4, p. 497) that  $q_0$  can be neglected except in the case of  $q$  vanishingly small. It is known that, for infinitely long wave-length ( $\lambda \rightarrow \infty, q \rightarrow 0$ ) 3 frequencies tend to zero, while the remaining  $3s - 3$  are non-vanishing (see M. Born "Atom, theorie des festen Zustandes," 'Enc. Math. Wiss.,' vol. 5, pp. 574-587). When  $\omega$  does not vanish,  $q_0$  does not vanish, and its presence will wipe out the derivatives of the term  $\frac{\exp \{iq(\mathbf{s} \cdot \mathbf{r})\}}{q^2 - q_0^2}$  occurring in  $\psi_1(\mathbf{r})$  and  $\bar{\psi}_1(\mathbf{r})$ .

The displacements corresponding to the vanishing frequencies are given by

$$\mathbf{u}_k = \mathbf{u} \exp \{iq(\mathbf{s} \cdot \mathbf{r}_k^0)\}, \quad (k = 1, 2, \dots s).$$

Substituting this in (5.22), it is found by straightforward algebra that the derivatives of the term  $\frac{\exp \{iq(\mathbf{s} \cdot \mathbf{r})\}}{q^2 - q_0^2}$  disappear from the coefficient of  $u_y$ , on account of the fact that the algebraic sum of the charges in a cell is identically zero ( $\sum e_k = 0$ ).

Thus the effect of  $q_0^2$  is that the term  $\frac{\exp \{iq(\mathbf{s} \cdot \mathbf{r})\}}{q^2 - q_0^2}$  in  $\psi_1(\mathbf{r})$  and  $\bar{\psi}_1(\mathbf{r})$  can be entirely omitted when  $q$  is vanishingly small.

# International Frequency Comparisons by Means of Standard Radio Frequency Emissions

By L. ESSEN, B.Sc, The National Physical Laboratory

(Communicated by Sir Joseph Petavel, F.R.S.—Received December 10, 1934)

## 1—INTRODUCTION

The Bureau of Standards, Washington, U.S.A., emits from its station at Beltsville, WWV, a few miles from Washington, a standard frequency of reference by which other organizations and individuals can measure the frequency of their own apparatus. The frequency is 5 million cycles per second, and its departure from the nominal value is not expected to exceed 1 cycle per second. The frequency of emission is compared continuously with that of the standard equipment at the Bureau and is monitored so as not to differ from that frequency by more than 1 part in  $10^8$ .

The value of the frequency has been determined at the National Physical Laboratory, Teddington, on a number of occasions. The observations have afforded information as to the agreement of standards of frequency in the two countries, and show with what accuracy the frequencies of two different standards can be compared by the use of emissions at a radio frequency. Some information is also obtained concerning the effect of the intervening medium on the propagation of an emission at this frequency.

## 2—METHOD OF MEASUREMENT

The frequency of the received signal was measured by the double beat method. The receiver, which consisted of 1 H.F., a detector, and 2 L.F. stages, was used in an oscillating condition and was adjusted to give a convenient beat note,  $f$ , of about 500 cycles per second with the incoming signal. The 250th harmonic of a 20 kc/s standard oscillator was selected, amplified and induced into the receiver, where it produced a beat note,  $f_1$ , with the oscillations of the receiver. The resultant beats obtained at a frequency  $f - f_1$  gave the frequency difference between the harmonic of the local standard and the received signal. The period of the beats was determined aurally by means of a stop-watch.

In order to determine the sign of the frequency difference, two 20 kc/s local standards differing in frequency by about 1 part in  $10^6$  were used in turn. When the sign had been determined, the observations were continued with the standard which gave the more convenient beat frequency.

Throughout the duration of the measurements, continuous observations were made of the frequency difference between the two local standards, to reveal any changes occurring in the frequency of the standard with which the signal was being compared.

The absolute frequency of the received signal was determined from the measured frequency difference and the absolute value of the frequency of the local standard, which was measured by comparison with Observatory time signals.

### 3—NATURE OF THE OBSERVATIONS

The emission was usually well received on an indoor aerial about 10 metres long. The reception on May 9 and subsequent occasions was so strong that no aerial was used. Fading of the received signal was always observed, usually with a period of about 4 seconds. If the beat frequency was less than 0.5 cycle per second, the fading prevented its measurement. The frequency difference which could be measured was limited to values between 0.5 and 6 beats per second, but the range could have been extended to 20 per second by automatic recording if this had been necessary. In general there was also a considerable amount of interference which prevented measurements at some periods. Owing to the fading, continuous measurements could at no time be made, but it was still usually possible to make four or five determinations of the beat frequency during each minute of the emission period. The observed beat frequency was usually very constant, although slow drifts of frequency were sometimes recorded, but at certain instants considerable changes in the rate of beat occurred, the duration of these changes always being short and usually less than 0.5 second. These disturbances were of a pronounced nature only during some of the emissions and at certain periods of them. They are probably to be explained by sudden changes in the path of the wave due to variations in the height of the reflecting layers. Owing to the short duration of the disturbances, they did not usually affect the measurements to an appreciable extent, as observations could be confined to periods of steady beat. During some of the emissions, the times at which the disturbances occurred and a rough estimate of the extent of the frequency change were recorded.

## 4—ACCURACY OF THE MEASUREMENTS

The comparisons between the two local standards showed that the frequency difference between them during the period occupied by the measurements was constant to  $\pm 0.1$  part in  $10^8$ . It can, therefore, be safely assumed that variations in the period of beat between the received signal and the local standard are the result of frequency variations in the signal and not in the standard.

Expressed as a fraction, the accuracy of measuring the difference between two frequencies which are producing beats is given by the expression  $\frac{\delta f \times \Delta t}{t}$ , where  $\delta f$  is the frequency difference,  $t$  the time over which beats are counted and  $\Delta t$  the error in the measurement of  $t$ .

In these measurements  $t$  was usually limited to about 3 seconds, owing to the fading of the signal; it was determined by means of a stop-watch with an accuracy,  $\Delta t$ , of 0.1 second.  $\delta f$  was usually of the order of 2 cycles per second. The accuracy of measurement was thus 1 in 15. This was the accuracy of the determination of a difference between two frequencies very near  $5 \times 10^6$  cycles per second, and the accuracy of the actual frequency comparison was therefore 1.3 in  $10^8$ . The values of  $\delta f$  and  $t$  were always such that an accuracy of at least  $\pm 2$  in  $10^8$  was attained in an individual observation lasting about 3 seconds.

The frequency of the local standard is determined by daily comparisons with Observatory time signals. Observations extended over a weekly period give the value of the average frequency during that period with an accuracy of 5 parts in  $10^8$ . Experience has shown that the stability of the standard is such that during the week the frequency does not depart from this mean value by more than  $\pm 2$  parts in  $10^8$ .

The final accuracy of the frequency comparisons is therefore  $\pm 2$  parts in  $10^8$ , and that of the absolute frequency measurements  $\pm 7$  parts in  $10^8$ .

## 5—RESULTS OF THE MEASUREMENTS

In column 2 of Table I the value given for the frequency of the received signal is the average of the whole of the measurements made.

In each case the measurements refer to the emission taking place from 0300 G.M.T. to 0500 G.M.T. In the fifth column are the values ascribed to the emission by the Bureau of Standards.

The results are given in more detail in fig. 1 in order to reveal the frequency stability of the received signal. The average frequency of

TABLE I—NOMINAL FREQUENCY 5,000,000 c/s

Date	N.P.L. measurements			Bureau of Standards values cycles per second	
	Frequency cycles per second	Number of measure- ments	Mean deviation from the mean : cycles per second	Maximum	Minimum
7.3.34	4,999,999·7	80	$\pm 0\cdot05$	5,000,000·1 <sub>6</sub>	5,000,000·1 <sub>1</sub>
14.3.34	5,000,000·4	130	$\pm 0\cdot05$	5,000,000·9 <sub>2</sub>	5,000,000·8 <sub>4</sub>
9.5.34	5,000,000·4	130	$\pm 0\cdot07$	5,000,000·5 <sub>2</sub>	5,000,000·4 <sub>4</sub>
30.5.34	4,999,999·4	150	$\pm 0\cdot05$	5,000,000·1 <sub>2</sub>	5,000,000·0 <sub>8</sub>
6.6.34	5,000,000·9	120	$\pm 0\cdot15$	5,000,000·4 <sub>4</sub>	5,000,000·3 <sub>6</sub>
13.6.34	5,000,000·6	130	$\pm 0\cdot10$	5,000,000·5 <sub>0</sub>	5,000,000·4 <sub>2</sub>

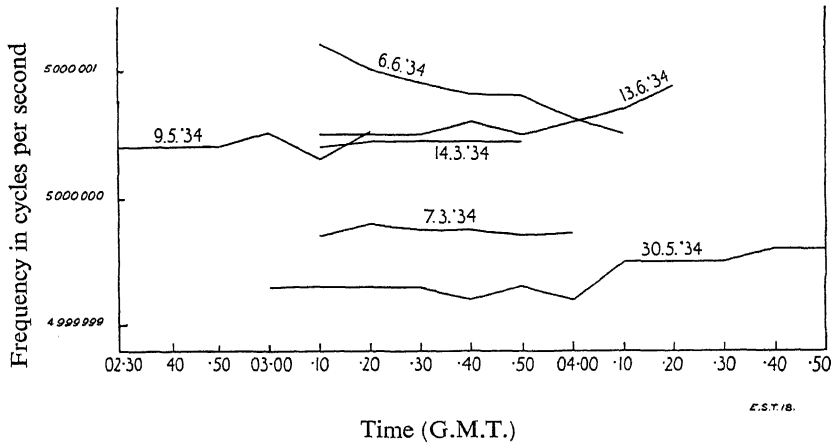


FIG. 1

each 10-minute dash is given, the time recorded being that of the middle of the dash.

During the emission of May 30, 1934, special notice was taken of the times at which sudden variations of the beat frequency occurred. Between 0350 and 0400 G.M.T. such changes amounting to  $\pm 1$  cycle per second were observed and near 0415 G.M.T. the disturbances were so numerous that, in spite of their short duration, the measurements of the beat frequency were somewhat uncertain. After 0430 G.M.T. the beats became very steady again. On June 6 sudden variations of short duration amounting to  $\pm 1$  cycle per second were observed between 0300 and 0330 G.M.T. The beats were then very steady till 0400 G.M.T. when some disturbances were again detected.



On June 13, the beats were very steady until 0350 G.M.T., when small disturbances were noticed.

The most probable explanation of these erratic frequency fluctuations is that sudden variations in the height of the reflecting layer change the length of the path of the waves with the production of corresponding frequency variations in accordance with the Doppler principle. If it is assumed that the wave is received after three reflections, then a change in the average height of the reflecting layer of 1 metre per second would produce a frequency change of roughly 1 part in  $10^8$ . A uniform movement would cause the frequency of the received signal to differ from that of the emitted signal by a constant amount and would have to be very considerable before it could be detected; but irregular movements would be readily detected by irregularities in the frequency curve. It appears from the results that at times there were upward and downward movements of the average height of the layer at a velocity of about 20 metres per second.

#### 6—CONCLUSIONS

The frequency comparison between the received signal and the local standard was effected with an accuracy of  $\pm 2$  parts in  $10^8$ . The accuracy of the absolute measurements was limited by the accuracy with which the local standard was known, which was  $\pm 5$  parts in  $10^8$ .

Frequency fluctuations probably caused by disturbances in the process of transmission were detected and estimated to be as large as  $\pm 20$  parts in  $10^8$ . These fluctuations were, however, of such short duration that they did not affect to an appreciable extent the accuracy of the results.

The accuracy of  $\pm 2$  parts in  $10^8$ , therefore, also applies to the comparison between the frequency emitted at Beltsville, U.S.A., and that of the standard at The National Physical Laboratory, Teddington.

---

## The Rotational Dispersion of Sound in Hydrogen

By ANGUS S. ROY, Ph.D.,<sup>†</sup> and MORRIS E. ROSE, University of Michigan

(Communicated by H. S. Allen, F.R.S.—Received December 13, 1934)

### INTRODUCTION

The development of the interferometric method originally due to Pierce<sup>‡</sup> has definitely established the existence of an acoustic dispersion phenomenon in gases at supersonic frequencies. The experimental investigations of Abello,<sup>§</sup> Kneser,<sup>||</sup> Richards and Reid<sup>¶</sup> and others have shown this dispersion to exist in CO<sub>2</sub>, C<sub>2</sub>H<sub>4</sub>, CS<sub>2</sub> and SO<sub>2</sub>. An explanation of the mechanism of the effect was advanced by Rice and Herzfeld<sup>\*\*</sup>; and on the basis of this mechanism the dispersion formula has been derived by Kneser,<sup>||</sup> Rutgers<sup>††</sup> and Bourgin.<sup>‡‡</sup> The density variations produced in the gas by the sound wave result in a disturbance of the equilibrium distribution of energy between the various degrees of freedom of the molecule, there being excess of translational energy in the compressional phase for example. This equilibrium is then re-established, after a certain length of time which is characteristic of the gas, by inelastic collisions. When the period of the wave is of the order of this characteristic time, this exchange becomes incomplete and the specific heat of the gas diminishes, the sound velocity therefore increases until, as the frequency increases further, there is no time during a cycle for energy to be transferred. The sound velocity then approaches a constant value.

In the case of all gases previously investigated it is quite certain that the dispersion is to be attributed to the failure of the vibrational energy exchanges to follow the acoustic cycle. However, recently Richards and Reid<sup>§§</sup> have reported certain effects which, they assert, indicate a dispersion region in hydrogen due to rotational energy lag and lying at

<sup>†</sup> Commonwealth Fellow.

<sup>‡</sup> 'Proc. Amer. Acad. Sci.,' vol. 60, p. 271 (1925).

<sup>§</sup> 'Proc. Nat. Acad. Sci. Wash.,' vol. 13, p. 699 (1927).

<sup>||</sup> 'Ann. Physik,' vol. 11, p. 761, 777 (1931); vol. 16, p. 337 (1933).

<sup>¶</sup> 'J. Chem. Phys.,' vol. 2, p. 193 (1934).

<sup>\*\*</sup> 'Phys. Rev.,' vol. 31, p. 691 (1928).

<sup>††</sup> 'Ann. Physik,' vol. 16, p. 350 (1933).

<sup>‡‡</sup> 'Nature,' vol. 122, p. 133 (1928); 'Phil. Mag.,' vol. 7, p. 821 (1929); 'Phys. Rev.,' vol. 34, p. 521 (1929).

<sup>§§</sup> 'J. Chem. Phys.,' vol. 2, p. 206 (1934).

least partly in frequency range 94–451 kc. However, on the basis of the classical kinetic theory of Jeans† one would expect to find such a dispersion only at frequencies of the order  $10^6$  kc. Further, Richards states that the experimental accuracy in the case of the hydrogen measurements was not very great. For these reasons it was considered advisable to investigate this problem further.

### THEORETICAL

The theory of the sound dispersion leads to the dispersion formula which may be written‡

$$f^2 = \frac{p}{\rho} \left\{ 1 + \frac{k}{C_\infty} - \frac{\varepsilon^2}{C_\infty^2 T^2} e^{-\varepsilon/kT} \left( 1 + \frac{\omega^2}{\omega_i^2} \right)^{-1} \right\}, \quad (1)$$

in which  $f$  is the sound velocity,  $p$  and  $\rho$  are pressure and density,  $C_\infty$  the specific heat of the gas for large frequencies,  $\varepsilon$  the energy difference between the ground state and excited level,  $\omega$  the frequency in radians per second, and  $k$  and  $T$  the Boltzmann constant and temperature respectively. The inflection frequency  $\omega_i$ ,  $(d/d \log \omega)^2 f^2 = 0$  determines centre of the dispersion region and is given by

$$\omega_i = \kappa_2 \frac{n}{V}. \quad (2)$$

$V$  and  $n$  are the total volume and total number of molecules. Prediction of the dispersion frequency, as is evident on *a priori* grounds, consists in the calculation of the parameter  $\kappa_2$  which enters in the theory through the reaction equation

$$V \, dn_1/dt = \kappa_1 n_0^2 - \kappa_2 n_0 n_1, \quad (3)$$

where  $n_0$ ,  $n_1$ , are the number of molecules in the ground and excited states respectively. It can be readily seen that the transition probabilities  $\kappa_1$  and  $\kappa_2$  are related with the cross-section for excitation  $Q$  by

$$\kappa_1 = \kappa_2 e^{-\varepsilon/kT} = \overline{vQ}, \quad (4)$$

where  $v$  is the relative velocity of the colliding molecules before collision. The bar indicates an average over the Maxwell-Boltzmann distribution. Our task is therefore to calculate the cross-section for excitation of rotational energy in hydrogen. Because of certain difficulties in the

† “Dynamical Theory of Gases,” Camb. Univ. Press, 2nd ed., 1916, pp. 374–378.

‡ For example, Kneser, *loc. cit.*; see also Rose, ‘J. Chem. Phys.’ vol. 2, p. 260 (1934).

collision theory no more than an order of magnitude result can be obtained; but this, as will be seen, is sufficient to substantiate the results of the experimental work.

### The Collision Theory

We consider a system of two diatomic rotators and choose as co-ordinates the relative position of the centre of gravity of one molecule referred to that of the other, these three co-ordinates being denoted by  $\mathbf{r}$ ; and the polar and azimuthal angles of the two molecules,  $\vartheta_1, \phi_1$ , and  $\vartheta_2, \phi_2$  with respect to the line joining the centres of gravity as polar axis. Then the wave equation may be written as follows:

$$\left\{ \frac{\hbar^2}{2\mu} \Delta - H + W - V(r, \vartheta_1, \vartheta_2, \phi) \right\} \Psi = 0, \quad (5)$$

in which  $W$  is the total energy of the system,  $\mu$  the reduced mass of the two molecules,  $\phi = |\phi_1 - \phi_2|$  and  $r = |\mathbf{r}|$ ;  $\Delta$  is the operator corresponding to the relative motion and  $H$  is the Hamiltonian for the system of two isolated rotators having eigenfunctions  $\psi_\nu$  with eigenvalues  $E_\nu$ , so that

$$H \psi_\nu = E_\nu \psi_\nu. \quad (6)$$

A solution of (5) is effected by expanding the total wave function  $\Psi$  in the normalized and orthogonal rotator wave functions  $\psi_\nu$  which are, of course, simply products of two spherical harmonics.

$$\Psi = \sum_\nu f_\nu(\mathbf{r}) \psi_\nu. \quad (7)$$

Combining (7) and (5), using (6) and then multiplying in turn by the complex conjugate wave functions  $\psi_0^*$  and  $\psi_n^*$ , there results, after integration over the solid angles  $d\Omega_1$ , and  $d\Omega_2$  of the two rotators, the wave equations for the relative motion in the initial and final states respectively,

$$\left. \begin{aligned} \Delta f_0 + (k_0^2 - U_{00}) f_0 &= 0 \\ \Delta f_n + (k_n^2 - U_{nn}) f_n &= U_{n0} f_0 \end{aligned} \right\} \quad (8)$$

$$k_\nu^2 = 2\mu/\hbar^2 (W - E_\nu) \quad (9)$$

$$U_{ik} = 2\mu/\hbar^2 \int \psi_i^* V \psi_k d\Omega_1 d\Omega_2. \quad (10)$$

In (8) the assumption has been made that the non-diagonal elements of the perturbation are small compared to the diagonal ones.† The

† "Method of Distorted Waves," Mott and Massey, "Atomic Collisions," Oxford Univ. Press (1933), p. 100. The criterion for the validity of this procedure, p. 105, is shown by later calculations to be fulfilled.

solutions of (8) must be found which behave, as usual, for large distances in the following manner

$$\left. \begin{aligned} f_0 &\sim e^{ik_0 z} + A_0(\theta) \frac{e^{ik_0 r}}{r} \\ f_n &\sim A_n(\theta) \frac{e^{ik_n r}}{r} \end{aligned} \right\}. \quad (11)$$

Then the cross-section for inelastic collisions is given by

$$Q = 2\pi k_n / k_0 \int_0^\pi |A_n(\theta)|^2 \sin \theta \, d\theta. \quad (12)$$

With the expansions

$$\left. \begin{aligned} f_0 &= \sum_0^\infty (2l+1) \gamma_l(r)/r P_l(\cos \theta) \\ f_n &= \sum_0^\infty (2l+1) g_l(r)/r P_l(\cos \theta) \end{aligned} \right\}, \quad (13)$$

we find for  $\gamma_l$  and  $g_l$  the differential equations

$$\frac{d^2 \gamma_l}{dr^2} + \left( k_0^2 - U_{00} - \frac{l(l+1)}{r^2} \right) \gamma_l = 0, \quad (14A)$$

$$\frac{d^2 g_l}{dr^2} + \left( k_n^2 - U_{nn} - \frac{l(l+1)}{r^2} \right) g_l = U_{n0} \gamma_l. \quad (14B)$$

In order to fulfil the requirement (11) we must choose the solution of (14A) which for large  $r$  has the behaviour

$$\gamma_l \sim k_0^{-1} e^{i\delta_l} (-i)^l \sin \left( k_0 r - \frac{l\pi}{2} + \delta_l \right), \quad (15)$$

in which  $\delta_l$  is a phase distortion due to the perturbing influence of  $U_{00}$ . The solution of (14B) can be given in terms of the solutions  $\Lambda_l$  and  $L_l$  of the homogeneous equation where for  $r \rightarrow \infty$

$$\left. \begin{aligned} \Lambda_l &\sim k_n^{-1} \sin \left( k_n r - \frac{l\pi}{2} + \beta_l \right) \\ L_l &\sim k_n^{-1} \exp i \left( k_n r - \frac{l\pi}{2} + \beta_l \right) \end{aligned} \right\}. \quad (16)$$

Then

$$\begin{aligned} g_l &= -k_n \Lambda_l \int_r^\infty L_l U_{n0} \gamma_l \, dr \\ &\quad - k_n L_l \int_0^r \Lambda_l U_{n0} \gamma_l \, dr^\dagger. \end{aligned} \quad (17)$$

† Mott and Massey, *loc. cit.*, p. 82.

Finally,

$$Q = 4\pi k_n/k_0 \sum_l (2l+1) |I_l|^2 \quad (18)$$

$$I_l = \int_0^\infty \Lambda_l U_{n0} \gamma_l dr. \quad (19)$$

In order to obtain solutions of the differential equations we must have suitable expressions for the matrix elements of the perturbation. We may obtain the angular dependence of the interaction quite in general in the following manner. We first write  $V$  as a sum of arbitrary radial interactions between the four pairs of hydrogen atoms in the two molecules. Then because the distance between centres,  $r$ , is always larger than the internuclear distance, we can expand each of these four interactions in a Taylor series about  $r$ . The result is†

$$V(r, \vartheta_1, \vartheta_2) = 4v(r) + 2R^2 v''(r) (\cos^2 \vartheta_1 + \cos^2 \vartheta_2), \quad (20)$$

where  $2R$  is the internuclear distance ( $\sim 0.75$  Å in  $H_2$ ) and  $v(r)$  is the interaction between two bound hydrogen atoms. The primes denote differentiation with respect to  $r$ . The integration over the angles gives

$$\left. \begin{aligned} V_{00} &= 4v(r) + 4/3 R^2 v''(r) \\ V_{nn} &= 4v(r) + 12/7 R^2 v''(r) \\ V_{n0} &= 5^{1/2} 4/15 v''(r) \end{aligned} \right\} \quad (21)$$

and the selection rules‡

$$\Delta l_1 = 0, \quad |\Delta l_2| = 0, 2, \quad \Delta m_1 = \Delta m_2 = 0, \quad (22)$$

$l_1 m_1$ ,  $l_2 m_2$  are the rotational quantum numbers of the two molecules. It has been assumed here that both molecules are originally in the normal state. Excitation involving higher states will be rare at ordinary temperatures.

### Application to Hydrogen

Although little is known concerning the actual interaction forces between two hydrogen molecules except for the general form,§ we may

† To this order of approximation  $V$  is independent of  $\phi$ .

‡ Because the Taylor expansion of  $V$  was broken off with the second term there is no cross-product term in  $\vartheta_1$  and  $\vartheta_2$ ; consequently, to this degree of approximation, the quantum numbers of only one molecule may change.

§ One does have a quantitative idea of certain parameters involved in this interaction function such as the molecular diameter and the interaction at large distances which can be given as  $\sim 3/4 \alpha^2 V_i r^{-6}$  in which  $V_i$  is the ionization potential and  $\alpha$  the polarizability. See e.g., Margenau, 'Phys. Rev.', vol. 36, p. 1782 (1930).

obtain plausible expressions for the wave functions and the matrix elements in the following manner. For the purpose of obtaining reasonable wave functions  $\gamma_l$  and  $\Lambda_l$  it will suffice to take for the field in which the two molecules move that of rigid spheres:

$$\left. \begin{aligned} V_{00} = V_{nn} = \infty & \quad r < \sigma \\ V_{00} = V_{nn} = 0 & \quad r > \sigma \end{aligned} \right\}. \quad (23)$$

Then,  $r > \sigma$

$$\left. \begin{aligned} \gamma_l &= \left( \frac{\pi r}{2k_0} \right)^{\frac{1}{2}} \frac{e^{i\delta_l}}{(1 + \xi_0^2)^{\frac{1}{2}}} \left[ J_{-l-\frac{1}{2}}(k_0 r) - \xi_0 J_{l+\frac{1}{2}}(k_0 r) \right] \\ \Lambda_l &= \left( \frac{\pi r}{2k_n} \right)^{\frac{1}{2}} \frac{1}{(1 + \xi_n^2)^{\frac{1}{2}}} \left[ J_{-l-\frac{1}{2}}(k_n r) - \xi_n J_{l+\frac{1}{2}}(k_n r) \right] \end{aligned} \right\} \quad (24)$$

$$\xi_i = \frac{J_{-l-\frac{1}{2}}(k_i \sigma)}{J_{l+\frac{1}{2}}(k_i \sigma)} \quad \tan \delta_l = (-1)^{l+1} \xi_0. \quad (25)$$

For the case of the matrix element  $V_{n0}$  we must choose a less schematic form for the interaction. We may take for the field in which the two normal molecules move a Morse potential

$$V_{00} = D e^{-2a(r-r_0)} - 2D e^{-a(r-r_0)}. \quad (26)$$

Combining this with the first equation of (21) we may determine  $v(r)$  and thus  $V_{n0}$ . We find

$$V_{n0} = \frac{4}{5^{\frac{1}{2}}} a^2 R^2 D \left[ \frac{e^{-a(r-r_0)}}{3 + a^2 R^2} - 2 \frac{e^{-2a(r-r_0)}}{3 + 4a^2 R^2} \right]. \quad (27)$$

Proceeding to the cross-section (18), it can be seen that we must consider terms up to  $l \sim k_0 r_m$ , where  $r_m$  is the distance at which  $V_{n0}$  has become inappreciable compared to  $D$ , say; for when  $l$  attains this value the distance of closest approach will be of the order  $r_m$  and then the wave functions in (19) will be small just in the region where  $V_{n0}$  has an appreciable value, that is for  $r < r_m$  ( $r_m \sim 4 \text{ \AA}$ ). Consequently  $I_l$  will be small for  $l > k_0 r_m$ . Stated otherwise, this means that for large  $l$  the centrifugal force prevents the molecules from approaching close to each other, so that the interaction forces do not become large enough to make the excitation process very probable. However, the number of terms left for consideration is still so large that in view of the approximations already made, a numerical evaluation of these is hardly worth while. For our purpose it is sufficient to establish a lower limit for the cross-

section and this can be done by considering only the first term in which the integral  $I_0$  can be done exactly.†

$$\left. \begin{aligned} Q > Q_0 &= \frac{2^{10} \mu^2 D^2 R^4 a^6}{5h^4} \frac{k_n}{k_0} [y(a) - 8y(2a)]^2 \\ y(a) &= \frac{1}{(3 + a^2 R^2)(\Delta k^2 + a^2)(K^2 + a^2)} \\ \Delta k^2 &= (k_0 - k_n)^2 \quad K = (k_0 + k_n)^2 \end{aligned} \right\} \quad (28)$$

The terms neglected ( $l > 0$ ) are not negligible compared to the first term. In fact we may estimate conservatively that the cross-section will be from 10 to 100 times  $Q_0$ . As far as order of magnitude is concerned we may put

$$Q \approx 10^{-18} \text{ cm}^2$$

and for  $T \sim 300^\circ \text{ A}$

$$\kappa_2 \approx 10^{-12} \text{ cm}^3 \text{ sec}^{-1}$$

and therefore

$$\omega_i \approx 10^7 \text{ sec}^{-1}.$$

With  $\omega_i = 10^7 \text{ sec}^{-1}$  the sound velocity at the frequency  $\omega = 10^6$  is little different from the classical value,  $f(\omega = 0)$ . On the basis of this calculation, therefore, we may expect that no dispersion should be observed in hydrogen at the frequency  $\omega \sim 10^6 \text{ sec}^{-1}$ .

## EXPERIMENTAL

The apparatus used in obtaining the experimental data was a modification of the acoustic interferometer used by Pierce. In a cylindrical tube of brass, 25 cm long and 8 cm in diameter the quartz oscillators were mounted. The positions of maximum reaction in the vibrating column were explored with a plane ground brass reflector and detected by means of the deflections on the microammeter in the plate circuit. A diagram of this part of the apparatus is shown in fig. 1.

The quartz oscillator rested on a bakelite plate  $a$ , which was set on three screws so placed that the upper face of the crystal was accurately

† The constants in the Morse potential have been given the values  $D = 1.5 \times 10^{-14}$  erg,  $a = 5 \times 10^8$  cm,  $r_0 = 3 \times 10^{-8}$  cm. The value of one of these is fixed by making  $V_{00}(\sigma) = 0$  with  $\sigma = 2.75 \times 10^{-8}$  cm. See Massey and Mohr, 'Proc. Roy. Soc.', A, vol. 141, p. 434 (1933). The other constants are chosen so that  $V_{00}$  approximates as closely as possible to the inverse sixth power curve for large  $r$ . Values for polarizability and ionization potential are to be found in Margenau's paper. See preceding footnote.



parallel to the brass reflector. The piezo electric quartz crystals were cut from the natural crystal of quartz so that their sides were parallel to the optic and electric axes. The exact mounting of the crystal depended on its size; for large crystals, that is, those vibrating with low frequency,

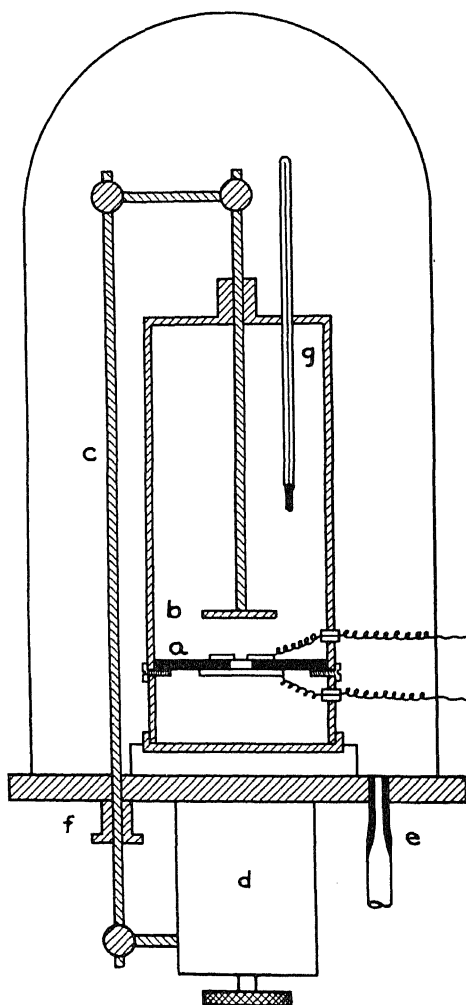


FIG. 1

the metal electrodes were placed vertically to the bakelite plate and the crystal placed in between so that the electrodes were perpendicular to the electric axis. The sides of the crystal only touched the electrodes and the crystal was free to execute mechanical vibrations perpendicular to the optic and electric axis. The method for mounting the high frequency

crystal, which was about 1 mm thick was slightly different; a hole was cut in the bakelite sufficiently large to contain the crystal and one electrode was fixed to the lower side of the bakelite plate. The other was made of a very thin aluminium plate and rested on the top of the crystal; a hole was cut in the latter plate to permit the radiation of the sound, which was in this case parallel to the electric axis.

The interferometer rested on a brass plate and was enclosed by a glass bell-jar. The brass reflector *b* was connected by the rod *c* to a fine micrometer screw *d*; one revolution of the screw corresponded to 0.5 mm, and could be read to  $5 \times 10^{-4}$  mm. By means of the copper-glass seal *e* the apparatus was joined to liquid air and charcoal traps

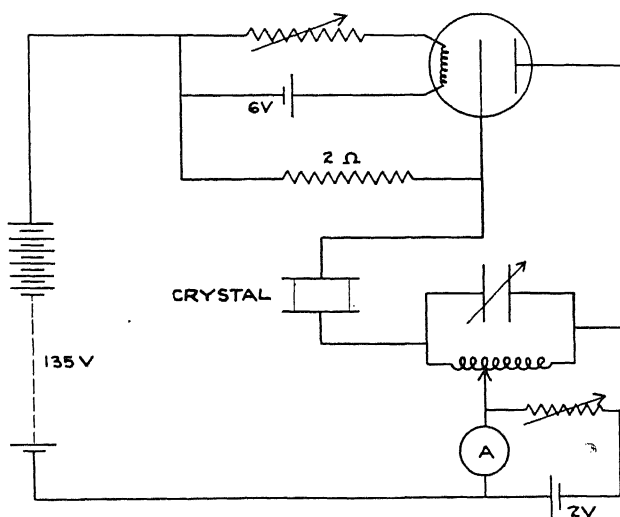


FIG. 2

and a system of drying tubes, then to a diffusion pump which was backed by a Hyvac pump. A wax made of beeswax and rosin was used at the base of the glass bell-jar and lubriseal was placed at the lower end of the tight fitting sleeve *f*. By this means a sufficient vacuum was obtained, and during 24 hours the gauges showed a rise less than  $2 \times 10^{-3}$  mm. To produce the vibrations either one of two circuits was used; in the case of the high frequency crystal a pentode oscillator was used, but for the low frequency a triode oscillator was sufficient. Fig. 2 shows the circuit; it consists of a UX 201 thermionic tube and a 135-volt B battery. The crystal was connected between the grid and the plate. Connected to the microammeter A and its shunts is a bias battery and a large variable resistance. This makes it possible to reduce the current through the ammeter to approximately zero. The sensitivity of the ammeter

could be increased to the desired value by the selection of the shunt and varying the resistance in the bias circuit; the sensitivity could be changed from  $10^{-4}$  amperes to  $10^{-7}$  amperes per millimetre deflection.

The dispersion of sound is sensitive to changes in pressure. The dispersive region shifts to higher frequencies with increasing pressure, or conversely at a given frequency the velocity of sound increases as the pressure is diminished until a constant of the velocity is reached. This means that instead of having many crystals in order to supply sufficient points on the dispersion curve a low frequency crystal can be used and readings taken at different pressures. Since the above apparatus could be conveniently used at low pressures, this method was used in attempting to find a dispersion region for hydrogen.

### *Procedure*

The hydrogen was supplied in a gas cylinder and was 99.5% pure, and was passed slowly through the drying system and charcoal traps into the interferometer chamber. At the required pressure the frequency of the crystal was measured immediately before the exploration of the vibrating column. This was done in two ways; the coil of the oscillating circuit was coupled with the coil of a standard wavemeter, and from the condenser readings of the latter the frequency was calculated; and secondly, the frequency was found by measuring the beat frequency of some harmonic of the crystal frequency with a certain radio frequency which was known to be correct to  $\pm 50$  cycles. The frequency therefore could be accurately measured to 0.05% at all temperatures. The oscillating column was then explored, the reflector moving about 0.015 mm between each reading; nearer the peaks more readings were taken. This was continued until sufficient peaks had been explored. The temperature was taken from the thermometer *g*, fig. 1, every 5 minutes and where the temperature varied by as much as  $0.1^\circ$ , the readings were discarded; at each pressure the vibrating column was explored several times. From the readings graphs were drawn of the peaks and from them the wave-length was calculated. Fig. 3 shows a few of the peaks obtained. Owing to the large deflections only the peaks are shown. It was necessary to change the resistance in order to keep the pointer on the scale when exploring the troughs of the sound wave.

The results obtained for the two crystals used and the different pressures are given in Table I. Each velocity is the average of several, the extremes of which did not differ from the average given by more than  $\pm 3$  kc.

TABLE I

At 388 kc and 30° C

$p$ in mm of Hg .....	424	487	576	648	764
$f$ in m sec <sup>-1</sup> .....	1319	1319	1320	1318	1318

At 1465 kc and 30° C

$p$ in mm of Hg .....	636	710	738	767	772
$f$ in m sec <sup>-1</sup> .....	1320	1320	1319	1320	1319

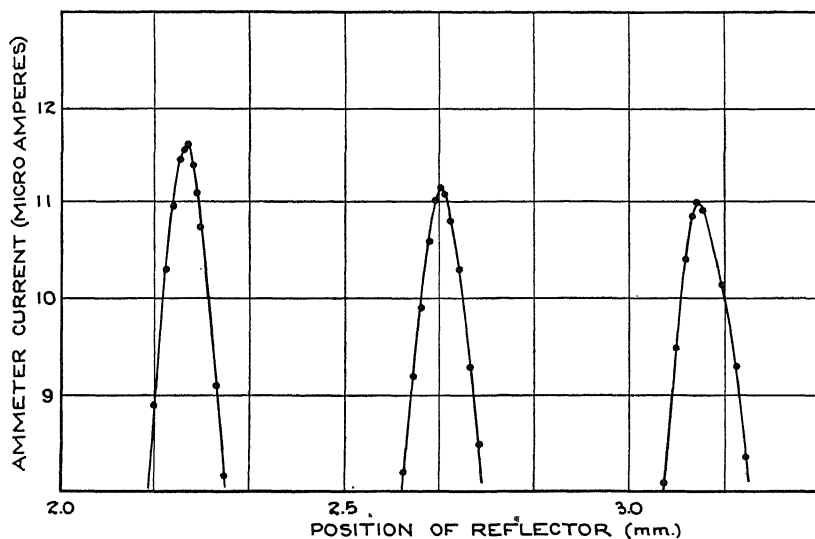


FIG. 3

The classical velocity calculated from

$$f^2 = p/\rho (1 + k/C_0),$$

for hydrogen with  $\rho = 8.41 \times 10^{-5}$  g cm<sup>-3</sup>, at  $T = 30^\circ$  C,  $p = 780$  mm Hg, and  $C_0/k = 2.46$ , is 1319 m sec<sup>-1</sup>. The experimental results for the velocity at the extreme frequencies used and at all pressures practically coincide with the computed value. The effect sought for is not a small one since the maximum possible change in the velocity is from 1319 m sec<sup>-1</sup> to 1440 m sec<sup>-1</sup>, so that we may conclude that at ordinary pressures the dispersion region lies at frequencies greater than  $1.5 \times 10^6$  cycles.†

† Since the completion of this work there has appeared a notice by Kneser and Wallmann, 'Naturwiss.', vol. 22, p. 510 (1934), reporting no dispersion in hydrogen up to 1481 kc.

We wish to express our gratitude to Professor G. E. Uhlenbeck for his many helpful suggestions and valuable advice so generously given throughout the course of this work.

One of the authors (A. S. R.) also wishes to express his indebtedness to the Commonwealth Fund of New York for a Fellowship.

#### SUMMARY

The dispersion of sound in hydrogen is investigated. The results show that no variation of velocity occurs below frequencies of the order  $10^6$  cycles per second. This is to be expected from the classical theory of Jeans as well as from the quantum treatment of the inelastic collision between two hydrogen molecules as the calculation shows.

---

## Artificial Radioactivity produced by Neutron Bombardment—II

By E. AMALDI, O. D'AGOSTINO, E. FERMI, B. PONTECORVO, F. RASETTI,  
and E. SEGRÈ

*(Communicated by Lord Rutherford, O.M., F.R.S.—Received  
February 15, 1935)*

#### INTRODUCTION

We describe in this paper some further results on artificial radioactivity induced by neutron bombardment, which have been obtained in the Physical Laboratory of the University of Rome, after the publication of our first paper on the same subject.\* Preliminary reports containing the main results have been already published by several of us.†

\* Fermi, Amaldi, D'Agostino, Rasetti, Segrè, 'Proc. Roy. Soc.,' A, vol. 146, p. 483 (1934).

† Fermi, Amaldi, Pontecorvo, Rasetti, Segrè, 'Ric. Scient.,' vol. 2, p. 280 (1934); Fermi, Pontecorvo, Rasetti, 'Ric. Scient.,' vol. 2, p. 380 (1934); Amaldi, D'Agostino, Segrè, 'Ric. Scient.,' vol. 2, p. 381 (1934); Amaldi, D'Agostino, Fermi, Pontecorvo, Rasetti, Segrè, 'Ric. Scient.,' vol. 2, p. 467 (1934); vol. 1, p. 123 (1935). Some of our experiments have been repeated with analogous results by Bjerger and Westcott 'Proc. Camb. Phil. Soc.,' vol. 31, p. 145 (1935); we thank them for having submitted their manuscript to us.

By far the most interesting new result concerns the effect of hydrogenated substances on the activation of several elements by neutron bombardment (§ 1). We give an interpretation of this phenomenon by assuming that neutrons are slowed down by impacts against hydrogen nuclei (§ 2). Some anomalously large absorption cross-sections for slow neutrons are discussed in § 3. In many cases the anomalous absorption is connected with the emission of  $\gamma$ -rays (§ 4). § 5 describes some attempts to get information about the energy of the slow neutrons. Scattering experiments on slow neutrons are described in § 6, while § 7 deals with the production of slow neutrons through the action of non-hydrogenated substances. In § 8 the above results are discussed from a theoretical point of view. §§ 9 and 10 are dedicated to chemical methods for the separation of radioactive isotopes, and to improvements in the technique of the measurements. Results of a systematic investigation of the different elements are given in § 11. These results are collected in a table at the end of the paper.

#### § 1—EFFECT OF HYDROGENATED SUBSTANCES ON THE ACTIVATION

In our previous work we had noticed some irregularities in the intensity of the activation of silver by neutrons from a radon + beryllium source, which apparently depended upon some not very clear geometrical factors. Further investigation showed that the activation was strongly influenced by objects surrounding the neutron source, and in particular that the activation could be enormously increased by surrounding the source and the activated substance with a large amount of water or paraffin wax. This effect appeared at once to be due to the presence of hydrogen, as other substances not containing hydrogen failed to give comparable effects (see § 7).

To ascertain whether these large activations were due to the neutrons or to the  $\gamma$ -rays emitted very strongly from our source, we repeated the experiment using as a source 100 mg radium, without beryllium, and found no induced radioactivity. It follows that the effect is actually connected with the neutrons. As a check on this point, we observed the same hydrogen effect with a Po + Be neutron source with an intensity in accordance with the number of neutrons emitted.

Not every substance which is activated by neutrons shows an increase in activity when irradiated under water. Among the strongly influenced activities are: Na (15 h); Al (2.3 m); V (3.75 m); Ag (22 s, 2.3 m); Cu (5 m); Rh (44 s, 3.9 m); I (25 m). The activation of other elements, or possibly of single decay periods, is not influenced by water; among

these are: Si (2.3 m); Al (10 m); Mg (40 s); Mn (3.75 m); Zn (5 m). We have observed that in every case where the active element is known to be an isotope of the bombarded one (about 20 cases), the activation is increased by the presence of water.

In order to measure approximately the sensitivity of the different activations to the action of water or paraffin, we express it in a conventional scale. A cylinder (about 2 cm in diameter and 5 cm in height) of the substance under investigation is irradiated by putting the source in its centre. Source and cylinder are sustained by thin metallic supports at some distance from other objects. The activity reached after a convenient time of irradiation is measured. Afterwards the same cylinder is irradiated with the same source in the same relative position for an equal length of time surrounding both with a large cylindrical block of paraffin 27 cm in diameter and 20 cm in height. The ratio of the activities with and without paraffin is taken as a measure of the sensitivity to hydrogenated substances and denoted by  $\alpha$ . In this scale  $\alpha = 1$  means that the substance shows no increase in activity when irradiated in paraffin. Of course this definition of the sensitivity coefficient is only an empirical one, as it depends somewhat on the geometrical conditions.

Sensitivity coefficients different from one have been observed ranging from  $\alpha = 1.6$  for U (13 m, 100 m) to  $\alpha = 40$  for V (3.75 m). However, it must be pointed out that the last figure may not be the largest, because many substances fail to show some activities when irradiated in air, and these activities appear only by irradiation under water, and then rather weakly.

The ratio of increase in activation due to the presence of paraffin or water is much larger if source and irradiated substance are kept some centimetres apart (see § 5).

## § 2—INTERPRETATION IN TERMS OF SLOW NEUTRONS

The experiments described in the preceding section can be explained on the hypothesis that the effect of water, or better of hydrogen, surrounding the source is due to scattering and slowing down of the primary neutrons by elastic collisions with hydrogen nuclei.

It is easily shown that an impact of a neutron against a proton reduces, on the average, the neutron energy by a factor  $1/e$ . From this it follows that 10 impacts reduce the energy to about  $1/20,000$  of its original value. Assuming the initial energy to be  $4 \cdot 10^6$  electron volts, the energy after 10 impacts would be about 200 electron volts; and less than 20 impacts would be necessary to reduce the energy to thermal equilibrium values.

The phenomena that we have described can now be explained on the assumption that slow neutrons are more easily captured by some nuclei than fast ones. In this and in the following sections we shall discuss our experiments in terms of this hypothesis.

The increase in activity through the action of hydrogen may be ascribed both to the scattering which causes an increased neutron flow through the substance to be activated and to the higher efficiency of the impact of a slow neutron as compared with that of a fast one. In order to show that this second factor is largely important, we performed the following experiment.

A silver cylinder was irradiated with a  $\text{Rn} + \text{Be}$  source containing 350 mC; the distance between source and cylinder was 20 cm. If nothing but air surrounded the source and the cylinder, no activity could be detected in this last after irradiation. Keeping the distance between the source and the irradiated cylinder constant, we then put round the source a cylinder (14 cm diameter and 14 cm depth) filled with water. A strong activity is shown by the silver irradiated in these conditions (about 100 impulses per minute in our counters). This experiment shows that the slow neutrons are much more effective than the fast ones. Indeed, the numbers of neutrons impinging on the silver per second is not increased (possibly slightly lowered through absorption) by the water surrounding the source. As the activation is much increased by the water in these conditions, we must conclude that the yield of activation per impinging neutron is very much enhanced by the slowing down of the neutrons.

### § 3—ABSORPTION OF SLOW NEUTRONS

From the result of the preceding section, that the collision cross-section of slow neutrons for the activation of many elements is much larger than that of fast neutrons, one is led to investigate whether slow neutrons are strongly absorbed by the elements which are most strongly activated by them. We therefore made a systematic investigation of the absorption of slow neutrons in the different elements.

The main purpose of this investigation was to find elements with anomalously large absorption coefficients for the slow neutrons, and hence we generally used fairly thin layers of absorbing material. The arrangement for these absorption measures is shown in fig. 1. The source of neutrons, a  $\text{Rn} + \text{Be}$  tube (S) is put inside a paraffin cylinder P (24 cm diameter, 14 cm height) about 2 cm under the upper surface. A second paraffin cylinder P' was put on P; in its lower surface a hole a few centimetres diameter and 2 or 3 cm in depth was excavated. The



detector of the slow neutrons, a rhodium plate (sometimes also a silver plate), was put inside this hole and its activation measured, after irradiation during a standard length of time, once without absorbing layers and once interposed between two layers A of the absorbing material, as shown in the figure. The ratio of the activities without or with absorbing layers gives the absorption. In these as well as in many other experiments, we generally used rhodium as detector of the slow neutrons, because the activity induced in this element is very large and can be measured very exactly with an ionization chamber; moreover, of the two periods of Rh, 44 s and 3.9 m, practically the first only is of importance, which makes the reduction of the measurements very easy.

As a result of these absorption measures, we found that the half-value thickness  $\delta$  for the absorption of slow neutrons for the different elements

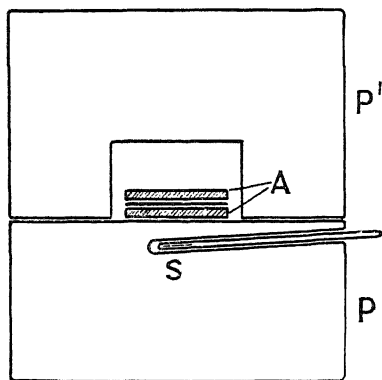


FIG. 1

varies over a very wide range. For several elements it is exceedingly small. As an example we found for boron  $\delta = 0.004 \text{ gm/cm}^2$ ; for yttrium  $\delta = 0.015 \text{ gm/cm}^2$ ; for cadmium  $\delta = 0.014 \text{ gm/cm}^2$ ; for some other elements instead,  $\delta$  is several thousands times larger; for instance, several centimetres of lead absorb less than a few milligrams per  $\text{cm}^2$  of boron.

Expressing the absorption coefficients in terms of a nuclear cross-section  $\sigma$  for the activating impact of a slow neutron,

we find in some cases surprisingly large values, *e.g.*,  $\sigma = 3000 \cdot 10^{-24}$  for B;  $\sigma = 7000 \cdot 10^{-24}$  for Y;  $10,000 \cdot 10^{-24}$  for Cd. This last is the largest cross-section as yet found. It is remarkable how much larger these cross-sections are than the geometrical cross-sections of nuclei, while, as is well known, fast neutrons have cross-sections comparable to the geometrical cross-sections.\* Indeed, we found directly that the absorption of boron for ordinary fast neutrons is at least 1000 times less than the absorption found for slow neutrons in the same element.

These absorption measurements do not refer to homogeneous neutrons. Indeed, the absorption curves are by no means exponentials; the absorption coefficient decreases with increasing thickness, as shown, for instance, by the absorption curve of cadmium, fig. 2. It must also be noticed that the half-value thickness depends to some extent upon the arrangement of

\* Dunning, 'Phys. Rev.', vol. 45, p. 586 (1934).

the paraffin, as this affects the average velocity of the neutrons. For instance absorption of the neutrons inside a hole in paraffin is larger than outside a paraffin block.

#### § 4—EMISSION OF $\gamma$ -RAYS THROUGH THE CAPTURE OF THE NEUTRON

In connection with the anomalous absorption of slow neutrons, one is led to investigate more closely the absorption process. The simplest assumption is to admit that the neutron is captured by the nucleus with formation of an isotope heavier by one mass unit. If this heavier isotope

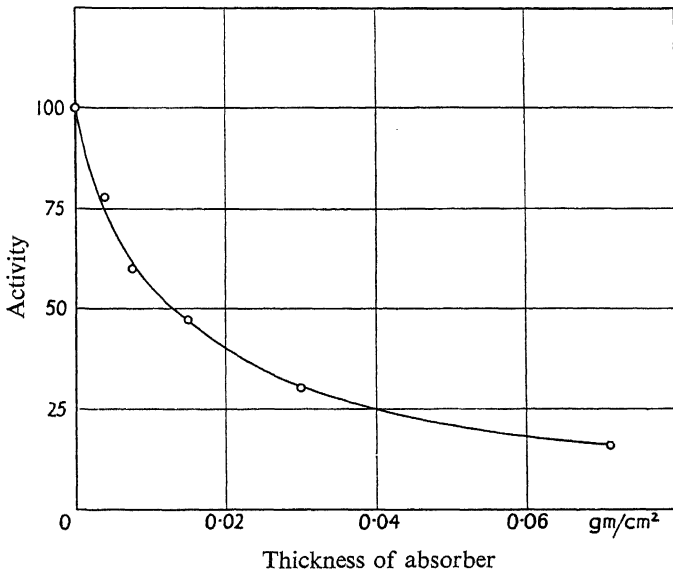


FIG. 2

is unstable, we might expect a strong induced radioactivity for the strongly absorbing elements. This occurs, for example, for indium and iridium, which are known to go over into radioactive isotopes. A rough evaluation of the intensity of the activation of the absorbing substance and of the number of the absorbed neutrons, shows that approximately an activated atom is formed in each absorption process. In other cases it is found that no activation, or at least no strong activation, corresponds to an anomalously large absorption (B, Y, Cd). In these cases we might expect that the capture of the neutron leads to the formation of a stable nucleus. It is obvious that this should happen more easily for elements with many stable isotopes differing in atomic weight by one unit (Cd, Hg).

In both cases, if the slow neutron is simply captured, we might expect that the absorption process should be accompanied by the emission of a  $\gamma$ -radiation, with energy corresponding to the binding energy of the neutron. For fast neutrons a  $\gamma$ -radiation of this type has already been announced by Lea.\*

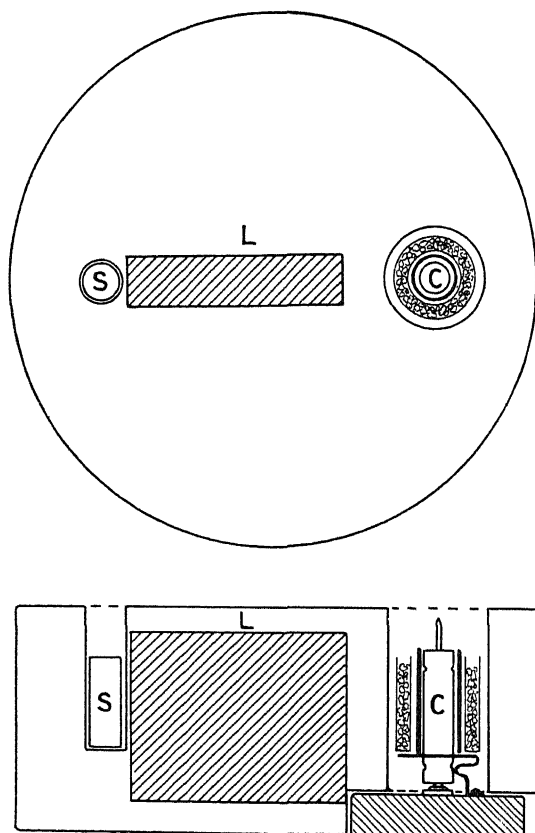


FIG. 3

In the case of the absorption of slow neutrons we were able to show for some elements the emission of a relatively strong  $\gamma$ -radiation of this type by the following experiment.

A  $\text{Po} + \text{Be}$  neutron source *S*, fig. 3, of about 60 millicuries was immersed in a paraffin block together with one of our standard Geiger Müller counters *C*. A lead absorber *L*, 10 cm thick, protected the counter from the direct  $\gamma$ -rays of the source. The counter was surrounded by a lead foil 2 mm thick. The counter registered in these conditions about

\* 'Nature,' vol. 133, p. 24 (1934).

30 counts per minute. Small cylindrical layers of the various substances were placed around the counter, outside the lead foil. We generally observed a very marked increase in the number of counts for the strongly absorbing substances. This was observed, for instance, for Co, Cd, Y, Cl, Ir, Au, Hg, when the number of counts was sometimes more than doubled. An exception to this behaviour is shown by boron and lithium, which, although showing a strong absorption for the slow neutrons, do not emit  $\gamma$ -rays. In these elements the absorption of the slow neutrons has been found to be connected instead to the emission of heavy particles (see § 11). This alternative possibility to the emission of  $\gamma$ -rays appears theoretically likely only for very light elements owing to the low potential barrier.

That the emission of  $\gamma$ -rays, as described before for some substances, was actually due to slow neutrons was shown by the fact that no emission was observed by removing the paraffin. Furthermore, the effect was very much reduced by surrounding substances and counters with a boron screen.

#### § 5—ENERGY OF THE SLOW NEUTRONS

It would be very important to evaluate somehow the mean energy of the slow activating neutrons, and we describe in this section some attempts to do this.

We have already stated that the mean energy of the neutrons is reduced by a factor  $1/e$  for each elastic collision against a proton, provided the values of the energy are large compared with the thermal energy. If the energy of the slow neutrons were really reduced down to this limit, one would expect that the diffusion process might be influenced by temperature. We made an attempt to find such an effect by the following experiment.

A rhodium or a silver detector was irradiated with the  $\text{Rn} + \text{Be}$  neutron source under the same geometrical conditions, once in hot paraffin at  $200^\circ \text{C}$ , and once at  $20^\circ \text{C}$  in a mixture of benzene and penthane having at this temperature the same density and elementary composition as paraffin at  $200^\circ \text{C}$ . No difference in the activation was found in the two tests, within the accuracy of 2%. The mixtures filled a cylinder 26 cm in diameter and 15 cm in height. The detector was on the axis of the cylinder 1 cm under the liquid surface; the source, also on the axis, 2 cm lower. It must be concluded that temperature, at least in these conditions, does not affect the activation, which might be interpreted to mean that the energy of the activating neutrons is higher than the thermal energy. This is, however, not quite conclusive, as the dependency

of both the cross-section for activation and the mean free path upon the velocity for very slow neutrons is unknown.

A direct method of measuring or at least of establishing an upper limit to the energy of the slow neutrons would be to measure the average ionization produced in each collision of a slow neutron against a hydrogen nucleus. This might be done either by measuring the total ionization in a hydrogen-filled chamber or by directly measuring the ionization in a single process by means of a linear amplifier. In both methods the action of the slow neutrons can be separated from that of the fast ones, by screening the chamber with a thin boron layer. Experiments of this kind are being attempted but have not yet led to definite results.

We have investigated whether the increase in activation produced by paraffin is also to be found with different sources of neutrons. We have done this with the neutrons emitted by beryllium irradiated with the  $\gamma$ -rays of radium,\* and found a large effect with this source. This shows that the slow neutrons of paraffin are slower than the neutrons emitted in this nuclear reaction.

#### § 6—SCATTERING AND DIFFUSION OF THE SLOW NEUTRONS

In connection with the absorption measurements described in § 4, we have made a rough survey of the scattering properties of the different substances. The experimental arrangement is shown in fig. 4. The source

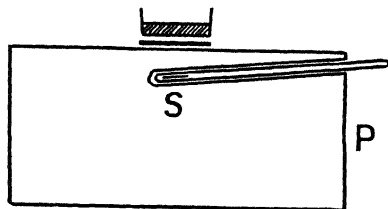


FIG. 4

S is enclosed in the cylindrical paraffin block P as described in § 4. The rhodium plate used as detector was activated by placing it on the top of this paraffin block. The activation was measured once with the substance to be investigated placed in a layer above the rhodium plate, and once without it. In some cases an increased activation was found when a substance was superimposed, indicating an action from slow neutrons scattered back from the substance. For instance, a layer of carbon a few centimetres thick increases the activation about five times. Similar

\* Szilard and Chalmers, 'Nature,' vol. 134, p. 494 (1934).

results are found with several light elements (Be, C, Si). Heavy elements generally produce a much smaller effect. Boron, which has a large absorption coefficient, does not produce any appreciable increase of activity. This shows that the anomalously large absorption of this element is mainly due to real absorption and not to scattering.

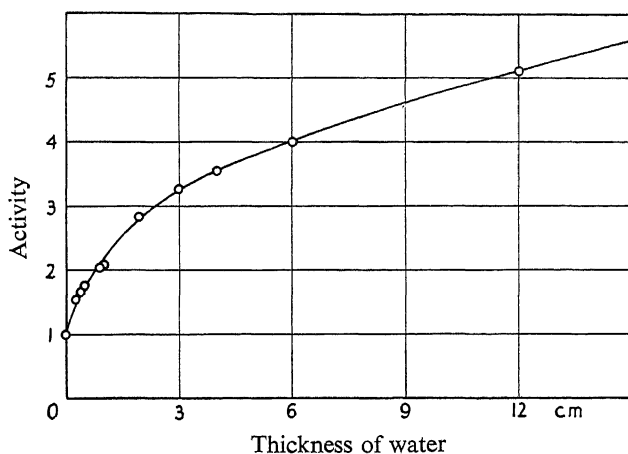


FIG. 5

We have repeated the same experiment with water, obtaining the curve reproduced in fig. 5 for the intensity of activation as a function of the thickness of the scattering layer. A similar result is obtained employing paraffin instead of water.

Other experiments on scattering have been made by the arrangement shown in fig. 6. A paraffin cylinder, 13 cm diameter and 11 cm high, contains in its centre the neutron source S. The detector, a silver or rhodium cylinder R, is kept at a distance of 30 cm from the source. A screen D of the scattering material is interposed between the source and the detector; its dimensions are such as to intercept exactly all the neutrons which might reach the detector from the paraffin block. The difference in the activity of the detector measured when irradiated with or without the screen D gives a measure of the effect of scattering + absorption. We found by this apparatus that a paraffin layer  $0.5 \text{ gm/cm}^2$  thick reduces the intensity of the silver activation to about one-half;

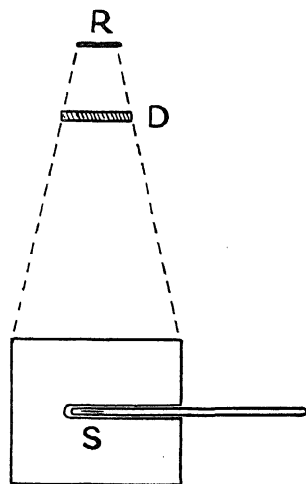


FIG. 6

here also we found that the absorption is not exponential. A similar result is obtained, using water as a scatterer. From this we might deduce the order of magnitude of the mean free path of slow neutrons in water or paraffin, this being comparable with the observed half-value thickness.

For carbon the half-value thickness is about 5 gm/cm<sup>2</sup>. Lead of a thickness of about 4 gm/cm<sup>2</sup> gave a slight decrease in intensity, which is mainly due to scattering.

Another set of experiments was made in order to determine how the intensity of the activation of rhodium in water decreases with the distance from the source. The source was immersed in a water basin of the dimensions 40 × 40 × 100 cm and the activity induced in rhodium at

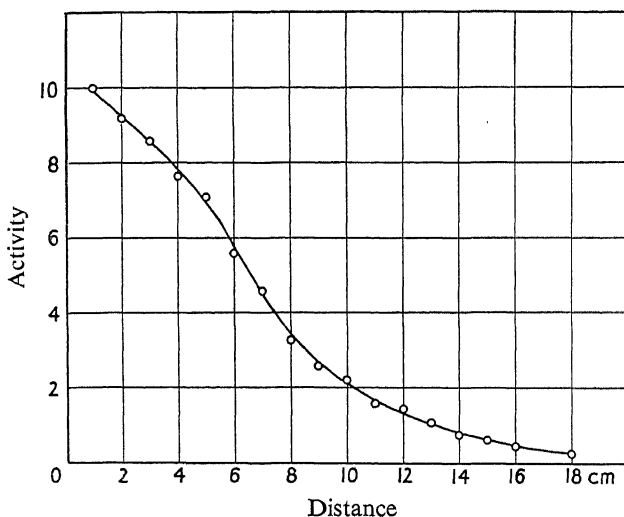


FIG. 7

different distances measured with an ionization chamber. The result is shown in fig. 7, where the activity is plotted as a function of the distance. A similar experiment was made with 2% boric acid dissolved in the water, obtaining a curve similar to the former, only very much reduced in intensity, owing to the absorption of boron.

The general picture of the slowing down process, which one gets from these experiments is the following. The largest part of the diffusion process takes place when the primary neutron still retains much of its original energy, having collided only a few times with hydrogen nuclei; as the velocity is reduced down to the value for which the absorption by boron becomes appreciable, the mean free path in hydrogen appears to

be fairly small, so that the diffusion process after this stage is contained in a small volume. This explains also the fact that the absorption coefficient of boron for the neutrons in water is fairly independent of the distance from the source.

#### § 7—EFFECT OF NON-HYDROGENATED SUBSTANCES ON THE ACTIVATION

We have tried if effects similar to that of water or paraffin could be obtained also with non-hydrogenated substances. Owing to the large amount of materials necessary for these experiments, only a few substances have been tested; Pb,  $\text{SiO}_2$ , C, Fe. In all these, with the exception of Fe, a definite increase of the activation of rhodium was observed. Under the geometrical conditions to be described later, the effect was increased by a factor two to five, while in water the factor would have been of some hundreds. That this increase in activity is not simply due to scattering of the neutrons but mainly to their loss in velocity, is proved by the fact that the activation of silicon under the same circumstances is not increased; moreover, very thin cadmium absorbers considerably reduced the activation of rhodium. These facts seem rather surprising chiefly for lead, as it would be difficult to explain the slowing down of neutrons as due to elastic collisions.

The details of these experiments were as follows. We built with lead blocks a cube with a side of about 50 cm. The neutron source was placed in the centre and the rhodium detector 10 cm apart. The activity is about three times larger than in the same geometrical conditions without lead. A similar result is obtained with silver as detector instead of rhodium, while a silicon detector shows no increase in the activity. This fact is to be taken as an indication that the velocity of the neutrons is reduced by the impact against lead nuclei. This view is confirmed by the observation that the activation of rhodium in lead is reduced to half value by an absorber of cadmium of 1 gm/cm<sup>2</sup>. Comparing this absorption of cadmium with that of the same element for the slow neutrons in water (half-value thickness 0.014 gm/cm<sup>2</sup>), one is led to assume that the average velocity of the neutrons in lead is not so low as in water.

A similar experiment was performed, using a graphite cylinder of 3 litres volume. The source was placed in the centre and the rhodium detector at 5 cm distance. The increase in activation was about the same as that produced by lead in the former experiment and the absorption of the neutrons in cadmium was certainly not smaller. Similar results were obtained with silica in the form of "Kieselguhr." The failure to



observe a similar effect with iron is probably due to its relatively large absorption.

We conclude from these experiments that the property of intensifying the activation is shown by most materials. The possible action of surrounding objects, possibly even of air, must always be considered, when experimenting quantitatively on the activation of some substances. For these reasons, the figures given above for the effect of some materials are to be taken only as an indication.

### § 8—THEORETICAL CONSIDERATIONS ON THE PROPERTIES OF SLOW NEUTRONS

In our first paper we left undecided the question whether whenever the neutron bombardment gives rise to a radio element isotopic with the original one, the neutron is captured or causes the expulsion of a neutron from the struck nucleus, *i.e.*, whether the atomic weight of the radioactive product is  $A + 1$  or  $A - 1$ . We believe that the evidence accumulated since then speaks all in favour of the first hypothesis. The main points of this evidence are the following.

(a) Two new weak activities have been recorded: one, a 15-hour period in sodium, the other a 2.3-minute period in aluminium. Both their identity with known periods, in the first case of aluminium and magnesium, in the second case of silicon and phosphorus, and the chemical evidence in the case of sodium (see § 11), show that the radio elements are respectively isotopes of Na and Al. As both these elements have only one stable isotope, *i.e.*,  $^{23}\text{Na}$  and  $^{27}\text{Al}$ , the choice remains for radio sodium between  $^{24}\text{Na}$  and  $^{22}\text{Na}$ , for radio aluminium between  $^{28}\text{Al}$  and  $^{26}\text{Al}$ . Now both the lighter isotopes  $^{22}\text{Na}$  and  $^{26}\text{Al}$  are known from other nuclear reactions to have different periods and to emit positrons instead of electrons, so that it seems well founded to admit that, at least in these cases, the neutron is captured.

(b) While there is no theoretical difficulty in understanding how a neutron with a negligible kinetic energy can be captured by a nucleus, it seems unlikely that it could knock out a stably bound neutron from the nucleus. Still more difficult it would be to understand that in the latter case energy could be left over to account for the emission of  $\gamma$ -rays.

We shall, then, discuss the experimental facts on the standpoint that the neutrons, and particularly slow ones, are easily captured by many nuclei.

There are, however, some theoretical difficulties in understanding this capture process, or at least to account for the large cross-sections that

have been experimentally observed in some cases. Nevertheless it may be worth while to state some general consequences of the theory, which must be always kept in mind in the discussion of this problem.

Let us admit, as it has been generally assumed, that the forces acting between the neutron and a nucleus extend about as far as the nuclear radius itself. If this is so, the de Broglie wave-length is, for fast neutrons, of the order of the radius of action, and consequently for slow neutrons is much larger. The well-known theory of the impact, in which the nucleus is treated as a potential hole, takes in this case an extremely simple form. Let  $\psi$  be the  $s$ -eigenfunction corresponding to zero energy. In fig. 8 the product  $r\psi$  is plotted as a function of the radius vector  $r$ , and  $\rho$  represents the radius of action. The curve has an irregular shape for  $r < \rho$ , while for  $r > \rho$  it becomes a straight line. We normalize  $\psi$  taking  $\psi(0) = 1$ . Let then the equation of the straight line into which  $r\psi$  goes over for large values of  $r$  be

$$r\psi \rightarrow \eta(a + r),$$

where the geometrical meaning of  $\eta$  and  $a$  is clear from the figure. The values of these two quantities could be easily calculated if one knew the form of the potential hole representing the nucleus. The cross-section for elastic collisions in the limit for low velocities is found to be

$$\sigma_{el} = 4\pi a^2, \quad (1)$$

while the density of probability for the neutron to be found in the centre of the nucleus is

$$P = n/\eta^2, \quad (2)$$

where  $n$  is the density of the neutrons outside of the nucleus.

Whatever the mechanism of capture may be, it is natural to assume that, at least to a certain approximation, the probability of capture of the neutron by a nucleus per unit time will be proportional to  $P$ , *i.e.*, that this probability will be given by  $kn/\eta^2$ , where  $k$  is a constant for each nucleus.

This probability can be expressed in terms of a cross-section  $\sigma_{ca}$  for the capture process through the relation

$$\sigma_{ca} = k/\eta^2 v, \quad (3)$$

where  $v$  is the velocity of the neutron. A limit to the validity of (3) is set by the fact that  $\sigma_{ca}$  can evidently be at most of the order of magnitude of the square of de Broglie wave-length. This allows one, considering the largest cross-sections found experimentally (Cd,  $\sigma_{ca} = 10^{-20}$ ), to set

an upper limit for the energy of the slow neutrons. This limit turns out to be a few hundred volts. However, it must be borne in mind that this deduction is valid only under the explicitly stated assumptions.

Formula (3), valid only for low velocities, gives a cross-section for capture for a given nucleus inversely proportional to the velocity of the neutron. This explains why the cross-section for capture is generally larger for slow neutrons than for fast ones. This result may also be expressed by saying that the mean life of a slow neutron in a substance is independent of its velocity. While the capture cross-section is inversely proportional to the velocity, the cross-section for elastic impact expressed

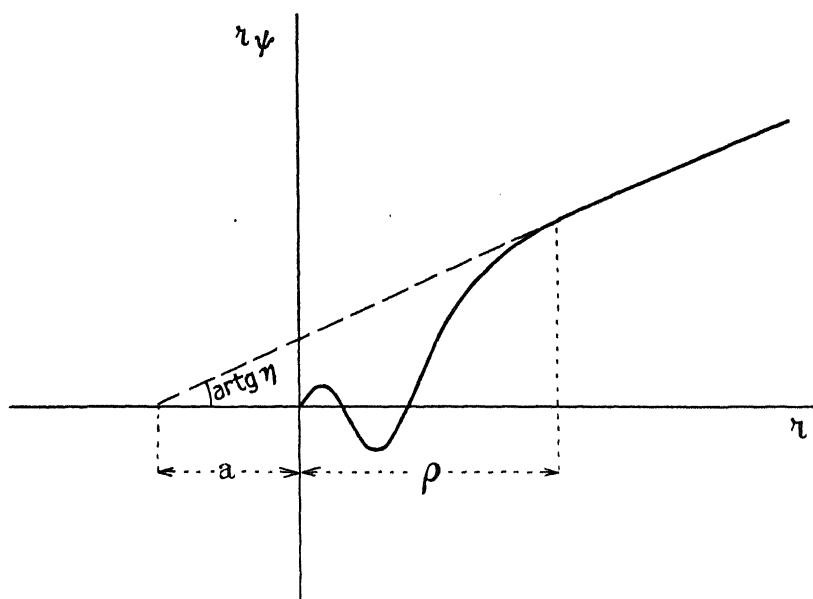


FIG. 8

by (1) is independent of the velocity, which means that the mean free path for this type of collisions is also independent of the velocity.

One more feature of (3) is that  $\sigma_{ca}$  is inversely proportional to  $v^2$ . The straight line of fig. 8 may occasionally be nearly parallel to the abscissæ axis. In this case  $\eta$  is very small and consequently the capture section becomes very large. This behaviour of the eigenfunction is probably responsible for the anomalously large cross-sections observed for a few nuclei.

In order to deduce from (3) the absolute values of the cross-sections, it would be necessary to know also the values of  $k$ , which quantity depends on the physical mechanism of the capture. We know from the experi-

ments that there are two different processes. In some light elements (Li, B) the capture of the neutron is followed by the emission of heavy particles; while in the heavier elements the normal process seems to be capture with emission of a  $\gamma$ -ray. The binding of an additional neutron to a nucleus sets free an amount of energy which, on the average, has a value about 7 million electron volts. This surplus energy might in some cases produce the emission of an  $\alpha$ -particle, provided the potential barrier surrounding the nucleus is low enough to allow for a quick escape of the particle. Therefore this process is expected to occur only for the lightest elements, whereas in the activation by fast neutrons, owing to the kinetic energy of the impinging neutron which is to be added to the binding energy, the emission of charged particles is possible also in elements of higher atomic weight.\*

In the case of capture with emission of a  $\gamma$ -ray, which is observed for elements of any atomic weight up to the highest, the ordinarily accepted mechanism of irradiation gives apparently rather too small a value for  $k$ .  $k$  depends upon two factors which are rather difficult to evaluate: matrix elements and energy of the emitted  $\gamma$ -quanta. As the probability of emission of a  $\gamma$ -quantum is *ceteris paribus* proportional to  $\nu^3$ , it is to be assumed that processes by which the binding energy of the neutron is very large ought to be preferred; this binding energy might in several cases considerably exceed 10 million volts. Nevertheless one ought probably to assume rather too high a value for the matrix elements in order to get a plausible interpretation of the relative frequency of the anomalously large cross-sections. From the theory one would also expect that generally anomalous cross-sections for the capture process were connected to anomalous elastic cross-sections. No experimental evidence has yet been found for this fact.

In this section we shall also discuss briefly the velocity distribution law for the slow neutrons in hydrogen. From the above theoretical considerations (formulae (1) and (3)), it seems plausible to assume that neutrons having velocities smaller than a certain limit have a constant mean free path  $\lambda$  for elastic collisions, and a constant mean life-time  $\tau$  before they are captured by the nuclei present in the medium. One can then easily show that the number of neutrons in a hydrogenated substance, having velocities between  $v$  and  $v + dv$ , is proportional, for  $v$  less than the above-stated limit to

$$\frac{v dv}{(v + \lambda/\tau)^3}. \quad (4)$$

\* Meitner, 'Naturwiss.,' vol. 45, p. 789 (1934).

This distribution law of the slow neutrons might be used for interpreting the fact that the absorption curves of the slow neutrons are not exponentials.

### § 9—SEPARATION OF RADIOACTIVE ISOTOPES

Szilard and Chalmers\* were the first to separate radioactive iodine from usual iodine by chemical methods. We have extended their procedure to some other cases, using also inorganic instead of organic compounds. The principle of the method is the following: let us suppose that the element before irradiation is bound in a molecule or radical which, once decomposed, has a practically negligible probability of being rebuilt. As the neutron strikes the atom, this is generally knocked out from the molecule, and has a tendency to remain in an atomic or ionic state. It follows that, after irradiation, the modified atoms are in a different chemical state from the main bulk of the unmodified ones, and can thus be separated by convenient reactions. The energy of the chemical bond is a few volts, and, even admitting that the impinging neutron might have a negligible energy, the recoil of the  $\gamma$ -quantum emitted in the capture of the neutron would be sufficient to overcome the binding chemical forces.

Szilard and Chalmers separated radioactive iodine from irradiated ethyl iodide adding a trace of free iodine, reducing and precipitating  $I^-$  with  $AgNO_3$ . The same method was applied by us to bromoform, chloroform, carbon tetrachloride and some other halogenic organic compounds. We were always able to separate almost completely the radioactive halogen from the bulk of the inactive substance.

We have also separated radioactive chlorine (35 m) starting from sodium chlorate. The chlorine atom is knocked out of the  $ClO_3^-$  ion by the neutron impact; adding a small trace of  $Cl^-$  to carry the radioactive isotope and precipitating carefully with  $AgNO_3$  with addition of  $HNO_3$  to prevent precipitation of  $AgClO_3$ , one finds the activity concentrated in the  $AgCl$  precipitate. Similar results are obtained also with bromates and iodates. In these last compounds the nitric acid was substituted with ammonia. From 70 to 90% of the total activity is concentrated in the precipitate.

Cacodylic acid  $(CH_3)_2AsOOH$  is a good starting substance for concentrating radioactive arsenic. By precipitating arsenic sulphide from irradiated cacodylic acid, it is possible to concentrate the activity.

Potassium permanganate irradiated and then filtered through an ordinary paper filter left much of the activity on the filter with manganese

\* 'Nature,' vol. 134, p. 462 (1934).

dioxide formed in the oxidation of the paper. About 80% of the total activity was separated, adding a trace of a manganous salt and precipitating the manganous carbonate. The  $\text{MnO}_4^-$  ion is dissociated by the neutron bombardment and the manganese atom is left in lower states of oxidation; these are collected with manganese peroxide on the filter, or precipitated by carbonates. We tried this separation starting either from solid salts or from solutions; there is no very remarkable difference between the two cases. Also no marked influence of the acidity or alkalinity of the irradiated solution was observed.

A physical method for separating radioactive isotopes is analogous to the well-known method of collecting the active deposit from the emanation. We tried this method with a gaseous iodine compound. A glass cylinder of about 1 litre volume with a large cylindrical aluminium electrode close to the wall and a nickel electrode along the axis was filled with methyl or ethyl iodide saturated vapour. The temperature of the cylinder was regulated so that the vapour pressure was about an atmosphere. The whole apparatus was immersed in hot water and a potential difference of 3000 volts applied to the electrodes. A  $\text{Rn} + \text{Be}$  source was placed outside the wall. After irradiation the nickel electrode was removed and showed an activity decaying with the iodine period. Nickel was used as a support because it does not become radioactive under neutron bombardment. The yield was rather a poor one. Inversion of the polarity of the electrodes gave no consistent results.

## § 10—METHODS OF MEASUREMENTS

The observed fact of the intense activating effect of the slow neutrons opened the possibility of obtaining stronger sources of the artificial radio elements than were available last year. This allows more accurate measurements of the constants of these substances by using an ionization chamber instead of Geiger Müller counters.

The ionization chamber was built of steel; the inner electrodes were a wire net and a brass rod. The  $\beta$ -rays entered the chamber through a circular window of 6 cm diameter on the top, closed by an aluminium foil 0.01 cm thick. The chamber was filled with  $\text{CO}_2$  at 3 atmospheres pressure. The chamber was connected to a Perucca electrometer, the total capacity of the system being about 20 cm, the electrometer sensitivity 0.02 volts per scale division. The system was perfectly constant both in its zero effect and in its sensitivity (as controlled by a uranium standard preparation). We reproduce in figs. 9 and 10 some decay curves obtained with this apparatus.

The same apparatus was used for measurements of the absorption of the  $\beta$ -rays. The window was protected with aluminium foils and the activity plotted as a function of the aluminium thickness. The absorption

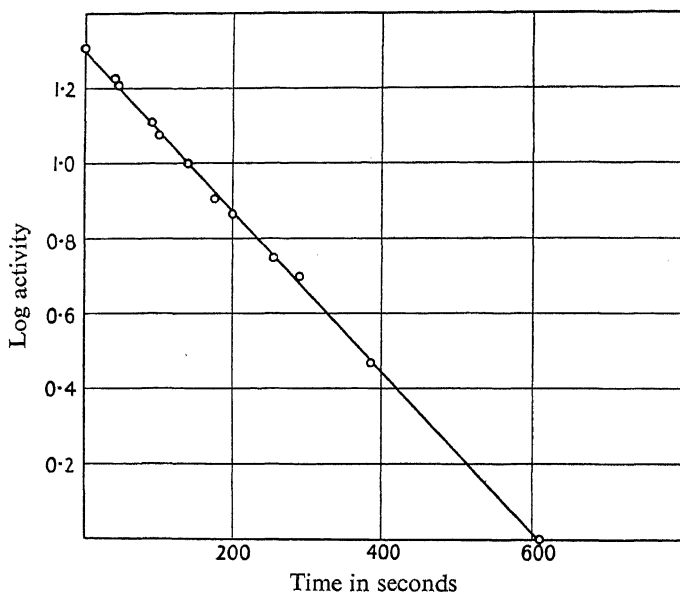


FIG. 9

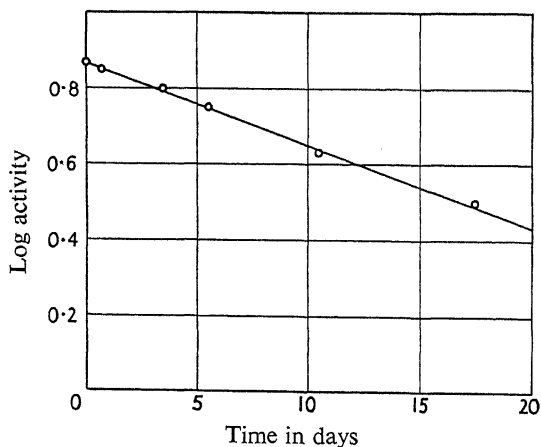


FIG. 10

curve was roughly exponential. Sometimes substances show besides the  $\beta$ -activity a strong  $\gamma$ -radiation. We conventionally attributed to  $\gamma$ -rays the residual ionization when the chamber was screened with 2 mm of lead. In the evaluation of the absorption coefficients for  $\beta$ -rays allow-

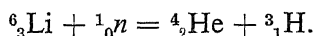
ance has been made for the  $\gamma$ -radiation. To check the measurements, the absorption coefficients of the  $\beta$ -rays of RaE and UX<sub>2</sub> have been measured and results obtained in accordance with the values commonly admitted.

### § 11—SYSTEMATIC INVESTIGATION OF ELEMENTS

In this section we shall report all the new data that we have found about each element, both as regards the induced activities and the properties with respect to slow neutrons. Some data differ slightly from our previous ones, owing to the increased precision of our measurements.

1—*Hydrogen*—No activity could be detected either in water or in paraffin irradiated in a large can of water with 500 millicuries Rn + Be for several days.

3—*Lithium*—Lithium hydroxide was found to be inactive after irradiation with slow neutrons (14 hours, 400 millicuries). Although lithium remains inactive, it strongly absorbs the slow neutrons; half-value thickness  $\delta = 0.05$  gm/cm<sup>2</sup>. This absorption is not accompanied by a  $\gamma$ -radiation. It was shown independently by Chadwick and Goldhaber\* and by us that when the slow neutrons are absorbed, heavy charged particles are emitted. According to Chadwick and Goldhaber, the nuclear process is represented by the following reaction,



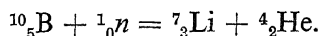
4—*Beryllium*—Metallic beryllium (purity 99%), strongly irradiated with slow neutrons, showed only an extremely weak activity possibly due to impurities. Owing to the very strong activation of several elements when irradiated under water, impurities might easily be misleading.

5—*Boron*—Metallic boron irradiated 14 hours under water with 500 millicuries was found inactive. Boron has the highest absorption coefficient as yet found for slow neutrons,  $\delta = 0.004$  gm/cm<sup>2</sup>, corresponding to a cross-section of about  $3 \cdot 10^{-21}$  cm<sup>2</sup>. No  $\gamma$ -rays have been found to accompany this absorption: instead of a  $\gamma$ -radiation in this case as well as for lithium,  $\alpha$ -particles are emitted, as was shown by Chadwick and Goldhaber\* and by us. This effect can be easily detected by the strong discharge in an ionization chamber filled with boron trifluoride surrounded by paraffin and irradiated with a Po + Be neutron source. Screening the ionization chamber with a thin cadmium foil

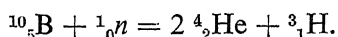
\* 'Nature,' vol. 135, p. 65 (1935).



in order to absorb the slow neutrons, reduces considerably the ionization current. The same effect was observed with the ionization chamber filled with air, some boron being spread on its floor. The emission of  $\alpha$ -particles was also detected with a small ionization chamber connected to a linear amplifier, either spreading some boron on its walls or filling it with boron trifluoride. In order to explain these phenomena we have proposed the nuclear reaction,



Chadwick and Goldhaber have proposed instead the reaction,



We do not think that there is at present sufficient evidence to decide between these two possibilities, and we are now experimenting to try to get a more exact measurement of the number of ions formed in each process in an ionization chamber containing boron either in a gaseous form (total process) or spread on its walls (effect of only one or two particles). We are also trying to observe the disintegration in a Wilson chamber containing a gaseous compound of boron.\*

6—*Carbon*—No activity; see hydrogen. For the scattering properties see § 6.

7—*Nitrogen*—Ammonium nitrate irradiated 12 hours with 600 millicuries under water showed no activity.

8—*Oxygen*—No activity, see hydrogen.

9—*Fluorine*—Both activities of this element (periods 9 seconds and 40 seconds)\* are not sensitive to hydrogenated substances.

11—*Sodium*—This element has two activities: one of these (period 40 seconds) is not sensitive to hydrogenated substances. A very weak activity with a long period was reported by Bjerger and Westcott.† As this activity is strongly enhanced by water, we were able to measure its period with reasonable accuracy and found it to be 15 hours. Owing to the theoretical importance of this activity (see § 8), we compared very carefully its decay curve with that of the long period of aluminium in order to check their identity. For a chemical investigation of the active substance we irradiated pure sodium carbonate (Kahlbaum). We dis-

\* [Note added in proof—Taylor and Goldhaber, 'Nature,' vol. 135, p. 341 (1935), have shown that the reaction takes place according to the first scheme.]

† Bjerger and Westcott, 'Nature,' vol. 134, p. 286 (1934).

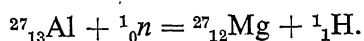
solved the irradiated substance in hydrochloric acid and added aluminium and magnesium chlorides. A precipitate of the hydroxides of the latter elements obtained by adding ammonia, was found inactive. Afterwards we added some sodium fluoride to the solution, and precipitated the fluorine as barium fluoride; this precipitate was also found inactive. The solution containing the original sodium was then evaporated and ignited gently, in order to eliminate neon, where an active isotope of this element would have been formed. The activity was found in the dried sodium salt. We conclude that the active product is an isotope of sodium,  $^{24}\text{Na}$ . The same isotope was produced by us last year by bombarding magnesium or aluminium with neutrons.  $^{24}\text{Na}$  has also been produced recently in considerable amounts and studied very completely by Lawrence\* bombarding several elements with artificially accelerated particles.

12—*Magnesium*—Pure magnesium oxide (Kahlbaum), especially tested by us in order to ensure that it was aluminium free, was irradiated under water. The substance was kept at some distance from the source in order to prevent the activation of the periods not sensitive to water. A new very weak activity with a period of about 10 minutes was found. As this period coincides with the 10-minute period of aluminium, which is known to be due to  $^{27}\text{Mg}$  (see aluminium), it is very likely that it is due to the same isotope formed by the capture of a neutron by  $^{26}\text{Mg}$  present in an amount of 11% in ordinary magnesium.

The 40-second period is insensitive to water.

13—*Aluminium*—Aluminium irradiated in water shows a fairly strong new activity decaying with a period of 2.3 minutes (measured with an ionization chamber). Irradiated outside of water, this activity is extremely weak. As the period of the new activity coincides with the 2.3-minute period of silicon, which is due to  $^{28}\text{Al}$ , we assume that this activity is also due to the same isotope formed by capture of a neutron from  $^{27}\text{Al}$ .

The second period of aluminium has been measured with the ionization chamber and found to be 10 minutes instead of 12. This activity is insensitive to water. A chemical separation of the carrier of this activity has been performed. Irradiated metallic aluminium was dissolved in a caustic soda solution and magnesium chloride was added. The precipitate of magnesium hydroxide carried the 10-minute activity. We assume that the active isotope is  $^{27}\text{Mg}$  formed according to the reaction,



\* 'Phys. Rev.', vol. 47, p. 17 (1935).

14—*Silicon*—We have determined with the ionization chamber the short period of this element, finding it to be 2·3 minutes. This activity is insensitive to water.

Besides this activity, we found a new longer period of some hours in fused silica irradiated in water. This activity is very weak and very sensitive to water. We think probably that its carrier is  $^{31}\text{Si}$  which is obtained by irradiated phosphorus and has a period of 2·4 hours.  $^{31}\text{Si}$  could be formed by capture of a neutron from  $^{30}\text{Si}$  present in an amount of 3%.

15—*Phosphorus*—The short-period activity of this element (2·3 minutes) is not enhanced by water. Curie, Joliot and Preiswerk\* ascribe this period to  $^{28}\text{Al}$ . A chemical test in favour of this hypothesis is the following: we irradiated phosphoric acid, neutralized the solution with sodium carbonate, and added aluminium chloride; the activity was found to be concentrated in the precipitated aluminium.

We have observed, with the aid of the ionization chamber, the decay-curve of the longer period of phosphorus. Its period is 2·4 hours instead of 3 as given before. We have also measured, with the ionization chamber, the half-value thickness of the corresponding  $\beta$ -rays and found it to be 0·15 gm/cm<sup>2</sup> Al.

16—*Sulphur*—We have determined in the ionization chamber the period of phosphorus extracted from irradiated sulphur. We found: period 14 days, half-value thickness of the  $\beta$ -rays 0·10 gm/cm<sup>2</sup> Al.

17—*Chlorine*—Chlorine irradiated under water showed a new period of 35 minutes measured electrometrically. For the chemical tests on the carrier of this activity see § 9.

Chlorine absorbs fairly strongly the slow neutrons (half-value thickness  $\delta = 0\cdot3$  gm/cm<sup>2</sup>). The process of absorption is accompanied by emission of  $\gamma$ -rays.

19—*Potassium*—We have found in irradiated potassium an induced activity strongly sensitive to water, decaying with a period of 16 hours. A chemical investigation of the carrier of the activity, performed by the same method described for sodium, excluded the elements Cl, A, Ca. We conclude therefrom that the activity is probably carried by an isotope of potassium. According to v. Hevesy†, this isotope is to be identified with a  $^{42}\text{K}$ , that was obtained by him by neutron bombardment of scandium, and has the same decay period.

\* 'C.R. Acad. Sci. Paris,' vol. 198, p. 2089 (1934).

† 'Nature,' vol. 135, p. 96 (1935).

20—*Calcium*—No activity was found in calcium fluoride irradiated 14 hours in water with a 600 millicuries source.

23—*Vanadium*—The decay of the activity induced in vanadium has been measured in the ionization chamber with the following results: half-value period 3.75 minutes; half-value thickness of the  $\beta$ -rays 0.17 gm/cm<sup>2</sup> Al. The  $\beta$ -rays are accompanied by a  $\gamma$ -radiation. The activation of vanadium is strongly sensitive to hydrogenated substances; with the definition of § 1,  $\alpha = 40$ .

24—*Chromium*—The activity of chromium is insensitive to water.

25—*Manganese*—The activity with short period (3.75 minutes) is insensitive to water ( $\alpha = 1$ ). On the other hand, the activity with longer period (2.5 hours measured in the ionization chamber) is strongly enhanced by water ( $\alpha = 23$ ). Half-value thickness of  $\beta$ -rays measured electrometrically is 0.14 gm/cm<sup>2</sup> Al; the disintegration is accompanied by  $\gamma$ -rays. The 2.5-hour product is known to be an isotope of manganese; in § 9 a method for concentrating the activity has been described. In order to get new evidence in favour of the fact that the active product is really an isotope of manganese, we first concentrated the activity obtained in irradiated manganese permanganate by a precipitation of manganese carbonate. The carbonate containing the activity was then dissolved in hydrochloric acid, and large amounts of chromium, vanadium and iron salts were added to the solution. Afterwards the manganese was separated once again as dioxide, with nitric acid and sodium chlorate. The manganese precipitate carried the activity, while the fractions containing chromium, vanadium and iron were found to be inactive.

26—*Iron*—The activity of this element (period 2.5 hours) is insensitive to water. Half-value thickness for the absorption of slow neutrons 8 gm/cm<sup>2</sup>.

27—*Cobalt*—This element absorbs fairly strongly the slow neutrons; half-value thickness 0.7 gm/cm<sup>2</sup>. The absorption is accompanied by the emission of a  $\gamma$ -radiation.

28—*Nickel*—Strongly irradiated nickel showed only a dubious trace of activity.

29—*Copper*—Both induced activities of this element (periods 5 minutes, measured electrometrically, and 10 hours) are strongly enhanced by water. For the first  $\alpha = 15$ . Copper absorbs the slow neutrons with a half-value thickness of about 3 gm/cm<sup>2</sup>; this absorption is accompanied by a weak  $\gamma$ -radiation.

Irradiated metallic copper was dissolved in hydrochloric acid, and small quantities of cobalt, nickel and zinc salts were added. Copper sulphide was precipitated from the acid solution and found to be active. The precipitates of the zinc, cobalt and nickel sulphides, obtained by neutralizing the solution and adding ammonium sulphide, were inactive. As the time employed for this test was rather long, the test refers only to the longer period. The carrier of this activity can then be assumed to be an isotope of copper, as suggested by Bjerger and Westcott (*loc. cit.*).

30—*Zinc*—The activity of the short period of zinc is not enhanced by water. The longer period was measured electrometrically and found to be 10 hours. The carrier of this activity has been investigated by means of the following test: irradiated metallic zinc was dissolved in hydrochloric acid, and a small quantity of copper, nickel and cobalt salts added. Copper was precipitated partially by reduction on small traces of undissolved metallic zinc and partially as sulphide in the acid solution. The collected copper was strongly active. Neutralizing the solution and adding ammonium sulphide, the other elements were precipitated and found to be inactive. This confirms the results of Bjerger and Westcott that the long period of zinc is due to copper, probably to the same isotope of copper which is responsible for the longer period of this element. There is only a certain difference between these authors and us with respect to the period (6 hours according to Bjerger and Westcott).

31—*Gallium*—The 20-minute period (measured electrometrically) is not very sensitive to water ( $\alpha = 3$ ). Half-value thickness of the corresponding  $\beta$ -rays is  $0.17 \text{ gm/cm}^2 \text{ Al}$ . The carrier of this activity is probably an isotope of gallium. In order to test this point, we irradiated gallium nitrate and afterwards added to the solution traces of copper and zinc. Copper was separated as a metallic deposit on zinc powder and zinc as zinc mercury sulphocyanate after adding mercury sulphocyanate. Both elements were found to be inactive.

Besides this 20-minute activity, we have also found, irradiating under water, a new activity which is accompanied by a rather strong  $\gamma$ -radiation; it decays with a period of 23 hours (measured electrometrically).

33—*Arsenic*—The activity of this element is strongly sensitive to water ( $\alpha = 6$ ). We have measured electrometrically its period (26 hours) and its half-value thickness of the  $\beta$ -rays ( $0.16 \text{ gm/cm}^2 \text{ Al}$ ). For a concentration of the activity, see § 9.

34—*Selenium*—The activity of this element (period 35 minutes) is sensitive to water ( $\alpha = 4$ ). Irradiated selenious anhydride was dissolved in 30% hydrochloric acid and some arsenious anhydride added to the

solution. We precipitated metallic selenium by reduction with gaseous sulphurous anhydride, and found it strongly active. We precipitated from the solution arsenic sulphide and found it inactive. This test seems to rule out also germanium, and we conclude that the activity is due to an isotope of selenium.

35—*Bromine*—Both activities of this element are sensitive to water. The short-period activity has  $\alpha = 10$ . The periods have been measured electrometrically; they are 18 minutes and 4.2 hours. The half-value thickness of the  $\gamma$ -rays is for both activities 0.12 gm/cm<sup>2</sup> Al, and both are accompanied by  $\gamma$ -rays. For the concentration of the activity see § 9.

38—*Strontium*—No activity was found after a long and strong irradiation under water.

39—*Yttrium*—Strongly irradiated yttrium oxide showed only a very weak activity possibly due to impurities. Yttrium absorbs very intensively the slow neutrons (half-value thickness  $\delta = 0.015$  gm/cm<sup>2</sup>). This absorption is accompanied by  $\gamma$ -rays.

40—*Zirconium*—Strongly irradiated zirconium nitrate showed only a very weak activity probably due to impurities.

41—*Niobium*—The same as zirconium.

43—*Rhodium*—The short-period activity is sensitive to water ( $\alpha = 15$ ). Period and half-value thickness of the  $\beta$ -rays have been determined electrometrically (44 seconds; 0.15 gm/cm<sup>2</sup> Al). We also made a more accurate measurement in the ionization chamber of the longer period and found it to be 3.9 minutes. The activity is accompanied by a weak  $\gamma$ -radiation. Rhodium absorbs fairly strongly the slow neutrons (half-value thickness 0.3 gm/cm<sup>2</sup>): the absorption probably corresponds to the formation of the active isotopes.

46—*Palladium*—Also the activities of this element are sensitive to water. We find at least two periods: a short one of about a quarter of an hour and one of about 12 hours. McLennan, Grimmett, and Read record a period of 14 hours, which is consistent with our precision.

47—*Silver*—The two periods have been redetermined with the ionization chamber. They are 22 seconds and 2.3 minutes. They are both very sensitive to water, having  $\alpha = 30$  and 15 respectively. To the strong activation of this element corresponds a considerable absorption for slow neutrons (half-value thickness  $\delta = 1.2$  gm/cm<sup>2</sup>).

We added palladium nitrate and rhodium chloride to a solution of irradiated silver nitrate. Adding hydrochloric acid, we precipitated silver which was found active. From the filtered solution we precipitated

palladium with dimethylglyoxime and rhodium by reduction. Both were inactive. This test is valid only for the longer period, owing to the time employed, and shows that the carrier of the activity is probably an isotope of silver.

48—*Cadmium*—Cadmium irradiation under different conditions showed several weak activities with various periods not yet identified. Cadmium absorbs with great intensity the slow neutrons. (Half-value thickness  $0.013 \text{ gm/cm}^2$ .) The corresponding cross-section is the largest as yet found for slow neutrons ( $\sigma = 10^{-20} \text{ cm}^2$ ). The absorption is accompanied by an intensive  $\gamma$ -radiation and probably corresponds to the transformation of a stable isotope of cadmium into another stable isotope of the same element.

49—*Indium*—The activity induced in indium shows three periods: the shortest period (13 seconds) corresponds to an activity sensitive to water ( $\alpha = 12$ ). Also the second period (54 minutes, measured electrometrically) is very sensitive to water. Magnetic deflection experiments show that the corresponding electrons are negative; their half-value thickness is  $0.045 \text{ gm/cm}^2 \text{ Al}$ . A still longer period of some hours is recorded by Szilard and Chalmers;\* this last activity is either insensitive to water or is only moderately sensitive.

Chemical tests have been made in order to identify the carriers of the last two activities. To a solution of irradiated indium nitrate, silver was added and precipitated as silver chloride; the precipitate was inactive. Afterwards we added to the solution tin, antimony and cadmium and precipitated them as sulphides with sulphuretted hydrogen. The acidity of the solution must be adjusted in such a way as to leave the indium in solution while precipitating the other metals. This precipitate also was inactive; neutralizing the solution, we precipitated the indium sulphide which carried the activity.

Corresponding to the strong activation of indium, it is found that this element has a considerable absorption power for the slow neutrons: half-value thickness  $\delta = 0.3 \text{ gm/cm}^2$ .

50—*Tin*—Tin strongly irradiated under water showed no activity.

51—*Antimony*—We have found an induced activity in this element, decaying with a period of 2.5 days; the activation is sensitive to hydrogenated substances. The half-value thickness for the emitted  $\beta$ -rays is  $0.09 \text{ gm/cm}^2 \text{ Al}$ . The following chemical test indicates that the carrier of this activity is probably an isotope of antimony. We dissolved metallic

\* 'Nature,' vol. 135, p. 493 (1935).

irradiated antimony in aqua regia and added some tin to the solution; after separation of tin as a sulphide according to Clarke, we found the activity in a precipitate of sulphide of antimony. The antimony sulphide was then dissolved again; indium was added to the solution and antimony separated as a sulphide in a moderately acid solution; the solution was neutralized and indium precipitated and found to be inactive. To a new solution of the antimony we added tellurium and iodine and separated the first by reduction and the second as a silver iodide. Both were inactive.

52—*Tellurium*—Shows a weak activity sensitive to water; the period resulted 45 minutes instead of 30 as given in our former paper.

53—*Iodine*—Period and half-value thickness of the  $\beta$ -rays were determined electrometrically: period 25 minutes; half-value thickness 0.11 gm/cm<sup>2</sup> Al. The activation is moderately sensitive to water ( $\alpha = 5$ ). For the concentration of the activity see § 9.

56—*Barium*—A new activity sensitive to water ( $\alpha = 8$ ) with a period of 80 minutes has been found. The following chemical test is in favour of the assumption that the carrier of this activity is an isotope of barium. We dissolved irradiated barium hydroxide in hydrochloric acid, and added a small quantity of sodium chloride and precipitated barium sulphate. The activity was carried by the precipitate; we evaporated the solution and found the residual sodium to be inactive.

57—*Lanthanum*—No activity was found after strong irradiation under water.

58—*Cerium*—Same as lanthanum.

59—*Praseodymium*—The short-period activity (5 minutes) is insensitive to water. Irradiating under water we have found a new water-sensitive activity decaying with a period of 19 hours; half-value thickness of the corresponding  $\beta$ -rays 0.12 gm/cm<sup>2</sup> Al (both measured electrometrically).

64—*Gadolinium*—We irradiated under water a very pure sample of gadolinium oxide kindly given to us, together with the other rare earths, by Professor L. Rolla. We found an activity, decaying with a period of 8 hours.

73—*Tantalum*—Only a dubious activity was found after 12 hours' irradiation under water with 500 millicuries.

74—*Tungsten*—Metallic tungsten was irradiated under water and showed an activity ( $\alpha = 15$ ) decaying with a period of about 1 day.\*

\* Cf. McLennan, Grimmett, and Read, 'Nature,' vol. 135, p. 147 (1935).



We irradiated tungstic anhydride, dissolved it in caustic soda and then added and separated tantalum pentoxide which was found to be inactive. To the tungstic solution we added a nitric rhenium solution and precipitated the tungstic anhydride adding hydrochloric acid. The precipitate carried the activity, while the rhenium, precipitated from the filtrate as sulphide, was inactive. As we have no hafnium, we have made the following experiment in order to exclude an isotope of this element as carrier of the activity. From a solution of irradiated tungstic anhydride in ammonia, we precipitated zirconium hydroxide. The precipitate was inactive. We conclude that the activity of tungsten is probably due to an isotope of this element.

75—*Rhenium*—We irradiated pure metallic rhenium under water; its activity is enhanced by water and decays with a period of about 20 hours. The half-value thickness of the electrons is  $0.12 \text{ gm/cm}^2 \text{ Al}$ . The activity is probably carried by an isotope of rhenium. Irradiated rhenium was dissolved in nitric acid; we added tantalum and tungsten and separated them as tantalum pentoxide and tungstic anhydride. Both were inactive, while rhenium conserved the activity.

77—*Iridium*—The activity induced in this element is strongly sensitive to water. Period and half-value thickness of the  $\beta$ -rays have been measured in the ionization chamber; period 19 hours, half-value thickness  $0.12 \text{ gm/cm}^2 \text{ Al}$ . To the strong activation of iridium corresponds a strong absorption of the slow neutrons; half-value thickness  $0.3 \text{ gm/cm}^2$ ; the absorption is accompanied by the emission of  $\gamma$ -rays.

78—*Platinum*—Very pure metallic platinum (Heraeus 4th purity standard) irradiated under water showed an activity decaying with a period of about 50 minutes. McLennan, Grimmett, and Read (*loc. cit.*) record a period of 36 minutes.

79—*Gold*—The activity of this element is sensitive to water; its period has been measured electrometrically and is 2.7 days. The  $\beta$ -rays were magnetically deflected and found to be negative. They have a very small penetrating power: half-value thickness  $0.04 \text{ gm/cm}^2 \text{ Al}$ .\*

80—*Mercury*—No activity was found after strong irradiation. This element absorbs intensely the slow neutrons, half-value thickness  $0.2 \text{ gm/cm}^2$ .  $\gamma$ -rays are emitted during the absorption.

81—*Thallium*—No activity was found after strong irradiation.

82—*Lead*—The same as thallium.

\* Gold bombarded with slow neutrons emits a strong  $\gamma$ -radiation.

83—*Bismuth*—The same as thallium.

90—*Thorium*—The 1-minute and 24-minute (measured electrometrically) periods are scarcely sensitive to water.

92—*Uranium*—We have also studied the influence of hydrogenated substances on the induced activities of this element. (Periods 15 seconds, 40 seconds, 13 minutes, 100 minutes.) The result was that while the activities corresponding to the first, third and fourth period are slightly increased by water, no increase was found for the activity corresponding to the 40-second period. We have measured the increase in activity for the 15-second, 13-minute, and 100-minute activities. We have found for all these  $\alpha$  = about 1.6. For the 15-second activity the measurement was made with the counters and, owing to the shortness of the period, is not very exact. The  $\alpha$  values for the other two activities have been measured in the ionization chamber, special care being taken in order to verify that the  $\alpha$  values for these two periods are equal. For this we compared three decay curves of the activity obtained by irradiating the same amount of uranium oxide for 14 hours, once in air placing the uranium around the source inside a test tube; once in the same geometrical disposition surrounding the test tube with paraffin, and once inside a large mass of paraffin placing the source at about 5 cm from the test tube containing the uranium. In all these tests we found that the decay curves were proportional, *i.e.*, showed the same ratio of the two activities. We think, therefore, that the test on the identity of the sensitivities to water for these two periods is rather more accurate than the absolute value of the sensitivity coefficient and also than the identity in sensitivity coefficient with the 15-second activity. It is now evident that all the active products arising from the same primary process must have the same sensitivity coefficient. We conclude, therefore, that the 40-second activity is due to an independent primary process while the other three activities are probably due to the same primary process. This conclusion is limited by the possibility of a chance coincidence of the sensitivity coefficients within the rather wide limits of our precision. In this assumption the three activities could either be chain products (the short-period activities being parents of the long-period activities) or their relations could be complicated by branching phenomena. A certain amount of evidence in favour of the former assumption, at least as regards the 13-minute and the 100-minute periods, is given by the following test. We have measured on the electrometer the decay curves of a thick layer of irradiated uranium; these curves analysed in exponentials with the periods 13 minutes and 100 minutes show that the initial activities are in the ratio of about

100:45. The half-value thickness for the  $\beta$ -rays of the 13-minute activity is  $0.14 \text{ gm/cm}^2 \text{ Al}$ ; for the longer period it could not be measured with any accuracy, but is definitely less than the former value and probably about a half. These results are consistent with the assumption that the number of disintegrations for the 13-minute and the 100-minute periods is equal.

In our former paper we gave some chemical evidence which seemed to indicate that the carriers of the 13- and the 100-minute activities were not isotopes of any of the known heaviest elements, and that they were probably due to transuranic elements. Our point of view has in the meantime been criticized by von Grosse and Agruss,\* who, although never having experimented on activated uranium, deduced from our chemical tests the opposite conclusion, that these activities were due to isotopes of protactinium. We have therefore performed some new chemical experiments on the behaviour of these activities.

The precipitation of the activity with a sulphide was repeated, precipitating several metals (silver, copper, lead, mercury); the acidity of the solution (hydrochloric acid) was about 20%; sometimes slightly varied in order to facilitate the precipitation of the sulphide of the metal used. The yield in activity of the precipitate was generally good—about 50%—and varied according to the conditions of the precipitation. Nitric acid lowers the yield of the reaction very much. The usual high yield of the sulphide reaction is also obtained in presence of a hydrofluoric solution of tantalum. We also made a test in order to see whether the induced activities presented a reaction which is given by von Grosse as the most characteristic of protoactinium.

We dissolved in a 25% hydrochloric acid solution uranium oxide which had been purified and irradiated; we added to the solution zirconium nitrate and phosphoric acid; the precipitate of zirconium phosphate was inactive. After the separation of zirconium we precipitated a sulphide from the filtered solution, and collected the activity in the sulphide with the usual yield. According to von Grosse and Agruss, this reaction must be considered a proof of the non-identity of the carrier of the activity with a protactinium isotope.

By different chemical experiments, Hahn and Meitner† conclude also that the 13- and 100-minute activities are very probably due to transuranic elements; we have repeated some of their experiments finding the same results.

\* 'Phys. Rev.', vol. 46, p. 241 (1934).

† 'Naturwiss.', vol. 23, p. 37 (1935).

The two activities have beyond doubt a similar chemical behaviour. Some slight evidence of a possible separation was obtained only in the following experiment. Carefully purified uranium oxide was irradiated and dissolved in hydrochloric acid. The solution was poured into an ammonium carbonate solution until the uranium precipitate was completely dissolved again. Adding lead or manganese nitrate, we collected the precipitate of carbonates and found it to carry a fraction of the 13- and 100-minute activities. In the filtrate we precipitated copper sulphide, and this also carried a fraction of the activities. It seems that the ratio of the two activities was somewhat different in the two precipitates, the 13-minute activity being more abundant in the sulphide precipitate.

Through these experiments our hypothesis that the 13-minute and 100-minute induced activities of uranium are due to transuranic elements seems to receive further support. The simplest interpretation consistent with the known facts is to assume that the 15-second, 13-minute and 100-minute activities are chain products, probably with atomic number 92, 93 and 94 respectively and atomic weight 239.

We express our warmest thanks to Professor G. C. Trabacchi who supplied us with the radon sources. Our thanks are due also to Professor L. Rolla who placed at our disposal some rare earths, to Dr. G. Fea for help in the experiments and to the Consiglio Nazionale delle Ricerche for making a grant.

## § 12—TABULAR SUMMARY

The main results of radioactivity induced by neutron bombardment are summarized in the table. Column 1 contains the atomic numbers and symbols of the elements investigated. Column 2 gives the isotopic constitution; numbers in bold type refer to isotopes which represent more than 20% of the element. Column 3 gives the observed half-value periods in order of increasing magnitude. Column 4 gives the half-value thickness of the  $\beta$ -rays in gm/cm<sup>2</sup> of aluminium; the mean energy of the  $\beta$ -rays in millions volts might be very roughly obtained by multiplying the figure of column 4 by 8. Column 5 indicates whether  $\gamma$ -rays have been observed to accompany the  $\beta$ -disintegration. Column 6 indicates the carrier of the activity. Column 7 gives the sensitivity of the activation to hydrogenated substances; this is given either by the numerical value of the sensitivity coefficient (for definition see § 1; sensitivity coefficient 1 means that the activation is not enhanced by hydrogenated substances) or by the letter *a*, which means that the activation is increased by hydrogenated substances, but the sensitivity

Element	Isotopes	Half-periods	Half-value thickness gm/cm <sup>2</sup> Al	$\gamma$ -rays	Sensitivity to hydrogen	Carrier of the activity	$\delta$ gm/cm <sup>2</sup>
1 H	1, 2, 3	—					0.05
2 He	3, 4	—					$>3$
3 Li	6, 7	—					0.004
4 Be	9	—					$>3$
5 B	10, 11	—					$>0.5$
6 C	12, 13	—					$>3$
7 N	14, 15	—					$>0.5$
8 O	16, 17, 18	—					$>3$
9 F	19	9 s; 40 s	0.24; —	yes	1; 1	<sup>16</sup> N (?)	$>3$
10 Ne	20, 21, 22	—					$>3$
11 Na	23	40 s; 15 h	—; 0.12	yes	1; a	<sup>20</sup> Ne (?) <sup>24</sup> Na	$>4$
12 Mg	24, 25, 26	40 s; 10 m; 15 h	—; 0.07; 0.12	yes	1; a	<sup>23</sup> Ne (?) <sup>27</sup> Mg; <sup>24</sup> Na	$>0.5$
13 Al	27	2.3 m; 10 m; 15 h	0.16; 0.07; 0.12	yes	a; 1	<sup>28</sup> Al; <sup>27</sup> Mg; <sup>24</sup> Na	$>7$
14 Si	28, 29, 30	2.3 m; 2.4 h	0.16; —	yes	1; a	<sup>28</sup> Al; <sup>31</sup> Si	$>5$
15 P	31	2.3 m; 2.4 h	0.16; 0.15	—	1; —	<sup>28</sup> Al; <sup>31</sup> Si	$>3$
16 S	32, 33, 34	14 d	0.10	—	a; —	<sup>32</sup> P	$>2$
17 Cl	35, 37	35 m; 14 d	—; 0.10	—	a; —	Cl; <sup>32</sup> p	0.3
18 A	36, 38, 40	—					$>1$
19 K	39, 41	16 h			a	<sup>42</sup> K	$>3$
20 Ca	40, 42, 43, 44	—					$>1$
21 Sc	45	16 h					$>3$
22 Ti	46, 47, 48, 49, 50	3 m					$>2$
23 V	51	3.75 m	0.17	yes	40	<sup>52</sup> V	$>1$
24 Cr	50, 52, 53, 54	3.75 m	0.17	yes	1	<sup>52</sup> V	$>2$
25 Mn	55	3.75 m; 2.5 h	0.17; 0.14	yes	1; 23	<sup>52</sup> V; <sup>56</sup> Mn	$>3$
26 Fe	54, 56	2.5 h	0.14	yes	1	<sup>56</sup> Mn	8
27 Co	59	2.5 h	0.14	yes	—	<sup>56</sup> Mn	0.7

28 Ni	56, <b>58</b> , <b>60</b> , 61, 62, 64	—							$\lambda^3$
29 Cu	<b>63</b> , <b>65</b>	5 m; 10 h	yes	15; <i>a</i>	Cu; Cu	3			3
30 Zn	<b>64</b> , <b>66</b> , 67, 68, 70	5 m; 10 h	yes	1; —	Cu; Cu	$\lambda^{10}$			$\lambda^{10}$
31 Ga	<b>69</b> , <b>71</b>	20 m; 23 h	yes	3; <i>a</i>	Ga; —	$\lambda^5$			$\lambda^5$
32 Ge	<b>70</b> , <b>72</b> , 73, <b>74</b> , 76	30 m (?)		0·17; —					
33 As	<b>75</b>	26 h	yes	0·16	<sup>76</sup> As	$\lambda^3$			$\lambda^3$
34 Se	74, 76, 77, <b>78</b> , <b>80</b> , 82	35 m			Se	4			4
35 Br	<b>79</b> , <b>81</b>	18 m; 4·2 h		0·12; 0·12	Br; Br	3			3
36 Kr	78, 80, 82, 83, <b>84</b> , 86								
37 Rb	<b>85</b> , <b>87</b>	? ?				$\lambda^2$			$\lambda^2$
38 Sr	86, 87, <b>88</b>	—				$\lambda^2$			$\lambda^2$
39 Y	<b>89</b>	—				0·015			0·015
40 Zr	<b>90</b> , 91, 92, <b>94</b> (96)	—				$\lambda^3$			$\lambda^3$
41 Nb	93	—				$\lambda^3$			$\lambda^3$
42 Mo	92, 94, 95, 96, 97, <b>98</b> , 100	30 m; 36 h							
43 Ma									
44 Ru	96, 98, 99, 100, <b>101</b> , <b>102</b> , 104	—				$\lambda^3$			$\lambda^3$
45 Rh		44 s; 3·9 m		0·15; —		0·3			0·3
46 Pd		15 m; 12 h				$\lambda^2$			$\lambda^2$
47 Ag	<b>107</b> , <b>109</b>	22 s; 2·3 m	yes	—; 0·08	—; Ag	1·2			1·2
48 Cd	106, 108, 110, 111, <b>112</b> , 113, <b>114</b> , 115, 116	? ?				0·013			0·013
49 In	113, <b>115</b>	13 s; 54 m; 3 h (?)	yes	—; 0·045; —	—; In; In	0·3			0·3
50 Sn	112, 114, 115, 116, 117, <b>118</b> , 119, <b>120</b> , 121, 122, 124					$\lambda^{10}$			$\lambda^{10}$
51 Sb	<b>121</b> , <b>123</b>	2·5 d	yes	0·09	Sb	$\lambda^{10}$			$\lambda^{10}$
52 Te	122, 123, 124, 125, <b>126</b> , (127), 128, 130	45 m				$\lambda^3$			$\lambda^3$
53 I	<b>127</b>	25 m	yes	0·11	<sup>128</sup> I	4			4

Element	Isotopes	Half-periods	Half-value thickness gm/cm <sup>2</sup> Al	$\gamma$ -rays	Sensitivity to hydrogen	Carrier of the activity	$\delta$ gm/cm <sup>2</sup>
54 Xe	124, 126, 128, <b>129</b> , 130, <b>131</b> , <b>132</b> , 134, 136 .....						
55 Cs	<b>133</b> .....	1.5 h (?) (?)					
56 Ba	135, 136, 137, <b>138</b> .....	3 m; 80 m			1; 8	—; Ba	>3
57 La	<b>139</b> .....	—					
58 Ce	<b>140</b> , 142 .....	—					
59 Pr	<b>141</b> .....	5 m; 19 h					
60 Nd	<b>142</b> , 143, <b>144</b> , 145, 146....	1 h			1; <i>a</i>		1.5
61			—; 0.12				
62 Sm	144, 147, 148, 149, 150, <b>152</b> , <b>154</b> .....	40 m					
63 Eu	<b>151</b> , <b>153</b> .....						
64 Gd	<b>155</b> , <b>156</b> , 157, <b>158</b> , 160....	8 h		<i>a</i>			
65 Tb	<b>159</b> .....						
66 Dy	<b>161</b> , <b>162</b> , <b>163</b> , <b>164</b> .....						
67 Ho	<b>165</b> .....						
68 Er	<b>166</b> , <b>167</b> , <b>168</b> , 170 .....						
69 Tu	<b>169</b> .....						
70 Yb	171, <b>172</b> , 173, <b>174</b> , 176 ..						
71 Lu	<b>175</b> .....						
72 Hf	176, 177, 178, 179, 180....						
73 Ta	<b>181</b> .....	?					
74 W	<b>182</b> , 183, <b>184</b> , <b>186</b> .....	1 d			15	W	
75 Re	<b>185</b> , <b>187</b> .....	20 h	0.12	<i>a</i>		Re.	
76 Os	<b>186</b> , 187, 188, 189, <b>190</b> , <b>192</b>	—					
77 Ir		19 h	0.12	<i>a</i>		Ir	0.3





coefficient has not been measured. Column 8 gives the half-value thickness for the absorption of the slow neutrons.

In a few cases the periods of products, known from chemical evidence to be equal, but obtained by bombardment of different atoms are given as equal, even when measured very accurately only in one case. The same holds for some half-value thicknesses of  $\beta$ -rays.

---

## The Theoretical Determination of the Lift Coefficient for a Thin Elliptic Cylinder

By L. HOWARTH, B.A., B.Sc., Busk Student

(Communicated by G. I. Taylor, F.R.S.—Received March 6, 1935)

### 1—INTRODUCTION

This paper is concerned with the calculation of the lift coefficient of an infinitely long, thin elliptic cylinder in a stream of viscous fluid moving with constant velocity at infinity, in a direction inclined at some angle to the major axis. The method used is a general one and may be applied to any cylinder with a stream-line section provided the potential flow past the cylinder, for a given value of the circulation, is calculable.

It is clear from experiment that two cases arise according as the flow in the boundary layer is fully laminar, or partly laminar and partly turbulent. It appears that experimental conditions have not yet been obtained capable of producing a boundary layer turbulent right from the forward stagnation point. Mathematically, however, the discussion of this latter problem is a necessary preliminary to the one in which both laminar and turbulent portions are present.

We shall, therefore, discuss the three cases in which the boundary layer (i) is entirely laminar; (ii) is entirely turbulent; (iii) contains both laminar and turbulent portions.

Joukowski has, of course, given an approximate solution of the problem indicated for the case when the section of the cylinder considered has a sharp trailing edge. The methods used in the present discussion are not dependent on such a salient point existing in the section of the cylinder, and indeed will give much more accurate results than Joukowski's method where that is applicable.

## 2—PRELIMINARY DETAILS AND ASSUMPTIONS

We consider any normal section of the cylinder and denote by—

$a, b,$	the semi-major and semi-minor axes of the ellipse.
$c,$	$(a^2 - b^2)^{\frac{1}{2}}.$
$\varepsilon = \operatorname{sech} \alpha,$	the eccentricity.
$\theta,$	the angle of incidence, <i>i.e.</i> , the angle between the major axis of the ellipse and the direction of motion of the fluid at infinity.
$\nu,$	the kinematic viscosity of the fluid.
$V,$	the undisturbed velocity of the fluid.
$R,$	the Reynolds' number $(Vc/\nu).$
$K,$	the circulation.
$\eta,$	the eccentric angle of a point on the periphery of the section, measured in the anti-clockwise direction from the trailing edge.
$X,$	the distance measured along the periphery of the section from the forward stagnation point.
$Y,$	the distance measured normal to the periphery.
$x, y,$	$X/c, R^{\frac{1}{2}}Y/c$ respectively.
$\bar{U},$	the velocity of the fluid at the edge of the boundary layer.
$U,$	$\bar{U}/V.$
$U', U'',$	$(dU/dx), (d^2U/dx^2).$
$\bar{u},$	the velocity, at any point of the boundary layer, parallel to the wall.
$u,$	$\bar{u}/V.$
$\delta,$	the thickness of the boundary layer.
$z,$	$V\delta^2/c\nu.$
$A,$	$K/2 cV\pi.$
$B,$	$e^{\alpha}.$
$D,$	$(\cosh^2 \alpha - \frac{1}{2}).$
$h,$	$(D - \frac{1}{2} \cos 2\eta)^{\frac{1}{2}}.$
$\lambda,$	$-\left(\frac{1}{\bar{U}\rho}\right)\left(\frac{dp}{dX}\right)\left(\frac{\delta^2}{\nu}\right) (= U'z).$
$p,$	the pressure distribution in the main stream at the edge of the boundary layer.
$\tau,$	the skin friction.
$\delta^*,$	$\int_0^{\delta} \left(1 - \frac{\bar{u}}{\bar{U}}\right) dY.$

$$\begin{aligned}
\vartheta, & \quad \int_0^\delta \left(1 - \frac{\bar{u}}{\bar{U}}\right) \frac{\bar{u}}{\bar{U}} dY. \\
H, & \quad \delta^*/\vartheta. \\
\Gamma, & \quad \frac{\bar{U}'\vartheta}{\bar{U}} \left(\frac{\bar{U}\vartheta}{\nu}\right)^{\frac{1}{2}}. \\
\zeta, & \quad \frac{\tau}{\rho \bar{U}^2} \left(\frac{\bar{U}\vartheta}{\nu}\right)^{\frac{1}{2}}. \\
\chi, & \quad R^{\frac{1}{2}} (\vartheta/c)^{5/4}. \\
R_\delta, & \quad \bar{U}\delta/\nu. \\
R_\vartheta, & \quad \bar{U}\vartheta/\nu.
\end{aligned}$$

The ratio of the major axis to the minor axis in the particular cylinder chosen for investigation was 6:1, so that  $\varepsilon = 0.9860$ ,  $\alpha = 0.16836$ ,  $B = 1.18328$ ,  $D = 0.52856$ .

In all three cases we shall make the assumptions of the boundary layer theory. Briefly summarized these are:—

- (1) The viscous forces are negligible everywhere except in a thin layer called the boundary layer, close to the surface of the cylinder. Thus, outside the boundary layer the flow can be discussed by means of the perfect fluid theory.
- (2) Inside the boundary layer, the viscous terms in the equation of motion are of the same order of magnitude as the inertia terms.
- (3) The curvature of the surface may be neglected inside the boundary layer. The error committed by neglecting the curvature is of the order of  $R^{-\frac{1}{2}} \sigma^{-1}$ , where  $\sigma$  is the ratio of the radius of curvature to  $c$ . At the nose or tail of the cylinder considered  $\sigma$  takes its minimum value (1/6) and so the error committed by neglecting the curvature is never greater than the order of  $6R^{-\frac{1}{2}}$ .

To determine conditions in the boundary layer we shall, in all cases, make use of Karman's momentum integral equation

$$\frac{\bar{U}d}{dX} \int_0^\delta \bar{u} dY - \frac{d}{dX} \int_0^\delta \bar{u}^2 dY = -\frac{\delta}{\rho} \frac{dp}{dX} + \frac{\tau}{\rho}. \quad (2.1)$$

We shall also assume that the vorticity is confined to a wake behind the cylinder and that the thickness of the wake is roughly defined by the positions of the points of separation. Outside the wake and the boundary layer the flow will therefore be assumed irrotational. The velocity distribution in the main stream at the edge of the boundary layer has,

in all cases, to be specified before the boundary layer equations can be solved and the point of separation determined theoretically. Where the wake is broad this involves an appeal to experiment. In the present problem it was assumed that a good approximation to this velocity distribution was given by the perfect fluid irrotational flow past the cylinder, provided the correct value of the circulation was chosen† and the wake so found was small. This involves assuming that the boundary layer is thin. The thickness of the boundary layer is of the order  $R^{-\frac{1}{2}}$  and hence, even if we restrict ourselves to the consideration of a laminar boundary layer, this assumption is valid for a considerable range of values of  $R$ . Further, the results obtained for small values of the angle of incidence gave points of separation near to the tail, and agreement was thus obtained between the initial assumption (that the wake was narrow) and the final result. Therefore for small values of the angle of incidence the results obtained should be in good agreement with those obtained in practice. The discussion of the results for larger angles of incidence is left until later (*see* section 8).

The object of the investigation is, therefore, the determination of the circulation in the irrotational flow past the cylinder.

### 3—THE CRITERION FOR DETERMINING THE CIRCULATION

- (i) We take, as an experimentally evident fact, that the average flux of vorticity out of some fixed circuit  $P$  (considering the cylinder as fixed also) enclosing the cylinder vanishes. Consider any other fixed circuit  $Q$  enclosing the cylinder. Since the average motion is steady, the average amount of vorticity contained between  $P$  and  $Q$  is constant. Therefore the average flux of vorticity out of  $Q$  is equal to the average flux of vorticity out of  $P$ , since vorticity is neither created nor destroyed in the region between  $P$  and  $Q$ .

Thus, by the experimental fact mentioned above, the average flux of vorticity out of  $Q$  vanishes. That is the average flux of vorticity out of any fixed circuit is zero, and therefore the average rate at which positive vorticity is transported from the upper surface of the cylinder into the wake is equal to the average rate at which negative vorticity is transported from the lower surface.

*Note*—It is necessary in considering conditions in the wake to take into account the average motion only because conditions in the wake are steady on the average only. From henceforward we shall consider the motion outside the wake as steady.

† Some justification for this assumption is given in Section 3 below.

- (ii) Betz† has shown that the rate at which vorticity is transported across any normal section of the boundary layer is proportional to the square of the velocity in the main stream at that section. For, denote by  $\bar{u}$  the velocity in the boundary layer parallel to the wall, then the vorticity at any point of the cross-section may be written  $\partial\bar{u}/\partial Y$ . Thus the rate at which vorticity is transported downstream is

$$\int_0^{\delta} \bar{u} \frac{\partial \bar{u}}{\partial Y} dY = \frac{\bar{U}^2}{2}.$$

Hence the magnitude of the vorticity transported into the wake is determined by the velocity in the main stream at the point of separation. Thus by (i) the velocities, and therefore the pressures, are the same at the points of separation on the upper and lower surfaces.

- (iii) Betz (*loc. cit.*, p. 289) has also shown, for a Joukowski aerofoil, that the observed pressure distribution and the pressure distribution, calculated from the inviscid flow past the aerofoil by choosing the circulation  $K$  so that it is related to the observed lift  $L$  by the relation

$$L = K\rho V, \quad (3.1)$$

are in good agreement when the wake is small. We assume this to be true also for the elliptic cylinder we consider. (It is evident that if a value of  $K$  exists such that the inviscid pressure distribution agrees with the observed one then the lift is given by (3.1). This can easily be shown by integrating the inviscid pressure distribution over the surface of the cylinder.)

- (iv) Further, by (ii), the actual pressure distribution satisfies the condition that the pressures at both points of separation are equal. Therefore, by choosing the circulation in the inviscid flow outside the boundary layer so that the pressures at both points of separation are the same then the pressure distribution will agree with the one actually found and the observed lift will be given by (3.1).

It should be pointed out at this stage that Fage‡ has published some experimental results of the pressure distribution around an elliptic cylinder and an aerofoil of infinite aspect ratio and compared these with

† 'Handbuch der Physik,' p. 223.

‡ 'Phil. Trans.,' A, vol. 227, p. 1 (1927).

pressure distributions calculated from inviscid flow as Betz did. The agreement found was not so good as that found by Betz, though the discrepancy was not large even at the larger angles of incidence and negligible at the smaller ones, say, for  $0 < \theta < 6^\circ$ .

Although not immediately necessary in determining the foregoing criterion, reference should be made at this stage to some experiments of Bryant and Williams<sup>†</sup> and a theorem due to Taylor.<sup>‡</sup> Bryant and Williams found that the circulation around any large circuit which cuts the wake in a line perpendicular to the direction of the undisturbed flow at infinity was the same for all such circuits and connected with the lift by the relation (3.1). Taylor gave a theoretical proof of this latter result for circuits chosen in this way.

The criterion established gives a trial and error method for determining the circulation. A value of the circulation is assumed and the velocity at the surface of the cylinder for the corresponding perfect fluid irrotational flow past the cylinder is determined. Using this velocity as the velocity in the main stream for the flow in the boundary layer, the points of separation on the upper and lower surfaces can be determined. The circulation has to be varied until the velocities at these points are the same.

#### 4—THE IRROTATIONAL FLOW PAST THE CYLINDER

The velocity potential for the irrotational motion of a perfect fluid past an elliptic cylinder can be written in the form§

$$\phi = -Vc e^{\alpha} \cos(\eta - \theta) + \frac{K\eta}{2\pi}. \quad (4.1)$$

The velocity potential used by the present writer has the opposite sign to that used by Lamb, and so there is a difference in sign between equation (4.1) and the one given by Lamb. Then

$$U = \frac{1}{Vc} \frac{\partial \phi}{\partial \eta} = + \left\{ \frac{A}{h} + \frac{B}{h} \sin \eta \cos \theta - \frac{B}{h} \cos \eta \sin \theta \right\}, \quad (4.2)$$

where  $A = K/2\pi cV$ ,  $B = e^{\alpha}$ ,  $h = (D - \frac{1}{2} \cos 2\eta)^{\frac{1}{2}}$  and  $D = (\cosh^2 \alpha - \frac{1}{2})$ . We have, therefore, to determine  $A$  in order to determine the circulation.

<sup>†</sup> 'Phil. Trans.,' A, vol. 225, p. 199 (1925).

<sup>‡</sup> 'Phil. Trans.,' A, vol. 225, p. 238 (1925).

§ See Lamb, "Hydrodynamics," 5th. Ed., pp. 79-84.

Further,

$$-U' = -\frac{\partial U}{h \partial \eta} = \frac{A \sin 2\eta}{2h^4} + \frac{\left(\frac{B}{2} - DB\right)}{h^4} \cos \eta \cos \theta - \frac{\left(\frac{B}{2} + DB\right)}{h^4} \sin \eta \sin \theta, \quad (4.3)$$

$$\begin{aligned} -U'' = -\frac{\partial U'}{h \partial \eta} = & A \frac{\left\{\frac{1}{4} \cos 4\eta + D \cos 2\eta - \frac{3}{4}\right\}}{h^7} \\ & + \cos \theta \frac{\left\{\left(\frac{3BD}{4} + BD^2 - \frac{5B}{8}\right) \sin \eta + \left(\frac{3BD}{4} - \frac{3B}{8}\right) \sin 3\eta\right\}}{h^7} \\ & + \sin \theta \frac{\left\{\left(\frac{3BD}{4} + \frac{5B}{8} - BD^2\right) \cos \eta - \left(\frac{3BD}{4} - \frac{3B}{8}\right) \cos 3\eta\right\}}{h^7}. \end{aligned} \quad (4.4)$$

The coefficients of  $A$ ,  $\cos \theta$  and  $\sin \theta$  in the expressions for  $U$ ,  $U'$  and  $U''$ , are functions of  $\eta$  only for any particular ellipse and can be tabulated. In the case considered this was done initially at intervals of  $15^\circ$  for  $\eta$ , except for  $20^\circ$  around the nose and tail where  $2^\circ$  intervals were used. Further values were added where they were found to be necessary.

Thus, for any values of  $\theta$  and  $A$  the values of  $U$ ,  $U'$  and  $U''$  can be obtained from these tables. With these values the boundary layer equations can be solved and the points of separation found. For any particular value of  $\theta$ ,  $A$  must be varied until the velocity in the main stream is the same at both points of separation.

We must now consider the actual solution of the boundary layer equations in order to find the velocities at the points of separation and therefore we must discuss each case separately.

## LAMINAR BOUNDARY LAYER

### 5—SOLUTION OF THE BOUNDARY LAYER EQUATIONS

Various methods of solution of the boundary layer equations have been described by the present writer in a previous paper,<sup>†</sup> referred to later as 1632. For the present work, in which  $U'$  and  $U''$  take large

<sup>†</sup> 'Rep. Memor. Aero. Res. Ctee. Lond.,' No. 1632 (1935).

values, the number of methods available is limited to Pohlhausen's method and Dryden's modification of it and also the modification of Falkner and Skan's method given by the present writer. These methods are described in paragraphs 3 and 8 respectively of 1632.

If we write  $z = V\delta^2/cv$ , Pohlhausen's method requires the solution of the differential equation

$$dz/dx = \frac{f(\lambda)}{U} + z^2 U'' g(\lambda), \quad (5.1)$$

where  $\lambda$  is the non-dimensional quantity

$$\left(\frac{d\bar{U}}{dX}\right) \frac{\delta^2}{v} = U'z.$$

The functions  $f(\lambda)$  and  $g(\lambda)$  are tabulated in 1632 and the initial value for starting the integration is given by  $U'z = 7.052$  at  $x = 0$ , the forward stagnation point.

This method was used wherever possible. In performing the integrations over the lower surface, however, when  $\theta = 8^\circ$  and  $8^\circ 30'$ , it was found that this method collapsed owing to  $\lambda$  becoming equal to 12. This difficulty was mentioned in 1632. Two alternative methods were used for performing these integrations, namely, Dryden's and the modified method of Falkner and Skan.

We consider now the application of the ordinary Pohlhausen method to the problem under discussion, when no difficulty arises. It was found convenient to use  $\eta$  instead of  $x$  as the independent variable in performing the integrations. A reason for this is given in section 7.

The condition for separation is given by

$$\lambda = U'z = -12. \quad (5.2)$$

With practice, the curves given by equation (5.2) for different values of  $A$  can be used, merely by inspection, to give a useful approximation to the correct value of  $A$ . The integrations over the upper and lower surfaces can be performed with this value of  $A$  and the velocities in the main stream at the points of separation obtained. If these are not equal, it appears that a better approximation can be obtained by assuming that the change required in the value of  $A$  does not alter appreciably the position of the point of separation but only the velocity there. This gives rise to the following approximate method for correcting values of  $A$ . Denote by  $U_1$  and  $U_2$  the velocities at the points of separation, by  $h_1$  and  $h_2$  the values of  $h$  at these points and by  $\epsilon'$  the error in the value of



A. The velocities at the points of separation when the change  $\varepsilon'$  is made in A are given by equation (4.2) as

$$\left(U_1 - \frac{\varepsilon'}{h_1}\right) \text{ and } \left(U_2 - \frac{\varepsilon'}{h_2}\right)$$

(since  $\theta$  is constant) on the assumption that the positions of the points of separation have not altered appreciably. Thus the condition for determining  $\varepsilon'$  is

$$U_1 - \frac{\varepsilon'}{h_1} = U_2 - \frac{\varepsilon'}{h_2}. \quad (5.3)$$

This condition is an approximate one only, but it was found by the present writer to be very useful. The values obtained for A by this method were checked by repeating the integrations and generally were found to be sufficiently accurate. If not, the process was repeated.

Typical integral curves for  $z$  are shown in figs. 1 and 2. Fig. 1 shows the integral for the upper surface of the cylinder when  $\theta = 6^\circ$  and the circulation has the correct value, whilst fig. 2 shows the corresponding integral for the lower surface. Figs. 3 and 4 show the integral curves over the upper surface when  $\theta = 7^\circ$  and  $8^\circ 30'$ , and illustrate the speed with which the separation on the upper surface moves forward as  $\theta$  is increased in this range.

#### 6—SPECIAL DIFFICULTY

As mentioned above, the ordinary Pohlhausen method breaks down when  $\theta = 8^\circ$  and  $8^\circ 30'$ , owing to  $\lambda$  becoming equal to 12. This difficulty occurred fairly near to the point of separation and was overcome, at first, in a crude fashion by neglecting that part of the curve where  $\lambda$  became nearly equal to 12 and by finishing the curve off so as to be similar to the ones already obtained when no difficulty occurred. The values of A obtained in this way have since been found to be in good agreement with those found by a less hazardous process. This is due, largely, to the condition for separation (5.2) giving a curve practically normal to the axis of  $x$  in the neighbourhood of the actual position of the point of separation.

Two alternative methods were used when this difficulty occurred. The first of these was Dryden's modification of Pohlhausen's method, whilst the second was the modification of Falkner and Skan's method suggested by the present writer. (Both these methods are described in 1632.) Actually, as far as the second method is concerned, it was joined on to the ordinary solution due to Pohlhausen some distance back from

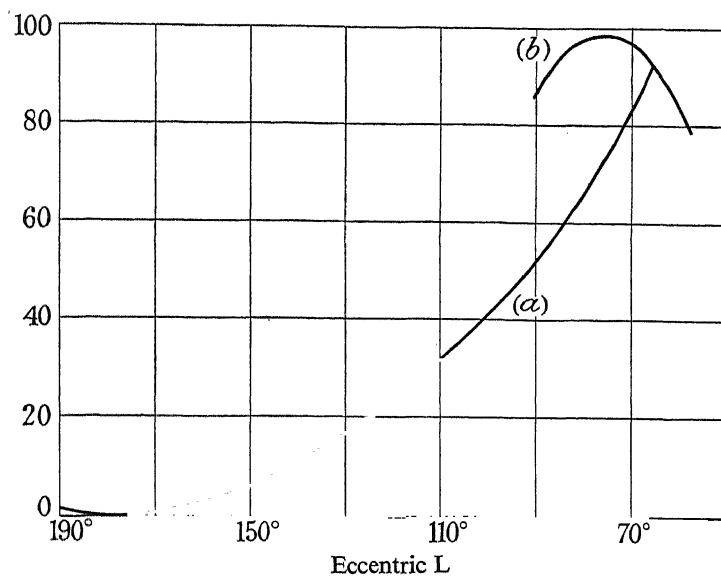


FIG. 1

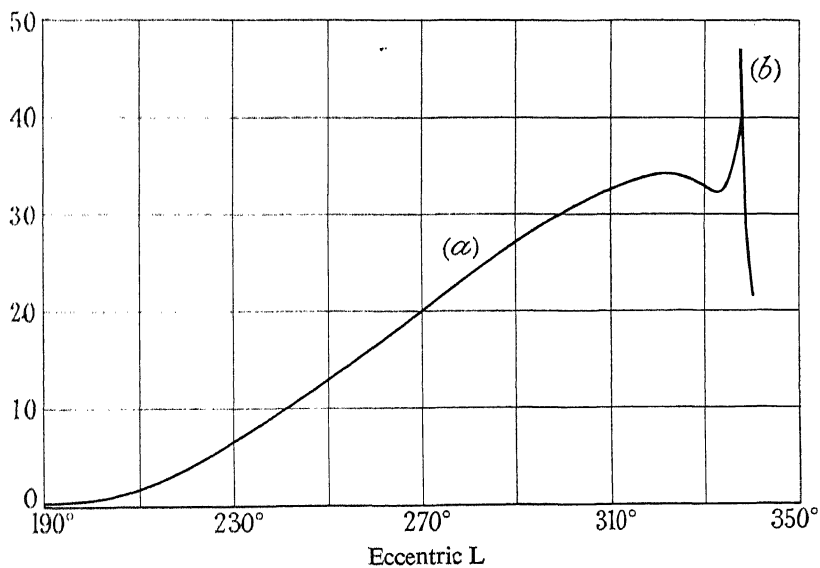


FIG. 2

FIGS. 1 and 2—Integral curve for  $z$  where  $\theta = 6^\circ$ ; fig. 1, top, fig. 2, bottom. (a) Integral curve for  $z$ ; (b) curve for  $U'z = -12$

where the difficulty occurred; it was used throughout the region of difficulty and then the ordinary Pohlhausen method was joined on again to complete the solution.

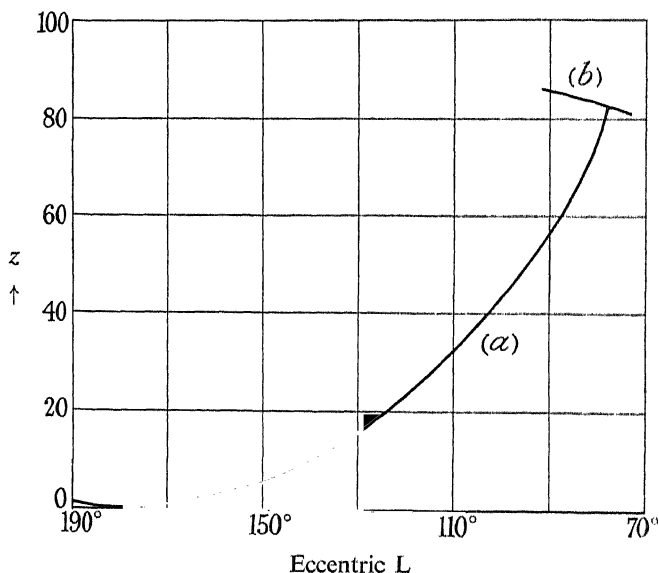


FIG. 3—Integral curve over top,  $\theta = 7^\circ$ . (a) Integral curve for  $z$ ; (b) curve for  $U'z = -12$

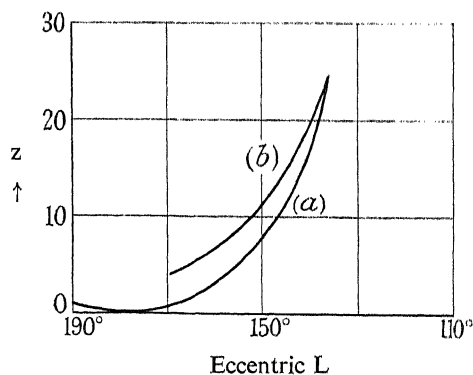


FIG. 4—Integral curve for  $z$ , top,  $\theta = 8^\circ 30'$ . (a) Integral curve for  $z$ ; (b) curve for  $U'z = -12$

These two methods were compared for  $\theta = 8^\circ 30'$  by plotting

$$\alpha = \frac{1}{2} \sqrt{\frac{vX}{U^3}} \left( \frac{\partial u}{\partial Y} \right)_{y=0} = \frac{1}{2} \sqrt{\frac{x}{U^3}} \left( \frac{\partial u}{\partial y} \right)_{y=0}$$

against  $x$ , see fig. 5. The results in the neighbourhood of the point of separation are shown in fig. 6. The agreement throughout the entire range will be seen to be remarkably good—the difference between the positions of the points of separation is almost within the limits of error of the graphical method used. The two methods are quite independent and the good agreement can be taken as an indication that they give good approximations to the correct value. Further, it was found by trial that Dryden's method gave the same point of separation when  $\theta = 7^\circ 30'$ , as did the ordinary method due to Pohlhausen. As Dryden's method is slightly easier to manipulate than the modification of Falkner and Skan's method, it was used elsewhere whenever Pohlhausen's method broke down.

As a matter of general interest, the curve for  $z$  given by the ordinary Pohlhausen method is shown in fig. 7 for  $\theta = 8^\circ 30'$ . The shaded region is the region in which  $z$  is imaginary. The part of the curve shown between the imaginary region and the point of separation was obtained, as indicated above, by joining on Pohlhausen's solution to Falkner and Skan's continuation.

#### 7—ACCURACY

It was thought preferable to use  $\eta$  as independent variable in the integration instead of  $x$ . Conditions vary so rapidly near the nose and tail that very small steps in  $x$  are required in performing the integration. However,  $dx = h d\eta$ , and in the neighbourhood of the nose and tail  $h$  is small and of the order of (0.2). Therefore a change of  $1^\circ$  in  $\eta$  corresponds to a very small change in  $x$ . Near the middle of the section  $h$  is of the order of 1 and the change in  $x$  corresponding to a change of  $1^\circ$  in  $\eta$  is larger. Hence the use of  $\eta$  instead of  $x$  magnifies the scale in those places where it is most needed.

The accuracy with which the position of the point of separation can be obtained is different for the upper and lower surfaces. For the lower surface the curve given by the condition (5.2) was found to cut the integral curve almost normally. Thus the point of separation could be given accurately. It was estimated that the method would give the point of separation to within  $\frac{1}{2}^\circ$  of eccentric angle and that the possible error in the eccentric angle chosen was  $\pm \frac{1}{4}^\circ$ . Now for separation it was found that  $U'$  was of the order of  $-0.3$ . The points of separation occur close together when  $\theta$  lies between  $2^\circ$  and  $8^\circ 30'$ , and in this region  $\eta = 340^\circ$  at the point of separation. For this value of  $\eta$ ,  $h$  is of the order of 0.4 and the change in  $U$  corresponding to a change of  $\frac{1}{4}^\circ$  in  $\eta$  is of the order of 0.00025. The change in  $A$  corresponding to this change in  $U$  is

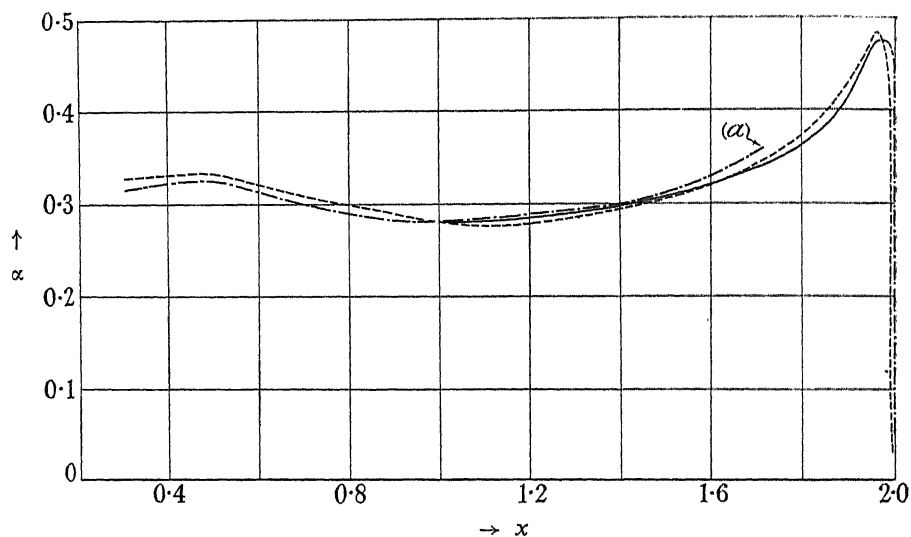


FIG. 5— $\alpha = \frac{1}{2} \sqrt{\frac{\nu X}{U_3}} \left( \frac{\partial \bar{u}}{\partial Y} \right)_0$ . ---, modified Pohlhausen; — . — . —, ordinary Pohlhausen; —, Falkner and Skan's continuation; (a) ordinary Pohlhausen breaks down

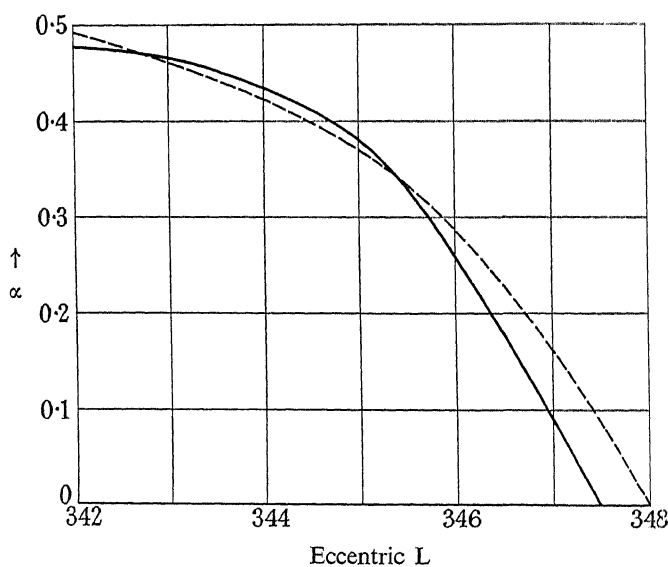


FIG. 6— $\alpha = \frac{1}{2} \sqrt{\frac{\nu X}{U_3}} \left( \frac{\partial \bar{u}}{\partial Y} \right)_0$ . —, Ordinary Polhausen joined to Falkner and Skan at  $342^\circ$ ; ---, modified Polhausen

obtainable from equation (4.2) and is given as of the order of 0.00015. The value of  $A$  varies between 0.028 when  $\theta = 2^\circ$  to a maximum of 0.14 when  $\theta = 7^\circ$ . Thus, for the lower surface the limits of error in  $A$  are  $\pm \frac{1}{2}\%$ .

The error on the upper surface can be estimated similarly and varies from  $\pm 3\%$  when  $\theta = 2^\circ$  to  $\pm 2\%$  when  $\theta = 6^\circ, 7^\circ$ , or  $8^\circ$ . Thus the maximum possible errors in the values of the circulation are  $\pm 3.5\%$  when  $\theta = 2^\circ$ , and  $\pm 2.5\%$  when  $\theta = 6^\circ, 7^\circ$ , or  $8^\circ$ .

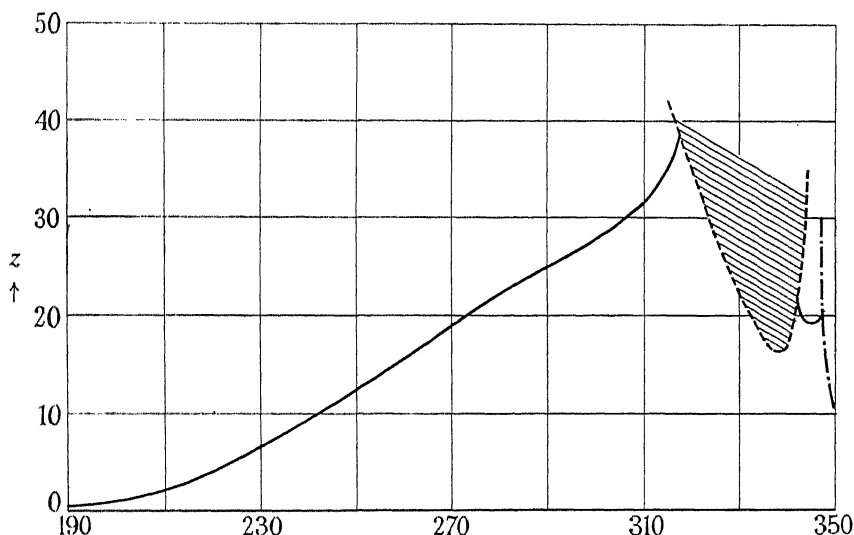


FIG. 7—0 to  $8^\circ 30'$  bottom. —, Integral curve; ---, boundary of imaginary region given by  $U'z = 12$ ; - · -, condition for separation  $U'z = -12$

## 8—CONCLUSION OF THE LAMINAR CASE

The lift coefficient is defined by  $(L/2a^2\rho V)$ , and in virtue of (3.1) this may be written  $(K/2aV)$ . This quantity, as determined by the method described, is shown plotted against  $\theta$  in fig. 8. The slope of the curve at the origin is 2.45 when  $\theta$  is expressed in radians. Fig. 9 shows the positions of the points of separation on both the upper and lower surfaces, when the circulation has the value given in fig. 8, for various angles of incidence. Thus, fig. 9 gives a rough idea of the size of the wake.

It will be noticed that the calculations made are independent of the Reynolds' number and so there is no scale effect on the lift coefficient.

Let us consider the assumptions involved in the method used. Denote by  $S_1$  and  $S_2$  the positions of the points of separation on the upper and lower surfaces respectively, by  $O$  the position of the forward stagnation

point, and by T the trailing edge. Further denote by  $S_1W_1$  and  $S_2W_2$  the boundaries of the wake in the neighbourhood of the points of separation.

Fundamentally, the method depends on the actual velocity distribution in the main stream over the regions  $OS_1$  and  $OS_2$  being the same as the velocity distribution over these regions found from the irrotational flow of a perfect fluid past the cylinder when the circulation is chosen to make the velocity at  $S_1$  and  $S_2$  the same. In effect, however, if we consider the wake as a "dead region," the boundary for the potential flow is  $W_1S_1OS_2W_2$  and not  $TS_1OS_2T$  as assumed in the calculations. Thus if

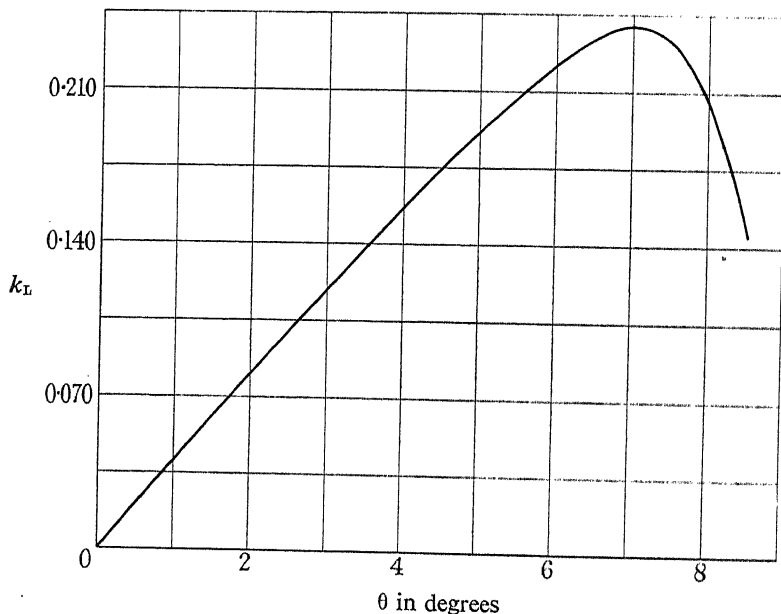


FIG. 8—Lift coefficient  $k_L = \frac{\text{circulation}}{(\text{major axis}) \times (\text{undisturbed velocity})}$

the distances  $S_1T$  and  $S_2T$  are small the discrepancy between the two potential flows should be small and the results obtained by the method discussed should be quantitatively good.  $S_1T$  and  $S_2T$  are small for small angles of incidence and, as anticipated earlier, the results for small angles of incidence should be reliable.†

For the larger angles of incidence, when  $S_1T$  and  $S_2T$  are no longer small, a considerable discrepancy arises between the two potential flows mentioned. We can show, however, that the fact of the rapid increase

† Evidence in support of this conclusion is given by Betz's experiments mentioned in section 3.

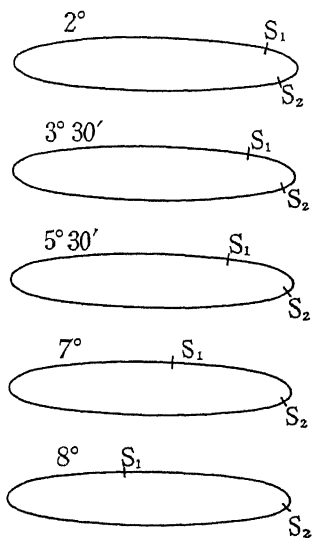
of either  $S_1T$  or  $S_2T$ , as given by the method considered, means that the cylinder is stalled.

It will be seen that the method considered will find the circulation and velocity distribution appropriate to a small wake, if there is one, since the assumed velocity distribution is obtained by neglecting the size of the wake. For suppose, if possible, that by considering the potential flow past a boundary of the type  $W_1S_1OS_2W_2$  it is possible to find a circulation satisfying the conditions of equal velocity in the main stream at  $S_1$  and  $S_2$  and with the distances  $S_1T$  and  $S_2T$  small when the method used above gives a large wake. Then the velocity distribution in the main stream over the region  $OS_1$  and  $OS_2$  is approximately the same as that originally assumed when the width of the wake was neglected since  $S_1T$  and  $S_2T$  are small. By hypothesis, however, the points of separation found from the assumed velocity distribution when the width of the wake is neglected are such that either  $S_1T$  or  $S_2T$  is no longer small. Thus a contradiction arises and therefore no velocity distribution and appropriate circulation exist giving a small wake.

Hence the rapid increase in the width of the wake given by the method considered means that, although the circulation and the size of the wake determined by this method may be incorrect, the wake found in practice increases rapidly. Experimentally this rapid increase in the area of the cylinder affected by the wake is known to be indicative of stalling. It is indeed clear that when the area of the upper surface affected by the wake is large the lift is small, since there is no suction to be obtained from the wake.

Thus we may say that for values of the Reynolds' number which give a fully laminar boundary layer the elliptic cylinder considered stalls at about  $7^\circ$  incidence and that for  $0 < \theta < 6^\circ$  the value of the lift coefficient will be given quite accurately in fig. 8.

We shall leave the discussion of the maximum Reynolds' number, for which the flow in the boundary layer remains laminar, until later and proceed now with a discussion of the conditions when the boundary layer is fully turbulent.



$S_1$  and  $S_2$  denote the points of separation

FIG. 9



## THE FULLY TURBULENT BOUNDARY LAYER

## 9—THE SOLUTION OF THE BOUNDARY LAYER EQUATIONS

The problem is precisely the same as the one just discussed apart from the solution of the boundary layer equations. We shall now discuss a method of solving the momentum integral equation (2.1) for a fully turbulent boundary layer. This method depends on the use of two empirical relations.

We write

$$\delta^* = \int_0^\delta \left(1 - \frac{\bar{u}}{\bar{U}}\right) dY \quad (9.1)$$

$$\vartheta = \int_0^\delta \left(1 - \frac{\bar{u}}{\bar{U}}\right) \frac{\bar{u}}{\bar{U}} dY \quad (9.2)$$

Then

$$H = \delta^*/\vartheta. \quad (9.3)$$

$$\begin{aligned} & \bar{U} \frac{d}{dX} \int_0^\delta \bar{u} dY - \frac{d}{dX} \int_0^\delta \bar{u}^2 dY \\ &= -\bar{U} \frac{d\bar{U}}{dX} \int_0^\delta \left(1 - \frac{\bar{u}}{\bar{U}} - 1\right) dY + \frac{d}{dX} \bar{U}^2 \int_0^\delta \left[\left(1 - \frac{\bar{u}}{\bar{U}}\right) \frac{\bar{u}}{\bar{U}} - \frac{\bar{u}}{\bar{U}} + 1 - 1\right] dY \\ &= \bar{U} \frac{d\bar{U}}{dX} (\delta^* - \delta) + 2\bar{U} \frac{d\bar{U}}{dX} \vartheta + \bar{U}^2 \frac{d\vartheta}{dX}. \end{aligned}$$

Therefore, since for steady motion  $-\frac{1}{\rho} \frac{dp}{dX} = \bar{U} \frac{d\bar{U}}{dX}$  we may write equation (2.1) in the form

$$\frac{d\vartheta}{dX} + \frac{1}{\bar{U}} \frac{d\bar{U}}{dX} (H + 2) \vartheta = \frac{\tau}{\rho \pi^2}. \quad (9.4)$$

Until a rational theory, which gives the velocity distribution through the boundary layer and the corresponding skin friction, is evolved, we must rely on two empirical relations to connect up  $H$  and  $\tau$  with  $\vartheta$  and  $X$ . It appears that if the form of the “mixing-length,” when a varying pressure gradient is present, could be determined this would suffice. No such form seems to have been obtained, so we are compelled to revert to experimental evidence, guided by dimensional considerations, to solve equation (9.4).

It seems to be fairly evident from dimensional considerations that

$$H = H\left(\frac{\bar{U}\vartheta}{\nu}, \frac{d\bar{U}}{dX} \frac{\vartheta}{\bar{U}}\right),$$

† The velocity  $\bar{u}$  in turbulent flow refers to the mean velocity.

and

$$\tau = \tau \left( \frac{\bar{U} \vartheta}{\nu}, \frac{d\bar{U}}{dX} \frac{\vartheta}{\bar{U}} \right).$$

Given sufficient experimental evidence, it should be possible to draw the families of curves for  $H$  and  $\tau$ . These families of curves would make the solution of (9.4) immediate by numerical means; for, given particular values of  $X$  and  $\vartheta$ ,  $H$  and  $\tau$  would be determined by these families of curves and thus the value of  $d\vartheta/dX$ , could be evaluated. Unfortunately, the experimental evidence available does not seem to be sufficient to permit the construction of the families of curves for  $H$  and  $\tau$ .

Buri† has suggested that there is some experimental evidence to show that if  $\zeta$  is defined by the relation

$$\zeta = \frac{\tau}{\rho U^2} \left( \frac{\bar{U} \vartheta}{\nu} \right)^{\frac{1}{2}},$$

then  $H$  and  $\zeta$  are functions of  $\Gamma = \left( \frac{\bar{U} \vartheta}{\nu} \right)^{\frac{1}{2}} \left( \frac{d\bar{U}}{dX} \frac{\vartheta}{\bar{U}} \right)$  only. The quantities  $H$  and  $\zeta$  are plotted against  $\Gamma$  in figs. 10 and 11 using the experimental results of Buri and Nikuradse.‡ It will be seen that, apart from some

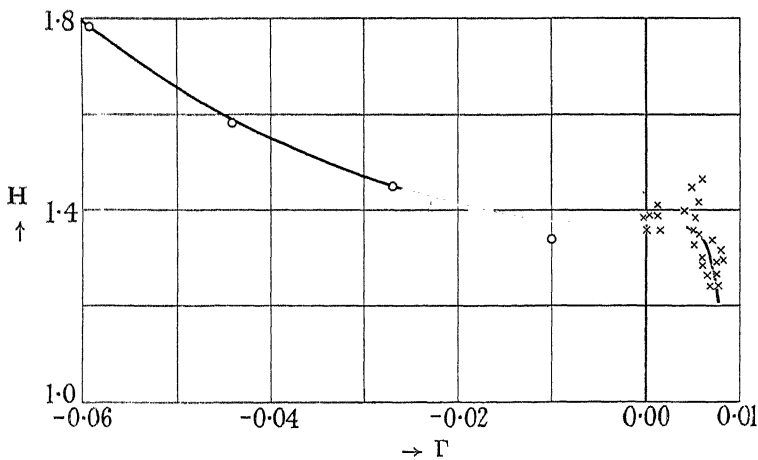


FIG. 10—O, Nikuradse's results as corrected by Buri; x, Buri's results

scattering, curves for  $H$  and  $\zeta$  are defined by this method of plotting. Certain results of Nikuradse have been omitted because they were far

† "Dissertation," Zürich, 1931.

‡ Forschungsarbeiten (Göttingen), No. 289.

from the curves defined by the other values, and it seemed probable to the present writer that the boundary layer was not fully turbulent for these measurements. (The measurements of Nikuradse were obtained from experiments in converging and diverging channels whilst those of Buri seem to be confined to converging channels.) The scattering leaves something to be desired, and indeed before the method can be used with confidence much additional experimental evidence is required.

In any case, there is obviously some relationship between the forms used by Buri for  $\zeta$  and  $\Gamma$  and the  $1/7$ th power law. One need only

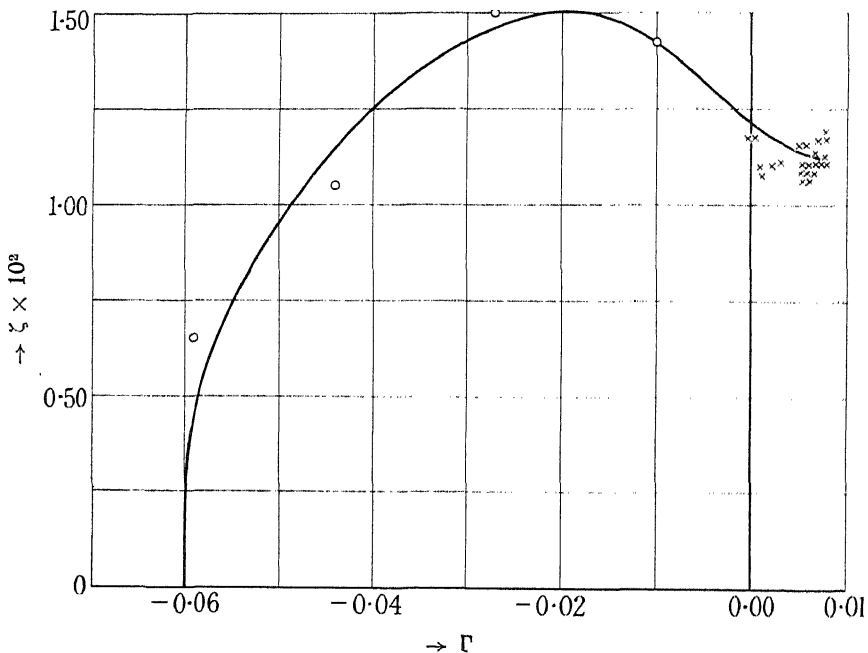


FIG. 11—○, Nikuradse's results corrected by Buri; ×, Buri's results

remark that the skin friction coefficient  $c_f$  for flow along a flat plate with a turbulent boundary layer may be written  $0.0116 / \left( \frac{\bar{U} g}{\nu} \right)^{\frac{1}{4}}$  when the  $1/7$ th power law is used to justify this statement. So far as the ideas underlying the forms assumed by Buri are correct, it is to be expected that better results will be obtained by generalizing Buri's forms so as to replace the  $1/7$ th power law by the corresponding logarithmic form. This can be done by a consideration of Karman's results for the skin friction for turbulent flow along a flat plate.

We consider now, in detail, the solution of (9.4).† For a given pair of values of  $X$  and  $\vartheta$ ,  $\Gamma$  is determined, thus giving the values of  $H$  and  $\zeta$  and hence the value of  $d\vartheta/dX$ . This is all that is required in order to solve (9.4) numerically apart from the value of  $\vartheta$  at the forward stagnation point. From (9.4),  $\vartheta$  is either zero or infinite when  $X = 0$ . We shall therefore assume that  $\vartheta = 0$  when  $X = 0$  and we find, on putting  $\bar{U} = \bar{U}_1 X$ , that

$$\vartheta^{5/4} = \frac{1}{(H_0 + 13/5)} \frac{\zeta_0}{(\bar{U}_1/\nu)^{1/2}} X^{1/2}$$

in the neighbourhood of the stagnation point where  $H_0$  and  $\zeta_0$  are the values of  $H$  and  $\zeta$  when  $\Gamma = 0$ .

We can transform (9.4) to a more convenient form by putting

$$\chi = R^{1/2} (\vartheta/c)^{5/4},$$

where

$$R = Vc/\nu.$$

Then

$$\Gamma = \left( \frac{d\bar{U}}{dX} \frac{\vartheta}{\bar{U}} \right) \left( \frac{\bar{U}\vartheta}{\nu} \right)^{1/2} = \frac{U'}{U^{1/2}} \chi,$$

where  $U = \bar{U}V$ ,  $X/c = x$ , and dashes denote differentiations with regard to  $x$ .

Equation (9.4) then takes the form

$$\frac{d\chi}{dx} + \frac{5}{4} (H + 2) \frac{U'}{U} \chi = \frac{5}{4} \frac{\zeta}{U^{1/2}}. \quad (9.9)$$

Thus tabulating  $5/4U^{1/2}$ ,  $5U'/4U$ ,  $U'/U^{1/2}$  the equation (9.9) can be solved immediately starting from the condition  $\chi = \vartheta = 0$  at the forward stagnation point ( $X = 0$ ).

From the graphs for  $\zeta$ ,  $\tau$  vanishes when  $\Gamma = -0.06$  and thus the point of separation is given by the intersection of the integral curve and the curve

$$U'\chi/U^{1/2} = -0.06. \quad (9.10)$$

Equations (9.9) and (9.10) are independent of  $R$  and therefore the value of  $x$  at the point of separation is independent of  $R$  and dependent on the values of  $U$ ,  $U'$  only. (It should be remembered that  $U = \bar{U}V$ .) Thus for the fully turbulent boundary layer the positions of the points of separation are independent of the Reynolds' number of the main flow

† Buri merely approximated to the solution by assuming a pair of constant values for  $H$  and  $\zeta$  when  $\Gamma > 0$  and a different pair for  $\Gamma < 0$  and thus obtained an analytic solution.

just as was found for laminar flow. That is, for fully turbulent flow in the boundary layer there is no scale effect on the positions of the point of separation, and therefore the same is true for the lift coefficient.

The method of solution follows exactly the same lines as for laminar flow; the value of  $K$  used to calculate  $U$ ,  $U'$  has to be varied until the values of  $U$  are the same at both points of separation.

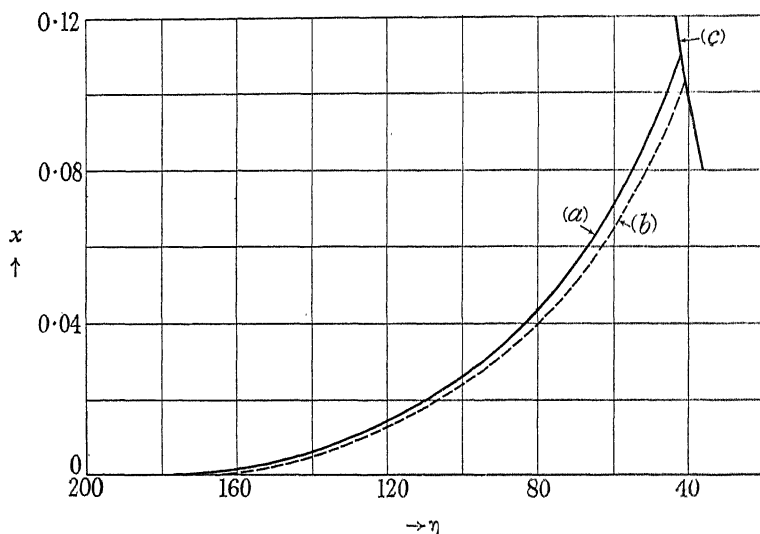


FIG. 12—12° incidence top. (a) Fully turbulent; (b) conditions when transition occurs at separation of laminar layer; (c) condition for separation

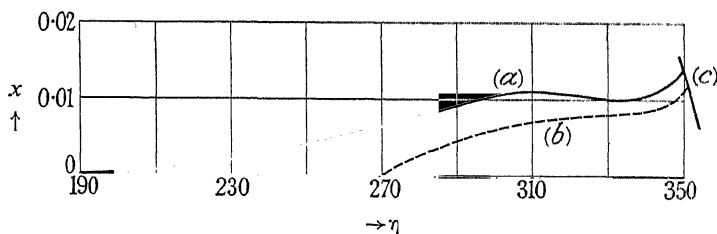


FIG. 13—12° incidence bottom. (a) Fully turbulent; (b) conditions when transition occurs at the point of separation of the laminar layer; (c) condition for separation

Typical integral curves, when  $K$  has the correct value, for the case  $\theta = 12^\circ$  and for both the upper and lower surfaces are shown in figs. 12 and 13 (full-line curves). Fig. 14 shows the curve of lift coefficient against incidence as obtained by this method. The errors committed in the method of graphical integration used may be discussed as for laminar motion, and give a possible error of  $\pm 1\%$  in the neighbourhood of  $20^\circ$  incidence and  $\pm 2\%$  in the neighbourhood of  $10^\circ$  incidence. It

will be noticed that for  $0^\circ < \theta < 20^\circ$  the graph is very accurately a straight line. The wake increases very rapidly in size when  $\theta$  is in the neighbourhood of  $22^\circ$  and as in laminar flow this may be taken to indicate stalling.

The straight line obtained for  $0^\circ < \theta < 20^\circ$  is in good qualitative agreement with experiments on aerofoils, but the value  $22^\circ$  for the stalling angle seems to be exceptionally high. Experiments do not seem to have been made on a thin elliptic cylinder, but a model aerofoil of roughly the same shape at the nose seems to stall at about  $16^\circ$  from zero incidence when tested in the compressed-air tunnel at a Reynolds' number of  $4 \times 10^6$  and when the effect of finite aspect ratio has been allowed

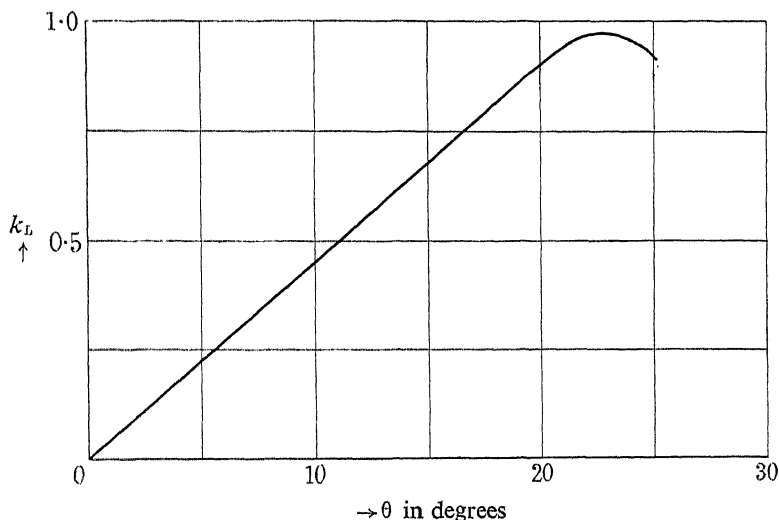


FIG. 14—Fully turbulent boundary layer. Lift coefficient and incidence curve

for. Further, there seems to be little evidence of such a large stalling angle for full-scale experiments with a Reynolds' number of  $3 \times 10^6$ . The slope of the straight line obtained theoretically is 2.70, whilst that obtained in the experiments referred to is 2.85. (The corresponding slope at the origin for laminar flow is 2.45.)

Experiments seem to suggest that at any rate up to Reynolds' numbers of the order of  $10^7$  a laminar portion of the boundary layer exists around the nose. We shall see in the next section that the existence of such a laminar portion would account for the cylinder stalling at smaller angles of incidence.

## THE CASE WHEN BOTH LAMINAR AND TURBULENT PORTIONS ARE PRESENT IN THE BOUNDARY LAYER

### 10—CONDITIONS AT THE POINT OF TRANSITION

We are here concerned with connecting the solution of the turbulent boundary layer equation on to the solution of the laminar boundary layer equation at the point of transition. If we assume that the position of the point of transition is known we experience little difficulty. We may make one of two assumptions suggested by various writers.

- (a) Physically, the more probable assumption seems to be that  $\delta$  is continuous at the point of transition. Having obtained the solution of the laminar boundary layer equation this gives immediately the value of  $\delta$  for starting the integration of the turbulent boundary layer equation.
- (b) A cruder assumption is to suppose that once transition has taken place the conditions in the boundary layer are the same as if it were fully turbulent right from the forward stagnation point.

We shall discuss both these assumptions at a later stage.

### 11—THE DETERMINATION OF THE POINT OF TRANSITION

For flow along a flat plate Karman gives

$$R_\delta = \bar{U}\delta/\nu = C \quad (11.1)$$

as the condition for determining the point of transition provided conditions with regard to turbulence in the oncoming stream remain similar.  $C$  is a constant which depends on the amount of turbulence in the main stream and seems to lie between 1600 and 6000.

$R_\delta$  is the only possible parameter for this condition. (There is  $Ud/\nu$ , where  $d$  is the distance from the leading edge, but on account of the relation between  $\delta$  and  $d$  the two parameters are equivalent.)

In flow past a cylinder we have to consider (i)  $R_\delta = \bar{U}\delta/\nu$ ; (ii) a parameter containing the velocity gradient such as  $\lambda = \frac{d\bar{U}}{dx} \frac{\delta^2}{\nu}$ ; (iii) a parameter containing  $c$  such as  $Vc/\nu$ .

The condition corresponding to (11.1) for this case is therefore

$$\Phi\left(\frac{\bar{U}\delta}{\nu}, \frac{d\bar{U}}{dx} \frac{\delta^2}{\nu}\right) = F(Vc/\nu), \quad (11.2)$$

where  $\Phi$  and  $F$  are undetermined functions.

The interesting systems from our point of view are flow in a wind tunnel and flow in full flight, when the velocity of flow or flight changes. Presumably conditions with regard to turbulence in the main stream change as the velocity changes, but this change can probably be allowed for in (11.2) by a suitable change in the function  $F(Vc/\nu)$ . Thus the form of (11.2) should be sufficient to give the transition point in the systems considered.

Stüper† in some experiments on an aerofoil finds that transition occurs for values of  $R_s = \bar{U}g/\nu$  lying between 250 and 650; thus it appears that for an aerofoil the values of  $R_s$  for transition are of the same order of magnitude as for flow along a plate.

In the problem considered, owing to the nature of the criterion established for determining the circulation, we are concerned wholly with the determination of the position of the points of separation. It appears by trial that the point of separation on the lower surface changes very little whether the boundary layer be fully laminar or fully turbulent. Further, if we assume that transition takes place, for any particular value of  $R$ , at a point corresponding to a value of  $R_s$ , of the same order of magnitude as that given by Stüper, using either of the assumptions (a) or (b) there is little change in the position of the point of separation. For the moment, therefore, we shall confine our attentions to conditions on the upper surface, since much greater changes take place there. By point of separation and point of transition we shall mean those points on the upper surface.

## 12—THE CRITICAL REYNOLDS' NUMBER

It seems probable that for any particular angle of incidence there will be a critical value  $R_c$  of  $R$  such that the point of separation of the laminar layer is coincident with the point of transition. Further, it will be expected that for values of  $R$  greater than  $R_c$  the transition to turbulent flow takes place before the laminar layer separates and that for values of  $R$  less than  $R_c$  the laminar layer separates before transition to turbulent flow in the boundary layer takes place. (This has not been proved, of course, and must be taken as a tentative suggestion.)

To determine  $R_c$  we must put, therefore,

$$\lambda = \frac{d\bar{U}}{dX} \frac{\delta^2}{\nu} = -12 \quad \text{see case (i).}$$

Thus (11.2) becomes

$$\Phi(R_{ss}, -12) = F(R_c),$$

† 'Luftfahrtforsch.', vol. 11, p. 26 (1934).



where the suffix  $s$  denotes that values are taken at the point of separation of the laminar layer

$$\text{or} \quad \Psi' (R_{\delta s}) = F (R_c),$$

$$\text{or} \quad R_{\delta s} = f(R_c) \quad \text{simply.} \quad (12.1)$$

It seems probable, too, that the curvature of the cylinder may have some effect on the point of transition. Due to this curvature there is a pressure gradient across the boundary layer and it seems probable that laminar flow will be less stable in the presence rather than the absence of this pressure gradient. The present theory does not take into consideration the effects of curvature except that they influence the pressure gradient parallel to the surface, and we return now to discussion of (12.1).

As we know nothing of the form of  $f(R_c)$ , all we can do at present is to assume simple forms for this function and test them by means of the results they give. First of all we make the simplest assumption, namely, that  $f(R_c)$  is a constant  $C$ .

Then

$$(\bar{U}\delta/\nu)_s = C,$$

*i.e.*,

$$\frac{cV}{\nu} U^2 \frac{V\delta^2}{\nu c} = C^2,$$

*i.e.*,

$$R_c (U^2 z)_s = C^2,$$

where  $z$  is defined in case (i). Thus

$$R_c = C^2 / (U^2 z)_s.$$

(It has been proved by trial that if the point of transition is given by  $R_s = C$ , whether the points of transition and separation coincide or not, then as  $R$  increases transition first takes place at the point of separation of the laminar layer. As the assumption mentioned here implies that the point of transition is not explicitly dependent on the pressure gradient, this is far less likely to be true than (12.2).)

We now fix our ideas by considering some angle of incidence, say  $12^\circ$ , between the angle when the cylinder with a fully laminar and fully turbulent boundary layer stalls. Integral curves for  $\chi$  for this case are shown dotted in figs. 12 and 13 when transition occurs at the point of separation of the laminar layer using assumption (a). The form of the lift coefficient-Reynolds' number curves is shown in fig. 15 on assumption (a), and on the further assumption that transition is determined by (12.2), whether it occurs at the point of separation or not. The curves on

assumption (b) consist of the two lines  $k_L = 0$  for  $R < R_c$  and  $k_L = k_{L_{\text{turb.}}}$  for  $R > R_c$ , where  $k_{L_{\text{turb.}}}$  denotes the value of  $k_L$  obtained from the fully turbulent boundary layer at the incidence considered. It will be seen that there is little difference between the two curves and for simplicity we shall therefore use assumption (b). The form of the curves is immediately evident from the assumptions made about  $R_c$ . For  $R < R_c$  separation takes place in the laminar layer before transition to turbulence and thus the cylinder is stalled since by supposition the angle of incidence considered is greater than the stalling angle for laminar

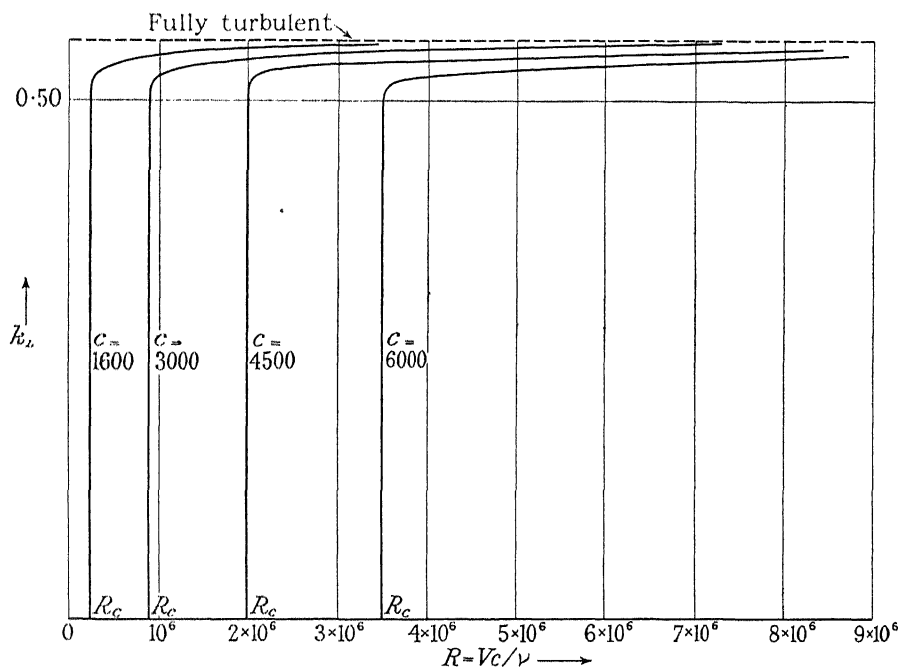


FIG. 15—12° incidence. Lift coefficient-Reynolds' number curves

flow. For  $R > R_c$  transition takes place before the laminar layer separates, and we have to use the solution of the turbulent boundary layer together with assumption (a) or (b).

If the angle is less than the stalling angle for the laminar boundary layer, the sole difference is that instead of having a very small value for  $R < R_c$  the lift coefficient is equal to the value obtained for the fully laminar boundary layer.

From a set of these lift coefficient-Reynolds number curves for various angles of incidence we can construct the curve of maximum lift coefficient plotted against Reynolds' number. This curve depends on the value

of  $C$ . The curves given in fig. 16 have been calculated on the assumption that  $R_c$  is given by (12.2) and for the values  $C$  1500, 3000, 4500 and 6000. The curves for different values of  $C$  are in fact transition curves for the maximum lift coefficient.

Apart from the sudden jump from a lift coefficient of about 0.7 to one of 1.0—a feature of all the curves—the results seem to be in fair agreement with experiment. The sudden jump occurs in all the curves at a Reynolds' number obtainable either in experiments in the compressed air tunnel or in full flight and would surely have been observed by experimenters if it were a reality.

We may either conclude that the method of solution of the turbulent boundary layer equation is wrong or that the form of the function  $f(R_c)$

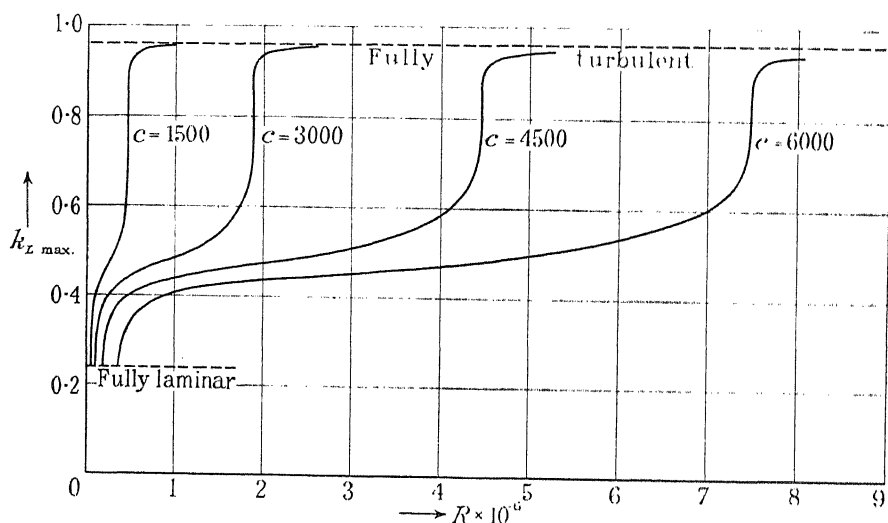


FIG. 16—Scale effect on maximum lift; first calculations

is not correct. It is known that a  $1/8$ th power law gives more accurate results than the  $1/7$ th power law as the Reynolds' number increases, but from a cursory examination it seems probable to the present writer that the same feature would be present in the maximum lift curves if this law were used instead of the  $1/7$ th power law.

The sudden jump in the curves shown in fig. 16 is due to the functions  $(U^2 z)_s$ , as found from the flow in the laminar portion round the nose, staying nearly constant over the range  $15^\circ$  to  $22^\circ$  of the angle of incidence. If we write

$$\left(\frac{\bar{U}\delta}{\nu}\right)_s = (C^2 + DR_c)^{\frac{1}{2}}, \quad (12.3)$$

where  $D$  is a constant, we find

$$R_c = \frac{C^2}{(U^2 z)_s - D}.$$

By choosing  $D$  to be nearly equal to the value of  $(U^2 z)_s$  for  $15^\circ < \theta < 22^\circ$ , the slight variations in the value of  $(U^2 z)_s$  produce greatly magnified effects in the values of  $R_c$ . The curves in fig. 17 were obtained in this way by putting  $D = 6.25$ .

Unfortunately, no experimental curves of scale effect on maximum lift coefficient for an elliptic cylinder seem to have been published. The curves in fig. 17 are physically more plausible than those in fig. 16, and, moreover, they seem to bear some resemblance to those found by Relf

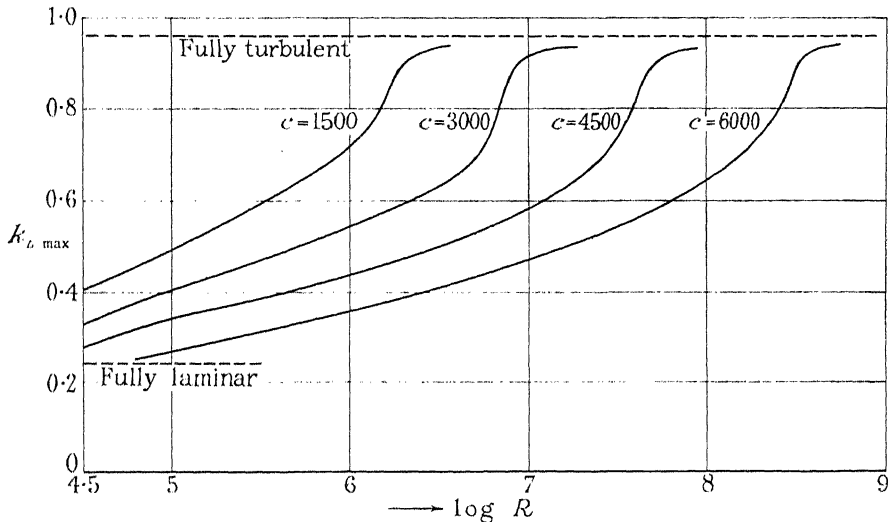


FIG. 17—Scale effect on maximum lift; second calculation

in some recent tests on a number of aerofoils in the compressed air tunnel for Reynolds numbers between  $10^6$  and  $7 \times 10^6$ . We cannot attempt a satisfactory determination of the function  $f(R_c)$  until experimental results are available. The form used in (12.3) was chosen to eliminate an improbable feature in the curves in fig. 16, but it does not appear possible to proceed further along these lines in the determination of  $f(R_c)$ .

For any particular value of the Reynolds' number, such that flow in the boundary layer is neither fully laminar nor fully turbulent, the lift coefficient-incidence curve is similar to the one given in fig. 14 except that stalling occurs earlier. The slope of the straight part has the same

value—2.70—as the fully turbulent case if we make assumption (b). The value given by assumption (a) is slightly less and is about 2.65.

It will be noticed from figs. 12 and 13 that the points of separation are further from the nose when transition takes place as late as possible than when the boundary layer is fully turbulent. Further, as the point of transition moves nearer to the nose the points of separation do as well. In effect, this means that, provided we may assume that the form of the pressure distribution remains the same as the Reynolds' number of the flow increases, the points of separation move nearer to the nose as the Reynolds' number increases once transition to turbulence has taken place. I have never seen any reference to such a phenomenon. It is possible, however, that slight changes in the pressure distribution as the Reynolds' number increases may more than counteract this tendency of the points of separation to move forward. This has been found to be so for a circular cylinder.

I wish to acknowledge my indebtedness to Dr. Goldstein for suggesting this paper and for the many helpful suggestions he has made.

#### SUMMARY

For a range of values of the angle of incidence, the circulation around an infinitely long thin elliptic cylinder has been determined theoretically. The calculations fall into three classes according as the boundary layer is fully laminar, fully turbulent or contains both laminar and turbulent portions.

---

## The Secondary Cathode Rays Expelled from Metals by Molybdenum $K\alpha$ Radiations

By H. R. ROBINSON, F.R.S., and C. J. B. CLEWS, B.Sc., A.Inst.P., Queen Mary College (University of London)

(Received March 7, 1935)

### § 1—INTRODUCTION

Kretschmar† has recently described a series of accurate measurements of the energies of the electrons expelled by molybdenum  $K\alpha_1$  radiations from targets of gold, platinum, silver and copper. He deduced his electron energies from deflections in an accurately known magnetic field, and it is obviously important to compare his results with those of similar recent work‡ § || in which other primary radiations (copper and chromium K-rays) were used to excite secondary electrons from the same targets.

Kretschmar† applies his results to the deduction of a value for the specific charge,  $e/m_0$ , of the electron. In doing this he has to assume a value for  $e/h$ , as well as values of X-ray wave-lengths. He eliminates part (not all) of the effect of uncertainty in the absolute values of the wave-lengths by using the X-ray (inverse photoelectric effect) value for  $e/h$ . He takes, in fact,  $e/h = 7.2796 \times 10^{16}$  e.s.u.  $\text{erg}^{-1} \text{sec}^{-1}$ —the mean of the values given by Duane, Palmer and Yeh¶ and by Feder.\*\* He then deduces, as the mean result of his own deflection experiments,  $1.757 \times 10^7$  e.m.u.  $\text{gm}^{-1}$  as the most probable value of  $e/m_0$ .

In papers†† ‡‡ §§ published from this laboratory, the experimental results are handled somewhat differently. It is shown, however (*see especially* §§), that with this value of  $e/m_0$  and a well-authenticated, if somewhat low, value of  $e/h$ , the photoelectric results can be brought into substantial agreement with the general body of standard (crystal) X-ray spectroscopic data. It would therefore appear at first sight that Kretschmar's

† 'Phys. Rev.', vol. 43, p. 417 (1933).

‡ Robinson, Andrews and Irons, 'Proc. Roy. Soc.', A, vol. 143, p. 48 (1933).

§ Robinson, 'Proc. Phys. Soc.', vol. 46, p. 693 (1934).

|| Robinson, 'Phil. Mag.', vol. 18, p. 1086 (1934).

¶ 'Proc. Nat. Acad. Sci. Wash.', vol. 7, p. 237 (1921).

\*\* 'Ann. Physik', vol. 1, p. 494 (1929).

†† Robinson, Andrews and Irons, 'Proc. Roy. Soc.', A, vol. 143, p. 48 (1933).

‡‡ Robinson, 'Proc. Phys. Soc.', vol. 46, p. 693 (1934).

§§ Robinson, 'Phil. Mag.', vol. 18, p. 1086 (1934).

work is in excellent accord with the measurements made here, especially as we use a very similar value ( $7.2827 \times 10^{10}$ ) of  $e/h$ .

The agreement is, however, only superficial, as we have taken appreciably different values for the X-ray energy levels used in the work. This fact is not immediately obvious from inspection of the papers, since Kretschmar quotes all X-ray data in terms of wave-length, while we always work in frequencies (Rydberg units). The differences have an important bearing on the comparison of the two sets of results, especially as our results, obtained with comparatively soft primary X radiations, are very sensitive to small changes in the level values.

Careful inspection of the two sets of results leads to the conclusion that our data indicate a rather higher scale of  $rH^\dagger$  values than those of Kretschmar. This conclusion also follows from the calculations given by Ruark $^\ddagger$  in an important recent paper. In view of the importance of this work in connection with the evaluation of the fundamental atomic constants, it was therefore decided to make as direct a comparison as possible with Kretschmar's work. Kretschmar's measurements with molybdenum K-rays have now been repeated in the same apparatus, and with the same plate-holder, as were used in our work with chromium and copper K-rays. The results of the new measurements are summarized in Table I. We are not able to give results for the gold and platinum  $M_{IV}$  levels, as these were not completely separated from  $M_V$  on our plates. Some of the results for platinum are duplicated in the table, as Kretschmar gives two different sets of values, based on two different plates.

## § 2—RESULTS

TABLE I

Element	Level	( $rH$ )	( $rH$ )'	$\Delta$	$\Delta \times 100$
		Present work	Kretschmar	( $rH$ )—( $rH$ )'	$\frac{\Delta}{rH}$ %
79 Gold .....	$M_I$	402.7 <sub>0</sub>	402.201	0.50	0.124
	$M_{II}$	406.7 <sub>8</sub>	406.240	0.54	0.133
	$M_{III}$	412.7 <sub>5</sub>	412.043	0.71	0.172
	$M_V$	419.7 <sub>7</sub>	419.741	0.03	0.007
78 Platinum (1) ..	$M_I$	404.4 <sub>2</sub>	404.317	0.10	0.025
	$M_{II}$	408.4 <sub>1</sub>	408.125	0.29	0.071
	$M_{III}$	413.9 <sub>7</sub>	413.588	0.38	0.092
	$M_V$	421.0 <sub>0</sub>	421.176	—0.18	—0.043

$^\dagger$  The results are most conveniently expressed in terms of the product  $rH$ , where  $r$  is the radius of curvature of the trajectory of the electron in a magnetic field of strength  $H$ , perpendicular to the plane of the trajectory.

$^\ddagger$  'Phys. Rev.', vol. 45, p. 827 (1934).

TABLE I—(continued)

Element	Level	( <i>rH</i> ) Present work	( <i>rH</i> )' Kretschmar	$\Delta =$ ( <i>rH</i> )—( <i>rH</i> )'	$\frac{\Delta \times 100}{rH}$ %
78 Platinum (2) ..	M <sub>I</sub>	404·4 <sub>2</sub>	404·165	0·26	0·064
	M <sub>II</sub>	408·4 <sub>1</sub>	407·868	0·54	0·132
	M <sub>III</sub>	413·9 <sub>7</sub>	413·318	0·65	0·157
47 Silver .....	L <sub>I</sub>	397·1 <sub>5</sub>	396·960	0·19	0·048
	L <sub>III</sub>	403·6 <sub>7</sub>	403·537	0·13	0·032
29 Copper .....	K	312·2 <sub>6</sub>	311·891	0·37	0·118

### § 3—ACCURACY OF RESULTS

The arrangement of Table I is almost self-explanatory. The first two columns give the element and level in which the photoelectron originates. Column 3 gives our value of (*rH*) in cm gauss; column 4 is the corresponding result of Kretschmar, which we have distinguished by accenting thus: (*rH*)'; column 5 gives  $\Delta = (rH) - (rH)'$ , and in the last column  $\Delta$  is expressed as a percentage of (*rH*).

Before discussing these results, it may be well to point out that, with the exception of those from the copper K level, all the photoelectrons listed above have energies outside the range for which our apparatus was originally designed. It was of the essence of this comparison that the photoelectrons expelled by the molybdenum K radiations should be examined under exactly the same geometrical conditions as those expelled by the copper and chromium radiations. It was therefore necessary to use fields corresponding to values of *r* in the neighbourhood of 5 cm, *i.e.*, fields of about 80 to 84 gauss. With weaker fields and larger *r* the corrections for inhomogeneity of field become much more important, and the comparison becomes in effect rather indirect.

In brief, the larger fields employed in the present work were approximately 50% greater than the strongest fields required in the earlier experiments; the heating effect in the Helmholtz coils was therefore approximately doubled. As a result it became much more difficult to maintain the field constant to the required degree of accuracy, and it was necessary to complete the longer exposures by instalments, in order to avoid excessive heating of the coils and their brass formers. Further, with these larger magnetic fields, the exact placing of the X-ray tube (which affects the focussing of the primary cathode stream upon the anticathode)



becomes much more critical. It may be recalled<sup>†</sup> that, in the interest of accuracy, no compensating coils are now used to neutralize the effect on the cathode beam of the non-axial components of the field. The absence of these coils certainly made adjustment more difficult in strong magnetic fields, and, we believe, it in part accounted for a certain capriciousness in the running of the tube.

The present experiments were therefore carried out under conditions less favourable to accuracy than those applying in previous work.<sup>† ‡ §</sup> Nevertheless, every care has been taken, and for every line given in Table I the result is the mean of at least 15 measurements on five or six different plates. In every test the element was used for the target, either in the form of leaf or of a film sputtered on aluminium, and precautions were taken to ensure that the target was in good electrical communication with the body of the metal plate-holder.

So far as can be judged from the internal consistency of the measurements, our *relative* values of ( $rH$ ) should not be in error by more than about 0.1 cm gauss; in quoting them to the nearest 0.01 cm gauss we follow common practice rather than the best precept.

#### § 4—DISCUSSION OF THE RESULTS

It will be seen that in general (in fact, with only one exception) our results are a little higher than those of Kretschmar. The differences are less regular than we should have anticipated, and certain features in their distribution appear to suggest a need for further investigation. With so few results, however, the only obvious course at the present stage is to take the mean value of the differences. There is no obvious reason for assigning different weights to different lines, as although there are minor differences in intensity and sharpness, the difficulties of measurement are not markedly different.

The average excess of our ( $rH$ ) values over those of Kretschmar is 0.081%, or very nearly 1 part in 1250. This is not perhaps a large difference, but unfortunately it implies a difference of 1 part in 625 in the energy or equivalent frequency, with which we are more directly concerned. It is, however, satisfactory to note that the discrepancy is exactly of the sign which would be expected to arise from certain differences in procedure between Kretschmar and ourselves.

<sup>†</sup> Robinson, Andrews and Irons, 'Proc. Roy. Soc.,' A, vol. 143, p. 48 (1933).

<sup>‡</sup> Robinson, 'Proc. Phys. Soc.,' vol. 18, p. 46 (1934).

<sup>§</sup> Robinson, 'Phil. Mag.,' vol. 18, p. 1086 (1934).

Kretschmar, in fact, used as targets very thin metallic films (sputtered or deposited from vapour), in which he assumed that there could be no appreciable retardation of any escaping photoelectrons, even from the deepest layers. He then, assuming that the "tail" on the low-velocity side of the spectral lines had been entirely suppressed, made his measurements between the centre of the slit and the centre of the line. Now, with the semicircular focussing method used in this work there is always, on account of the finite width of the target, a slight broadening of the lines on their low-velocity sides. Moreover, there is another broadening of the line in the same sense, which depends on a quite different feature of the geometry of the method, namely, the nature of the paths pursued by photoelectrons which start off in directions slightly inclined to the plane of symmetry of the apparatus.

From both these causes there results a displacement, towards the low-velocity end of the spectrum, of what may be called the centre of gravity of a spectral line. In brief, Kretschmar's method of procedure tends to give too low values of ( $rH$ ).

In our work we measure from the high-velocity edge of the "line" to the nearer edge of the slit. Measurement to an edge is admittedly more difficult—and therefore less accurate—than measurement to the apparent centre of a sharp and narrow band, but we believe that in this type of work the result of the former measurement approximates more closely to the quantity sought.

On the other hand, there are two physical factors which tend to "spread" the lines also on their high-velocity sides.† Firstly, there is a factor due to the imperfect homogeneity of the effective constituent of the primary X-rays—the factor which is most conveniently expressed by the "natural width" of the corresponding line in the X-ray spectrum. Moreover, this almost certainly has its counterpart in the level from which the electron is extracted. Secondly, there may be a little spread due to the penetration of the electrons into, and scattering in, the photographic emulsion. This is not likely to be large with the plates used in most of our work—Hilger Schumann plates—and we have no evidence of systematic differences in the results obtained with plates differing widely in thickness of emulsion (Ilford X-ray, Paget Half-Tone and Hilger Schumann). We do not think that the combined effect of these two factors can be large—in fact we scarcely think it large enough to have any measurable influence on our results—but at least theoretically it means that we are tending to measure upper limits for the electron velocities.

† Robinson, 'Proc. Phys. Soc.,' vol. 46, p. 693 (1934).

Kretschmar's measurements will scarcely be affected by these physical factors, as their effect will presumably be an almost symmetrical broadening of the lines.

Most of the levels measured by Kretschmar are of (negative) energy, too low to admit of easy separation of the lines due to the two components of  $\text{Mo K}\alpha$ . We have, however, using a thin film of copper sputtered on aluminium, clearly separated the two lines produced in this way by electrons from the copper K level. We have therefore been able to measure accurately the "centre" of the line due to  $\text{Mo K}\alpha_1$ , and hence to deduce a value of  $(rH)$  which should be comparable with that given by Kretschmar.

The result is of considerable interest in connection with the preceding discussion: measurement from edge of line to edge of slit gives  $(rH) = 312.2_8$  while that from centre of line to centre of slit on the same plate gives  $311.9_8$ . The latter value differs only by one part in 3500 from Kretschmar's  $311.891$ —a remarkably close agreement when it is considered that there are minor differences in the geometry of the two experimental arrangements, which would cause slightly different amounts of geometrical broadening of the lines.

It does therefore appear highly probable that the discrepancy of 1 part in 1250 between our results and those of Kretschmar may be almost entirely attributable to the circumstance that we are tending to measure upper, and Kretschmar lower, limits to the electron velocities. If this can be accepted, it means that there can be no serious disagreement between the two magnetic standardizations, viz., of Kretschmar's solenoid and our Helmholtz coil. The comparison therefore turns out much more satisfactorily than at first appeared likely. Unless the agreement is a mere coincidence, it clearly makes it probable that neither set of  $(rH)$  values is far from the truth—that, for example, the mean of the two should not be in error by more than 1 part in 2000.

#### § 5—RELATION OF THE RESULTS TO OTHER PHOTOELECTRIC RESULTS AND TO THE ATOMIC CONSTANTS

There is one further way in which we may apply our results. First we calculate the energies from the  $(rH)$  values and express them as equivalent frequencies  $(\nu^*/R)$  in Rydberg units. To do this we assume, as in the earlier work†‡  $e/m_0 = 1.757 \times 10^7$  e.m.u.  $\text{gm}^{-1}$ ,

† Robinson, 'Proc. Phys. Soc.,' vol. 46, p. 693 (1934).

‡ 'Phil. Mag.,' vol. 18, p. 1086 (1934).

and  $e/h = 7 \cdot 2827 \times 10^{16}$  e.s.u. erg<sup>-1</sup> sec<sup>-1</sup>. The resulting values of  $\nu^*/R$  are :—

Au M <sub>I</sub> 1037·6	Pt M <sub>I</sub> 1046·4
M <sub>II</sub> 1058·5	M <sub>II</sub> 1066·9
M <sub>III</sub> 1089·3	M <sub>III</sub> 1095·7
M <sub>V</sub> 1126·2	M <sub>V</sub> 1132·7
Ag L <sub>I</sub> 1009·6	
L <sub>III</sub> 1042·6	

The copper K level is omitted, as it has no application here.

We can now combine these, as in the previous paper,<sup>†</sup> with the results obtained with copper and chromium K rays. Thus, take for example the  $(\nu^*/R)$  for the gold M<sub>I</sub> level (1037·6). The corresponding value of  $\nu^*/R$  for the photoelectrons ejected from the same level by copper K $\alpha_1$  rays is 340·8. The difference between these two figures (696·8) is to be compared with the difference between the two primary frequencies, *i.e.*, Mo K $\alpha_1$  — Cu K $\alpha_1$  = 1287·42 — 592·74 = 694·7 Rydbergs. The corresponding values for chromium K $\alpha_1$  are  $\Delta(\nu^*/R) = 1037 \cdot 6 - 146 \cdot 5 = 891 \cdot 1$ , and Mo K $\alpha_1$  — Cr K $\alpha_1$  = 1287·42 — 398·80 = 888·6.

Taking the necessary data from Robinson,<sup>‡</sup> and using all available level values, we have:—

Mo — Cu, $\Delta(\nu^*/R)$			
Au M <sub>I</sub>	696·8 = 694·7 + 2·1	Pt M <sub>I</sub>	695·7 = 694·7 + 1·0
M <sub>II</sub>	697·1 = 694·7 + 2·4	M <sub>II</sub>	696·2 = 694·7 + 1·5
M <sub>III</sub>	698·0 = 694·7 + 3·3	M <sub>III</sub>	696·9 = 694·7 + 2·2
M <sub>V</sub>	695·1 = 694·7 + 0·4	M <sub>V</sub>	695·2 = 694·7 + 0·5
Ag L <sub>I</sub> 696·9 = 694·7 + 2·2			
L <sub>III</sub> 696·2 = 694·7 + 1·5			

The mean value of  $\Delta(\nu^*/R)$  is 694·7 + 1·7; that is, the “photo-electric” difference,  $\Delta(\nu^*/R)$ , exceeds the corresponding X-ray (“crystal”) value by 0·2<sub>4</sub>%.

Similarly, the comparison with the chromium results gives:—

Mo — Cr, $\Delta(\nu^*/R)$			
Au M <sub>I</sub>	891·1 = 888·6 + 2·5	Pt M <sub>I</sub>	890·1 = 888·6 + 1·5
M <sub>II</sub>	891·4 = 888·6 + 2·8	M <sub>II</sub>	890·3 = 888·6 + 1·9
M <sub>III</sub>	892·3 = 888·6 + 3·7	M <sub>III</sub>	891·3 = 888·6 + 2·7
M <sub>V</sub>	889·6 = 888·6 + 1·0	M <sub>V</sub>	889·7 = 888·6 + 1·1
Ag L <sub>I</sub> 891·0 = 888·6 + 2·4			
L <sub>III</sub> 890·4 = 888·6 + 1·8.			

<sup>†</sup> ‘Phil. Mag.’ vol. 18, p. 1086 (1934).

<sup>‡</sup> ‘Phil. Mag.’ vol. 18, p. 1097 (1934).

Mean value,  $888.6 + 2.1$ , *i.e.*, the photoelectric value exceeds the crystal value by  $0.2_4\%$ .

Paired in the same way,† the copper and chromium results show a difference of  $0.12_4\%$  in the same sense.

This method of expressing the results is very sensitive to small changes in the values adopted for the constants and primary X-ray frequencies, and to small errors in the measurements of ( $rH$ ). In fact, for all the data used in the last comparison, an error of 1 part in 2000 in the measurement of ( $rH$ ) affects the equivalent frequency by more than one Rydberg. When this is kept in mind, it appears that the photoelectric results are remarkably consistent, and could be made even more so by quite trivial manipulation of the X-ray frequencies. The most unsatisfactory feature, from the point of view of our present measurements, is that our values for the  $M_{III}$  levels of gold and platinum come out rather excessively high, both in the comparison with Kretschmar's results and with the work with copper and chromium K rays. This may be a matter for further examination, but all that need be said at present is that these anomalous values do not seriously affect the average result.

We do not propose here to discuss in detail the relation of the photoelectric results to the general problem of X-ray data and atomic constants. We may, however, recall that all the photoelectric measurements from this Laboratory are in agreement on one point—namely, that they can only, if at all, be reconciled with X-ray measurements and with widely accepted values of the atomic constants by taking something very near to lower limits of  $e/m_0$  and  $e/h$ . Even so, it is necessary to retain the “crystal” values of the X-ray wave-lengths, as the agreement, already imperfect, is made worse if the “grating” values are taken. These conclusions are strengthened, rather than weakened, by the results of the present comparison with Kretschmar's work.

The existing difficulty is emphasized in two directions by the most recent work on the subject. In the first place, it seems clear that, as was previously suspected, the true value of  $e/m_0$  is appreciably greater than  $1.757 \times 10^7$ . Shane and Spedding,‡ from a very careful comparison of  $H^1\alpha$  with  $H^2\alpha$ , find  $e/m_0 = (1.7579 \pm 0.0003) \times 10^7$ , which is in very close agreement with Kirchner's§ value  $(1.7585 \pm 0.0012) \times 10^7$ .

In the second place, the latest evidence is in favour of the ruled grating wave-lengths. Bearden and Shaw|| now find that X-ray wave-lengths

† Robinson, 'Phil. Mag.', vol. 18, p. 1097 (1934).

‡ 'Phys. Rev.', vol. 47, p. 33 (1935).

§ 'Ann. Physik,' vol. 12, p. 503 (1932).

|| 'Phys. Rev.', vol. 46, p. 759 (1934).

deduced from the refraction in quartz are in close agreement with the grating values, and it appears from their measurements that the X-unit is very nearly  $1.0023 \times 10^{-11}$  cm. The most recent "ruled grating" results are in substantial agreement with much of the earlier work with gratings; Bäcklin† finds the wave-length of  $\text{Al K}\alpha_{1,2}$  to be  $8.3395 \text{ \AA} \pm 0.012\%$  (mean of 56 concordant measurements with a ruled grating), and Södermann‡ finds for the same line  $(8.340 \pm 0.001) \text{ \AA}$ . Comparison of these with the crystal value of Larsson gives for the X unit  $1.00218$  and  $1.00225 \times 10^{-11}$  cm respectively.

Our photoelectric results cannot be brought into line with these values of  $e/m_0$  and the X unit without an almost iconoclastic revision of certain of the constants. We have to thank Professor Arthur E. Ruark for his kindness in sending to one of us, at about the time when this work was being completed, an advance copy of a note on a particularly appropriate method of recalculating the atomic constants in a suitable form for application to X-ray and photoelectric data. This will doubtless form the best basis for the further discussion of our results.

#### SUMMARY

The energies of the photoelectrons expelled from targets of gold, platinum, silver, and copper by molybdenum  $\text{K}\alpha$  rays have been measured in the magnetic spectrometer. The results are compared with those of Kretschmar for the same elements, and briefly discussed in their relation to the absolute values of X-ray wave-lengths and the principal atomic constants.

† 'Nature,' vol. 135, p. 32 (1935).

‡ 'Nature,' vol. 135, p. 67 (1935).

## The Kinetics of Photosynthesis

(Abstract)

By E. C. C. BALY, F.R.S.

(Received December 4, 1934)

It has been proved that the primary process in photosynthesis is an oxidation-reduction reaction. Expressing this in the simplest terms of chlorophyll, a complex of chlorophyll A and hydrated  $\text{CO}_2$  is converted by the action of light into chlorophyll B and activated formaldehyde which at once undergoes polymerization into hexoses. The chlorophyll B thereby produced undergoes the dark or Blackman reaction and is reduced to chlorophyll A. There are, therefore, three separate processes involved in the photosynthetic cycle, namely, the primary photosynthetic reaction, the Blackman reaction, and the formation of the photosensitive complex of chlorophyll A and hydrated  $\text{CO}_2$ .

Since the Blackman reaction regenerates chlorophyll A from the chlorophyll B produced in the primary reaction, a photostationary state will be established which is determined by the intensity of irradiation, the temperature and the external concentration of hydrated  $\text{CO}_2$ . In this communication the equation for the photostationary state is derived, and shown to express correctly the variation in the rate of photosynthesis with temperature.

In view of the evidence that the primary photosynthetic process consists of two consecutive light reactions, one promoted by blue light and the other by red light, the equations for the photostationary state are modified by the substitution of the term  $I_1 I_2 / (I_1 + I_2)$  in which  $I_1$  and  $I_2$  are the intensities of the blue and red rays, respectively. The equations give a satisfactory explanation of (1) the effect of changing the four variables, temperature,  $\text{CO}_2$  concentration, total light intensity, and the relative intensities of blue and red light, (2) the effect of irradiation by flashing light, and (3) the effect of poisons, in the case of the uni-cellular alga *Chlorella*.

(The full paper is published in 'Proc. Roy. Soc.,' B, vol. 117, p. 218 (1935))

---

## INDEX TO VOLUME CXLIX (A)

- Acetaldehyde, thermal decomposition (Winkler and Hinshelwood), 355.
- Acetone vapour, thermal decomposition (Winkler and Hinshelwood), 340.
- Alty (T.) and Mackay (C. A.) The accommodation coefficient and the evaporation coefficient of water, 104.
- Aluminium, single crystals, behaviour in fatigue under complex stresses (Cox and Clenshaw), 312.
- Amaldi (E.), D'Agostino (O.), Fermi (E.), Pontecorvo (B.), Rasetti (F.) and Segrè (E.) Artificial radioactivity produced by neutron bombardment, II, 522.
- Angus (W. R.) and Leckie (A. H.) Investigations of Raman Spectra. I—The Raman spectra of sulphuric, nitric and nitrosylsulphuric acids, 327.
- Aston (F. W.) The isotopic constitution and atomic weights of hafnium, thorium, rhodium, titanium, zirconium, calcium, gallium, silver, carbon, nickel, cadmium, iron and indium, 396.
- Atomic weights and isotopic constitution of hafnium, thorium, rhodium, titanium, zirconium, calcium, gallium, silver, carbon, nickel, cadmium, iron and indium (Aston), 396.
- Barrer (R. M.) and Rideal (E. K.) The interaction of hydrogen with micro-crystalline charcoal, I, 231.
- Barrer (R. M.) Interaction of hydrogen with micro-crystalline charcoal. II—Activated sorption of hydrogen and methane by carbon, 253.
- Bastings (L.) Shear waves through the earth's core, 88.
- Bethe (H.) and Peierls (R.) The scattering of neutrons by protons, 176.
- Blackman (M.) Contributions to the theory of specific heat. III—On the existence of pseudo- $T^3$  regions in the specific heat curve of a crystal, 117.
- Blackman (M.) Contributions to the theory of specific heat. IV—On the calculation of the specific heat of crystals from elastic data, 126.
- Buckingham (R. A.) *See* Hulme and others.
- Cathode rays, secondary, expelled from metals by molybdenum  $K\alpha$  radiations (Robinson and Clews), 587.
- Charcoal, micro-crystalline, interaction with hydrogen, I (Barrer and Rideal, and Barrer), 231, 253.
- Clark (R. E. D.) *See* Palmer and Clark.
- Clenshaw (W. J.) *See* Cox and Clenshaw.
- Clews (C. J. B.) *See* Robinson and Clews.
- Cloud-track method of investigating transmutation of heavy hydrogen (Dee and Gilbert), 200.
- Coefficient, accommodation, of hydrogen, effect of temperature (Gregory), 35.
- Coefficient, accommodation, of water (Alty and Mackay), 104.
- Copper, X-ray study of inter-diffusion with zinc (Owen and Pickup), 282.
- Counting experiments, statistical error (Peierls), 467.
- Cox (H. L.) and Clenshaw (W. J.) The behaviour of three single crystals of aluminium in fatigue under complex stresses, 312.
- Crystals, specific heat (Blackman), 117, 126.
- Cylinder, thin elliptic, lift coefficient (Howarth), 558.



- D'Agostino (O.) *See* Amaldi and others.
- Dee (P. I.) and Gilbert (C. W.) Transmutation of heavy hydrogen investigated by the cloud-track method, 200.
- Disturbance, magnetic, diurnal variation in high latitudes (Stagg), 298.
- Eastwood (E.) and Snow (C. P.) Electronic spectra of polyatomic molecules. I—Saturated aldehydes, II—Acrolein, 434, 446.
- Error, statistical, in counting experiments (Peierls), 467.
- Essen (L.) International frequency comparisons by means of standard radio frequency emissions, 506.
- Evaporation coefficient of water (Alty and Mackay), 104.
- Fermi (E.) *See* Amaldi and others.
- Fowler (R. H.) A theory of the rotations of molecules in solids and of the dielectric constant of solids and liquids, 1.
- Fowler (R. H.) *See also* Hulme and others.
- Frequency comparisons by means of standard radio frequency emissions (Essen), 506.
- Gamma rays, photoelectric absorption in heavy-elements (Hulme and others), 131.
- Gauss' theorem and concept of mass in general relativity (Whittaker), 384.
- Gilbert (C. W.) *See* Dee and Gilbert.
- Gregory (H. S.) Effect of temperature on the thermal conductivity and the accommodation coefficient of hydrogen, 35.
- Hartree (D. R.) and Hartree (W.) Results of calculations of atomic wave functions. III—Results for Be, Ca and Hg, 210.
- Hartree (W.) *See* Hartree and Hartree.
- Havelock (T. H.) Ship waves : the relative efficiency of bow and stern, 417.
- Hinshelwood (C. N.) *See* Winkler and Hinshelwood.
- Howarth (L.) The theoretical determination of the lift coefficient for a thin elliptic cylinder, 558.
- Hulme (H. R.), McDougall (J.), Buckingham (R. A.) and Fowler (R. H.) Photoelectric absorption of  $\gamma$ -rays in heavy elements, 131.
- Hydrogen, effect of temperature on thermal conductivity and accommodation coefficient (Gregory), 35.
- Hydrogen, heavy, transmutation investigated by cloud-track method (Dee and Gilbert), 200.
- Hydrogen, interaction with micro-crystalline charcoal, I, II (Barrer and Rideal, and Barrer), 231, 253.
- Hydrogen, rotational dispersion of sound (Roy and Rose), 511.
- Iodine, nuclear spin, I (Tolansky), 269.
- Ions, gaseous, variation of mobility (Tyndall and Pearce), 426.
- Isotopic constitution and atomic weights of hafnium, thorium, rhodium, titanium, zirconium, calcium, gallium, silver, carbon, nickel, cadmium, iron and indium (Aston), 396.
- Kempton (A. R.) *See* Oliphant and others.
- Krishnamurty (S. G.) and Rao (K. R.) Investigations on the spectrum of selenium. V—Structure of Se II, 56.
- Kurti (N.) and Simon (F.) Experiments at very low temperatures obtained by the magnetic method. I—The production of the low temperatures, 152.

- Lattice, polar crystal, spectrum of normal frequencies (Thompson), 487.
- Leckie (A. H.) *See* Angus and Leckie.
- Lee (A. W.) Direction of approach of microseismic waves, 183.
- Lift coefficient for a thin elliptic cylinder, theoretical determination (Howarth), 558.
- Liquids, dielectric constant (Fowler), 1.
- London (F. and H.) Electromagnetic equations of the supraconductor, 71.
- London (H.) *See* London (F. and H.).
- Mackay (C. A.) *See* Alty and Mackay.
- McDougall (J.) *See* Hulme and others.
- Microseismic waves, direction of approach (Lee), 183.
- Molecules, polyatomic, electronic spectra, I and II (Eastwood and Snow), 434, 446.
- Molecules, theory of rotations in solids (Fowler), 1.
- Molybdenum  $K\alpha$  radiations, expulsion of secondary cathode rays from metals (Robinson and Clews), 587.
- Neutron bombardment, production of artificial radioactivity (Amaldi and others), 522.
- Neutrons, scattering by protons (Bethe and Peierls), 176.
- Nuclear transformations, accurate determination of energy released (Oliphant and others), 406.
- Oliphant (M. L. E.), Kempton (A. R.) and Rutherford (Lord) Accurate determination of the energy released in certain nuclear transformations, 406.
- Owen (E. A.) and Pickup (L.) X-ray study of the inter-diffusion of copper and zinc, 282.
- Pai (N. Gopala) Raman spectra of certain organo-metallic compounds, 29.
- Palmer (W. G.) and Clark (R. E. D.) Adsorption of measured surfaces of vitreous silica, 360.
- Pearce (A. F.) *See* Tyndall and Pearce.
- Peierls (R.) Statistical error in counting experiments, 467.
- Peierls (R.) *See* Bethe and Peierls.
- Pickup (L.) *See* Owen and Pickup.
- Pontecorvo (B.) *See* Amaldi and others.
- Protons scattering neutrons (Bethe and Peierls), 176.
- Radio frequency emissions, standard, frequency comparisons by means of (Essen), 506.
- Radioactivity, artificial, produced by neutron bombardment (Amaldi and others), 522.
- Raman spectra of sulphuric, nitric, and nitrosylsulphuric acids (Angus and Leckie), 327.
- Rao (K. R.) *See* Krishnamurty and Rao.
- Rasetti (F.) *See* Amaldi and others.
- Relativity, general, concept of mass (Whittaker), 384.
- Rideal (E. K.) *See* Barrer and Rideal.
- Robinson (H. R.) and Clews (C. J. B.) The secondary cathode rays expelled from metals by molybdenum  $K\alpha$  radiations, 587.
- Rose (M. E.) *See* Roy and Rose.
- Rotation of molecules (Fowler), 1.
- Roy (A. S.) and Rose (M. E.) The rotational dispersion of sound in hydrogen, 511.

Rutherford (Lord) *See* Oliphant and others.

Segrè (E.) *See* Amaldi and others.

Selenium, investigations on the spectrum (Krishnamurty and Rao), 56.

Ship waves, relative efficiency of bow and stern (Havelock), 417.

Silica, vitreous, adsorption of measured surfaces (Palmer and Clark), 360.

Simon (F.) *See* Kurti and Simon.

Snow (C. P.) *See* Eastwood and Snow.

Solids, rotations of molecules and dielectric constant (Fowler), 1.

Sound, rotational dispersion in hydrogen (Roy and Rose), 511.

Specific heat, contributions to theory, III and IV (Blackman), 117, 126.

Spectra, electronic, of polyatomic molecules, I and II (Eastwood and Snow), 434, 446.

Spectra, Raman, of certain organo-metallic compounds (Pai), 29.

Spectrum of normal frequencies of a polar crystal lattice (Thompson), 487.

Spectrum of selenium (Krishnamurty and Rao), 56.

Spectrum, spark of iodine (Tolansky), 269.

Stagg (J. M.) Diurnal variation of magnetic disturbance in high latitudes, 298.

Supraconductor, electromagnetic equations (London), 71.

Temperatures, very low, obtained by the magnetic method, I (Kurti and Simon), 152.

Thermal conductivity and accommodation coefficient of hydrogen, effect of temperature (Gregory), 35.

Thompson (J. H. C.) On the spectrum of the normal frequencies of a polar crystal lattice. I—General theory, 487.

Tolansky (S.) The nuclear spin of iodine. I—Fine structure in the first spark spectrum, 269.

Transmutation of heavy hydrogen, cloud-track method of investigation (Dee and Gilbert), 200.

Tyndall (A. M.) and Pearce (A. F.) The variation of the mobility of gaseous ions with temperature. I—Positive ions in their own gas, 426.

Water, accommodation coefficient and evaporation coefficient, (Alty and Mackay), 104.

Wave functions, atomic, for Be, Ca, and Hg, III (Hartree and Hartree), 210.

Waves, microseismic, direction of approach (Lee), 193.

Waves, shear, through the earth's core (Bastings), 88.

Waves, ship (Havelock), 417.

Whittaker (E. T.) On Gauss' theorem and the concept of mass in general relativity, 384.

Winkler (C. A.) and Hinshelwood (C. N.) Thermal decomposition of acetone vapour, 340.

Winkler (C. A.) and Hinshelwood (C. N.) Thermal decomposition of acetaldehyde, 355.

Zinc, X-ray study of inter-diffusion with copper (Owen and Pickup), 282.





I. A. R. I. 75

IMPERIAL AGRICULTURAL RESEARCH  
INSTITUTE LIBRARY  
NEW DELHI.

[illegible]